

Reactivity in the Gas Phase and in Solution of Group 9 Metal Olefin Complexes

Simone Thewissen

Reactivity in the Gas Phase and in Solution of Group 9 Metal Olefin Complexes

(Reactiviteit van Groep 9 Metaal Olefine Complexen
in de Gasfase en in Oplossing)

Simone Thewissen

Reactivity in the Gas Phase and in Solution of Group 9 Metal Olefin Complexes
Thewissen, S.
Thesis Radboud University Nijmegen, **2005**
ISBN 90-9019497-5
Cover design Bas Vanmeulebrouk
Cover photos The Atlantic Ocean as viewed from Dias Beach
(situated at 34º 21' 15" south latitude and 18º 29' 02" east longitude)

Reactivity in the Gas Phase and in Solution of Group 9 Metal Olefin Complexes

(met een samenvatting in het Nederlands)

Een wetenschappelijke proeve op het gebied van de
Natuurwetenschappen, Wiskunde en Informatica

Proefschrift

ter verkrijging van de graad van doctor
aan de Radboud Universiteit Nijmegen,
op gezag van de Rector Magnificus, prof. dr. C.W.P.M. Blom
volgens besluit van het College van Decanen
in het openbaar te verdedigen op
woensdag 6 juli 2005
des namiddags om 1.30 uur precies

door

Simone Thewissen

Geboren op 10 november 1975 te Geleen

Promotores

Prof. Dr. R.J.M. Nolte

Prof. Dr. P. Chen *(Swiss Federal Institute of Technology Zurich, Switzerland)*

Prof. Dr. D.A. Plattner *(Albert Ludwigs University Freiburg, Germany)*

Copromotor

Dr. B. de Bruin

Manuscriptcommissie

Prof. Dr. A.E. Rowan

Prof. Dr. A.J.R. Heck *(Utrecht University)*

Dr. R. de Gelder

Een glimlach is een licht
In het venster van het gezicht,
Dat aangeeft dat het hart thuis is.
Japans gezegde

Mysterie is het mooiste dat een mens kan ervaren.
De erkenning dat het universum een mysterie is,
is de weg van alle ware wetenschap.
Albert Einstein (1879-1955)

Paranimfen

Etienne Thewissen

Sander Graswinckel

Contents

Voorwoord

Toen ik met mijn promotie begon zei iemand tegen mij: "Tijdens je AIO-schap zul je heel veel leren en je heel veel dingen eigen maken. Maar het meeste nog zul je leren over jezelf." Beter had het niet geformuleerd kunnen worden. Het is inderdaad een hele leerzame tijd geweest van het me eigen maken van nieuwe technieken en nieuwe chemie, het switchen tussen onderzoek in twee landen en twee laboratoria tot het begeleiden van studenten toe.

Dat ik met tevredenheid op mijn AIO-schap terug kan kijken is niet alleen mijn eigen verdienste geweest. Ik ben in de luxe positie geweest dat er altijd mensen in mijn omgeving zijn geweest die mij verder hebben geholpen op mijn pad, zowel op wetenschappelijk als op persoonlijk gebied.

I would like to thank Prof. Ton Gal and Prof. Peter Chen for making it possible for me to perform this inter-university PhD project and for giving me the freedom to give my own direction to my research. Bas, ik heb jouw aanbod om mijn co-promotor te worden en jouw daaruit vloeiende hulp bij mijn onderzoek in de vorm van steun, discussies en nieuwe ideëen heel erg gewaardeerd. Peter, je bent dan geen promotor of co-promotor van mij geworden, maar jouw bijdrage kwalificeert je er zeker voor: zowel op chemisch gebied als daarbuiten heb je mij menigmaal gestimuleerd of een hart onder de riem gestoken door het formuleren van jouw visie op dingen. Ik waardeer het heel erg hoe jullie beide op het einde, toen de tijd krap begon te worden, toch zoveel tijd vrij wisten te maken om mij door de laatste loodjes heen te helpen! Dietmar, ich möchte mich herzlich bei Dir bedanken für Deine Stütze und für Deine Hilfe bei alles (ob es über Chemie oder etwas anderes ginge). Auch Du hast am Ende, als die Zeit kurz wurde, Zeit für mich frei gemacht um den letzeten Korrekturen in Zeit durch zu führen zu können, das schätze ich sehr. Ik ben Prof. Nolte erkentelijk dat hij erin toe heeft gestemd om mijn Nijmeegse promotor te zijn. De reden hiervoor was niet leuk en ik had het graag anders gezien, maar ik ben blij dat voor mijn promotie zo alles goed geregeld heeft kunnen worden.

Jos, Maike, Theo en Tsi-Wai wil ik bedanken voor de bijdrage die ieder van hen geleverd heeft aan mijn promotie onderzoek.

Daarnaast ben ik alle mensen die werkzaam zijn en waren op de beide afdelingen, waar ik tijdens mijn promotie heb gewerkt, dankbaar voor hun hulp tijdens het dagelijks leven op het lab en voor het creëeren van een erg prettige werksfeer. Alle Mitarbeitern und Mitarbeiterinnen in der Chen Gruppe, die während all diese Jahren in der Gruppe gearbeitet haben, bin ich dankbar dafür, dass sie dafür gesorgt haben dass ich mich bei jedem Besuch an Zürich zu Hause gefühlt habe. Een paar mensen wil ik met name noemen.

Paul, het samen runnen van de Synthese III praktika zal me altijd bijblijven als heel erg gezellig en inspirerend. Ik heb het altijd heel erg fijn gevonden dat ik met jou over alles kon praten (zelfs tot Pergamano'en toe!). Koos, ik denk met veel plezier terug aan onze leerzame gesprekken die varieerden van lesgeven tot interpretaties van bijbelvoorstellingen. Trudy en Ingrid, na mekaar steun en toeverlaat van de afdeling. Informatie, dingen regelen, of gewoon een goed gesprek (over vanalles: kleinkinderen, creatieve inspiraties), ik kon altijd bij jullie terecht, echt geweldig! Jaap, ik waardeer het heel erg dat jij contactpersoon van de afdeling wilde zijn bij het regelen van de laatste dingen voor mijn promotie tijdens mijn verblijf in Kaapstad. Derek, Christian H., Christian A., Rolf und Ruedi, für Fragen oder wenn es sich ein Problem gäbe mit dem Gerät, immer seit ihr bereit gewesen um mir zu helfen. Das habe ich sehr geschätzt! André, Du hast mir jedes Mal geholfen um inert kurzem einen wirkenden Arbeitzplatz auf zu

bauen. Annette, es hat mir immer sehr gefreut um Dir zu e-mailen zu können dass ich wieder nach Zurich käme: alles war immer so gut versorgt und es hat mir immer sehr gefreut Dir wieder zu sehen.

Niet alleen op wetenschappelijk gebied, ook in spiritueel opzicht heb ik mij de afgelopen jaren zoveel mogen ontplooien. Ik wil in dit verband graag Jorike, Juliette en Joyce graag bedanken voor jullie vriendschap en voor de mogelijkheid die we kregen om ons gezamenlijk te ontwikkelen. Het is heerlijk om met gelijkgestemden over dergelijke zaken te kunnen praten en ervaringen uit te kunnen wisselen.

Ook wil ik Harriët en Iousha heel hartelijk bedanken voor hun hulp en steun die precies op die momenten kwam dat ik het nodig had.

Al dat ontwikkelen en groeien in de afgelopen tijd kon natuurlijk niet plaats hebben gevonden zonder de nodige ontspanning op z'n tijd. Hierin hebben mijn familie en vrienden natuurlijk een hele belangrijke rol gespeeld of het nu was met wandelingen, naar concerten gaan, heerlijk kwebbelen, een goed gesprek of wat dan ook. Ik ben dankbaar dat ik Sander, Anja, Timo, Jorike, Ingeborg, Maurice P., Angelique, Miranda en vele anderen tot mijn vrienden mag rekenen. Auch während meinen Besuchen an der Schweiz bin ich immer umringd gewesen von guten Freunden: Derek und Simone, Aswin, Carolien ich will euch danken für euren Freundschaft. Es hat mir immer sehr gefreut euch wieder zu sehen! Und ich hoffe, daß auch in der Zukunft wir uns regelmäßig besuchen bleiben.

Lieve papa en mama, zonder jullie steun door de jaren heen zou ik nooit zo ver gekomen zijn. Jullie hebben mij altijd gestimuleerd en 100% achter mij gestaan, welke beslissing ik ook nam in mijn leven. Hiervoor ben ik jullie heel erg dankbaar. Lieve Etienne, Andrea, Patrick, Marilène en Cyriel, ik prijs mij gelukkig met zo'n lieve familie. Heerlijk samen kletsen, samen kamperen, samen spelen, samen lachen, wat wenst een mens zich nog meer!

Tot slot wil ik mijn paranimfen, Sander en Etienne, nog extra hartelijk bedanken voor hun hulp bij het organiseren van alles wat met promoveren te maken heeft! Vanuit Kaapstad zou dit allemaal niet zo goed gelukt zijn.

Bas, miene leeve jóng, wae hei dat gedach, dat 't allemaol zoa zoe loupe. Veer saame mèt ós twièkes op avontuur… En ich geneet eeder moment d'rvan. V'r höbben 't zoa heerlik saame. En in de lètste tied veurdat v'r noa Kaapstad kaome, höbste mich zoa ontzeen, mich zoa de ruimte gegaeve óm alles op tied aaf te kriege en mich weer opgehólpe es ich 't èch aeve neet miè zooch zitte. Miene leeve jóng, ich houwt ongeluifelik vèùl van dich.

List of Abbreviations

bpa	*N*,*N*-di(2-pyridylmethyl)amine
bpa-Me	*N*-methyl-*N*,*N*-di(2-pyridylmethyl)amine
bpa-Bz	*N*-benzyl-*N*,*N*-di(2-pyridylmethyl)amine
Me_2-bpa	*N*,*N*-di[(6-methyl-2-pyridyl)methyl]amine
Me_2-bpa-Me	*N*-methyl-*N*,*N*-di[(6-methyl-2-pyridyl)methyl]amine
Me_2-bpa-Bz	*N*-benzyl-*N*,*N*-di[(6-methyl-2-pyridyl)methyl]amine
tpa	*N*,*N*,*N*-tri(2-pyridylmethyl)amine
Me-tpa	*N*-[(6-methyl-2-pyridyl)methyl]-*N*,*N*-di(2-pyridylmethyl)amine
Me_2-tpa	*N*,*N*-di[(6-methyl-2-pyridyl)methyl]-*N*-(2-pyridylmethyl)amine
Me_3-tpa	*N*,*N*,*N*-tri[(6-methyl-2-pyridyl)methyl]amine
tia	*N*,*N*,*N*-tri[(1-methyl-1*H*-2-imidazolyl)methyl]amine
coe	*Z*-1-cyclooctene
cod	*Z*,*Z*-1,5-cyclooctadiene
$HBAr^F_4$	oxonium acid $[H(OEt_2)_2]^+[(3,5\text{-}(CF_3)_2C_6H_3)_4B]^-$
RC 1	Reaction Chamber 1, the region before the second quadrupole mass analyzer, this corresponds to the 24-pole region of the Finnigan TSQ 700 and to the first octopole region of the Finnigan TSQ 7000
RC 2	Reaction Chamber 2, the region after the second quadrupole mass analyzer, this corresponds to the octopole region of the Finnigan TSQ 700 and to the seconc octopole region of the Finnigan TSQ 7000
CID	Collision Induced Dissociation (in the octopole region, RC 2)
CA	Collisional Activation (in the tube lens region)

List of Compound Numbers

[**1**]$^{+}$	[(κ^4-Me$_3$-tpa)Rh^{I}(C$_2$H$_4$)]$^{+}$
[**2**]$^{+}$	[(κ^4-Me$_2$-tpa)Rh^{I}(C$_2$H$_4$)]$^{+}$
[**3**]$^{+}$	[(κ^3-Me$_3$-tpa)Ir^{I}(C$_2$H$_4$)$_2$]$^{+}$
[**4**]$^{+}$	[(κ^4-Me$_3$-tpa)Ir^{I}(C$_2$H$_4$)]$^{+}$
[**5**]$^{+}$	[(κ^4-C,N,N',N''-Me$_3$-tpa)Ir^{III}(H)(CD$_3$CN)]$^{+}$
[**6**]$^{+}$	[(κ^4-Me$_2$-tpa)Ir^{I}(C$_2$H$_4$)]$^{+}$
[**7**]$^{+}$	[(κ^3-Me$_2$-bpa-Me)Ir^{I}(C$_2$H$_4$)$_2$]$^{+}$
[**8**]$^{+}$	[(κ^3-Me$_2$-bpa-Me)Ir^{I}(C$_2$H$_4$)]$^{+}$
[**9**]$^{+}$	[(κ^3-Me$_2$-bpa-Me)Ir^{III}(C$_2$H$_5$)(η^1-CH=CH$_2$)(CD$_3$CN)]$^{+}$
[**10**]$^{+}$	[(κ^3-Me$_2$-bpa-Bz)Ir^{I}(C$_2$H$_4$)$_2$]$^{+}$
[**11**]$^{+}$	[(κ^4-C,N,N'-Me$_2$-bpa-Bz)Ir^{III}(H)(C$_2$H$_4$)]$^{+}$
[**12**]$^{+}$	[(κ^4-C,N,N'-Me$_2$-bpa-Bz)Ir^{III}(H)(CD$_3$CN)]$^{+}$
[**13**]$^{+}$	[(κ^3-bpa)Ir^{I}(C$_2$H$_4$)$_2$]$^{+}$
[**14**]$^{2+}$	[{(bpa$^{\#}$)Ir^{III}(C$_2$H$_5$)(CH$_3$CN)}$_2$]$^{2+}$
[**15**]$^{+}$	[(κ^3-bpa-Me)Ir^{I}(C$_2$H$_4$)$_2$]$^{+}$
[**16**]$^{+}$	[(κ^3-bpa-Bz)Ir^{I}(C$_2$H$_4$)$_2$]$^{+}$
[**17**]$^{2+}$	[{(κ^4-C,N,N'-bpa-Bz)Ir^{III}(μ_2-H)}$_2$]$^{2+}$
[**18**]$^{+}$	[(κ^4-C,N,N'-bpa-Bz)Ir^{III}(H)(CD$_3$CN)]$^{+}$
[**19**]$^{2+}$	Asymmetric [(κ^4-C,N,N'-bpa-Bz)Ir^{III}(μ_2-H)(μ_2-H)Ir(κ^4-C,N,N'-bpa-Bz)]$^{2+}$
[**20**]$^{+}$	[(κ^3-Me$_2$-bpa-Me)Rh^{I}(C$_2$H$_4$)(CD$_3$CN)]$^{+}$
[**21**]$^{+}$	[(κ^3-Me$_2$-bpa-Bz)Rh^{I}(C$_2$H$_4$)(CD$_3$CN)]$^{+}$
[**22a**]$^{+}$	[(κ^3-Me$_2$-bpa-Me)Rh^{I}(C$_2$H$_4$)(acetone-d6)]$^{+}$ (asymmetric)
[**22b**]$^{+}$	[(κ^3-Me$_2$-bpa-Me)Rh^{I}(C$_2$H$_4$)]$^{+}$ (symmetric)
[**23a**]$^{+}$	[(κ^3-Me$_2$-bpa-Bz)Rh^{I}(C$_2$H$_4$)(acetone-d6)]$^{+}$ (asymmetric)
[**23b**]$^{+}$	[(κ^3-Me$_2$-bpa-Bz)Rh^{I}(C$_2$H$_4$)]$^{+}$ (symmetric)
[**24**]$^{+}$	[(κ^4-C,N,N',N''-bpa-Bz)Rh^{III}(C$_2$H$_5$)(acetone-d6)]$^{+}$
[**25**]$^{+}$	[(κ^3-bpa)Rh^{I}(C$_2$H$_4$)]$^{+}$
[**26**]$^{+}$	[(κ^3-bpa-Me)Rh^{I}(C$_2$H$_4$)]$^{+}$
[**27**]$^{+}$	[(κ^3-bpa-Bz)Rh^{I}(C$_2$H$_4$)]$^{+}$

[**28**]$^{+}$ [(κ^3-Me_3-tpa)Ir^{III}(C_2H_4)(O_2)]$^{+}$

[**29**]$^{+}$ [(κ^3-Me_2-bpa-Me)Ir^{III}(C_2H_4)(O_2)]$^{+}$

[**30**]$^{+}$ [(κ^4-Me_3-tpa)Rh^{III}(O_2)]$^{+}$

[**31**]$^{+}$ [(κ^4-Me_2-tpa)Rh^{III}(O_2)]$^{+}$

[**32**]$^{+}$ [(κ^4-Me_3-tpa)Rh^{III}($Cl)_2$]$^{+}$

[**33**]$^{2+}$ [(κ^4-Me_2-tpa)Rh^{III}(ethanimidoyl peroxy)]$^{2+}$

[**34**]$^{+}$ [(κ^3-Me_2-bpa-Me)Rh^{III}(O_2)(CD_3CN)]$^{+}$

[**35**]$^{+}$ [(κ^3-Me_2-bpa-Bz)Rh^{III}(O_2)(CD_3CN)]$^{+}$

[**36**]$^{2+}$ [(κ^4-Me_3-tpa)Ir^{II}(C_2H_4)]$^{2+}$

[**37**]$^{2+}$ [(κ^4-Me_2-tpa)Ir^{II}(C_2H_4)]$^{2+}$

[**38**]$^{4+}$ [(κ^4-Me_3-tpa)(CH_3CN)Ir^{III}(μ_2-η^1,η^1-C_2H_4)Ir^{III}(κ^4-Me_3-tpa)(CH_3CN)]$^{4+}$

[**39**]$^{4+}$ [(κ^4-Me_2-tpa)(CH_3CN)Ir^{III}(μ_2-η^1,η^1-C_2H_4)Ir^{III}(κ^4-Me_2-tpa)(CH_3CN)]$^{4+}$

[**40**]$^{4+}$ [(κ^4-Me_3-tpa)(Cl)Ir^{III}(μ_2-η^1,η^1-C_2H_4)Ir^{III}(κ^4-Me_3-tpa)(Cl)]$^{4+}$

[**41**]$^{2+}$ [(κ^4-Me_3-tpa)Ir^{III}(formylmethyl)(CD_3CN)]$^{2+}$

[**42**]$^{2+}$ intermediate in the reaction of [**36**]$^{2+}$ with O_2 to form [**41**]$^{2+}$

[**43**]$^{2+}$ [(κ^4-Me_3-tpa)Ir^{III}(H)(C_2H_4)]$^{2+}$

[**44**]$^{2+}$ [(κ^4-Me_3-tpa)Ir^{III}(C_2H_5)(CH_3CN)]$^{2+}$

[**A1**]$^{+}$ [(κ^4-tpa)Rh^{I}(C_2H_4)]$^{+}$

[**A2**]$^{+}$ [(κ^4-tpa)Rh^{III}(κ^2-O,C-2-oxoethyl)]$^{+}$

[**A3**]$^{+}$ [(κ^4-tpa)Rh^{III}(2-peroxyethyl-κ^2-C^1,O^2)]$^{+}$ (isomer 1)

[**A4**]$^{+}$ [(κ^4-tpa)Rh^{III}(2-peroxyethyl-κ^2-C^1,O^2)]$^{+}$ (isomer 2)

[**B1**]$^{+}$ [(κ^4-Me-tpa)Rh^{I}(C_2H_4)]$^{+}$

[**B2**]$^{+}$ [(κ^4-Me-tpa)Rh^{III}(κ^2-O,C-2-oxoethyl)]$^{+}$

[**C1**]$^{+}$ [(κ^4-tpa)Ir^{I}(C_2H_4)]$^{+}$

[**C2**]$^{+}$ [(κ^4-tpa)Ir^{III}(κ^2-O,C-2-oxoethyl)]$^{+}$

[**C3**]$^{+}$ [(κ^4-tpa)Ir^{III}(2-peroxyethyl-κ^2-C^1,O^2)]$^{+}$ (isomer 1)

[**C4**]$^{+}$ [(κ^4-tpa)Ir^{III}(2-peroxyethyl-κ^2-C^1,O^2)]$^{+}$ (isomer 2)

[**D1**]$^{+}$ [(κ^4-Me-tpa)Ir^{I}(C_2H_4)]$^{+}$

[**D2**]$^{+}$ [(κ^4-Me-tpa)Ir^{III}(κ^2-O,C-2-oxoethyl)]$^{+}$

[**E**]$^{2+}$ [κ^2-*N*,*C*-2-(acetimidoyl oxy)ethyl)Rh(κ^4-tpa)]$^{2+}$

Chapter 1

Introduction

1.1 Introduction

Most reactions of organometallic chemistry and catalysis are carried out in solution. In this medium it is possible to mix reactant and catalyst homogeneously, increasing the reaction rate. The polarity and coordinating properties of a solvent can influence both the activity and deactivation of a catalyst. The balance between these two can be very subtle. Also, a solvent can affect both binding preferences of ligands [1] and the final geometry of the complexes. [2] The importance of the influence of the solvent on structure and inter- and intramolecular reactivities is reflected by the increasing amount of reports on this topic. [3] – [71] If ionic complexes are used, counterions will be present, and these too are known to affect reactions. [33], [72] – [79]

Since they can have such an influence, solvents and counterions make it impossible to study the intrinsic reactivity of a catalyst in solution. Going to the gas phase where these complications are absent, will present a "purer" picture of reactivity. However, translation back to solution-phase chemistry may still be difficult.

An interesting example is given by Vachet and co-workers. Once they had developed new methods [80], [81] to determine the coordination number of a complex in the gas phase, they wanted to predict the interactions between novel multidentate ligands and metals in solution on the basis of gas-phase measurements. However, they soon [82], [83] found that for a number of nickel(II) and copper(II) complexes that coordination numbers differ on going from one phase to the other. Figure 1.1 and Table 1.1 summarize their results.

As expected, for the tridentate L_N ligands **4** and **5** produced six-coordinate $[(L_N)_2M]^{2+}$ (M = Ni, Cu) complexes in all three phases (solid state, solution, gas phase). For nickel in the solid state and in solution in all cases octahedrally surrounded complexes were obtained. For ligands **2** and **3**, solvent molecules were bound to complete the coordination sphere; upon transferring these complexes to the gas-phase coordinated solvent molecules were removed.

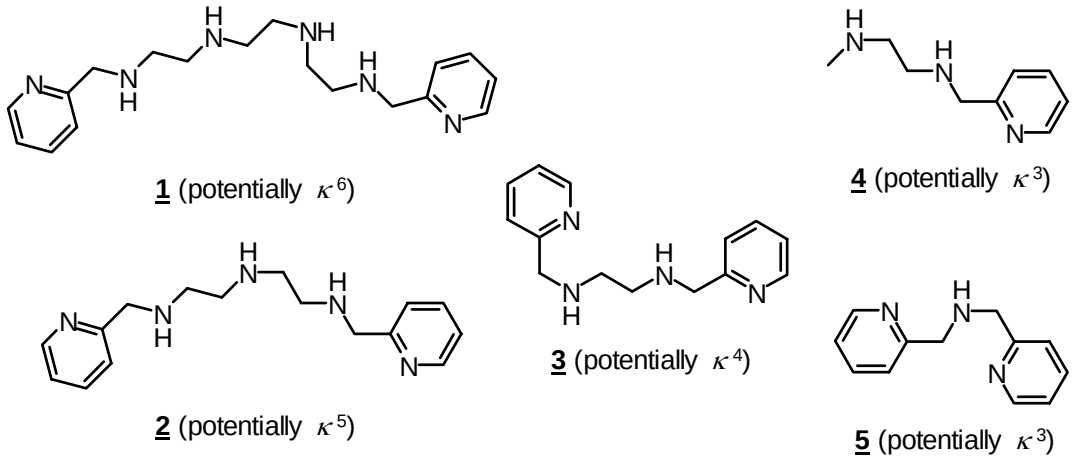

Figure 1.1 *Ligands (L_N) used by Vachet et al.* [82], [83] *to synthesize nickel and copper complexes*

Table 1.1 *Coordination numbers (CN) observed for complexes of* **1** - **6**

Ligand	Metal	Solid State		Solution		Gas phase	
		Structure	CN	Structure	CN	Structure	CN
1	Ni	$[(L_N)M]^{2+}$	6	$[(L_N)M]^{2+}$	6	$[(L_N)M]^{2+}$	5
	Cu	$[(L_N)M]^{2+}$	6 [a]	$[(L_N)M]^{2+}$	fluxional	$[(L_N)M]^{2+}$	4 or 5 [b]
2	Ni	$[(L_N)M(solv)^{]2+}$	6	$[(L_N)M(solv)^{]2+}$	6	$[(L_N)M]^{2+}$	5
	Cu	$[(L_N)M]^{2+}$	5	$[(L_N)M]^{2+}$	4 and higher	$[(L_N)M]^{2+}$	4
3	Ni	$[(L_N)M(solv)_2]^{2+}$	6	$[(L_N)M(solv)_2]^{2+}$	6	$[(L_N)M]^{2+}$	4
	Cu	$[(L_N)M]^{2+}$	4	$[(L_N)M]^{2+}$	4	$[(L_N)M]^{2+}$	4
4	Ni	$[(L_N)_2M]^{2+}$	6	$[(L_N)_2M]^{2+}$	6	$[(L_N)_2M]^{2+}$	6
	Cu	$[(L_N)_2M]^{2+}$	6	$[(L_N)_2M]^{2+}$	6	$[(L_N)_2M]^{2+}$	5 or 6 [c]
5	Ni	$[(L_N)_2M]^{2+}$	6	$[(L_N)_2M]^{2+}$	6	$[(L_N)_2M]^{2+}$	6
	Cu	$[(L_N)_2M]^{2+}$	6	$[(L_N)_2M]^{2+}$	6	$[(L_N)_2M]^{2+}$	6

[a] *The two axial bonds in this octhahedral complex are very long, making it likely that in the more dynamic solution and gas-phase structures a pyridyl-Cu bond is completely broken and one secondary amine bond is weakened.*

[b] *This complex is borderline reactive in the gas phase. This may suggest that the fifth coordination site is weakly bound*

[c] *For this complex the mass spectrometric method of Vachet* [80] *et al. had difficulties distinguishing between a five and six-coordinate Cu(II) complex in the gas phase.*

The nickel complex of potentially κ^6 ligand **1** is interesting. In solution and in the solid state it is six-coordinate, whereas gas-phase studies indicate that only five nitrogen atoms are coordinated (one of the two outermost secondary amines appears not to coordinate Ni). For the corresponding copper complex of **1** an even more fluxional behavior is observed: it is 6-coordinate in the solid state, fluxionally coordinated in solution and four- or five-coordinate in the gas phase. This same fluxionality was also observed for the copper complex of ligand **2**: a coordination number of 5 in the solid state, 4 and higher in solution and only 4 in the gas phase.

Another example, which shows that conclusions regarding solution phase reactivities based on those observed in the gas phase have to be drawn with caution, comes from Wu and co-workers [70].
They investigated the kinetic stability of non-covalent complexes between bovine carbonic anhydrase II and *para*-substituted benzenesulfonamide inhibitors. They found that in solution dissociation rates are mainly affected by hydrophobic interactions between the inhibitor and the enzyme, while in the gas phase they are primarily determined by polar surface interactions.
And Daniel *et al.* [84] concluded in their review article on determining non-covalent binding energies using soft ionization mass spectrometry that, with a few exceptions, no agreement exists between solution-phase and gas-phase binding energies, the main reason being that electrostatic and polar non-covalent interactions are strengthened in the absence of solvent shielding, while other non-covalent interactions, particular hydrophobic interactions, become less important in the absence of a solvent.
The presence of a solvent can also be important in catalytic reactions. Hinderling *et al.* [85] reported that ring-opening olefin metathesis of a certain ruthenium-carbene complex was faster in the gas phase than in solution

by a factor of up to 10^4. Both the similarities and the differences between gas-phase and solution-phase chemistry hold information useful to the analysis of complex reaction pathways. [86] – [89]

In the present thesis, we have used gas-phase reactivity studies to improve our understanding of a complex reaction *par excellence*, namely the oxidation of group 9 metal-olefin complexes with molecular oxygen. [90] – [116] The complexes involved are cationic and are therefore well suited for mass spectrometric studies. Oxygen is a convenient reactant that can easily be introduced in various stages of a mass spectrometer. Finally, a considerable amount of solution-phase data already exists for this reaction (and more was generated in the course of this work), providing extensive reference material. Thus, the system seems to be well suited for a gas-phase reactivity study, and a comparison with condensed-phase data might result in new insights. Before explaining the approach taken in the present work, the next section introduces the topic of olefin complex oxidation and summarizes a part of the relevant chemistry.

1.2 Oxidation of transition metal olefin complexes

Oxygenation of olefins using transition metals

Transition metal catalyzed oxygenation of olefins using molecular oxygen, hydrogen peroxide or water as an oxidant has received considerable attention from a synthetic, mechanistic and industrial point of view already from the 70's on. [90] – [106] Especially the Wacker [107] – [110] type of oxidation[1] at palladium has been extensively studied over the last decades. This process has, however, a few drawbacks. And over the last decade it has become more and more clear that, give the right choice of ligand, rhodium and iridium can also catalyze olefin oxygenation with dioxygen, although lower rates and faster deactivation are usually observed.

Dioxygen can in principle be used with high atom efficiency and in many reactions produces either water as the only by-product, or no by-product at all. This makes it a cheap and environmentally benign oxidant. However, it can be difficult to prevent overoxidation of the substrate and decomposition of the catalyst. For example, in a catalytic cycle proposed by Read [104], in which one mol of terminal or cyclic olefin is oxidized by one mol of dioxygen (Figure 1.2), a co-oxidant like triphenylphosphine is necessary to get rid of the surplus oxygen atom.

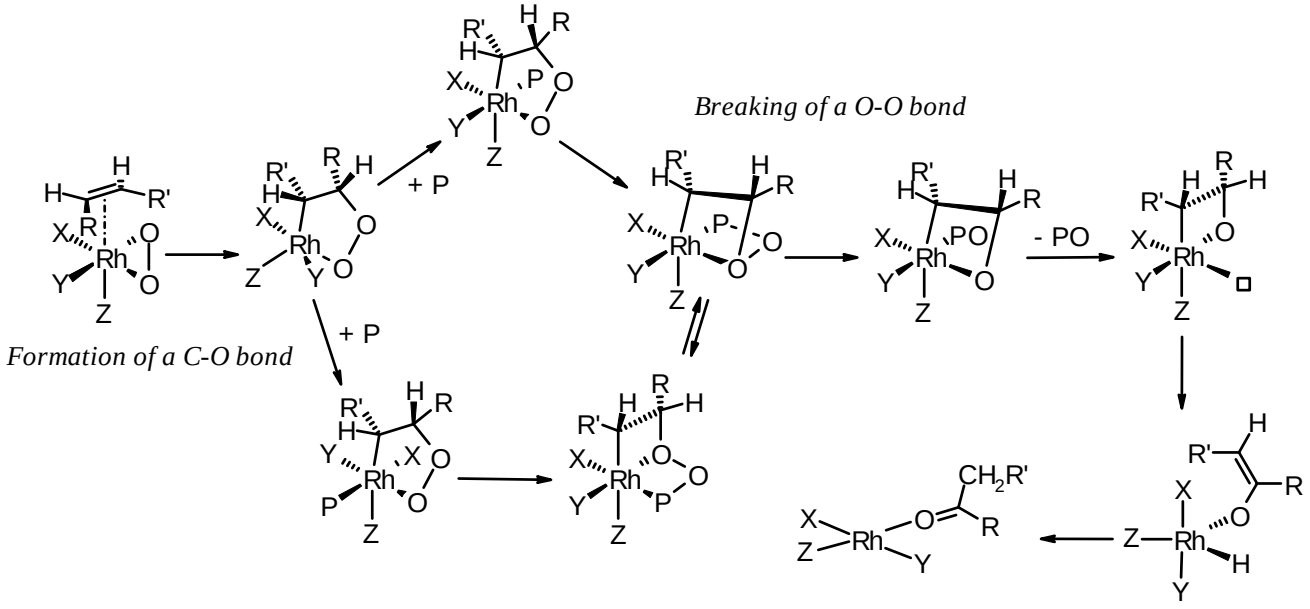

Figure 1.2 *Mechanism of rhodium-catalyzed co-oxygenation of olefins and $P(Ph)_3$ proposed by Read* [104]

[1] The Wacker process encompasses Pd/Cu catalyzed oxidation of ethene by O_2 to acetaldehyde.

In late transition metal (LTM) catalyzed oxidation of olefins, peroxo and olefin-peroxo complexes, [91] – [101], [105] 3-metalla-1,2-dioxolanes, [90] – [101], [105], [106] and 2-metallaoxetanes [102] – [104], [111], [112] have been proposed as crucial intermediates (see for example Figure 1.2).

Stoichiometric studies of oxygenation of rhodium(I) and iridium(I) olefin complexes have proved useful in establishing the viability of these proposed intermediates and elucidated their chemistry. [105] In particular several dioxolane [106], [113] – [115] and oxetane species [111], [112], [116] have been prepared and their reactivity has been studied. However, one of the crucial steps in the oxygenation reaction, *viz.* the formation of the first C-O bond, still remains unclear. It might occur via direct attack of O_2 on a coordinated olefin, or via peroxo-olefin complexes, or via even more complicated mechanisms.

An example, which shows that mechanistically reactions with dioxygen are still not completely understood, was a report [116], [117] on bpa-type[2] *Z,Z*-1,5-cyclooctadiene complexes. Their exposure to dioxygen in solution consumes 1 mol of rhodium/iridium center but results in the incorporation of only one oxygen atom to give metal(III) oxabicyclononadiyl complexes, which subsequently rearrange to metal(III) hydroxycyclooctenediyl complexes. Where the second oxygen atom goes to is still unclear. It is highly probably that the solvent is involved, since only in dichloromethane selective oxidation could be obtained.

In oxidation reactions with dioxygen not only the solvent, but also the counterion can be of influence, even in the solid state. This is shown in the reaction of tpa[3]-type olefin complexes with dioxygen to give 3-metalla-1,2-dioxolanes. [106], [113] – [115] For these complexes it was found that the counterion (PF_6^- or BPh_4^-) determines the selectivity of the reaction: formation of a mixture of two isomers or of only a *single* isomer.

The mechanism of this reaction is still unclear. One possibility is that in the solid state first single-electron transfer takes place from the metal(I) center to a dioxygen molecule. The resulting metal(II) species would then react with a second dioxygen molecule to form a dioxolane radical species, and the superoxide anion (which should have a low mobility in the solid state) would reduce this to a metal(III) dioxolane species. The idea of open-shell intermediates in this type of reactions does not seem to have received serious attention, and it opens up exciting possibilities.

Since solvent and counterions are important in oxygenation chemistry, the intrinsic reactivity of organometallic complexes in the ***absence*** of these species becomes very interesting. Also the (possible) role of open-shell olefin-metal(II) complexes in olefin oxidation reactions is intriguing.

Mononuclear, open-shell organometallic complexes

Traditionally, most well-understood catalytic reactions mediated by *organometallic* complexes proceed via closed-shell species. For the transition metals rhodium and iridium the +1 (d^8) and the +3 (d^6) oxidation states are the most common ones. Many catalytic pathways involve two-electron redox steps (oxidative addition/reductive elimination).

Redox pathways in principle allow formation of oxidation state +2 complexes. These species are considered to be highly reactive, following uncommon reaction pathways such as radical abstraction, radical coupling or disproportionation. Although isolated examples of these species are quite rare, they could well be intermediates in various reactions.[4] Only a few stable open-shell olefin complexes are known. [124] – [131] Most previous examples are stabilized by bulky di-anionic porphyrinate ligands (por^{2-}). To our best knowledge, only one stable mononuclear iridium(II)-*olefin* complex has been reported, *viz.* $[(C_6Cl_5)_2Ir^{II}(cod)]$ (cod= *Z,Z*-1,5-cyclooctadiene). [129]

[2] bpa = *N,N*-di(2-pyridylmethyl)amine

[3] tpa = *N,N,N*-tri(2-pyridylmethyl)amine

[4] NOTE: The rhodium(II) and iridium(II) (d^7) oxidation states are well established in dimeric metal-metal bonded complexes in which the metals share their unpaired electrons. [118] – [123]

Nevertheless, factors that stabilize these species are more and more understood. Ligands that are sufficiently bulky can protect the d^7 metal from external attack. [121], [122], [132], [133] In addition to steric protection, polydentate ligands can impose coordination environments that destabilize the +1 and/or +3 oxidation state. [134], [135] Ligands can also increase stability by delocalizing the unpaired electron away from the metal center. [121], [134], [136]

Recently, [(por)M^{II}(ethene)] (M= Rh [137], Ir [122], por^{2-} = a bulky meso-tetra-arylporphyrinate dianion), formed *in situ* from [(por)M^{II}] and ethene, have been reported to undergo bimolecular C-C radical coupling to butylene bridged dinuclear complexes, implying that in these complexes the unpaired spin-density is not located on the metal, but on the olefin moiety, leaving the metal in the usual closed shell configuration. Also for other metal(II) complexes dimerization via coupling reactions has been observed. [138] – [143]

A comparison between solution phase and gas phase could help in establishing the involvement of redox pathways. According to the Marcus theory, reorganization of both the reactants (inner sphere) and the solvent shell (outer sphere) contributes to the activation energy of a reaction. [144] – [147] In the absence of solvent influences it is expected that single-electron-transfer (SET) reactions will proceed differently.

Distinguishing between reaction paths

Even ignoring the possibility of SET reactions, one could envisage different pathways for olefin oxygenation. This is illustrated by the formation of peroxo complexes [**B**]$^+$ from metal-olefin complexes [**A**]$^+$ and dioxygen (see Figure 1.3). Starting from a coordinatively unsaturated (16 VE) olefin complex, possible routes are either adduct formation (A^1) followed by dissociation of the olefin (D^2), or first a dissociation step (D^1) followed by coordination of the dioxygen molecule (A^2).
For a coordinatively saturated (18 VE) complex like a N_4 metal-olefin complex, either a donor (D^1) or the olefin itself (D^2) has to dissociate to enable a reaction with dioxygen.

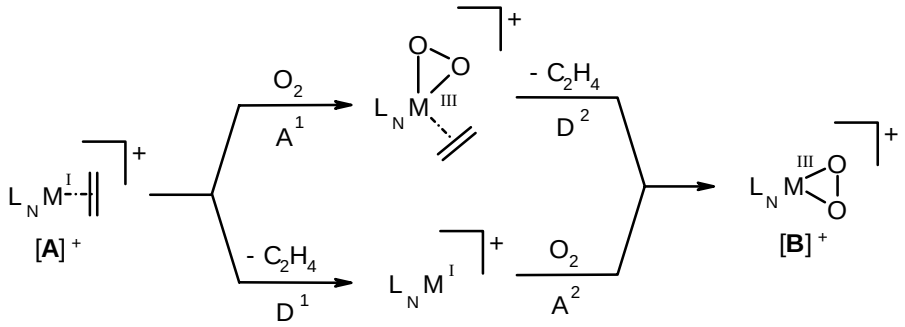

Figure 1.3 *Associative (A) versus dissociative (D) pathways*

In solution it is often difficult to distinguish between these reaction paths, since intermediates are too reactive to be observed directly. In contrast associative and dissociative processes can be (more or less) separated in the gas phase. For example, Bossio *et al.* [148] collided *trans*-[$Rh(PPh_3)_2(CO)$(4-picoline)]$^+$ with pyridine in the gas phase. They observed not only substitution of pyridine for 4-picoline but also loss of CO. On the basis of their gas-phase measurements, and supported by DFT calculations[5], they conclude that the primary substitution pathway for this reaction proceeds dissociatively not associatively, unlike almost all solution-phase ligand-substitution reactions of Pt(II) and Pd(II).

[5] DFT calculations revealed that the bond energies of Rh-4-picoline, Rh-pyridine, and Rh-CO are similar enough that CO loss might be expected.

Gas-phase studies of oxidation reactions

The study of gas-phase chemistry of "real" transition metal complexes is still in its infancy. Several groups have studied the chemistry of isolated metal atoms or diatomic "molecules" with oxygen-containing molecules like H_2O_2, N_2O or O_3. [149] – [160]

However, such small systems can hardly be considered as representative of "real" transition metal complexes. Naked atoms are much more unsaturated: they will bind any molecule they encounter and are capable of breaking most chemical bonds. In contrast, "stable" complexes often need to overcome a barrier even for binding a reactant, let alone undergoing subsequent reactions. [157] This might limit the possibilities for gas-phase reactivity studies, since that requires reactions at the mass spectrometric time scale (~ milliseconds).

Nevertheless, a few gas-phase studies of the reaction of organometallic fragments with O_2 have yielded interesting results. Collision of $[(bipy)_2M]^{2+}$ (M = Cr, Ru, Os)[6] and $[(bipy)M]^+$ (M = Co, Ni) with dioxygen ($E_{(lab)}$ = 1.0 eV, dioxygen pressure ca. 3.0 mTorr) [161] results in the formation of the corresponding dioxygen adducts. When these adducts are collided with argon to induce fragmentation, the dioxygen molecule can dissociate again as a whole.

The influence of ligands coordinated to the metal center on the reactivity is shown in a study by Caraiman and Bohme. [162] Collision experiments of benzene complexes of first second and third row transition metal cations, $[(C_6H_6)_pM]^+$ (p = 1, 2), with dioxygen were compared with experiments of the bare metal cations. Bare metal cations appear to yield either $[MO]^+$ or $[MO_2]^+$ species, the first species being produced for early transition metals and the latter for late transition metals. [149] For the benzene-containing complexes O-O cleavage [7] by early transition metal cations still occurs in the presence of one benzene ligand but is largely suppressed in the presence of a second benzene ligand. For the mono-benzene complexes, on moving from left to right through the periodic table a shift in reactivity is observed. Oxidation of the benzene ligand and displacement of benzene by O_2 disappear, and $[MC_6H_6O_2]^+$ becomes the sole product.

Collision of $[(C_5H_5)Fe]^+$ with N_2O [163] produces only the adduct $[(C_5H_5)Fe(N_2O)]^+$. In contrast, with NO_2 oxidation of iron by oxygen-atom transfer becomes the main reaction path.

1.3 Scope of this thesis

The aim of the PhD research described in this thesis was to compare solution and gas-phase reactivities and from this increase our insight in reaction mechanisms. In particular we have focused on the reaction of rhodium(I) and iridium(I) complexes of bpa-type and tpa-type ligands[8] with dioxygen.

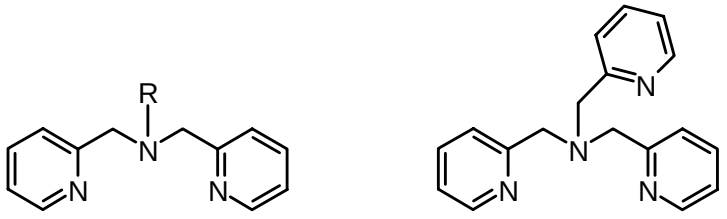

bpa **tpa**

Figure 1.4 *Nitrogen donor ligands used in this thesis*

[6] bipy = 4,4'-bipyridine

[7] This can be determined from the presence of species like $[MC_6H_6O]^+$ (O-transfer, observed for M = group 3 to 6 transition metals), $[MC_6H_4O]^+$ (addition/dehydration, M = V, Cr, Re, Fe) and $[MC_4H_4]^+$ (acetylene elimination, M = Os).

[8] bpa = *N*,*N*-di(2-pyridylmethyl)amine, tpa = *N*,*N*,*N*-tri(2-pyridylmethyl)amine

Chapter 2 introduces the mass-spectrometric equipment used and the ionization technique, electrospray ionization (ESI), and points out some of its important characteristics. Also a few phenomena will be described that one can encounter when using ESI-MS for analysis and reactivity studies.

In chapter 3 the synthesis and stability of some new rhodium and iridium ethene complexes with tri- and tetradentate nitrogen donor ligands will be described. Their reactivity towards oxidizing agents like dioxygen in solution and in the solid state are the subject of chapter 4.

In chapter 5 the synthesis and characterization of new open-shell organometallic olefin species $[(Me_n\text{-tpa})Ir^{II}(ethene)]^{2+}$ (n = 2, 3) are described. These are the first examples of stable iridium(II) ethene species. Although these are stable by themselves, they can be triggered to undergo radical-type reactions by addition of donor reagents. Their reactivity towards dioxygen will be discussed.

The behavior of tri- and tetradentate rhodium and iridium ethene complexes under ESI-MS conditions is discussed in chapter 6. Once we know the characteristic behavior of the complexes themselves, the reactivity towards dioxygen or air in the different regions of the mass spectrometer can be studied. As will be shown in chapter 7, each region has its own characteristics and as a result has its own group of compounds that react in it.

The results described in chapters 2 to 7 will be used in chapter 8 to make a comparison between solution, solid-state and gas-phase reactivity and draw some conclusions about the type of reactivity one can expect in each phase.

In order to get a feeling for the stability of the species involved in the oxidation reactions proposed in this thesis, several N_3 and N_4 rhodium and iridium complexes and their possible intermediates in associative and dissociative reactions have been studied by DFT methods. The results are presented in Appendix A and will be used throughout this thesis for the interpretation of results obtained.

1.4 References

[1] Y. Takeda, *Cation Binding by Macrocycles*, Vol. Eds. Y. Inoue and G. W. Gokel, Marcel Dekker, New York, **1990**, 150-151

[2] R. Machida, E. Kimura and Y. Kushi, *Inorg. Chem.*, **1986**, *25 (19)*, 3461-3466

[3] L. J. Leroux, C. S. Lu, S. Sugden and R. H. K. Thomson, *J. Chem. Soc.*, **1945**, 586-588

[4] P. C. Goswami, *J. Indian Chem. Soc.*, **1947**, *24 (10)*, 379-382

[5] A. Meretoja, *Acta Chem. Scand.*, **1948**, *2 (4)*, 352-357

[6] K. J. Laidler and P. A. Landskroener, *Trans. Faraday Soc.*, **1956**, *52 (2)*, 200-210

[7] V. Gutmann, *Angew. Chem. - Int. Edit.*, **1967**, *6 (3)*, 271

[8] P. E. M. Allen and R. M. Lough, *J. Organomet. Chem.*, **1973**, *61 (1)*, 7-8

[9] J. F. Coetzee and Chattopa.Pk, *Abstr. Pap. Am. Chem. Soc.*, **1974**, 130-130

[10] L. I. Kopylova, V. B. Pukhnarevich, Tsykhanskaya, II, E. N. Satsuk, B. V. Timokhin, V. I. Dmitriev, V. Khvalovskii, M. Chapka, A. V. Kalabina and M. G. Voronkov, *Zhurnal Obshchei Khimii*, **1981**, *51 (8)*, 1851-1855

[11] P. Sevcik and J. Tkac, *Coll. Czech. Chem. Commun.*, **1981**, *46 (7)*, 1554-1559

[12] J. D. Samuilov, S. E. Solovieva and A. I. Konovalov, *Doklady Ak. Nauk Sssr*, **1980**, *255 (3)*, 606-609

[13] M. M. Elsemongy and M. F. Amira, *J. Indian Chem. Soc.*, **1980**, *57 (5)*, 506-512

[14] V. F. Gromov and P. M. Khomikovskii, *Uspekhi Khimii*, **1979**, *48 (11)*, 1943-1967

[15] C. F. Wells, *J. Chem. Soc. - Faraday Trans. I*, **1977**, *73*, 1851-1859

[16] R. J. P. Corriu and B. J. L. Henner, *J. Organomet. Chem.*, **1974**, *71 (3)*, 393-397

[17] M. J. Weaver and T. Gennett, *Chem. Phys. Lett.*, **1985**, *113 (2)*, 213-218

[18] E. Dumitriu, V. Hulea and P. Moreau, *Rev. Roum. Chim.*, **1999**, *44 (11-12)*, 1073-1083

[19] G. Chambard, B. Klumperman and A. L. German, *Macromolecules*, **2000**, *33 (12)*, 4417-4421

[20] J. M. G. Cowie, I. J. McEwen and D. J. Yule, *Eur. Polym. J.*, **2000**, *36 (9)*, 1795-1803

[21] H. Jensen and K. Daasbjerg, *J. Chem. Soc. - Perkin Trans. 2*, **2000**, *6*, 1251-1257

[22] K. M. Morgan and S. Gronert, *J. Org. Chem.*, **2000**, *65 (5)*, 1461-1466

[23] W. J. Kinart, C. M. Kinart and I. Tylak, *J. Organomet. Chem.*, **1999**, *590 (2)*, 258-260

[24] A. Srivastava, A. Darszon and R. J. Strasser, *Arch. Sci.*, **1999**, *52 (2)*, 73-99

[25] M. M. A. Talpur, A. Kaim, T. Kaspryzycka-Guttman and T. Pirzada, *Arab. J. Sci. Eng.*, **1999**, *24 (2A)*, 133-140

[26] A. Kaim and P. Oracz, *Polymer*, **1999**, *40 (25)*, 6925-6932

[27] M. Barra, E. D. Harder and J. P. Balfe, *J. Chem. Soc. - Perkin Trans. 2*, **1999**, *(7)*, 1439-1441

[28] S. Schneider, B. Brem, W. Jager, H. Rehaber, D. Lenoir and R. Frank, *Chem. Phys. Lett.*, **1999**, *308 (3-4)*, 211-217
[29] O. F. Olaj and I. Schnoll-Bitai, *Mon. Chem.*, **1999**, *130 (6)*, 731-740
[30] L. Lassova, H. K. Lee and T. S. A. Hor, *J. Mol. Catal. A - Chem.*, **1999**, *144 (3)*, 397-403
[31] M. Banziger, S. Klein and G. Rihs, *Helv. Chim. Acta*, **2002**, *85 (5)*, 1399-1406
[32] E. Eder and C. Deininger, *Mutat. Res. - Genet. Toxicol. Environ. Mutagen.*, **2002**, *516 (1-2)*, 81-89
[33] W. P. Su, M. C. Hong, J. B. Weng, Y. C. Liang, Y. J. Zhao, R. Cao, Z. Y. Zhou and A. S. C. Chan, *Inorg. Chim. Acta*, **2002**, *331*, 8-15
[34] P. M. Mancini, G. Fortunato, C. Adam, L. R. Vottero and A. J. Terenzani, *J. Phys. Org. Chem.*, **2002**, *15 (5)*, 258-269
[35] J. Gonzalez-Benito, A. Aznar and J. Baselga, *J. Fluoresc.*, **2001**, *11 (4)*, 307-314
[36] B. Bleisteiner, T. Marian, S. Schneider, A. M. Brouwer and J. W. Verhoeven, *Phys. Chem. Chem. Phys.*, **2001**, *3 (24)*, 5383-5392
[37] T. Yasin, Z. Q. Fan, Y. B. Zhu and L. X. Feng, *Chem. Res. Chin. Univ.*, **2001**, *17 (4)*, 445-451
[38] L. V. Mel'nik, M. N. Khvatova, Y. A. Moskvichev, S. S. Srednev and L. M. Egorova, *Petrol. Chem.*, **2001**, *41 (4)*, 277-280
[39] V. Ramesh, M. Sumathy, K. Karunakaran and K. P. Elango, *Oxid. Commun.*, **2001**, *24 (2)*, 241-247
[40] H. Yekeler and D. Ozbakir, *J. Mol. Model.*, **2001**, *7 (4)*, 103-111
[41] K. P. Elango, *J. Serb. Chem. Soc.*, **2001**, *66 (6)*, 359-365
[42] J. Barluenga, J. Alonso and F. J. Fananas, *J. Am. Chem. Soc.*, **2003**, *125 (9)*, 2610-2616
[43] N. I. Yanchuk, I. N. Grod and L. N. Ivanets, *Russ. J. Gen. Chem.*, **2002**, *72 (11)*, 1784-1789
[44] Y. Zimmermann and S. Spange, *J. Phys. Chem. B*, **2002**, *106 (48)*, 12524-12530
[45] C. Bianchini, A. Meli, G. Muller, W. Oberhauser and E. Passaglia, *Organometallics*, **2002**, *21 (23)*, 4965-4977
[46] J. M. Fraile, J. I. Garcia, M. A. Harmer, C. I. Herrerias, J. A. Mayoral, O. Reiser and H. Werner, *J. Mater. Chem.*, **2002**, *12 (11)*, 3290-3295
[47] M. A. Bonache, G. Gerona-Navarro, M. Martin-Martinez, M. T. Garcia-Lopez, P. Lopez, C. Cativiela and R. Gonzalez-Muniz, *Synlett*, **2003**, *(7)*, 1007-1011
[48] H. Y. Shen, G. L. Tian, A. X. Yan, Y. Jia, Y. Y. Hong and Y. H. Ye, *Acta Chim. Sin.*, **2003**, *61 (7)*, 1144-1148
[49] I. V. Pobelov, Z. V. Kuz'minova, G. A. Tsirlina and O. A. Petrii, *Russ. J. Electrochem.*, **2003**, *39 (8)*, 828-838
[50] K. Anbalagan, K. A. Danishad and S. P. R. Poonkodi, *Indian J. Chem. Sect A - Inorg. Bio-Inorg. Phys. Theor. Anal. Chem.*, **2003**, *42 (5)*, 1040-1043
[51] M. C. Iovu, N. G. Maithufi and S. F. Mapolie, *Polym. Int.*, **2003**, *52 (6)*, 899-907
[52] M. C. Capel-Sanchez, J. M. Campos-Martin and J. L. G. Fierro, *J. Catal.*, **2003**, *217 (1)*, 195-202
[53] A. Wolfson, I. F. J. Vankelecom, S. Geresh and P. A. Jacobs, *J. Mol. Catal. A - Chem.*, **2003**, *198 (1-2)*, 39-45
[54] W. J. Kinart and C. M. Kinart, *Phys. Chem. Liq.*, **2003**, *41 (2)*, 173-176
[55] T. Paczesniak and A. Sobkowiak, *J. Mol. Catal. A - Chem.*, **2003**, *194 (1-2)*, 1-11
[56] J. B. Nikolic, G. S. Uscumlic and V. V. Krstic, *Indian J. Chem. Sect B - Org. Chem. Incl. Med. Chem.*, **2004**, *43 (9)*, 1995-2000
[57] S. F. Ledenkov, V. A. Sharnin and G. V. Chistyakova, *Russ. Chem. Bull.*, **2004**, *53 (4)*, 758-765
[58] M. Winterbottoma, H. Marwan and R. Natividad, *Can. J. Chem. Eng.*, **2003**, *81 (3-4)*, 838-845
[59] X. D. Yang, J. D. Ranford and J. J. Vittal, *Cryst. Growth Des.*, **2004**, *4 (4)*, 781-788
[60] I. S. Lee, D. M. Shin and Y. K. Chung, *Chem. - Eur. J.*, **2004**, *10 (13)*, 3158-3165
[61] S. E. Shim, S. Oh, Y. H. Chang, M. J. Jin and S. Choe, *Polymer*, **2004**, *45 (14)*, 4731-4739
[62] R. W. Gora, W. Bartkowiak, S. Roszak and J. Leszczynski, *J. Chem. Phys.*, **2004**, *120 (6)*, 2802-2813
[63] R. N. Butler, W. J. Cunningham, A. G. Coyne and L. A. Burke, *J. Am. Chem. Soc.*, **2004**, *126 (38)*, 11923-11929
[64] V. P. Krasnov, G. L. Levit, M. A. Korolyova, I. M. Bukrina, L. S. Sadretdinova, I. N. Andreeva, V. N. Charushin and O. N. Chupakhin, *Russ. Chem. Bull.*, **2004**, *53 (6)*, 1253-1256
[65] H. Li, W. J. Zhao, S. X. Cao, K. Lu and Y. F. Zhao, *Chem. J. Chin. Univ. - Chin.*, **2004**, *25 (10)*, 1866-1868
[66] M. A. Esteruelas, A. M. Lopez, E. Onate and E. Royo, *Organometallics*, **2004**, *23 (23)*, 5633-5636
[67] H. Chen, H. W. Chen, R. G. Cooks and H. Bagheri, *J. Am. Soc. Mass Spectrom.*, **2004**, *15 (11)*, 1675-1688
[68] R. Gupta, S. M. Hamdan, N. E. Dixon, M. M. Sheil and J. L. Beck, *Protein Sci.*, **2004**, *13 (11)*, 2878-2887
[69] N. R. Walker, R. R. Wright, P. E. Barran, J. N. Murrell and A. J. Stace, *J. Am. Chem. Soc.*, **2001**, *123 (18)*, 4223-4227
[70] Q. Y. Wu, J. M. Gao, D. JosephMcCarthy, G. B. Sigal, J. E. Bruce, G. M. Whitesides and R. D. Smith, *J. Am. Chem. Soc.*, **1997**, *119 (5)*, 1157-1158
[71] G. Gerdes and P. Chen, *Organometallics*, **2003**, *22 (11)*, 2217-2225
[72] G. A. Russell and W. Baik, *J. Chem. Soc. - Chem. Commun.*, **1988**, *(3)*, 196-198
[73] H. P. Lin, C. P. Kao, C. Y. Mou and S. B. Liu, *J. Phys. Chem. B*, **2000**, *104 (33)*, 7885-7894
[74] B. Dutta, B. Adhikary, P. Bag, U. Florke and K. Nag, *J. Chem. Soc. - Dalton Trans.*, **2002**, *(13)*, 2760-2767
[75] A. L. van den Brenk, J. D. A. Tyndall, R. M. Cusack, A. Jones, D. P. Fairlie, L. R. Gahan and G. R. Hanson, *J. Inorg. Biochem.*, **2004**, *98 (11)*, 1857-1866
[76] S. Abaci, L. S. Zhang and C. Shannon, *Journal of Electroanalytical Chemistry*, **2004**, *571 (2)*, 169-176
[77] Z. T. Xu, K. Vanka and T. Ziegler, *Macromol. Symp.*, **2004**, *206*, 457-469
[78] Z. T. Xu, K. Vanka and T. Ziegler, *Organometallics*, **2004**, *23 (1)*, 104-116
[79] S. D. Ittel, L. K. Johnson and M. Brookhart, *Chem. Rev.*, **2000**, *100 (4)*, 1169-1203
[80] R. W. Vachet, J. A. R. Hartman and J. H. Callahan, *J. Mass Spectrom.*, **1998**, *33 (12)*, 1209-1225

[81] R. W. Vachet, J. R. Hartman, J. W. Gertner and J. H. Callahan, *Int. J. Mass Spectrom.*, **2001**, *204 (1-3)*, 101-112
[82] J. R. Hartman, R. W. Vachet and J. H. Callahan, *Inorg. Chim. Acta*, **2000**, *297 (1-2)*, 79-87
[83] J. R. Hartman, R. W. Vachet, W. Pearson, R. J. Wheat and J. H. Callahan, *Inorg. Chim. Acta*, **2003**, *343*, 119-132
[84] J. M. Daniel, S. D. Friess, S. Rajagopalan, S. Wendt and R. Zenobi, *Int. J. Mass Spectrom.*, **2002**, *216 (1)*, 1-27
[85] C. Hinderling, C. Adlhart and P. Chen, *Angew. Chem. - Int. Edit.*, **1998**, *37 (19)*, 2685-2689
[86] C. Hinderling, D. Feichtinger, D. A. Plattner and P. Chen, *J. Am. Chem. Soc.*, **1997**, *119 (44)*, 10793-10804
[87] C. Adlhart, C. Hinderling, H. Baumann and P. Chen, *J. Am. Chem. Soc.*, **2000**, *122 (34)*, 8204-8214
[88] D. Feichtinger and D. A. Plattner, *Chem. - Eur. J.*, **2001**, *7 (3)*, 591-599
[89] D. Feichtinger, D. A. Plattner and P. Chen, *J. Am. Chem. Soc.*, **1998**, *120 (28)*, 7125-7126
[90] G. Strukul and R. A. Michelin, *J. Am. Chem. Soc.*, **1985**, *107 (25)*, 7563-7569
[91] K. Takao, M. Wayaku, Y. Fujiwara, T. Imanaka and S. Teranishi, *Bull. Chem. Soc. Jpn*, **1970**, *43*, 3898
[92] K. Takao, Y. Fujiwara, T. Imanaka and Teranish.S, *Bull. Chem. Soc. Jpn*, **1970**, *43 (4)*, 1153
[93] G. Read and P. J. C. Walker, *J. Chem. Soc. - Dalton Trans.*, **1977**, *(9)*, 883-888
[94] G. Read and M. Urgelles, *J. Chem. Soc. - Dalton Trans.*, **1985**, *(8)*, 1591-1596
[95] H. Mimoun, M. M. P. Machirant and I. Sereederoch, *J. Am. Chem. Soc.*, **1978**, *100 (17)*, 5437-5444
[96] H. Mimoun, *Pure Appl. Chem.*, **1981**, *53 (12)*, 2389-2399
[97] F. Igersheim and H. Mimoun, *Nouv. J. Chim. - New J. Chem.*, **1980**, *4 (3)*, 161-166
[98] C. Dudley and G. Read, *Tetrahedron Lett.*, **1972**, *(52)*, 5273
[99] F. Di Furia and G. Modena, *Pure Appl. Chem.*, **1982**, *54 (10)*, 1853-1866
[100] L. Carlton, G. Read and M. Urgelles, *J. Chem. Soc. - Chem. Commun.*, **1983**, *(10)*, 586-588
[101] O. Bortolini, F. Difuria, G. Modena and R. Seraglia, *J. Mol. Catal.*, **1984**, *22 (3)*, 313-317
[102] K. A. Jorgensen and B. Schiott, *Chem. Rev.*, **1990**, *90 (8)*, 1483-1506
[103] K. A. Jorgensen, *Chem. Rev.*, **1989**, *89 (3)*, 431-458
[104] G. Read, *J. Mol. Catal.*, **1988**, *44 (1)*, 15-33
[105] B. de Bruin, P. H. M. Budzelaar and A. W. Gal, *Angew. Chem. - Int. Edit.*, **2004**, *43 (32)*, 4142-4157
[106] M. Krom, T. P. J. Peters, R. G. E. Coumans, T. J. J. Sciarone, J. Hoogboom, S. I. ter Beek, P. P. J. Schlebos, J. M. M. Smits, R. de Gelder and A. W. Gal, *Eur. J. Inorg. Chem.*, **2003**, *6*, 1072-1087
[107] R. Jira, W. Blay and G. Grimm, *Hydrocarbon Process*, **1975**, *55*, 97
[108] B. Cornils and W. A. Hermann, *"Applied Homogeneous Catalysis with Organometallic Compounds"*, Eds., VCH, Weinheim, **1996**
[109] L. I. Simandi, *"Activation of Dioxygen by Metal Complexes"*, Kluwer Academic Publishers, **1992**
[110] J. March, *"Advanced Organic Chemistry; Reactions, Mechanisms and Structure"*, John Wiley & Sons, New York, **1992**
[111] B. de Bruin, M. J. Boerakker, J. A. W. Verhagen, R. de Gelder, J. M. M. Smits and A. W. Gal, *Chem. - Eur. J.*, **2000**, *6 (2)*, 298-312
[112] B. de Bruin, M. J. Boerakker, J. J. J. M. Donners, B. E. C. Christiaans, P. P. J. Schlebos, R. de Gelder, J. M. M. Smits, A. L. Spek and A. W. Gal, *Angew. Chem. - Int. Edit.*, **1997**, *36 (19)*, 2064-2067
[113] M. Krom, *PhD Thesis "Mono- and Dioxygenation of Rhodium and Iridium Olefin Fragments, Solution versus Solid State Reactivity"*, **2003**
[114] M. Krom, R. G. E. Coumans, J. M. M. Smits and A. W. Gal, *Angew. Chem. - Int. Edit.*, **2001**, *40 (11)*, 2106-2108
[115] M. Krom, R. G. E. Coumans, J. M. M. Smits and A. W. Gal, *Angew. Chem. - Int. Edit.*, **2002**, *41 (4)*, 576-579
[116] R. J. N. A. M. Kicken, *PhD Thesis "Oxidation of Iridium Olefin Complexes by H_2O_2 and O_2"*, **2001**
[117] B. de Bruin, J. A. Brands, J. J. J. M. Donners, M. P. J. Donners, R. de Gelder, J. M. M. Smits, A. W. Gal and A. L. Spek, *Chem. - Eur. J.*, **1999**, *5 (10)*, 2921-2936
[118] M. Moszner, *Inorg. Chim. Acta*, **2004**, *357 (12)*, 3613-3620
[119] E. B. Boyar and S. D. Robinson, *Coord. Chem. Rev.*, **1983**, *50*, 109
[120] T. R. Felthouse, *Prog. Inorg. Chem.*, **1982**, *29*, 73
[121] D. G. de Wit, *Coord. Chem. Rev.*, **1996**, *147*, 209-246
[122] H. L. Zhai, A. Bunn and B. Wayland, *Chem. Commun.*, **2001**, *(14)*, 1294-1295
[123] K. S. Chan and Y. B. Leung, *Inorg. Chem.*, **1994**, *33 (14)*, 3187-3187
[124] D. G. H. Hetterscheid, J. M. M. Smits and B. de Bruin, *Organometallics*, **2004**, *23 (18)*, 4236-4246
[125] M. A. Casado, J. J. Perez-Torrente, J. A. Lopez, M. A. Ciriano, P. J. Alonso, F. J. Lahoz and L. A. Oro, *Inorg. Chem.*, **2001**, *40 (18)*, 4785-4792
[126] M. J. Shaw, W. E. Geiger, J. Hyde and C. White, *Organometallics*, **1998**, *17 (25)*, 5486-5491
[127] M. P. Garcia, M. V. Jimenez, L. A. Oro, F. J. Lahoz, J. M. Casas and P. J. Alonso, *Organometallics*, **1993**, *12 (8)*, 3257-3263
[128] D. G. H. Hetterscheid, B. de Bruin, J. M. M. Smits and A. W. Gal, *Organometallics*, **2003**, *22 (15)*, 3022-3024
[129] M. P. Garcia, M. V. Jimenez, L. A. Oro, F. J. Lahoz and P. J. Alonso, *Angew. Chem. - Int. Edit.*, **1992**, *31 (11)*, 1527-1529
[130] B. de Bruin, T. P. J. Peters, S. Thewissen, A. N. J. Blok, J. B. M. Wilting, R. de Gelder, J. M. M. Smits and A. W. Gal, *Angew. Chem. - Int. Edit.*, **2002**, *41 (12)*, 2135-2138
[131] B. de Bruin, S. Thewissen, T. W. Yuen, T. P. J. Peters, J. M. M. Smits and A. W. Gal, *Organometallics*, **2002**, *21 (21)*, 4312-4314

[132] M. P. Garcia, M. V. Jimenez, L. A. Oro, F. J. Lahoz, M. C. Tiripicchio and A. Tiripicchio, *Organometallics*, **1993**, *12 (11)*, 4660-4663
[133] M. P. Garcia, M. V. Jimenez, A. Cuesta, C. Siurana, L. A. Oro, F. J. Lahoz, J. A. Lopez, M. P. Catalan, A. Tiripicchio and M. Lanfranchi, *Organometallics*, **1997**, *16 (5)*, 1026-1036
[134] Y. P. Ni, J. P. Fitzgerald, P. Carroll and B. B. Wayland, *Inorg. Chem.*, **1994**, *33 (9)*, 2029-2035
[135] E. T. Singewald, C. S. Slone, C. L. Stern, C. A. Mirkin, G. P. A. Yap, L. M. LiableSands and A. L. Rheingold, *J. Am. Chem. Soc.*, **1997**, *119 (13)*, 3048-3056
[136] J. P. Collman and R. Boulatov, *J. Am. Chem. Soc.*, **2000**, *122 (48)*, 11812-11821
[137] D. G. DeWit, *Coord. Chem. Rev.*, **1996**, *147*, 209-246
[138] C. F. Zou, K. J. Ahmed and M. S. Wrighton, *J. Am. Chem. Soc.*, **1989**, *111 (3)*, 1133-1135
[139] L. N. Novikova, B. A. Mazurchik, N. A. Ustynyuk, Y. F. Oprunenko, V. Y. Rochev and V. G. Bekeshev, *J. Organomet. Chem.*, **1995**, *498 (1)*, 25-27
[140] T. D. Newbound, A. M. Arif, D. R. Wilson, A. L. Rheingold and R. D. Ernst, *J. Organomet. Chem.*, **1992**, *435 (1-2)*, 73-84
[141] L. Brammer, N. G. Connelly, J. Edwin, W. E. Geiger, A. G. Orpen and J. B. Sheridan, *Organometallics*, **1988**, *7 (6)*, 1259-1265
[142] R. D. Ernst, H. Ma, G. Sergeson, T. Zahn and M. L. Ziegler, *Organometallics*, **1987**, *6 (4)*, 848-853
[143] W. E. Geiger, T. Gennett, G. A. Lane, A. Salzer and A. L. Rheingold, *Organometallics*, **1986**, *5 (7)*, 1352-1359
[144] R. A. Marcus, *J. Electroanal. Chem.*, **1997**, *438 (1-2)*, 251-259
[145] H. Imahori, H. Yamada, D. M. Guldi, Y. Endo, A. Shimomura, S. Kundu, K. Yamada, T. Okada, Y. Sakata and S. Fukuzumi, *Angew. Chem. - Int. Edit.*, **2002**, *41 (13)*, 2344-2347
[146] K. M. Rosso and J. J. Morgan, *Geochim. Cosmochim. Acta*, **2002**, *66 (24)*, 4223-4233
[147] M. J. Weaver, *J. Mol. Liq.*, **1994**, *60 (1-3)*, 57-71
[148] R. E. Bossio, N. W. Hoffman, T. R. Cundari and A. G. Marshall, *Organometallics*, **2004**, *23 (1)*, 144-148
[149] G. K. Koyanagi, D. Caraiman, V. Blagojevic and D. K. Böhme, *J. Phys. Chem. A*, **2002**, *106 (18)*, 4581-4590
[150] D. Schröder and H. Schwarz, *Angew. Chem. - Int. Edit.*, **1990**, *29 (12)*, 1433-1434
[151] G. K. Koyanagi, D. K. Böhme, I. Kretzschmar, D. Schröder and H. Schwarz, *J. Phys. Chem. A*, **2001**, *105 (17)*, 4259-4271
[152] J. J. S. Tokos, B. Hall, J. A. Calhoun and E. M. Prestbo, *Atmosph. Environ.*, **1998**, *32 (5)*, 823-827
[153] H. H. Cornehl, R. Wesendrup, M. Diefenbach and H. Schwarz, *Chem. - Eur. J.*, **1997**, *3 (7)*, 1083-1090
[154] C. A. Schalley, R. Wesendrup, D. Schröder and H. Schwarz, *Organometallics*, **1996**, *15 (2)*, 678-683
[155] D. Schröder, A. Fiedler, W. A. Herrmann and H. Schwarz, *Angew. Chem. - Int. Edit.*, **1995**, *34 (22)*, 2517-2520
[156] D. Stöckigt and H. Schwarz, *Liebigs Ann.*, **1995**, *(2)*, 429-431
[157] D. Stöckigt and H. Schwarz, *Chem. Berichte*, **1994**, *127 (12)*, 2499-2503
[158] D. Stöckigt and H. Schwarz, *Chem. Berichte*, **1994**, *127 (4)*, 791-793
[159] D. Schröder and H. Schwarz, *Angew. Chem. - Int. Edit.*, **1993**, *32 (10)*, 1420-1422
[160] D. Schröder and H. Schwarz, *Angew. Chem. - Int. Edit.*, **1990**, *29 (12)*, 1431-1433
[161] H. Molina-Svendsen, G. Bojesen and C. J. McKenzie, *Inorg. Chem.*, **1998**, *37 (8)*, 1981-1983
[162] D. Caraiman and D. K. Böhme, *J. Phys. Chem. A*, **2002**, *106 (42)*, 9705-9717
[163] V. Baranov and D. K. Böhme, *Int. J. Mass Spectrom.*, **2001**, *204 (1-3)*, 209-221

Chapter 2

Characteristics of Electrospray Ionization Mass Spectrometry

2.1 Introduction

Application of Electrospray Ionization Tandem Mass Spectrometry (ESI-MS/MS) in the characterization of (in)organic species [1] – [13] is a growing field. This is a result from:

(i) The possibility to analyze highly diluted solutions.

(ii) The mild conditions used for the transfer of charged species from solution to the gas phase.

Applications exploiting these advantages for ESI-MS are numerous:

- The first application is the most frequently used one: analysis of the m/z of all the species present in solution to get an idea of the type of products that are formed in a reaction or to get information about the elemental composition and mass of a certain compound.
- Being able to work directly from a dilute solution is a major advantage for catalysis because the active species often exist only under these conditions.
- The gentleness by which ions are formed makes that proteins can be ionized without denaturation and that non-covalent receptor-substrate/cofactor complexes e.g. in enzymes and proteins [14] – [20] remain intact.
- Elucidation of 3-D structures [21]: on the basis of collision experiments the folding of peptides can be determined. [22] – [27] For example, in the case of α-dendrotoxin (see picture beside for a 3-D representation) Belva *et al.* [28] have been able to determine by means of ESI-MS 1) which residues are hidden in the core of the structure, 2) which S-linkages are less accessible for reduction and are therefore responsible for a compact fold of the peptide and 3) the amount of hydrogens involved in hydrogen bonds. This information provides more insight in the folding of this peptide.
  ESI-MS has also been very useful for the determination of supramolecular structures of coordination polymers and multinuclear metal clusters. [2], [4], [7], [8], [11], [29]

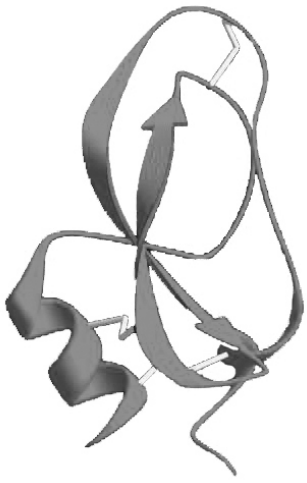

- Fragmentation behavior observed in ESI tandem MS can provide useful information on decomposition pathways of compounds in solution. [30] – [33]
- Gas-phase ion-molecule reactions can also be used to obtain more insight in the mechanisms of reactions in solution. [34] – [42].
  This is especially the case since it is possible to mass select the species of interest and allow only this species to react with the reactant gas in a collision cell enabling identification of the gas-phase products of only this particular species (instead of the products of all possible species present in solution).
- ESI-MS/MS has been used in high-throughput screening of homogeneous catalysts. [39], [43] – [45]
- With electrospray mass spectrometry subtle differences in reactivities can be observed. This allowed Schwarz [46] – [48] to get a feeling for the influences of relativistic effects on certain reactions.

Often, the species detected by ESI-MS are considered to represent the charged species in solution. Nevertheless, one has to keep in mind that reactions might occur within the ion source, especially at higher tube lens voltages [6], [30], [49] (see also § 2.3 and Chapter 7).

In this chapter we will describe characteristics of the mass spectrometric equipment used throughout this thesis. We will also show that performing ESI-MS/MS measurements is not always straightforward.

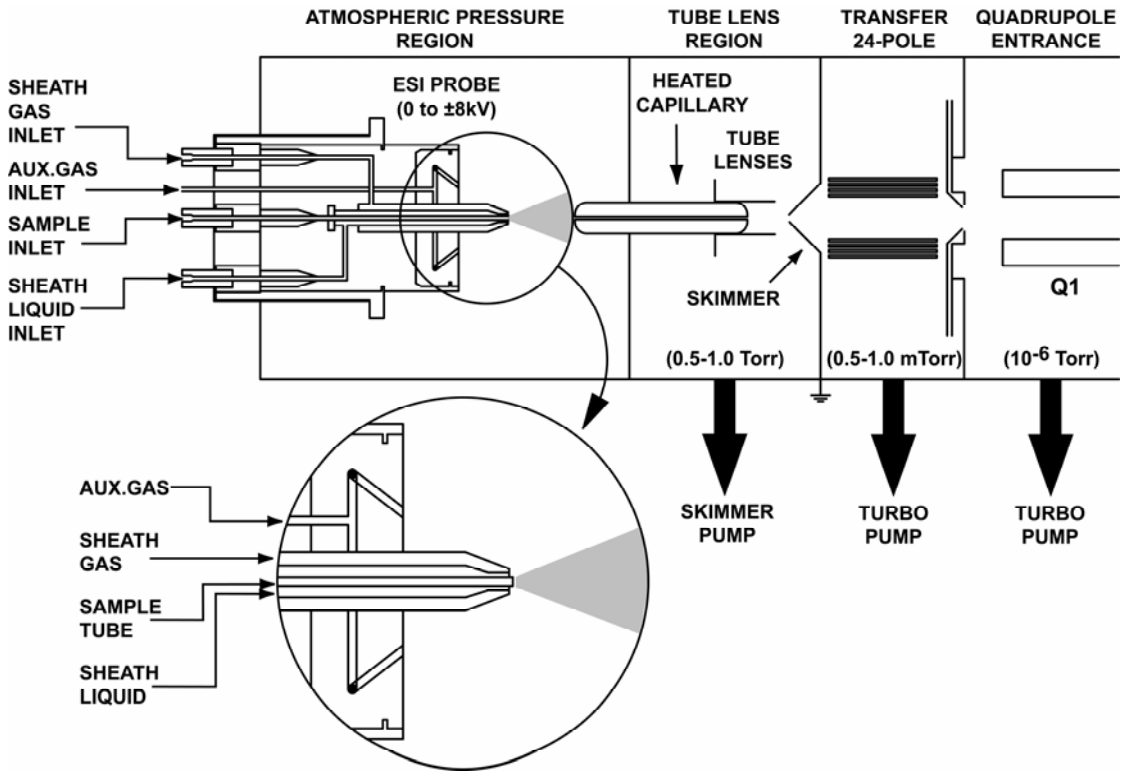

Figure 2.1 *Schematic representation of the electrospray source* [50] [1]

2.2 Description of the MS equipment

2.2.1 The electrospray ion source

For all mass spectrometric measurements discussed in this thesis electrospray ionization (ESI) was used to transfer the ionic complexes to the gas phase. This technique is capable of transferring intact molecular ions from a dilute solution *directly* to the gas phase by a complicated multi-step process: charged droplet formation, droplet fission at the Rayleigh limit and/or direct field desorption. [51] – [54] Thorough discussions of the electrospray process and everything related to it have been published [1], [55] – [57] and will not be repeated in detail here. [2]

[1] The sheath liquid inlet can be used to co-spray a second solution without mixing it in the tubing with the analyte solution in the sample inlet. It could also be just a solvent that facilitates the electrospray process for the analyte solution. The auxiliary gas can be used to facilitate droplet formation.

[2] The basic electrospray source for mass spectrometry is described by Whitehouse *et al.* [50]

Typically, a 10^{-4} to 10^{-5} M solution of the ionic compound in a (usually somewhat polar) organic solvent is pressed through a capillary at a flow rate of 3-15 μl/min and electrosprayed in the atmospheric pressure chamber in contact with air at a potential of 3 - 5 kV (Figure 2.1). By adjusting the electrospray voltage, the concentration of the dissolved compound, the flow, the use of sheath gas (to improve droplet formation [59]) stability of the electrospray can be achieved.

Only a very small amount of the ions that are sprayed in this way enter the mass spectrometer, the rest hits the ground plate around the heated capillary.

The ion beam thus produced enters the heated capillary (typically at 150-200 °C) where the ions are declustered and the remaining solvent molecules are evaporated. After that the ions enter the first stage of the mass spectrometer that is already at a somewhat reduced pressure (0.5 - 1.0 Torr [3]): the tube lens region. A positive potential is applied to the tube lenses to converge the diverging ion beam and bend it in such a way that the ions can pass through the entrance of the skimmer, which is situated a bit below the exit of the heated capillary (Figure 2.2).

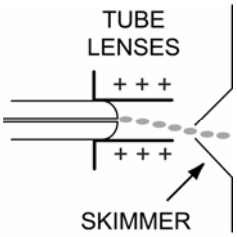

Figure 2.2 *Schematic view of the ion beam passing via the tube lens region into the skimmer*

By doing so the neutral particles entering the tube lens region (which are not analyzed anyway since they don't posses any charge) will not enter the high-vacuum part of the mass spectrometer, preventing excessive pollution and decreasing the pressure load on the pumps connected to the high-vacuum part of the mass spectrometer.

For every mass-over-charge ratio (m/z) there is a tube lens potential for which the number of the ions passing the skimmer entrance is maximal. Also the extent of desolvation and collisional activation, CA (e.g. generation of coordinatively unsaturated complexes by removal of the most weakly bound ligand), can be controlled by the height of the tube lens potential. The higher the applied potential, the more the ions are accelerated towards the center of the tube lens region and the more and the harder they will collide with background gas molecules [4] and other ions. In these collisions the kinetic energy of the ions, obtained by this positive tube lens potential, can be converted into internal energy, which can be used to overcome activation barriers for fragmentation (Chapter 6) or in some cases a reaction with dioxygen, which is also present in the background gas (Chapter 7).

Typical tube lens potential ranges are between 35 V (mild conditions) to 140 V (harsh conditions).

Although little is known of the reaction conditions in the tube lens region or of the number of collisions ions undergo in this region, it is certain that in the tube lens region *high-energy collisions at high collision gas pressures* can be performed.

[3] 1 Torr corresponds to 1.33322 mbar

[4] The background gas in the tube lens region consists of air and gaseous solvent molecules, all of which have entered through the heated capillary along with the gaseous ions. The exact composition of the background gas cannot be determined. Neither can it be varied at will.

2.2.2 Mass spectrometric analyzers

A few of the analysis and fragmentation experiments presented in this PhD thesis were performed on a Finnigan MAT 900 XL: a double focusing magnetic sector analyzer with with a Nier-Johnson geometry: first the ions pass the electrostatic analyzer and then the magnetic sector (see a book by Chapman [60] for a more detailed description of such an analyzer).

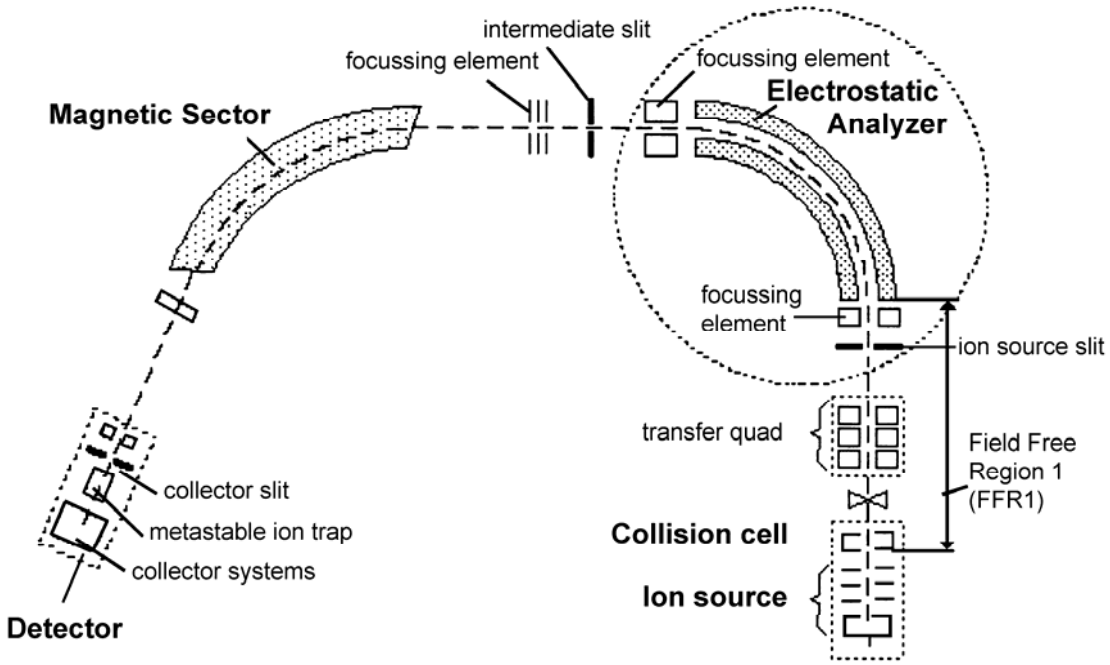

Figure 2.3 *Schematic representation of the MAT 900 XL*

A result of this geometry is that the only place where the collision cell can be located is before the electrostatic analyzer and the magnetic sector, right at the end of the ion source. Therefore, it is not possible to first mass select ions with only one m/z and then allow selective collision of these ions with a gas: all ions that have been transferred to the gas phase enter the collision cell. Only helium can be used as a collision gas; an unknown pressure can be bled into the collision cell to induce fragmentation. These collision-induced-dissociation (CID) experiments are performed at *very high collision energies* (in the order of magnitude of keV). The collision energy cannot be adjusted in any way. Therefore this setup can only be used to analyze the species present in solution and look at their fragmentation behavior.

Real gas-phase reactivity studies were performed on a modified Finnigan MAT TSQ 700 or a slightly modified Finnigan MAT TSQ 7000. [5] The only difference between the setup of the two mass spectrometers is that the first octopole in the TSQ 7000 (reaction chamber 1, RC 1) has been replaced by an rf 24-pole in the TSQ 700. Since the TSQ 7000 is nearly identical except for this difference, we will only describe the setup of the TSQ 700 in detail.

The ESI-MS equipment used during this PhD project was already previously described in detail by members of the group of Prof. Chen. [38] – [45], [58], [61] – [70] Therefore only the important issues that are relevant for this thesis will be addressed in the following paragraph.

[5] The only modification of the TSQ 7000 is that the first octopole (RC 1) has been fitted with an open cylindrical sheath around the rods into which a collision gas could be bled for thermalization or reaction pressures. As a result both TSQ's have two reaction chambers: RC 1 and RC 2.

2.2.3 Layout of the modified TSQ 700

A schematic representation of the layout of the Finnigan MAT TSQ 700 mass spectrometer is shown in Figure 2.4.

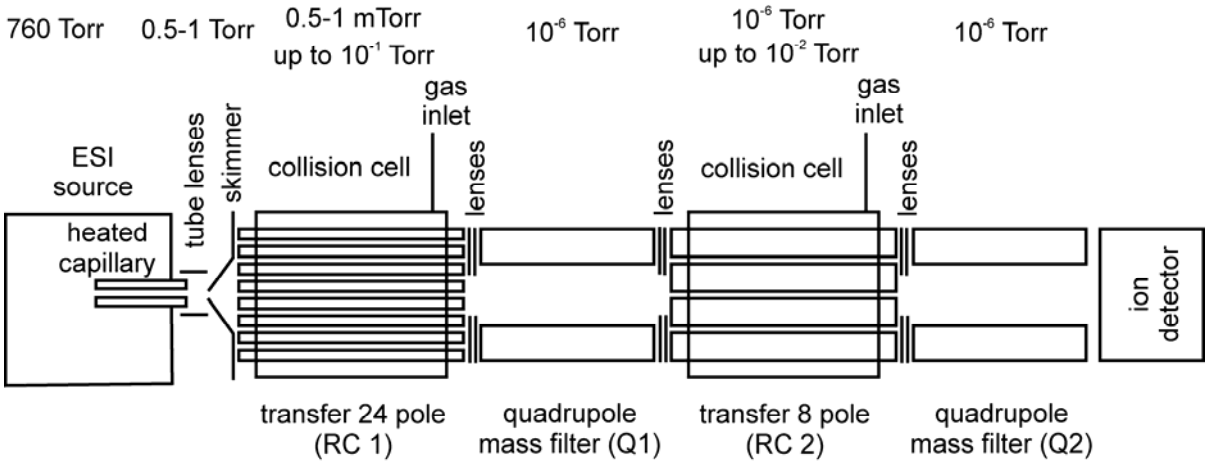

Figure 2.4 *Schematic representation of the modified TSQ 700 ESI tandem mass spectrometer* [71]

The two radio-frequency (rf) multipoles (RC 1 and RC 2) serve as reaction "vessels" for collision of the ions with neutral gaseous reagents. After each stage of reaction, product identification and/or selection is carried out in a quadrupole mass analyzer.

Reaction chamber 1 (RC 1): the rf 24-pole region

Every gaseous ion produced in the tube lens region enters the next region: the radio-frequency (rf) 24-pole. It acts as an ion guide to separate the ions from the neutral molecules, which are pumped off by a turbopump located underneath the 24-pole. The pressure in this region is still relatively high (about 0.5 - 1.0 mTorr). It is fitted with an open cylindrical sheath around the rods into which, depending on the setup, a collision gas can be bled for thermalization or reaction at pressures up to 100 mTorr.[6]

The 24-pole lies at -3 V with respect to the skimmer in order to pull the cations inside. Theoretically, the ions have a kinetic energy of 3 eV (laboratory frame) upon entering the 24-pole. However, this initial kinetic energy is already lost in the first few collisions, due to the relatively high pressure at the entrance region of the 24-pole where the ions pass this potential difference of -3 V. As a result the ions will enter the 24-pole region with near-zero kinetic energy[7], which cannot be adjusted in any way. [8]

Although there is no applied longitudinal electric field, the continuous ion current into the 24-pole creates by way of space-charge effects a slight longitudinal potential that drives the ions through. The 24-pole serves as an ion guide which confines the ions in the radial direction. Once the ions have entered the 24-pole, they sort of "diffuse" through the 24-pole.

Collision frequencies of 10^6 - 10^7 s^{-1} (corresponding to around 10^5 collisions) can be achieved in this region. As a result efficient thermalization to 70 °C can take place. Species formed in exothermic reactions can easily get rid of their excess of energy.

---

[6] In RC 1 of the Finnigan MAT TSQ 7000 (the first octopole) up to 20 mTorr of collision gas can be bled.

[7] Of course the ions always have a thermal energy of $3RT$ = 0.03 eV (at 70 ºC manifold temperature)[72]. However, this amount of energy is negligible compared to the amount of energy the ions can receive upon entering RC 2, for example.

[8] Attempts by Adlhart [71] to induce ligand dissociation in the 24-pole region by changing the potential difference between the 24-pole and the skimmer from -3 V to -10 V were not successful. This implies that the ions really have lost all their kinetic energy once they enter the 24-pole region.

In other words, *zero-collision-energy collisions at high collision gas pressures* can be performed in the 24-pole region.

Quadrupole mass filters

Once the ions have left the 24-pole region, they enter the last part of the mass spectrometer, which is at 10^{-6} Torr and 70 °C manifold temperature during operation. The configuration is quadrupole/octopole/quadrupole (Q1/RC 2/Q2), with the two quadrupoles as mass selection stages and the octopole operating as a collision-induced-dissociation (CID) cell.

Spectra were recorded in two different modes:

- In the normal ESI-MS mode (MS), only one quadrupole is operated (either Q1 or Q2) as a mass analyzer, and a mass spectrum of the electrosprayed ions is recorded. This mode serves primarily to characterize the ions produced by a given set of conditions.
- In the daughter-ion mode (MS/MS or tandem-MS), Q1 is used as a mass filter to mass-select ions of a single m/z from among all of the ions coming out of RC 1. These ions are then collided with a target gas in RC 2, and finally mass analyzed by Q2. This mode is used to obtain structural information (by analysis of the fragments) or investigate the specific reactivity of a species of a given m/z towards a certain collision gas.

Reaction chamber 2 (RC 2): the octopole region

The octopole region can be operated as a conventional collision-induced-dissociation (CID) cell. It differs from the 24-pole region in two ways:

- Collision gas pressures of only up to 5 mTorr can be applied (c.f. up to 100 mTorr in RC 1). [9]
- The kinetic energy of the ions can be varied up to about 150 eV (laboratory conditions). Compare this to RC 1 in which the kinetic energy of the ions cannot be changed and is near zero-collision-energy.

In other words, in the octopole region ***tunable*** *low and high-energy collision experiments at low collision gas pressures* can be carried out.

Number of collisions with gas molecules in the different regions

Monte Carlo simulations by Adlhart [71] indicate that under the reaction conditions employed in the octopole, the ions have a "temperature" of 70 ºC and undergo about 5000 collisions with the reactant gas. The simulated retention time for the ions in the collision cell is ≈ 1 – 10 ms depending on the pressure of the collision gas and the initial kinetic energy of the ions.

The number of collisions in the 24-pole can be 100 times as high. Thus, reactions performed here will be more similar to condensed-phase chemistry in the gas-phase because of efficient thermalization of chemically activated intermediates produced in exothermic reactions. However, the stabilizing effect of the solvent is still absent. In other words, by looking at reactions in the 24-pole region we are able to separate these two properties of a solvent.

[9] This latter part of the mass spectrometer (the so-called manifold) has to be kept at high-vacuum (required for among other things the ion multiplier). Any raise in collision gas pressure has directly its influence on the manifold pressure. Since the 24-pole is separated from the manifold by differential pumping, the influence of increased collision gas pressure on the manifold is much less and therefore higher collision gas pressures can be applied to this region.

2.3 Possibilities and difficulties encountered when using ESI^+-MS

The ESI process does not always "magically" transfer intact sample ions into the gas phase. The following sections describe some of the peculiarities one might encounter in ESI-MS studies. In this chapter only measurements in the positive ion mode (ESI^+) will be discussed, since this is the mode in which all spectra in this thesis have been measured. In most cases the issues discussed can be easily reformulated for the negative ion mode (ESI^-).

2.3.1 Spraying of neutral compounds

One of the requirements for the use of ESI^+-MS is that the compounds to be transferred to the gas phase are cationic. Neutral molecules can also be analyzed by ESI^+-MS, provided they have high proton affinity [59], [73] or form stable complexes with ions (the so-called "coordination ion-spray mass spectrometry", CIS-MS). [74] – [84] Especially MS analyses via the formation of cation adducts (e.g. with Na^+, K^+, Li^+, Ag^+, Ca^{2+}, Co^{2+}, Cu^{2+}) is a growing field and is mainly used to investigate peptides, proteins or polymer mixtures. [78], [82], [85] – [89]

For this technique, the neutral molecules must have sites suitable for coordination of the cation, like aromatic ring systems, olefinic bonds [90] or functional groups containing oxygen, nitrogen [14], [85], [90], [91] or halides.

For example, we found that Na^+ coordination worked for the chloride-containing neutral organometallic complex [(pmdta)$Rh^{III}Cl_3$]. [10] When a DMSO-d6 solution was co-sprayed with $NaBPh_4$ (Rh:Na = 1:1), the ion-molecule complex {[(pmdta)$Rh^{III}Cl_3$]Na}$^+$ and its solvent adducts could be observed. However, the related complex [(pmdta)$Rh^{III}(Me)_3$] did not form any sodium adducts, demonstrating the importance of the presence of the chlorides for Na^+ coordination. Apparently none of the three amine groups of this N_3 ligand is accessible for sodium coordination.

2.3.2 Single-electron transfer during the spraying process

Since sodium coordination seemed to work for chloride-containing organometallic complexes, we tried to analyze the neutral complexes [(*i*Pr-Brookhart)$Co^{I}Cl$] [11] and [(*i*Pr-Brookhart)$Co^{II}Cl_2$] in the same manner. The [(*i*Pr-Brookhart)$Co^{I}Cl$] complex surprisingly gave mono-cationic species [(*i*Pr-Brookhart)$Co^{II}Cl]^+$ as base peak in the mass spectra. Apparently, single-electron transfer (SET) from the cobalt complex had taken place during the spraying process. This was probably induced by the high spraying voltage (3-5 kV) at the capillary tip, which is necessary to obtain a stable spray.

Upon co-spraying the neutral complex [(*i*Pr-Brookhart)$Co^{II}Cl_2$] with $NaBPh_4$, we again did not observe any sodium adducts. The same mono-cationic cobalt(II) species, [(*i*Pr-Brookhart)$Co^{II}Cl]^+$, was the base peak in the spectra. This behavior was not too surprising, since ionization via loss of the halide ligand is a very common phenomenon observed when using electrospray as ionization method. [3], [12] Also, it was already reported [92], [93] that one of the two chlorides can dissociate easily in solution. Finally, any Na^+ adduct formed may easily lose NaCl.

In order to find out whether single-electron-transfer reactions can occur for other complexes as well, we sprayed MeCN solutions of both [$(Cp)_2Co$] and [$(Cp)_2Fe$]. Again the corresponding mono-oxidized species were the base peaks in the mass spectra, confirming that SET can take place during the process of transferring

[10] pmdta = *N*1-[2-(dimethylamino)ethyl]-*N*1,*N*2,*N*2-trimethyl-1,2-ethanediamine

[11] *i*Pr-Brookhart = *N*1-((*E*)-1-6-[(2-isopropylphenyl)ethanimidoyl]-2-pyridylethylidene)-2,6-diisopropylaniline

species to the gas phase in the electrospray source. The signal of the cobaltocenium ion was much more stable and intense than that of the ferrocenium ion. Also, because the ferrocene measurements were performed after those of cobaltocene there was a large memory effect of the cobaltocenium ion.
The relative ionization efficiencies of different species in the electrospray source is a function of the oxidation potentials of the species, with large differences (> 0.2 V), resulting in the nearly exclusive production of the analyte of lower oxidation potential. [84] Since cobaltocene is oxidized much more easily than ferrocene[12], even traces of cobaltocene remaining in the ESI area will suppress ferrocene ionization, which explains the memory effect.

In the literature one can find quite a few reports concerning similar redox reactions: ferrocene derivatives [95], metalloporphyrins [84], metal complexes of L-histidine [96], fullerenes [97], [98] (negative ion mode) and some organic molecules. [99] – [101]
Van Berkel [99], [100], [102], [103] has studied redox reactions taking place when using ESI-MS in detail. He found that oxidation reactions in the positive ion mode and reduction reactions in the negative ion mode dominate at the emitter electrode (the tip of the capillary where the solution is sprayed), whereas reduction reactions in positive ion mode and oxidation reactions in negative ion mode can dominate at the counter electrode (the entrance of the heated capillary). Mainly reactions at the emitter are reported, although a few reports describe electron capture in the positive ion mode. [96], [104] Charbonnier *et al.* [101] have even tried to differentiate between these oxidation and reduction processes taking place simultaneously.
Redox reactions can both take place in the tube lens region and under influence of the source voltage (at the counter electrode). [105]
In the *tube lens region* redox reactions are usually a matter of a ligand-to-metal electron transfer (after which the ligand can dissociate) or the analyte can transfer an electron to a gaseous solvent molecule [106] or another analyte molecule. For these reactions the ionization potentials of the solvents (which lie usually in the 9-12 eV range[13] [107]) and of the analytes are important.

Thus, the electrochemical reactions that take place at the ESI emitter electrode [100] may influence the gas-phase ions formed and ultimately analyzed by mass spectrometry. [99] Of particular interest are those electrochemical reactions and compositional changes that directly involve the analytes. [108] These reactions include electrochemical ionization that can be exploited to ionize neutral electroactive analytes that would otherwise go undetected in ESI-MS as shown above. Other reactions include those that modify the mass, structure, or charge of the analyte [109] and those that can remove analytes from solution. [110] Reactions of the latter type might be troublesome for analyses involving unknown analytes or quantification. The ability to control the extent of any or all of these electrochemical reactions would be an analytical advantage.
According to Van Berkel, a lot of factors affect the reactions occurring at the emitter electrode: the magnitude of the electrospray current, the redox character[14] and concentrations of all species in the system, the solution flow rate, solvent polarity, the spraying voltage, temperature, solvent dielectric constant, the electrode material [108], geometry and any other parameters that affect the flux of reactive species to the electrode surface. [1], [103], [111]

Similar redox reactions could theoretically also occur when spraying cationic instead of neutral complexes. However, for the mono-cationic N_3 and N_4 rhodium(I) and iridium(I) ethene complexes described in this thesis

[12] Electrochemical data reported [94] for $[Cp_2Co]$: $E_{½}$ = -0.94 V (against $[Cp_2Fe]/[Cp_2Fe]^+$ reference).
[13] Ionization potentials: 9.1 eV for DMSO, 9.2 eV for THF and pyridine, 9.4 eV for Et_2O, 9.7 eV for acetone, 10.8 eV for methanol, 12.2 eV for acetonitrile and 12.6 eV for water.
[14] For example, ionization of metalloporphyrins in the positive ion mode appears to be a direct function of their oxidation potentials. [84]

dicationic species were never observed in the mass spectra.
Either it is difficult to oxidize these species, or the amount of metal(II) species formed is so small, that they are suppressed by the mono-cationic species (the dominant-ion effect described in § 2.3.4), or they are so reactive that they react with anything that comes in their way.

2.3.3 Reaction with air in the ESI-source

Using ESI^+-MS for analysis of extremely air-sensitive organometallic species can be problematic. Especially in a dilute solution such compounds will react rapidly with air, to which they are exposed during the nebulization process in the ESI source. A reaction with gaseous molecules present in the atmospheric pressure chamber was already observed by Ikonomou *et al.* [59] It will result either in the observation of a lot of unknown oxidized or oxygenated species in the mass spectra, or simply in a decrease of the signal intensity and stability.

One way to circumvent this problem is the use of sheath gas, which would protect the complexes from a reaction with air during nebulization. However, this has never had any visible influence at all on any of the mass spectra we obtained.

One could also to try to prevent reaction with air by going to higher flow rates. This will increase the droplet size [112] and decrease the surface-to-volume ratio. Provided the reaction with dioxygen only takes place at the droplet surfaces, increasing the flow rate reduces contact of the organometallic molecules with air.
Whether or not this works depends strongly on the ESI source: each has its own droplet-size distribution. Although the sources of the sector machine and of the quadrupoles used throughout this thesis look quite alike and are from the same factory, for the sector machine we had to go to flow rates of at least 40 µl/min if we wanted to be able to spray really air-sensitive complexes and get good signal-to-noise ratios. For the TSQ's we never had to go higher than 10 µl/min.

A last way to keep the droplet size relatively large is to go to less volatile solvents like acetonitrile. For example, it was impossible to obtain mass spectra from iridium(II) ethene complex $[(Me_3\text{-tpa})Ir^{II}(C_2H_4)]^{2+}$ [15] using acetone (b.p. 56 ºC) as a solvent. However, when acetonitrile (b.p. 81 ºC) was used, very intense signals were obtained of which the iridium(II) species (without coordinated acetonitrile) was the base peak.

2.3.4 Dominant-ion effect

During the electrospray process droplets shrink to the point where repulsive coulombic forces approach the level of droplet cohesive forces (e.g., surface tension). There is still no consensus on the mechanism by which solute ions are transferred to the gas phase from charged droplets. Two mechanisms are commonly cited for ion formation from charged droplets; droplet fission at the Rayleigh limit and direct field desorpion of ions:

Droplet fission at the Rayleigh limit [113] – [116]

For large (> 1µm) droplets most probably the Rayleigh limit applies, where droplets explode, typically shedding more than 10% of their charge and about an order of magnitude less mass [117]. These droplets undergo a cascade of fission processes yielding smaller and smaller droplets until the electric field at the droplet surface is sufficient for ion desorption to take place.

[15] $[(Me_3\text{-tpa})Ir^{II}(C_2H_4)]^{2+}$ is a complex with a N_4 ligand, which will be discussed in more detail in Chapter 5

Direct Field Desorption [53], [54]

> Desorption of ions is an activated process that can be characterized by the product of two terms [52]: the concentration of the desorbing species at the surface and a rate constant depending exponentially on the difference between the lift force on the ions and the solvation forces holding the ion to the droplet. The lift force is proportional to both the charge of the molecule [53] and the intensity of the electric field at the droplet surface. [52] The solvation force depends on the composition of both the ion and solvent and is proportional to the ion's "wetted area".

A high charge of the analytes that are being sprayed can also be disadvantageous. It makes the desorption process more difficult due to stronger interaction with the solvent. As a result, when an equimolar mixture of mono- and dicationic species is sprayed, the signals corresponding to the mono-cationic species will dominate in the mass spectra (the *dominant-ion* effect).

For species having long tails (e.g. oligomers) in polar solvents solvophobicity increases with increasing tail length, thus decreasing the work needed to remove an ion from the liquid. [52] Also, due to their tail such ions will have a higher concentration on the surface of the droplets. As a result, in an equimolar mixture of solvophobic and solvophilic compounds, the solvophobic ones will be overrepresented in the mass spectra. Quaternary ammonium salts behave in the same manner.

An other important factor is the surface tension[16]: the higher it is, the higher the activation energy for the transfer of the ions to the gas phase and thus the lower the efficiency of ion desorption. [59]

The dominant ion effect can be relevant to the chemistry of the mono-cationic ethene complexes discussed in this thesis. If single-electron transfer (as described in § 2.3.2) would take place somewhere in the electrospray source, it would result in the formation of a small amount of dicationic species. Both because of their low concentration and their higher charge, their abundance in the mass spectra will be negligible; the mono-cationic species will suppress their desorption.

2.3.5 Ion pairs

Another phenomenon that can be observed when spraying multiple cationic species is the presence of ion pairs in the mass spectra. Ion pairs are commonly observed in the electrospray mass spectra of transition metal complexes. Their relative abundance in the ESI mass spectra of low-concentration solutions suggests that the electrospray process in some way favors the formation of these less charged species. Polar solvents, that exhibit stronger solvating powers towards cations, appear to reduce the amount of ion pairing observed. [118] Other solvent properties that are known to affect ESI mass spectra (e.g. volatility) appear not to be important here. Upon increase of the analyte concentration an increased ion pairing is observed. [17] The coordinating properties of the counterion are important: trifluoroacetate appeared to have a higher affinity for diquaternary ammonium ions than chloride.

Vachet *et al.* [119] investigated the chemistry of ion-pair complexes[18] systematically by ion-molecule reactions and CID. They were not only able to establish whether the counterion in an ion pair is an inner- or outer-

[16] For a list of the surface tensions of some commonly used solvents see Table 2.1 in § 2.3.6.

[17] Upon increase of the concentration of the analyte ion pairing in solution will also increase.

[18] $[ML_2X]^+$, M = Mn(II), Fe(II), Co(II), Ni(II), Cu(II), Zn(II); L = 1,10-phenantroline, 2,2'-bipyridine, ethylenediamine, diethylenetriamine, 1,4,8,11-tetraazacyclotetradecane; X = Cl^-, NO_3^-, acetylacetonate, ClO_4^-, acetate, SCN^-.

sphere ligand, but also found unique coordination modes for some of the ions[19] and interesting reactivities of some of these ion pairs.

2.3.6 Reaction with the solvent

There is one other factor one has to take into account, when using ESI^+-MS: the solvent.

In general one can use most solvents to perform ESI^+-MS measurements, as long as the compound of interest dissolves in it with a concentration of at least 10^{-5} M. Usually these solvents are somewhat polar, but an apolar solvent like toluene can also be used. [97], [98], [120] When spraying neutral compounds a protic solvent is often used to generate ions through protonation (as described in § 2.3.1).

The conductivity of the solution must be less than 10^{-5} Ω^{-1} [116] and the surface tension of the solvent must be not too high. [59] The higher the surface tension, the higher the spraying voltage V_{on} needed for a stable spray [20]; see Table 2.1. [59], [121]

The spraying voltage used must not be too high, because else so-called "corona discharges" [21] take place, which disturb the ESI-MS measurement. These discharges are especially problematic when water is used as a solvent. The influence of the boiling point of the solvent on the minimum spraying voltage is relatively unimportant (Table 2.1). [121], [122]

Table 2.1 *Surface tensions, minimum spraying voltages and boiling points for some solvents*

Solvent	Surface tension (10^{-3} N·m^{-1}, at 20 ºC)	V_{on} (kV)	Boiling point (ºC)
Methanol	22.61	2.2	65
Acetone	23.7	2.3	56
Dichloromethane	26.52	2.4	40
Chloroform	27.14	2.4	61
Acetonitrile	29.3	2.5	81
DMSO	43	3.0	189
Water	73.05	4.0	100

The above solvent requirements are mostly independent of the analyte and are mainly physical properties. However, the solvent is also a chemical compound and can undergo chemical reactions with the analyte.

---

[19] SCN^-, displaying mainly a monodentate coordination mode, behaved like a bidentate ligand in nickel(II) and zink(II) complexes, as did also ClO_4^- in nickel(II) complexes.

[20] V_{on} increases with the square root of the surface tension of the solvent. [121] Below V_{on} the liquid surface is electrohydrodynamically stable: even though the surface may be charged, the charge is not sufficient to produce droplets.

[21] A corona discharge is a process by which a current develops between two high-potential electrodes in a neutral medium, usually air, by ionizing that medium so as to create a plasma around one electrode, and by using the ions generated in plasma-processes as the charge carriers to the other electrode.

Corona discharge usually involves two asymmetric electrodes, one highly curved (such as the tip of or a narrow wire; here the capillary tip) and one of low curvature (such as a plate, or the ground; here the entrance to the high-vacuum part of the mass spectrometer). The high curvature ensures a high potential gradient around the capillary electrode, for the generation of a plasma. An electrical discharge occurs when this potential gradient exceeds a certain value.

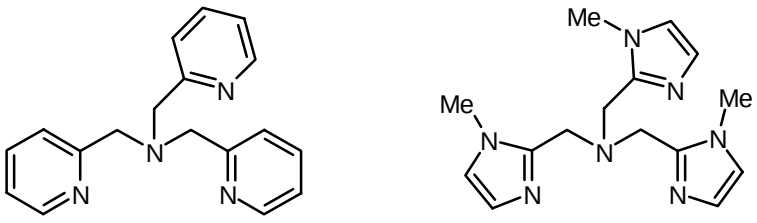

Figure 2.5 *Ligands used in the complexes that reacted with CH_2Cl_2 when analyzing them with ESI-MS*

To illustrate this we now discuss the ESI^+ mass spectra of $[(N_4)Rh(C_2H_4)]^+$ (N_4 = tpa or tia, see Figure 2.5)[22] complexes in some detail. When solutions of these compounds in CH_2Cl_2 are sprayed no olefin complex can be observed in the mass spectrum!

Instead only a species with an isotope pattern and an m/z corresponding to $[(N_4)RhC_2H_2Cl_2]^+$ is present. In other words, during the spraying process in the ESI source both the olefin complexes have been fully converted to an unknown chloride-containing species.

At first we believed that the $C_2H_2Cl_2$ moiety was a π-coordinated olefin. From the presence of $[(N_4)Rh^I]^+$ in the daughter spectrum of the tpa complex (Figure 2.6, signal **2**), one could conclude that $C_2H_2Cl_2$ can dissociate as a whole, which is in favor of such an olefin complex. Another fragmentation that could explain the presence of signal **2**, first loss of C_2H_2 and then loss of Cl_2, seems less likely.

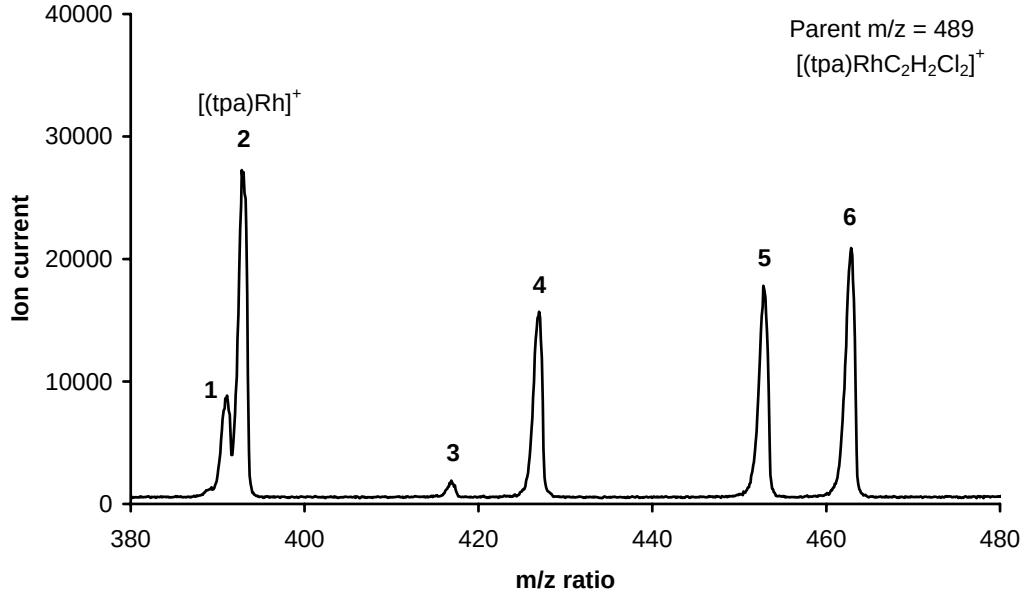

Figure 2.6 *Fragmentation behavior of $[(tpa)RhC_2H_2Cl_2]^+$* [23]

However, some of the other fragmentations observed[24] would not have been expected for an olefin complex:

- First loss of C_2H_2 (signal **6**), and then twice loss of HCl (signal **4** and **1**)
- Or first loss of HCl (signal **5**), then C_2H_2 (signal **4**) and then HCl (signal **1**)
- Or twice loss of HCl (signal **5** and **3**) and then C_2H_2

[22] tpa (= *N*,*N*,*N*-tri(2-pyridylmethyl)amine); tia (=*N*,*N*,*N*-tri[(1-methyl-1*H*-2-imidazolyl)methyl]amine).

[23] Collision with 0.4 mTorr argon at 50 eV (laboratory conditions). The fragmentation behavior of the $[(tpa)RhC_2H_2Cl_2]^+$ species is similar to that obtained for the corresponding tia complex.

[24] For each of the daughter ions in Figure 2.6 the fragmentation behavior is measured separately as well to confirm the different fragmentation pathways.

Especially the loss of C_2H_2 (leaving $[(tpa)RhCl_2]^+$ behind) is most puzzling. On the basis of this fragmentation behavior one could propose several structures for $[(N_4)RhC_2H_2Cl_2]^+$ (in Figure 2.7 some of them are shown for the tpa complex).

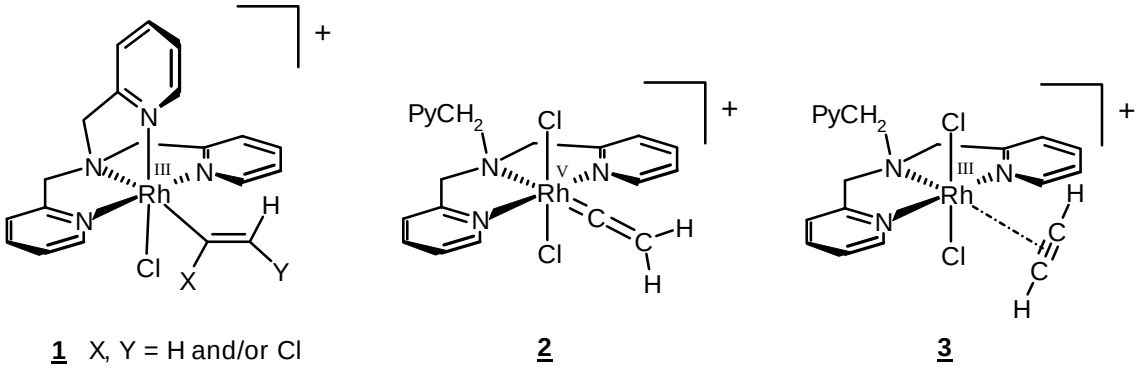

1 X, Y = H and/or Cl **2** **3**

Figure 2.7 *Possible structures of $[(tpa)RhC_2H_2Cl_2]^+$*

There are arguments against each of these structures:

- Structure **1** seems very reasonable. However, loss of C_2H_2 from **1** seems not to be very straightforward. The alternative structure with the vinylic chloride *cis* to the metal center should β-eliminate very rapidly and will therefore not be observed. A $[(N_4)Rh(H)(CCl=CHCl)]^+$ isomer will undergo easy reductive elimination and (or) *β*-elimination.
- For structure **2** it is difficult to picture loss of HCl with the proton stemming from the $C_2H_2Cl_2$ moiety instead of from the N_4 ligand (loss of DCl was observed for the corresponding $C_2D_2Cl_2$ species, as will be shown later on).
- Intact transfer of species **3** to the gas phase does not seem plausible due to the weak coordination of acetylene. Also, for structure **3** one would have expected the signal corresponding to loss of C_2H_2 be even more intense.

We do not know anything about the mechanism via which these chlorinated species are formed.
What we do know about the reaction is that:

- HCl is not necessary for the reaction to proceed. If CH_2Cl_2 is stirred with Na_2CO_3 before use, the reaction still proceeds in the same high yields.[25]
- When CD_2Cl_2 is used as a solvent instead of CH_2Cl_2 for the tia rhodium ethene complex, the reaction produces $[(tia)RhC_2\mathbf{D}_2Cl_2]^+$. In other words, at least the hydrogen atoms (but most probably also the carbon atoms) of the $C_2\mathbf{D}_2Cl_2$ moiety stem from the solvent.
  The reaction with CD_2Cl_2 instead of CH_2Cl_2 appears to be somewhat different, since now also a second species is present: $[(tia)Rh(C_2DCl_3)]^+$ (intensity about 20% of that of the corresponding $C_2\mathbf{D}_2Cl_2$ species). In other words, for some reason when using the deuterated solvent it is possible to incorporate in more than two chlorine atoms. [26]
  The fragmentation behavior of the $C_2\mathbf{D}_2Cl_2$ species is comparable with that of the corresponding $C_2H_2Cl_2$ species. Only now in the first step either $C_2\mathbf{D}_2$ or **D**Cl is lost (in other words, the corresponding deuterated species).

[25] If CD_2Cl_2 that contains a lot of impurities is used almost full conversion to an ethyl-chloride species is observed if stirring with Na_2CO_3 before use is ommited.

[26] There was also a signal as large as the one for $[(tia)RhC_2D_2Cl_2]^+$ present in the mass spectra corresponding to a species with an m/z and fragmentation behavior corresponding to $\{[(tia)Rh]+76\}^+$. Its structure is completely a mystery. The only thing we know is that it can fragment losing a particle with a mass of 76. Whether this species is due to impurities in the CD_2Cl_2 we do not know.

- The most remarkable, and also most puzzling behavior was observed when $CHCl_3$ and 1,2-dichloroethane solutions of $[(tia)Rh(C_2H_4)]^+$ were sprayed (both the solvents were stirred with Na_2CO_3 before use). Again in both these solvents the mysterious $[(tia)Rh(C_2H_2Cl_2)]^+$ is the base peak of the spectrum (among a few other unknown chlorinated species).
  Do these reactions proceed via the same (unknown) reaction mechanism as for CH_2Cl_2 and does this result indeed point to a melting pot of reactions taking place simultaneously of which only the observed $C_2H_2Cl_2$ product is stable?
- Similar reaction products were also observed for some of the N_3 rhodium and iridium ethene complexes described in this thesis, although the yields were much lower than for the tpa and tia complexes and in some cases the reaction only oxidative addition of a C-Cl bond of CH_2Cl_2 was obtained.

At first we thought that oxidative addition of the C-Cl bond to the rhodium center was the first step in the reaction:

- Collision experiments in which the tpa rhodium ethene complex was collided with 0.45 mTorr CH_2Cl_2 in RC 2 resulted in the formation of a species with the m/z of the oxidative addition product $[(tpa)Rh(CH_2Cl)(Cl)]^+$ and of $[(tpa)Rh(Cl)]^+$.[27]
- During ESI^+-MS measurements of the tia rhodium ethene complex performed in CH_2Br_2 (also stirred with Na_2CO_3) the main product formed was $[(tia)Rh(CH_2Br)(Br)]^+$. In other words, for CH_2Br_2 with its more polarizable C-Br bonds, the reaction with the solvent stops after oxidative addition of the carbon-halide bond to the metal center.

However, when the tpa and tia species $[(N_4)Rh(CH_2Cl)(Cl)]^+$ were sprayed in CH_2Cl_2 (1 % of methanol was added to the solution due to solubility problems) no reaction with the chlorinated solvent took place at all. Either $[(N_4)Rh(CH_2Cl)(Cl)]^+$ is no intermediate in the formation of $[(N_4)RhC_2H_2Cl_2]^+$ or the presence of methanol suppresses further reaction.

In any case, it is not clear whether or not oxidative addition of a C-Cl bond to the metal center is the first step in the formation of these $C_2H_2Cl_2$ species, neither do we have any information on the mechanism via which these $C_2H_2Cl_2$ species are formed.

Since the tpa and tia rhodium ethene complexes are relatively stable in CH_2Cl_2, the reaction with the solvent observed during electrospray ionization must be induced or accelerated by either the unusual reaction conditions during scattering of the droplets (high positive charge density at the surface, high concentrations) or by the high spraying voltage.

What can be learned from all this is that if unexpected species show up in the mass spectra, the solvent may be involved in a "mass-spectrometer-induced" chemical reaction.

2.3.7 Rearrangements in the gas phase

Once the species with the desired mass-over-charge-ratio have been successfully transferred to the gas phase, one might think that all problems have been conquered.

There is, however, one last thing that has to be kept in mind. Although the m/z of a mass-selected species is known, its exact structure is not known at all in some cases.

To illustrate this problem, we will now discuss the gas-phase reaction of rhodium alkyl complexes with 1-butene. We wanted to find out how such coordinatively unsaturated species react with olefins if no solvent

[27] When $[(tpa)Rh(C_2H_4)]^+$ was collided in the 24-pole region of TSQ 700 (RC 1) with CH_2Cl_2 at pressures of up to 45 mTorr no reaction occurred. In other words, at zero-collision-energy no reaction can take place, the ions need to have a certain amount of kinetic energy to allow a reaction with CH_2Cl_2 to occur.

molecules or counterions are around that can block vacant coordination sites. In order to be able to generate such highly reactive, coordinatively unsaturated species in the gas phase, solutions of the compounds in coordinating solvents are sprayed and in the tube lens region one or more of the coordinating solvent molecules are removed by collisional activation. Subsequently the cations are collided with 1-butene in RC 2. [28]

For early transition metal (ETM) alkyls this type of experiment has allowed the observation of successive 1-butene insertions. [123], [124] For zirconocene complex $[(Cp)_2Zr(Me)]^+$ it has been reported [41] that up to four insertions of 1-butene into the Zr-C bond could be observed in RC 2 of the TSQ 7000.

As an example of a late transition metal (LTM), for iron it was demonstrated both by mass spectrometric measurements and by calculations that the interconversion of $[Fe(C_2H_5)]^+$ into $[Fe(H)(C_2H_4)]^+$ is facile and reversible and occurs well below the respective dissociation asymptotes. [125] The ethyl complex corresponds to the global minimum on the $[Fe,C_2H_5]^+$ potential energy surface. The ethene hydride complex is 13 kcal/mol less stable.

For rhodium, on the other hand, unsaturated alkyls are usually less stable than their olefin-hydride counterparts resulting in immediate β-hydrogen elimination to obtain the more stable complex. [30]

Also, the barriers for insertion of the C=C bond into the metal-carbon bond are known to be higher for LTM (> 16 kcal/mol) [126] – [131] than for ETM complexes (7-10 kcal/mol). [123], [124]

These factors combine to make it more difficult to observe insertion of an olefin into the Rh-C bond in a mass spectrometer.

As reported previously [132] – [135] $[(Me_n\text{-tpa})M(C_2H_4)]^+$ complexes (M = Rh, Ir and n = 1, 0) can easily be protonated with HCl or $HBAr^F{}_4.2Et_2O$ [136] to form ethene-hydride complexes.

In acetonitrile these complexes rapidly rearrange to the corresponding ethyl complexes in which the solvent occupies any vacant site left at the octahedrally surrounded metal(III) center.

A similar reaction was also observed for some of the N_3 rhodium ethene complexes described in this thesis and for some other rhodium-olefin complexes. [137], [138] Apparently the β-diketonato rhodium(III) alkyl complexes reported by Ohrstrom [137] are even stable against degradation by β-hydride elimination.

One equivalent of $HBAr^F{}_4.2Et_2O$ was added to acetonitrile solutions of some N_3 and N_4 rhodium ethene complexes. This resulted in the formation of the coordinatively saturated species $[(N_3)Rh(C_2H_5)(CH_3CN)_2]^{2+}$ [29] and $[(N_4)Rh(C_2H_5)(CH_3CN)]^{2+}$.[30]

In solution these alkyl complexes did not display any polymerization reactivity towards ethene. [139]

When only one solvent molecule was removed by collisional activation in the tube lens region, none of the complexes reacted with 1-butene upon collision in RC 2. Fragmentation was the only reaction that took place.

---

[28] Although it is known that ethene is usually polymerized 100 to 1000 times faster than the more substituted olefins, we decided to use 1-butene as a reagent gas. This was done, because it was hoped that the longer tail would help in stabilizing the products by dissipating the excess of internal energy after the reaction (see § 2.3.8 for an explanation of the "kinetic shift").

The internal energy of the complex increases upon olefin insertion; or β-elimination. If this energy becomes too high and cannot be dissipated, the product ion will fragment again, e.g. by undergoing the backward reaction.

[29] N_3 = pmdta, bpa, bpa-Bz and app-Bz^- (in this case the ethyl complex is mono-cationic).

pmdta = *N*1-[2-(dimethylamino)ethyl]-*N*1,*N*2,*N*2-trimethyl-1,2-ethanediamine, bpa = *N*,*N*-di(2-pyridylmetyl)amine and app-Bz^- = deprotonated *N*-benzyl-*N*-(1*H*-2-pyrrolylmethyl)-2-pyridylmethanamine.

[30] N_4 = tia, Me_3-tpa and the pyridinophane N_4Me_2.

tia (=*N*,*N*,*N*-tri[(1-methyl-1*H*-2-imidazolyl)methyl]amine), Me_3-tpa = *N*,*N*,*N*-tri[(6-methyl-2-pyridyl)methyl]amine, N_4Me_2 = *N*,*N*'-dimethyl-2,11-diaza[3,3](2,6)pyridinophane.

When a second MeCN-molecule was removed (this appeared not to be possible for every N_3 complex) the formation of species with an m/z corresponding to butyl complexes was observed.

This behavior can only by explained by assuming that after removal of the first MeCN-molecule the ethyl complexes rearrange via β-hydrogen elimination to the corresponding ethene-hydride species before entering RC 2 (Figure 2.8). These coordinatively saturated species will not be reactive towards butene, since they lack a vacant site. After removal of the second solvent molecule the ethene-hydride complexes have one vacant site to which 1-butene can coordinate. Associative or dissociative displacement of ethene by 1-butene can then lead to "butyl" complexes, which are in fact butene-hydride complexes.

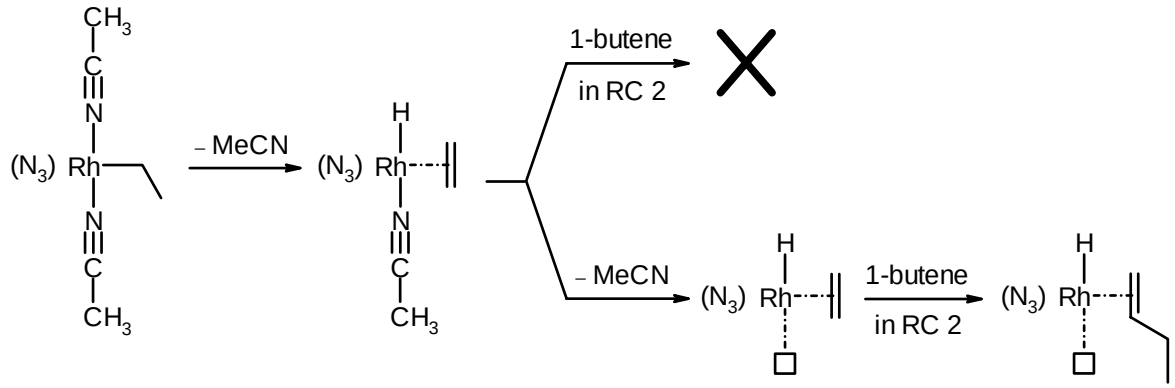

Figure 2.8 *Reaction of rhodium ethyl complexes with 1-butene*

We were still interested in the gas-phase reaction of alkyl complexes towards olefins, but we needed alkyls that would not β-hydrogen eliminate.

To obtain these, the complexes $[(tpa)M(hydroxy)(formylmethyl)]^+$ (M = Rh, Ir) were protonated using one equivalent of $HBAr^F_4.2Et_2O$ in CH_3CN. This resulted in the formation of dicationic species $[(tpa)M(S)(formylmethyl)]^{2+}$ (S = H_2O, MeCN). [140]

In the mass spectrometer the solvent molecule S was removed by collisional activation and the dicationic formylmethyl species was collided with 1-butene in RC 2. Again no reaction towards 1-butene was observed.

The best explanation for this behavior is that, after removal of S these formylmethyl species rearrange to the corresponding oxo-allyl species (Figure 2.9). Such a bonding mode has been reported for palladium [141] – [146] and rhenium [147].

Again, it appears that during their flight from the ESI source to RC 2 the ions have rearranged to a thermodynamically more favorable form.

This could not be deduced from the m/z and not even from the fragmentation behavior of the species.

Clearly, the m/z ratio and fragmentation patterns determined with mass spectrometry are not highly informative of the absolute structure and isomeric descriptions should always be considered.

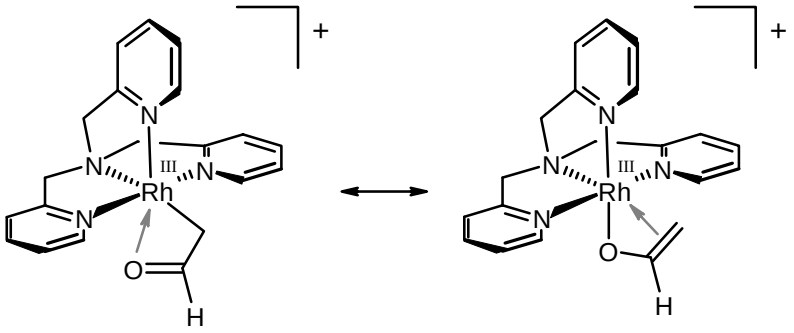

Figure 2.9 *Structure of $[(tpa)Rh(formylmethyl)]^{2+}$*

2.3.8 Kinetic shift

A last phenomenon one has to reckon with when interpreting the outcome of gas-phase ion-molecule reactions is the so-called kinetic shift. "Kinetic shift" is the term applied to experimentally observed ionization onsets, which are higher than the thermodynamic onset energy.

When looking at, for example, fragmentation reactions, this means that fragmentation of an ion having "just enough" energy for fragmentation is slow on the instrument time scale (microseconds). [148] As a result one has to go to even higher collision energies to observe the fragments of these ions. Especially when detection of the products takes place within a short timeframe (for example when quadrupole Q2 analyzes the reaction mixture coming out of RC 2), the measured threshold energy can be much higher than the true activation energy for the process. Changing from a quadrupole mass spectrometer to an FT-ICR MS [31] could greatly reduce the kinetic shift observed due to longer reaction times (ranging from milliseconds to seconds).

Kinetic shifts depend on the actual bond-dissociation enthalpy and on the number and type of internal degrees of freedom in the reactant ion. [150] Kinetic shifts will be greatest for large molecules [73] or for molecules having high dissociation energies or many low-frequency vibrations, and smallest for relatively small or rigid molecules or molecules having weak bonds. Therefore, the kinetic shift will not be important in every measurement, [150], [151] but when interpreting the results from gas-phase collision experiments one has to be aware of it. Unexpected peak broadening could be an indication. The kinetic shift is proportional to the number of degrees of freedom of the reactant ion. For organometallic complexes with only a few ligands it can already be of the order of magnitude of the measured onset energies and can therefore be quite significant. [121]

Of course a kinetic shift is not only observed in fragmentation reactions. Also in other types of reactions that are slow on the instrument time scale performed in RC 2 this phenomenon can play an important role.

One approach for getting around this problem is an analysis based on the determination of the so-called rate-energy curve for a given fragmentation; in this approach, the rate constant of fragmentation of the ion is determined as a function of energy. Fragmentation has also been studied as a function of time using time-resolved photodissociation and time-resolved photoionization mass spectrometry. [152] Alternatively, one can calculate an estimate of the kinetic shift using the CRUNCH program developed by Armentrout and co-workers. [153] – [159]

It is also possible to turn the occurrence of the kinetic shift into an advantage:
When reactions are performed in RC 2, the products might be so unstable (e.g. due to a too high amount of internal energy in the case of exothermic reactions) that they fragment already before leaving RC 2. In this case we will only be able to observe these fragments, not the real products.
Upon increase of the number of degrees of freedom of the product, the number of vibrational modes over which the internal energy can be dissipated will increase as well. As a result a higher amount of internal energy will be needed before any of the vibrational modes is saturated and the corresponding bond dissociates, for example. This can slow down the reaction enough for the metastable ion to be detected.
A way to create such a metastable ion is by adding a "tail" to either the reactant or the collision gas. For example, in the reaction of $[(Cp)_2ZrMe]^+$ with an olefin [41] on going from ethene to butene the quality of the mass spectra increased dramatically.

[31] FT-ICR = Fourier Transform Ion Cyclotron Resonance. For a review on this ion storage device see "FT-ICR MS: Analytical Applications of Fourier Transform Ion Cyclotron Resonance Mass Spectrometry" edited by Bruce Asamoto. [149] It allows both observation of fragmentation reactions at relatively low collision energies and a study of the lifetime effect on the dissociation pattern of large ions due to the possibility of longer residence times of the ions compared to for example triple quadrupoles.

2.3.9 Fragment-ion intensities using different collision gasses

One generally assumes that the nature of the collision gas does not affect the specificity of cleavage, i.e. the relative abundances of the fragment ions. However, recent investigations [160], [161] show that the nature and intensities of the fragment ions can depend on the reagent gas used.

This is especially true when the molecular structures of the collision gasses used are very different [160] (e.g. O_2 *vs.* methanol). The difference in the number of degrees of freedom and vibrational modes of the collision gas molecules can have an influence on the ***amount*** of energy that is being transferred to the ionic complex upon collision and ***how*** it is transferred.

But even if the molecular structures of the collision gasses used are not very different (e.g. O_2 *vs.* N_2), it is possible for certain compounds they induce a different fragmentation behavior. It has been reported [161] that for certain radical cations[32] using dioxygen as a collision gas can induce rearrangements and/or simple cleavage reactions. Maybe the initial formation of O_2-cation complexes could account for these differences in behavior, although they were never observed in the mass spectra.

Whether or not the fragmentation behavior changes upon changing the collision gas depends strongly on the molecular structure of the radical cation, since for related cations [33] no spectral changes are observed.

2.4 Conclusions

Electrospray Ionization Mass Spectrometry is an analytical tool with widespread possibilities. As for each technique one has to be keep in mind that under certain measuring conditions one can run into problems. However, in some cases they can be turned to advantages.

- Formation of cation adducts with Lewis acids like Na^+, K^+, Ag^+, enables the analysis of otherwise undetected neutral species.
- Oxidation of neutral complexes resulting in mono-cationic species can occur in solution at the capillary tip before droplet formation takes place.
- In the ESI source a reaction with air can take place.
- Multiply charged species are less easily transferred to the gas phase than singly charged species. This is due to the so-called "dominant-ion effect".
- Especially when using halogenated solvents, the solvent may be involved in a mass-spectrometer-induced chemical reaction.
- The m/z ratio determined with mass spectrometry is not highly informative of the absolute structure and isomeric descriptions should always be considered.

Apart from simple analysis of mixtures, ESI-MS can be used to study gas-phase ***reactions***.

The mass spectrometers we used for gas-phase reactions have three regions in which collisions can be performed:

- In the tube lens region, collisions with air (N_2 and O_2) occur whether one wants it or not. Control of collision conditions (except for the tube lens potential) in this region is not possible with most spectrometers.
- In reaction chamber 1 (RC 1, the 24-pole region in the Finnigan MAT TSQ 700) "zero-collision-energy" collisions at high collision gas pressures can be performed.

[32] $[HN=C=O]^+$, $[HN=C=C=NH]^+$, H-C≡C-C≡N and ethyl cations substituted at the carbenium center by groups like OH, NH_2, SH or CH_3.

[33] $[HN=C=C=S]^+$, aliphatic nitriles, $H_2C=C(H)(CN)$ or N≡C-C≡N.

– In reaction chamber 2 (RC 2, the octopole region) *tunable* low and high-energy collision experiments at low collision gas pressures can be carried out.

In principle it should be possible to deduce not only reaction stoichiometry, but also activation parameters from collision studies. However, experimentally observed onset energies are often higher than true barriers due to the "kinetic shift".

2.5 Experimental section

2.5.1 General methods

All procedures were performed under a nitrogen atmosphere using standard Schlenck techniques, unless indicated otherwise. Solvents (p.a.) were deoxygenated by bubbling through a stream of nitrogen or by the freeze-pump-thaw method. Some solvents were distilled under a nitrogen atmosphere to remove last traces of water and dioxygen: acetonitrile was distilled over potassium, THF over CaH_2 and CH_2Cl_2 also over CaH_2. The temperature indication r.t. corresponds to ca. 20 ºC.

NMR experiments were carried out on a Bruker DPX200 (200 MHz and 50 MHz for ^1H and ^{13}C respectively), a Bruker AC300 (300 MHz and 75 MHz for ^1H and ^{13}C respectively), a Varian Inova 400 (400 MHz and 100 MHz for ^1H and ^{13}C respectively). Solvent shift references for ^1H-NMR are: CD_2Cl_2 δ (^1H) = 5.31 ppm, CD_3CN δ (^1H) = 1.94 ppm, methanol-d4 δ (^1H) = 3.35 ppm and acetone-d6 δ (^1H) = 2.05 ppm. Solvent shift references for ^{13}C-NMR are: CD_3CN δ (^{13}C) = 1.24 (and 118.25), CD_2Cl_2 δ (^{13}C) = 54.20, methanol-d4 δ (^{13}C) = 49.3 ppm and acetone-d6 δ (^{13}C) = 29.83 ppm (and 206.18 ppm). Abbreviations used are: s = singlet, d = doublet, dd = double doublet, ddd = double doublet of doublets, t = triplet, dt = double triplet, q = quartet, qq = quartet of quartets, m = multiplet, dm = double multiplet, br. = broad.

Tpa [162], tia [163], pmdta [139], bpa-Bz [164], app-Bz [165], N_4Me_2 [166], $[(tpa)Rh(C_2H_4)]PF_6$ [134], $[(tia)Rh(C_2H_4)]PF_6$ [140], $[(bpa\text{-}Bz)Rh(C_2H_4)]PF_6$ [31], $[(pmdta)Rh(Cl)_3]$ [139], $[(pmdta)Rh(Me)_3]$ [139], [(i-Pr-Brookhart)$CoCl_2$] [167], $[(app\text{-}Bz)Rh(C_2H_4)]$ [139], $[(tpa)Rh(OH)(formylmethyl)]^+$ [166], [168], [169], [(*i*Pr-Brookhart)CoCl] [139], $HBAr^F{}_4.2Et_2O$ [136], $[(Cp)_2Fe]$ [170], $[(Cp)_2Co]$ [171], $[(pyridinophane)Rh(C_2H_4)]PF_6$ [166] and $[\{(C_2H_4)_2Rh(\mu\text{-}Cl)\}_2]$ [172] were prepared according to literature procedures.

All other chemicals are commercially available and were used without further purification, unless stated otherwise.

2.5.2 ESI^+-MS measurements

General ESI^+-MS setup for the experiments

Many electrospray ionization (ESI) mass spectra were measured on both a slightly modified Finnigan MAT TSQ 7000 and a modified Finnigan MAT TSQ 700 as previously described. [38] – [45], [58], [61] – [70] Other spectra have been measured on a Finnigan MAT 900 XL (only analysis of the species present in solution and of fragmentation behavior).

Typically solutions with a concentration of 10^{-5} M of the desired compounds (prepared in the glove-box under a nitrogen atmosphere) were electrosprayed at a flow-rate of 3 – 15 µl/min at 3 – 5 kV and a capillary temperature of 150 ºC. In some cases dinitrogen was used as a sheath gas. The tube lens potential was varied between 35 and 140 V(referenced to m/z = 500) depending on the complex.

Daughter-ion spectra were recorded in daughter-ion mode, that is, the first quadrupole was used to mass select ions of a single mass-over-charge ratio, which were then collided with a target gas in the second reaction chamber (RC 2). The second quadrupole was operated in scanning mode in order to detect the ionic fragments. The collision energy could be varied by applying different potentials (to a lens in front of the second octopole), which altered the velocity of the ions on their way into the collision region (the collision energies are given in eV, lab frame).

Determining collision gas pressures in RC 1 and RC 2.

The pressure in the collision cell (RC 2) was read both from a Pirani gauge and with a Capacitance gauge. The pressure in the 24-pole (RC 1) was read from a Pirani gauge. The pressures of the Pirani gauges were calibrated to those displayed by the Capacitance gauge. All gauges are directly attached to the housing of the two multipoles.

Pirani and thermocouple gauges actually measure thermal conductivity rather than pressure. Because thermal conductivity is proportional to the product of the heat capacity and pressure, two different collision gasses should have the same actual pressure when the gauge readings are normalized by the ratio of their heat capacities. In other words, for a gas with a heat

capacity twice as high as for dinitrogen the gas pressure reading will be twice as high as the actual pressure. Therefore, computation of the heat capacities from scaled harmonic vibrational frequencies was done and produced the C_V[collision gas] / C_V[dinitrogen] ratios shown in Table 2.2, which we used to normalize the gauge readings. This calibration method was published by Gerdes *et al.* [63]

Table 2.2 *Heat capacities of collision gasses used*

Collision gas	Calculated C_V in cal/(mol∗K) (at 343 Kelvin, 0.00010 atm.)	Ratio of heat capacities C_V[collision gas] / C_V[dinitrogen]
Dioxygen	5.06	1.017
Dinitrogen	4.975	1
1-Butene	20.182	4.057
Propene	13.979	2.810
Ethene	9.106	1.830
Methanol	9.534	1.916
Dichloromethane	11.08	2.227
Chloroform	14.754	2.966
PMe_3	25.875	5.201
Ethylvinylether	23.831	4.790
N_2O	7.591	1.526

For a few gasses (argon, dinitrogen, dioxygen and 1-butene) we have been able to measure the gas pressure in RC 2 also with a capacitance gauges. With these measurements we were able to correlate the pressure readings of the Pirani gauges in the 24-pole (RC 1) and in the octopole (RC 2) to the real gas pressure and to verify that the method of normalizing gauge readings by means of head capacities is correct. Apparently for dinitrogen the pressure readings of the Pirani gauge are exactly the same as for the Capacitance gauge.

Collision gas pressures read from the Pirani gauge, which are gas-dependent, attached to the octopole were later also compared with those read from a Capacitance gauge, which is capable of measuring absolute pressures. This comparison was used to calibrate all gas pressures read from the Pirani gauges.

Collision gas pressures used for the collision experiments in RC 2: 0.25 mTorr 1-butene (TSQ 700) and 0.5 mTorr CH_2Cl_2 (TSQ 7000).

2.5.3 Synthesis

[(tia)Rh(CH_2Cl)(Cl)]Cl

81.2 mg (0.2088 mmol) $[(C_2H_4)_2Rh(\mu\text{-}Cl)]_2$ is added to 10 ml CH_2Cl_2. For 15 minutes propene is bubbled through the solution, then 125 mg (0.4176 mmol) tia[34] is added. For another 30 min. propene is bubbled through the reaction mixture. The red-brown suspension is filtered and the residue is washed three times with 0.5 ml dichloromethane. In the filtrate a solid precipitates during this washing procedure. Therefore it is put in the freezer (-20 ºC) for 4 days. Now the solvent is removed with a pipette. The remaining solid is washed three times with 2 ml CH_2Cl_2. The solid is dried. Yield: 105 mg (48%).

^{1}H-NMR (400 MHz, methanol-d4, 294K): δ(ppm) = 7.37 (d, 1H, Im-*H*), 7.01 (d, 5H, Im-*H*), 6.05 (d, $^2J_{Rh\text{-}H}$ = 3.1 Hz, 2H, Rh-C*H*$_2$Cl), 5.14 (d[AB], $^2J_{H\text{-}H}$ = 15.4 Hz, 2H, N-C*H*$_2$-Im$_{equatorial}$), 5.07 (d[AB], $^2J_{H\text{-}H}$ = 15.1 Hz, 2H, N-C*H*$_2$-Im$_{equatorial}$), 4.89 (s, 2H, N-C*H*$_2$-Im$_{axial}$), 3.77 (s, 6H, N$_{equatorial}$-C*H*$_3$), 3.56 (s, 3H, N$_{axial}$-C*H*$_3$).

^{13}C-NMR (100 MHz, methanol-d4, 294K): δ(ppm) = 150.2 (s, Im$_{equatorial}$-*C1*), 150.0 (s, Im$_{axial}$-*C1*), 127.4 (s, Im$_{equatorial}$-*C*), 127.3 (s, Im$_{axial}$-*C*), 124.5 (s, Im$_{axial}$-*C*), 123.6 (s, Im$_{equatorial}$-*C*), 60.8 (s, N-C*H*$_2$-Im$_{equatorial}$), 59.6 (s, N-C*H*$_2$-Im$_{axial}$), 41.1 (d, $^1J_{Rh\text{-}C}$ = 27.7 Hz, Rh-*C*H$_2$Cl), 34.8 (s, N$_{equatorial}$-*C*H$_3$), 34.6 (s, N$_{axial}$-*C*H$_3$).

ESI$^+$-MS: 486 [(tia)Rh(CH_2Cl)(Cl)]$^+$.

[34] tia (=*N*,*N*,*N*-tri[(1-methyl-1*H*-2-imidazolyl)methyl]amine)

[(tpa)Rh(CH_2Cl)(Cl)]Cl

The synthesis of this compound is similar to the one described above for the corresponding tia complex, only now tpa[35] was used as a nitrogen donor ligand, the reaction time was about a month and the yield was extremely low: only a few percentages of a pink-like solid could be obtained. However, this was enough for the ESI^+-MS measurements.

ESI^+-MS: 477 $[(tpa)Rh(CH_2Cl)(Cl)]^+$.

Synthesis of the rhodium ethyl compounds

For the synthesis of the rhodium ethyl complexes as mentioned in § 2.3.6 in all cases to 10 mg of the corresponding rhodium ethene complex a MeCN-solution of 1 equivalent of $HBAr^F_4.2Et_2O$ was added at -30 ºC and allowed to react for about 30 minutes. The resulting reaction mixture was diluted to a solution with a concentration of ca. 10^{-5} M.

Pay attention: The MeCN used for these measurements was not only dried by distillation over potassium but also right before use the amount of solvent needed was filtered over aluminum oxide to remove the last traces of water, which could cause the ethyl complexes to decompose.

Table 2.3 *M/z of rhodium alkyl complexes measured with ESI^+-MS*

Ethyl compound	$[(L_N)Rh(alkyl)(MeCN)_2]^{2+}$	$[(L_N)Rh(alkyl)(MeCN)]^{2+}$	$[(L_N)Rh(alkyl)]^{2+}$
$[(bpa)Rh(C_2H_5)(MeCN)_2]^{2+}$	206.5	186	165.5
$[(bpa\text{-}Bz)Rh(C_2H_5)(MeCN)_2]^{2+}$	251.5	231	210.5 (trace)
$[(Me_2\text{-}bpa\text{-}Bz)Rh(C_2H_5)(MeCN)_2]^{2+}$	265.5	245	224.5
$[(pyridinophane)Rh(C_2H_5)(MeCN)_2]^{2+}$		220.5	200
$[(Me_3\text{-}tpa)Rh(C_2H_5)(MeCN)_2]^{2+}$		252.5	232
$[(tia)Rh(C_2H_5)(MeCN)_2]^{2+}$		236	215.5
$[(pmdta)Rh(C_2H_5)]^{2+}$	193.6	173	152.5 (trace)
$[(app\text{-}Bz)Rh(C_2H_5)(MeCN)_2]^{+}$	490	449	408
$[(tpa)Rh(formylmethyl)(MeCN)]^{2+}$		238.5	218
$[(tpa)Ir(formylmethyl)(MeCN)]^{2+}$		283.5	263

Since app-Bz is a mono-anionic ligand, this ethyl complex is mono-cationic. All other alkyl complexes are dicationic.

2.6 References

[1] R. B. Cole, *"Electrospray ionization mass spectrometry, Fundamentals, Instrumentation & Applications"*, John Wiley & Sons, New York, **1997**

[2] P. Bussian, F. Sobott, B. Brutschy, W. Schrader and F. Schuth, *Angew. Chem. - Int. Edit.*, **2000**, *39 (21)*, 3901

[3] W. Henderson and C. Evans, *Inorg. Chim. Acta*, **1999**, *294 (2)*, 183-192

[4] E. Coronado, M. Feliz, A. Forment-Aliaga, C. J. Gomez-Garcia, R. Llusar and F. M. Romero, *Inorg. Chem.*, **2001**, *40 (24)*, 6084

[5] C. Evans, K. M. Mackay and B. K. Nicholson, *J. Chem. Soc. - Dalton Trans.*, **2001**, *(10)*, 1645-1649

[6] D. Mansfeld, M. Mehring and M. Schurmann, *Inorg. Chim. Acta*, **2003**, *348*, 82-90

[7] H. Nierengarten, J. Rojo, E. Leize, J. M. Lehn and A. Van Dorsselaer, *Eur. J. Inorg. Chem.*, **2002**, *(3)*, 573-579

[8] H. Nierengarten, E. Leize, E. Breuning, A. Garcia, F. Romero-Salguero, J. Rojo, J. M. Lehn and A. Van Dorsselaer, *J. Mass Spectrom.*, **2002**, *37 (1)*, 56-62

[9] A. W. G. Platt, J. Fawcett, R. S. Hughes and D. R. Russell, *Inorg. Chim. Acta*, **1999**, *295 (2)*, 146-152

[10] A. M. J. Lees, J. M. Charnock, R. A. Kresinski and A. W. G. Platt, *Inorg. Chim. Acta*, **2001**, *312 (1-2)*, 170-182

[11] H. W. Yim, K. C. Lam, A. L. Rheingold and D. Rabinovich, *Polyhedron*, **2000**, *19 (7)*, 849-853

[12] J. S. L. Yeo, J. J. Vittal, W. Henderson and T. S. A. Hor, *J. Chem. Soc. - Dalton Trans.*, **2002**, *(3)*, 328-336

[13] P. D. Mlynek and L. F. Dahl, *Organometallics*, **1997**, *16 (8)*, 1641-1654

[14] S. D. Friess, J. M. Daniel, R. Hartmann and R. Zenobi, *Int. J. Mass Spectrom.*, **2002**, *219 (1)*, 269-281

[15] M. I. Catalina, N. J. de Mol, M. J. E. Fischer and A. J. R. Heck, *Phys. Chem. Chem. Phys.*, **2004**, *6 (10)*, 2572-2579

[35] tpa (= *N*,*N*,*N*-tri(2-pyridylmethyl)amine)

[16] R. H. H. van den Heuvel, A. H. Westphal, A. J. R. Heck, M. A. Walsh, S. Rovida, W. J. H. van Berkel and A. Mattevi, *J. Biol. Chem.*, **2004**, *279 (13)*, 12860-12867
[17] J. A. A. Demmers, A. van Dalen, B. de Kruijff, A. J. R. Heck and J. A. Killian, *FEBS Lett.*, **2003**, *541 (1-3)*, 28-32
[18] A. P. M. de Brouwer, C. Versluis, J. Westerman, B. Roelofsen, A. J. R. Heck and K. W. A. Wirtz, *Biochemistry*, **2002**, *41 (25)*, 8013-8018
[19] P. J. Vollmerhaus, F. W. A. Tempels, J. J. Kettenes-van den Bosch and A. J. R. Heck, *Electrophoresis*, **2002**, *23 (6)*, 868-879
[20] H. Rogniaux, A. Van Dorsselaer, P. Barth, J. F. Biellmann, J. Barbanton, M. van Zandt, B. Chevrier, E. Howard, A. Mitschler, N. Potier, L. Urzhumtseva, D. Moras and A. Podjarny, *J. Am. Soc. Mass Spectrom.*, **1999**, *10 (7)*, 635-647
[21] D. Schröder, K. Schroeter and H. Schwarz, *Int. J. Mass Spectrom.*, **2001**, *212 (1-3)*, 327-336
[22] J. Banoub, A. Cohen, A. Mansour and P. Thibault, *Eur. J. Mass Spectrom.*, **2004**, *10 (1)*, 121-134
[23] J. Banoub, P. Thibault, A. Mansour, A. Cohen, D. H. Heeley and D. Jackman, *Eur. J. Mass Spectrom.*, **2003**, *9 (5)*, 509-524
[24] N. J. de Mol, M. I. Catalina, M. J. E. Fischer, I. Broutin, C. S. Maier and A. J. R. Heck, *Biochim. Biophys. Acta - Proteins and Proteomics*, **2004**, *1700 (1)*, 53-64
[25] E. T. J. van den Bremer, A. H. Keeble, W. Jiskoot, R. E. J. Spelbrink, C. S. Maier, A. van Hoek, A. Visser, R. James, G. R. Moore, C. Kleanthous and A. J. R. Heck, *Protein Sci.*, **2004**, *13 (5)*, 1391-1401
[26] A. J. Kleinnijenhuis, M. C. Duursma, E. Breukink, R. M. A. Heeren and A. J. R. Heck, *Anal. Chem.*, **2003**, *75 (13)*, 3219-3225
[27] J. A. A. Demmers, D. T. S. Rijkers, J. Haverkamp, J. A. Killian and A. J. R. Heck, *J. Am. Chem. Soc.*, **2002**, *124 (37)*, 11191-11198
[28] H. Belva, C. Lange and I. Segalas, *Eur. J. Mass Spectrom.*, **2001**, *7 (4-5)*, 373-383
[29] M. W. H. Pinkse, C. S. Maier, J. I. Kim, B. H. Oh and A. J. R. Heck, *J. Mass Spectrom.*, **2003**, *38 (3)*, 315-320
[30] D. Dakternieks, A. E. K. Lim and K. F. Lim, *Chem. Commun.*, **1999**, *(15)*, 1425-1426
[31] B. de Bruin, J. A. W. Verhagen, C. H. J. Schouten, A. W. Gal, D. Feichtinger and D. A. Plattner, *Chem. - Eur. J.*, **2001**, *7 (2)*, 416-422
[32] K. Schroeter, R. Wesendrup and H. Schwarz, *Eur. J. Org. Chem.*, **1998**, *(4)*, 565-571
[33] D. Schröder, J. Loos, M. Semialjac, T. Weiske, H. Schwarz, G. Hohne, R. Thissen and O. Dutuit, *Int. J. Mass Spectrom.*, **2002**, *214 (1)*, 155-170
[34] D. Schröder, C. Trage, H. Schwarz, D. Danovich and S. Shaik, *Int. J. Mass Spectrom.*, **2000**, *200 (1-3)*, 163-173
[35] S. Barsch, D. Schröder and H. Schwarz, *Helv. Chim. Acta*, **2000**, *83 (4)*, 827-835
[36] C. A. Schalley, M. Dieterle, D. Schröder, H. Schwarz and E. Uggerud, *Int. J. Mass Spectrom. Ion Process.*, **1997**, *163 (1-2)*, 101-119
[37] C. A. Schalley, R. Wesendrup, D. Schröder and H. Schwarz, *Organometallics*, **1996**, *15 (2)*, 678-683
[38] C. Adlhart and P. Chen, *Helv. Chim. Acta*, **2003**, *86 (4)*, 941-949
[39] M. A. O. Volland, C. Adlhart, C. A. Kiener, P. Chen and P. Hofmann, *Chem. - Eur. J.*, **2001**, *7 (21)*, 4621-4632
[40] D. Feichtinger and D. A. Plattner, *Chem. - Eur. J.*, **2001**, *7 (3)*, 591-599
[41] D. Feichtinger, D. A. Plattner and P. Chen, *J. Am. Chem. Soc.*, **1998**, *120 (28)*, 7125-7126
[42] C. Hinderling, D. Feichtinger, D. A. Plattner and P. Chen, *J. Am. Chem. Soc.*, **1997**, *119 (44)*, 10793-10804
[43] C. Hinderling and P. Chen, *Angew. Chem. - Int. Edit.*, **1999**, *38 (15)*, 2253-2256
[44] C. Adlhart and P. Chen, *Helv. Chim. Acta*, **2000**, *83 (9)*, 2192-2196
[45] P. Chen, *Angew. Chem. - Int. Edit.*, **2003**, *42 (25)*, 2832-2847
[46] D. Schröder, M. Diefenbach, H. Schwarz, A. Schier and H. Schmidbaur, "*Experimental Probes for Relativistic Effects in the Chemistry of Heavy d and f Elements*", Vol. 123, Eds. B. A. Hess, **2003**, 247-299
[47] H. Schwarz, *Angew. Chem. - Int. Edit.*, **2003**, *42 (37)*, 4442-4454
[48] C. Heinemann, H. Schwarz, W. Koch and K. G. Dyall, *J. Chem. Phys.*, **1996**, *104 (12)*, 4642-4651
[49] G. A. Lawrance, M. J. Robertson, Sutrisno and E. I. von Nagy-Felsobuki, *Inorg. Chim. Acta*, **2002**, *328*, 159-168
[50] D. A. Plattner, *Int. J. Mass Spectrom.*, **2001**, *207 (3)*, 125-144
[51] C. M. Whitehouse, R. N. Dreyer, M. Yamashita and J. B. Fenn, *Anal. Chem.*, **1985**, *57 (3)*, 675-679
[52] J. B. Fenn, J. Rosell and C. K. Meng, *J. Am. Soc. Mass Spectrom.*, **1997**, *8 (11)*, 1147-1157
[53] J. V. Iribarne and B. A. Thomson, *J. Chem. Phys.*, **1976**, *64 (6)*, 2287-2294
[54] B. A. Thomson and J. V. Iribarne, *J. Chem. Phys.*, **1979**, *71 (11)*, 4451-4463
[55] J. B. Fenn, J. Rosell, T. Nohmi, S. Shen and F. J. Banks, "*Electrospray ion formation: Desorption versus desertion*", *Biochemical and Biotechnological Applications of Electrospray Ionization Mass Spectrometry*, Vol. Vol. 619, Eds. American Chemical Society, Washington, **1996**, 60-80
[56] H. Wollnik, *J. Mass Spectrom.*, **1999**, *34 (10)*, 991-1006
[57] A. P. Bruins, *J. Chromatogr. A*, **1998**, *794 (1-2)*, 345-357
[58] P. Kebarle, *J. Mass Spectrom.*, **2000**, *35 (7)*, 804-817
[59] M. G. Ikonomou, A. T. Blades and P. Kebarle, *Anal. Chem.*, **1991**, *63 (18)*, 1989-1998
[60] J. R. Chapman, *"Practical Organic Mass Spectrometry, A Guide for Chemical and Biochemical Analysis"*, John Wiley & Sons, New York, *Second Edition*, **1998**
[61] C. Hinderling, D. A. Plattner and P. Chen, *Angew. Chem. - Int. Edit.*, **1997**, *36 (3)*, 243-244
[62] C. Hinderling and P. Chen, *Int. J. Mass Spectrom.*, **2000**, *196*, 377-383

[63] G. Gerdes and P. Chen, *Organometallics*, **2003**, *22 (11)*, 2217-2225
[64] C. Hinderling, C. Adlhart and P. Chen, *Angew. Chem. - Int. Edit.*, **1998**, *37 (19)*, 2685-2689
[65] C. Adlhart, M. A. O. Volland, P. Hofmann and P. Chen, *Helv. Chim. Acta*, **2000**, *83 (12)*, 3306-3311
[66] Y. M. Kim and P. Chen, *Int. J. Mass Spectrom.*, **2000**, *202 (1-3)*, 1-7
[67] G. Gerdes and P. Chen, *Organometallics*, **2004**, *23 (12)*, 3031-3036
[68] D. A. Plattner, D. Feichtinger, J. El-Bahraoui and O. Wiest, *Int. J. Mass Spectrom.*, **2000**, *196*, 351-362
[69] D. Feichtinger and D. A. Plattner, *J. Chem. Soc. - Perkin Trans. 2*, **2000**, *5*, 1023-1028
[70] D. Feichtinger and D. A. Plattner, *Angew. Chem. - Int. Edit.*, **1997**, *36 (16)*, 1718-1719
[71] C. Adlhart, *PhD Thesis ETH No. 15073, 2003* http://e-collection.ethbib.ethz.ch/show?type=diss&nr=15073 *"Intrinsic Reactivity of Ruthenium Carbenes: A Combined Gas-Phase and Computational Study"*, **2003**
[72] P. W. Atkins, *"Physical Chemistry"*, Oxford University Press, Oxford, **1994**
[73] M. J. Polce, D. Ren and C. Wesdemiotis, *J. Mass Spectrom.*, **2000**, *35 (12)*, 1391-1398
[74] J. R. Seal and N. A. Porter, *Anal. Bioanal. Chem.*, **2004**, *378 (4)*, 1007-1013
[75] K. Yamaguchi and S. Sakamoto, *JEOL News*, **2002**, *28A (1)*, 2-5
[76] P. Sandra, A. Medvedovici, Y. Zhao and F. David, *J. Chromatogr. A*, **2002**, *974 (1-2)*, 231-241
[77] A. von Brocke, G. Nicholson and E. Bayer, *Electrophoresis*, **2001**, *22 (7)*, 1251-1266
[78] H. Y. Yin, D. L. Hachey and N. A. Porter, *J. Am. Soc. Mass Spectrom.*, **2001**, *12 (4)*, 449-455
[79] C. Rentel, P. Gfrorer and E. Bayer, *Electrophoresis*, **1999**, *20 (12)*, 2329-2336
[80] E. Bayer, P. Gfrorer and C. Rentel, *Angew. Chem. - Int. Edit.*, **1999**, *38 (7)*, 992-995
[81] G. Hopfgartner, F. Vilbois and C. Piguet, *Rapid Commun. Mass Spectrom.*, **1999**, *13 (5)*, 302-306
[82] H. Hayen, M. M. Alvarez-Grima, S. C. Debnath, J. W. M. Hoordermeer and U. Karst, *Anal. Chem.*, **2004**, *76 (4)*, 1063-1068
[83] P. Timmerman, K. A. Jolliffe, M. C. Calama, J. L. Weidmann, L. J. Prins, F. Cardullo, B. H. M. Snellink-Ruel, R. H. Fokkens, N. M. M. Nibbering, S. Shinkai and D. N. Reinhoudt, *Chem. - Eur. J.*, **2000**, *6 (22)*, 4104-4115
[84] V. E. Vandell and P. A. Limbach, *J. Mass Spectrom.*, **1998**, *33 (3)*, 212-220
[85] O. Laine, T. Laitinen and P. Vainiotalo, *Anal. Chem.*, **2002**, *74 (16)*, 4250-4258
[86] A. von Brocke, D. Wistuba, P. Gfrorer, M. Stahl, V. Schurig and E. Bayer, *Electrophoresis*, **2002**, *23 (17)*, 2963-2972
[87] A. Medvedovici, K. Lazou, A. d'Oosterlinck, Y. N. Zhao and P. Sandra, *J. Sep. Sci.*, **2002**, *25 (3)*, 173-178
[88] K. Yamaguchi, S. Sakamoto, T. Imamoto and T. Ishikawa, *Anal. Sci.*, **1999**, *15 (10)*, 1037-1038
[89] K. M. Koshy and J. M. Boggs, *J. Biol. Chem.*, **1996**, *271 (7)*, 3496-3499
[90] N. Morisaki, H. Kobayashi, Y. Yamamura, M. Morisaki, K. Nagasawa and Y. Hashimoto, *Chem. Pharm. Bull.*, **2002**, *50 (7)*, 935-940
[91] H. A. Cox, R. R. Julian, S. W. Lee and J. L. Beauchamp, *J. Am. Chem. Soc.*, **2004**, *126 (20)*, 6485-6490
[92] G. J. P. Britovsek, V. C. Gibson, S. K. Spitzmesser, K. P. Tellmann, A. J. P. White and D. J. Williams, *J. Chem. Soc. - Dalton Trans.*, **2002**, *(6)*, 1159-1171
[93] K. Kreischer, J. Kipke, M. Bauerfeind and J. Sundermeyer, *Z. Anorg. Allg. Chem.*, **2001**, *627 (5)*, 1023-1028
[94] J. D. L. Hollaway and W. E. Gieger, *J. Am. Chem. Soc.*, **1979**, *101*, 2038
[95] L. A. P. Kane-Maguire, R. Kanitz and M. M. Sheil, *Inorg. Chim. Acta*, **1996**, *245 (2)*, 209-214
[96] H. Lavanant, E. Hecquet and Y. Hoppilliard, *Int. J. Mass Spectrom.*, **1999**, *187*, 11-23
[97] Z. Y. Suo, X. W. Wei, Y. H. Mei, K. Lin and Z. Xu, *Fullerene Sci. Technol.*, **2001**, *9 (2)*, 211-223
[98] L. Qi, C. Zhang, X. W. Wei, M. F. Wu, Z. Xu, K. Y. Zhou and Y. C. Cao, *Acta Chim. Sin.*, **1997**, *55 (5)*, 498-502
[99] G. J. Van Berkel, K. G. Asano and V. Kertesz, *Anal. Chem.*, **2002**, *74 (19)*, 5047-5056
[100] G. J. Van Berkel, K. G. Asano and M. C. Granger, *Anal. Chem.*, **2004**, *76 (5)*, 1493-1499
[101] F. Charbonnier, L. Berthelot and C. Rolando, *Anal. Chem.*, **1999**, *71 (8)*, 1585-1591
[102] G. J. Van Berkel, K. G. Asano and P. D. Schnier, *J. Am. Soc. Mass Spectrom.*, **2001**, *12 (7)*, 853-862
[103] G. J. Van Berkel, G. E. Giles, J. S. Bullock and L. J. Gray, *Anal. Chem.*, **1999**, *71 (23)*, 5288-5296
[104] H. Lavanant, H. Virelizier and Y. Hoppilliard, *J. Am. Soc. Mass Spectrom.*, **1998**, *9 (11)*, 1217-1221
[105] J. F. de la Mora, G. J. Van Berkel, C. G. Enke, R. B. Cole, M. Martinez-Sanchez and J. B. Fenn, *J. Mass Spectrom.*, **2000**, *35 (8)*, 939-952
[106] M. C. B. Moraes, J. Neto and C. L. do Lago, *Int. J. Mass Spectrom.*, **2000**, *198 (1-2)*, 121-132
[107] A. A. Shvartsburg and K. W. M. Siu, *J. Am. Chem. Soc.*, **2001**, *123 (41)*, 10071-10075
[108] V. Kertesz and G. J. Van Berkel, *J. Mass Spectrom.*, **2001**, *36 (2)*, 204-210
[109] T. Karancsi, P. Slegel, L. Novak, G. Pirok, P. Kovacs and K. Vekey, *Rapid Commun. Mass Spectrom.*, **1997**, *11 (1)*, 81-84
[110] G. J. Van Berkel, *J. Mass Spectrom.*, **2000**, *35 (7)*, 773-783
[111] G. J. Van Berkel, *J. Am. Soc. Mass Spectrom.*, **2000**, *11 (11)*, 951-960
[112] T. T. Hoang, S. W. May and R. F. Browner, *J. Anal. Atom. Spectrom.*, **2002**, *17 (12)*, 1575-1581
[113] J. W. S. Rayleigh, *Philosoph. Mag.*, **1882**, *14*, 184
[114] L. L. Mack, P. Kralik, A. Rheude and M. Dole, *J. Chem. Phys.*, **1970**, *52 (10)*, 4977
[115] M. Dole, L. L. Mack and R. L. Hines, *J. Chem. Phys.*, **1968**, *49 (5)*, 2240
[116] R. D. Smith, J. A. Loo, C. G. Edmonds, C. J. Barinaga and H. R. Udseth, *Anal. Chem.*, **1990**, *62 (9)*, 882-899
[117] D. C. Taflin, T. L. Ward and E. J. Davis, *Langmuir*, **1989**, *5 (2)*, 376-384
[118] G. D. Wang and R. B. Cole, *J. Am. Soc. Mass Spectrom.*, **1996**, *7 (10)*, 1050-1058

[119] R. W. Vachet and J. H. Callahan, *J. Mass Spectrom.*, **2000**, *35 (3)*, 311-320
[120] T. Pintauer, C. B. Jasieczek and K. Matyjaszewski, *J. Mass Spectrom.*, **2000**, *35 (11)*, 1295-1299
[121] D. Feichtinger, *PhD Thesis ETH No. 13595 "Untersuchung der intrinsischen Reaktivitaet von metallorganischen Katalysatoren mittels Elektrospray Tandem Massenspektrometrie"*, **2000**
[122] *"Handbook of Chemistry and Physics, 1913-1995 Special Student Edition"*, Eds. D. R. Lide and H. P. R. Frederikse, CRC Press, London, **1994**
[123] L. Q. Deng, T. Ziegler, T. K. Woo, P. Margl and L. Y. Fan, *Organometallics*, **1998**, *17 (15)*, 3240-3253
[124] P. Margl, J. C. W. Lohrenz, T. Ziegler and P. E. Blochl, *J. Am. Chem. Soc.*, **1996**, *118 (18)*, 4434-4441
[125] A. Fiedler, D. Schröder, W. Zummack and H. Schwarz, *Inorg. Chim. Acta*, **1997**, *259 (1-2)*, 227-235
[126] J. M. Malinoski and M. Brookhart, *Organometallics*, **2003**, *22 (25)*, 5324-5335
[127] E. L. Dias, M. Brookhart and P. S. White, *Organometallics*, **2000**, *19 (24)*, 4995-5004
[128] D. J. Tempel, L. K. Johnson, R. L. Huff, P. S. White and M. Brookhart, *J. Am. Chem. Soc.*, **2000**, *122 (28)*, 6686-6700
[129] S. D. Ittel, L. K. Johnson and M. Brookhart, *Chem. Rev.*, **2000**, *100 (4)*, 1169-1203
[130] M. J. Tanner, M. Brookhart and J. M. DeSimone, *J. Am. Chem. Soc.*, **1997**, *119 (32)*, 7617-7618
[131] L. Q. Deng, P. Margl and T. Ziegler, *J. Am. Chem. Soc.*, **1997**, *119 (5)*, 1094-1100
[132] R. J. N. A. M. Kicken, *PhD Thesis "Oxidation of Iridium Olefin Complexes by H_2O_2 and O_2"*, **2001**
[133] B. de Bruin, *PhD Thesis "Oxidation of Rhodium-Olefin Complexes via 2-Rhodaoxetanes"*, **1999**
[134] B. de Bruin, M. J. Boerakker, J. A. W. Verhagen, R. de Gelder, J. M. M. Smits and A. W. Gal, *Chem. - Eur. J.*, **2000**, *6 (2)*, 298-312
[135] B. de Bruin, M. J. Boerakker, J. J. J. M. Donners, B. E. C. Christiaans, P. P. J. Schlebos, R. de Gelder, J. M. M. Smits, A. L. Spek and A. W. Gal, *Angew. Chem. - Int. Edit.*, **1997**, *36 (19)*, 2064-2067
[136] M. Brookhart, B. Grant and A. F. Volpe, *Organometallics*, **1992**, *11 (11)*, 3920-3922
[137] L. Ohrstrom, S. Stromberg, J. Glaser and K. Zetterberg, *Journal of Organometallic Chemistry*, **1998**, *558 (1-2)*, 123-130
[138] L. P. Seiwell, *Inorg. Chem.*, **1976**, *15 (10)*, 2560-2563
[139] T. M. Kooistra, *PhD Thesis "Olefin polymerisation with late transition metals and nitrogen donor ligands"*, **2005**
[140] M. Krom, *PhD Thesis "Mono- and Dioxygenation of Rhodium and Iridium Olefin Fragments, Solution versus Solid State Reactivity"*, **2003**
[141] M. Sodeoka, K. Ohrai and M. Shibasaki, *J. Org. Chem.*, **1995**, *60 (9)*, 2648-2649
[142] F. R. Lemke and C. P. Kubiak, *J. Organomet. Chem.*, **1989**, *373 (3)*, 391-400
[143] Y. Ito, H. Aoyama, T. Hirao, A. Mochizuki and T. Saegusa, *J. Am. Chem. Soc.*, **1979**, *101 (2)*, 494-496
[144] N. Yoshimura, S. I. Murahashi and I. Moritani, *J. Organomet. Chem.*, **1973**, *52 (2)*, C58-C60
[145] A. Fujii, E. Hagiwara and M. Sodeoka, *J. Am. Chem. Soc.*, **1999**, *121 (23)*, 5450-5458
[146] A. C. Albeniz, N. M. Catalina, P. Espinet and R. Redon, *Organometallics*, **1999**, *18 (26)*, 5571-5576
[147] G. L. Hillhouse, *J. Am. Chem. Soc.*, **1985**, *107 (25)*, 7772-7773
[148] J. H. Ren, C. J. Cramer and R. R. Squires, *J. Am. Chem. Soc.*, **1999**, *121 (11)*, 2633-2634
[149] *"FT-ICR MS: Analytical Applications of Fourier Transform Ion Cyclotron Resonance Mass Spectrometry"*, Eds. B. Asamoto, VCH Publishers, Weinheim, **1991**
[150] P. G. Wenthold and R. R. Squires, *J. Am. Chem. Soc.*, **1994**, *116 (14)*, 6401-6412
[151] J. C. Poutsma, J. J. Nash, J. A. Paulino and R. R. Squires, *J. Am. Chem. Soc.*, **1997**, *119 (20)*, 4686-4697
[152] S. G. Lias and J. E. Bartmess, *"Gas-Phase Ion Thermochemistry"*, *http://webbook.nist.gov/chemistry/ion/*,
[153] M. T. Rodgers and P. B. Armentrout, *J. Chem. Phys.*, **1998**, *109 (5)*, 1787-1800
[154] M. T. Rodgers, K. M. Ervin and P. B. Armentrout, *J. Chem. Phys.*, **1997**, *106 (11)*, 4499-4508
[155] A. A. Shvartsburg, K. M. Ervin and J. H. Frederick, *J. Chem. Phys.*, **1996**, *104 (21)*, 8458-8469
[156] N. F. Dalleska, K. Honma, L. S. Sunderlin and P. B. Armentrout, *J. Am. Chem. Soc.*, **1994**, *116 (8)*, 3519-3528
[157] R. H. Schultz, K. C. Crellin and P. B. Armentrout, *J. Am. Chem. Soc.*, **1991**, *113 (23)*, 8590-8601
[158] M. E. Weber, J. L. Elkind and P. B. Armentrout, *J. Chem. Phys.*, **1986**, *84 (3)*, 1521-1529
[159] K. M. Ervin and P. B. Armentrout, *J. Chem. Phys.*, **1985**, *83 (1)*, 166-189
[160] Z. Zencak, M. Oehme and S. Skopp, *Rapid Commun. Mass Spectrom.*, **2001**, *15 (18)*, 1719-1725
[161] R. Flammang, L. Gallez, Y. VanHaverbeke, M. W. Wong and C. Wentrup, *Rapid Commun. Mass Spectrom.*, **1996**, *10 (2)*, 232-234
[162] G. Anderegg and F. Wenk, *Helv. Chim. Acta*, **1967**, *50 (8)*, 2330
[163] K. J. Oberhausen, R. J. Obrien, J. F. Richardson and R. M. Buchanan, *Inorg. Chim. Acta*, **1990**, *173 (2)*, 145-154
[164] B. de Bruin, J. A. Brands, J. J. J. M. Donners, M. P. J. Donners, R. de Gelder, J. M. M. Smits, A. W. Gal and A. L. Spek, *Chem. - Eur. J.*, **1999**, *5 (10)*, 2921-2936
[165] B. de Bruin, R. Kicken, N. F. A. Suos, M. P. J. Donners, C. J. den Reijer, A. J. Sandee, R. de Gelder, J. M. M. Smits, A. W. Gal and A. L. Spek, *Eur. J. Inorg. Chem.*, **1999**, *(9)*, 1581-1592
[166] M. Krom, T. P. J. Peters, R. G. E. Coumans, T. J. J. Sciarone, J. Hoogboom, S. I. ter Beek, P. P. J. Schlebos, J. M. M. Smits, R. de Gelder and A. W. Gal, *Eur. J. Inorg. Chem.*, **2003**, *6*, 1072-1087
[167] T. M. Kooistra, Q. Knijnenburg, J. M. M. Smits, A. D. Horton, P. H. M. Budzelaar and A. W. Gal, *Angew. Chem. - Int. Edit.*, **2001**, *40 (24)*, 4719
[168] M. Krom, R. G. E. Coumans, J. M. M. Smits and A. W. Gal, *Angew. Chem. - Int. Edit.*, **2002**, *41 (4)*, 576-579
[169] M. Krom, R. G. E. Coumans, J. M. M. Smits and A. W. Gal, *Angew. Chem. - Int. Edit.*, **2001**, *40 (11)*, 2106-2108

[170] W. L. Jolly, *"The Synthesis and Characterization of Inorganic Compounds"*, Prentice-Hall, New Jersey, **1970**
[171] R. B. King and F. G. A. Stone, *Inorg. Synth.*, **1963**, *7*, 99-115
[172] R. Cramer, J. A. McCleverty and J. Bray, *Inorg. Synth.*, **1990**, *28*, 86

Chapter 3

Synthesis and Reactivity of N_3 and N_4 Rhodium and Iridium Olefin Complexes

3.1 Introduction

In this chapter the synthesis and solution-phase stability of rhodium and iridium ethene complexes with tri- and tetradentate nitrogen donor ligands (as shown in Figure 3.1) will be discussed. These complexes were originally intended as starting points for a study of oxidation chemistry, as described in Chapters 4-7. However, we found that they also have a rich chemistry of their own, in the absence of added reactants, and this is the subject of the present chapter.

Nitrogen donor ligands could help in stabilizing higher oxidation states on the metal center, enabling us to "trap" intermediates in the oxidation reaction of metal-coordinated olefins with dioxygen. Another advantage of nitrogen donor ligands is that, unlike their phosphorous donor analogues, they are not easily oxidized themselves (see Chapter 4 and 5).

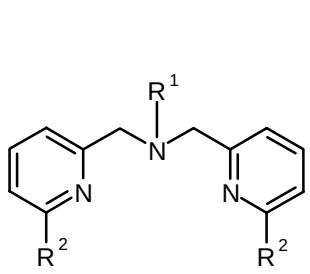

bpa-R : R^2 = H

Me$_2$-bpa-R : R^2 = Me

R = R^1 = H, Me, Bz

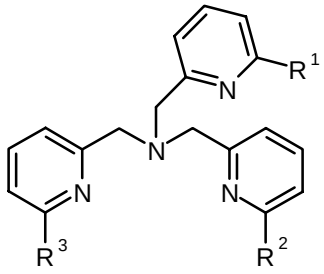

Me$_n$-tpa

n = 0 : $R^1 = R^2 = R^3$ = H

n = 1 : R^1 = Me, $R^2 = R^3$ = H

n = 2 : $R^1 = R^2$ = Me, R^3 = H

n = 3 : $R^1 = R^2 = R^3$ = Me

Figure 3.1 *Ligands used for the synthesis of rhodium and iridium ethene complexes* [1]

Both tri- and tetradentate ligands were used to investigate the influence of the coordination geometry and the number of vacant sites at the metal center on the reactivity. In order to vary the steric bulk around the metal center, methyl substituents were attached to the 6-position of some or all of the pyridine rings.

Analogous ethene complexes of both rhodium and iridium were synthesized, because it was expected that upon switching between these elements different intermediates in oxidation reactions would become isolable.

---

[1] bpa = *N,N*-di(2-pyridylmethyl)amine and tpa = *N,N,N*-tri(2-pyridylmethyl)amine

All cases in which the L_N ligand is modified in the course of the reaction (by for example deprotonation or aromatic C-H activation) the L_N ligand is depicted as $L_N^{\#}$.

The isolation of such intermediates would give more information on the reaction steps via which metal(I) ethene complexes react with dioxygen.

In Appendix A theoretical calculations are presented that were performed on some of the N_3 and N_4 metal-olefin complexes (and their oxidation products) to get an idea of their stability and reactivity; they will be used now and then in this thesis for the interpretation of results obtained.

Some of the results presented in this chapter have already been published. [1]

3.2 Synthesis and reactivity of N_4 rhodium(I) ethene complexes

The synthetic procedure for the rhodium ethene complex cations $[(\kappa^4\text{-Me}_3\text{-tpa})\text{Rh}^{\text{I}}(\text{C}_2\text{H}_4)]^+$ ([**1**]$^+$) and $[(\kappa^4\text{-Me}_2\text{-tpa})\text{Rh}^{\text{I}}(\text{C}_2\text{H}_4)]^+$ ([**2**]$^+$) is similar to that of their tpa rhodium ethene analogue reported by de Bruin *et al.* [2]; we used KPF_6 to precipitate them as [**1**]PF_6/[**2**]PF_6 respectively (Figure 3.2).

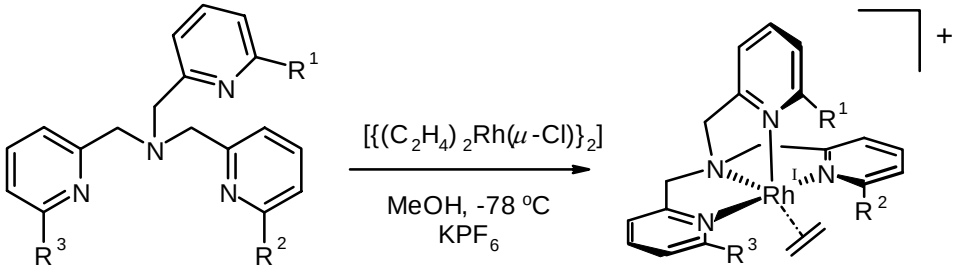

Figure 3.2 *Preparation of the Me_2-tpa and Me_3-tpa rhodium(I) mono-ethene complexes*

In both cases the spectra are consistent with a trigonal-bipyramidal structure of the mono-ethene complexes. For Me_3-tpa a symmetric complex is obtained. At room temperature the ^{1}H- and ^{13}C-NMR spectra of [**1**]$^+$ show two types of N-CH_2-Py^{Me} fragments in the ratio 2:1, which corresponds to two axial and one equatorial N-CH_2-Py^{Me} fragment. For Me_2-tpa an asymmetric complex is obtained with its strongest donor, the picolyl group, at an axial position. These trigonal-bipyramidal structures are comparable to the ones reported for tpa ($R^1 = R^2 = R^3 = H$,) and Me-tpa ($R^1 = Me$, $R^2 = R^3 = H$). [2] For the Me-tpa complex the weaker 6-methyl-picolyl group also occupies an equatorial position.

The tpa and Me-tpa rhodium ethene complexes showed a broad singlet was obtained for the olefin in the ^{1}H-NMR spectra, indicating fluxional behavior (e.g. rotation of the olefin around the metal-olefin bond or dissociation/recoordination [3] – [5]). In contrast, for Me_2-tpa and Me_3-tpa the coordinated ethene appears as several multiplets with rhodium couplings, indicating that the orientation of the olefin is frozen out on the NMR-timescale.

Clear NOE contacts are observed between one of the =CH_2 groups of the olefin and one of the N-CH_2-Py methylene protons, indicating that the olefin lies below the plane defined by the amine-nitrogen and the axial pyridine rings (see picture on the right).

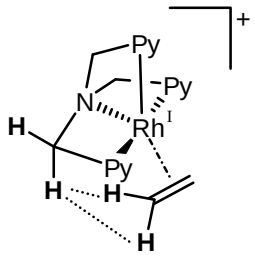

All N_4 rhodium mono-ethene complexes are stable under an inert atmosphere at room temperature (r.t.) both in solution and in the solid state.

3.3 Synthesis and reactivity of N_4 iridium(I) ethene complexes

In analogy with literature procedures for tpa and Me-tpa iridium ethene complexes [6] $[(C_2H_4)_4Ir^I(Cl)]$ [7] (generated *in situ* from reaction of $[\{(coe)_2Ir^I(\mu\text{-}Cl)\}_2]$ [8] with ethene; coe = 1-cyclooctene) was allowed to react in MeOH with Me_2-tpa and Me_3-tpa, respectively.

Me_3-tpa iridium(I) ethene complex

Although for rhodium only mono-ethene complex ([**1**]$^+$) can be isolated, the bis-ethene complex cation $[(\kappa^3\text{-}Me_3\text{-tpa})Ir^I(C_2H_4)_2]^+$ ([**3**]$^+$) is initially formed for iridium. It was isolated via precipitation with KPF_6 as [**3**]PF_6 (Figure 3.3). This difference in reactivity is probably due to the better π-back-donating ability of iridium, which results in a stronger iridium-olefin bond. Such initial formation of iridium bis-ethene complexes was also reported for the corresponding tpa [6] and Me-tpa [9] complexes.

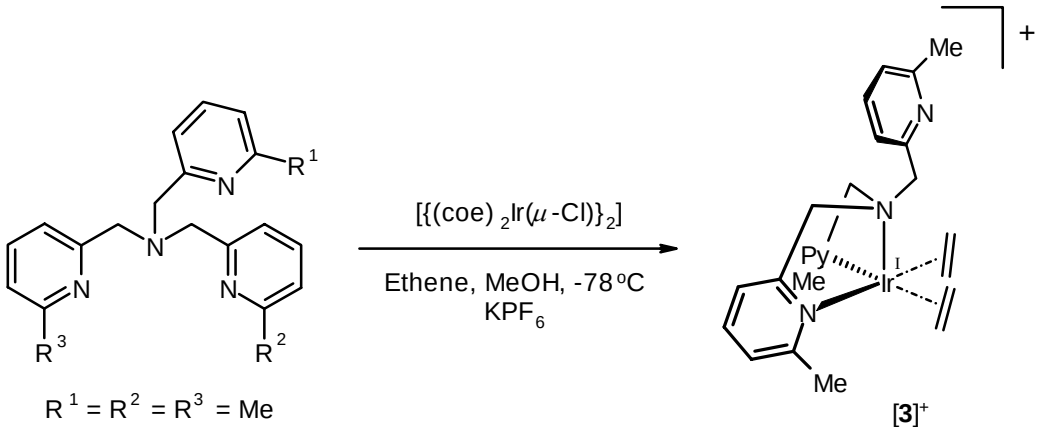

Figure 3.3 *Synthetic procedure for $[(\kappa^3\text{-}Me_3\text{-tpa})Ir^I(C_2H_4)_2]^+$ ([**3**]$^+$)*

^{1}H- and ^{13}C-NMR data of $[(\kappa^3\text{-}Me_3\text{-tpa})Ir^I(C_2H_4)_2]]^+$ reveal two basal N-CH_2-Py^{Me} groups. The ^{1}H-NMR methyl signals of these two groups have shifted approx. 0.7 ppm downfield relative to the free ligand. As expected, the diastereotopic methylene protons of these N-CH_2-Py^{Me} groups give rise to an AB pattern in the ^{1}H-NMR. The ^{1}H-NMR methyl signal of the third N-CH_2-Py^{Me} group of [**3**]$^+$ at 2.6 ppm is close to the value for the free ligand (2.56 ppm). In the ^{1}H-NMR spectra the ethene fragments are observed as two broad signals between 2.1-1.6 ppm at r.t., which can most probably be ascribed to fast rotation around the iridium-olefin bond.

The X-ray structure of [**3**]$^+$ was determined (Figure 3.4). Despite the poor quality of the data-set obtained, the X-ray analysis clearly establishes the presence of the κ^3-*N,N,N-fac* coordinated Me_3-tpa ligand with a non-coordinated 6-methyl-pyridyl group. The structure is in good agreement with the NMR data in solution and is best described as a distorted square pyramidal (*sqpy*) coordination geometry with the two ethene fragments and two 6-methyl-picolyl groups in the basal plane and the amine nitrogen at the apical position.

Such a facial coordination of the Me_3-tpa ligand is in contrast with the meridional coordination mode reported for tpa in the trigonal-bipyramidal bis-ethene complex, $[(\kappa^3\text{-tpa})Ir^I(C_2H_4)_2]^+$ (Figure 3.5). [6]

The change in coordination mode on going from tpa to Me_3-tpa is probably due to steric hindrance caused by the methyl substituents at the coordinated pyridine rings. The olefins need to bend away from them, but in the meridional structure the olefin cis to the dangling pyridyl-arm cannot bend away far enough. In the facial bis-ethene structure there is almost no steric hindrance between the olefins and the nitrogen donor ligand.

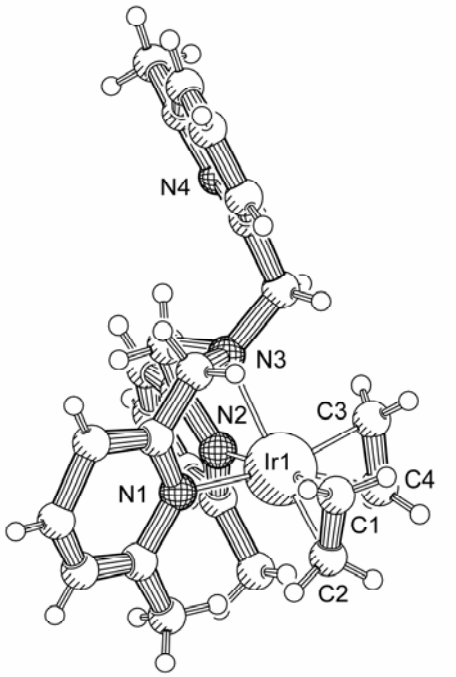

Figure 3.4 *X-ray structure of $[(\kappa^3\text{-}Me_3\text{-}tpa)Ir^I(C_2H_4)_2]PF_6.CH_3OH.½H_2O$*
Anion and solvent molecules omitted for clarity

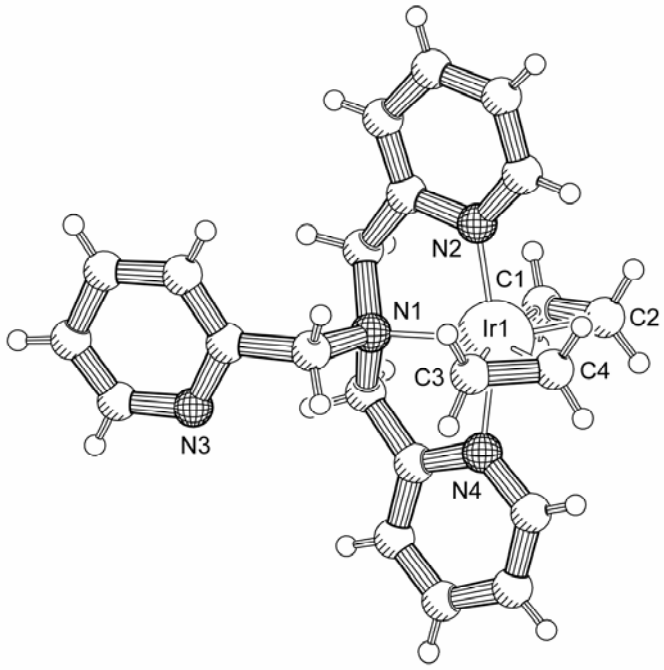

Figure 3.5 *X-ray structure reported for $[(\kappa^3\text{-}tpa)Ir^I(C_2H_4)_2]PF_6$ by Krom.* [6]
Anion omitted for clarity

Table 3.1 *Selected bond lengths and angles of $[\mathbf{3}]^+$ and $[(\kappa^3\text{-}tpa)Ir^I(C_2H_4)_2]^+$*

$[\mathbf{3}]^+$	Length [Å]	$[\mathbf{3}]^+$	Angle [°]	κ^3-tpa	Length [Å]	κ^3-tpa	Angle [°]
Ir1-N1	2.124(18)	N1-Ir1-N2	88.3(8)	Ir1-N1	2.175(8)	N1-Ir1-N2	82.2(3)
Ir1-N2	2.14(3)	N1-Ir1-N3	75.6(7)	Ir1-N2	2.027(10)	N1-Ir1-N4	82.1(3)
Ir1-N3	2.346(19)	N2-Ir1-N3	77.0(9)	Ir1-N4	2.056(8)	N2-Ir1-N4	164.1(4)

[**3**]$^+$	Length [Å]	[**3**]$^+$	Angle [°]	κ^3-tpa	Length [Å]	κ^3-tpa	Angle [°]
Ir1-C1	2.05(3)	C1-Ir1-C2	38.0(10)	Ir1-C1	2.164(11)	C1-Ir1-C2	38.6(4)
Ir1-C2	2.13(3)	C3-Ir1-C4	35.7(10)	Ir1-C2	2.126(13)	C3-Ir1-C4	38.7(4)
Ir1-C3	2.09(3)	C1-Ir1-C3	91.2(13)	Ir1-C3	2.157(11)	C2-Ir1-C4	91.9(4)
Ir1-C4	2.13(3)	C1-Ir1-N1	90.7(11)	Ir1-C4	2.118(10)	C3-Ir1-N1	95.2(4)
C1-C2	1.36(4)	C3-Ir1-N1	167.1(11)	C1-C2	1.419(16)	C1-Ir1-N1	95.7(4)
C3-C4	1.29(4)	C3-Ir1-N2	90.7(12)	C3-C4	1.416(16)	C1-Ir1-N2	89.4(4)
						C3-Ir1-N2	92.6(4)

The iridium(I) bis-ethene complexes are not stable at r.t. in solution: they readily lose the olefin. For tpa and Me-tpa this reaction is fast and is driven to completion by bubbling nitrogen through the solution for a few minutes.[2] For Me_3-tpa complex [**3**]$^+$, bubbling through nitrogen does not have any effect. It takes about 4 hours at r.t. in acetone-d6, CD_2Cl_2 or MeCN to substitute one of the ethene fragments by the dangling 6-methylpyridyl group resulting in mono-ethene complex [(κ^4-Me_3-tpa)Ir^I(ethene)]$^+$ ([**4**]$^+$), which is the iridium analogue of [**1**]$^+$ (Figure 3.6).

Apparently, in the *fac*-square-pyramidal Me_3-tpa complex the olefin can be less easily replaced by a pyridine ring than in the *mer*-trigonal-bipyramidal tpa or Me-tpa complexes. Possibly dissociation of the olefin from the meridional complex is easier because it can smoothly lead to a square planar structure, whereas olefin dissociation from the square pyramid structure would initially produce a *cis*-divacant octahedron. Also, in [**3**]$^+$ the remaining olefin would have to slip <u>*between*</u> the two 6-methyl-picolyl groups all the way to a position <u>*trans*</u> to the dangling picolyl group to allow coordination of this dangling group. A similar difficult loss of one ethene molecule was observed in the square pyramidal complex [(pyridinophane)$Rh(C_2H_4)_2$]$^+$. [10]

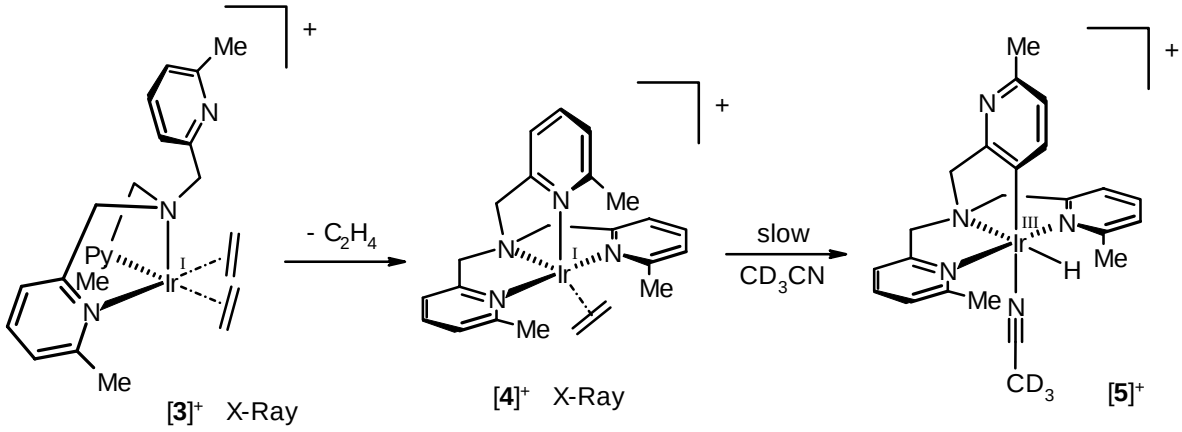

Figure 3.6 *Ethene dissociation from iridium(I) bis-ethene complex [**3**]$^+$ resulting in mono-ethene complex [**4**]$^+$ and cyclometallated complex [**5**]$^+$*

At room temperature the ^{1}H- and ^{13}C-NMR spectra of [**4**]$^+$ show two axial and one equatorial N-CH_2-Py^{Me} fragment, consistent with a κ^4-coordination mode of the Me_3-tpa ligand. Triplet signals were obtained with ^{1}H-NMR for the coordinated ethene molecule indicating that the orientation of the olefin is frozen out on the NMR timescale.

This distorted trigonal-bipyramidal (*tbp*) structure of [**4**]$^+$ was confirmed by X-ray diffraction (Figure 3.7). In [**4**]$^+$, the Ir1-C2 distance is approx. 0.1 Å longer than the Ir1-C1 distance, probably because the axial Py-Me substituents of the Me_3-tpa ligand hinder a closer approach of C2 to the iridium center.

[2] This process is reversible: when C_2H_4 is bubbled through the solution the bis-ethene complexes are obtained again.

Complex [**4**]$^+$ is only moderately stable at r.t. in solution. This is in marked contrast to the less substituted tpa and Me-tpa iridium(I) mono-ethene complexes, which are stable in solution over a period of days. [11] In CD_3CN complex [**4**]$^+$ selectively converts within 72 hours to cyclometallated complex [**5**]$^+$, presumably via chelate ring opening, oxidative addition of the 6-methylpyridyl C3-H bond to the iridium(I) center and substitution of CD_3CN for ethene (Figure 3.6). The hydride in [**5**]$^+$ is observed as a sharp ^{1}H-NMR singlet at δ = -18.6 ppm. The presence of a coordinated CD_3CN was confirmed by ESI$^+$-MS and elemental analysis. The observed cyclometallation also occurs in acetone or CH_2Cl_2. In these solvents however, ^{1}H-NMR indicates that the 6th coordination site is still occupied by ethene.

From MO calculations it is known that a distortion towards a mono-vacant trigonal-bipyramidal coordination geometry increases the reactivity of d^8-metal centers towards oxidative addition of a C-H bond. [12] Dissociation of the equatorial 6-methyl-pyridyl fragment of [**4**]$^+$ would lead to a similar distorted square planar geometry, thus accounting for its intramolecular C-H activation.

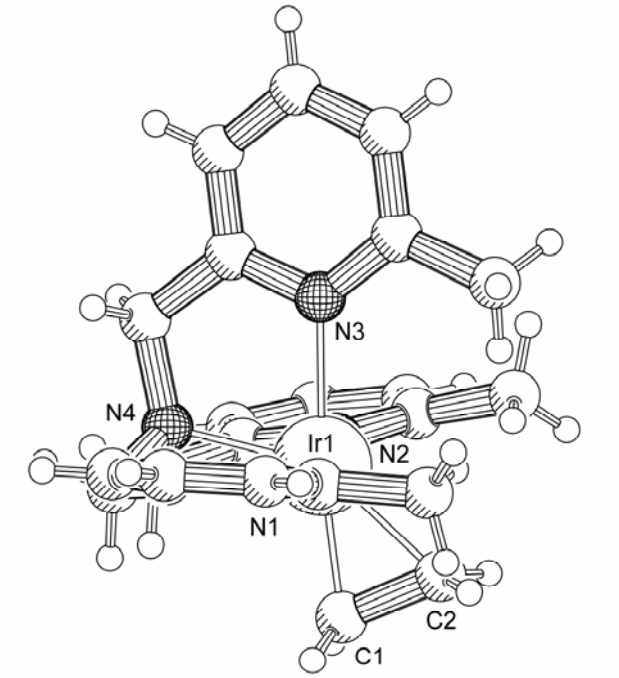

Figure 3.7 *X-ray structure of [(κ^4-Me$_3$-tpa)Ir^I(C_2H_4)]PF_6. Anion omitted for clarity*

Table 3.2 *Selected bond lengths and angles of [**4**]$^+$*

Bond length [Å]		Angle [°]	
Ir1-N1	2.075(7)	N1-Ir1-N2	164.9(3)
Ir1-N2	2.043(8)	N1-Ir1-N3	88.3(3)
Ir1-N3	2.260(7)	N1-Ir1-N4	83.1(3)
Ir1-N4	2.154(8)	N2-Ir1-N3	88.2(3)
Ir1-C1	2.042(9)	N2-Ir1-N4	81.8(3)
Ir1-C2	2.143(9)	N3-Ir1-N4	77.4(3)
C1-C2	1.451(13)	C1-Ir1-C2	40.5(4)
		C1-Ir1-N1	93.5(4)
		C1-Ir1-N4	109.2(4)

Me_2-tpa iridium(I) ethene complex

When Me_2-tpa is allowed to react with $[(C_2H_4)_4Ir^I(Cl)]$ generated *in situ* [7], only the mono-ethene complex $[(\kappa^4\text{-}Me_2\text{-tpa})Ir^I(C_2H_4)]^+$ ($[\mathbf{6}]^+$) can be isolated. Contrary to the Me_3-tpa complex, no signals corresponding a bis-ethene complex were observed in the ^{1}H-NMR spectra.

The trigonal-bipyramidal mono-ethene complex ($[\mathbf{6}]^+$) obtained is asymmetric, as was also the case for the corresponding rhodium complex $[\mathbf{2}]^+$ (Figure 3.2). Its structure was confirmed by X-ray diffraction (Figure 3.8).

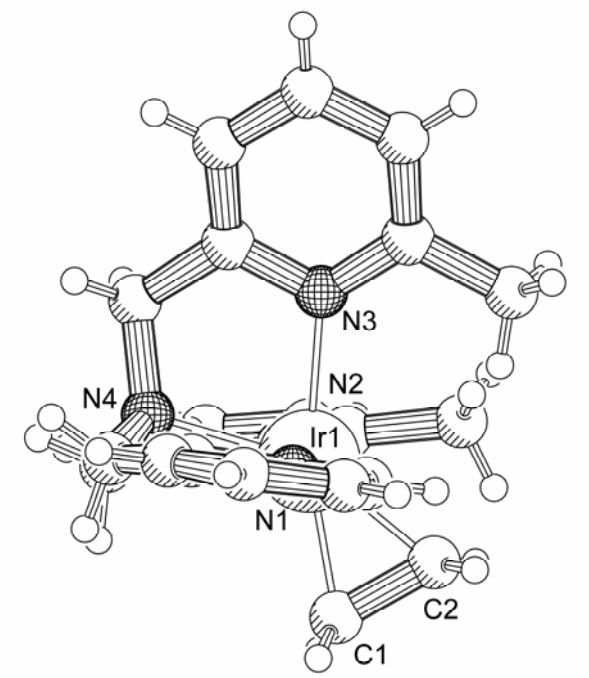

Figure 3.8 *X-ray structure of $[(\kappa^4\text{-}Me_2\text{-ta})Ir^I(C_2H_4)]PF_6$. Anion omitted for clarity*

Table 3.3 *Selected bond lengths and angles of $[\mathbf{6}]^+$*

Bond length [Å]		Angle [°]	
Ir1-N1	2.039(6)	N1-Ir1-N2	164.5(2)
Ir1-N2	2.066(5)	N1-Ir1-N3	84.2(2)
Ir1-N3	2.219(6)	N1-Ir1-N3	83.8(3)
Ir1-N4	2.153(5)	N2-Ir1-N3	95.5(2)
Ir1-C1	2.051(7)	N2-Ir1-N4	81.0(2)
Ir1-C2	2.073(7)	N3-Ir1-N4	78.0(2)
C1-C2	1.442(11)	C1-Ir1-C2	40.9(3)
		C1-Ir1-N1	90.7(3)
		C1-Ir1-N4	116.0(3)

The structure of $[\mathbf{6}]^+$ is similar to that of $[\mathbf{4}]^+$. One significant difference is that the equatorial pyridine ring is somewhat tilted towards the unsubstituted pyridine ring (probably to reduce the steric hindrance between the Py-Me groups). In $[\mathbf{6}]^+$ the Ir1-C1 and Ir1-C2 distances are comparable, contrary to $[\mathbf{4}]^+$ (which has an elongated Ir1-C2 bond). This is probably a result of the reduced steric hindrance between the axial Py-Me substituents of the Me_2-tpa ligand and the olefin due to the presence of one unsubstituted pyridine ring.

Shortening of the Ir1-N3 distance by ~0.04 Å on going from [**4**]$^+$ to [**6**]$^+$ probably reflects the stronger binding of the N_4 ligand in the latter, which has one unsubstituted pyridine ring, which is a much stronger σ-donor than a substituted pyridine ring and which also decreases the steric hindrance around the metal center hereby allowing N3 to approach the iridium center at a closer distance. This is also reflected in the decreasing C1-Ir1-N4 angle: [**6**]$^+$ (116.0(3) º) to [**4**]$^+$ (109.2(4) º).

The structures described here for [**4**]$^+$ and [**6**]$^+$ are similar to the one reported for the corresponding tpa iridium(I) mono-ethene complex. [13]

Unlike [**4**]$^+$, [**6**]$^+$ is stable in solution under an inert atmosphere at r.t.; no activation of a pyridine C-H bond was observed.

3.4 Synthesis and reactivity of N_3 iridium(I) ethene complexes

3.4.1 Iridium(I) ethene complexes with sterically demanding Me_2-bpa-R ligands

In the case of the Me_2-bpa-R (R = Me, Bz) complexes, the same synthetic route is used as for the N_4 iridium ethene complexes (§ 3.3). This yields the bis-ethene iridium complexes [(κ^3-Me_2-bpa-Me)$Ir^I(C_2H_4)_2]^+$ ([**7**]$^+$) and [(κ^3-Me_2-bpa-Bz)$Ir^I(C_2H_4)_2]^+$ ([**10**]$^+$), respectively (Figure 3.9). They were isolated as PF_6-salts by precipitation with KPF_6.

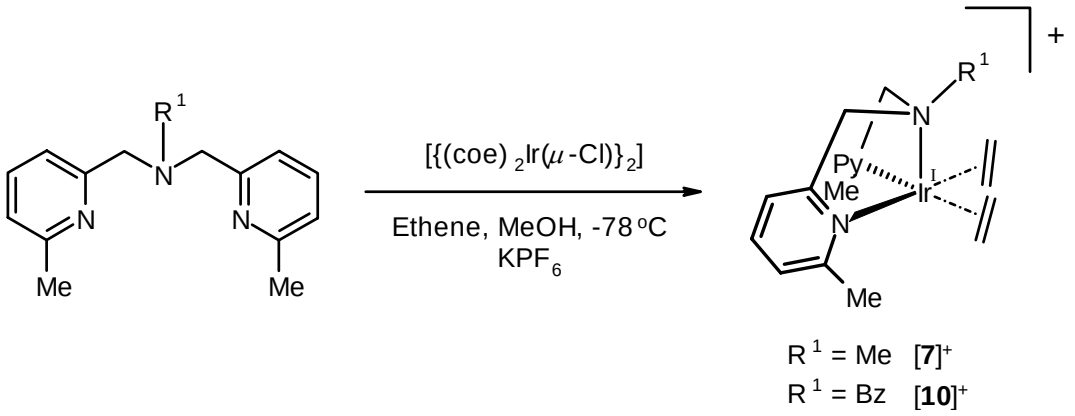

Figure 3.9 *Synthesis of [(κ^3-Me_2-bpa-R)$Ir^I(C_2H_4)_2]^+$ (R = R^1 = Me, Bz)*

The ^{1}H-NMR data of [**7**]$^+$ and [**10**]$^+$ reveal two axial N-CH_2-Py^{Me} groups. The ^{1}H-NMR methyl signals of these two groups have shifted approx. 0.7 ppm downfield relative to the free ligand. As expected, the diastereotopic methylene protons of the two axial N-CH_2-Py^{Me} groups give rise to two AB-type doublets. In the ^{1}H-NMR spectra of [**7**]$^+$ and [**10**]$^+$ the ethene fragments are observed as two broad signals between 2.2-1.6 ppm at r.t.

Since for [(κ^3-Me_3-tpa)$Ir^I(C_2H_4)_2]^+$ ([**3**]$^+$) a distorted square-pyramidal structure is obtained with the N_4-ligand κ^3-coordinated in a facial manner, based on analogy, the bis-ethene complexes [**7**]$^+$ and [**10**]$^+$ will most probably be square pyramidal too.

These bis-ethene complexes are not stable at all at r.t. in solution.

Me_2-bpa-Me iridium(I) ethene

In the case of Me_2-bpa- complex [**7**]$^+$ one of the two ethene fragments dissociates in acetone-d6, CD_2Cl_2 or MeCN within 4 hours at r.t. (Figure 3.10). This results in the formation of four-coordinate mono-ethene complex [**8**]$^+$.

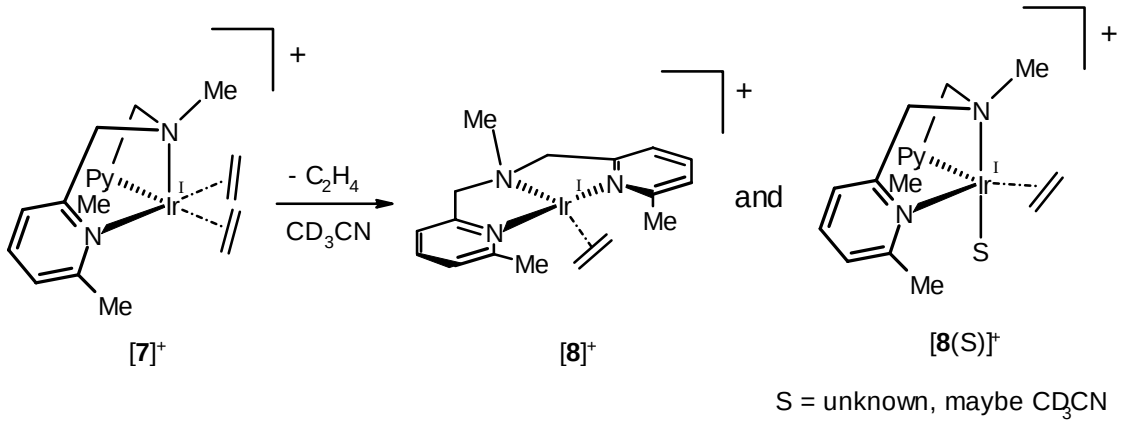

Figure 3.10 *Ethene dissociation from iridium(I) bis-ethene complex [**7**]$^+$ resulting in [**8**]$^+$*

The ^{1}H- and ^{13}C-NMR spectra of [**8**]$^+$ show signals for two equivalent N-CH_2-Py^{Me} groups. The ethene signals are observed as two sharp triplets, indicating that the position of the ethene fragment is fixed on the NMR time-scale.

The ^{1}H-NOE patterns of [**8**]$^+$ are characteristic of a *mer*-coordination mode of the Me_2-bpa-Me ligand. Clear NOE contacts are observed between N-*CH_3* and one of the two N-*CH_2*-Py^{Me} methylene protons. The latter also show NOE contacts with the Py^{Me}-*H3* protons. The other N-*CH_2*-Py^{Me} methylene proton does not show NOE contacts with either N-*CH_3* or Py^{Me}-*H3*.

A solution of [**8**]$^+$ in CD_2Cl_2 contains only [**8**]$^+$. In CD_3CN however, [**8**]$^+$ and [**8**(S)]$^+$ are present in a ratio of 3:1. Although they have separate ^{1}H-NMR signals, they show exchange signals in the EXSY spectrum, indicating that [**8**]$^+$ and [**8**(S)]$^+$ are in slow exchange on the ^{1}H-NMR time-scale. The ethene ^{1}H-NMR signals of [**8**(S)]$^+$ are very similar to those of the Me_3-tpa iridium mono-ethene complex ([**4**]$^+$). The ethene signals of [**8**]$^+$, both in CD_3CN and CD_2Cl_2, have clearly shifted downfield relative to those of [**8**(S)]$^+$. Computer generated space-filling models of [**8**]$^+$ obtained for a structure optimized by DFT (Appendix A) indicate that the methyl substituents on the pyridyl fragments prevent the complex from adopting a true square-planar coordination geometry. DFT-calculations also indicate that only the position *trans* to the amine-substituent (as shown in Figure 3.10) is suitable for ethene coordination. At the *cis*-position the serious steric hindrance between the olefin and the N_{amine}-Me and Py-Me groups causes large structural deformations of the N_3-ligand. Therefore we propose [**8**]$^+$ to have a distorted square planar geometry, in which the ethene fragment has moved to a position below the *mer*-(Me-bpa-Me)Ir plane, away from the N_{amine}-Me and the methyl substituents at the 6-position of the pyridine rings (Figure 3.10).

A structure for [**8**(S)]$^+$ in which the N_3 ligand is coordinated in a facial fashion as shown in Figure 3.10, would explain why there is a slow equilibrium between [**8**]$^+$ and [**8**(S)]$^+$. In such a structure coordination of a fifth ligand S is required. The identity of S is not known: it is probably CD_3CN or H_2O.

Mono-ethene complex [**8**]$^+$ is only moderately stable at r.t. in solution. Easy C-H activation (c.f. complex [**3**]$^+$) could explain its apparent instability.

Solid state rearrangement of iridium(I) bis-ethene complex [7]$^+$

When complex [**7**]$^+$ is exposed to a dioxygen atmosphere for about 3 months at r.t. no reaction with dioxygen takes place. Instead the complex reacts intramolecularly, possibly under the influence of light. Product analysis was performed by dissolving the solid in CD_3CN and follow its solution-phase stability in time. At first it seemed as if at least four different products had been formed. However, after 12 hours in solution at -20 ºC one single product was left behind: ethyl-vinyl complex [**9**]$^+$ (Figure 3.11).

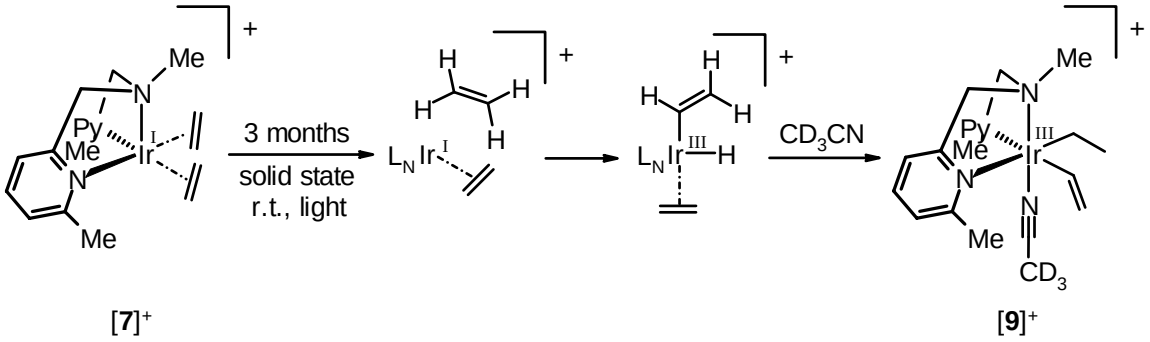

Figure 3.11 *Proposed solid-state reaction of [7]$^+$*

Characteristic ^{1}H-NMR signals are the vinylic signals and the diastereotopic methylene protons of the coordinated ethyl moiety. Since [**9**]$^+$ is asymmetric, we propose a facial coordination mode of the Me_2-bpa-Me ligand.

In other words, one of the vinylic C-H-bonds has oxidatively added to the iridium center in the course of the reaction. It is likely that in the solid state three geometrically different ethene-vinyl-hydride complexes are formed. Upon dissolving them in CD_3CN they will probably all rearrange to form ethyl-vinyl complex [**9**]$^+$.

Similar reactions were previously reported (in solution) both for an square pyramidal pyridinophane iridium(I) bis-ethene complex [11], which rearranges at r.t. spontaneously to an ethyl-vinyl complex, and for a Tp* iridium bis-ethene[3] complex complex [14], for which the corresponding hydrido-vinyl ethene complex could be isolated. The latter can be generated either thermally or photochemically.

Me_2-bpa-Bz iridium(I) ethene

Me_2-bpa-Bz iridium(I) bis-ethene complex [**10**]$^+$ is not stable at r.t. in solution. It presumably loses ethene, but the resulting mono-ethene complex cannot be isolated, since aromatic C-H activation at the 2-position of the phenyl ring is fast, as found earlier for [**4**]$^+$. Upon dissolving [**10**]$^+$ in acetone-d6 or CD_2Cl_2 at r.t. the reaction is complete after 2 hours and the resulting Me_2-bpa-Bz$^{\#}$ iridium(III) ethene-hydride species ([**11**]$^+$) can be isolated (Figure 3.12).

Apparently [(Me_2-bpa-Bz)Ir^I(C_2H_4)]$^+$ is more reactive than the Me_3-tpa iridium(I) mono-ethene complex ([**4**]$^+$), since the latter needs up to 72 hours instead of 2 to complete the aromatic C-H activation reaction.

This is most likely because the N_4 ligand has to become κ^3-coordinated before it can undergo oxidative addition of the pyridine C-H bond to the iridium(I) center. However, we do not have any information at all on the mechanism via which these aromatic C-H activation reactions takes place.

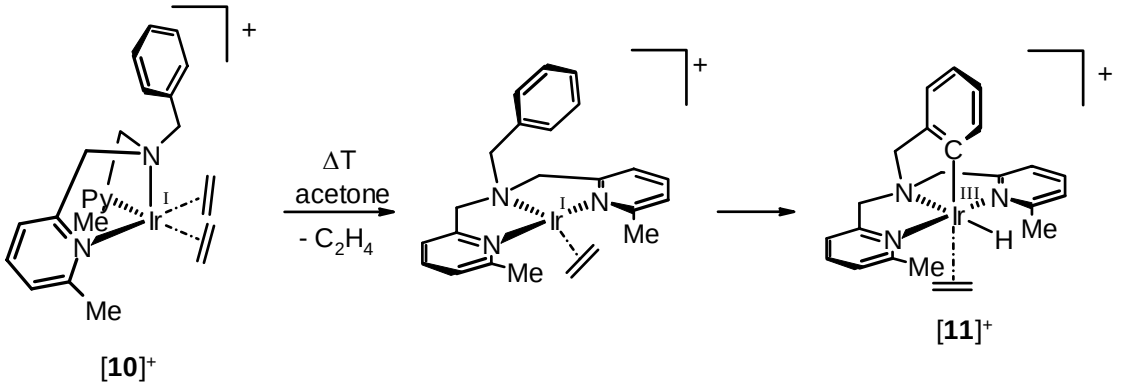

Figure 3.12 *Reaction of iridium(I) bis-ethene complex [**10**]$^+$ in acetone-d6 and CD_2Cl_2 to form [**11**]$^+$*

[3] Tp* = hydridotriss(3,5-dimethyl-1-pyrazolyl)borate

Oxidative addition of the aromatic C-H bond while the N_3 ligand is still coordinated in a meridional fashion does not seem very plausible: only in a *fac* coordination mode can the C-H bond be brought in such a position that oxidative addition is possible.
Work by Karen Goldberg [15] – [17] shows that for platinum systems a three-coordinate 14 VE metal complex is needed for oxidative addition. To what extent this is applicable to our iridium species is not clear, but at least it shows that the mechanism of aromatic C-H activation in [**4**]$^+$ and [**10**]$^+$ can be quite complicated.

The structure of the intermediate mono-ethene complex is proposed to be similar to that of [**8**]$^+$: a mono-vacant trigonal-bipyramidal complex due to the steric hindrance caused by the methyl substituents at the 6-position of the pyridine rings.
The symmetric ethene-hydride complex [**11**]$^+$ is the main product obtained in acetone-d6 after 2 hours. On the basis of ^{1}H-NMR, NOESY and COSY it can be concluded that in this symmetric complex the nitrogen donors all must lie in one plane, as depicted in Figure 3.12. In order to undergo aromatic C-H activation it is probably not possible for the N_3 ligand to remain meridionally coordinated. Due to the large trans-effect of the coordinated hydride and the carbon-atom after oxidative addition rearrangements will eventually take place, resulting in a symmetric structure for [**11**]$^+$ as shown in Figure 3.12.
The hydride in [**11**]$^+$ is observed as a sharp singlet at δ = -15.45 ppm in acetone-d6 and the olefin gives rise to a somewhat broader singlet at δ = 3.66 ppm, indicating fast rotation of C_2H_4 around the iridium-olefin bound. The reaction is, however, not completely selective: on the basis of the intensities of the hydride signals in the ^{1}H-NMR spectra it can be deduced that approx. 10 % consists of four different other hydride species with ^{1}H-signals at δ = -16.22 ppm, -17.73 ppm, -18.45 ppm and -19.11 ppm. The signal at -17.73 ppm probably corresponds to [(Me_2-bpa-$Bz^{\#}$)Ir(H)(acetone-d6)]$^+$ (*vide infra*). The exact nature of the other species could not be determined, because their intensities are too low and none of them could be isolated.
On going from bis-ethene complex [**10**]$^+$ to mono-ethene-hydride complex [**11**]$^+$ in CD_2Cl_2 the N-C*H_2*-Py^{Me} methylene signals shift up to 1.6 ppm to low field. Also the signal corresponding to the coordinated olefin shifts up to 1.5 ppm to low field, and the Ph-*H6* proton shifts 0.6 ppm downfield, whereas the other four phenylic protons shift about the same amount upfield.
Clear ^{1}H-NOE signals can be observed between the olefin protons and one of the two N-C*H_2*-Py^{Me} methylene protons, indicating that the olefin is coordinated *trans* to the benzyl-ring at an axial position. The other diastereotopic N-C*H_2*-Py^{Me} methylene proton displays a NOE contact with the N-C*H_2*-Ph protons.
Ethene-hydride complex [**11**]$^+$ is not air stable: upon contact with air, the light-yellow solution becomes brownish and by ^{1}H-NMR a mixture of unidentifiable products can be observed.
[**11**]$^+$ also slowly decomposes in acetone solution under an inert atmosphere (even at -20 ºC), as monitored by the rise of a hydride signal at δ = -17.73 ppm at the cost of the signal at -15.45. This signal is ascribed to [(Me_2-bpa-$Bz^{\#}$)Ir(H)(acetone-d6)]$^+$.

When iridium(I) bis-ethene complex [**10**]$^+$ is dissolved in acetonitrile, again a symmetric complex is obtained. Just like ethene-hydride complex [**11**]$^+$, the obtained compound has a characteristic doublet in the ^{1}H-NMR at low field in the aromatic region (δ = 8.2 ppm), corresponding to the Ph-H6 of the C-H activated product and a signal corresponding to a hydride at δ = -18.32 ppm. However, in this case the olefin is no longer observed in the ^{1}H-NMR spectrum. Therefore we propose iridium(III) hydride complex [(Me_2-bpa-$Bz^{\#}$)Ir(H)(CD_3CN)]$^+$ ([**12**]$^+$) to be formed in CD_3CN.

3.4.2 Iridium(I) ethene complexes with sterically less demanding bpa-R ligands

Also the bpa-R ligands (R = H, Me, Bz) were allowed to react with *in situ* generated $[(C_2H_4)_4Ir^I(Cl)]$ [7] in MeOH. Just like for the Me_2-bpa-R ligands, this results in the formation of bis-ethene complexes: $[(bpa)Ir^I(C_2H_4)_2]^+$ ([**13**]$^+$), $[(bpa\text{-}Me)Ir^I(C_2H_4)_2]^+$ ([**15**]$^+$) and $[(bpa\text{-}Bz)Ir^I(C_2H_4)_2]^+$ ([**16**]$^+$).

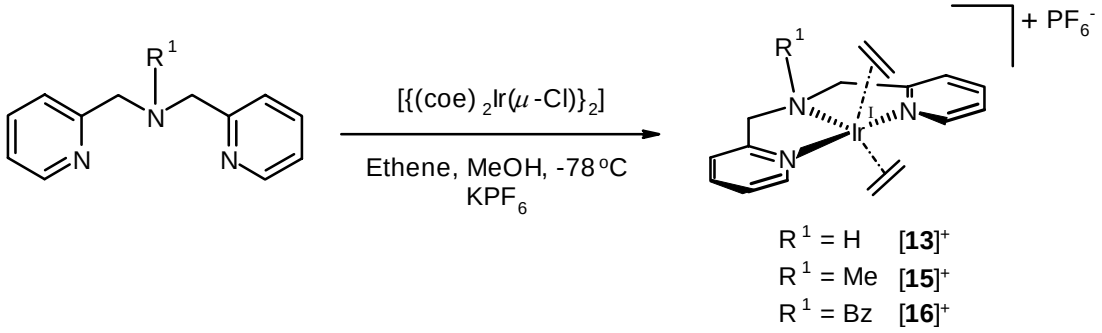

Figure 3.13 *Synthesis of $[(\kappa^3\text{-bpa-R})Ir^I(C_2H_4)_2]^+$ (R = R^1 = H, Me, Bz)*

^{1}H-NMR data of [**13**]$^+$, [**15**]$^+$ and [**16**]$^+$ reveal two equivalent N-C*H*$_2$-Py groups. As expected, the diastereotopic methylene protons of the two equivalent N-C*H*$_2$-Py groups give rise to an AB pattern.

The ^{1}H-NOE patterns of these bis-ethene complexes are characteristic of a *mer*-coordination mode of the bpa-R ligands. Clear NOE contacts are observed between only one of the two coordinated ethene molecules ("above" the plane formed by the bpa-R ligand and the metal center) and the amine-R group. The two types of N-CH_2-Py protons each show a NOE contact with a *different* ethene molecule. NOE contacts are also observed between the Py-H6 and *both* ethene molecules. No direct exchange is observed between the two ethene molecules, they only exchange with a trace of free ethene present in solution.

From these results, a trigonal-bipyramidal coordination geometry is proposed for the bis-ethene complexes [**13**]$^+$, [**15**]$^+$ and [**16**]$^+$, in which the N_3-ligand is coordinated in a meridional fashion. The trigonal plane is formed by the two ethene molecules and the amine-N donor. The axial positions are taken by the pyridyl donors. This structure is in contrast with the square-pyramidal structures proposed for the Me_2-bpa-R iridium(I) bis-ethene complexes [**7**]$^+$ and [**10**]$^+$. Such a change in coordination mode of the ligand from meridional to facial upon increase of the steric bulk around the metal center was also observed for the N_4 iridium(I) bis-ethene complexes (§ 3.3).

The ethene molecules are not equivalent and are observed as four triplet-like signals in the ^{1}H-NMR, indicating that the ethene moieties do not to rotate rapidly on the NMR time-scale. The ethene molecule that has NOE contacts with the amine-R group (i.e. positioned *cis* to the R group) gives rise to broader triplet-like signals (i.e. close to coalescence on the NMR timescale), which indicates that this fragment is somewhat more fluxional and perhaps more weakly coordinated to the iridium centre than the ethene molecule positioned "below" the plane.

All three iridium(I) bis-ethene complexes are stable in solution at r.t. under an inert atmosphere.

Bubbling nitrogen through a solution of the corresponding complex for a few minutes or heating the solution did not result in clear ethene dissociation.

Upon heating a solution of the bpa-Me iridium(I) bis-ethene complex no reaction was observed at al with ^{1}H-NMR: this bis-ethene complex is apparently too stable. In the case of the bpa and bpa-Bz complexes heating resulted in other reactions taking place, possibly as a follow-up reaction from the expected formation of $[(bpa\text{-}R)Rh^I(C_2H_4)]^+$ (R = H, Bz).

Reactivity of bpa iridium(I) bis-ethene upon heating: N-H activation

When a solution of bpa iridium(I) bis-ethene complex [**13**]$^+$ in CD_3CN is heated to approximately 70 ºC for two hours, a single product can be isolated in 81 % yield. This was identified as a dinuclear iridium(III) ethyl complex [**14**]$^{2+}$ in which the amine-nitrogen of the bpa ligand is deprotonated and coordinated to both iridium(III) centers.

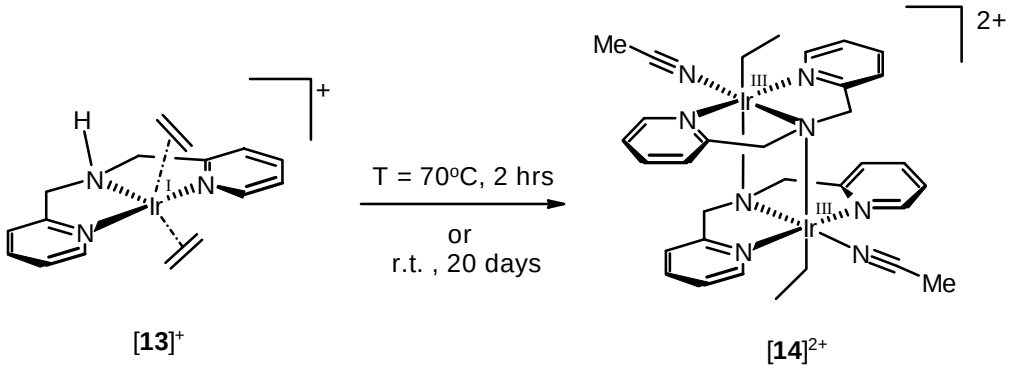

Figure 3.14 *Reactivity of [13]$^+$ upon heating in solution: formation of [14]$^{2+}$*

When the reaction is carried out in CH_3CN, solvent coordination is clearly recognized by a ^{1}H-NMR signal at 2.70 ppm. Upon dissolving the CH_3CN-coordinated complex in CD_3CN no exchange between coordinated CH_3CN and the solvent seems to take place, indicating a very strong bond between the iridium(III) center and the nitrile.

It was also possible to perform the synthesis of [**14**]$^{2+}$ at r.t. in CH_3CN. After 20 days the bis-ethene complex was completely converted to the dinuclear complex. According to ^{1}H-NMR again no by-products were formed.

^{1}H-NOE contacts are characteristic of a dinuclear complex with a *mer*-coordination mode of the deprotonated bpa-ligand with the ethyl-group at an axial position. An indication of the presence of a dinuclear complex can be obtained from NOE contacts between one of the N-C*H*$_2$-Py methylene protons and two of the pyridine protons (Py-*H3* and -*H6*), which would have been impossible in a mononuclear complex.

Solutions of dinuclear complex [**14**]$^{2+}$ are air stable.

When the reaction is carried out in CD_3CN, again the only product obtained is [**14**]$^{2+}$ with only hydrogen atoms, not any deuterium atom, at the ethyl moiety. It seems therefore plausible that the proton used to convert the olefin into ethyl group stems from the amine-nitrogen. Therefore, we propose following mechanism for the formation of [**14**]$^{2+}$ (Figure 3.15).

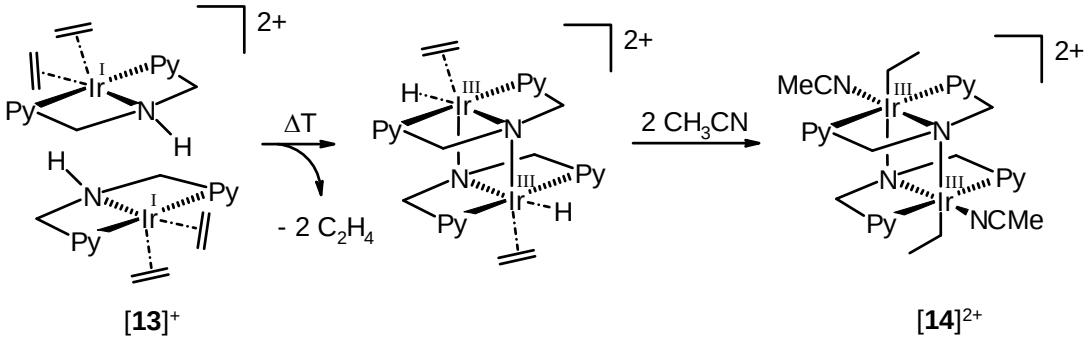

Figure 3.15 *Formation of [14]$^{2+}$*

It involves N-H activation of the bpa ligand, e.g. deprotonation of the amine-nitrogen, and oxidative protonation of iridium(I) to form a iridium(III)-hydrido complex. Migratory insertion of the coordinated ethene fragment into the iridium hydride bond then yields the ethyl fragment of [**14**]$^{2+}$.[4]

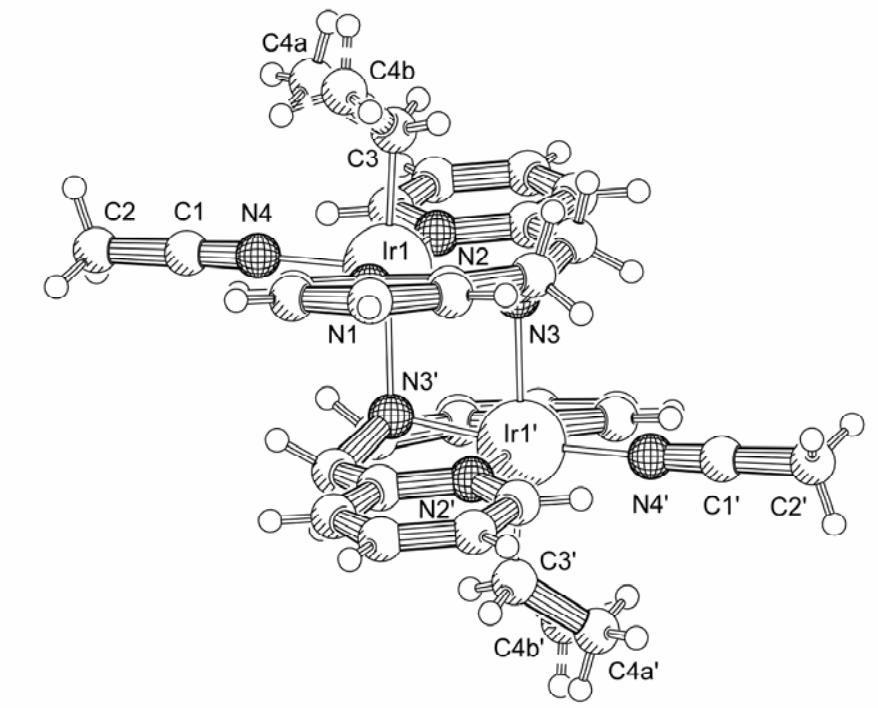

Figure 3.16 *X-ray structure of [{(bpa$^{\#}$)Ir(C_2H_5)(CH_3CN)}$_2$](PF_6)$_2$*
Anions omitted for clarity

Table 3.4 *Selected bond lengths and angles of [**14**]$^{2+}$*

	Bond length [Å]		Angle [°]		Angle [°]
Ir1-N1	2.034(8)	N1-Ir1-N2	163.7(3)	N4-Ir1-C3	90.8(4)
Ir1-N2	2.011(8)	N1-Ir1-N3	83.4(3)	N3'-Ir1-N1	94.5(3)
Ir1-N3	2.036(7)	N1-Ir1-N4	98.7(3)	N3'-Ir1-N2	93.2(3)
Ir1-N4	2.014(8)	N2-Ir1-N3	83.8(3)	N3'-Ir1-N3	79.7(3)
Ir1-C3	2.113(10)	N2-Ir1-N4	95.2(3)	N3'-Ir1-C3	175.9(3)
Ir1-N3a	2.266(8)	N1-Ir1-C3	85.8(4)	Ir1-N3-Ir1a	100.3(3)
Ir-Ir1	2.6877(6)	N2-Ir1-C3	85.6(4)	Torsion: N1-Ir1-Ir1'-N2'	-8.40
		N3-Ir1-C3	96.2(4)		

Crystals suitable for X-ray diffraction were obtained from vapor diffusion of diethylether into an acetonitrile solution. The X-ray structure of [**14**]$^{2+}$ is shown in Figure 3.16.

Dinuclear iridium complex [**14**]$^{2+}$ has an inversion center and a slightly distorted octahedral geometry around each metal center with the N_3 ligand still coordinated in a meridional fashion. As proposed in Figure 3.14 and Figure 3.15 the only dinuclear complex present in the crystal is the one with the ethyl group occupying an

[4] This reaction can take place both via an inter- and via an intramolecular pathway. There is no proof for either of them.

axial position. The end-of-chain carbon atom C4 is rather disordered and has been split up over two separate positions; it proved to be impossible to refine these two positions anisotropically. The pyridine rings are positioned in such a way that π-stacking between the two N_3 ligands is optimal, which could be one of the driving forces for the reaction.

Reactivity of bpa-Bz iridium(I) bis-ethene upon heating: C-H activation

Upon heating a saturated solution of bpa-Bz iridium(I) bis-ethene ([**16**]$^+$) for at least 24 hours at 50 ºC, a yellow solid precipitates. It appears to be one single species: a dinuclear iridium(III) hydride species with bridging hydrogen atoms ([**17**]$^{2+}$).

Table 3.5 *Selected bond lengths and angles of [**17**]$^{2+}$*

Bond length [Å]			Angle [º]
Ir1-Ir1a	2.6877(6)	N1-Ir1-C37	87.3(2)
Ir1-N1	2.043(6)	N2-Ir1-C37	86.1(2)
Ir1-N2	2.036(6)	N4-Ir1-N1	81.1(2)
Ir1-N4	2.070(6)	N4-Ir1-N2	81.8(2)
Ir1-C37	2.005(7)	N1-Ir1-N2	162.4(2)
		Torsion: N1-Ir1-Ir1'-N2'	16.23

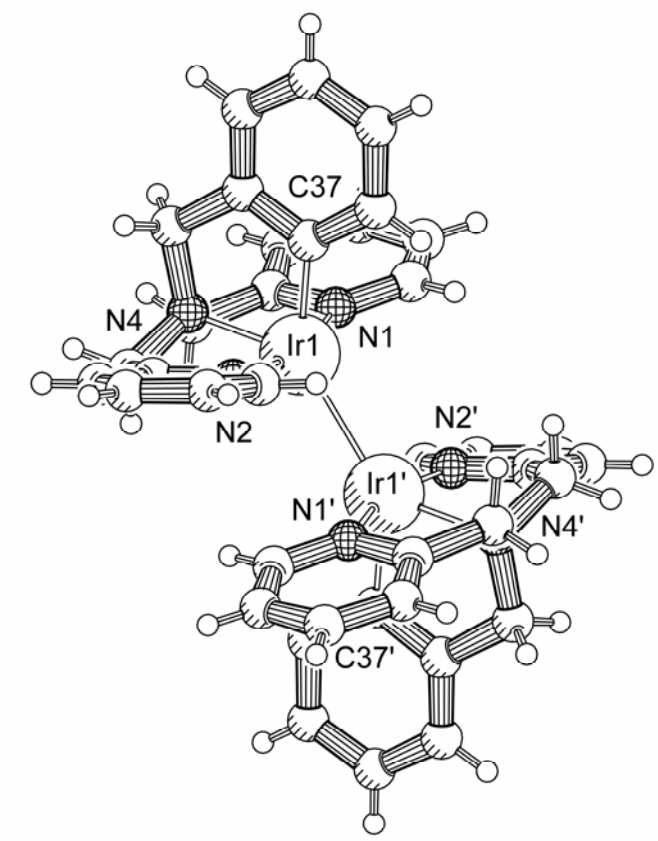

Figure 3.17 *X-ray structure of [{(bpa-Bz$^{\#}$)Ir(H)}$_2$](PF$_6$)$_2$.4(CH$_3$)$_2$CO*
Anions and solvent molecules omitted for clarity

Crystals of [**17**]$^{2+}$ suitable for X-ray diffraction were obtained when an acetone solution of iridium(I) bis-ethene complex [**16**]$^+$ was allowed to stand at r.t. for three weeks. The X-ray structure obtained is shown in

Figure 3.17. Unfortunately, it was not possible to locate the bridging hydrogen atoms in $[\mathbf{17}]^{2+}$ by X-ray diffraction, but they are clearly observed as a sharp ^{1}H-NMR signal at δ = -14.73 ppm in acetone-d6.

The structure of $[\mathbf{17}]^{2+}$ consists of the iridium dimer positioned at an inversion center, four acetone moieties and two rather disordered PF_6 moieties. The Ir-Ir distance is 2.6877(6) Å. Complex $[\mathbf{17}]^{2+}$ has a distorted octahedral coordination geometry around each iridium(III) center and the N_3 ligands are coordinated in a *mer*-fashion. The C-H bond at the 2-position of the benzyl-ring has oxidatively added to the iridium center resulting in an iridium(III) hydride species. Two of these have dimerized to form the hydride-bridged species $[\mathbf{17}]^{2+}$. The olefin is no longer coordinated. Similar aromatic C-H activation was already observed for the Me_2-bpa-Bz and the Me_3-tpa iridium(I) ethene complexes, although for these complexes the olefin remained coordinated to the metal center in acetone and no dimerization was observed.

A clear indication of a dinuclear structure comes also from NOESY experiments in which NOE contacts are observed between the Py-*H6* and both the Py-*H3* and one of the N-C*H*$_2$-Py methylene protons. A Py-*H6* proton can only display such NOE contacts if two N_3 ligands are in close proximity of one another, like in Figure 3.17. Also, the upfield shift of more than 0.7 ppm in the ^{1}H-NMR for most of the aromatic benzyl signals of $[\mathbf{17}]^{2+}$ as compared to $[\mathbf{16}]^{+}$ is indeed a clear indication that the benzyl ring is coordinated to the iridium(III) centre. The pyridine rings and their methylene groups have remained equivalent in the ^{1}H-NMR.

Short Ir-Ir contacts bridged solely by hydrides are uncommon, but some examples of (poly) hydride bridged iridium complexes are known. [18] – [22] Similar hydrogen bridged dinuclear iridium(III) complexes containing additional diphosphine bridges were reported by Fujita *et al.* [23] – [25] For these complexes (Figure 3.18) the bridging hydrogen atoms can be observed at δ = -17.82 ppm in acetone-d6.

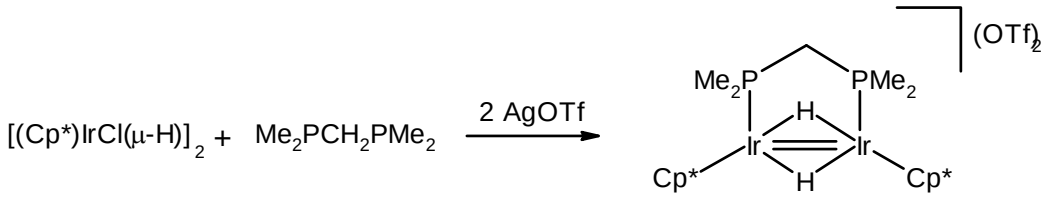

Figure 3.18 *Dinuclear iridium complexes with bridging hydrogen atoms by Fujita et al.*

Addition of ethyne to this dinuclear iridium hydride complex gives a μ-vinyl complex $[(Cp^*Ir)_2(\mu\text{-dmpm})(\mu^2,\eta^1,\eta^2\text{-}CH{=}CH_2)(\mu\text{-H})]^{2+}$ via addition of one of the iridium-hydrides to the carbon-carbon triple bond. In this complex the bridging hydride can be found at δ = -20.36 ppm (in acetone-d6). When *tert*-butylisocyanide is added, one of the iridium-hydride bonds is broken and the isocyanide coordinates to one of the iridium centers. The chemical shift of the bridging hydride in this case is -24.00 ppm and that of the terminal hydride is -15.51 ppm (in CD_2Cl_2).

When the reaction of $[\mathbf{16}]^{+}$ is performed at 50 ºC for 24 hours, $[\mathbf{17}]^{2+}$ is the only species present both in the precipitated solid and in the supernatant. However, when the reaction is performed for only a few hours at 50 ºC, or at 35 ºC for several hours or at r.t. for a few weeks the reaction does not go to completion (starting material remains present) and is less selective.

The mechanism proposed for this reaction (depicted in Figure 3.19) is similar to that proposed for the Me_2-bpa-Bz iridium complex.

Again the formation of an intermediate mono-ethene complex is proposed. By ^{1}H-NMR, however, this complex was never observed in the reaction mixture. For the Me_2-bpa-Bz iridium complex it was proposed that formation of the corresponding mono-vacant trigonal-bipyramidal mono-ethene complex was the reason for the observed oxidative addition of the C-H bond at the 2-position of the benzylic ring. However, for bpa-R rhodium(I) and iridium(I) mono-ethene complexes square planar geometries are expected (see also § 3.5.2 for Rh), since such mono-vacant trigonal-bipyramidal geometry should be able to rearrange barrierless to the corresponding square planar structure. Apparently the square planar iridium(I) mono-ethene complex is so

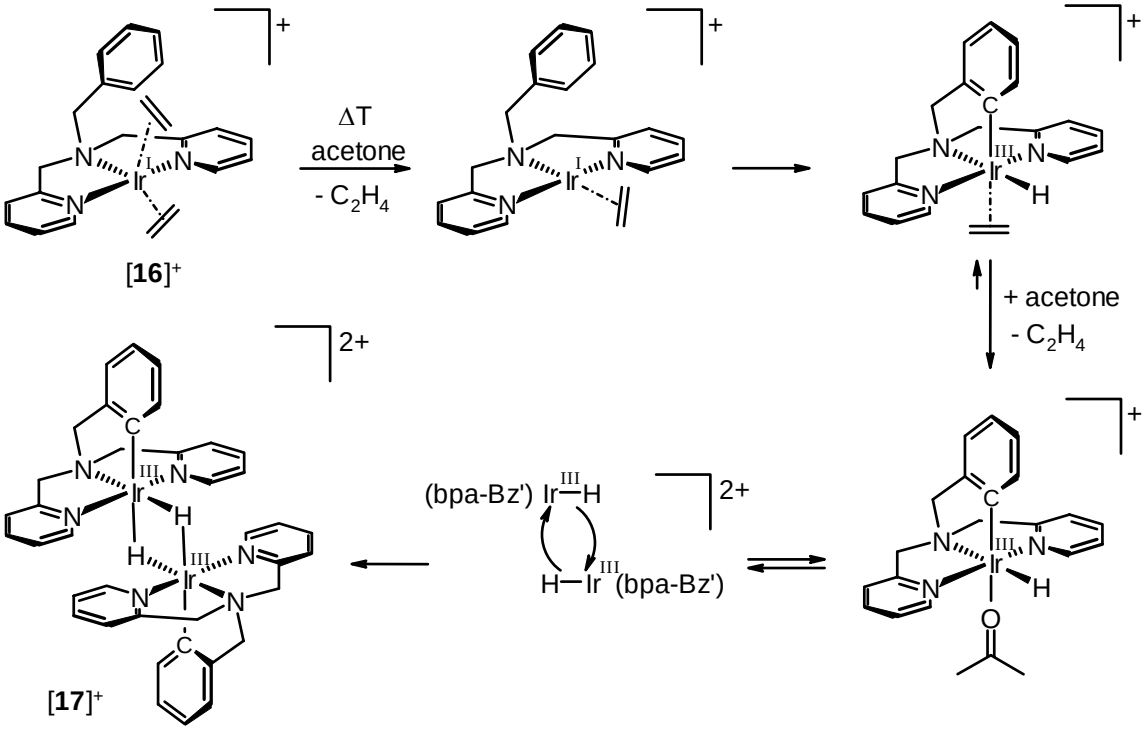

Figure 3.19 *Mechanism proposed for the formation of [**17**]$^{2+}$ from [**16**]$^{+}$*

high in energy, that immediately oxidative addition of an aromatic C-H bond takes place. It is possible that also for the Me_2-bpa-Bz complex the instability of a square planar iridium(I) complex is the main reason why aromatic C-H activation takes place, instead of the previously proposed instability of a mono-vacant trigonal-bipyramidal complex.

In CD_3CN dinuclear complex [**17**]$^{2+}$ forms the acetonitrile-coordinated mono-nuclear iridium(III) hydride species, [(bpa-Bz$^{\#}$)Ir^{III}(H)(CD_3CN)]$^{+}$ ([**18**]$^{+}$). The ^{1}H-signal signal of the original dinuclear complex (δ = -14.73 ppm in acetone-d6, δ = -15.12 in CD_3CN) disappears very rapidly after dissolving, whereas a new hydride signal comes up at δ = -18.30 ppm. After 25 minutes the original dinuclear complex [**17**]$^{2+}$ has converted for 87 % to [**18**]$^{+}$ and goes to completion within an hour. On the basis of ^{1}H-NMR it can be said that for 95 % [**18**]$^{+}$ is formed and that the remaining 5 % consists of an unknown species with a hydride signal at -18.82. This could be the other mononuclear isomer of [**18**]$^{+}$: the one with the hydride *trans* to the carbon instead of *trans* to the amine-nitrogen.
Also ESI^{+}-MS measurements confirm that [**18**]$^{+}$ is a mononuclear complex. Complex [**18**]$^{+}$ is stable at r.t. in CD_3CN.

Dinuclear complex [**17**]$^{2+}$ is stable in acetone in the dark.
However, as soon as an acetone-solution of the complex is exposed to glass-filtered daylight, it starts to react. Within a few hours almost all of the symmetric dinuclear complex [**17**]$^{2+}$ is converted into a new compound, [**19**]$^{2+}$. Based on ^{1}H-COSY, ^{1}H-NOESY and ESI^{+}-MS we propose for [**19**]$^{2+}$ the asymmetric, dinuclear structure displayed in Figure 3.20.
We propose that upon irradiation one of the Ir-H bonds is broken (most probably the one with the carbon *trans* coordinated, which is the weakest Ir-H bond due to the carbon *trans*-effect). Hereafter the dinuclear complex rearranges to the much more stable [**19**]$^{2+}$ in which only one of the bridging hydrides has a carbon *trans* to it. The ^{1}H-NMR signal at δ = -14.90 will probably correspond to the hydride with the carbon *trans* (only a shift of 0.2 ppm to higher field compared to the original dinuclear complex [**17**]$^{2+}$, in which both hydrides have

carbons *trans* coordinated). The hydride with only nitrogen atoms *trans* coordinated will then lie at a chemical shift of -23.92 ppm.

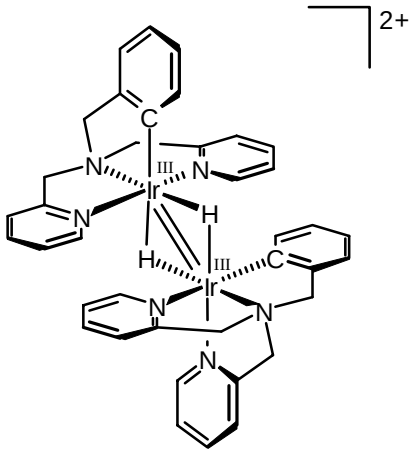

Figure 3.20 *Dinuclear iridium-complex [**19**]$^{2+}$ formed upon irradiation of [**17**]$^{2+}$ with daylight*

Since the latter hydride does not have any carbon-atoms *trans* coordinated anymore, this hydride bridge will be much stronger, therefore making the dinuclear complex more stable.

ESI$^+$-MS measurements show that complex [**19**]$^{2+}$ fragments much less easily than [**17**]$^{2+}$. This seems to confirm that in [**19**]$^{2+}$ the hydride bridge is much stronger than in [**17**]$^{2+}$.

Formation of [**19**]$^{2+}$ stops when a solution of [**17**]$^{2+}$ is no longer exposed to daylight. Upon further exposure of an acetone solution of [**19**]$^{2+}$ to daylight no further rearrangements take place: the other benzyl-ring remains *trans* coordinated to one of the hydrides.

Another indication that the bridge in [**19**]$^{2+}$ is stronger than in [**17**]$^{2+}$ comes from the fact that upon addition of CD_3CN to an acetone-d6 solution of [**19**]$^{2+}$ the dinuclear complex does not fall apart to form [**18**]$^+$ but seems to remain intact. The hydride signals are now observed at δ = -15.05 and -24.06 ppm (instead of -14.90 and -23.92) and the other signals have shifted up to 0.1 ppm to higher field compared to [**19**]$^{2+}$ in acetone-d6. This small shift in the ^{1}H-NMR is probably only due to solvent effects (comparable to the hydride shifts of [**17**]$^{2+}$ in acetone-d6 and CD_3CN).

Also ESI$^+$-MS measurements confirm that the bulk amount present in solution corresponds to the intact dicationic complex [**19**]$^{2+}$.

In addition to [**19**]$^{2+}$ ESI$^+$-MS spectra measured in CH_3CN show the presence of a small amount of an unknown species. It has an m/z and isotope pattern corresponding to {[**19**](CD_3CN)}$^{2+}$. The fact that absolutely no exchange at all has occurred with CH_3CN (which is present in much larger amounts after a 100-fold dilution of the NMR-solution with CH_3CN) is remarkable, since this exchange should be quite rapid and is quite frequently observed. Such exchange was in fact observed for [**18**]$^+$, though for [**14**]$^{2+}$ this exchange with the solvent was not observed at all.

The coordination mode of CD_3CN remains a mystery. It seems very strongly bound to an iridium center, although in [**19**]$^{2+}$ the iridium(III) centers already have a coordination number of 6. Any higher number would be highly unusual. A very slow equilibrium (no exchange with CH_3CN) between [**19**]$^{2+}$ and some seven-coordinate species {[**19**](CD_3CN)}$^{2+}$ seems highly unlikely. Another possibility could be that one of the pyridine rings (preferably the one coordinated *trans* to the benzyl) dissociates from the iridium(III) center and is replaced by CD_3CN. However, this species should then again be in very slow equilibrium with [**19**]$^{2+}$.

^{1}H-NMR spectra do not indicate the presence of {[**19**](CD_3CN)}$^{2+}$ at all.

Apparently we do not look at the same species with NMR as with MS.

One possible (but admittedly unsatisfactory) explanation could be that $\{[\mathbf{19}](CD_3CN)\}^{2+}$ is only present in very small amounts, which could explain its invisibility in the ^{1}H-NMR. Its observation in the mass spectra could then be explained by the fact that apparently $\{[\mathbf{19}](CD_3CN)\}^{2+}$ is better transferred to the gas phase using ESI^+-MS than $[\mathbf{19}]^{2+}$.

The proton spin-lattice relaxation times (T1) were measured for $[\mathbf{17}]^{2+}$ (acetone-d6), $[\mathbf{18}]^+$ (CD_3CN), $[\mathbf{19}]^{2+}$ (both in acetone-d6 and in acetone-d6/CD_3CN). The results are shown in Table 3.6. From such relaxation times one can deduce whether the hydride atoms are terminal or bridging. Bakhmutov *et al.* [26] were even able to calculate metal-hydride and hydride-hydride distances in $[Cp_2NbH^X{}_2H^A]$ on the basis of both selective and nonselective T1 relaxation times.

Table 3.6 *T1 of the hydride signals of the bpa-Bz$^{\#}$ iridium(III) hydride complexes*

Compounds	δ (ppm)	T1 (mseconds)	δ (ppm)	T1 (mseconds)
$[\mathbf{17}]^{2+}$ (acetone-d6)	-14.7	650		
$[\mathbf{18}]^+$ (CD_3CN)	-18.3	2300		
$[\mathbf{19}]^{2+}$ (acetone-d6)	-14.9	725	-23.89	725
$[\mathbf{19}]^{2+}$ (mixture of acetone-d6 and CD_3CN)	-15.0	700	-24.0	700

Since these relaxation times are mainly determined by H-H spin-spin relaxation processes, the large difference in T1 between mononuclear complex $[\mathbf{18}]^+$ and the dinuclear complexes is quite normal and indicates there is no large change in H-H distance on going from $[\mathbf{17}]^{2+}$ to $[\mathbf{19}]^{2+}$, supporting our assumption that not only $[\mathbf{17}]^{2+}$ but also $[\mathbf{19}]^{2+}$ has two bridging hydrides.

3.5 Synthesis and reactivity of N_3 rhodium(I) ethene complexes

3.5.1 Rhodium ethene complexes with sterically demanding Me_2-bpa-R ligands

The Me_2-bpa-R rhodium(I) ethene complexes were synthesized analogously to the N_4 rhodium(I) ethene complexes (§ 3.2) [2]. The resulting products could be precipitated by the addition of KPF_6 as PF_6-salts.
It is likely that, in analogy to the corresponding Me_2-bpa-R iridium complexes, initially rhodium(I) bis-ethene complexes are formed. An indication of this is the color change of the precipitated solid upon removal of the solvent under vacuum from yellow to orange for the Me_2-bpa-Me complex, indicating a change in the coordination surroundings of the metal center.
Also the presence of free ethene in solution upon redissolving the precipitated complexes indicates that the starting material was (or at least contained) the bis-ethene complex.
However, we never observed a rhodium bis-ethene complex in the ^{1}H-NMR. The most likely reason for this is, that mono-cationic rhodium(I) bis-ethene complexes are too unstable to ever be observed in solution at r.t. To our knowledge the only mono-cationic complex for which initial formation of a rhodium(I) bis-ethene complex is reported is a N,N-dimethyl-2,11-diaza[3,3](2,6)pyridinophane complex. [6]
Most of the other 18 VE rhodium(I) bis-olefin complexes reported are neutral complexes with an anionic ligand coordinated to the metal center resulting in a stronger π-backdonation to the olefin. Cyclopentadienyl [27] – [30], indenyl [31] – [33], hydrotris(3,5-dimethylpyrazolyl)borate ligand [34] or even chloride [35] – [38].

Reaction in acetonitrile-d3

Upon dissolving these Me_2-bpa-R rhodium(I) ethene complexes (R = R^1 = Me, Bz) in CD_3CN asymmetric rhodium(I) mono-ethene-CD_3CN complexes, $[(Me_2\text{-bpa-Me})Rh^I(C_2H_4)(CD_3CN)]^+$ ([**20**]$^+$) and $[(Me_2\text{-bpa-Bz})Rh^I(C_2H_4)(CD_3CN)]^+$ ([**21**]$^+$), are obtained (Figure 3.21).

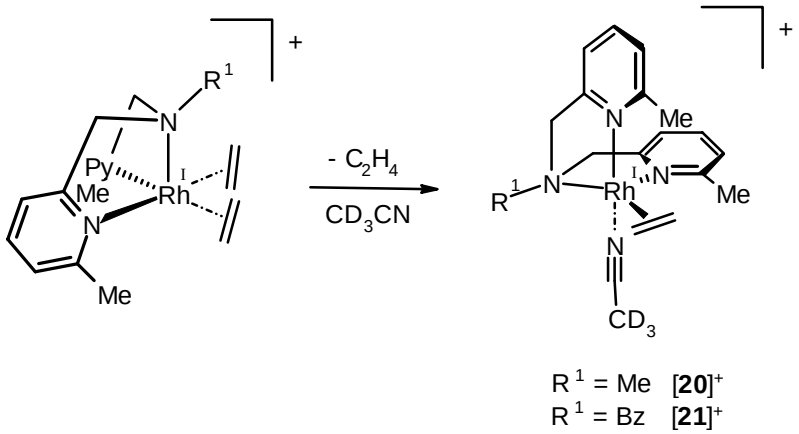

Figure 3.21 *Reaction of $[(\kappa^3\text{-}Me_2\text{-bpa-R})Rh^I(C_2H_4)]^+$ in CD_3CN to form [**20**]$^+$ and [**21**]$^+$*

^{1}H-NMR data of [**20**]$^+$ and [**21**]$^+$ reveal two non-equivalent N-CH_2-Py groups. The diastereotopic methylene protons of the two non-equivalent N-CH_2-Py groups give rise to four AB-type doublets. In the case of the rhodium Me_2-bpa-Bz complex also the N-CH_2-Ph protons have become diastereotopic. For both complexes the orientation of the olefin is frozen out on the NMR timescale: four multiplets with rhodium coupling can be observed between δ = 1.0 and 2.5 ppm.

Therefore we propose for the asymmetric complexes [**20**]$^+$ and [**21**]$^+$ the ligand to be facially coordinated and that there is no exchange between the coordinated ethene fragment and CD_3CN molecule. Whether these five-coordinate complexes have a trigonal-bipyramidal (as shown in Figure 3.21) or a square-pyramidal structure could not be determined.

From ^{1}H-NMR it can be concluded that for both Me_2-bpa-R compounds a small amount of a second, symmetric species is also present, which does not have an olefin coordinated anymore. This is probably $[(Me_2\text{-bpa-R})Rh(CD_3CN)]^+$, since upon measuring an ESI$^+$-MS spectrum of these compounds in CH_3CN the base peak in the MS spectrum corresponds to this same solvent-coordinated complex, indicating that the olefin in the ethene-MeCN complex is not very strongly bound to the metal center.

Reaction in acetone-d6

In acetone-d6 the Me_2-bpa-R rhodium(I) ethene complexes (R = R^1 = Me, Bz) behave quite differently than in CD_3CN. For both complexes initially two mono-ethene complexes, a symmetric and an asymmetric one, can be observed by ^{1}H-NMR. The structures proposed for these complexes are displayed in Figure 3.22.

In the case of the asymmetric complexes [**22a**]$^+$ and [**23a**]$^+$ the N_3 ligand must be facially coordinated. However, whether in the case of the symmetric complexes [**22b**]$^+$ and [**23b**]$^+$ the N_3 ligand is facially or meridionally coordinated, cannot be deduced from ^{1}H-NMR, NOESY or COSY. In a *mer* geometry solvent coordination is not necessary, however in the *fac*-trigonal-bipyramidal structure the fifth coordination site needs to be occupied by some donor S. In the asymmetric complexes also coordination of S is necessary.

Whether S is a solvent molecule, H_2O or something else is unknown for all structures. For solvents with strong coordinating properties like acetonitrile, such coordination is well known and also observed in [**20**]$^+$ and [**21**]$^+$. However, for a weakly coordinating solvent like acetone such coordination in 18 VE complexes is remarkable and has not been reported before.

Only a few complexes in which acetone is coordinated to the metal center have been reported: all are highly reactive four-coordinate 16 VE rhodium(I) species. [39] – [42]

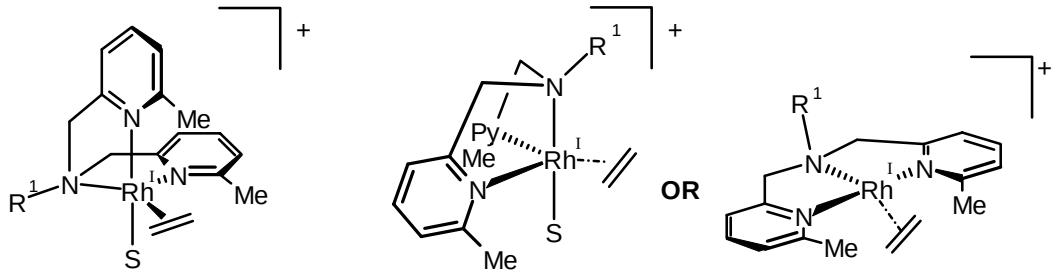

R^1 = Me [**22a**]$^+$
R^1 = Bz [**23a**]$^+$

R^1 = Me [**22b**]$^+$
R^1 = Bz [**23b**]$^+$

Figure 3.22 *Reaction products from dissolving [(Me_2-bpa-R)$Rh^I(C_2H_4)_2$]PF_6 in acetone-d6*

It is strange that for Me_2-bpa-Me and for Me_2-bpa-Bz in acetone-d6 both the symmetric and the asymmetric mono-ethene complex present, whereas in CD_3CN only the asymmetric mono-ethene complex can be observed.
If the symmetric mono-ethene complexes in acetone-d6 ([**22b**]$^+$ and [**23b**]$^+$) have a coordination number of four and not five (i.e. no solvent coordinated), it can be expected that in the weaker coordinating acetone-d6 these species are present in much larger quantities than in the strongly coordinating CD_3CN. Otherwise the stronger preference for the symmetric compound in acetone-d6 compared to CD_3CN cannot easily be explained.

The Me_2-bpa-Me rhodium mono-ethene complexes [**22a**]$^+$ and [**22b**]$^+$ are only moderately stable: after a few days in solution in acetone-d6 they decompose, leaving a mixture of unidentifiable products behind.
The Me_2-bpa-Bz rhodium(I) mono-ethene complexes [**23a**]$^+$ and [**23b**]$^+$, however, are not stable at all in acetone. Within about an hour both mono-ethene species seem to have disappeared and the major product formed in about 55 % yield (on the basis of ^{1}H-NMR) is an asymmetric ethyl complex, [(Me_2-bpa-Bz$^{\#}$)Rh(C_2H_5)(acetone-d6)]$^+$ ([**24**]$^+$), which must be the result of aromatic C-H activation and subsequent insertion of the olefin into the rhodium-hydride bond (Figure 3.23).
Among the rest of the signals 2 symmetric species, [**Y**]$^+$ and [**X**]$^+$, can be identified as being present in largest amounts. Complex [**Y**]$^+$ seems to have an olefin coordinated to the metal center, though its chemical shifts are a bit different from [**23b**]$^+$. For complex [**X**]$^+$ it was not possible to identify the olefin; this might be [(Me_2-bpa-Bz)Rh(acetone-d6)]$^+$. What is clear from NOESY spectra, is that these two symmetric species exchange on the NMR timescale. The structure of these two symmetric species could not be further elucidated, since they could not be isolated and their intensity in the ^{1}H-NMR is too low to distinguish them from the other signals present in the NMR spectra.

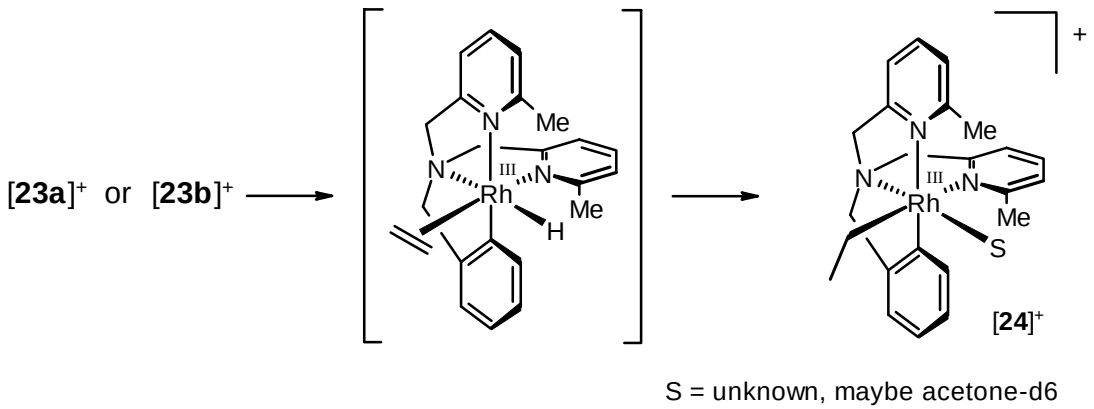

Figure 3.23 *Reaction of Me_2-bpa-Bz rhodium(I) ethene in acetone*

NOE contacts of one of the diastereotopic methylene protons of the Rh-ethyl group of [**24**]$^+$ with two AB-doublets, indicate that the ethyl group must be *cis*-coordinated to the amine-nitrogen atom.

The reaction of the Me_2-bpa-Bz rhodium(I) ethene complexes in acetone-d6 occurs very rapidly. Already 10 minutes after dissolving the ratio between the major species present in solution is
[**23a**]$^+$ **:** [**23b**]$^+$ **:** [**24**]$^+$ **:** [**X**]$^+$ = 54 : 24 : 16 : 7.
After 2 hours this ratio has become [**24**]$^+$: [**X**]$^+$: [**Y**]$^+$ = 55 : 27 : 17.
Apparently the ratio between symmetric and asymmetric species remains about fifty-fifty. This could imply that [**24**]$^+$ is only formed from a reaction of the asymmetric mono-ethene complex [**23a**]$^+$ and not from the symmetric mono-ethene complex [**23b**]$^+$.

Apparently for these mono-cationic rhodium(III) complexes the ethene-hydride species is less stable than for iridium: For the corresponding Me_2-bpa-Bz$^{\#}$ iridium complex the ethene-hydride species could be isolated (§ 3.4.1). In the case of the Me_2-bpa-Bz$^{\#}$ rhodium species no hydride signal can be observed by ^{1}H-NMR, insertion of the olefin into the Ir-H bond immediately takes place. Apparently the electron density on the mono-cationic rhodium(III) center is too low to facilitate olefin coordination. That it should be possible for rhodium to isolate an ethene-hydride species provided the electron density on the metal center is high enough, is shown by Ruiz *et al.* [43], who were able to isolate an
(η^2-ethene)hydrido(η^5-pentamethylcyclopentadienyl)(silyl)rhodium species.

3.5.2 Rhodium(I) ethene complexes with sterically less demanding bpa-R ligands

The synthesis of [(bpa-Me)$Rh^I(C_2H_4)$]$^+$ ([**26**]$^+$) and [(bpa-Bz)$Rh^I(C_2H_4)$]$^+$ ([**27**]$^+$) was already described in literature. [44] The analogous bpa rhodium ethene complex ([**25**]$^+$) was prepared accordingly. The resulting products could be precipitated by the addition of KPF_6 or $NaBPh_4$ as PF_6 or BPh_4 salts.
Again there are indications that initially rhodium(I) bis-ethene complexes are formed. In the case of the bpa-Me complex there is a color-change from light yellow to orange upon removal of the solvent from the precipitated salt by applying vacuum. However, we did not observe any rhodium bis-ethene complexes with ^{1}H-NMR at r.t. [5]

Such bpa-R rhodium(I) bis-ethene complexes will most probably have the N_3 ligand coordinated in a meridional fashion, analogously to the corresponding bpa-R iridium(I) bis-ethene complexes ([**13**]$^+$, [**15**]$^+$ and [**16**]$^+$).

When the obtained products are dissolved in CD_2Cl_2 or acetone-d6 clearly mono-ethene complexes like the ones depicted in Figure 3.24 are visible in the ^{1}H- and ^{13}C-NMR.

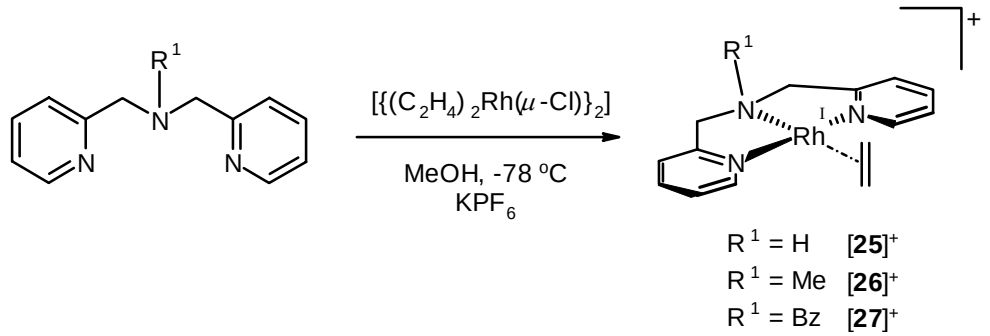

Figure 3.24 *Synthesis of [(κ^3-bpa-R)$Rh^I(C_2H_4)_2$]$^+$ (R = R^1 = H, Me, Bz)*

[5] Measuring NMR spectra at -60 °C under an ethene atmosphere could have resulted in the observation of *mer*-N_3 bis-ethene complexes, in analogy with the bpa-R iridium complexes.

The ^{1}H-NOE patterns of [**25**]$^+$, [**26**]$^+$ and [**27**]$^+$, are characteristic of a *mer*-coordination mode of the bpa-R ligand. Clear NOE contacts are observed between the coordinated ethene molecule and the Py-*H6*. No NOE contact is observed between the coordinated olefin and one of the N-C*H*$_2$-Py methylene protons. This is in contrast with for example Me$_2$-bpa-Me iridium mono-ethene complex [**8**]$^+$, in which the ethene fragment has moved to a position below the *mer*-(Me$_2$-bpa-Me)Ir plane, away from the methyl substituents at the 6-position of the pyridine rings, which does show NOE contacts between the olefin and one of the N-C*H*$_2$-Py protons. Therefore, it can be concluded that the bpa-R rhodium mono-ethene complexes have a less distorted square planar geometry.

Acetone-d6 solutions of [**25**]$^+$ and [**27**]$^+$ were heated to about 50 ºC for about a day in order to check whether similar reactivity could be observed as was seen for the corresponding iridium complexes, [**13**]$^+$ and [**16**]$^+$ (§ 3.4.2). The reactions were followed in time. The bpa rhodium ethene complex ([**25**]$^+$) decomposed upon heating, whereas the bpa-Bz rhodium ethene complex did not react at all.

In acetonitrile the bpa-R rhodium ethene complexes are not stable at all. All three readily lose the olefin. In the case of [**26**]$^+$ and [**27**]$^+$ the acetonitrile adduct [(L$_N$)Rh(CD$_3$CN)]$^+$ is selectively formed, whereas for [**25**]$^+$ a complex mixture is obtained.

3.6 DFT-calculations on the stability of mono- *versus* bis-ethene complexes

In order to obtain more insight in the observed differences between the N_3 complexes in the observed formation of mono- or bis-ethene complexes and in the type of bis-ethene complexes obtained (e.g. N_3 coordinated in a meridional or a facial fashion, Figure 3.25) DFT calculations were performed (for details see Appendix A). In Table 3.7 the free energies $\Delta G_{298\ K,\ 1\ bar.}$ and free enthalpies $\Delta H_{0\ K}$ for four types of mono- and bis-ethene complexes for rhodium and iridium are presented.

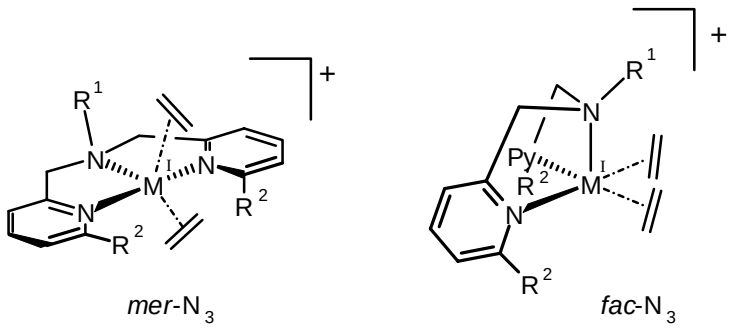

Figure 3.25 *Types of bis-ethene complexes obtained for [(N$_3$)M(C$_2$H$_4$)$_2$]$^+$*

Table 3.7 *Computational results for N_3 mono- and bis-ethene complexes: free energies (relevant to reactions in solution) and enthalpies (relevant to collision-induced reactions) in kcal/mol*

Complex	Rhodium		Iridium	
	$\Delta G_{298\ K,\ 1\ bar}$	$\Delta H_{0\ K}$	$\Delta G_{298\ K,\ 1\ bar}$	$\Delta H_{0\ K}$
[(bpa)M]$^+$	(0.0)	(0.0)	(0.0)	(0.0)
[(bpa)M(C$_2$H$_4$)]$^+$	-18.1	-30.2	-27.3	-39.5
[(bpa)M(C$_2$H$_4$)$_2$]$^+$ (*fac*)	-3.7	-26.5	-17.1	-40.7
[(bpa)M(C$_2$H$_4$)$_2$]$^+$ (*mer*)	-5.0	-29.7	-18.1	-42.9

Complex	Rhodium		Iridium	
	$\Delta G_{298\ K,\ 1\ bar}$	$\Delta H_{0\ K}$	$\Delta G_{298\ K,\ 1\ bar}$	$\Delta H_{0\ K}$
$[(bpa\text{-}Me)M]^+$	(0.0)	(0.0)	(0.0)	(0.0)
$[(bpa\text{-}Me)M(C_2H_4)]^+$	-18.7	-30.6	-27.3	-39.3
$[(bpa\text{-}Me)M(C_2H_4)_2]^+$ (*fac*)	-2.0	-25.3	-14.2	-38.6
$[(bpa\text{-}Me)M(C_2H_4)_2]^+$ (*mer*)	-4.8	-29.5	-17.1	-41.9
$[(Me_2\text{-}bpa)M]^+$	(0.0)	(0.0)	(0.0)	(0.0)
$[(Me_2\text{-}bpa)M(C_2H_4)]^+$	-1.3	-13.9	-7.0	-20.5
$[(Me_2\text{-}bpa)M(C_2H_4)_2]^+$ (*fac*)	8.2	-16.4	-4.4	-29.9
$[(Me_2\text{-}bpa)M(C_2H_4)_2]^+$ (*mer*)	9.2	-16.2	-4.0	-29.3
$[(Me_2\text{-}bpa\text{-}Me)M]^+$	(0.0)	(0.0)	(0.0)	(0.0)
$[(Me_2\text{-}bpa\text{-}Me)M(C_2H_4)]^+$	-2.5	-14.9	-8.1	-21.2
$[(Me_2\text{-}bpa\text{-}Me)M(C_2H_4)_2]^+$ (*fac*)	9.4	-15.3	-3.6	-28.1
$[(Me_2\text{-}bpa\text{-}Me)M(C_2H_4)_2]^+$ (*mer*)	10.4	-14.9	-2.1	-27.4

The binding energy of the second ethene molecule is lower for the bpa-R complexes than for the Me_2-bpa-R complexes. For bpa-R *mer* bis-ethene complexes are more stable than *fac* ones, whereas for Me_2-bpa-R this stability is reversed. Finally iridium binds the second ethene stronger than rhodium.

The enthalpies $\Delta H_{0\ K}$ of the bis-ethene complexes are similar or lower than those of the corresponding mono-ethene complexes, indicating that in the gas phase bis-ethene complexes should be stable.

According to the free energies $\Delta G_{298\ K,\ 1\ bar}$, which should describe solution phase behavior, all bis-ethene complexes are less stable than the corresponding mono-ethene complexes.
This is in contrast to the reactivities observed in solution. For iridium very stable *mer* bpa-R bis-ethene complexes were obtained, whereas for Me_2-bpa-R somewhat less stable *fac* bis-ethene complexes could be isolated. For rhodium the Me_2-bpa-R bis-ethene complexes could only be observed with ^{1}H-NMR in solution, and for bpa-R we only have indirect indications that bis-ethene complexes are formed initially.
Possibly the metal-olefin binding energies are underestimated due to the fact that not all relativistic effects have been accounted for in our calculations. [6]

3.7 Conclusions

A few interesting observations can be made when an overview of the reactivities described in this chapter is made:

– Iridium complexes seem to have a stronger tendency to remain five-coordinate (to form very stable bis-ethene complexes) than their corresponding rhodium analogues.
– Potentially square planar N_3 metal-olefin complexes are unexpectedly reactive with regard to intramolecular C-H and N-H activation.

[6] Calculations were carried out with a non-relativistic formalism, but using relativistic effective core potentials for Rh and Ir. This means that indirect relativistic effects like changes of d-orbital levels are included in an approximate way, but spin-orbit coupling is not included at all.

This reactivity decreases on going from iridium to rhodium and on going from the sterically bulky Me_2-bpa-R complexes to the sterically less demanding bpa-R complexes.

– Methyl substituents at the 6-position of the pyridine rings of the nitrogen donor ligands seem to increase the reactivity of the metal-olefin complexes

– Although the radii of the rhodium and iridium centers are similar, there is a clear difference in behavior between analogous complexes. Iridium has a stronger tendency to the formation of 18 VE complexes, and undergoes more easily aromatic C-H or N-H activation.

3.8 Experimental section

3.8.1 General methods

All procedures were performed under a nitrogen atmosphere using standard Schlenck techniques, unless indicated otherwise. Solvents (p.a.) were deoxygenated by bubbling through a stream of nitrogen or by the freeze-pump-thaw method. The temperature indication r.t. corresponds to ca. 20 ºC.

NMR experiments were carried out on a Bruker DPX200 (200 MHz and 50 MHz for ^1H and ^{13}C respectively), a Bruker AC300 (300 MHz and 75 MHz for ^1H and ^{13}C respectively), a Varian Inova 400 (400 MHz and 100 MHz for ^1H and ^{13}C respectively). Solvent shift references for ^1H-NMR are: CD_2Cl_2 δ (^1H) = 5.31 ppm, CD_3CN δ (^1H) = 1.94 ppm, methanol-d4 δ (^1H) = 3.35 ppm and acetone-d6 δ (^1H) = 2.05 ppm. Solvent shift references for ^{13}C-NMR are: CD_3CN δ (^{13}C) = 1.24 (and 118.25), CD_2Cl_2 δ (^{13}C) = 54.20, methanol-d4 δ (^{13}C) = 49.3 ppm and acetone-d6 δ (^{13}C) = 29.83 ppm (and 206.18 ppm). Abbreviations used are: s = singlet, d = doublet, dd = double doublet, ddd = double doublet of doublets, t = triplet, dt = double triplet, q = quartet, qq = quartet of quartets, m = multiplet, dm = double multiplet, br. = broad.

Spin-lattice relaxation times (T1) were measured at 298 K and at 500 MHz.

Since the κ^4-N_4 mono-ethene complexes have one equatiorial pyridine ring and two axial pyridine rings, the NMR signals belonging to the different rings will be assigned as shown below. In the case of the asymmetric Me_2-tpa complexes a third type of pyridine-assignment will be introduced (Figure 3.26). And since the κ^3-bpa-R iridium(I) bis-ethene complexes have two chemically different ethene molecules (one above the trigonal plane having NOE contacts with the amine-R group (C_2H_4, A), the other below this plane (C_2H_4, B)), the NMR signals belonging to the different olefins and the diastereotopic methylene protons of the N-CH_2-Py groups will be assigned as shown in Figure 3.26.

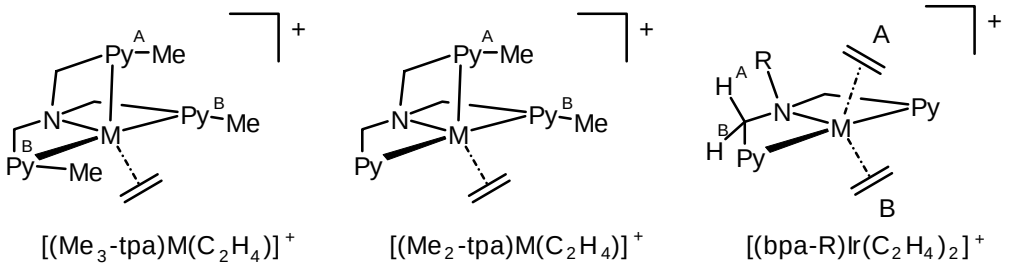

Figure 3.26 *Assignment of NMR signals of different groups*

Elemental analysis (C,H,N) were carried out on a Carlo Erba NCSO-analyser.

Mass spectra (ESI- or FAB-MS) were recorded on a Finnigan MAT 900S (Radboud University Nijmegen), a Finnigan TSQ 700 (ETH-Zurich) or a Finnigan TSQ 7000 (ETH-Zurich). All spectra were obtained in the positive ion mode. Daughter ion spectra were measured on the TSQ 700 and TSQ 7000 using argon as a collision gas.

Bpa-Me [44], bpa-Bz [45], tpa [46], Me-tpa [47], Me_3-tpa [47], [(bpa-Me)Rh(C_2H_4)]PF_6 [44], [(bpa-Bz)Rh(C_2H_4)]PF_6 [44], [(tpa)Rh(C_2H_4)]PF_6 [2], [(Me-tpa)Rh(C_2H_4)]PF_6 [2], [(tpa)Ir(C_2H_4)]PF_6 [6], [(Me-tpa)Ir(C_2H_4)]PF_6 [6], [{(C_2H_4)$_2$Rh(μ-Cl)}$_2$] [48] and [{(coe)$_2$Ir(μ-Cl)}$_2$] [8] were prepared according to literature procedures.

All other chemicals are commercially available and were used without further purification, unless stated otherwise.

We thank Johnson Matthey Ltd for a generous loan of $RhCl_3.H_2O$.

3.8.2 X-ray diffraction

*[(Me$_3$-tpa)Ir^I(C$_2$H$_4$)$_2$]PF$_6$ ([**3**]PF$_6$)*

Crystals suitable for X-ray diffraction were obtained from crystallization from methanol at -20 ºC.

A single crystal was mounted in air on a glass fiber. Intensity data were collected at 293 K. An Enraf-Nonius CAD4 single-crystal diffractometer was used, applying graphite monochromatized CuK_α radiation. Unit cell dimensions were determined from the angular setting of 22 reflections for [**3**]PF$_6$. Intensity data were corrected for Lorentz and polarisation effects. Semi-empirical absorption correction (ψ-scan) was applied. [49] The structure was solved by the program system DIRDIF [50] using the program PATTY [51] to locate the heavy atoms. Its structure was refined with standard methods (refinement against F^2 of reflections with Io > 2σ (Io) using SHELXL97 [52]) with anisotropic parameters for the nonhydrogen atoms. Hydrogen atoms were placed at calculated positions and were subsequently refined isotropically in riding mode.

The assignment of atomic species has been made on the basis of prior occupancy factor refinement and comparison of thermal displacement parameters.

The structure determination was hampered by the poor quality of the data caused by the inferior quality of the crystals, which was, unfortunately, the best that could be achieved. The crystal diffracted very weakly, and no reliable data could be collected above 55 degrees theta (resolution 0.95 A). Moreover a more than average crystal decay was observed, up to 17%. No attempt was made to locate the hydrogen atoms attached to the disordered CH_3OH and partially occupied H_2O moieties: they cannot be calculated and no indication whatsoever of their location was found in the difference fourier map. From the anisotropic thermal displacement parameters for the PF_6 moiety it is clear that these atoms show a large positional disorder. Although it is possible to use several partially occupied positions for these atoms, no physically reasonable model results from these parameters, at least not any better than the model presented here.

Because the EMPABS procedure [49] by itself was not adequate enough, caused presumably by the poor quality of the data and hence of the ψ-scans, an additional absorption correction was applied using the DIFABS procedure. [53] Even then it was necessary to use the SIMU option in the least-squares refinement to end up with physically acceptable anisotropic thermal displacement parameters. Geometrical calculations (PLATON-93) [54] revealed neither unusual geometric features, nor unusual short intermolecular contacts. The calculations revealed no higher symmetry and no (further) solvent accessible areas.

*[(Me$_3$-tpa)Ir^I(C$_2$H$_4$)]PF$_6$ ([**4**]PF$_6$)*

Transparent brown-red crystals suitable for X-ray diffraction were obtained from a dichloromethane solution top-layered with hexane at 4 ºC.

A single crystal was mounted in air on a glass fiber. Intensity data were collected at 293 K. An Enraf-Nonius CAD4 single-crystal diffractometer was used, applying graphite monochromatized MoK_α radiation. Unit cell dimensions were determined from the angular setting of 25 reflections. The structure was solved by the program system DIRDIF [50] using the program PATTY [51] to locate the heavy atoms. The structure was refined with standard methods (refinement against F^2 of reflections with $I_o > 2\sigma$ (I_o) using SHELXL97 [52]) with anisotropic temperature factors for the nonhydrogen atoms. The hydrogen atoms were placed at calculated positions, refined isotropically in riding mode, and were subsequently refined freely. The EMPABS procedure [49] by itself was not adequate enough. The difference fourier map showed peaks up to 3.6 e.A^{-3} close to the Ir atom. Therefore an additional absorption correction was applied using the DIFABS procedure [53], resulting in final residual peaks up to 2.3 e.A^{-3}.

Based on geometrical considerations alone, the unit cell could be transformed to a orthorhombic C-cell (a = 9.1795(19), b = 46.2562(78), c = 11.5840(17) Å), but this transformation is not supported by the symmetry of the data (R(int) = 0.549) nor by the unit cell contents.

Geometrical calculations [54] revealed neither unusual geometric features, nor unusual short intermolecular contacts. The calculations revealed no higher symmetry and no (further) solvent accessible areas.

*[(Me$_2$-tpa)Ir^I(C$_2$H$_4$)]PF$_6$ ([**6**]PF$_6$)*

Crystals suitable for X-ray diffraction were obtained from vapor diffusion of hexane into an acetone solution.

A single crystal was mounted in air on a glass fiber. Intensity data were collected at 293 K. An Enraf-Nonius CAD4 single-crystal diffractometer was used, applying graphite monochromatized MoK_α radiation. Unit cell dimensions were determined from the angular setting of 25 reflections. The structure was solved by the program system DIRDIF [50] using the program PATTY [51] to locate the heavy atoms. The structure was refined with standard methods (refinement against F^2 of reflections with Io > 2σ (Io) using SHELXL97 [52]) with anisotropic temperature factors for the nonhydrogen atoms. The hydrogen atoms were placed at calculated positions and refined isotropically in riding mode.

Geometrical calculations [54] revealed neither unusual geometric features, nor unusual short intermolecular contacts. The calculations revealed no higher symmetry and no (further) solvent accessible areas.

*[{(bpa$^{\#}$)Ir^{III}(C$_2$H$_5$)(CH$_3$CN)}$_2$](PF$_6$)$_2$ ([**14**](PF$_6$)$_2$)*

Crystals suitable for an X-ray structure determination were obtained from vapor diffusion of diethylether into an acetonitrile solution at r.t.

A single crystal was mounted in air on a glass fiber. Intensity data were collected at 150 K. A Nonius KappaCCD with area detector, φ and ω scans, was used, applying graphite monochromatized MoK_α radiation. Unit cell dimensions were determined from the angular setting of 12483 reflections. The structures were solved by the program system DIRDIF [50] using the program PATTY [51] to locate the heavy atoms. The structure was refined with standard methods (refinement against F^2 of reflections with $I_o > 2\sigma(I_o)$ using SHELXL97 [52]). All nonhydrogen atoms were refined with anisotropic temperature factors, except C4A and C4B. The hydrogen atoms were placed at calculated positions, and refined isotropically in riding mode.

The compound crystallizes in the rather highly symmetrical space group I 4$_1$/acd. The dinuclear iridium complex forms a dimer around an inversion center. The end-of-chain carbon atom C4 is rather disordered and has been split up over two separate positions. However, it proved to be impossible to refine these two positions anisotropically. The hydrogen atoms calculated on C4A, C4B and C3 should be considered unreliable.

The space group has a multiplicity of the general position of 32 and thus the cell unit contains 16 molecules (Z=16) $C_{32}H_{40}N_8Ir_2.2(PF_6)$. The P atoms of the PF_6 moieties occupy three special positions and especially the PF_6 moieties around P2 and P3 are highly disordered and should be considered very unreliable. Lowering the symmetry did not solve any of the problems described here. On the contrary, various atoms got unacceptable thermal displacement parameters (non-positive definite) or could not be located at all in the fourier map.

Geometrical calculations with PLATON [54] revealed neither unusual geometric features, nor unusual short intermolecular contacts. The calculations revealed no higher symmetry and no (further) solvent accessible areas.

*[{(bpa-Bz$^{\#}$)Ir^{III}(H)}$_2$](PF$_6$)$_2$ ([**17**](PF$_6$)$_2$)*

Crystals suitable for X-ray diffraction of this same compound were obtained when an acetone solution of [**16**]$^+$ was allowed to stand at r.t. for three weeks.

A single crystal was mounted in air on a glass fiber. Intensity data were collected at 208 K. A Nonius KappaCCD with area detector, φ and ω scans, was used, applying graphite monochromatized MoK_α radiation. Unit cell dimensions were determined from the angular setting of 31699 reflections. The structure was solved by the program system DIRDIF [50] using the program PATTY [51] to locate the heavy atoms. The structure was refined with standard methods (refinement against F^2 of reflections with $I_o > 2\sigma(I_o)$ using SHELXL97 [52]). All nonhydrogen atoms were refined with anisotropic temperature factors. The hydrogen atoms were placed at calculated positions, and refined isotropically in riding mode.

The structure consists of the Ir-complex dimerized via an inversion center, two acetone moieties and a rather disordered PF_6 moiety. The Ir-Ir distance is 2.6877(6) Å.

Geometrical calculations with PLATON [54] revealed neither unusual geometric features, nor unusual short intermolecular contacts. The calculations revealed no higher symmetry and no (further) solvent accessible areas.

Selected bond lengths and angles are summarized in Tables 3.1 - 3.6. Drawings were generated with the program PLATON. [54] Other relevant crystal data are summarized in Table 3.8 and Table 3.9.

Table 3.8 *Crystallographic data for [**3**]PF$_6$, [**14**](PF$_6$)$_2$ and [**17**](PF$_6$)$_2$*

	[**3**]PF$_6$.CH$_3$OH.½H$_2$O	[**14**](PF$_6$)$_2$	[**17**](PF$_6$)$_2$.4(CH$_3$)$_2$CO
Empirical formula	$C_{25.5}H_{36}F_6O_{1.5}N_4PIr$	$C_{32}H_{40}F_{12}Ir_2N_8P_2$	$C_{25}H_{30}F_6Ir_1N_3O_2P_1$
Crystal size [mm]	0.63x0.28x0.13	0.62 x 0.50 x 0.39	0.70 x 0.70 x 0.22
Crystal color	Transparent yellow	Light yellow-green	Transparent brown-red
Formula weight	759.75	1211.06	741.69
T [K]	293(2)	150(2)	208(2)
Crystal system	Orthorhombic	Tetragonal	Monoclinic
Space group	Pbcn	I 4$_1$/a c d	P 2$_1$/c

	[**3**]$PF_6.CH_3OH.½H_2O$	[**14**]$(PF_6)_2$	[**17**]$(PF_6)_2.4(CH_3)_2CO$
a [Å]	31.9939(19)	21.8924(7)	12.0391(14)
b [Å]	12.1203(8)	21.8924(7)	15.756(2)
c [Å]	14.7332(8)	32.8309(8)	14.3507(18)
α [°]	90	90	90
β [°]	90	90	94.045(11)
γ [°]	90	90	90
V [$Å^3$]	5713.2(6)	15735.1(8)	2715.3(6)
$\rho_{calcd.}$ [gcm^{-3}]	1.767	2.045	1.814
Z	8	16	4
Diffractometer (scan)	Enraf-Nonius CAD4 (ω-scan)	Nonius KappaCCD area detector ϕ and ω scan	Nonius KappaCCD area detector ϕ and ω scan
Radiation	CuK_α	MoK_α (graphite mon.)	MoK_α (graphite mon.)
Wavelength [Å]	1.54184	0.71073	0.71073
F(000)	3000	9280	1452
θ range [°]	3.90 to 54.96	1.81 to 25.12	3.13 to 25.00
Index ranges	$-33 \le h \le 0$	-25<=h<=22	-14<=h<=14
	$-12 \le k \le 0$	-26<=k<=26	-18<=k<=18
	$-15 \le l \le 0$	-38<=l<=39	-17<=l<=17
Measured reflections	3586	12483	31699
Unique reflections	3586	2952	4656
Observed refl. [$I_o > 2\sigma(I_o)$]	1688	2406	3811
Refined parameters	357	259	384
Goodness-of-fit on F^2	1.110	1.029	1.110
R [$I_o > 2\sigma(I_o)$]	0.0844	0.0585	0.0381
WR^2 [all data]	0.2202	0.1142	0.1285
ρ_{fin} (max/min) [e. $Å^{-3}$]	1.017 / -0.891	2.222 / -1.219	1.969 / -2.221

Table 3.9 *Crystallographic data for [**4**]PF_6, and [**6**]PF_6*

	[**4**]PF_6	[**6**]PF_6
Empirical formula	$C_{23}H_{28}F_6IrN_4P$	$C_{22}H_{26}F_6IrN_4P$
Crystal size [mm]	0.45 x 0.21 x 0.12	0.53 x 0.48 x 0.26
Crystal color	Transparent brown-red	Transparent red-brown
Formula weight	697.66	683.64
T [K]	293(2)	293(2)
Crystal system	Monoclinic	Monoclinic
Space group	P 21/c	P 21/c
a [Å]	9.1802(19)	13.9423(10)
b [Å]	11.5828(18)	13.2295(14)
c [Å]	23.581(4)	14.7294(15)
α [°]	90	90
β [°]	101.193(19)	116.392(10)
γ [°]	90	90
V [$Å^3$]	2459.7(7)	2433.7(4)

	[**4**]PF_6	[**6**]PF_6
$\rho_{calcd.}$ [gcm^{-3}]	1.884	1.866
Z	4	4
Diffractometer (scan)	Enraf-Nonius	Enraf-Nonius
	CAD4 ($\omega/2\theta$-scan)	CAD4 ($\omega/2\theta$-scan)
Radiation	MoK_α (graphite mon.)	MoK_α (graphite mon.)
Wavelength [Å]	0.71073	0.71073
F(000)	1360	1328
θ range [°]	2.87 to 27.49	2.78 to 27.49
Index ranges	0<=h<=11	-18<=h<=0
	-15<=k<=0	-17<=k<=0
	-30<=l<=30	-17<=l<=19
Measured reflections	5961	5783
Unique reflections	5616	5560
Observed refl. [$I_o > 2\sigma(I_o)$]	3815	4362
Refined parameters	319	309
Goodness-of-fit on F^2	1.064	1.106
R [$I_o > 2\sigma(I_o)$]	0.0529	0.0444
wR^2 [all data]	0.1314	0.1140
ρ_{fin} (max/min) [e. $Å^{-3}$]	2.249 and -2.322	2.909 and -1.382

3.8.3 Synthesis

N-methyl-N,N-di[(6-methyl-2-pyridylmethyl)]amine (Me_2-bpa-Me)

To 300 ml. CH_3CN, 7.98 gram (44.8 mmol) 2-chloromethyl-6-methylpyridine.HCl, [55] 2.27 gram (33.6 mmol) CH_3NH_2.HCl, 25.00 gram Na_2SO_4 and 47.50 gram Na_2CO_3 were added. The resulting suspension was heated to reflux for 16 hours. The mixture was filtered and the filtrate was evaporated yielding a brown oil, to which 100 ml. Et_2O was added. Partial evaporation of the solvent resulted in precipitation of Me_2-dpa-Me as a white solid (> 95% pure according to GC), which was crystallised as white crystals from a saturated hexane solution at -20°C. Yield 2.52 gram (16.8 mmol, 50%). An alternative synthetic route to Me_2-dpa-Me has been reported, mentioning its melting point and C, H, N analysis. [56]

^{1}H-NMR (200.13 MHz, $CDCl_3$, 289 K): δ (ppm) = 7.54 (t, 2H, ^3J(H,H)= 7.7 Hz, Py-H4), 7.34 (d, 2H, ^3J(H,H)= 7.7 Hz, Py-H3), 7.00 (d, 2H, ^3J(H,H)= 7.7 Hz, Py-H5), 3.74 (s, 4H, N-*C*H_2-Py^{Me}), 2.54 (s, 6H, Py-*C*H_3), 2.30 (s, 3H, N-*C*H_3).

^{13}C{^{1}H}-NMR (75.47 MHz, $CDCl_3$, 289 K): δ (ppm) = 158.6 (Py-*C2*), 157.4 (Py-*C6*), 136.4 (Py-*C4*), 121.2 (Py-*C5*), 119.6 (Py-*C3*), 63.6 (N-*C*H_2-Py^{Me}), 42.6 (N-*C*H_3), 24.3 (Py-*C*H_3).

N-benzyl-N,N-di[(6-methyl-2-pyridylmethyl)]amine (Me_2-bpa-Bz)

This ligand was synthesized according to the procedure described by de Bruin. [57]

To 100 ml. acetonitrile, 150 gram 2-chloromethyl-6-methylpyridine, 0.43 gram (4.01 mmol) benzylamine and 12 gram (140 mmol) Na_2CO_3 dissolved in 10 ml. water, were added. The resulting suspension was heated to reflux for 16 hours. The mixture was filtered and the filtrate was evaporated yielding a yellow oil, to which 100 ml. Et_2O was added. Partial evaporation of the solvent resulted in precipitation of Me_2-bpa-Bz as a white solid, which was recrystallized as white crystals from a saturated hexane solution at -20 ºC. Yield 0.44 gram (36 %).

Mp 76.9 ºC.

^{1}H-NMR (200.13 MHz, $CDCl_3$, 298K): δ (ppm) = 7.62 - 7.00 (m, 11H, Py-*H3*, -*H4*, -*H5*, all five Ph-*H*)3.86 (s, 4H, N-CH_2-Py), 3.75 (s, 2H, N-CH_2-Ph), 2.54 (s, 6H, Py-CH_3).

^{1}H-NMR (200.13 MHz, CD_3CN, 298K): δ (ppm) = 7.59 (t, 2H, J(H,H) = 7.71 Hz, Py-*H4*), 7.5 - 7.2 (m, 7H, all five Py-*H*, Py-*H3* or -*H5*), 7.04 (d, 2H, J(H,H) = 7.95 Hz, Py-*H3* or -*H5*), 3.66 (s, 4H, N-CH_2-Py), 3.63 (s, 2H, N-CH_2-Ph), 2.44 (s, 6H, Py-CH_3).

$^{13}C\{^1H\}$-NMR (50.32 MHz, acetone-d6, 298 K): δ (ppm) = 160.4 (Py-*C2*), 158.5 (Py-*C6*), 140.6 (Ph-*C1*), 137.7 (Py-*C4*), 130.0 (Ph-*C2*, Ph-*C3*), 128.1 (Ph-*C4*), 122.3 (Py-*C5*), 120.6 (Py-*C3*), 61.0 (N-*C*H_2-Py), 59.3 (N-*C*H_2-Ph), 24.8 (Py-*C*H_3)

N-[(6-methyl-2-pyridyl)methyl]-N-(2-pyridylmethyl)amine (PLA)

Dissolve 5.5 g (53.3 mmol) 2-pyridylmethylamine in 50 ml. of methanol. Add 6.25 g (51.6 mmol) 6-methyl-2-pyridinecarbaldehyde and heat the reaction mixture up to 60 ºC. Allow it to cool off again while stirring the mixture. Add carefully 1.9 g $NaBH_4$ at r.t. and stir until the reaction has ended, e.g. no more gas evolves anymore. Add 5 ml. of water and evaporate all the solvent. Add 50 ml. of water and extract the water layer three times with 50 ml. of dichloromethane. Combine the CH_2Cl_2 fractions and dry with Na_2SO_4. Filter it and remove the solvent by evaporation. Yield 7.80 g (83%). The PLA was not further purified but used directly for the synthesis of Me_2-tpa.

^1H-NMR (200.13 MHz, $CDCl_3$, 289 K): δ (ppm) = 8.54 (d, 1H, J(H,H) = 3.24 Hz, Py-*H6*), 7.63 (dt, 1H, J(H,H) = 5.12 Hz, J(H,H) = 1.36 Hz, Py-*H4*), 7.51 (t, 1H, J(H,H) = 5.12 Hz, Py'-*H4*), 7.35 (d, 1H, J(H,H) = 5.12 Hz, Py-*H3*), 7.17 - 7.12 (m, 2H, Py-*H5* and Py'-*H3*), 7.00 (d, 1H, J(H,H) = 5.12 Hz, Py'-*H5*), 3.98 (s, 2H, N-CH_2-Py or -Py'), 3.94 (s, 2H, N-CH_2-Py or -Py'), 3.11 (s, 1H, N-*H*), 2.52 (s, 3H, Py-CH_3).

$^{13}C\{^1H\}$-NMR (50.32 MHz, acetone-d6, 298 K): δ (ppm) = 159.9 (Py- or Py'-*C2*), 159.0 (Py- or Py'-*C2*), 157.8 (Py'-*C6*), 149.2 (Py-*C6*), 136.6 (Py- or Py'-*C4*), 136.4 (Py- or Py'-*C4*),122.2 (Py- or Py'-*C3* or Py-*C5*), 121.9 (Py- or Py'-*C3* or Py-*C5*), 119.1 (Py'-*C5*), 54.9 (N-*C*H_2-Py or -Py'), 54.8 (N-*C*H_2-Py or -Py'), 24.5 (Py'-*C*H_3)

N,N-di[(6-methyl-2-pyridyl)methyl]-N-(2-pyridylmethyl)amine (Me_2-tpa)

In order to synthesize the Me_2-tpa ligand, first N-[(6-methyl-2-pyridyl)methyl]-N-(2-pyridylmethyl)amine (PLA) has to be synthesized. Then dissolve 7.80 g (36.6 mmol) PLA in 150 ml. of methanol. Bubble dinitrogen through for about 1 hour. Then add 5.43 g (44.8 mmol) 6-methyl-2-pyridinecarbaldehyde and 6 g of acetic acid. Cool the mixture down to 0 ºC, add 2.31 g $NaCNBH_3$ and allow the reaction mixture to stir overnight. Then add concentrated HCl to quench the remaining $NaCNBH_3$ and remove the solvent by evaporation. Add 75 ml. of water to the reaction mixture and subsequently add Na_2CO_3 until the reaction mixture is basic. Extract the water layer 3 times with 75 ml. of chloroform. Combine the chloroform fractions and dry them with Na_2SO_4. Filter it off and evaporate the solvent. Purify the crude yellow product by recrystallization from n-heptane. Yield 10.2 g (87%).

^1H-NMR (200.13 MHz, $CDCl_3$, 289 K): δ (ppm) = 8.54 (dm, 1H, J(H,H) = 5.0 Hz, Py-*H6*), 7.72 - 7.62 (m, 3H, Py- and Py'-*H4*), 7.57 (d, 1H, J(H,H) = 7.6 Hz, Py-*H3*), 7.45 (d, 2H, J(H,H) = 7.3 Hz, Py'-*H3*), 7.20 - 7.12 (m, 1H, Py-*H5*), 7.03 (d, 2H, J(H,H) = 7.3 Hz, Py'-*H5*), 3.99 (s, 6H, N-CH_2-Py and -Py'), 2.55 (s, 6H, Py-CH_3).

$^{13}C\{^1H\}$-NMR (50.32 MHz, $CDCl_3$, 289 K): δ (ppm) = 159.8 (Py- or Py'-*C2*), 159.1 (Py- or Py'-*C2*), 157.8 (Py'-*C6*), 149.2 (Py-*C6*), 137.0 (Py'-*C4*), 136.7 (Py-*C4*), 123.1 (Py-*C3* or -*C5*), 122.2 (Py-*C3* or -*C5*), 121.7 (Py'-*C3*), 119.8 (Py'-*C5*), 60.6 (N-*C*H_2-Py or -Py'), 60.4 (N-*C*H_2-Py or -Py'), 24.7 (Py'-*C*H_3).

*[(κ^4-Me_3-tpa)Rh^I(C_2H_4)]PF_6 ([**1**1]PF_6)*

270 mg (0.69 mmol) $[(C_2H_4)_2Rh(\mu\text{-}Cl)]_2$ and 375 mg (1.13 mmol) Me_3-tpa were stirred in 55 ml. MeOH at -78°C for about 4 hours until a clear solution was obtained. Subsequently 127 mg (0.69 mmol) KPF_6 was added. Partial evaporation of the solvent caused the precipitation of [**1**]PF_6 as a yellow powder, which was collected by filtration dried under vacuum. Yield 370 mg (0.61 mmol, 63%).

^1H-NMR (200.13 MHz, CD_2Cl_2, 298K): δ (ppm) = 7.42 (t, 3H, ^3J(H,H) = 7.8 Hz, Py^A-H4 and Py^B-H4); 7.16 (d, 1H, ^3J(H,H) = 7.3 Hz, Py^B-H3 or Py^B-H5); 7.04 (d, 2H, ^3J(H,H) = 7.6 Hz, Py^A-H3 or Py^B-H5); 6.89 (d, 3H, ^3J(H,H) = 7.6 Hz, Py^B-H3 or -H5 or Py^A-H3 or -H5); 5.63 (d[AB], 2H, ^2J(H,H) = 15.3 Hz, N-CH_2-Py^A); 4.80 (d[AB], 2H, ^2J(H,H) = 15.3 Hz, N-CH_2-Py^A); 4.41 (s, 2H, N-CH_2-Py^B); 3.71 (s, 3H, Py^B-CH_3); 2.87 (s, 6H, Py^A-CH_3); 2.54-2.34 (m, 2H, CH_2=CH_2); 2.25-2.05 (m, 2H, CH_2=CH_2).

$^{13}C\{^1H\}$-NMR (50.32 MHz, CD_2Cl_2, 298 K): δ (ppm) = 163.8 (Py^B-*C*2); 163.6 (Py^A-*C*2); 161.0 (Py^B-*C*6); 159.6 (Py^A-*C*6); 138.0 (Py^B-*C*4); 137.8 (Py^A-*C*4); 125.5 (Py^A-*C*3); 124.5 (Py^B-*C*3); 120.5 (Py^A-*C*5); 119.9 (Py^B-*C*5); 70.5 (N-*C*H_2-Py^A); 63.7 (N-*C*H_2-Py^B); 31.7 (Py^B-*C*H_3); 29.5 (d, ^1J(Rh,H) = 16.9 Hz; CH_2=CH_2); 28.2 (Py^A-*C*H_3); 26.3 (d, ^1J(Rh,H) = 19.9 Hz; CH_2=CH_2).

ESI^+-MS: m/z = 463 $[\mathbf{1}]^+$, 435 $\{[\mathbf{1}]\text{-}C_2H_4\}^+$.

Calculated for $C_{23}H_{28}N_4RhPF_6$ (608.37): C 45.41, H 4.64, N 9.21; Found: C 45.18, H 4.71, N 9.40.

*[(κ^4-Me_2-tpa)Rh^I(C_2H_4)]BPh_4 ([**2**1]BPh_4)*

This compound was prepared by a procedure similar to that of [(Me_3-tpa)Rh(C_2H_4)]PF_6, using Me_2-tpa and 1 eq. $NaBPh_4$. A yellow powder was obtained. Yield 59%.

^{1}H-NMR (200.13 MHz, CD_2Cl_2, 298K): δ (ppm) = 7.85 (d, ^{3}J(H, H) = 5.6 Hz, 1H; Py^A-*H*6); 7.6-7.2 (Py-, Py^A- and Py^B-*H4*); 7.2-6.7 (Py-, Py^A- and Py^B-*H3*, Py-, Py^A- and Py^B-*H5*); 7.29 (m, 8H; BAr-*H2*); 7.03 (t, ^{4}J(B,H) = 7.3 Hz, 8H; BAr-*H3*); 6.88 (t, ^{5}J(B,H) = 7.4 Hz, 4H; BAr-*H4*); 5.40 (d[AB], ^{2}J(H,H) = 14.4 Hz, 1H; N-CH_2-Py^B); 4.90 (d[AB'], ^{2}J(H,H) = 16.5 Hz, 1H; N-CH_2-Py); 4.37 (d[AB], ^{2}J(H,H) = 17.7 Hz, 1H; N-CH_2-Py^B); 4.07 (d[AB'], ^{2}J(H,H) = 16.5 Hz; N-CH_2-Py); 4.07 (d[AB''], ^{2}J(H,H) = 17.0 Hz, 1H; N-CH_2-Py^A); 3.96 (d[AB''], ^{2}J(H,H) = 17.1 Hz, 1H; N-CH_2-Py^A); 3.52 (s, 3H; Py^A-CH_3); 2.75 (s, 3H; Py^B-CH_3); 2.61-2.47 (m, 1H; C_2H_4); 2.06-1.77 (m, 3H; C_2H_4).

^{13}C{^{1}H}-NMR (50.31 MHz, CD_2Cl_2, 298K): δ (ppm) = 164.8 (m, ^{1}J(B,C) = 49.5 Hz; BAr-*C1*); 164.3, 163.3, 162.7, 161.0, 158.3 (s; Py-, Py^A- and Py^B-*C2*, Py^A- and Py^B-*C6*); 151.0 (s; Py-*C6*);138.0 (s; Py^A-*C4*); 137.8 (s; Py^B-*C4*); 137.1 (s; Py-*C4*); 136.7 (s; BAr-*C2*); 126.5 (s; BAr-*C3*); 125.6 (s; Py^B-*C3*); 124.8 (s; Py-*C3*); 124.5 (s; Py^A-*C3*); 122.6 (s; BAr-*C4*); 122.3, 121.0, 119.9 (s; Py-, Py^A- and Py^B-*C5*); 70.5, 68.4 (s; N-*C*H_2-Py and -Py^B); 64.2 (s; N-*C*H_2-Py^A); 29.5 (s; Py^A-*C*H_3); 28.8 (d, ^{1}J(Rh,C) = 20.8 Hz; *C*$_2$H$_4$); 27.6 (s; Py^B-*C*H_3); 27.1 (d, ^{1}J(Rh,C) = 17.6 Hz; *C*$_2$H$_4$).

ESI^+-MS: m/z = 449 [**2**]$^+$, 421 {[**2**]-C_2H_4}$^+$.

*[(κ^3-Me_3-tpa)Ir^I(C_2H_4)$_2$]PF_6 ([**3**]PF_6)*

350 mg (0.39 mmol) of [Ir(coe)$_2$(μ-Cl)]$_2$ was dissolved in 14 ml. methanol. Ethene was bubbled through the solution until a clear solution was obtained. The solution was cooled to -30 °C and 260 mg (0.78 mmol) of Me_3-tpa was added under an ethene atmosphere. The reaction mixture was stirred until the Me_3-tpa had dissolved. Subsequently 170 mg (0.92 mmol) of KPF_6 was added and the solution was stirred for 1 hour at -30 °C after which the solution was cooled to -78 °C causing precipitation of [**3**]PF_6. A second portion was obtained by adding 25 mg (0.14 mmol) of KPF_6 to the filtrate, stirring for one hour at -50°C, and standing overnight at -20°C. The thus obtained yellow solid was collected by filtration, washed three times with cold methanol (-78°C) under a nitrogen atmosphere and dried under vacuum. Yield 311 mg (0.43 mmol, 55%).

^{1}H-NMR (200.13 MHz, CD_2Cl_2, 298 K): δ (ppm) = 7.80 (t, 1H, ^{3}*J*(H,H) = 7.7 Hz, Py^B-H4), 7.71 (t, 2H, ^{3}*J*(H,H) = 7.7 Hz, Py^A-H4), 7.38 (d, 2H, ^{3}*J*(H,H) = 7.7 Hz, $Py^{A/B}$-H3/5), 7.34 (d, 2H, ^{3}*J*(H,H) = 7.7 Hz, $Py^{A/B}$-H3/5), 7.24 (d, 2H, ^{3}*J*(H,H) = 7.7 Hz, $Py^{A/B}$-H3/5), 5.26 (d[AB], 2H, ^{2}*J*(H,H) = 16.0 Hz, N-*CH*$_2$-Py^A), 4.94 (s, 2H, N-*CH*$_2$-Py^B), 3.92 (d[AB], 2H, ^{2}*J*(H,H) = 16.0 Hz, N-*CH*$_2$-Py^A), 3.28 (s, 6H, CH_3-Py^A). 2.62 (s, 3H, CH_3-Py^B), 2.02 (br, 4H, CH_2=CH_2), 1.81 (br, 4H, CH_2=CH_2).

Calculated for $C_{25}H_{32}N_4IrPF_6$ (725.74): C 41.38, H 4.44, N 7.72, Found C 41.19, H 4.20, N 7.80.

X-Ray diffraction: for a structure see Figure 3.4.

*[(κ^4 -Me_3-tpa)Ir^I(C_2H_4)]PF_6 ([**4**]PF_6)*

100 mg (0.14 mmol) of [**3**]PF_6 was dissolved in 5 ml. of acetone and stirred for 4 hours under nitrogen atmosphere at r.t. The atmosphere was flushed with fresh nitrogen every hour. Subsequently 25 ml. of hexane was added causing precipitation of [**4**]PF_6. The thus obtained orange solid was collected by filtration, washed 3 times with cold hexane and dried under vacuum. Yield 42 mg (0.07 mmol, 50 %).

^{1}H-NMR (200.13 MHz, CD_3CN, 298 K) δ (ppm) = 7.54 (t, 1H, ^{3}*J*(H,H) = 7.7 Hz, Py^B-H4), 7.50 (t, 2H, ^{3}*J*(H,H) = 7.7 Hz, Py^A-H4), 7.24 (d, 2H, ^{3}*J*(H,H) = 7.7 Hz, Py^A-H3/Py^B-H3&H_5), 7.09 (d, 2H, ^{3}*J*(H,H) = 7.7 Hz, Py^A-H5/H3/Py^B-H3&H5), 7.02 (d, 2H, ^{3}*J*(H,H) = 7.7 Hz, Py^A-H5/Py^B-H3&H5), 5.29 (d[AB], ^{2}*J*(H,H) = 15.3 Hz, N-*CH*$_2$-Py^A), 4.85 (d[AB], ^{2}*J*(H,H) = 15.3 Hz N-*CH*$_2$-Py^A), 4.64 (s, N-*CH*$_2$-Py^B), 3.65 (s, 3H, Py^B-CH_3), 2.85 (s, 6H, Py^A-CH_3), 1.85 (t, 2H, ^{3}*J*(H,H) =8.6 Hz, *CH*$_2$=CH_2), 1.37 (t, 2H, ^{3}*J*(H,H) =8.58 Hz, CH_2=*CH*$_2$).

^{1}H-NMR (400.14 MHz, acetone-d6, 298 K): δ (ppm) = 7.72 (t, 1H, ^{3}*J*(H,H) = 7.8 Hz, Py^B-H4), 7.60 (t, 2H, ^{3}*J*(H,H) = 7.8 Hz, Py^A-H4), 7.35 (d, 1H, ^{3}*J*(H,H) = 7.2 Hz, Py^B-H3), 7.26 (d, 2H, ^{3}*J*(H,H) = 7.6 Hz, Py^A-H3), 7.15 (d, 1H, ^{3}*J*(H,H) = 7.3 Hz, Py^B-H5), 7.81 (d, 2H, ^{3}*J*(H,H) = 7.8 Hz, Py^A-H5), 5.49 (d[AB], ^{2}*J*(H,H) = 15.2 Hz, N-*CH*$_2$-Py^A), 5.11 (d[AB], ^{2}*J*(H,H) = 15.2 Hz, N-*CH*$_2$-Py^A), 4.90 (s, N-*CH*$_2$-Py^B), 3.75 (s, 3H, Py^B-*CH*$_3$), 2.94 (s, 6H, Py^A-*CH*$_3$), 1.89 (t, 2H, ^{3}*J*(H,H) =8.6 Hz, *CH*$_2$=CH_2), 1.47 (t, 2H, ^{3}*J*(H,H) =8.79 Hz, CH_2=*CH*$_2$).

^{13}C{^{1}H}-NMR (100.61 MHz, acetone-d6, 298 K) δ (ppm) = 164.6 (Py^A-*C6*), 163.2 (Py^A-*C2*), 161.8 (Py^B-*C6*), 160.2 (Py^B-*C2*), 138.4 (Py^B-*C4*), 136.9 (Py^A-*C4*), 124.7 (Py^A-*C5*), 123.5 (Py^B-*C5*), 119.8 (Py^A-*C3*), 118.9 (Py^B-*C3*), 71.7 (N-*C*H_2-Py^A), 65.2 (N-*C*H_2-Py^B), 32.5 (Py^B-*C*H_3), 27.2 (Py^A-*C*H_3), 3.7 (*C*H_2=CH_2), 0.2 (CH_2=*C*H_2).

ESI^+-MS: m/z = 553 [**4**]$^+$, 525 {[**4**]-C_2H_4}$^+$.

Calculated for $C_{23}H_{28}N_4IrPF_6$ (697.69): C 39.60, H 4.04, N 8.03; Found: C 39.43, H 4.17, N 8.20.

X-Ray diffraction: for a structure see Figure 3.7.

*[(κ^4-C,N,N',N''-Me_3-tpa)Ir^{III}(H)(CD_3CN)]PF_6 (or [(Me_3-$tpa^{\#}$)Ir^{III}(H)(CD_3CN)]PF_6 or [**5**]PF_6)*

20 mg (0.03 mmol) of [**4**]PF_6 was dissolved in 1 ml. MeCN and was kept for 3 days under a nitrogen atmosphere. The color of the solution remains yellow.

Sample prepared in CD_3CN:

CPy represents the equatorial cyclo-metallated pyridyl group (at C3).

^{1}H-NMR (500 MHz, CD_3CN, 298 K): δ (ppm) = 7.81 (d, ^3J(H,H) = 7.7 Hz, CPy-*H4*), 7.63 (t, 2H, ^3J(H,H) = 7.7 Hz, Py^A-*H4*), 7.25 (d, 2H, ^3J(H,H) = 7.2 Hz, Py^A-*H3*), 7.23 (d, 2H, ^3J(H,H) = 7.7 Hz, Py^A-*H5*), 6.48 (d, ^3J(H,H) = 7.7 Hz, CPy-*H5*), 5.09 (d[AB], 2H, ^2J(H,H) = 15.3 Hz, N-CH_2-Py^A), 5.04 (d[AB], 2H, ^2J(H,H) = 15.3 Hz, N-CH_2-Py^A), 4.41 (s, 2H, N-CH_2-CPy), 2.81 (s, 6H, Py^A-CH_3), 2.13 (s, 3H, CPy-CH_3), -18.58 (s, Ir-*H*).

^{13}C{^{1}H}-NMR (75.47 MHz, CD_3CN, 298 K): δ (ppm): 169.6 (CPy-*C6*), 167.0 (Py^A-*C6*), 164.6 (CPy-*C2*), 151.8 (CPy-*C5*), 151.2 (Py^A-*C2*), 139.0 (Py^A-*C4*), 127.3 (CPy-*C3*-Ir), 124.9 (Py^A-*C5*), 121.9 (CPy-*C4*), 121.7 (Py^A-*C3*), 70.4 (N-CH_2-Py^A), 68.8 (N-CH_2-CPy), 31.6 (CH_3-Py^A), 23.2 (CH_3-CPy).

ESI^+-MS: m/z = 569 $[\mathbf{5}]^+$

Sample prepared in CH_3CN instead of CD_3CN:

ESI^+-MS: m/z = 566 $[\mathbf{5}]^+$.

Calculated for $C_{23}H_{27}N_5IrPF_6$ (710.68): C 38.87, H 3.83, N 9.85; Found: C 39.07, H 4.01, N 9.99.

[(κ^4-C,N,N',N''-Me_3TPA)Ir^{III}(H)(C_2H_4)]PF_6 (or [(Me_3-$tpa^{\#}$)Ir^{III}(H)(C_2H_4)]PF_6)

10 mg (0.015 mmol) of [**4**]PF_6 was dissolved in 1 ml. CD_2Cl_2 and was kept for 3 days under nitrogen atmosphere. The color of the solution remains yellow.

CPy represents the equatorial cyclo-metallated pyridyl group (at C3).

^{1}H-NMR: (200MHz, CD_2Cl_2, 298 K) δ (ppm): 8.23 (d, CPy-*H4*, ^3J(H,H) = 7.4 Hz), 7.58 (t, 2H, Py^A-*H4*, ^3J(H,H) =7.9 Hz), 7.22 (d, 2H, Py-*H3*, ^3J(H,H) =7.7 Hz), 7.13 (d, 2H, Py^A-*H5*, ^3J(H,H) =7.7 Hz), 6.70 (d, CPy-*H5*, ^3J(H,H) =7.7 Hz), 5.50 (d[AB], N-CH_2-Py^A, ^2J(H,H) =16.0 Hz), 5.27 (d[AB], N-CH_2-Py^A, ^2J(H,H) =16.0 Hz), 4.68 (s, 2H, N-CH_2-CPy), 3.53 (s, 4H, CH_2=CH_2), 2.75 (s, 6H, Py^A-CH_3), 2.22 (s, 3H, CPy-CH_3), -15.87 (s, Ir-*H*).

*[(κ^4 -Me_2-tpa)Ir^I(C_2H_4)]PF_6 ([**6**]PF_6)*

This compound was prepared analogously to a literature method of Blake et al.[57] by bubbling ethene through solution of 310 mg (0.34 mmole) $[Ir(coe)_2(\mu\text{-}Cl)]_2$ in 25 ml. MeOH at 298 K for about 15 minutes. The resultant yellow solution was cooled down to a temperature of -78°C during which a white powder, $Ir(C_2H_4)_4Cl$, precipitated. Subsequently 220 mg (0.68 mmole) Me_2-tpa was added and the mixture was stirred at -78°C for about an hour. The addition of 230 mg (0.67 mmole) $NaBPh_4$ caused the precipitation of $[(Me_2\text{-tpa})Ir(C_2H_4)]BPh_4$ as a yellow powder, which was filtered and vacuum dried. Yield 350 mg (59%).

^{1}H-NMR (200.13 MHz, CD_2Cl_2, 298K): δ (ppm) = 8.10 (d, ^{3}J(H,H) = 5.8 Hz, 1H; Py-*H6*); 7.52-7.29 (m, 3H; Py- and Py^A- and Py^B-*H4*); 7.37 (m, 8H; BAr-*H2*); 7.15-6.73 (m, 6H; Py-, Py^A- and Py^B-*H3*, Py-, Py^A- and Py^B -*H5*); 7.01 (t, ^{4}J(B,H) = 7.3 Hz, 8H; BAr-*H3*); 6.86 (t, ^{5}J(B,H) = 7.3 Hz, 4H; BAr-*H4*); 5.00 (d[AB], ^{2}J(H,H) = 14.6 Hz, 1H; N-CH_2-Py or -Py^B); 4.53 (d[AB'], ^{2}J(H,H) = 16.1 Hz, 1H; N-CH_2-Py or -Py^B); 4.39 (d[AB], ^{2}J(H,H) = 14.6 Hz, 1H; N-CH_2-Py or -Py^B); 4.24 (d[AB''], ^{2}J(H,H) = 17.0 Hz, 1H; N-CH_2-Py^A); 4.04 (d[AB''], ^{2}J(H,H) = 17.0 Hz, 1H; N-CH_2-Py^A); 4.01 (d[AB'], ^{2}J(H,H) = 16.1 Hz, 1H; N-CH_2-Py or -Py^B); 3.39 (s, 3H; Py^A-CH_3); 2.73 (s, 3H; Py^B-CH_3); 1.84 (dd, J(H,H) = 8.6 Hz, J(H,H) = 4.2 Hz, 1H; C_2H_4); 1.28 (m, 3H; C_2H_4).

^{13}C{^{1}H}-NMR (50.31 MHz, CD_2Cl_2, 298K): δ (ppm) = 164.7 (m, ^{1}J(B,C) = 49 Hz; BAr-C*1*); (s; Py-, Py^A- and Py^B-*C2*, Py-, Py^A and Py^B-*C6*); 151.3 (s; Py-*C6*); 137.5 (s; Py^B-*C4*); 137.3 (s; Py-*C4*); 135.8 (s; Py^A-*C4*); 136.7 (s; BAr-*C2*); 126.5 (m; BAr-*C3*); 125.5, 125.4 (s; Py- and Py^B-*C3*); 124.4 (s; Py^A-*C3*); 122.7 (s; BAr-*C4*); 120.9, 119.8, 119.4 (s; Py-, Py^A- and Py^B-*C5*); 72.5, 70.5 (s; N-CH_2-Py and -Py^B); 66.3 (s; N-CH_2-Py^A); 30.9 (s; Py^A-CH_3); 28.2 (s; Py^B-CH_3); 4.6 (s; C_2H_4); 3.7 (s; C_2H_4).

ESI^+-MS: m/z = 539 $[\mathbf{6}]^+$, 511 $\{[\mathbf{6}]\text{-}C_2H_4\}^+$.

Calculated for $C_{22}H_{26}N_4Ir_1P_1F_6$: C, 38.65; H, 3.83; N, 8.20; Found: C, 38.43; H, 3.66; N, 8.05.

X-Ray diffraction: for a structure see Figure 3.8.

*[(κ^3-Me_2-bpa-Me)Ir^I(C_2H_4)$_2$]PF_6 ([**7**]PF_6)*

350 mg (0.39 mmol) of $[Ir(coe)_2(\mu\text{-}Cl)]_2$ was dissolved in 14 ml. of methanol, ethene was bubbled through the solution until a clear solution was obtained. The solution was cooled down to -30°C and 190 mg (0.79 mmol) of Me_2-bpa-Me was added under

an ethene atmosphere. The reaction mixture was stirred until the Me_2-bpa-Me had dissolved. Subsequently 170 mg (0.92 mmol) of KPF_6 was added and the solution was stirred for 1 hour at -30 °C after which the solution was cooled to -78 °C causing precipitation of [**7**]PF_6. A second portion was obtained by adding 25 mg (0.14 mmol) of KPF_6 to the filtrate, stirring for one hour at -50°C, and standing overnight at -20°C. The thus obtained yellow solid was collected by filtration, washed three times with cold methanol (-78°C) under a nitrogen atmosphere and dried under vacuum. Yield 234 mg (0.37 mmol, 47 %).

^{1}H-NMR (200.13 MHz, CD_3CN, 298 K): δ (ppm) = 7.73 (t, 2H, ^{3}J(H,H) = 7.7 Hz, Py-H4), 7.37 (d, 2H, ^{3}J(H,H) = 7.7 Hz, Py-H3/5), 7.27 (d, 2H, ^{3}J(H,H) = 7.7 Hz, Py-H3/5), 4.64 (d[AB], 2H, ^{2}J(H,H) =15.8 Hz, CH_2-Py), 4.10 (d[AB], 2H, ^{2}J(H,H) =15.8 Hz, CH_2-Py), 3.34 (s, 3H, CH_3-N), 3.18 (s, 6H, CH_3-Py), 1.83 (br, 4H, CH_2=CH_2), 1.67 (br, 4H, CH_2=CH_2).

ESI^+-MS: m/z = 490 [**7**]$^+$, 462 [**8**]$^+$, 434 {[**8**]-C_2H_4}$^+$.

Calculated for $C_{19}H_{27}N_3IrPF_6$ (634.63): C 35.96, H 4.29, N 6.62 Found: C 35.66, H 4.10, N 6.39.

*[(κ^3-Me_2-bpa-Me)Ir^I(C_2H_4)]PF_6 ([**8**]PF_6)*

Dissolving [**7**]PF_6 in CD_2Cl_2 results in formation of [**8**]PF_6 within 2 hours. The color of the solution remains yellow.

^{1}H-NMR (200.13 MHz, CD_2Cl_2, 298 K): δ (ppm) = 7.59 (t, 2H, ^{3}J(H,H) = 7.7 Hz, Py-H4), 7.17 (d, 2H, ^{3}J(H,H) = 7.5 Hz, Py-H3), 7.05 (d, 2H, ^{3}J(H,H) = 7.9 Hz, Py-H5), 5.07 (d[AB], ^{2}J(H,H) = 14.9 Hz, N-CH_2-Py), 4.75 (d[AB], ^{2}J(H,H) = 14.9 Hz, N-CH_2-Py), 3.59 (t, 2H, ^{3}J(H,H) = 9.7 Hz, CH_2=CH_2), 3.15 (s, 3H, N-CH_3), 2.66 (s, 6H, Py-CH_3), 2.36 (t, 2H, ^{3}J(H,H) = 9.7 Hz, CH_2=CH_2).

^{1}H-NMR (400.14 MHz, CD_3CN, 298 K): δ (ppm) = 7.63 (t, 2H, ^{3}J(H,H) = 7.9 Hz, Py-H4), 7.18 (d, 2H, ^{3}J(H,H) = 7.4 Hz, Py-H3), 7.11 (d, 2H, ^{3}J(H,H) = 7.9 Hz, Py-H5), 5.06 (d[AB], ^{2}J(H,H) = 15.1 Hz, N-CH_2-Py), 4.71 (d[AB], ^{2}J(H,H) = 15.1 Hz, N-CH_2-Py), 3.54 (t, 2H, ^{3}J(H,H) = 9.7 Hz, CH_2=CH_2), 3.11 (s, 3H, N-CH_3), 2.64 (s, 6H, Py-CH_3), 2.34 (t, 2H, ^{3}J(H,H) = 9.7 Hz, CH_2=CH_2).

^{13}C{^{1}H}-NMR (75.47 MHz, CD_3CN, 298 K): δ (ppm) = 166.6 (Py-C6), 164.4 (Py-C2), 138.7 (Py-C4), 127.2 (Py-C5), 121.9 (Py-C3), 72.2 (N-CH_2-Py), 52.4 (N-CH_3), 37.0 (CH_2=CH_2), 27.1 (Py-CH_3), 25.1 (CH_2=CH_2).

ESI^+-MS: m/z = 462 [**8**]$^+$, 434 {[**8**]-C_2H_4}$^+$.

Due to the instability of [**8**]PF_6, reliable elemental analytical data were not obtained.

*[(κ^3-Me_2-bpa-Me)Ir^I(C_2H_4)(CD_3CN]PF_6 ([**8**(S)]PF_6)*

Dissolving [**7**]PF_6 in CD_3CN results in a 3:1 mixture of [**8**]PF_6 and [**8**(MeCN)]PF_6 within 2 hours.

^{1}H-NMR (400.14 MHz, CD_3CN, 298 K): δ (ppm) = 7.63 (t, 2H, ^{3}J(H,H) = 7.8 Hz, Py-H4), 7.20 (d, 2H, ^{3}J(H,H) = 7.9 Hz, Py-H3), 7.16 (d, 2H, ^{3}J(H,H) = 7.8 Hz, Py-H5), 4.95 (d[AB], ^{2}J(H,H) = 14.9 Hz, N-CH_2-Py), 4.57 (d[AB], ^{2}J(H,H) = 14.9 Hz, N-CH_2-Py), 2.91 (s, 6H, Py-CH_3), 2.78 (s, 3H, N-CH_3), 1.94 (t, 2H, ^{3}J(H,H) = 8.7 Hz, CH_2=CH_2), 1.28 (t, 2H, ^{3}J(H,H) = 8.7 Hz, CH_2=CH_2).

^{13}C{^{1}H}-NMR (75.47 MHz, CD_3CN, 298 K): δ (ppm) = 166 (Py-C6), 164 (Py-C2), 137.0 (Py-C4), 127.2 (Py-C5), 120.0 (Py-C3), 72.6 (N-CH_2-Py), 51.4 (N-CH_3), 27.6 (Py-CH_3), ^{13}C signals of the ethene fragment could not be observed at 289 K.

Due to the instability of [**8**(MeCN)]PF_6, reliable elemental analytical data were not obtained.

*[(Me_2bpa-Me)Ir^{III}(η^1-vinyl-ethene)(ethyl)(CD_3CN)]PF_6 ([**9**]PF_6)*

When solid [**7**]PF_6 is allowed to stand under a dioxygen atmosphere at r.t. for three months one single, yellow product is obtained: [**9**]PF_6. Upon dissolving in CD_3CN at first it seems as if at least four products were formed. However, after allowing the solution to stand overnight at -20 ºC the signals of only one single product could be observed anymore. Atom numbering for NMR is shown beside.

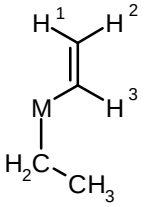

^{1}H-NMR (200.13 MHz, CD_3CN, 298 K): δ (ppm) = 7.74 (m, 2H, Py-*H4*), 7.29 (m, 4H, Py-*H3* or -*H5*), 5.15 (dd, 1H, J(H,H) = 10.01 Hz, J(H,H) = 2.74 Hz, vinyl-*H2*), 4.32 (d[AB], 2H, J(H,H) = 16.45 Hz, N-CH_2-Py), 4.2 (m, 4H, N-CH_2-Py and vinyl-*H3* an -*H1*), 2.75 (s, 9H, Py-CH_3 and N-CH_3), 1.65 (m, 1H, Ir-CH^4H-CH_3), 1.50 (m, 1H, Ir-CHH^5-CH_3) 0.33 (t, 3H, J(H,H) = 7.77 Hz, Ir-CH_2-CH_3).

*[(κ^3-Me_2-bpa-Bz)Ir^I(C_2H_4)$_2$]PF_6 ([**10**]PF_6)*

150 mg (0.17 mmol) of [Ir(coe)$_2$(μ-Cl)]$_2$ was dissolved in 5 ml. of methanol, ethene was bubbled through the solution until a clear solution was obtained. 107 mg (0.34 mmol) of Me_2-bpa-Bz was added under an ethene atmosphere. Under bubbling through ethene the reaction mixture was stirred for 5 minutes until all the Me_2-bpa-Bz has dissolved. Subsequently 83 mg (0.45

mmol) of KPF_6 was added and the solution was stirred for 45 minutes at r.t. Precipitation of white/yellow solid already starts to take place. Then the solution was cooled to -78 °C causing precipitation of [**10**]PF_6. The thus obtained yellow solid was collected by filtration, washed three times with ice-cold methanol under a nitrogen atmosphere and dried under vacuum. Yield 196 mg (82 %).

^{1}H-NMR (200.13 MHz, CD_2Cl_2, 298 K): δ (ppm) = 7.71 (t, 2H, ^{3}J(H,H) = 7.7 Hz, Py-*H4*), 7.7 - 7.5 (m, 6H, Ph-*H2*, -*H3*, -*H4*, -*H5* and -*H6*), 7.37 (d, 2H, ^{3}J(H,H) = 7.7 Hz, Py-*H3/5*), 7.23 (d, 2H, ^{3}J(H,H) = 7.0 Hz, Py-*H3/5*), 4.84 (d[AB], 2H, ^{2}J(H,H) = 15.6 Hz, N-CH_2-Py), 4.85 (s, 2H, N-CH_2-Ph), 3.73 (d[AB], 2H, ^{2}J(H,H) =15.6 Hz, N-CH_2-Py), 3.26 (s, 6H, Py-CH_3), 2.00 (m (br), 4H, C_2H_4), 1.82 (m (br), 4H, C_2H_4).

ESI$^+$-MS: m/z = 566 [**10**]$^+$, 538 {[**10**]-C_2H_4}$^+$, 510 {[**10**]-2∗C_2H_4}$^+$.

Calculated for $C_{25}H_{31}N_3Ir_1P_1F_6$: C, 42.25; H, 4.40; N, 5.91; Found: C, 42.34; H, 4.41; N, 5.89.

*[(κ^4-C,N,N'-Me_2-bpa-Bz)Ir^{III}(H)(C_2H_4)]PF_6 (or [(Me_2-bpa-$Bz^{\#}$)Ir^{III}(H)(C_2H_4)]PF_6 or [**11**]PF_6)*

Dissolving [**10**]PF_6 in acetone-d6 results in the formation of yellow [**11**]PF_6 within 2 hours.

The phenyl group is cyclo-metallated at C2.

^{1}H-NMR (200.13 MHz, acetone-d6, 298 K): δ (ppm) = 8.23 (d, 1H, J(H,H) = 7.20 Hz, Ph-*H3*), 7.70 (t, 2H, J(H,H) = 7.77 Hz, Py-*H4*), 7.41 (d, 2H, J(H,H) = 7.83 Hz, Py-*H3*), 7.29 (d, 2H, J(H,H) = 7.83 Hz, Py-*H5*), 6.83 (m, 2H, Ph-*H4* and -*H6*), 6.71 (m, 1H, Ph-*H5*), 5.77 (d[AB], 2H, J(H,H) = 16.15 Hz, N-CH_2-Py), 5.53 (d[AB], 2H, J(H,H) = 16.01 Hz, N-CH_2-Py), 4.88 (s, 2H, N-CH_2-Ph), 3.66 (s, 4H, C_2H_4), 2.88 (s, 6H, Py-CH_3), -15.45 (s, 1H, Ir-*H*).

^{13}C{^{1}H}-NMR (75.47 MHz, acetone-d6, 298 K): δ (ppm) = 166.43 (s, 1C, Py-*C6*), 163.05 (s, 2C, Py-*C2*), 152.46 (s, 1C, Ph-*C1*), 149.11 (s, Ph-*C2*), 144.46 (s, 1C, Ph-*C6*), 139.39 (s, 2C, Py-*C4*), 128.03 (s, 1C, Ph-*C3*/*C5*), 125.49 (s, 2C, Py-*C5*), 123.67 (s, 1C, Ph-*C4*), 123.46 (s, ?), 122.26 (s, 2C, Py-*C3*), 121,44 (s, 1C, Ph-*C3*/*C5*), 74.06 (s, 1C, N-*C*H_2-Ph), 73.02 (s, 2C, N-*C*H_2-Py), 60.62 (s, 2C, *C*$_2$H$_4$), 29.82 (s, 2C, Py-*C*H3).

ESI$^+$-MS: m/z = 551 [**11**]$^+$, 510 {[**11**]-CH_3CN}$^+$.

*[(κ^4-C,N,N'-Me_2-bpa-Bz)Ir^{III}(H)(CD_3CN)]PF_6 (or [(Me_2-bpa-$Bz^{\#}$)Ir^{III}(H)(CD_3CN)]PF_6 or [**12**]PF_6)*

Dissolving [**10**]PF_6 in CD_3CN results in the formation of yellow [**12**]PF_6 within 2 hours.

The phenyl group is cyclo-metallated at C2.

^{1}H-NMR (400.14 MHz, CD_3CN, 298 K): δ (ppm) = 7.72 (d, 1H, J(H,H) = 7.32 Hz, Ph-*H6*), 7.59 (t, 2H, J(H,H) = 7.56 Hz, Py-*H4*), 7.22 (d, 2H, J(H,H) = 10,96 Hz, Py-*H3*), 7.20 (d, 2H, J(H,H) = 11.7 Hz, Py-*H5*), 6.67 – 6.60 (m, 2H, Ph-*H3* and -*H5*), 6.55 (m, 1H, Ph-*H4*), 5.12 (d[AB], 2H, J(H,H) = 15.41 Hz, N-CH_2-Py), 5.03 (dd[AB], 2H, J(H,H) = 15.36 Hz, J(H,H) = 1.0 Hz, N-CH_2-Py), 4.48 (s, 2H, N-CH_2-Ph), 2.86 (s, 6H, Py-CH_3), -18.32 (s, 1H, Ir-*H*).

^{13}C{^{1}H}-NMR (75.47 MHz, CD_3CN, 298 K): δ (ppm) = 167.19 (s, 2C, Py-*C6*), 164.55 (s, 2C, Py-*C2*), 150.78 (s, 2C, Ph- *C1* and -*C2*), 144.01 (s, 1C, Ph-*C6*), 138.72 (s, 2C, Py-*C4*), 126.41 (s, 1C, Ph-*C3* or *C5*), 124.72 (s, 2C, Py-*H5*), 122.79 (s, 1C, Ph-*C4*), 121.41 (s, 2C, Py-*C3*), 120, 80 (s, 1C, Ph-*C3* or *C5*), 70.38 (s, 2C, N-*C*H_2-Py), 69.08 (s, 1C, N-*C*H_2-Ph), 31.51 (s, 2C, Py-*C*H_3).

ESI$^+$-MS: m/z = 538 [**12**]$^+$, 510 {[**12**]-C_2H_4}$^+$.

*[(κ^3-bpa)Ir^I(C_2H_4)$_2$]PF_6 ([**13**]PF_6)*

155 mg (0.17 mmol) [Ir(coe)$_2$(μ-Cl)]$_2$ was dissolved in 5 ml. of methanol, ethene was bubbled through the solution at room temperature until a clear solution was obtained. Under ethene atmosphere a solution of 120 mg (0.60 mmol, about 1.7 equiv.) of bpa in 1,5 ml. methanol was added and stirred for a few minutes while bubbling through ethene. Subsequently 100.0 mg (0.54 mmol) of KPF_6 was added and the solution was stirred for 45 minutes under an ethene atmosphere. The solution was cooled down to -78°C to allow precipitation of [**13**]PF_6. The thus obtained yellow-green solid was collected by filtration, washed three times with ice-cold methanol under a nitrogen atmosphere and dried under vacuum. Yield 115 mg (0.20 mmol, 61 %).

This complex was also synthesised using 70 mg (0.43 mmol) NH_4PF_6 instead of KPF_6

^{1}H-NMR: (400.15 MHz, CD_3CN, T= 298 K) δ (ppm) = 7.73 (dt, 2H, J(H,H)$_{triplet}$ = 7.82 Hz and J(H,H)$_{doublet}$ = 1.71 Hz, Py-*H4*), 7.63 (d, 2H, J(H,H) = 5.62 Hz, Py-*H6*), 7.31 (d, 2H, J(H,H) = 7.82 Hz, Py-*H3*), 7.38 (s, 1H, N-*H*), 7.11 (t, 2H, J(H,H) = 6.72 Hz, Py-*H5*), 4.99 (dd[AB], 2H, J(H,H) = 15.76 Hz and J(H,H) = 5.50 Hz, Py-CH^AH-N), 4.65 (dd[AB], 2H, J(H,H) = 16.13 Hz and J(H,H) = 10.26, Py-CHH^B-N), 3.02 (t, 2H, J(H,H) = 10.14 Hz, $C_2H_4{}^A$), 2.89 (t, 2H, J(H,H) = 9.53 Hz, $C_2H_4{}^B$), 1.77 (t, 2H, J(H,H) = 9.53 Hz, $C_2H_4{}^B$ and $C_2H_4{}^A$).

$^{13}C\{^1H\}$-NMR (50.03 MHz, CD_3CN, T= 298 K) δ (ppm) = 167.54 (s, 2C, Py-*C2*), 150.58 (s, 2C, Py-*C6*), 138.53 (s, 2C, Py-*C4*), 126.29 (s, 2C, Py-*C3*), 123.08 (s, 2C, Py-*C5*), 60.97 (s, 2C, Py-*C*H_2-N), 36.64 (s, 2C, *C*$_2H_4$), 31.01 (s, 1C, *C*$_2H_4^A$), 25.61 (s, 1C, *C*$_2H_4^B$).

ESI^+-MS: m/z = 448 [**13**]$^+$, 420 {[**13**]-C_2H_4}$^+$, 392 {[**13**]-2∗C_2H_4}$^+$.

Calculated for $C_{16}H_{21}N_3IrPF_6$: C 32.43, H 3.57, N 7.09. Found: C 32.25, H 3.55, N 6.99.

*[{(bpa$^{\#}$)Ir^{III}(C$_2$H$_5$)(CH$_3$CN)}$_2$](PF$_6$)$_2$ ([**14**](PF$_6$)$_2$)* [7]

115 mg (0.19 mmol) of [**13**]PF_6 was dissolved in acetonitrile, heated to approximately 70° C under stirring for 2 hours. The solvent was removed and the product was analyzed. In another experiment [**13**]PF_6 was dissolved in acetonitrile-d3 and left standing at room temperature for 2 weeks. Here also dark-green product [**14**]$(PF_6)_2$ was found. Crystallisation was performed in a damp-diffusion experiment with acetonitrile and diethylether. Yield 73.5 mg (81.5 %)

1H-NMR: (400.15 MHz, CD_3CN, T = 298 K) δ (ppm) = 8.49 (d, 4H, J(H,H) = 5.08 Hz, Py-*H6*), 7.50 (dt, 4H, $J(H,H)_{triplet}$ = 7.80 Hz, $J(H,H)_{doublet}$ = 1.49 Hz, Py-*H4*), 7.08 (t, 4H, J(H,H) = 6.54 Hz, Py-*H5*), 6.84 (d, 4H, J(H,H) = 7.84 Hz, Py-*H3*), 4.75 (d[AB], 4H, J(H,H) = 17.57 Hz, Py-CH*H*^{B}-N), 4.62 (d[AB], 4H, J(H,H) = 17.57, Py-C*H*^{A}H-N), 2.70 (s, 6H, coordinated CH_3CN), 1.06 (q, 4H, J(H,H) = 7.63 Hz, -C*H*$_2$CH$_3$), 0.01 (t, 6H, J(H,H) = 7.62 Hz, -CH$_2$C*H*$_3$).

$^{13}C\{^1H\}$-NMR (50.03 MHz, CD_3CN, T= 298 K) δ (ppm) = 172.39 (s, 4C, Py-*C2*), 150.39 (s, 4C, Py-*C6*), 137.66 (s, 4C, Py-*C4*), 124.96 (s, 4C, Py-*C5*), 122.73 (s, 4C, Py-*C3*), 119.02 (s, 2C, coordinated CH_3CN), 69.36 (s, 4C, Py-*C*H_2-N), 15.10 (s, 2C, -CH$_2$*C*H$_3$), 4.78 (s, 2C, coordinated *C*H_3CN), -10.29 (s, 2C, -*C*H_2CH_3).

ESI^+-MS: m/z = 463.5 [**14**]$^{2+}$

Calculated for $C_{32}H_{40}N_8Ir_2P_2F_{12}CH_3CN$: C, 32.61; H, 3.46; N, 10.07. Found: C, 32.62; H, 3.31; N, 9.87.

X-Ray diffraction: for a structure see Figure 3.16.

*[(κ^3-bpa-Me)Ir^I(C$_2$H$_4$)$_2$]PF$_6$ ([**15**]PF$_6$)*

150 mg (0.17 mmol) $[Ir(coe)_2(\mu\text{-}Cl)]_2$ was dissolved in 5 ml. of methanol, ethene was bubbled through the solution at room temperature until a clear solution was obtained. Under ethene atmosphere a solution of 71 mg (0.33 mmol) of bpa-Me in 1,5 ml. methanol was added and stirred for a few minutes while bubbling through ethene. Subsequently 80.0 mg (0.43 mmol) of KPF_6 was added and the solution was stirred for 45 minutes under an ethene atmosphere. The solution was cooled down to -78°C to allow precipitation of [**15**]PF_6. The thus obtained light-green solid was collected by filtration, washed three times with ice-cold methanol under a nitrogen atmosphere and dried under vacuum. Yield 66.8 mg (0.11 mmol, 33 %).

^{1}H-NMR: (400.15 MHz, CD_3CN, T= 298 K) δ (ppm) = 7.79 (dt , 2H, $J(H,H)_{triplet}$ = 7.68 Hz and $J(H,H)_{doublet}$ = 1.63 Hz, Py-*H4*), 7.70 (d, 2H, J(H,H) = 5.62 Hz, Py-*H6*), 7.40 (d, 2H, J(H,H) = 8.30 Hz, Py-*H3*), 7.19 (t, 2H, J(H,H) = 6.72 Hz, Py-*H5*), 4.98 (d[AB], 2H, J(H,H) = 15.15 Hz, Py-CH*H*^{B}-N), 4.78 (d[AB], 2H, J(H,H) = 15.39 Hz, Py-C*H*^{A}H-N), 3.32 (t, 2H, J(H,H) = 10.14 Hz, $C_2H_4^A$), 3.18 (s, 3H, N-C*H*$_3$), 3.03 (t, 2H, J(H,H) = 9.65 Hz, $C_2H_4^B$), 1.87 (t, 2H, J(H,H) = 9.65 Hz, $C_2H_4^B$), 1.76 (t, 2H, J(H,H) = 9.77 Hz, $C_2H_4^A$).

$^{13}C\{^1H\}$-NMR (50.03 MHz, CD_3CN, T= 298 K) δ (ppm) = 166.07 (s, 2C, Py-*C2*), 150.40 (s, 2C, Py-*C6*), 138.67 (s, 2C, Py-*C4*), 126.62 (s, 2C, Py-*C5*), 124.61 (s, 2C, Py-*C3*), 71.05 (s, 2C, Py-*C*H_2-N), 53.81 (s, 1C, N-*C*H_3), 39.67 (s, 1C, *C*$_2H_4^A$), 36.38 (s, 1C, *C*$_2H_4^A$), 33.97 (s, 1C, *C*$_2H_4^B$), 28.53 (s, 1C, *C*$_2H_4^B$).

ESI^+-MS: m/z = 462 [**15**]$^+$, 434 {[**15**]-C_2H_4}$^+$, 406 {[**15**]-2∗C_2H_4}$^+$.

Calculated for $C_{17}H_{23}N_3IrPF_6$: C 33.66, H 3.82, N 6.93. Found: C 33.72, H 3.86, N 7.07.

*[(κ^3-bpa-Bz)Ir^I(C$_2$H$_4$)$_2$]PF$_6$ ([**16**]PF$_6$)*

150 mg (0.17 mmol) $[Ir(coe)_2(\mu\text{-}Cl)]_2$ was dissolved in 5 ml. of methanol, ethene was bubbled through the solution at room temperature until a clear solution was obtained. Under ethene atmosphere a solution of 97 mg (0.34 mmol) of bpa-Bz in 1,5 ml. methanol was added and stirred for a few minutes while bubbling through ethene. Subsequently 80.0 mg (0.43 mmol) of KPF_6 was added and the solution was stirred for 45 minutes under an ethene atmosphere. The solution was cooled down to -78°C to allow precipitation of [**16**]PF_6. The thus obtained light-yellow solid was collected by filtration, washed three times with ice-cold methanol under a nitrogen atmosphere and dried under vacuum. Yield 123.7 mg (0.18 mmol, 54 %).

[7] bpa$^{\#}$ = *N,N*-di(2-pyridylmetyl)amine (= bpa) with the amine-nitrogen deprotonated

^{1}H-NMR: (400.15 MHz, CD_2Cl_2, T= 298 K) δ (ppm) = 7.85 (t, 2H, J(H,H) = 7.77 Hz, Py-*H4*), 7.70 (d, 2H, J(H,H) = 5.57 Hz, Py-*H6*), 7.58 (m, 3H, Ph-*H3*, Ph-*H4* and Ph-*H5*), 7.50 (d, 2H, J(H,H) = 7.92 Hz, Py-*H3*), 7.24 (m, 4H, Py-*H5*, Ph-*H2* and Ph-*H6*), 5.39 (s, 4H, free C_2H_4), 5.10 (d[AB], 2H, J(H,H) = 15.53 Hz, Py-CH^AH-N), 4.64 (d[AB], 2H, J(H,H) = 15.68 Hz, Py-CHH^B-N), 4.36 (s, 2H, N-CH_2-Ph), 3.44 (t, 2H, J(H,H) = 10.11 Hz, $C_2H_4{}^A$), 3.27 (t, 2H, J(H,H) = 9.67 Hz, $C_2H_4{}^B$), 2.03 (t, 2H, J(H,H) = 9.67 Hz, $C_2H_4{}^B$), 1.94 (t, 2H, J(H,H) = 9.89 Hz, $C_2H_4{}^A$).

^{13}C{^{1}H}-NMR (50.03 MHz, CD_3CN, T= 298 K) δ I(ppm) = 165.62 (s, 2C, Py-C2), 150.65 (s, 2C, Py-C6), 138.97 (s, 2C, Py-C4), 133.32 (s, 2C, Ph-C2, Ph-C6), 132.25 (s, 1C, Ph-C1), 130.04 (d, 3C, Ph-C3, Ph-C4, Ph-C5), 126.82 (s, 2C, Py-C5), 125.04 (s, 2C, Py-C3), 64.92 (s, 1C, Ph-CH_2-N), 64.47 (s, 2C, Py-CH_2-N), 35.00 (s, 2C, $C_2H_4{}^A$), 30.60 (s, 2C, $C_2H_4{}^B$).

ESI$^+$-MS: m/z = 538 [**16**]$^+$, 510 {[**16**]-C_2H_4}$^+$, 482 {[**16**]-2 ∗C_2H_4}$^+$.

Calculated for $C_{23}H_{27}N_3IrPF_6$: C 40.47, H 3.99, N 6.16. Found: C 40.53, H 4.03, N 6.05.

*[{(κ^4-C,N,N'-bpa-Bz)Ir^{III}(μ^2-H)}$_2$]PF_6 (or [{(bpa-Bz$^{\#}$)Ir^{III}(μ^2-H)}$_2$]PF_6 or [**17**]$(PF_6)_2$)* [8]

A saturated solution of 100 mg (0.15 mmol) [**16**]$^+$ in 15 ml. acetone was prepared. Subsequently this solution is heated to 50 ºC for about 3 days. Meanwhile a fine light-yellow powder of [**17**]$(PF_6)_2$ has precipitated. The solution is removed from the powder with a syringe and the product is subsequently washed twice with acetone at −30 ºC.
Yield 33.6 mg (0.027 mmol, 18 %).

The phenyl group is cyclo-metallated at C2.

^{1}H-NMR (400.14 MHz, acetone-d6, 298 K): δ (ppm) = 7.94 (td, 4H, $J(H,H)_{doublet}$ = 5.68 Hz, $J(H,H)_{triplet}$ = 1.16 Hz, Py-*H6*), 7.8 - 7.7 (m, 8H, Py-*H3* and -*H4*), 7.55 (dd, 2H, J(H,H) = 7.42 Hz, J(H,H) = 0.96 Hz, Ph-*H3*), 6.65 (dt, 2H, $J(H,H)_{triplet}$ = 9.56 Hz, $J(H,H)_{doublet}$ = 1.56 Hz, Ph-*H4*), 6.62 (m, 4H, Py-*H5*), 6.58 (dt, 2H, $J(H,H)_{triplet}$ = 7.40 Hz, $J(H,H)_{doublet}$ = 1.36 Hz, Ph-*H5*), 6.45 (dd, 2H, J(H,H) = 7.14 Hz, J(H,H) = 1.00 Hz, Ph-*H6*), 6.15 (d[AB], 4H, J(H,H) = 14.85 Hz, N-CH_2-Py), 5.64 (d[AB], 4H, J(H,H) = 15.05 Hz, N-CH_2-Py), 4.67 (s, 4H, N-CH_2-Ph), −14.73 (s, 2H, Ir-*H*-Ir).

Due to the extremely low solubility in acetone-d6 it was not possible to measure a ^{13}C-NMR spectrum However, it was possible to measure gHSQC and gHMBC (C-H correlation spectra) from which some of the ^{13}C chemical shifts could be deduced.

^{13}C{^{1}H}-NMR (50.03 MHz, acetone-d6, 298 K): δ (ppm) = 166.1 (Py-C2), 155.8 (Py-*C6*), 148.8 (Ph-*C2*), 138.64 (Ph-*C3*), 138.52 (Py-*C3* or -*C4*), 134.9 (Ph-*C1*), 126.73 (Py-*C5*), 126.40 (Ph-*C4*), 124.69 (Py-*C3* or -*C4*), 124.40 (Ph-*C5*), 119.87 (Ph-*C6*), 73.45 (N-*C*H_2-Py), 68.52 (N-*C*H_2-Ph).

ESI$^+$-MS (acetone-d6 solution diluted with acetone) : m/z = 481 [**17**]$^{2+}$ (dicationic dinuclear complex), 482 [(bpa-Bz$^{\#}$)Ir(H)]$^+$ (monocationic, monomeric complex), 540 [(bpa-Bz$^{\#}$)Ir(H)(acetone)]$^+$.

Calculated for $C_{38}H_{38}N_6Ir_2P_2F_{12}$: C, 36.42; H, 3.06; N, 6.71; Found: C, 36.25; H, 3.12; N, 6.81.

X-Ray diffraction: for a structure see Figure 3.17.

*[(κ^4-C,N,N'-bpa-Bz)Ir^{III}(H)(CD_3CN)]PF_6 (or [(bpa-Bz$^{\#}$)Ir^{III}(H)(CD_3CN)]PF_6 or [**18**]PF_6)*

Upon dissolving [**17**]$^+$ in CD_3CN the conversion to [**18**]$^+$ takes place very rapidly. After 25 minutes only 13 % of the original dinuclear complex is present anymore. Eventually, according to ^{1}H-NMR full conversion to [**18**]$^+$ has taken place. The color of the solution is still yellow.

The phenyl group is cyclo-metallated at C2.

^{1}H-NMR (400.14 MHz, CD_3CN, 298 K): δ (ppm) = 8.66 (dd, 2H, J(H,H) = 5.60 Hz, J(H,H) = 0.48 Hz, Py-*H6*), 7.74 (dt, 2H, $J(H,H)_{triplet}$ = 7.82 Hz, $J(H,H)_{doublet}$ = 1.68 Hz, Py-*H4*), 7.65 (d, 1H, J(H,H) = 7.58 Hz, Ph-*H3*), 7.40 (dd, 2H, J(H,H) = 7.84 Hz, J(H,H) = 0.48 Hz, Py-*H3*), 7.08 (mt, 2H, J(H,H) = 8.56 Hz, Py-*H5*), 6.68 – 6.63 (m, 1H, Ph-*H4*), 6.60 (dt, $J(H,H)_{triplet}$ = 7.56 Hz, $J(H,H)_{doublet}$ = 1.48 Hz, Ph-*H5*), 6.58 (m, 1H, Ph-*H6*), 5.09 (d[AB], 2H, J(H,H) = 15.41 Hz, N-CH_2-Py), 5.02 (d[AB], 2H, J(H,H) = 15.41 Hz, N-CH_2-Py), 4.47 (s, 2H, N-CH_2-Ph), -18.30 (s, 1H, Ir-H).

^{13}C{^{1}H}-NMR (50.03 MHz, CD_3CN, 298 K): δ (ppm) = 166.89 (s, Py-*C2*), 158.23 (s, Py-*C6*), 149.85 (s, Ph-*C2*), 139.56 (s, Ph-*C1*), 142.17 (s, Ph-*C3*), 138.04 (s, Py-*C4*), 126.64 (s, Ph-*C4*), 126.46 (s, Py-*C5*),124.08 (s, Py-*C3*), 123.02 (s, Ph-*C5*), 120.14 (s, Ph-*C6*), 69.92 (s, N-CH_2-Py), 69.75 (s, N-CH_2, Ph).

ESI$^+$-MS (CD_3CN solution diluted with CH_3CN):

[(bpa-Bz$^{\#}$)Ir^{III}(H)(CH_3CN)]$^+$: m/z = 523 [**18**]$^+$, 482 {[**18**]-CH_3CN}$^+$.

Calculated for $C_{21}H_{22}IrN_4$: 523.14745; Found: 523.14433 (Δ = -5.8 ppm).

[8] bpa-Bz$^{\#}$ = *N*-benzyl-*N*,*N*-di(2-pyridylmethyl)amine (= bpa-Bz) with the benzyl ring deprotonated at C2.

$[(bpa\text{-}Bz^{\#})Ir^{III}(H)(CD_3CN)]^+$: m/z = 526 [**18**]$^+$, 482 {[**18**]-CD_3CN}$^+$.

Calculated for $C_{21}H_{19}IrN_4D_3$: 526.16626; Found: 526.16337 (Δ = -5.3 ppm).

*[(bpa-Bz$^{\#}$)Ir^{III}(μ^2-H)Ir(H)(bpa-Bz$^{\#}$)](PF$_6$)$_2$ ([**19**](PF$_6$)$_2$)*

Upon exposing an acetone-d6 solution of [**17**]$^+$ for about 5 hours to glass-filtered light the asymmetric product [**19**]$^{2+}$ is the only product formed according to ^{1}H-NMR. The color of the solution has now become somewhat darker yellow.

The phenyl group is cyclo-metallated at C2. Py, Py'' and Ph' belong to the asymmetrically coordinated N_3 ligand and Py', Py''' and Ph belong to the symmetrically coordinated N_3 ligand.

^{1}H-NMR (400.14 MHz, acetone-d6, 298 K): δ (ppm) = 9.22 (d, 1H, J(H,H) = Hz, Py'''-*H6*), 8.11 (td, ^{1}H, J(H,H)$_{doublet}$ = 5.36 Hz, J(H,H)$_{triplet}$ = 1.20 Hz, Py-*H6*), 7.95 (m, 1H, Py'-*H6*), 7.88 - 7.85 (m, 2H, Py-*H3* and -*H4*), 7.81 - 7.78 (m, 2H, Py'-*H3* and -*H4*), 7.72 - 7.66 (m, 3H, Py'''-*H3* and *H4*, Py''-*H4*), 7.38 (td, ^{1}H, J(H,H)$_{doublet}$ = 5.64 Hz, J(H,H)$_{triplet}$ = 0.96 Hz, Py''-*H6*), 7.23 (dd, J(H,H) = 7.68 Hz, J(H,H) = 1.20 Hz, Ph-*H3*), 7.21 - 7.15 (m, 2H, Py''-*H3*, Py'''-*H5*), 7.08 (d, ^{1}H, J(H,H) = 7.32 Hz, Ph'-*H6*), 6.9 (m, 1H, Py-*H5*), 6.69 (m, 1H, Py'-*H5*), 6.66 (m, 1H, Ph-*H4*), 6.65 - 6.55 (m, 3H, Py''-*H5*, Ph-*H5*, Ph'-*H5*), 6.52 (dd, ^{1}H, J(H,H) = 7.58 Hz, J(H,H) = 1.00 Hz, Ph'-*H3*), 6.39 (dd, ^{1}H, J(H,H) = 7.32 Hz, J(H,H) = 1.24 Hz, Ph-*H6*), 6.2 - 6.1 (m, 2H, N-C*H*$_2$-Py' and Ph'-*H4*, 6.01 (d[AB]$^{Py\ and\ Py'''}$, 1H, J(H,H) = 16.61 Hz, N-C*H*$_2$-Py and -Py'''), 5.67 (d[AB]$^{Ph'}$, 1H, J(H,H) = 12.68 Hz, N-C*H*$_2$-Ph'), 5.61 (d[AB]^{Py}, 1H, J(H,H) = 14.93 Hz, N-C*H*$_2$-Py), 5.36 (d[AB]$^{Py'}$, 1H, J(H,H) = 14.89 Hz, N-C*H*$_2$-Py'), 5.30 (d[AB]$^{Py'''}$, 1H, J(H,H) = 14.65 Hz, N-C*H*$_2$-Py'''), 5.20 (d[AB]$^{Ph'}$, 1H, J(H,H) = 12.96 Hz, N-C*H*$_2$-Ph'), 4.95 (d[AB]$^{Py''}$, 1H, J(H,H) = 19.29 Hz, N-C*H*$_2$-Py''), 4.88 (d[AB]$^{Py''}$, 1H, J(H,H) = 19.05 Hz, N-C*H*$_2$-Py''), 4.63 (s, 2H, N-C*H*$_2$-Ph), -14.90 (s, 1H, Ir-*H*-Ir), -23.92 (s, 1H, Ir-*H'*-Ir).

Due to the extremely low solubility in acetone-d6 it was not possible to measure a ^{13}C-NMR spectrum.

ESI$^+$-MS (actone-d6 solution diluted with acetone) : m/z = 481 [**19**]$^{2+}$ (dicationic dinuclear complex), 482 [(bpa-Bz$^{\#}$)Ir(H)]$^+$ (monocationic, monomeric complex), 540 [(bpa-Bz$^{\#}$)Ir(H)(acetone)]$^+$. In contrast to [**17**]$^+$ much less [(bpa-Bz$^{\#}$)Ir(H)]$^+$ is present in the mass spectrum, indicating a much more strongly bound dinuclear complex.

Upon addition of 0.3 ml. CD_3CN to a solution of [**19**]$^+$ in acetone-d6 no significant changes in the ^{1}H-NMR spectra or in the color of the solution are observed. The hydrides are now observed at δ = 15.05 and -24.06 ppm (instead of -14.90 and -23.92). The other signals have shifted up to 0.1 ppm to higher field.

ESI$^+$-MS (acetone-d6/CD_3CN solution diluted with CH_3CN) : m/z = 481 [**19**]$^{2+}$, 503 {[**19**](CD_3CN)}$^{2+}$, 523 [(bpa-Bz$^{\#}$)Ir(H)(CH_3CN)]$^+$, 526 [(bpa-Bz$^{\#}$)Ir(H)(CD_3CN)]$^+$. In contrast with previous ESI$^+$-MS measurements of [**17**]$^+$ and [**19**]$^+$ in acetone no [(bpa-Bz$^{\#}$)Ir(H)(solvent)]$^+$ and hardly any [(bpa-Bz$^{\#}$)Ir(H)]$^+$ is present in the spectrum.

*{[**19**](CD$_3$CN)}$^+$*

Upon dilution of the acetone-d6/CD_3CN NMR-solution of [**19**]$^{2+}$ with CH3CN for ESI$^+$-MS an interesting isotope pattern was observed: it corresponded to {[**19**](CD_3CN)}$^+$. Apparently no exchange of CD_3CN with CH_3CN had taken place. This is quite extraordinary, since such exchange has been observed for [**18**]$^+$ and other complexes., however for [**14**]$^{2+}$ this exchange was not observed either.

Calculated for $C_{40}H_{38}{}^{191}Ir^{193}IrN_7D_3$: 1006.285; found: 10062888 (Δ = 4.1 ppm)

[(κ^3-Me$_2$-bpa-R)Rh^I(C$_2$H$_4$)$_2$]PF$_6$

To a suspension of 0.87 mmol {[Rh(C_2H_4)$_2$(Cl)]$_2$} in 10 ml. of MeOH at -78 ºC was added 0.99 mmol Me_2-bpa-R (R = Me, Bz). The reaction mixture was stirred for 2 hours: there is still a lot of solid reactants present. Therefore the temperature of the reaction mixture is shortly allowed to go up to about 0 ºC. Immediately nearly all the reactants dissolve and presumably react. The reaction mixture is cooled down again to -78 ºC and the reaction mixture is filtered to remove all unreacted {[Rh(C_2H_4)$_2$(Cl)]$_2$}. Subsequently 1 equivalent of KPF_6 is added and a yellow/orange precipitate is formed, which is collected by filtration and dried under reduced pressure. Yield: 208 mg (for Me_2-bpa-Me) and 285 mg (for Me_2-bpa-Bz).

Since a mixture of both the bis- and the mono-ethene complex is obtained, the percentage yield cannot be determined.

Dissolving the precipitated solids in either CD_3CN or acetone-d6 did not help in determining the ratio between the bis- and the mono-ethene complexes, because in all cases unexpected reactions occurred.

*[(κ^3-Me$_2$-bpa-Me)Rh^I(C_2H_4)(CD_3CN)]PF_6 (asymmetric, [**20**]PF_6)*

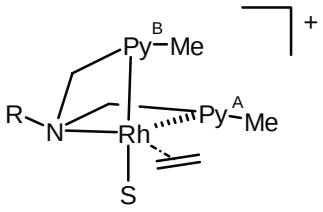

S = CD_3CN or acetone-d6

45 mg of [(Me$_2$-bpa-Me)Rh(C_2H_4)$_2$]PF_6 was dissolved in 1 ml. CD_3CN and the orange-yellow solution was kept for 2 hours under nitrogen atmosphere.

The assignment of Py^A and Py^B in [**20**]$^+$ was done in analogy with [**21**]$^+$.

^{1}H-NMR (400.14 MHz, CD_3CN, 298 K): δ (ppm) = 7.70 (t, ^{1}H, J(H,H) = 7.64 Hz, Py^B-*H4*), 7.60 (t, ^{1}H, J(H,H) = 7.60 Hz, Py^A-*H4*), 7.42 (d, 1H, J(H,H) = 7.64 Hz, Py^B-*H5*), 7.25 (dd, 1H, J(H,H) = 7.62 Hz, J(H,H) = 0.60 Hz, Py^A-*H3*), 7.11 (d, 1H, J(H,H) = 4.48 Hz, Py^B-*H3*), 7.09 (d, 1H, J(H,H) = 4.48 Hz, Py^A-*H5*), 5.34 (d[AB'], 1H, J(H,H) = 14.65 Hz, N-CH_2-Py^A), 4.35 (d[AB'], 1H, J(H,H) = 14.65 Hz, N-CH_2-Py^A), 3.73 (d[AB], 1H, J(H,H) = 16.00 Hz, N-CH_2-Py^B), 3.42 (d[AB], 1H, J(H,H) = 15.65 Hz, N-CH_2-Py^B), 3.41 (s, 3H, Py^B-CH_3), 3.09 (s, 3H, N-CH_3), 2.83 (s, 3H, Py^A-CH_3), 2.28 (m, 1H, C_2H_4), 2.16 (m, 1H, C_2H_4), 2.00 (m, 1H, C_2H_4), 1.04 (m, 1H, C_2H_4).

The ethene signals at δ = 2.16 and 1.04 show exchange signals in the NOESY spectrum indicating that although the olefin does not seems to be fluxional on ^{1}H-NMR timescale, the olefin is still a bit fluxionally bound to the rhodium center.

^{13}C{^{1}H}-NMR (50.03 MHz, CD_3CN, 298 K): δ (ppm) = 163.33 (s, Py^A- or Py^B-*C2* or -*C6*), 161.97 (s, Py^A- or Py^B-*C2* or -*C6*), 161.87 (s, Py^A- or Py^B-*C2* or -*C6*), 160.38 (s, Py^A- or Py^B-*C2* or -*C6*), 138.50 (s, Py^B-*C4*), 138.09 (s, Py^A-*C4*), 125.71 (Py^A-*C5*), 125.13 (Py^B-*C5*), 121.37 (s, Py^A-*C3*), 120.72 (s, Py^B-*C3*), 68.78 (s, N-*C*H$_2$-Py), 61.76 (s, N-*C*H$_2$-Py), 48.56 (s, N-*C*H$_3$), 28.91 (s, *C*$_2$H$_4$ (belonging to δ = 2.28 and 2.16 ppm in the ^{1}H-NMR), 28.51 (s, Py^B-*C*H$_3$), 28.17 (s, *C*$_2$H$_4$ (belonging to δ = 2.00 and 1.04 in the ^{1}H-NMR), 27.38 (s, Py^A-*C*H$_3$).

Upon dissolving the Me$_2$-bpa-Me rhodium bis-ethene complex in acetone-d6 the 2 major species present in solution are a symmetric mono-ethene complex, [(Me$_2$-bpa-Me)Rh(C_2H_4)]PF_6, and an asymmetric mono-ethene complex [(Me$_2$-bpa-Me)Rh(C_2H_4)(acetone-d6)]PF_6 in the ratio of ca. 2:1.

*[(κ^3-Me$_2$-bpa-Me)Rh^I(C_2H_4)(acetone-d6)]PF_6 (asymmetric, [**22a**]$^+$)*

^{1}H-NMR (400.14 MHz, acetone-d6, 298 K): δ (ppm) = 7.58 (t, 1H, J(H,H) = 7.84 Hz, Py^B-*H4*), 7.55 (t, 1H, J(H,H) = 7.80 Hz, Py^A-*H4*), 7.31 (d, 1H, J(H,H) = 7.84 Hz, Py^B-*H5*), 7.26 (d, 1H, J(H,H) = 7.44 Hz, Py^A-*H3*), 7.08 (d, 1H, J(H,H) = 7.80 Hz, Py^A-*H5*), 7.02 (d, 1H, J(H,H) = 8.00 Hz, Py^B-*H3*), 5.45 (d[AB], 1H, J(H,H) = 14.45 Hz, N-CH_2-Py^A), 4.37 (d[AB], 1H, J(H,H) = 14.28 Hz, N-CH_2-Py^A), 3.62 (d[AB], 1H, J(H,H) = 15.45 Hz, N-CH_2-Py^B), 3.56 (s, 3H, Py^B-Me), 3.39 (d[AB], 1H, J(H,H) = 15.21 Hz, N-CH_2-Py^B), 3.06 (s, 3H, N-Me), 2.99 (Py^A-Me), 2.53 (m, 1H, C_2H_4), 2.12 (m, 1H, C_2H_4), 1.97 (m, 1H, C_2H_4), 0.81 (m, 1H, C_2H_4).

*[(κ^3-Me$_2$-bpa-Me)Rh^I(C_2H_4)]PF_6 (symmetric, [**22b**]$^+$)*

^{1}H-NMR (400.14 MHz, acetone-d6, 298 K): δ (ppm) = 7.62 (t, 2H, J(H,H) = 7.80 Hz, Py-*H4*), 7.22 (d, 2H, J(H,H) = 7.64 Hz, Py-*H3*), 7.02 (d, 1H, J(H,H) = 8.00 Hz, Py-*H5*), 5.43 (d[AB], 2H, J(H,H) = 14.69 Hz, N-CH_2-Py), 4.41 (d[AB], 2H, J(H,H) = 14.45 Hz, N-CH_2-Py), 2.72 (s, 6H, Py-Me), 2.50 (s, 3H, N-Me), 2.39 (d, 4H, J(H,H) = 6.48 Hz, C_2H_4).

ESI$^+$-MS: m/z = 372 [(Me$_2$-bpa-Me)Rh(C_2H_4)]$^+$, 344 [(Me$_2$-bpa-Me)Rh]$^+$.

*[(κ^3-Me$_2$-bpa-Bz)Rh^I(C_2H_4)(CD_3CN)]PF_6 ([**21**]PF_6)*

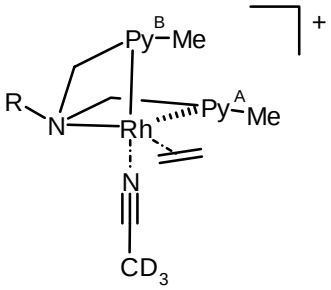

52 mg of [(Me$_2$-bpa-Bz)Rh(C_2H_4)$_2$]PF_6 was dissolved in 1 ml. CD_3CN and the red-orange solution was kept for 2 hours under nitrogen atmosphere.

Py^A and Py^B were assigned on the basis of NOESY measurements.

^{1}H-NMR (400.14 MHz, CD_3CN, 298 K): δ (ppm) = 7.76 (t, 1H, J(H,H) = 7.70 Hz, Py^B-*H4*), 7.6 - 7.5 (m, 6H, Py^A-*H4* and Ph-*H2*, *-H3*, *-H4*, *-H5* and *-H6*), 7.47 (d, 1H, J(H,H) = 8.08 Hz, Py^B-*H5*), .7.19 (d, 1H, J(H,H) = 7.40 Hz, Py^B-*H3*), 7.13 (d, 1H, J(H,H) = 7.60 Hz, Py^A-*H3*), 7.08 (d, 1H, J(H,H) = 7.70Hz, Py^A-*H5*), 5.57 (d[AB''], 1H, J(H,H) = 14.69 Hz, N-CH$_2$-Py^A), 4.93 (dd[AB'], 1H, J(H,H) = 14.43 Hz, J(H,H) = 1.68 Hz, N-CH_2-Ph), 4.19 (d[AB']or d[AB''], 1H, J(H,H) = 14.41 Hz, N-CH_2-Py^A or N-CH_2-Ph), 4.18 (d[AB'] or d[AB''], 1H, J(H,H) = 14.41 Hz, N-CH_2-Py^A or N-CH_2-Ph), 3.95 (d[AB], 1H, J(H,H) = 16.13 Hz, N-CH_2-Py^B), 3.46 (s, 3H, Py^B-CH_3), 2.98 (d[AB], 1H, J(H,H) = 16.12 Hz, N-CH_2-Py^B)2.87 (s, 3H, Py^A-CH_3) 2.47 (m, 1H, C_2H_4), 2.28 (m, 1H, C_2H_4), 2.13 (m, 1H, C_2H_4), 1.10 (m, 1H, C_2H_4).

^{13}C{^{1}H}-NMR (50.03 MHz, CD_3CN, 298 K): δ (ppm) = 163.28 (s, 2C, Py^A- and Py^B-*C2*), 161.96 (s, 1C, Py^A-*C6*), 160.11 (s, 1C, Py^B-*C6*), 138.70 (s, 1C, Py^A-*C4*), 138.08 (s, 1C, Py^B-*C4*), 133.64 (s, 1C, Ph-*C1*), 132.51 (s, 2C, Ph-*C2* and *-C6*), 129.74 (s,

2C, Ph-*C3* and -*C5*), 129.11 (s, 1C, Ph-*C4*), 125.77 (s, 1C, Py^A-*C5*), 125.36 (s, 1C, Py^B-*C5*), 121.75 (s, 1C, Py^A-*C3*), 121.15 (s, 1C, Py^B-*C3*), 65.92 (s, 1C, N-*C*H_2-Py^A), 62.71 (s, 1C, N-*C*H_2-Ph), 55.18 (s, 1C, N-*C*H_2-Py^B), 30.07 (d, 1C, J(Rh,C) = 28.16 Hz, *C*$_2$H$_4$), 29.13 (d, 1C, J(Rh,C) = 25.16 Hz, *C*$_2$H$_4$), 27.49 (s, 1C, Py^B-*C*H_3), 26.50 (s, 1C, Py^A-*C*H_3).

ESI^+-MS (in CH_3CN, thus coordinated CH_3CN, not CD_3CN): m/z = 489 [**20**]$^+$, 461 {[**20**]-C_2H_4}$^+$, 448 {[**20**]-CH_3CN}$^+$, 420 {[**20**]-CH_3CN-C_2H_4}$^+$.

*Reaction of [**21**]$^+$ in acetone-d6*

Upon dissolving [**21**]PF_6 in acetone-d6 immediately a red-orange colored mixture is formed of [**23a**]$^+$, [**23b**]$^+$, [**24**]$^+$. After 1 hour a mixture of products, with major product [**24**]$^+$ together with two symmetric complexes (in minor amounts) are present. ESI^+-MS measurements within 15 minutes (when still mainly ethene complexes are present) and 2 hours after dissolving (when [**24**]$^+$ is the major species present) give the same spectrum. The only difference observed is that after 2 hours the signal is more stable than at first: this could be due to the fact that the ethyl complex is much more stable than the ethene complexes.

ESI^+-MS (in acetone): m/z = 448 [**complex**]$^+$, 420 {[**complex**]-C_2H_4}$^+$ ([**complex**]$^+$ is a species with an m/z corresponding to [**21**]$^+$ but with unknown structure)

*[(κ^3-Me_2-bpa-Bz)Rh^I(C_2H_4)(acetone-d6)]PF_6 (asymmetric, [**23a**]$^+$)*

Since at first a mixture is obtained of 4 compounds, two of which are asymmetric (one of which is [**23a**]$^+$) and present in the smallest amounts, is it not possible to fully identify all ^{1}H-signals belonging to [**23a**]$^+$.

^{1}H-NMR (200.13 MHz, acetone-d6, 298 K): δ (ppm) = 7.7- 6.6 (m , 5.7 - 3.8 (d[AB] and d[AB'] and d[AB''], 6H, N-CH_2-Py^A, N-CH_2-Py^B, N-CH_2-Ph), 3.61 (s, 3H, Py-CH_3), 3.03 (s, 3H, Py-CH_3), 2.45 (m, 1H, C_2H_4), 2.22 (dd, 1H, J(H,H) = 9.11 Hz, J(H,H) = 2.32 Hz, C_2H_4), 2.06 (dd, 1H, J(H,H) = 10.15 Hz, J(H,H) = 2.32 Hz, C_2H_4), 0.86 (dd, 1H,J(H,H) = 8.02 Hz, J(H,H) = 1.70 Hz, C_2H_4).

*[(κ^3-Me_2-bpa-Bz)Rh^I(C_2H_4)]PF_6 (symmetric, [**23b**]$^+$)*

Since at first a mixture is obtained of 4 compounds, two of which are asymmetric, is it not possible to fully identify all ^{1}H-signals belonging to [**23b**]$^+$.

^{1}H-NMR (200.12 MHz, acetone-d6, 298 K): δ (ppm) = 7.51 (t, 2H, J(H,H) = 7.34 Hz, Py-*H4*), 7.6 - 6.6 (5H, m, Ph-*H2*, -*H3*, -*H4*, -*H5* and -*H6*), 7.27 (d, 2H, J(H,H) = 7.71 Hz, Py-*H3* or -*H5*), 7.07 (d, 2H, J(H,H) = 7.46 Hz, Py-*H3* or -*H5*), , 5.32 (d[AB], J(H,H) = 15.53 Hz, N-C*H*$_2$-Py), 4.65 (d[AB], J(H,H) = 15.29 Hz, N-C*H*$_2$-Py), 3.78 (s, 2H, N-C*H*$_2$-Ph), 2.84 (s, 6H, Py-C*H*$_3$), 2.68 (s(br), 4H, C_2H_4).

*[(κ^4-C,N,N',N''-bpa-Bz)Rh^{III}(C_2H_5)(acetone-d6)]PF_6 (or [(κ^4-Me_2-bpa-Bz$^{\#}$)Rh^{III}(C_2H_5)(acetone-d6)]PF_6 or [**24**]PF_6)*

The NMR signals of the two symmetric complexes present in solution 1 hour after dissolving could not be determined due to the large number of signals in the ^{1}H-NMR spectrum. For [**24**]$^+$ it was difficult, yet possible up to some extent. Due to the large number of proton signals in the aromatic region the chemical shift of only one of the phenyl-protons could be determined.

^{1}H-NMR (400.14 MHz, acetone-d6, 298 K): δ (ppm) = 7.64 (t, 1H, J(H,H) = 7.60 Hz, Py^A-*H4*), 7.28 (m, Ph-*H3*), 7.35 - 7.25 (m, Py^B-*H4* and Py^A-*H3*), 6.96 (d, 1H, J(H,H) = 7.60 Hz, Py^B-*H5*), 6.78 (d, 1H, J(H,H) = 7.60 Hz, Py^B-*H3*), 4.99 (d[AB''], 1H, J(H,H) = 14.65 Hz, N-C*H*$_2$-Ph), 4.75 (d[AB'], 1H, J(H,H) = 15.25 Hz, N-C*H*$_2$-Py^A), 4.42 (dd[AB''], 1H, J(H,H) = 14.65 Hz, J(H,H) = 2.12 Hz, N-C*H*$_2$-Ph), 4.30 (d[AB], 1H, J(H,H) = 15.25 Hz, N-C*H*$_2$-Py^B), 4.21 (d[AB], 1H, J(H,H) = 15.25 Hz, N-C*H*$_2$-Py^B), 3.90 (dd[AB'], 1H, J(H,H) = 14.06 Hz, J(H,H) = 2.76 Hz, N-C*H*$_2$-Py^A), 3.13 (s, 3H, Py^B-C*H*$_3$), 2.92 (s, 3H, Py^A-C*H*$_3$), 2.45 (m, 1H, Rh-CH*H*-CH_3), 1.86 (m, 1H, Rh-C*H*H-CH_3), 0.61 (t, 3H, J(H,H) = 7.46 Hz, Rh-CH_2-C*H*$_3$).

ESI^+-MS (in acetone): m/z = 448 [**24**]$^+$, 420 {[**24**]-C_2H_4}$^+$.

*[(κ^3-bpa)Rh^I(C_2H_4)]BPh_4 ([**25**]BPh_4)*

[**25**]BPh_4 was prepared by a procedure similar to that reported for [(κ^3-bpa-Me)Rh(C_2H_4)]PF_6 ([**26**]PF_6) and [(κ^3-bpa-Bz)Rh(C_2H_4)]PF_6 ([**27**]PF_6) [13], using bpa and 1 eq. $NaBPh_4$. A green-yellow solid was obtained. Yield 517 mg (80 %) starting from 1.00 mmol [(C_2H_4)$_2$Rh(μ-Cl)]$_2$.

^{1}H-NMR: (400.15 MHz, acetone-d6, T= 298 K) δ (ppm) = 7.89 (dt, J(H,H)$_{triplet}$ = 8.02 Hz, J(H,H)$_{doublet}$ = 1.56 Hz, 2H, Py-*H4*), 7.61 (dd, J(H,H)$_{doublet}$ = 5.64 Hz, J(H,H)$_{doublet}$ = 0.56 Hz, 2H, Py-*H6*), 7.45 (d, J(H,H) = 8.04 Hz, 2H, Py-*H3*), 7.37 - 7.31 (m, 8H, BAr-*H2* and t, 2H, Py-*H5*), 6.92 (t, J(H,H) = 7.24 Hz, 8H, BAr-*H3*), 6.78 (tt, J(H,H) = 7.04 Hz, J(H,H) = 1.4 Hz, 4H, BAr-

H4), 4.73 (d[AB], J(H,H) = 16.21 Hz, 2H, N-CH_2-Py), 4.66 (d[AB], J(H,H) = 16.04 Hz, 2H, N-CH_2-Py), 3.51, (s (br), 4H, C_2H_4).

$^{13}C\{^1H\}$-NMR (50.03 MHz, acetone-d6, T= 298 K) δ (ppm) = 166.37 (s, 2C, Py-*C2*), 163.94 (d, $^1J(B,C)$ = 49.3 Hz, 4C BAr-*C1*), 149.44 (s, 2C, Py-*C6*), 138.19 (s, 2C, Py-*C4*), 137.00 (q, J(B,C) = 1.09 Hz, 8C, BAr-*C2*), 126.05 (q, J(B,C) = 2.08 Hz, 8C, BAr-*C3*), 125.20 (s, 2C, Py-*C5*), 122.64 (s, 2C, Py-*C3*), 122.30 (s, 4C, BAr-*C4*), 58.21 (s, 2C, N-*C*H_2-Py). The ethene signal cannot be observed at r.t., it probably is too fluxional to be observed on the NMR timescale.

ESI^+-MS: m/z = 330 [**25**]$^+$, 302 {[**25**]-C_2H_4}$^+$, 328 {[**25**]-H_2}$^+$, 300 {[**25**]-C_2H_4-H_2}$^+$.

Calculated for $C_{38}H_{37}N_3Rh_1B_1$: C, 70.28; H, 5.74; N, 6.47. Found: C, 70.03; H, 5.67; N, 6.52.

3.9 References

[1] B. de Bruin, T. P. J. Peters, J. B. M. Wilting, S. Thewissen, J. M. M. Smits and A. W. Gal, *Eur. J. Inorg. Chem.,* **2002**, *(10)*, 2671-2680

[2] B. de Bruin, M. J. Boerakker, J. A. W. Verhagen, R. de Gelder, J. M. M. Smits and A. W. Gal, *Chem. - Eur. J.,* **2000**, *6 (2)*, 298-312

[3] E. B. Wickenheiser and W. R. Cullen, *Inorg. Chem.,* **1990**, *29 (23)*, 4671-4676

[4] B. Akermark, J. Glaser, L. Ohrstrom and K. Zetterberg, *Organometallics,* **1991**, *10 (3)*, 733-736

[5] C. L. Xie, D. Campbell and J. Jonas, *J. Chem. Phys.,* **1988**, *88 (5)*, 3396-3398

[6] M. Krom, T. P. J. Peters, R. G. E. Coumans, T. J. J. Sciarone, J. Hoogboom, S. I. ter Beek, P. P. J. Schlebos, J. M. M. Smits, R. de Gelder and A. W. Gal, *Eur. J. Inorg. Chem.,* **2003**, *6*, 1072-1087

[7] A. L. Onderlinden and A. van der Ent, *Inorg. Chim. Acta,* **1972**, *6*, 420-426

[8] J. L. Herde, J. C. Lambert and C. V. Senoff, *Inorg. Synth.,* **1974**, *15*, 18-20

[9] T. P. J. Peters, *Quarterly Report Q4 2000*, Department of Metal-Organic Chemistry, University of Nijmegen, the Netherlands, **2000**

[10] T. Sciarone, J. Hoogboom, P. P. J. Schlebos, P. H. M. Budzelaar, R. de Gelder, J. M. M. Smits and A. W. Gal, *Eur. J. Inorg. Chem.,* **2002**, *(2)*, 457-464

[11] M. Krom, *PhD Thesis "Mono- and Dioxygenation of Rhodium and Iridium Olefin Fragments, Solution versus Solid State Reactivity"*, **2003**

[12] J. Y. Saillard and R. Hoffmann, *J. Am. Chem. Soc.,* **1984**, *106 (7)*, 2006-2026

[13] R. J. N. A. M. Kicken, *PhD Thesis "Oxidation of Iridium Olefin Complexes by H_2O_2 and O_2"*, **2001**

[14] P. J. Perez, M. L. Poveda and E. Carmona, *J. Chem. Soc. - Chem. Commun.,* **1992**, *(1)*, 8-9

[15] D. M. Crumpton-Bregel and K. I. Goldberg, *J. Am. Chem. Soc.,* **2003**, *125 (31)*, 9442-9456

[16] U. Fekl and K. I. Goldberg, *"Homogeneous hydrocarbon C-H bond activation and functionalization with platinum", Advances in Inorganic Chemistry: Including Bioinorganic Studies*, *Volume 54*, Eds., Academic Press Inc., San Diego, **2003**

[17] M. P. Jensen, D. D. Wick, S. Reinartz, P. S. White, J. L. Templeton and K. I. Goldberg, *J. Am. Chem. Soc.,* **2003**, *125 (28)*, 8614-8624

[18] F. L. Taw, H. Mellows, P. S. White, F. J. Hollander, R. G. Bergman, M. Brookhart and D. M. Heinekey, *J. Am. Chem. Soc.,* **2002**, *124 (18)*, 5100-5108

[19] M. J. Chen, L. Nunez, J. W. Rathke and R. D. Rogers, *Organometallics,* **1996**, *15 (9)*, 2338-2344

[20] R. C. Schnabel, P. S. Carroll and D. M. Roddick, *Organometallics,* **1996**, *15 (2)*, 655-662

[21] D. M. Heinekey, D. A. Fine, T. G. P. Harper and S. T. Michel, *Can. J. Chem. - Rev. Can. Chim.,* **1995**, *73 (7)*, 1116-1125

[22] G. B. Robertson and P. A. Tucker, *Austr. J. Chem.,* **1984**, *37 (2)*, 257-263

[23] K. Fujita, T. Hamada and R. Yamaguchi, *J. Chem. Soc. - Dalton Trans.,* **2000**, *(12)*, 1931-1936

[24] K. Fujita, H. Nakaguma, T. Hamada and R. Yamaguchi, *J. Am. Chem. Soc.,* **2003**, *125 (41)*, 12368-12369

[25] K. Fujita, H. Nakaguma, F. Hanasaka and R. Yamaguchi, *Organometallics,* **2002**, *21 (18)*, 3749-3757

[26] V. I. Bakhmutov, E. V. Vorontsov, G. I. Nikonov and D. A. Lemenovskii, *Inorg. Chem.,* **1998**, *37 (2)*, 279-282

[27] A. Daugulis and M. Brookhart, *Organometallics,* **2004**, *23 (3)*, 527-534

[28] D. H. Woodmansee, X. H. Bu and G. C. Bazan, *Chem. Commun.,* **2001**, *(7)*, 619-620

[29] J. Muller, T. Akhnoukh, P. E. Gaede, A. L. Guo, P. Moran and K. Qiao, *J. Organomet. Chem.,* **1997**, *541 (1-2)*, 207-217

[30] R. Blom, D. W. H. Rankin, H. E. Robertson and R. N. Perutz, *J. Chem. Soc. - Dalton Trans.,* **1993**, *(13)*, 1983-1986

[31] P. Binger, B. Biedenbach, R. Mynott, R. Benn, A. Rufinska, P. Betz and C. Kruger, *J. Chem. Soc. - Dalton Trans.,* **1990**, *(6)*, 1771-1777

[32] D. T. Clark, M. Mlekuz, B. G. Sayer, B. E. McCarry and M. J. McGlinchey, *Organometallics,* **1987**, *6 (10)*, 2201-2207

[33] P. Caddy, M. Green, L. E. Smart and N. White, *J. Chem. Soc. - Chem. Commun.,* **1978**, *(19)*, 839-841

[34] M. C. Nicasio, M. Paneque, P. J. Perez, A. Pizzano, M. L. Poveda, L. Rey, S. Sirol, S. Taboada, M. Trujillo, A. Monge, C. Ruiz and E. Carmona, *Inorg. Chem.,* **2000**, *39 (2)*, 180-188

[35] R. Bencheikh, M. C. Bonnet, R. Chaabouni and F. Dahan, *J. Organomet. Chem.,* **1992**, *438 (1-2)*, 217-228

[36] M. Cocivera, A. J. McAlees, R. McCrindle and P. Szczecinski, *J. Organomet. Chem.,* **1982**, *235 (1)*, 97-104

[37] M. Hidai, Y. Uchida, K. Ishimi and M. Iwase, *Bull. Chem. Soc. Jpn,* **1972**, *45 (9)*, 2935

[38] J. C. Choi and T. Sakakura, *Organometallics,* **2004**, *23 (15)*, 3756-3758
[39] R. Boca, J. Kozisek and D. Steinborn, *J. Mol. Catal.,* **1993**, *84 (3)*, 261-265
[40] E. Krukowka, R. Taube and D. Steinborn, DD 296 909, **1988**
[41] H. Werner, G. Canepa, K. Ilg and J. Wolf, *Organometallics,* **2000**, *19 (23)*, 4756-4766
[42] H. Werner, M. E. Schneider, M. Bosch, J. Wolf, J. H. Teuben, A. Meetsma and S. I. Troyanov, *Chem. - Eur. J.,* **2000**, *6 (16)*, 3052-3059
[43] J. Ruiz, P. O. Bentz, B. E. Mann, C. M. Spencer, B. F. Taylor and P. M. Maitlis, *J. Chem. Soc. - Dalton Trans.,* **1987**, *(11)*, 2709-2713
[44] B. de Bruin, J. A. W. Verhagen, C. H. J. Schouten, A. W. Gal, D. Feichtinger and D. A. Plattner, *Chem. - Eur. J.,* **2001**, *7 (2)*, 416-422
[45] B. de Bruin, J. A. Brands, J. J. J. M. Donners, M. P. J. Donners, R. de Gelder, J. M. M. Smits, A. W. Gal and A. L. Spek, *Chem. - Eur. J.,* **1999**, *5 (10)*, 2921-2936
[46] G. Anderegg and F. Wenk, *Helv. Chim. Acta,* **1967**, *50 (8)*, 2330
[47] H. Nagao, N. Komeda, M. Mukaida, M. Suzuki and K. Tanaka, *Inorg. Chem.,* **1996**, *35 (23)*, 6809-6815
[48] R. Cramer, J. A. McCleverty and J. Bray, *Inorg. Synth.,* **1990**, *28*, 86
[49] A. C. T. North, D. C. Phillips and F. S. Mathews, *Acta Crystallogr. Sect. A,* **1968**, *A 24*, 351
[50] P. T. Beurskens, G. Beurskens, W. P. Bosman, R. de Gelder, S. Garcia-Granda, R. O. Gould, R. Israel and J. M. M. Smits, *"DIRDIF-96. A computer program system for crystal structure determination by Patterson methods and direct methods applied to difference structure factors"*; Laboratory of Crystallography, Department of Inorganic Chemistry, University of Nijmegen: The Netherlands, **1996**
[51] P. T. Beurskens, G. Beurskens, M. Strumpel and C. E. Nordman, *Patterson and Pattersons*, Vol. Eds. J. P. Glusker, B. K. Patterson and M. Rossi, Clarendon Press, Oxford, **1987**, page 356
[52] G. M. Sheldrick, *"SHELXL-97. Program for the refinement of crystal structures"*; University of Goettingen, Germany, **1997**
[53] N. Walker and D. Stuart, *Acta Crystallogr.,* **1983**, *A39*, 158-166
[54] A. L. Spek, *"PLATON-93. Program for display and analysis of crystal and molecular structures"*; University of Utrecht, The Netherlands, **2003**
[55] W. Baker, K. M. Buggle, J. F. W. McOmie and D. A. M. Watkins, *J. Chem. Soc.,* **1958**, *(OCT)*, 3594-3603
[56] M. M. Damota, J. Rodgers and S. M. Nelson, *J. Chem. Soc. A - Inorg. Phys. Theor.,* **1969**, *(13)*, 2036-2044
[57] B. de Bruin, *PhD Thesis "Oxidation of Rhodium-Olefin Complexes via 2-Rhodaoxetanes"*, **1999**

Chapter 4

Solution and Solid-State Reaction of N_3 and N_4 Rhodium and Iridium Olefin Complexes towards Dioxygen

4.1 Introduction

Mechanistically olefin oxygenation by dioxygen is poorly understood. In late transition metal (LTM) catalyzed oxidation of olefins, peroxo and olefin-peroxo complexes, [1] – [12] 3-metalla-1,2-dioxolanes, [1] – [13] and 2-metallaoxetanes [14], [15], [16] have been proposed as crucial intermediates. Stoichiometric studies of oxygenation of rhodium(I) and iridium(I) olefin complexes have proved useful in establishing the viability of these proposed intermediates and elucidating their chemistry.

Previous studies from our group involving stoichiometric oxygenation of metal-olefin complexes by O_2 and H_2O_2 focused on relatively unhindered bpa and tpa-type of complexes. [17] – [21] They indeed led to several 2-metallaoxetane and 3-metalla-1,2-dioxolane derivatives:

– Selective oxygenation of cationic rhodium(I) and iridium(I)-ethene complexes [**A1**]$^+$-[**D1**]$^+$ by H_2O_2 *in solution* (various solvents) results in 2-rhoda(III)- and 2-irida(III)-oxetanes (1-oxa-2-metalla(III)cyclobutanes) [**A2**]$^+$-[**D2**]$^+$ (Figure 4.1). [17], [22] – [25]

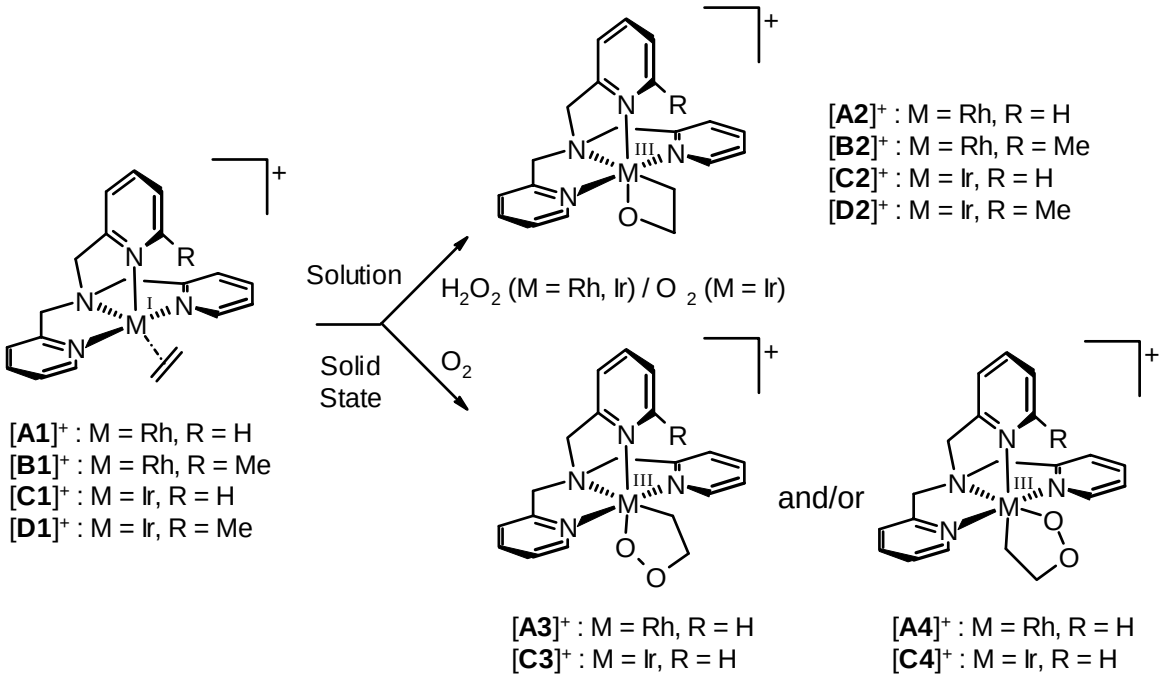

Figure 4.1 *Mono- and dioxygenation of rhodium(I)- and iridium(I)-ethene complexes by O_2*

- For a few cationic iridium(I)-ethene complexes mono-oxygenation is also observed with molecular oxygen instead of H_2O_2: reaction of [**D1**]$^+$ with air or O_2 in CH_2Cl_2 led to formation of approx. 25 % of [**D2**]$^+$. [17]
- Slow, selective dioxygenation of *solid* [**A1**]$^+$ with air or O_2 to the 3-metalla-1,2-dioxolanes [**A3**]$^+$ and [**A4**]$^+$ has been observed. The ratio between these geometrical isomers proved to be counter-ion dependent. [19] Similar reactions were observed for iridium(I) analogue [**C1**]$^+$ yielding [**C3**]$^+$ and [**C4**]$^+$. [20]

Formation of these 4- and 5-membered ring compounds in stoichiometric model reactions indicates that these species may also be important in catalytic reactions. However, the mechanism by which 2-metallaoxetanes and 3-metalla-1,2-dioxolanes are formed from O_2 is still unclear.

In the present chapter we will study the influence of steric bulk by using the more highly substituted Me_2-bpa-R (R = Me, Bz), Me_2-tpa and Me_3-tpa ligands. Where relevant, results are compared with those for more open systems ([**A1**]$^+$-[**D1**]$^+$).

Some of the results presented in this chapter have already been published. [26]

4.2 Reaction of N_3 and N_4 iridium(I) ethene complexes towards dioxygen

4.2.1 Me_3-tpa and Me_2-bpa-Me iridium(I) ethene

Reaction in solution of Me_3-tpa and Me_2-bpa-Me iridium(I) ethene with dioxygen

When 1.2 bar of dioxygen is put on a CD_2Cl_2-solution of the Me_3-tpa or the Me_2-bpa-Me iridium(I) mono-ethene complex, non-selective reactions take place.

In the case of Me_3-tpa complex [**4**]$^+$ the ^{1}H-NMR shows intense signals of peroxo-ethene complex [**28**]$^+$ (Figure 4.2) and very broad signals, probably from paramagnetic species. Based on the intensity of the ^{1}H-NMR signals of [**28**]$^+$ relative to the internal standard dichloroethane, the starting complex [**4**]$^+$ has been converted for approx. 25 % to [**28**]$^+$, and for approx. 70 % to one or more paramagnetic compounds.

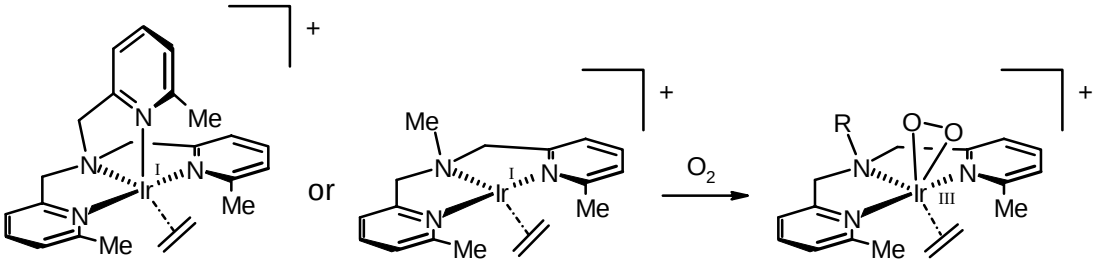

Figure 4.2 *Reaction of Me_3-tpa and Me_2-bpa-Me iridium(I) ethene ([**4**]$^+$ and [**8**]$^+$) with dioxygen*

The reaction of Me_2-bpa-Me complex [**8**]$^+$ proceeds similar to that of [**4**]$^+$. Again approx. 25 % of the peroxo-ethene complex [**29**]$^+$ and approx. 70 % of unidentified paramagnetic species are formed (Figure 4.2).

Attempts to improve the selectivity of these reactions, e.g. by treatment of [**4**]PF_6 or [**8**]PF_6 with only one equivalent O_2 or by performing the reactions at lower temperatures, were not successful. Nevertheless, we succeeded in isolating pure [**28**]PF_6 and [**29**]PF_6 through crystallization.

The ^{1}H- and ^{13}C-NMR spectra of peroxo-ethene complexes [**28**]$^+$ and [**29**]$^+$ show signals for two equivalent N-CH_2-Py^{Me} groups. The dangling N-CH_2-Py^{Me} group of [**28**]$^+$ gives rise to a ^{1}H-NMR methyl signal at 2.65 ppm, close to the value for the free ligand (2.56 ppm). The methyl signals of the two equivalent

6-methyl-pyridyl groups of [**28**]$^+$ and [**29**]$^+$ are approx. 0.4 ppm downfield from those in the free ligand. The diastereotopic methylene protons of the two axial N-CH_2-Py^{Me} groups give rise to an AB pattern.

Solid state structures of [28]$^+$ and [29]$^+$

The structures of peroxo-ethene complexes [**28**]PF_6 (Figure 4.3) and [**29**]PF_6 (Figure 4.4) were determined by single crystal X-ray diffraction. The structure of [**29**]$^+$ reveals a κ^3-*mer* coordinated Me_3-tpa ligand with a non-coordinated 6-methyl-pyridyl group, in accord with the NMR data. It seems reasonable to assume that for [**4**]$^+$ dissociation of the equatorial pyridyl group precedes reaction with O_2; this would explain why the reactions of [**4**]$^+$ and [**8**]$^+$ with O_2 are very similar.

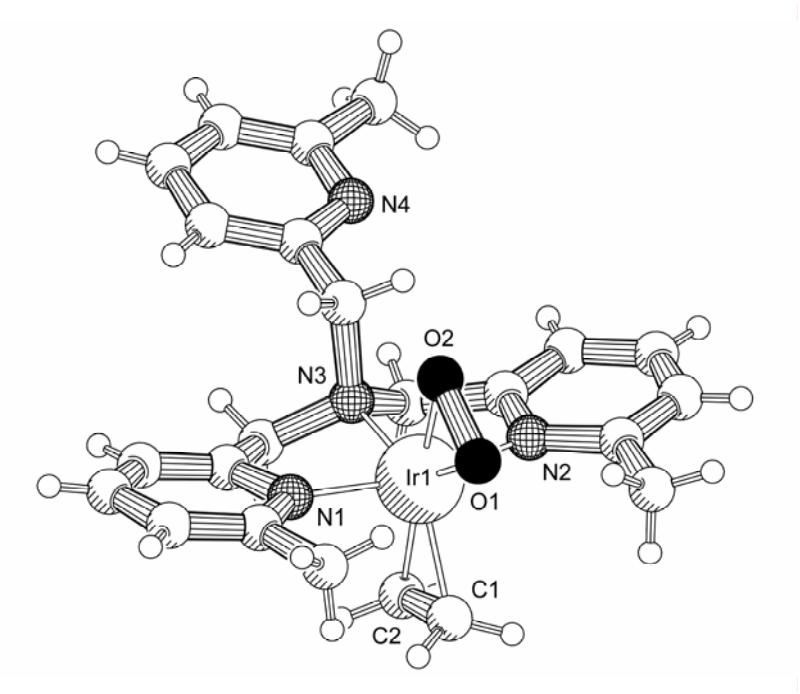

Figure 4.3 *X-ray structure of [(κ^3-Me_3-tpa)Ir(C_2H_4)(O_2)]PF_6 .½H_2O. Anion and crystal water omitted for clarity*

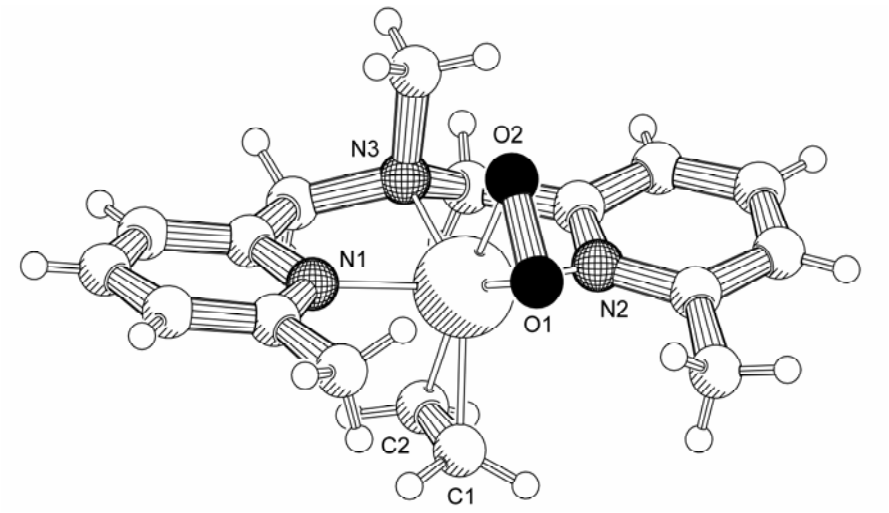

Figure 4.4 *X-ray structure of [(κ^3-Me_2-bpa-Me)Ir(C_2H_4)(O_2)]PF_6. Anion omitted for clarity*

Table 4.1 *Selected bond lengths [Å] and angles [°] of [**28**]$^+$ and [**29**]$^+$*

	[**28**]$^+$	[**29**]$^+$		[**28**]$^+$	[**29**]$^+$
Ir1-N1	2.071(12)	2.083 (6)	N1-Ir1-N2	162.3 (5)	164.0 (2)
Ir1-N2	2.085 (12)	2.076 (5)	N1-Ir1-N3	80.7 (5)	81.5 (2)
Ir1-N3	2.073 (11)	2.098 (5)	N2-Ir1-N3	81.6 (5)	82.7 (2)
Ir1-O1	2.014 (10)	2.046 (5)	O1-Ir1-N3	136.7 (4)	136.0 (2)
Ir1-O2	2.011 (9)	2.023 (5)	O2-Ir1-N3	95.1 (4)	94.4 (2)
Ir1-C1	2.119 (14)	2.122 (7)	C1-Ir1-N3	128.4 (5)	127.1 (3)
Ir1-C2	2.162 (14)	2.136 (7)	C2-Ir1-N3	90.1 (5)	88.8 (3)
O1-O2	1.430 (13)	1.446 (8)	O1-Ir1-C1	94.9 (5)	96.8 (3)
C1-C2	1.40 (2)	1.404 (11)	O1-Ir1-C2	133.1 (5)	135.1 (3)
			O2-Ir1-C1	136.5 (5)	138.4 (3)
			O2-Ir1-C2	174.6 (5)	176.1 (5)

The O-O distances in [**28**]$^+$ (1.430(13) Å) and [**29**]$^+$ (1.446(8) Å) indicate that the coordinated η^2-O_2 is best described as a η^2-peroxo fragment.[1] Consequently the iridium center is formally in the +3 oxidation state. The errors in the C=C distances are too large to draw any conclusions about the ethene-metal interaction.[2] Also the lack of suitable reference compounds complicates this assignment.

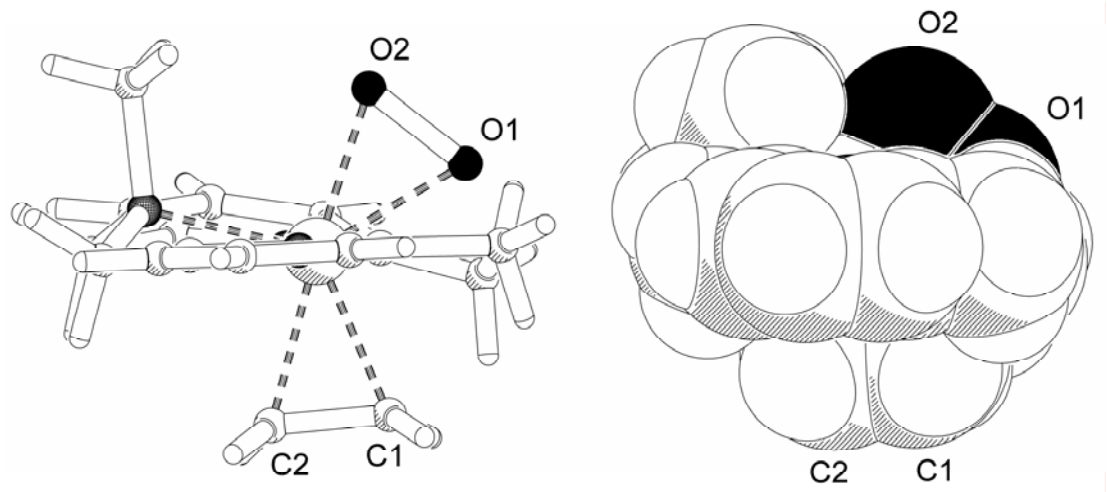

Figure 4.5 *Left: Structure of [**29**]$^+$ in the solid state viewed along the N1-Ir1-N2 axis. Right: Space-filling model of this structure*

A view of the ethene-peroxo complex [**28**]$^+$ along the N1-Ir1-N2 axis (see Figure 4.5) reveals that Me_2-dpa-Me in its *mer*-coordination mode leaves a relatively small compartment for coordination *cis* to the N3-Me fragment and a much larger one *trans* to it.

[1] Typical O-O distances for metal-peroxo complexes are 1.4 - 1.6 Å [27], [28] and for metal-superoxo complexes 1.26 - 1.33 Å.[29] – [33] The O-O distance calculated for free dioxygen is 1.17 Å.

[2] Ranges found in the Cambridge Structural Database, Ir^I-C: 2.036-2.191 Å, C-C: 1.351-1.444 Å.

C=C distance calculated for free ethene: 1.34 Å. The C=C distance in the Me_2-tpa and Me_3-tpa iridium(I) mono-ethene complexes is 1.442(11) Å and 1.451(13) Å respectively.

As already discussed in Chapter 3, on the basis of DFT-calculations for [**8**]$^+$ a mono-vacant trigonal bipyramidal coordination geometry can be assumed, with ethene coordinated *trans* to the N3-Me fragment, close to the structure of [**29**]$^+$ without the peroxo-fragment. Binding of O_2 to [**8**]$^+$ would thus involve only small structural rearrangements.

Complexes [**28**]$^+$ and [**29**]$^+$ are rare examples of peroxo-olefin complexes. In complexes [**F**] [34] and [**G**]$^+$ [35] – [37] (Figure 4.6) olefin coordination is promoted by the chelate effect:

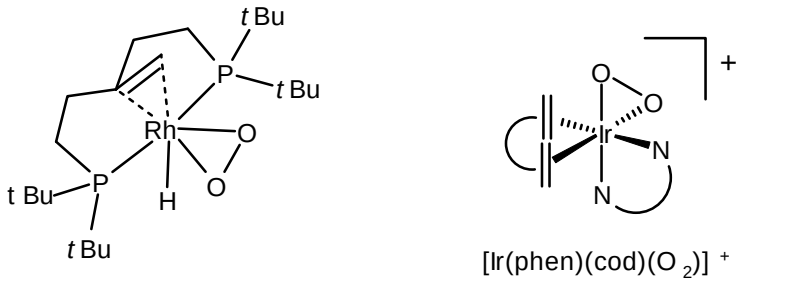

[**F**] [**G**]$^+$

Figure 4.6 *Peroxo-olefin rhodium complexes [**F**] and [**G**]$^+$*

Brown *et al.* reported formation of [(Cl)Ir(PPh_3)$_2$(O_2)(C_2H_4)] [38], a complex in which the chelating effect is absent, but this compound was not structurally characterized.
[**28**]$^+$ and [**29**]$^+$ are the first examples of structurally characterized peroxo-ethene complexes.

It is remarkable that the olefin fragment of [**28**]$^+$, [**29**]$^+$, [**F**] and [**G**]$^+$ does not insert into the M-O bond of the η^2-peroxo fragment. The approach of the peroxo fragment by the olefin fragment might be hindered by geometrical constraints, i.e. the fixed position of the olefin in [**F**] and [**G**]$^+$ and for steric reasons in [**28**]$^+$ and [**29**]$^+$. However, there seems to be no obvious geometrical constraint preventing movement of the peroxo fragment towards the olefin. Nevertheless, intramolecular C-O bond formation is not observed, both [**28**]$^+$ and [**29**]$^+$ are stable.
[(Cl)Ir(PPh_3)$_2$(O_2)(C_2H_4)], on the other hand, decomposes in solution in the absence of ethene forming some Ph_3PO and CH_3CHO, which indicates C-O bond formation. The complex appears to be also capable of promoting the oxidation of 1-octene and styrene by dioxygen.

Reduced π-backdonation to the olefin?

One would expect a weakening of the iridium-ethene coordination on going from the mono-ethene complexes to the peroxo-ethene complexes. Unfortunately this cannot be established from the X-ray data, because of the relatively large error bounds in the C=C bond lengths and the lack of suitable reference compounds. However, the ^{1}H-NMR data provide clear evidence for this weakening.
When comparing the ^{1}H-NMR chemical shifts of the olefin of [**4**]$^+$ and [**8**]$^+$ with those of [**28**]$^+$ and [**29**]$^+$ (see Table 4.2 on the next page), a clear shift towards free ethene can be observed.
Of course, ^{1}H chemical shifts are not only determined by π-backdonation from the metal, but also by anisotropy effects due to the solvent and nearby π-systems.
From Table 4.2 it is clear that changing the solvent does not account for this large shift upon going from a mono-ethene complex to the corresponding peroxo-ethene complex.
In both the mono-ethene and the corresponding peroxo-ethene complexes the olefin takes up the same position, e.g. below the N_{amine}-Ir-$N_{pyridine}$ plane (see the solid-state structures of [**28**]$^+$ and [**29**]$^+$, the solid-state structure of [**4**]$^+$ in § 3.3 and the DFT-calculated structures for [**8**]$^+$ in Appendix A). Therefore the shielding/deshielding should be very similar in all cases.

Table 4.2 *^{1}H-chemical shifts of the ethene signals in different solvents in ppm (200 MHz, 298K)*

	^{1}H in Acetone-d6	^{1}H in CD_3CN	^{1}H in CD_2Cl_2
$[(Me_3\text{-tpa})Ir^{I}(C_2H_4)]^+$ ([**4**]$^+$)	1.89 (t), 1.47 (t)	1.85 (t), 1.37 (t)	
$[(Me_3\text{-tpa})Ir^{III}(C_2H_4)(O_2)]^+$ ([**28**]$^+$)	4.48 (s(broad))		
$[(Me_2\text{-bpa-Me})Ir^{I}(C_2H_4)]^+$ ([**8**]$^+$)		3.54 (t), 2.34 (t)	3.59 (t), 2.36 (t)
$[(Me_2\text{-bpa-Me})Ir^{III}(C_2H_4)(O_2)]^+$ ([**29**]$^+$)	4.36 (s(broad))	4.22 (s(broad))	
Free ethene	4.5	4.5	4.5

Thus it seems safe to state that the downfield shift of the ethene protons upon going from a mono-ethene to the corresponding peroxo-ethene complex is mainly due to a decreased π-backdonation from the metal to the olefin on going from iridium(I) to iridium(III).

The large downfield shift in both the ^{1}H- and the ^{13}C-NMR[3] on going from five-coordinate [**4**]$^+$ to four-coordinate [**8**]$^+$ must be due to electronic reasons only, since the geometry of the (bpa)Ir(ethene) part of the molecule hardly changes on going from [**4**]$^+$ to [**8**]$^+$. For the peroxo-ethene complexes [**28**]$^+$ and [**29**]$^+$, which are both κ^3-coordinated, the electronic influence of the N-donor ligands seem similar, since there is no significant difference in the ^{1}H chemical shift observed.

Another indication of this phenomenon comes from the rate of ethene rotation (around the iridium-olefin bond). On going from iridium(I)-ethene compounds [**4**]$^+$ and [**8**]$^+$ to the peroxo-ethene iridium(III) species [**28**]$^+$ and [**29**]$^+$, the rate of ethene rotation increases. In the 200 MHz ^{1}H-NMR spectra of [**28**]$^+$ and [**29**]$^+$ at r.t., the ethene fragments are observed as very broad signals at 4.48 ppm and 4.22 ppm, respectively. At 500 MHz, the broad signals have split into two sharp triplets at 233 K, for both [**28**]$^+$ (δ = 4.84 and 4.14 ppm, ^3J(H,H) = 9.70 Hz) and [**29**]$^+$ (δ = 4.56 and 3.77 ppm, ^3J(H,H) = 9.40 Hz). For both [**28**]$^+$ and [**29**]$^+$ at 500 MHz, coalescence of these triplets into one signal occurs at T_c= 273 K. From these data, the free energy of activation ($\Delta G_c^{\neq}$) for ethene rotation in [**28**]$^+$ and [**29**]$^+$ at T_c was estimated to be ~12 kcal/mol. The ethene fragments of [**4**]$^+$ and [**8**]$^+$ do not rotate on the ^{1}H-NMR timescale at r.t. (298 K, 200 MHz). The free energy of activation for ethene rotation ($\Delta G_c^{\neq}$) of [**4**]$^+$ and [**8**]$^+$, as estimated from line-width analysis of the ethene ^{1}H-NMR signals, must be at least 17 kcal/mol.

The increased rate of ethene rotation on going from iridium(I)-ethene compounds [**4**]$^+$ and [**8**]$^+$ to peroxo-ethene iridium(III) species [**28**]$^+$ and [**29**]$^+$ most likely results from decreased Ir→C=C π-back bonding for iridium(III) relative to iridium(I), since the C=C→Ir σ-donation should be nearly independent of the orientation of the olefin.

Reactivity of [(Me$_2$-bpa-Me)Ir^{III}(C$_2$H$_4$)(O$_2$)]$^+$ ([29]$^+$)

Binding of O_2 to a transition metal is accompanied by electron transfer from the metal to O_2 (to form superoxo or peroxo complexes), making the coordinated oxygen fragments more nucleophilic. This can be useful for attack at electrophilic carbon centers. However, if *oxidation* of organic substrates is intended, an electrophilic oxygen moiety is required, so the usual binding of dioxygen to the metal center in fact *deactivates* the O_2 molecule. Therefore, effective metal-mediated oxygenation reactions usually require additional activation of

[3] ^{13}C chemical shifts of ethene-carbons in [**4**]$^+$ (acetone-d6): 3.7 and 0.2 ppm; in [**8**]$^+$ (CD_3CN): 37.0 and 25.1 ppm. Since the shifts in the ^{13}C-NMR due to electronic or structural reasons are much larger than those observed for changing the solvent (only 1-2 ppm), the solvent effect is negligible. Unfortunately the ^{13}C-shift of the ethene-carbons for the peroxo-ethene complexes could not be observed. They are too fluxional at this temperature, as was already observed in the ^{1}H-NMR.

superoxo or peroxo ligands, which converts the nucleophilic oxygen moiety into an electrophilic species. For example in the well-studied cytochrome P-450 system it is proposed that protonation of the η^2-peroxo intermediates gives the η^1-hydroperoxo species, which is converted into the higher valent, highly electrophilic oxo intermediate by protonation followed by the elimination of water. [39] – [42]

It was hoped that activation of [**29**]$^+$ could lead to formation of a C-O bond between a coordinated olefin and one of the oxygen-atoms of the peroxo moiety. The reactivity of [**29**]$^+$ was tested under various conditions in CD_2Cl_2.

- Since the O-O bond in 3-rhoda-1,2-dioxolanes is cleaved when they are irradiated with glass-filtered daylight ($\lambda > 320$ nm) [20], [21] the same conditions were applied to peroxo-ethene complex [**29**]$^+$ in CD_2Cl_2. According to ^{1}H-NMR no reaction seems to take place. The trivial explanation would be the absence of an absorbance above 320 nm. However, the visual color is similar to that of the 3-rhoda-1,2-dioxolane (which is light-yellow).
- No reaction was observed with triphenylphosphine.
- Burger [43] found that addition of H_2 can activate some peroxo complexes for olefin oxidation. But [**29**]$^+$ did not seem to react with H_2 at all.
- Conversion of a peroxo species into a hydroperoxo species via protonation is a common activation pathway. This has been proposed for metalloporphyrin systems including hemoproteins [41], [42], [44] and also for some rhodium peroxo complexes reported by Morvillo *et al.* [45]
  Addition of one equivalent of oxonium acid $[H(OEt_2)_2]^+[(3,5\text{-}(CF_3)_2C_6H_3)_4B]^-$ ($HBAr^F_4$) [46] to a solution of [**28**]$^+$ produced a white precipitate is formed and a clear solution.
  From ^{1}H-NMR it can be concluded that the reaction with $HBAr^F_4$ is not selective.
  Interestingly, a small multiplet can be observed around 9.8 ppm, which could correspond to either a trace of acetaldehyde or some formylmethyl species. Apparently, it is possible to activate the peroxo moiety to such extent that C-O bond formation can take place (although in an aselective reaction).

Solid state reaction of Me_3-tpa mono-ethene and Me_2-bpa-Me bis-ethene complexes with dioxygen

In the solid state Me_3-tpa iridium(I) mono-ethene complex [**4**]$^+$ does not react at in the solid state with dioxygen.

As already described in § 3.4.1, when the Me_2-bpa-Me iridium(I) bis-ethene complex [**7**]$^+$ is exposed to a dioxygen atmosphere for about 3 months at r.t. no reaction with dioxygen takes place at all. Instead the bis-ethene complex reacts intramolecularly (maybe under the influence of light) to form a vinyl-ethene-hydride complex, which rearranges to the corresponding ethyl-vinyl complex [**9**]$^+$ upon dissolving in CD_3CN.

4.2.2 Reaction of bpa-R iridium(I) bis-ethene (R = H, Me, Bz) towards dioxygen

Reactions of bpa-R complexes [**13**]$^+$, [**15**]$^+$ and [**16**]$^+$ (R = H, Me, Bz respectively) towards dioxygen were performed both in acetonitrile and in dichloromethane to investigate the influence of the coordinating properties of the solvent on the type of products formed. Product analysis was performed by ^{1}H-NMR and ESI^+-MS.

In all cases non-selective reactions with dioxygen were observed, but similar reactions seem to have taken place for all bpa-R complexes. For all three compounds very broad ^{1}H-NMR signals were obtained, probably indicating the presence of paramagnetic species.

Upon exposure of solid [**13**]$^+$, [**15**]$^+$ and [**16**]$^+$ to dioxygen, no reaction took place for the bpa-Me and the bpa-Bz iridium(I) bis-ethene complexes. The bpa complex had not reacted after a week; it had completely decomposed after a year.

4.3 Reaction of N_3 and N_4 rhodium ethene complexes with dioxygen

4.3.1 Me_n-tpa rhodium ethene complexes (n = 2, 3)

Treatment of CD_2Cl_2 solutions of rhodium(I) complexes [**1**]$^+$ or [**2**]$^+$ with O_2 resulted in selective formation of rhodium(III) peroxo complexes [**30**]$^+$ and [**31**]$^+$, respectively, according to ^{1}H-NMR and ESI$^+$-MS (Figure 4.7).

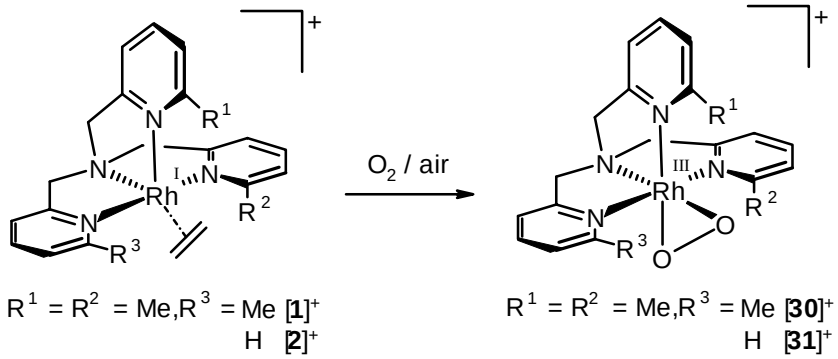

Figure 4.7 *Reaction of N_4 rhodium ethene complexes with dioxygen: formation of peroxo complexes*

Ethene is cleanly displaced by dioxygen. Loss of ethene was confirmed by ^{1}H-NMR. The ^{1}H- and ^{13}C-NMR data of [**30**]$^+$, showing two equivalent and one unique N-CH_2-Py^{Me} fragment, are in accordance with a κ^4-coordination mode of the Me_3-tpa ligand. In the case of [**2**]$^+$ an asymmetric peroxo complex [**31**]$^+$ is obtained, indicating that the geometry of the Me_2-tpa complex does not change during the reaction.
Interestingly, air can also be used as a dioxygen source for these reactions. For the formation of the iridium peroxo-ethene complexes [**28**]$^+$ and [**29**]$^+$ the presence of H_2O and CO_2 would have interfered too much.
In contrast, dissolved rhodium Me_n-tpa complexes with fewer Me subsituents, *viz.* [(Me_n-tpa)$Rh^I(C_2H_4)$]$^+$ (n = 0, 1), upon contact with O_2 or air lose ethene in an aselective reaction. [18]

The reaction path via which rhodium peroxo complexes [**30**]$^+$ and [**31**]$^+$ are formed is not known; it could be either via the formation of a peroxo-ethene complex (as observed for iridium, § 4.2.1) or via dissociation of the ethene and subsequent coordination of dioxygen.
Some insight into this could be retrieved from the reaction rates observed: for the Me_3-tpa ethene complex [**1**]$^+$ the reaction is complete within 30 minutes, whereas for Me_2-tpa ([**2**]$^+$) the reaction takes about 4 hours.
Since both the olefin and the N_4-ligand are probably more strongly coordinated to the metal center in the case of Me_2-tpa complex [**2**]$^+$ than for Me_3-tpa complex [**1**]$^+$ (analogous to what was concluded from the structures obtained by X-ray diffraction of the corresponding iridium complexes [**4**]$^+$ and [**6**]$^+$ in Chapter 3), the reaction would only be slowed down if first a dissociation reaction has to take place (either of the olefin or of one of the pyridyl-arms of the N_4-ligand).

In the solid state the Me_2-tpa and Me_3-tpa rhodium ethene complexes [**1**]$^+$ and [**2**]$^+$ do not react with dioxygen. This is in contrast with the tpa and Me-tpa complexes, for which formation of 3-metalla-1,2-dioxolane species upon a solid state reaction with dioxygen was reported. [19] – [21]

Reactivity of the N_4 rhodium peroxo complexes

Since peroxo complexes have been proposed as important intermediates in the rhodium-catalysed oxidation of olefins [1] – [12], [16] we have tested the reactivity of the N_4 rhodium peroxo complexes towards various substrates.

When one equivalent of triphenylphosphine (δ = -7.75 ppm in ^{31}P-NMR) was added to a methanolic solution of [**30**]$^+$ or [**31**]$^+$ under an inert atmosphere, quantitative conversion to O=P(Ph)$_3$ (δ = 30.4 ppm) took place. In the ^{1}H-NMR in both cases a mixture of unidentifiable species is left behind.

Me_2-tpa complex [**31**]$^+$ reacts much faster than the Me_3-tpa complex [**30**]$^+$: After 40 minutes already 25 % of the P(Ph)$_3$ had been converted to the phosphine oxide, whereas in the case of [**30**]$^+$ less than 2 % had been converted. Measuring a ^{31}P-NMR spectrum after 1 day revealed that for both peroxo complexes all of the added phosphine was converted to triphenylphosphine oxide.

This difference in reaction rate may reflect the difference in steric hindrance caused by the methyl-substituents around the peroxo moiety. For Me_2-tpa the steric hindrance is less, since only one of the axial pyridine rings has a methyl substituent at the 6-position. This will render the peroxo moiety more accessible for an electrophilic attack by triphenylphosphine.

Complexes [**30**]$^+$ and [**31**]$^+$ do not react with C_2H_4 present in solution. Since ethene is considered to be one of the most reactive species, apparently these peroxo complexes are not very reactive towards olefins.

Not only peroxo [7] but also hydroperoxo complexes [47] have been proposed as reactive intermediates in rhodium catalysed oxidation reactions. Bressan *et al.* [48], [49] reported that in the presence of acid oxygen transfer from peroxo complex can become catalytic. Once a peroxo species is converted into a hydroperoxo species by protonation, it is possible for the latter to be protonated again yielding a highly electrophilic, high valent oxometal species via heterolytic O-O bond cleavage (dehydration). [50]

Since our peroxo complexes appeared to be not very reactive, we tried to activate them by protonation.

When HCl is bubbled through a solution of [**30**]$^+$ in dichloromethane, at first a yellow suspension is formed, which quickly turns into a yellow solution of [(Me_3-tpa)Rh(Cl)$_2$]PF$_6$ [**32**]$^+$ when an excess of HCl is added. The initial precipitate is probably hydroperoxo complex [(Me_3-tpa)Rh(OOH)(Cl)]PF$_6$, which reacts further with HCl to form hydrogen peroxide and [**32**]$^+$.

When <u>one</u> equivalent of HBAr$^F_4$.2Et$_2$O is added to a CD_3CN solution of [**30**]$^+$ at low temperature, a mixture of compounds is obtained. The major species (ca. 70 %) is proposed to be [**33**]$^+$, a κ^2-*N,O*-2-ethanimidoyl peroxy complex (Figure 4.8). The reaction is proposed to proceed in analogy with the reaction reported by de Bruin *et al.* [22] of tpa 2-rhodaoxetane species [**A2**]$^+$ with one equivalent of NH_4PF_6 in CH_3CN resulting in product [**E**]$^{2+}$. The only difference is that we propose a hydroperoxo species as the intermediate species instead of a protonated oxetane.

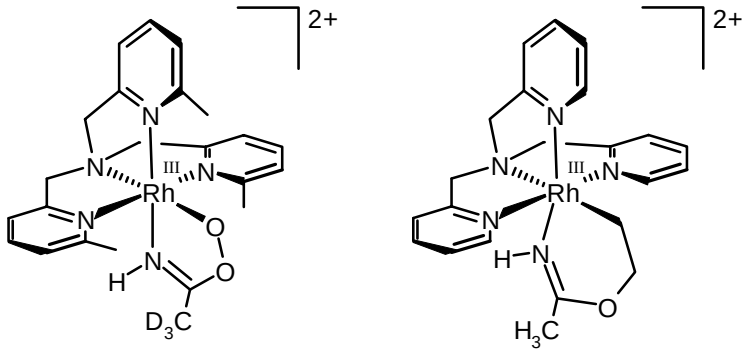

[**33**]$^{2+}$ [**E**]$^{2+}$

Figure 4.8 *Proposed structure of [**33**]$^{2+}$*

For [**E**]$^{2+}$ the imide proton is visible in ^{1}H-NMR at δ = 8.35 ppm in DMSO-d6 (not visible in CD_3CN). For [**33**]$^{2+}$ a broad singlet is observed at δ = 8.33 ppm in CD_3CN, which we also ascribe to an imide-proton.

When <u>two</u> equivalents of $HBAr^F_4.2Et_2O$ are added another product is obtained. Again we see a broad singlet at 8.37 ppm (an imide proton?) and a new singlet at δ = 6.93 ppm (a hydroxo or hydroperoxo proton? [4] The latter is sensitive to the presence of Et_2O in solution: removal results in an upfield shift of 0.21 ppm). After formation of [**33**]$^+$ with the first equivalent of acid, one would expect protonation of the most nucleophilic O-atom of [**33**]$^+$ and subsequent opening of the Rh-O bond (formation of an ethanimidoly hydroperoxy complex?).
The structure of the new compound could not be established unambiguously.

In conclusion, we have been able to activate the peroxo group of N_4 rhodium peroxo complexes, but we were not able to oxidize olefins with them.

4.3.2 Reaction of Me_2-bpa-R rhodium ethene complexes (R = Me, Bz) towards dioxygen

When solid Me_2-bpa-R rhodium ethene complexes (R = Me, Bz) are exposed to dioxygen no reaction takes place at all.
However, when the solid (mixtures of mono- and bis-ethene) is dissolved in CD_3CN under a dioxygen atmosphere the corresponding peroxo-CD_3CN complexes are among the products formed (Figure 4.9). For Me_2-bpa-Bz, the formation of [**34**]$^+$ is very selective. For Me_2-bpa-Me [**35**]$^+$ was only obtained in approx. 17 % yield (on the basis of ^{1}H-NMR).

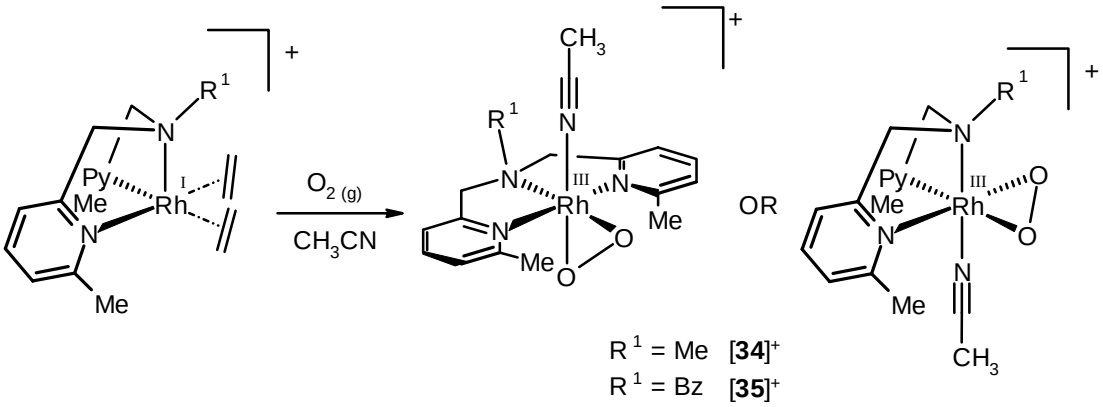

Figure 4.9 *Formation of peroxo complexes [**34**]$^+$ and [**35**]$^+$*

From ^{1}H-NMR it is clear that [**34**]$^+$ and [**35**]$^+$ have a symmetric structure. Whether the N_3 ligand is meridionally or facially coordinated could not be determined. Neither could be determined whether the amine-substituent is directed upward towards the CD_3CN molecule (as depicted) or directed below the pyridine plane towards the peroxo moiety.
The solvent molecule is not bound very tightly, since when solutions of the Me_2-bpa-R rhodium peroxo complexes are prepared in CD_3CN and diluted 100 times for ESI$^+$-MS only peroxo complexes with CH_3CN coordinated were observed in the mass spectra.

When prior to a reaction with dioxygen the Me_2-bpa-R rhodium ethene complexes were dissolved in CD_3CN and allowed to form the asymmetric ethene-acetonitrile complexes [**20**]$^+$ and [**21**]$^+$ (§ 3.5.1), a much less selective reaction took place. In both cases signals of the symmetric peroxo-acetonitrile complexes [**34**]$^+$ and [**35**]$^+$ could be observed in the ^{1}H-NMR spectrum, but these species were present in just about 6 % yield. The rest of the products consist of a mixture of unidentifiable products.

[4] Typical chemical shifts for hydroperoxo protons in organic compounds can be found between 7.6 and 8.3 ppm; hydroxyl protons between 5.3 and 6.2 ppm. [51] – [53]

Stability of N_3 rhodium peroxo complexes [34]$^+$ and [35]$^+$

Both N_3 rhodium(III) peroxo complexes are unstable in solution.

The Me_2-bpa-Bz complex is the most stable one: decomposition (to a mixture of unidentifiable species) requires a few days. From fragmentation behavior under ESI$^+$-MS conditions it was clear that peroxo complex [**35**]$^+$ remained stable as long as the solvent molecule remained coordinated. Once CH_3CN has dissociated the peroxo complex immediately starts losing H_2O.[5]

The Me_2-bpa-Me rhodium(III) peroxo complex is much less stable. Upon removal of the dioxygen atmosphere [**34**]$^+$ (upon transferring the reacted solution to an NMR tube filled with dinitrogen) decomposed completely within 14 hours leaving a mixture of unidentifiable species behind. When the NMR tube was filled with dioxygen instead, the peroxo complex remained stable for about a day and seemed to decompose in a somewhat more selective fashion (still a lot of products were formed).

A possible explanation for the observed higher stability of the Me_2-bpa-Me rhodium peroxo complex upon application of a dioxygen atmosphere can be that these peroxo species somehow catalytically oxidize compounds present in solution and are reformed again due to the oxygen-atmosphere.

According to DFT calculations (Appendix A) it is not likely that the increased stability under O_2-atomosphere has anything to do with a reversible binding process of O_2; O_2 should be more strongly bound than C_2H_4 in this complex.

This high reactivity of the Me_2-bpa-Me peroxo complex in solution is in line with its gas-phase reactivities towards 1-butene (as will be further discussed in § 7.6.1). [(Me_2-bpa-Me)Rh(O_2)]$^+$ was the only peroxo complex capable of losing 'O' (a single oxygen atom), possibly to the collision gas. All other peroxo complexes that were reactive formed 1-butene adducts or exchange products, but none of them was capable of losing a single oxygen atom.

If such an 'O' abstraction would also easily take place in solution, the highly reactive oxo species left behind will react with anything that comes along its way, hereby explaining the fast decomposition of [**34**]$^+$ in the absence of O_2.

Interestingly, neither of the two N_3 rhodium(III) peroxo complexes reacts with C_2H_4 in solution (no aldehyde signals are present in the ^{1}H-NMR spectra). This is quite remarkable, considering the high reactivity of [**34**]$^+$ in the gas phase and the low stability in solution.

4.3.3 Reaction of bpa-R rhodium ethene complexes (R = H, Me, Bz) towards dioxygen

Reactions of bpa-R complexes [**25**]$^+$, [**26**]$^+$ and [**27**]$^+$ (R = H, Me, Bz respectively) towards dioxygen were performed both in acetonitrile and in dichloromethane to investigate the influence of the coordinating properties of the solvent on the type of products formed. Product analysis was performed by ^{1}H-NMR and ESI$^+$-MS.

Just as for the analogous iridium bis-ethene complexes the bpa-R rhodium mono-ethene complexes do not react selectively with dioxygen. For all three compounds very broad signals were obtained in the ^{1}H-NMR spectra, probably indicating the presence of paramagnetic species.

[5] As will be shown in Chapter 6 loss of H_2O from our peroxo complexes is unusual and only observed for the benzyl-containing N_3 rhodium peroxo complexes. For the other N_3 and N_4 peroxo complexes loss of O_2 is observed. This difference is probably due to the fact that aromatic C-H activation takes place resulting in the formation of a hydroperoxo species, which is much more prone to lose H_2O upon fragmentation.

Since paramagnetic species seemed to be among the products formed, EPR spectra were measured of acetone-methanol (ratio = 2:3) solutions of the bpa-R rhodium(I) ethene complexes which had been exposed to air, to see if species with unpaired electrons could be identified.[6]

From the EPR-spectra shown in Figure 4.10 can be concluded that in all cases a rhodium complex with one unpaired electron was formed upon exposure to air. For the bpa complex the intensity of the product signal was weaker and decreased after longer exposure to air; for bpa-Bz and bpa-Me it remained constant. The shapes of the EPR spectra obtained look similar for all three bpa-R complexes.

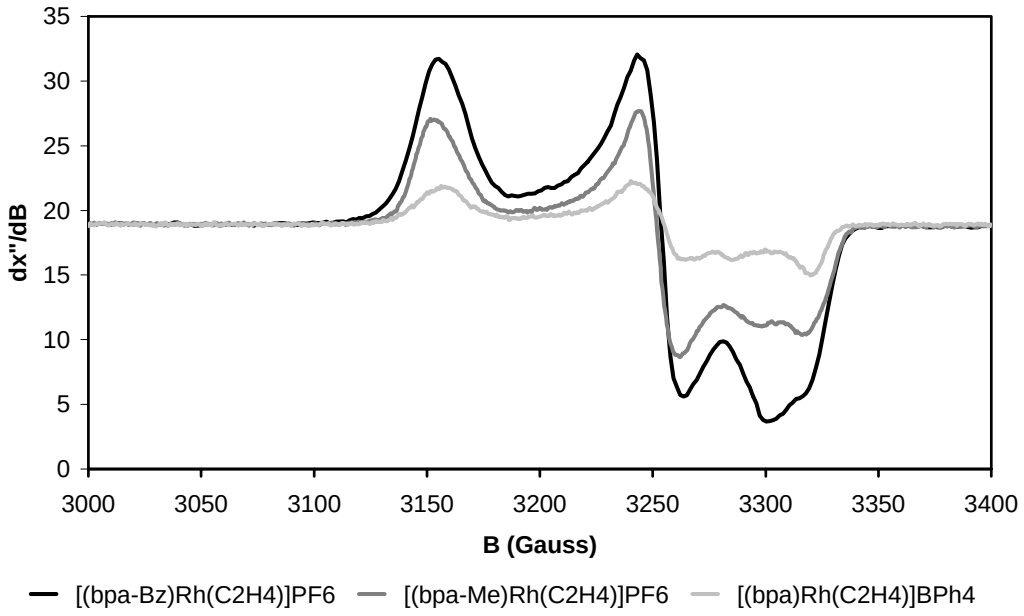

Figure 4.10 *EPR-spectra of the products upon exposure of [**26**]$^+$ and [**27**]$^+$ to air*

The EPR spectra shown seem to be rhombic (i.e. they show three different g-values). The absorbance around 3300 Gauss seems to have a rhodium coupling on it. The unpaired electron must therefore be at least partially located at the rhodium center.

For bpa complex [**25**]BPh_4 only very low concentrations of odd electron species are formed. The EPR signal disappeared after about 1 minute in contact with air at r.t. In contrast, for bpa-Me complex [**26**]PF_6 the EPR signal intensity increases in time to the intensity shown in Figure 4.10. And for bpa-Bz complex [**27**]PF_6 a very strong EPR signal was observed, which did not disappear even after having been at r.t. for a few minutes. The shape and the intensity of the signal changed somewhat, though. It seems as if in time some sort of rearrangements take place.

In other words, for all three bpa-R rhodium(I) ethene compounds single-electron-transfer reactions between dioxygen and the rhodium complex take place. The stability of the rhodium(II) complexes formed depends on the bpa-R ligand.

Upon exposure of solid [**25**]$^+$, [**26**]$^+$ and [**27**]$^+$ to dioxygen, immediately a reaction took place according to the color change. Analysis of the solid with ^{1}H-NMR and ESI$^+$-MS reveals no selective reaction. Just as for the reaction in solution single-electron-transfer reaction seems to have taken place. No product could be isolated from the dissolved solid after reaction.

[6] For all compounds an EPR spectrum was measured before contact with air and in all cases at this point no unpaired electrons were present in the samples. Upon first contact with air, the solutions were immediately cooled down to 4 K and an EPR spectrum was measured. After that the EPR-tube was warmed up to r.t. for a few seconds and cooled down again. This process was repeated a few times, depending on the EPR-behavior of the compound.

4.4 DFT-calculations on the reaction of N_3 complexes with dioxygen

In most square-planar systems, ligand exchange in solution occurs via an associative mechanism (most kinetic studies of this kind are based on Pt(II) and Pd(II) systems). A five-coordinate intermediate forms first, followed by departure of the leaving ligand. Dissociative substitution at square planar d8 transition metal complexes is a not as common, but still there are numerous examples involving dissociation to a T-shaped 3-coordinate intermediate. [54] – [74]

For $^3O_2$ to react with a closed shell organometallic complex a singlet-triplet crossing has to take place at some stage of the reaction. Upon approach of a triplet dioxygen molecule to a metal center the metal-dioxygen interaction becomes more and more repulsive. Only for $^1O_2$ (which is 22-24 kcal/mol [75] higher in energy than $^3O_2$), the interaction between the metal center and molecular oxygen can become attractive upon decrease of the metal-dioxygen distance. If heavy atoms like iridium are involved, spin-orbit coupling can become important, which destroys the strict separation between singlet and triplet states. However, in the present case we are mainly concerned with a spin flip *on the O_2 fragment*, so that the transition state that would one would find when *including* spin-orbit coupling can reasonably be approximated by the minimum-energy singlet-triplet crossing point calculated *ignoring* spin-orbit coupling.[7]

Somewhere along the reaction coordinate a triplet-singlet crossing is required to obtain a stable metal peroxo(-ethene) complex. However, before this can happen, the reactants have to rearrange their geometry.

It is possible to get an idea of the structure of the transition metal complex at this singlet-triplet crossing point by calculating the "Minimum Energy Crossing Point" (MECP) of the reaction. This point is similar to a transition state, only that the MECP is at the crossing point between two potential energy surfaces. [8] We were able to calculate these crossing points for the bpa-Me and the Me_2-bpa-Me rhodium and iridium ethene complexes; as mentioned above, we consider them to be reasonable approximations of the "real" transition states that would be obtained from a fully relativistic calculation.[9] In Figure 4.11 on the next page the obtained MECP structures are shown. The free energies $\Delta G_{298\ K,\ 1\ bar.}$ and free enthalpies $\Delta H_{0\ K}$ for all the species involved in an associative pathway are presented in Figure 4.12a, Figure 4.12b and Appendix A. [10, 11, 12]

Once the reactants have assumed a geometry equal to that at the MECP of the reaction, there will be no further barrier for the triplet-singlet crossing.

[7] A fully relativistic transition-state search, including spin-orbit coupling, is at present completely unfeasible for systems of this size.

[8] For more background information on calculations of spin-forbidden reactions see reference 76.

[9] Calculations were carried out with a non-relativistic formalism, but using relativistic effective core potentials for Rh and Ir. This means that indirect relativistic effects like changes of d-orbital levels are included in an approximate way, but spin-orbit coupling is not included at all.

[10] For all L_N metal complexes, the energy of corresponding naked species, $[(L_N)M]^+$, is set to zero kcal/mol.

[11] The reference energy of $^3O_2$ is adjusted upwards by 18 kcal/mol when calculating relative energies (see Appendix A for an explanation).

[12] As already mentioned in Appendix A, the most appropriate energy quantity for a description of reactions occurring in solution is the Gibbs free energy at (in this case) 25 ºC: $\Delta G_{298\ K,\ 1\ bar}$.

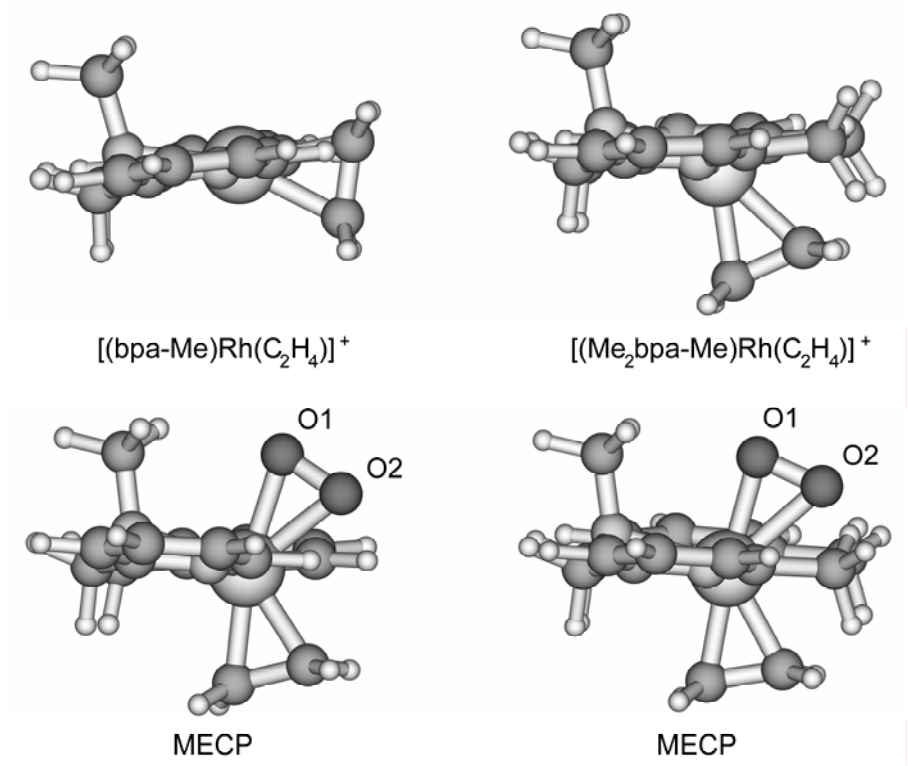

Figure 4.11 *DFT-optimized structures for $[(bpa\text{-}Me)Rh(C_2H_4)]^+$ and $[(Me_2\text{-}bpa\text{-}Me)Rh(C_2H_4)]^+$ and the corresponding MECP structures for the reaction with dioxygen*

Upon comparison of the MECP structures for the reaction with dioxygen (see Figure 4.11) with those of the optimized mono-ethene complexes, one can see that the olefin has to 'bend down', i.e. the angle between the olefin, the metal center and the amine-nitrogen has to decrease.

For the bpa-Me complex the calculated barrier for the reaction with dioxygen is about 8 kcal/mol higher than for the corresponding Me_2-bpa-Me complex. This difference is solely caused by the fact that the ethene molecule in the Me_2-bpa-Me complex is already completely pre-organized to capture the dioxygen molecule and the bpa-Me complex is not pre-organized at all.

Such a difference in barrier for formation of the peroxo-ethene complex can be translated to a reaction rate decrease by a factor of 100 to 1000 at r.t.

For iridium the bpa-Me MECP even lies about 12 kcal/mol higher than that of the corresponding Me_2-bpa-Me complex.

Table 4.3 *Metal-oxygen distances in the MECP structures*

MECP structures	Metal-O1 distance (Å)	Metal-O2 distance (Å)
bpa-Me rhodium	2.191	2.241
Me_2-bpa-Me rhodium	2.142	2.325
bpa-Me iridium	2.235	2.316
Me_2-bpa-Me iridium	2.172	2.427

The structures of the MECP's for iridium are similar to those obtained for rhodium, except for the fact that the metal-oxygen bonds are longer for iridium than for rhodium (Table 4.3). This probably reflects the fact that for iridium the crossing is more 'early' than for rhodium (compare this to an 'early' transition state).

All MECP structures are fairly similar to the optimized peroxo-ethene complexes.

In order to be better able to compare the different reaction pathways, the energies of the different species involved in both the dissociative and the associative substitution reactions are displayed in Figure 4.12a and Figure 4.12b for the bpa-Me and Me_2-bpa-Me species (see also Appendix A).

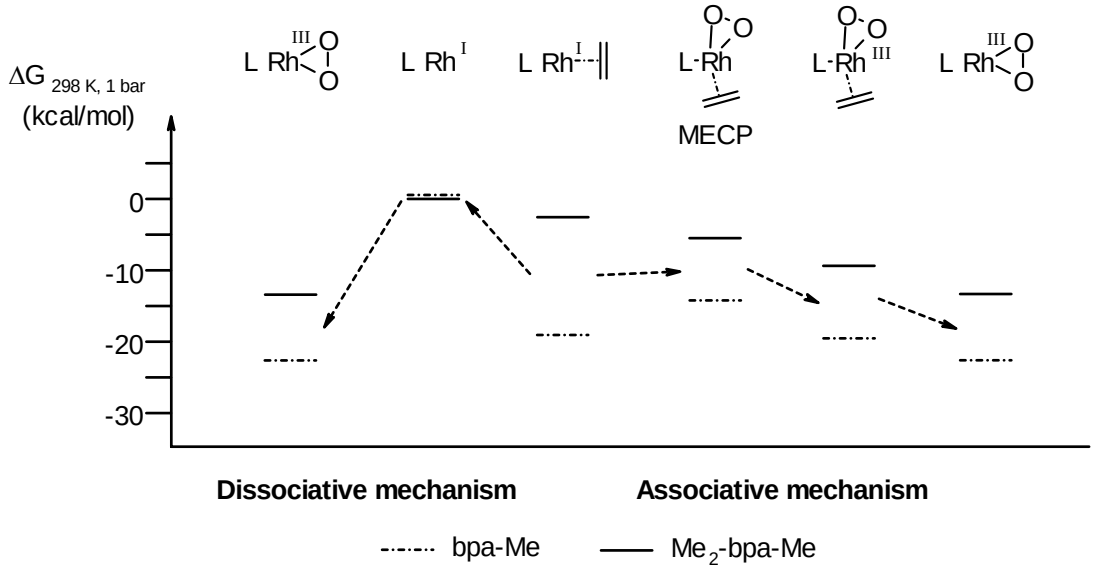

Figure 4.12a *Computational results ($\Delta G_{298\ K,\ 1bar}$) for the bpa-Me and Me_2-bpa-Me rhodium species* [13]

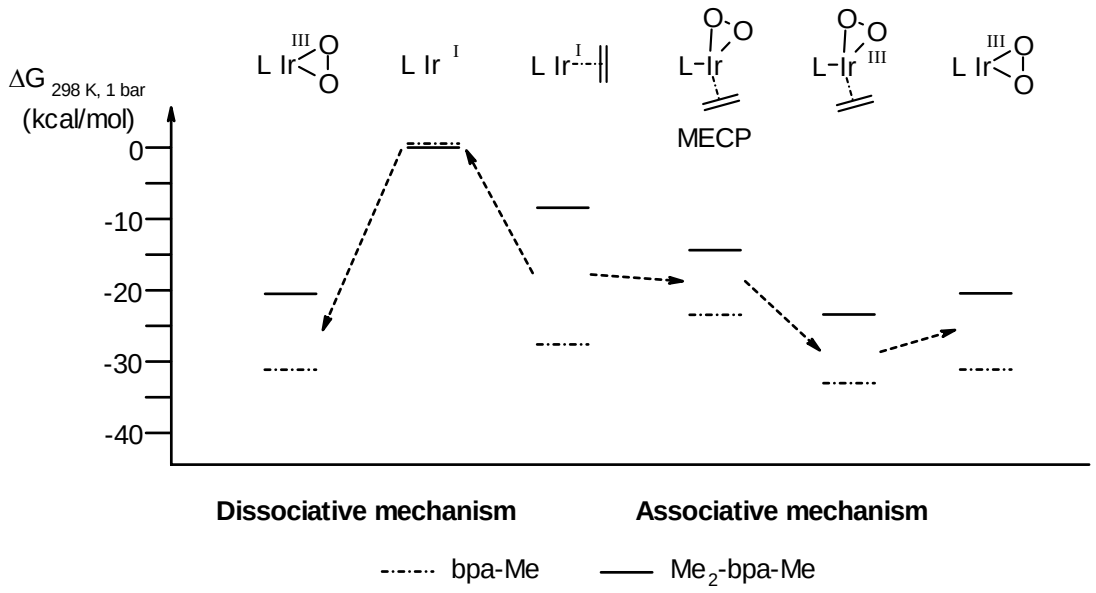

Figure 4.12b *Computational results ($\Delta G_{298\ K,\ 1bar}$) for the bpa-Me and Me_2-bpa-Me iridium species*

For all complexes the energy of the MECP lies below that of the corresponding naked species $[(L_N)M]^+$, this energy difference being larger for iridium than for rhodium. For the Me_2-bpa-Me complexes the energy of the MECP structure is even lower than that of the corresponding ethene complex, making a reaction with dioxygen energetically favorable.

We do not have any information on the barriers associated with the dissociative pathway.[14]

[13] The MECP structures are not stationary points on any potential energy surface, so the standard formulas for thermal corrections cannot be applied. In order to obtain approximate free energies for the MECP structures, we added the thermal correction calculated for the peroxo-ethene complex to the $\Delta H_{0\ K}$ for the MECP structure.

However, on the basis of our calculations for both the rhodium and the iridium N_3 complexes the associative pathway seems to be more favorable than the dissociative one.

The reactivity observed in solution is in accord with the computational results. For *iridium* the peroxo complexes lies somewhat higher in energy than the corresponding peroxo-ethene species and indeed we were only able to isolate the latter species. For *rhodium*, on the other hand, the peroxo complexes lie somewhat lower in energy than the peroxo-ethene complexes. In solution we have only observed the formation of peroxo complexes.

4.5 Conclusions

The use of nitrogen donor ligands with methyl-substituents at the 6-position of the pyridine rings to increase the steric bulk around the metal center results in a number of characteristic reactivities:

- The use of sterically hindered nitrogen donor ligands enables the isolation of rhodium peroxo complexes from solution.
- Iridium, on the other hand, is capable of keeping the olefin in the coordination sphere as well. This probably reflects a stronger metal-olefin bond for iridium.
- For rhodium the presence of four nitrogen donor atoms around the metal center is necessary to stabilize the peroxo complex obtained. The N_3 peroxo complexes with a labile fourth nitrogen donor are less stable than the N_4 species.
- The peroxo complexes obtained are not reactive towards olefins.

For nearly all L_N M ethene complexes there are two types of products possible in the reaction with dioxygen: diamagnetic or paramagnetic products (resulting from SET from the TM complex to O_2). The ratio between these products depends on the ligand bulk.
In *solution* well-defined products can only for be isolated the sterically hindered complexes, whereas in the *solid state* only N_4-ligand complexes with fewer substituents give rise to a selective reaction.

The reaction steps via which the diamagnetic products are formed in *solution* are not clear yet.
Do they proceed via associative or dissociative pathways? On the basis of the calculations presented in § 4.4 an associative mechanism seems more favorable than a dissociative one for the N_3 rhodium and iridium ethene complexes. For the bpa-R complexes the barrier for the associative reaction with dioxygen seems to be higher than for the Me_2-bpa-R complexes.
For the N_4 complexes dissociation has to be the first step (either of the olefin or of one of the pyridyl arms of the nitrogen donor ligand). In the *solid state* SET reactions seem to take place very frequently.

[14] We do not have any information on the barriers related to the formation of $[(L_N)M]^+$. One could imagine that for naked T-shaped $[(N_3)M]^+$ species no rearrangement due to steric hindrance is necessary, since dioxygen can easily approach the metal centre. There should be no barrier for the binding interaction for either $^1O_2$ or $^3O_2$.

4.6 Experimental section

4.6.1 General methods

All procedures were performed under a nitrogen atmosphere using standard Schlenck techniques, unless indicated otherwise. Solvents (p.a.) were deoxygenated by bubbling through a stream of nitrogen or by the freeze-pump-thaw method. The temperature indication r.t. corresponds to ca. 20 ºC.

NMR experiments were carried out on a Bruker DPX200 (200 MHz and 50 MHz for ^{1}H and ^{13}C respectively), a Bruker AC300 (300 MHz and 75 MHz for ^{1}H and ^{13}C respectively), a Varian Inova 400 (400 MHz and 100 MHz for ^{1}H and ^{13}C respectively). Solvent shift references for ^{1}H-NMR are: CD_2Cl_2 δ (^{1}H) = 5.31 ppm, CD_3CN δ (^{1}H) = 1.94 ppm, methanol-d4 δ (^{1}H) = 3.35 ppm and acetone-d6 δ (^{1}H) = 2.05 ppm. Solvent shift references for ^{13}C-NMR are: CD_3CN δ (^{13}C) = 1.24 (and 118.25), CD_2Cl_2 δ (^{13}C) = 54.20, methanol-d4 δ (^{13}C) = 49.3 ppm and acetone-d6 δ (^{13}C) = 29.83 ppm (and 206.18 ppm). Abbreviations used are: s = singlet, d = doublet, dd = double doublet, ddd = double doublet of doublets, t = triplet, dt = double triplet, q = quartet, qq = quartet of quartets, m = multiplet, dm = double multiplet, br. = broad.

Since the κ^4-N_4 mono-ethene complexes have one unique pyridine ring and two axial pyridine rings, the NMR signals belonging to the different rings will be assigned as shown below. In the case of the asymmetric Me_2-tpa complexes a third type of pyridine-assignment will be introduced (Figure 4.13).

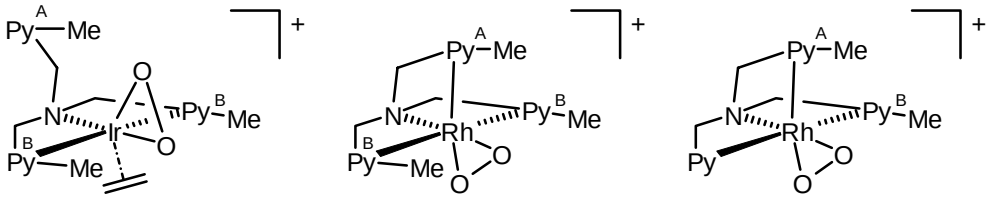

[**28**]$^+$ [**30**]$^+$ [**31**]$^+$

Figure 4.13 *Assignment of NMR signals of different groups*

Elemental analysis (C,H,N) were carried out on a Carlo Erba NCSO-analyser.

Mass spectra (ESI- or FAB-MS) were recorded on a Finnigan MAT 900S (Radboud University Nijmegen), a Finnigan TSQ 700 (ETH-Zurich) or a Finnigan TSQ 7000 (ETH-Zurich). All spectra were obtained in the positive ion mode. Daughter ion spectra were measured on the TSQ 700 and TSQ 7000 using argon as a collision gas.

Experimental X-band EPR spectra were recorded on a Bruker ER220 spectrometer.

Bpa-Me [77], bpa-Bz [25], tpa [78], Me-tpa [79], Me_3-tpa [79], [(bpa-Me)Rh(C_2H_4)]PF_6 [77], [(bpa-Bz)Rh(C_2H_4)]PF_6 [77], [(tpa)Rh(C_2H_4)]PF_6 [24], [(Me-tpa)Rh(C_2H_4)]PF_6 [24], [(tpa)Ir(C_2H_4)]PF_6 [21], [(Me-tpa)Ir(C_2H_4)]PF_6 [21], $HBAr^F{}_4.2Et_2O$ [46], [{(C_2H_4)$_2$Rh(μ-Cl)}$_2$] [80] and [{(coe)$_2$Ir(μ-Cl)}$_2$] [81] were prepared according to literature procedures.

All other chemicals are commercially available and were used without further purification, unless stated otherwise.

4.6.2 X-ray diffraction

Single crystals were mounted in air on glass fibers. Intensity data were collected at room temperature. An Enraf-Nonius CAD4 single-crystal diffractometer was used, applying graphite monochromatized MoK_α radiation. Unit cell dimensions were determined from the angular setting of 24 reflections for [**28**]PF_6 and 25 reflections for [**29**]PF_6. Intensity data were corrected for Lorentz and polarisation effects. Semi-empirical absorption correction (ψ-scan) was applied for all compounds. [82] The structures were solved by the program system DIRDIF [83] using the program PATTY [84] to locate the heavy atoms. All structures were refined with standard methods (refinement against F^2 of all reflections with SHELXL97 [85]) with anisotropic parameters for the nonhydrogen atoms. Hydrogen atoms were placed at calculated positions and were subsequently refined isotropically in riding mode.

For [**28**]PF_6 and [**29**]PF_6 geometrical data with regard to O1, O2, C1 and C2 are rather similar. The assignment of atomic species has been made on the basis of prior occupancy factor refinement and comparison of thermal displacement parameters.

*[(κ^3-Me_3-tpa)Ir^{III}(C_2H_4)(O_2)]PF_6 ([**28**]PF_6)*

Unfortunately the crystal structure determination was influenced by a rather severe but regular crystal decay up to 43 %. From the anisotropic thermal displacement parameters for the PF_6 moiety it is clear that these atoms show a large positional disorder. Although it is possible to use several partially occupied positions for these atoms, no physically reasonable model results from

these parameters, at least not any better than the model presented here. Moreover, the model presented here was the only one which was stable to refinement without the need of additional restraints.
Calculations (PLATON-93) [86] showed a small void of 162 Å^3, containing at least 6 electrons, around 0, 1/2, 0. This electron density is assumed to be a disordered water molecule, and the SQUEEZE (PLATON-93) [86] procedure was applied to account for this electron density. This assumption accounts for the physical molecular properties as given in Table 4.4.

*[(κ^3-Me$_2$-bpa-Me)Ir^{III}(C$_2$H$_4$)(O$_2$)]PF$_6$ ([**29**]PF$_6$)*
Geometrical calculations (PLATON-93) [86] revealed neither unusual geometric features, nor unusual short intermolecular contacts. The calculations revealed no higher symmetry and no solvent accessible areas.

Selected bond lengths and angles are summarized in Tables 4.1-4.3. Drawings were generated with the program PLATON. [86] Other relevant crystal data are summarized in Table 4.4.

Table 4.4 *Crystallographic data for [**28**]PF$_6$ and [**29**]PF$_6$*

	[**28**]PF$_6$.½H$_2$O	[**29**]PF$_6$
Empirical formula	$C_{23}H_{29}F_6O_{2.5}N_4PIr$	$C_{17}H_{23}F_6O_2N_3PIr$
Crystal size [mm]	0.36x0.11x0.10	0.52x0.38x0.20
Crystal color	Transparent light yellow-brown	Transparent brown
Formula weight	738.67	638.55
T [K]	293(2)	293(2)
Crystal system	Monoclinic	Triclinic
Space group	P 2$_1$/c	P -1
a [Å]	9.583(2)	7.001(3)
b [Å]	24.768(5)	12.081(4)
c [Å]	12.0374(13)	12.414(3)
α [°]	90	90.91(2)
β [°]	100.420(12)	90.74(2)
γ [°]	90	100.699(17)
V [Å^3]	2809.8(9)	1031.5(6)
$\rho_{calcd.}$ [gcm^{-3}]	1.746	2.056
Z	4	2
Diffractometer (scan)	Enraf-Nonius	Enraf-Nonius
	CAD4 (ω-scan)	CAD4 (ω/2θ-scan)
Radiation	Mo-K$_\alpha$	Mo-K$_\alpha$
Wavelength [Å]	0.71073	0.71073
F(000)	1444	616
θ range [°]	3.11 to 27.49	2.96 to 27.48
Index ranges	$-12 \le h \le 12$	$0 \le h \le 9$
	$0 \le k \le 32$	$-15 \le k \le 15$
	$0 \le l \le 15$	$-16 \le l \le 16$
Measured reflections	6705	5112
Unique reflections	6408	4724
Observed refl. [$I_o > 2\sigma(I_o)$]	2563	4273
Refined parameters	337	274
Goodness-of-fit on F^2	0.907	1.142

	[**28**]PF_6.½H_2O	[**29**]PF_6
R [Io > 2σ(Io)]	0.0784	0.0423
wR^2 [all data]	0.1808	0.1111
ρ_{fin} (max/min) [e. Å^{-3}]	0.784 / -0.785	2.889 / -3.954

4.6.3 Calculations

DFT calculations

Minimum-energy crossing points were determined by minimizing the average energy of the singlet and triplet states subject to the constraint that the energies of the two states are equal. These constrained optimizations were carried out by iterative minimization within the null-space of the constraint and simultaneous Newton zeroing along the constraint direction, using a newly written external optimizer (still under development). P.H.M. Budzelaar, to be published.

*Calculation of the rotation rate of the coordinated ethene in [**28**]$^{+}$ and [**29**]$^{+}$*

At 500 MHz, the broad ethene signals have split into two sharp triplets at 233 K, for both [**28**]$^+$ (δ = 4.84 and 4.14 ppm, ^3J(H,H) = 9.70 Hz, $\Delta\nu$ = 349.14 Hz) and [**29**]$^+$ (δ = 4.56 and 3.77 ppm, ^3J(H,H) = 9.40 Hz, $\Delta\nu$ = 397.96 Hz). For both [**28**]$^+$ and [**29**]$^+$ at 500 MHz, coalescence of these triplets into one signal occurs at T_c= 273 K.

From these measurements it is possible to calculate the rotation rate k_c of the coordinated ethene (equation 4.1), resulting in a K_c for [**28**]$^+$ of 777.4 s^{-1} and for [**29**]$^+$ of 885.5 s^{-1}.

$$k_c = \frac{\pi}{\sqrt{2}}\sqrt{\left(\Delta\nu^2 + 6J^2\right)} \qquad (4.1)$$

From these data, the free energy of activation ($\Delta G_c^{\neq}$) for ethene rotation in [**28**]$^+$ and [**29**]$^+$ at T_c was estimated to be ~12 kcal/mol using the Eyring equation (equation 4.2):

$$k = \frac{k_B \cdot T}{h} \cdot e^{\frac{-\Delta G^{\neq}}{R \cdot T}} \qquad (4.2)$$

The ethene fragments of [**4**]$^+$ and [**8**]$^+$ do not rotate on the ^{1}H-NMR timescale at r.t. (298 K, 200 MHz). The free energy of activation for ethene rotation ($\Delta G_c^{\neq}$) of [**4**]$^+$ and [**8**]$^+$, as estimated from line-width analysis of the ethene ^{1}H-NMR signals, must be at least 17 kcal/mol.

4.6.4 Synthesis

*[(κ^3-Me_3-tpa)Ir^{III}(C_2H_4)(O_2)]PF_6 ([**28**]PF_6)*

40 mg (0.06 mmol) of [**4**]PF_6 was dissolved in 4 ml dichloromethane, and placed under an atmosphere of 1.6 bar O_2 for 30 minutes. The solution was filtered and dried under vacuum. Yellow/brown crystals of [**28**]PF_6, suitable for X-ray diffraction, were obtained by vapor-vapor diffusion of diethylether and a solution of [**28**]PF_6 in MeCN. A separate volumetric gas-uptake measurement indicated consumption of 1 mol O_2 per mol [**4**]PF_6 during this reaction (150 mg (0.15 mmol) [**4**]PF_6 consumes ~3.40 ml (0.14 mmol) O_2). Isolated yield 7.3 mg (0.01 mmol, 16 %).

^{1}H-NMR (400.14 MHzo, acetone-d6, 289 K): δ (ppm)= 7.97 (t, 2H, ^3J(H,H)= 7.8 Hz, Py^A-*H4*), 7.82 (t, 1H, ^3J(H,H)= 7.6 Hz, Py^B-*H4*), 7.63 (d, 2H, ^3J(H,H)= 7.8 Hz, Py^A-*H3*), 7.43 (d, 1H, ^3J(H,H)= 7.4 Hz, Py^B-*H5*), 7.41 (d, 2H, ^3J(H,H)= 7.8 Hz, Py^A-H5), 7.37 (d, 1H, ^3J(H,H)= 7.6 Hz, Py^B-H3), 5.79 (d[AB], 2H, ^3J(H,H)= 16.0 Hz, Py^A-*CH_2*-N), 5.05 (d[AB], 2H, ^3J(H,H)= 16.0 Hz, Py^A-*CH_2*-N), 4.80 (s, 2H, Py^B-*CH_2*-N), 4.48 (br, 4H, *CH_2=CH_2*), 2.96 (s, 6H, Py^A-CH_3), 2.65 (s, 3H, Py^B-CH_3).

^{13}C{^{1}H}-NMR (75.47 MHz, acetone-d6, 289 K) δ (ppm)= 166 (Py^A-*C2*), 166 (Py^A-*C2*), 165 (Py^A-*C6*), 159.5 (Py^B-*C6*), 151 (Py^B-*C2*), 140.2 (Py^A-*C4*), 137.9 (Py^B-*C4*), 128 (Py^A-*C5*), 124.5 (Py^B-*C3*), 124 (Py^B-*C5*), 122 (Py^A-*C3*), 65.5 (N-*C*H_2-Py^A), 62.7 (N-*C*H_2-Py^B), 22.0 (Py^A-*C*H_3 & Py^B-*C*H_3), ^{13}C signals of the ethene fragment could not be observed at 289 K

ESI$^+$-MS: 585 [**28**]$^+$, 557 {[**28**]-C_2H_4}$^+$, 553 {[**28**]-O_2}$^+$, 566 {[**28**]-O_2-C_2H_4+CH_3CN}$^+$.

Calculated for $C_{23}H_{28}N_4O_2IrPF_6$ (729.68): C 37.86, H 3.87, N 7.68, Found: C 38.05, H 4.03, N 7.85.

*[(κ^3-Me$_2$-bpa-Me)Ir^{III}(C_2H_4)(O_2)]PF_6 ([**29**]PF_6)*

40 mg (0.112 mmol) of [**7**]PF_6 was dissolved in 4 ml of dichloromethane, and placed under an atmosphere of 1.6 bar O_2 for 30 minutes. The solution was filtered and dried under vacuum. Light-brown crystals of [**29**]PF_6, suitable for X-ray diffraction, were obtained by vapor-vapor diffusion of hexane and a solution of [**29**]PF_6 in acetone. Isolated yield 7.7 mg (0.012 mmol, 16 %).

^{1}H-NMR (400.14 MHz, CD_3CN, 289 K): δ (ppm)= 7.78 (t, 2H, ^3J(H,H)= 7.8 Hz, Py-*H4*), 7.35 (d, 1H, ^3J(H,H)= 7.8 Hz, Py-*H3*), 7.22 (d, 2H, ^3J(H,H)= 8.1 Hz, Py-*H5*), 4.93 (d[AB], 2H, ^2J(H,H)= 15.6 Hz, N-CH_2-Py), 4.86 (d[AB], 2H, ^2J(H,H)= 15.6 Hz, N-CH_2-Py), 4.22 (br, 4H, C_2H_4), 3.23 (s, 3H, N-CH_3), 2.82 (s, 6H, Py-CH_3).

^{1}H-NMR (400.14 MHz, acetone-d6, 289 K): δ (ppm)= 7.93 (t, 2H, ^3J(H,H)= 7.8 Hz, Py-*H4*), 7.56 (d, 1H, ^3J(H,H)= 7.8 Hz, Py-*H3*), 7.37 (d, 2H, ^3J(H,H)= 7.8 Hz, Py-*H5*), 5.53 (d[AB], 2H, ^2J(H,H)= 15.6 Hz, N-CH_2-Py), 5.21 (d[AB], 2H, ^2J(H,H)= 15.6 Hz, N-CH_2-Py), 4.36 (br, 4H, C_2H_4), 3.41 (s, 3H, N-CH_3), 2.92 (s, 6H, Py-CH_3).

^{13}C{^{1}H}-NMR (75.47 MHz, CD_3CN, 289 K): δ (ppm)= 166.1 (Py-*C2*), 165.5 (Py-*C6*), 140.7 (Py-*C4*), 128.6 (Py-*C5*), 122.5 (Py-*C3*), 71.3 (N-*C*H_2-Py), 52.7 (N-*C*H_3), 23.0 (Py-*C*H_3), ^{13}C signals of the ethene fragment could not be observed at 289 K

ESI$^+$-MS: 494 [**29**]$^+$, 466 {[**29**]-C_2H_4}$^+$, 462 {[**29**]-O_2}$^+$, 434 {[**29**]-O_2-C_2H_4}$^+$.

Calculated for $C_{17}H_{23}N_3O_2IrPF_6$ (638.57): C 31.98, H 3.63, N 6.58; Found: C 32.14, H 3.61, N 6.38.

*Reaction of [**13**]$^{\pm}$, [**15**]$^{\pm}$, [**16**]$^{\pm}$, [**25**]$^{\pm}$, [**26**]$^{\pm}$ and [**27**]$^{\pm}$ with dioxygen*

In all cases the products were analysed by ^{1}H-NMR and ESI$^+$-MS.

Reaction in dichloromethane

Approximately 20 mg of [**13**]PF_6, [**15**]PF_6 and [**16**]PF_6, [**25**]PF_6, [**26**]PF_6 and [**27**]PF_6 was dissolved in 2 ml dichloromethane under nitrogen atmosphere. A Schlenck tube was placed under dioxygen and the solution was transferred to this Schlenck tube. After stirring for 30 minutes the solvent was removed and the product mixture was dried under vacuum.

Reaction in acetonitrile

Approximately 30 mg of [**13**]PF_6, [**15**]PF_6, [**16**]PF_6, [**25**]PF_6, [**26**]PF_6 and [**27**]PF_6 was placed in a Schlenck tube under nitrogen atmosphere. The nitrogen atmosphere then was replaced by dioxygen (approximately 0.5 bar) and the solvent, acetonitrile, was added. After stirring for 30 minutes the solvent was removed and the product mixture was dried under vacuum.

Reaction in the solid state

Approximately 20 mg of [**13**]PF_6, [**15**]PF_6, [**16**]PF_6, [**25**]PF_6, [**26**]PF_6 and [**27**]PF_6 was placed in a Schlenck tube under nitrogen atmosphere. The nitrogen atmosphere was replaced by dioxygen. The Schlenck tube was allowed to stand for a year at room temperature and was exposed to glass filtered light.

*[(κ^4-Me$_3$-tpa)Rh^{III}(O_2)]PF_6 ([**30**]PF_6)*

A solution of 50 mg (0.082 mmol) of [**1**]PF_6 in 2 ml CH_2Cl_2 was vigorously stirred at room-temperature in contact with O_2 for about 30 minutes. The peroxo complex [**30**]$^+$ was formed in 100 % yield. Addition of hexane to the solution caused precipitation of [**30**]PF_6 as a light-brown solid, which was collected by filtration and dried under vacuum.

^{1}H-NMR (200.13 MHz, CD_2Cl_2, 298K): δ (ppm) = 7.63 (t, 2H, ^3J(H,H) = 7.7 Hz, Py^A-*H4*); 7.60 (t, 1H, ^3J(H,H) = 7.7 Hz, Py^B-*H4*); 7.34 (d, 1H, ^3J(H,H) = 7.6 Hz, Py^B-*H3* or -*H5*); 7.24 (d, 2H, ^3J(H,H) = 7.6 Hz, Py^A-*H3* or -*H5*); 7.11 (d, 1H, ^3J(H,H) = 7.8 Hz, Py^B- *H3* or -*H5*); 7.10 (d, 2H, ^3J(H,H) = 8.1 Hz, Py^A- *H3* or -*H5*); 5.64 (d[AB], 2H, ^2J(H,H) = 15.5 Hz, N-CH_2-Py^A); 5.15 (d[AB], 2H, ^2J(H,H) = 15.5 Hz, N-CH_2-Py^A); 4.68 (s, 2H, N-CH_2-Py^B); 3.56 (s, 3H, Py^B-CH_3); 3.03 (s, 6H, Py^A-CH_3).

^{13}C{^{1}H}-NMR (50.31 MHz, CD_2Cl_2, 298K): δ (ppm) = 165.4, 162.7, 162.6, 160.3 (Py^B- and Py^A-*C2*, Py^B- and Py^A-*C6*); 139.8 (Py^A-*C4*); 139.5 (Py^B-*C4*); 127.6 (Py^A-*C3*); 126.3 (Py^B-*C3*); 120.8 (Py^A-*C5*); 119.9 (Py^B-*C5*); 72.0 (N-*C*H_2-Py^A); 67.5 (N-*C*H_2-Py^B); 31.3 (Py^B-*C*H_3); 24.2 (Py^A-*C*H_3);

ESI$^+$-MS: m/z = 467 [**30**]$^+$, 435 {[**30**]-O_2}$^+$

Calculated for $C_{21}H_{24}N_4O_2RhPF_6$ (612.32): C 41.19, H 3.95, N 9.15; Found: C 40.29, H 4.72, N 8.46.

*[(κ^4-Me_2-tpa)$Rh^{III}(O_2)$]BAr^F_4 ([**31**]BAr^F_4)*

A solution of 50 mg (0.082 mmol) of [**2**]PF_6 in 2 ml CH_2Cl_2 was vigorously stirred at room-temperature in contact with O_2 for about 4 hours. The peroxo complex [**31**]$^+$ was formed in 100 % yield. Addition of hexane to the solution caused precipitation of [**31**]PF_6 as a light-brown solid, which was collected by filtration and dried under vacuum.

^{1}H-NMR (300.13 MHz, CD_2Cl_2, 298K): δ (ppm) = 8.41 (d, J_{H-H} = 5.7 Hz, 1H; Py-*H6*); 7.8-7.1 (Py-, Py^A- and Py^B-*H3*; Py-, Py^A- and Py^B-*H4*; Py-, Py^A- and Py^B-*H5*); 7.71 (m, 8H; BAr^F-*H2*) ; 7.53 (m, 4H; BAr^F-*H4*); 7.00 (d, J_{H-H} = 7.7 Hz, 1H; Py-*H3*); 5.70 (d[AB], $^2J_{H-H}$ = 14.9 Hz, 1H; N-C*H*$_2$-Py^A or Py^B); 5,57 (d[AB'], $^2J_{H-H}$ = 17.3 Hz, 1H; N-C*H*$_2$-Py^A or -Py^B); 5.06 (d[AB], $^2J_{H-H}$ = 14.5 Hz, 1H; N-C*H*$_2$-Py^A or Py^B); 4.82 (d[AB'], $^2J_{H-H}$ = 16.9 Hz, 1H; N-C*H*$_2$-Py^A or -Py^B); 4.53 (d[AB''], $^2J_{H-H}$ = 16.9 Hz, 1H; N-C*H*$_2$-Py); 4.42 (d[AB''], $^2J_{H-H}$ = 17.6 Hz, 1H; N-C*H*$_2$-Py); 3.37 (s, 3H; Py^A-C*H*$_3$); 2.98 (s, 3H; Py^B-C*H*$_3$).

^{13}C{^{1}H}-NMR (75.45 MHz, CD_2Cl_2, 298K): δ (ppm) = 165.2, 163.4, 163.1, 160.8, 158.0 (s; Py-, Py^A- and Py^B-*C2* ; Py-, Py^A- and Py^B-*C6*); 162.5 (m, $^1J_{B-C}$ = 50 Hz; BAr^F-*C1*); 150.6 (s; Py-*C6*); 140.3, 140.2, 139.8 (s; Py- and Py^A- and Py^B-*C4*); 135.5 (s; BAr^F-*C2*); 129.6 (q, $^2J_{F-C}$ = 32 Hz; BAr^F-*C3*); 127.8 (s; Py^B-*C3*); 126.9 (s; Py-*C3*); 126.3 (s; Py^A-*C3*); 125.3 (q, $^1J_{F-C}$ = 272 Hz; BAr^F-*C*F_3); 122.4 (s; Py^B-*C5*); 121.3 (s; Py-*C5*); 119.7 (s; Py^A-*C5*); 118.3 (s; BAr^F-*C4*); 72.4 (s; N-*C*H_2-Py^B), 70.6 (s; N-*C*H_2-Py); 68.6 (s; N-*C*H_2-Py^A); 28.7 (s; Py^A-*C*H_3); 24.8 (s; Py^B-*C*H_3).

ESI$^+$-MS: m/z = 453 [**31**]$^+$, 421 {[**31**]-O_2}$^+$

Due to the hygroscopic nature of the compound reliable elemental analytical data were not obtained.

*Reaction of [**30**]PF_6 or [**31**]PF_6 with PPh_3*

One equivalent of $P(Ph)_3$ was added to a solution of 0.015 mmole of [**30**]PF_6 or [**31**]PF_6 in 0.5 ml. methanol-d4 at r.t.

^{31}P{^{1}H}-NMR (): d = 30.36 (O=*P*Ph_3), -7.95 (*P*Ph_3, decreasing in time until finally gone).

*Reaction of [**30**]PF_6 with HCl in CD_2Cl_2 : Formation of [(κ^4-Me_3-tpa)$Rh^{III}(Cl)_2$]PF_6 ([**32**]PF_6)*

At room-temperature 94 mg (0.15 mmole) [(Me_3-tpa)Rh(C_2H_4)]PF_6 was dissolved on the air in 10 ml. dichloromethane and stirred for about half an hour to complete the formation of the peroxo complex. After that HCl was bubbled through the solution. At first a suspension was formed which quickly turned into a clear yellow solution of [(Me_3-tpa)Rh($Cl)_2$]PF_6 when an excess of HCl was added. By the addition of hexane the complex was precipitated as a yellow powder, which then could be isolated and vacuum dried.

^{1}H-NMR (200.13 MHz, CD_2Cl_2, 298K): δ (ppm) = 7.71 (t, ^{2}J(H,H) = 7.7 Hz, 2H; Py^B-*H4*); 7.61 (t, ^{2}J(H,H) = 7.6 Hz, 1H; Py^A-*H4*); 7.31 (d, ^{2}J(H,H) = 7.9 Hz, 2H; Py^B-*H3* or -*H5*); 7.24 (d, ^{2}J(H,H) = 6.8 Hz, 1H;Py^A-*H3* or -*H5*); 7.20 (s, ^{2}J(H,H) = 7.0 Hz, 1H;Py^A-*H3* or -*H5*); 7.17 (Py^B-*H3* or -*H5*); 6.02 (d[AB], ^{2}J(H,H) = 15.5 Hz, 2H; N-C*H*$_2$-Py^B); 4.96 (s, 2H; N-C*H*$_2$-Py^A); 4.78 (d[AB], ^{2}J(H,H) = 15.5 Hz, 2H; N-C*H*$_2$-Py^B); 3.65 (s, 3H; Py^A-C*H*$_3$); 3.16 (s, 6H; Py^B-C*H*$_3$).

FAB$^+$-MS: m/z = 505 [**32**]$^+$

*Reaction of [**30**]PF_6 with 1 eq. $HBAr^F_4$.2Et_2O in CD_3CN, formation of ([**33**]PF_6)*

At -20°C 17 mg (0.028 mmole) [**30**]PF_6 was dissolved in 0.5 ml CD_3CN. Subsequently 29 mg (0.028 mmole) $HBAr^F_4$.2Et_2O was added slowly. During the next two hours the temperature of the yellow-colored reaction mixture was allowed to rise to 0°C. The reaction was not selective, however the five-membered ring seemed to be formed in majority.

^{1}H-NMR (200.13 MHz, CD_3CN, 298K): δ (ppm) = 8.33 (s(br), 1H; imide N-*H*); 8.0-7.8 (Py^A- and Py^B-*H4*); 7.73 (m, 8H; BAr^F-*H2*); 7.71 (m, 4H; BAr^F-*H4*); 7.6-7.1 (Py^A- and Py^B-*H3*, Py^A- and Py^B-*H5*); 5.34 (d[AB], ^{2}J(H,H(= 16.2 Hz, 2H; N-C*H*$_2$-Py^B); 5,00 (d[AB], ^{2}J(H,H) = 16.2 Hz, 2H; N-C*H*$_2$-Py^B); 4.88 (s, 2H; N-C*H*$_2$-Py^A); 3.17 (s, 3H; Py^A-C*H*$_3$); 2.85 (s, 6H; Py^B-C*H*$_3$).

*Reaction of [**30**]BAr^F_4 with 2 eq. $HBAr^F_4$.2Et_2O in CD_3CN*

At -20°C 60 mg (0.045 mmole) [**30**]BAr^F_4 was dissolved in 1 ml CD_3CN. Subsequently 89 mg (0.089 mmole) $HBAr^F_4$.2Et_2O dissolved in 1 ml CD_3CN was added slowly. During the next two hours the temperature of the reaction-mixture was allowed to rise to 0°C. The solvent was evaporated and the yellow product was collected.

^{1}H-NMR (200.13 MHz, CD_3CN, 298K): δ (ppm) = 8.37 (s(br), 0.9H; imide N-*H*); 8.07 (t, J_{H-H} = 7.7 Hz, 2H; Py_b-H_4); 7.9-7.6 (Py_a-H_4); 7.77 (m, 8H; BAr^F-H_2) ; 7.71 (m, 4H; BAr^F-H_4); 7.7-7.2 (Py_a- and Py_b-H_3, Py_a- and Py_b-H_5); 6.93 (s(br), 1.6H; hydroperoxo-*H*); 5.54 (d[AB], $^2J_{H-H}$ = 16.9 Hz, 2H; N-C*H*$_2$-Py_b); 5,10 (s, 2H; N-C*H*$_2$-Py_a); 4.97 (d[AB], $^2J_{H-H}$ = 16.9 Hz, 2H; N-C*H*$_2$-Py_b); 3.31 (s, 3H; Py_a-C*H*$_3$); 2.97 (s, 6H; Py_b-C*H*$_3$).

$^{13}C\{^1H\}$-NMR (50.31 MHz, CD_3CN, 298K): δ (ppm) = 165.5 (s; Py_b-*C*$_2$);164.3 (s; Py_a-*C*$_2$); 162.0 (s; Py_b-*C*$_6$); 158.0 (s; Py_a-*C*$_6$); 161.6 (m, $^1J_{B-C}$ = 51 Hz; BAr^F-*C*$_1$); 158.0 (s; Py_a-*C*6); 142.4 (s; Py_b-*C*$_4$); 141.4 (s; Py_a-*C*$_4$); 134.7 (s; BAr^F-*C*$_2$); 129.5 (s; Py_a-*C*$_3$); 129.3 (s; Py_b-*C*$_3$); 129.0 (q, $^2J_{F-C}$ = 31 Hz; BAr^F-*C*$_3$); 124.5 (q, $^1J_{F-C}$ = 272 Hz; BAr^F-*C*F_3); 122.8 (s; Py_b-*C*$_5$); 121.2 (s; Py_a-*C*$_5$); 117.7 (s; BAr^F-*C*$_4$); 71.0 (s; N-*C*H_2-Py_a), 70.3 (s; N-*C*H_2-Py_b); 27.1 (s; Py_a-*C*H_3); 26.2 (s; Py_b-*C*H_3). Two broad signals at 134.2 and 134.0 ppm could not be interpretated. Could they belong to an ethanimidoyl peroxy fragment?

FAB^+-MS: mz/ = 1375 {[**33**](BAr^F_4)}$^+$.

*[(κ^3-Me$_2$-bpa-Bz)Rh^{III}(O$_2$)(CD$_3$CN)]PF$_6$ ([**34**]PF$_6$)*

50 mg of [(Me_2-bpa-Bz)Rh(C_2H_4)$_2$]PF_6 was put under a dioxygen atmosphere and immediately 1.5 ml. of CD_3CN was added. The reaction mixture was stirred for about 30 minutes and the solvent was removed under a reduced pressure. A brown solid was obtained. Yield: > 95 % on the basis of ^{1}H-NMR.

^{1}H-NMR (200.13 MHz, CD_3CN, 298K): δ (ppm) = 7.89 (t, 2H, J(H,H) = 7.83 Hz, Py-*H4*), 7.55 (m, 3H, Ph-*H4* and Ph-*H2*/*H6* or Ph-*H3*/*H5*), 7.46 (d, 2H, J(H,H) = 7.22 Hz, Py-*H3* or -*H5*), 7.39 (d, 2H, J(H,H) = 7.95 Hz, Py-*H3* or -*H5*), 7.27 (m, 2H, Ph-*H2*/*H6* or -*H3*/*H5*), 4.84 (s, 4H, N-CH_2-Py), 3.88 (s, 2H, N-C*H*$_2$-Ph), 3.00 (s, 6H, Py-CH_3).

^{13}C-NMR (50.03 MHz, CD_3CN, 298K): δ (ppm) = 164.62 (Py-*C2*), 163.04 (Py-*C6*), 140.62 (Py-C4), 133.31 (Ph-*C2*/*C6*), 131.01 (Ph-C1), 130.34 (Py-*C3*/*C5* and -*C4*), 130.16 (Ph-*C2*/*C6* or -*C3*/*C5*), 126.99 (Py-*C3*), 121.68 (Py-*C5*), 118.27 (), 65.15 (N-*C*H_2-Py), 60.15 (N-*C*H_2-Ph), 23.81 (Py-*C*H_3).

For the ESI^+-MS measurement was [**34**]$^+$ prepared in CD_3CN. Subsequently the CD_3CN-solution was diluted with CH_3CN to a concentration of 10^{-5}. Only the peroxo complex with CH_3CN coordinated was observed in the mass spectrum, indicating a fast exchange of the coordinated acetonitrile molecule with the surrounding solvent.

ESI^+-MS: m/z = 493 [(Me_2-bpa-Bz)Rh(O_2)(CH_3CN)]$^+$, 452 [(Me_2-bpa-Bz)Rh(O_2)]$^+$, 434 [(Me_2-bpa-Bz)Rh(O_2)]-H_2O}$^+$.

Calculated for $C_{23}H_{26}O_2N_4Rh$: 493.1111; Found: 493.10996 (Δ = –2.3 ppm).

*[(κ^3-Me$_2$-bpa-Me)Rh^{III}(O$_2$)(CD$_3$CN)]PF$_6$ ([**35**]PF$_6$)*

50 mg of [(Me_2-bpa-Bz)Rh(C_2H_4)$_2$]PF_6 was put under a dioxygen atmosphere and immediately 1.5 ml. of CD_3CN was added. The reaction mixture was stirred for about 30 minutes and the solvent was removed under a reduced pressure. A brown solid was obtained.

From the mixture of products we were able to identify most of the ^{1}H-signals belonging to complex [**35**]$^+$ (in approx. 17 % yield on the basis of ^{1}H-NMR).

^{1}H-NMR (200.13 MHz, CD_2Cl_2, 298K): δ (ppm) = 7.81 (t, 2H, J(H,H) = 7.83 Hz, Py-*H4*), 7.4 - 7.25 (m, Py-*H3* and -*H5*), 5.41 (free C_2H_4), 5.20 (d[AB], 2H, J(H,H) = 15.53 Hz, N-C*H*$_2$-Py), 4.71 (d[AB], 2H, J(H,H) = 15.39 Hz, N-C*H*$_2$-Py), 2.96 (s, 6H, Py-C*H*$_3$), 2.65 (s, 3H, N-C*H*$_3$).

For the ESI^+-MS measurement [**35**]$^+$ was prepared in CD_3CN. Subsequently the CD_3CN-solution was diluted with CH_3CN to a concentration of 10^{-5}. Only the peroxo complex with CH_3CN coordinated was observed in the mass spectrum, indicating a fast exchange of the coordinated acetonitrile molecule with the surrounding solvent.

ESI^+-MS: m/z = 417 [(Me_2-bpa-Me)Rh(O_2)(CH_3CN)]$^+$, 376 [(Me_2-bpa-Me)Rh(O_2)]$^+$, 344 [(Me_2-bpa-Me)Rh]$^+$.

Calculated for $C_{17}H_{22}O_2N_4Rh$: 417.0798; Found: 417.07979 (Δ = 0.0 ppm).

*EPR measurements for [**25**]BPh$_4$, [**26**]PF$_6$ and [**27**]PF$_6$ upon exposure to air*

Solutions of ca. 10^{-3} M are prepared under an inert atmosphere for all three compounds. The total volume of the solution is 1 ml. For [**25**]BPh_4 a mixture of acetone-methanol (3:1) was used as a solvent. For [**26**]PF_6 and [**27**]PF_6 a ratio of 2:3 was used. The ratios were changed for [**25**]BPh_4 to circumvent solvation problems.

For all compounds an EPR spectrum was measured before contact with air and in all cases at this point no unpaired electrons were present in the samples. Upon first contact with air, the solutions were immediately cooled down to 4 K and an EPR spectrum was measured. After that the EPR-tube was warmed up to r.t. for a few seconds and cooled down again. This process was repeated a few times, depending on the EPR-behavior of the compound.

For [**25**]BPh_4 only in very low concentrations species with unpaired electrons are formed. The EPR signal disappeared after about 1 minute in contact with air at r.t.

For [**26**]PF_6 the EPR signal intensity increased in time

For [**27**]PF_6 a very strong EPR signal was observed, which did not disappear even after having been at r.t. for a few minutes. The shape and the intensity of the signal changed a little bit during this time, though. It seems as if in time some sort of rearrangements take place.

4.7 References

[1] G. Read and M. Urgelles, *J. Chem. Soc. - Dalton Trans.*, **1985**, *(8)*, 1591-1596
[2] O. Bortolini, F. Difuria, G. Modena and R. Seraglia, *J. Mol. Catal.*, **1984**, *22 (3)*, 313-317
[3] L. Carlton, G. Read and M. Urgelles, *J. Chem. Soc. - Chem. Commun.*, **1983**, *(10)*, 586-588
[4] F. Di Furia and G. Modena, *Pure Appl. Chem.*, **1982**, *54 (10)*, 1853-1866
[5] H. Mimoun, *Pure Appl. Chem.*, **1981**, *53 (12)*, 2389-2399
[6] F. Igersheim and H. Mimoun, *Nouv. J. Chim. - New J. Chem.*, **1980**, *4 (3)*, 161-166
[7] H. Mimoun, M. M. P. Machirant and I. Sereederoch, *J. Am. Chem. Soc.*, **1978**, *100 (17)*, 5437-5444
[8] G. Read and P. J. C. Walker, *J. Chem. Soc. - Dalton Trans.*, **1977**, *(9)*, 883-888
[9] C. Dudley and G. Read, *Tetrahedron Lett.*, **1972**, *(52)*, 5273
[10] K. Takao, Y. Fujiwara, T. Imanaka and Teranish.S, *Bull. Chem. Soc. Jpn*, **1970**, *43 (4)*, 1153
[11] K. Takao, M. Wayaku, Y. Fujiwara, T. Imanaka and S. Teranishi, *Bull. Chem. Soc. Jpn*, **1970**, *43*, 3898
[12] B. de Bruin, P. H. M. Budzelaar and A. W. Gal, *Angew. Chem. - Int. Edit.*, **2004**, *43 (32)*, 4142-4157
[13] G. Strukul and R. A. Michelin, *J. Am. Chem. Soc.*, **1985**, *107 (25)*, 7563-7569
[14] K. A. Jorgensen and B. Schiott, *Chem. Rev.*, **1990**, *90 (8)*, 1483-1506
[15] K. A. Jorgensen, *Chem. Rev.*, **1989**, *89 (3)*, 431-458
[16] G. Read, *J. Mol. Catal.*, **1988**, *44 (1)*, 15-33
[17] R. J. N. A. M. Kicken, *PhD Thesis "Oxidation of Iridium Olefin Complexes by H_2O_2 and O_2"*, **2001**
[18] M. Krom, *PhD Thesis "Mono- and Dioxygenation of Rhodium and Iridium Olefin Fragments, Solution versus Solid State Reactivity"*, **2003**
[19] M. Krom, R. G. E. Coumans, J. M. M. Smits and A. W. Gal, *Angew. Chem. - Int. Edit.*, **2001**, *40 (11)*, 2106-2108
[20] M. Krom, R. G. E. Coumans, J. M. M. Smits and A. W. Gal, *Angew. Chem. - Int. Edit.*, **2002**, *41 (4)*, 576-579
[21] M. Krom, T. P. J. Peters, R. G. E. Coumans, T. J. J. Sciarone, J. Hoogboom, S. I. ter Beek, P. P. J. Schlebos, J. M. M. Smits, R. de Gelder and A. W. Gal, *Eur. J. Inorg. Chem.*, **2003**, *6*, 1072-1087
[22] B. de Bruin, M. J. Boerakker, R. de Gelder, J. M. M. Smits and A. W. Gal, *Angew. Chem. - Int. Edit.*, **1999**, *38 (1-2)*, 219-222
[23] B. de Bruin, M. J. Boerakker, J. J. J. M. Donners, B. E. C. Christiaans, P. P. J. Schlebos, R. de Gelder, J. M. M. Smits, A. L. Spek and A. W. Gal, *Angew. Chem. - Int. Edit.*, **1997**, *36 (19)*, 2064-2067
[24] B. de Bruin, M. J. Boerakker, J. A. W. Verhagen, R. de Gelder, J. M. M. Smits and A. W. Gal, *Chem. - Eur. J.*, **2000**, *6 (2)*, 298-312
[25] B. de Bruin, J. A. Brands, J. J. J. M. Donners, M. P. J. Donners, R. de Gelder, J. M. M. Smits, A. W. Gal and A. L. Spek, *Chem. - Eur. J.*, **1999**, *5 (10)*, 2921-2936
[26] B. de Bruin, T. P. J. Peters, J. B. M. Wilting, S. Thewissen, J. M. M. Smits and A. W. Gal, *Eur. J. Inorg. Chem.*, **2002**, *(10)*, 2671-2680
[27] M. H. Dickman and M. T. Pope, *Chem. Rev.*, **1994**, *94 (3)*, 569-584
[28] J. S. Valentine, *Chem. Rev.*, **1973**, *73 (3)*, 235-245
[29] G. A. Rodley and W. T. Robinson, *Nature*, **1972**, *235*, 438
[30] W. P. Schaefer, *Inorg. Chem.*, **1968**, *7*, 725
[31] W. P. Schaefer and R. E. Marsh, *J. Am. Chem. Soc.*, **1966**, *88*, 178
[32] W. P. Schaefer and R. E. Marsh, *Acta Crystallogr.*, **1966**, *21*, 735
[33] L. Vaska, *Accounts Chem. Res.*, **1976**, *9*, 175-183
[34] A. Vigalok, L. J. W. Shimon and D. Milstein, *Chem. Commun.*, **1996**, *(14)*, 1673-1674
[35] D. J. A. de Waal, T. I. A. Gerber, W. J. Louw and R. Van Eldik, *Inorg. Chem.*, **1982**, *21 (5)*, 2002-2006
[36] W. J. Louw, D. J. A. De Waal, T. I. A. Gerber, C. M. Demanet and R. G. Copperthwaite, *Inorg. Chem.*, **1982**, *21 (4)*, 1667-1668
[37] G. Mestroni and A. Camus, *Inorg. Nucl. Chem. Lett.*, **1973**, *9 (2)*, 261-263
[38] J. M. Brown, R. A. John and A. R. Lucy, *J. Organomet. Chem.*, **1985**, *279 (1-2)*, 245-257
[39] *"Cytochrome P-450"*, Eds. R. Sato and T. Omura, Kodansha, Tokyo, **1978**
[40] P. R. O. d. Montellano, *"Cytochrome P-450: Structure, Mechanism and Biochemistry"*, Plenum, New York, **1986**
[41] Y. Watanabe and J. T. Groves, *"The Enzymes"*, Eds. B. Sigman, Academic Press, Orlando, **1992**
[42] M. Sono, M. P. Roach, E. D. Coulter and J. H. Dawson, *Chem. Rev.*, **1996**, *96 (7)*, 2841-2887
[43] P. Burger, *Lecture at the Nijmegen NSR Reseach Center*, **2002**, *January 14*
[44] P. R. O. de Montellano, *"Cytochrome P-450: Structure, Mechanism and Biochemistry"*, Plenum Press, New York, **1986**
[45] A. Morvillo and M. Bressan, *J. Organomet. Chem.*, **1987**, *332 (3)*, 337-343
[46] M. Brookhart, B. Grant and A. F. Volpe, *Organometallics*, **1992**, *11 (11)*, 3920-3922
[47] R. S. Drago, A. Zuzich and E. D. Nyberg, *J. Am. Chem. Soc.*, **1985**, *107 (10)*, 2898-2903

[48] M. Bressan, F. Morandini and P. Rigo, *Inorg. Chim. Acta - Lett.*, **1983**, *77 (4)*, L139-L142
[49] M. Bressan, F. Morandini and P. Rigo, *J. Organomet. Chem.*, **1983**, *247 (1)*, C8-C10
[50] Y. Takahashi, M. Hashimoto, S. Hikichi, Y. Moro-oka and M. Akita, *Inorg. Chim. Acta*, **2004**, *357 (6)*, 1711-1724
[51] G. A. Abakumov, N. N. Vavilina, Y. A. Kurskii, V. I. Nevodchikov, V. K. Cherkasov and A. S. Shavyrin, *Russ. Chem. Bull.*, **2003**, *52 (8)*, 1847-1853
[52] K. Tanaka, Y. Yamamoto and S. Ohba, *Chem. Commun.*, **2003**, *(15)*, 1866-1867
[53] E. Liepinsh, G. Otting and K. Wüthrich, *J. Biomol. NMR*, **1992**, *2 (5)*, 447-465
[54] O. Groning, T. Drakenberg and L. I. Elding, *Inorg. Chem.*, **1982**, *21 (5)*, 1820-1824
[55] N. Hallinan, V. Besancon, M. Forster, G. Elbaze, Y. Ducommun and A. E. Merbach, *Inorg. Chem.*, **1991**, *30 (5)*, 1112-1114
[56] P. E. Garrou, *Adv. Organomet. Chem.*, **1984**, *23*, 95-129
[57] R. L. Rominger, J. M. McFarland, J. R. Jeitler, J. S. Thompson and J. D. Atwood, *J. Coord. Chem.*, **1994**, *31 (1)*, 7-18
[58] R. Romeo, L. M. Scolaro, M. R. Plutino, F. F. de Biani, G. Bottari and A. Romeo, *Inorg. Chim. Acta*, **2003**, *350*, 143-151
[59] R. Romeo, *Comments Inorg. Chem.*, **2002**, *23 (1)*, 79-100
[60] A. L. Casado, A. A. Casares and P. Espinet, *Inorg. Chem.*, **1998**, *37 (16)*, 4154-4156
[61] A. Gelling, K. G. Orrell, A. G. Osborne and V. Sik, *J. Chem. Soc. - Dalton Trans.*, **1998**, *(6)*, 937-945
[62] B. B. Coussens, F. Buda, H. Oevering and R. J. Meier, *Organometallics*, **1998**, *17 (5)*, 795-801
[63] M. W. Holtcamp, J. A. Labinger and J. E. Bercaw, *Inorg. Chim. Acta*, **1997**, *265 (1-2)*, 117-125
[64] L. M. Rendina and R. J. Puddephatt, *Chem. Rev.*, **1997**, *97 (6)*, 1735-1754
[65] S. S. Stahl, J. A. Labinger and J. E. Bercaw, *J. Am. Chem. Soc.*, **1996**, *118 (25)*, 5961-5976
[66] J. A. Casares, S. Coco, P. Espinet and Y. S. Lin, *Organometallics*, **1995**, *14 (6)*, 3058-3067
[67] A. Yamamoto, T. Yamamoto, S. Komiya and F. Ozawa, *Pure Appl. Chem.*, **1984**, *56 (11)*, 1621-1634
[68] J. D. Scott and R. J. Puddephatt, *Organometallics*, **1983**, *2 (11)*, 1643-1648
[69] R. S. Paonessa and W. C. Trogler, *J. Am. Chem. Soc.*, **1982**, *104 (12)*, 3529-3530
[70] G. M. Whitesides, *Pure Appl. Chem.*, **1981**, *53 (1)*, 287-292
[71] R. Romeo, G. Alibrandi and L. M. Scolaro, *Inorg. Chem.*, **1993**, *32 (22)*, 4688-4694
[72] R. Romeo and G. Alibrandi, *Inorg. Chem.*, **1997**, *36 (21)*, 4822-4830
[73] M. R. Plutino, L. M. Scolaro, R. Romeo and A. Grassi, *Inorg. Chem.*, **2000**, *39 (13)*, 2712-2720
[74] R. Romeo, M. R. Plutino and L. I. Elding, *Inorg. Chem.*, **1997**, *36 (25)*, 5909-5916
[75] F. Wilkinson, W. P. Helman and A. B. Ross, *J. Phys. Chem. Ref. Data*, **1995**, *24 (2)*, 663-1021
[76] "*Chapter 12: Spin-Forbidden Reactions in Transition Metal Chemistry*", *Computational Organometallic Chemistry*, Vol. Eds. T. R. Cundari, Marcel Dekker, Inc., New York, **2001**, 291-321
[77] B. de Bruin, J. A. W. Verhagen, C. H. J. Schouten, A. W. Gal, D. Feichtinger and D. A. Plattner, *Chem. - Eur. J.*, **2001**, *7 (2)*, 416-422
[78] G. Anderegg and F. Wenk, *Helv. Chim. Acta*, **1967**, *50 (8)*, 2330
[79] H. Nagao, N. Komeda, M. Mukaida, M. Suzuki and K. Tanaka, *Inorg. Chem.*, **1996**, *35 (23)*, 6809-6815
[80] R. Cramer, J. A. McCleverty and J. Bray, *Inorg. Synth.*, **1990**, *28*, 86
[81] J. L. Herde, J. C. Lambert and C. V. Senoff, *Inorg. Synth.*, **1974**, *15*, 18-20
[82] A. C. T. North, D. C. Phillips and F. S. Mathews, *Acta Crystallogr. Sect. A*, **1968**, *A 24*, 351
[83] P. T. Beurskens, G. Beurskens, W. P. Bosman, R. de Gelder, S. Garcia-Granda, R. O. Gould, R. Israel and J. M. M. Smits, *"DIRDIF-96. A computer program system for crystal structure determination by Patterson methods and direct methods applied to difference structure factors"*; Laboratory of Crystallography, Department of Inorganic Chemistry, University of Nijmegen: The Netherlands, **1996**
[84] P. T. Beurskens, G. Beurskens, M. Strumpel and C. E. Nordman, *Patterson and Pattersons*, Vol. Eds. J. P. Glusker, B. K. Patterson and M. Rossi, Clarendon Press, Oxford, **1987**, page 356
[85] G. M. Sheldrick, *"SHELXL-97. Program for the refinement of crystal structures"*; University of Goettingen, Germany, **1997**
[86] A. L. Spek, *"PLATON-93. Program for display and analysis of crystal and molecular structures"*; University of Utrecht, The Netherlands, **2003**

Chapter 5

Synthesis and Reactivity of N_4 Iridium(II) Olefin Complexes

5.1 Introduction

The reactions of the N_3 and N_4 rhodium(I) and iridium(I) ethene complexes with molecular oxygen, as described in Chapter 4, seem to involve paramagnetic as well as diamagnetic species. The complicated nature of these reactions made it impossible to establish the reaction patterns of these interesting odd-electron species. Therefore, we attempted to independently synthesize metal(II) olefin complexes and study their reactivity towards oxygen and other small molecules. As the present chapter shows, steric hindrance turns out to be the key to isolation of stable metal(II) ethene complexes of tpa-type ligands.

Mononuclear complexes of rhodium(II) [1] – [3] and particularly iridium(II) [4], [5] are rare. Most previous examples are stabilized by bulky di-anionic porphyrinate ligands (por^{2-}). To our best knowledge, only one stable mononuclear iridium(II)-*olefin* complex has been reported, *viz.* $[(C_6Cl_5)_2Ir^{II}(cod)]$ (cod= *Z,Z*-1,5-cyclooctadiene). [6]

$[(por)Rh^{II}]$ complexes are known for their remarkable reactivity towards a variety of otherwise rather inert substrates: activation under mild conditions of H_2, Si-H and Sn-H bonds, benzylic and allylic C-H bonds, and even methane have been reported. [1]

Recently, $[(por)M^{II}(ethene)]$ complexes (M= Rh [1], [2], Ir [5], por^{2-} = a bulky meso-tetra-arylporphyrinate dianion), formed *in situ* from $[(por)M^{II}]$ and ethene, have been reported to undergo bimolecular M-C coupling reactions to form (diamagnetic) ethylene bridged species $[(por)M\text{-}CH_2CH_2\text{-}M(por)]$ and, upon increase of the steric bulk of the por^{2-} ligand, C-C coupling reactions to form butylene bridged species $[(por)M\text{-}CH_2CH_2\text{-}CH_2CH_2\text{-}M(por)]$ (Figure 5.1).

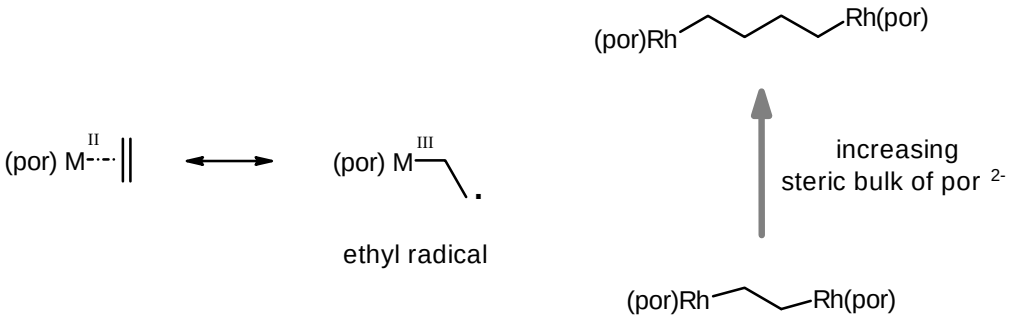

Figure 5.1 *Reactivity of $[(por)M^{II}(ethene)]$ complexes*

Apparently, in $[(por)M^{II}(ethene)]$ the unpaired electron has a relatively high density on the ethene substrate, imposing some M^{III}-ethyl-radical character on these transient species. Also for other metal(II) complexes dimerization reactions have been observed. [3], [7] – [11]

The metal(II)-ethene complexes also reacted readily with CO, forming metal(II)-CO complexes and free to ethene. [12]

In the remainder of this chapter we will compare the chemistry of our tpa-type metal(II)-ethene complexes with that of the [(por)M^{II}(ethene)] mentioned above. Parts of described in this chapter have already been published. [13] – [15]

5.2 Synthesis of N_4 iridium(II) ethene complexes

5.2.1 Reaction of $[4]^+$ and $[6]^+$ towards $[Fc]PF_6$

Treatment of [**4**]PF_6 and [**6**]PF_6 with ferrocenium hexafluorophoshate ([Fc]PF_6) in CH_2Cl_2 results in precipitation of [**36**]$(PF_6)_2$ and [**37**]$(PF_6)_2$ respectively. (Figure 5.2).

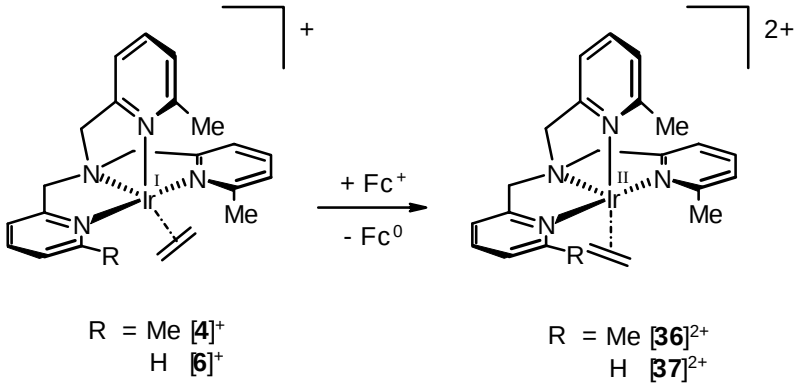

Figure 5.2 *Synthesis of N_4 iridium(II) ethene complexes*

The reaction rate increases with increasing substitution of the tpa ligand. For $[\mathbf{6}]^+$ the reaction takes about 1.5 hour, whereas for $[\mathbf{4}]^+$ the reaction is complete after 30 minutes.

This is in line with the electrochemical data presented in Table 5.1, which show that $[\mathbf{4}]^+$ is easier to oxidize than $[\mathbf{6}]^+$.[1]

Table 5.1 *Electrochemical data for $[(Me_n\text{-tpa})Ir^I(ethene)]^+$ (n= 0, 1, 2, 3)* [2]

Compound	Solvent	E_p^a	$E_{½}$	ΔE	I_b/I_f
$[(Me_3\text{-tpa})Ir^I(ethene)]^+$ ($[\mathbf{4}]^+$)	CH_2Cl_2	-255	-289	68	1.0
	Acetone	-334	-368	70	1.0
	MeCN	-330	-365	69	1.0
$[(Me_2\text{-tpa})Ir^I(ethene)]^+$ ($[\mathbf{6}]^+$)	CH_2Cl_2	-138	-173	68	1.0
	Acetone	-213	-249	70	1.0
	MeCN	-198	-240	84	0.4

[1] The 6-methyl-pyridyl group is a weaker donor than the unsubstituted pyridyl group, because the methyl group hinders approach of the nitrogen atom to the metal. [16] – [20] Therefore, one would expect the more substituted complexes to be *more resistant* to oxidation. The data in Table 5.1 not only disagree with this expectation, but do not even show a clear trend, with Me_3-tpa < Me_2-tpa ~ tpa < Me-tpa. At present, we have no explanation for this observation. However, the irreversibility of the oxidation of tpa and Me-tpa complexes and the strong solvent dependence make interpretation of the redox potentials difficult.

[2] E in mV versus Fc/Fc^+. E_p^a: anodic peak potential, $E_{½}$: half-wave potential in mV, ΔE: peak separation in mV, I_b/I_f: cathodic peak current/anodic peak current, scan-rate 100 mV/second.

Compound	Solvent	E_p [a]	$E_{½}$	ΔE	I_b/I_f
$[(Me\text{-}tpa)Ir^{I}(ethene)]^+$	CH_2Cl_2	-43	--	--	0
	Acetone	-122	--	--	0
	MeCN	-93	--	--	0
$[(tpa)Ir^{I}(ethene)]^+$	CH_2Cl_2	-136	--	--	0
	Acetone	-144	--	--	0
	MeCN	-10	--	--	0

For the redox couple $[\mathbf{4}]^+/[\mathbf{36}]^{2+}$ electrochemically reversible oxidation-reduction waves (ΔE = 68-70 mV, I_b/I_f = 1.0) were observed in CH_2Cl_2, acetone and acetonitrile. The redox couple $[\mathbf{6}]^+/[\mathbf{37}]^{2+}$ also gives rise to reversible waves in CH_2Cl_2 and acetone, but in acetonitrile oxidation of $[\mathbf{6}]^+$is much less reversible (I_b/I_f = 0.4). The reason for this behavior will become apparent in § 5.3.

In agreement with the electrochemical data, both $[\mathbf{36}]^{2+}$ and $[\mathbf{37}]^{2+}$ are stable in acetone judging from the persistence of their paramagnetically shifted and broadened ^{1}H-NMR signals. Complex $[\mathbf{36}]^{2+}$ is stable in acetone for over 48 hours, but a slight degradation of $[\mathbf{37}]^{2+}$ was observed after 2 hours at room temperature. Complete degradation of $[\mathbf{37}]^{2+}$ in acetone requires more than 24 hours, and results in a complex mixture of diamagnetic products. This process is accelerated upon passing N_2 through the solution (complete degradation within 30 minutes), and is therefore probably related to ethene loss.

Remarkably, both $[\mathbf{36}]^{2+}$ and $[\mathbf{37}]^{2+}$ do not appear to react with CO, apart from the degradation due to ethene loss also observed with N_2. This is surprising in view of the reported higher affinity of $[(por)Rh^{II}]$ for CO relative to ethene. [12]
A steric explanation for this difference between our tpa-type complexes and the porphyrin complexes is unlikely, so we believe that the weaker σ-donor character of the neutral Me_n-tpa ligand relative to the dianionic por^{2-} is responsible.

As can be seen in Table 5.1, less substituted analogues of $[\mathbf{4}]^+$, e.g. $[(tpa)Ir^{I}(ethene)]^+$ and $[(Me\text{-}tpa)Ir^{I}(ethene)]^+$, show entirely irreversible oxidation waves even in the weakly coordinating solvents CH_2Cl_2 and acetone. In line with these observations, attempts to prepare the corresponding iridium(II)-ethene species (less substituted analogues of $[\mathbf{36}]^{2+}$ and $[\mathbf{37}]^{2+}$) were not successful.
Apparently, steric shielding of the iridium(II) centre is important to stabilize iridium species in the unusual oxidation state +2.

Comparison of X-ray structures

We were able to isolate crystals suitable for X-ray diffraction for $[\mathbf{36}](PF_6)_2$. The structure obtained is shown in Figure 5.3 side by side with the analogous iridium(I) complex $[\mathbf{4}]^+$. Table 5.2 gives selected bond lengths for $[\mathbf{36}]^{2+}$ and the iridium(I) ethene complexes $[\mathbf{4}]^+$ and $[\mathbf{6}]^+$ (for more details about the last two structures see Chapter 3).

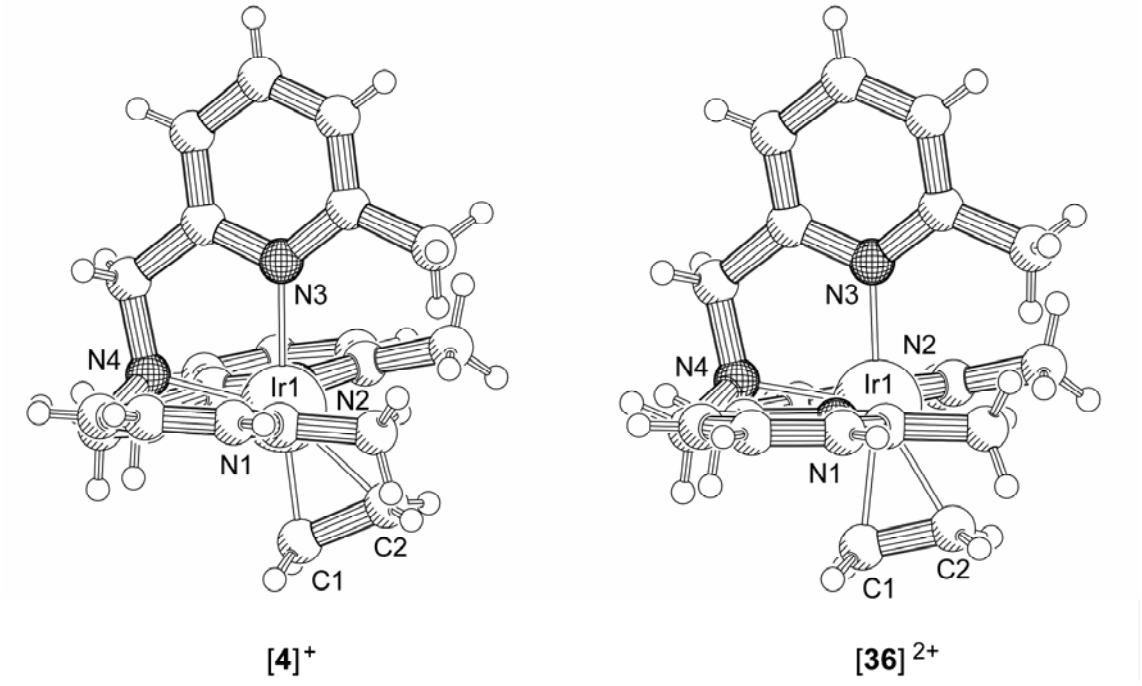

Figure 5.3 *X-ray structures of [**4**]PF_6 and [**36**]$(PF_6)_2$*
Anions omitted for clarity

Table 5.2 *Selected bond lengths (Å) in [**6**]$^+$, [**4**]$^+$ and [**36**]$^{2+}$*

	[$(Me_2$-tpa$)Ir^I(C_2H_4)]^+$ ([**6**]$^+$)	[$(Me_3$-tpa$)Ir^I(C_2H_4)]^+$ ([**4**]$^+$)	[$(Me_3$-tpa$)Ir^{II}(C_2H_4)]^+$ ([**36**]$^{2+}$)
Ir1-N1	2.039(6)	2.075(7)	2.071(5)
Ir1-N2	2.066(5)	2.043(8)	2.062(5)
Ir1-N3	2.219(6)	2.260(7)	2.136(5)
Ir1-N4	2.153(5)	2.154(8)	2.146(5)
Ir1-C1	2.051(7)	2.042(9)	2.136(6)
Ir1-C2	2.073(7)	2.143(9)	2.149(6)
C1-C2	1.442(11)	1.451(13)	1.380(9)

As shown in Chapter 3, the structures of [**4**]$^+$ and [**6**]$^+$ are best described as distorted trigonal bipyramidal (*tbp*), with N1 and N2 at the axial positions and N3, N4 and ethene in the equatorial plane. Remarkably, upon one-electron oxidation of [**4**]$^+$ to [**36**]$^{2+}$, the ethene ligand moves to a position *cis* to the amine-nitrogen, changing the coordination geometry from *tbp* to distorted square pyramidal (*sqpy*), with N4 at the apical position and N1, N2, N3 and ethene in the basal plane. This is clearly shown by the decreasing C1-Ir1-N4 angle on going from [**6**]$^+$ (116.0(3) º) and [**4**]$^+$ (109.2(4) º) to [**36**]$^+$ (92.4(2) º).

From Table 5.2 it is clear that oxidation of [**4**]$^+$ to [**36**]$^{2+}$ results in a stronger binding of N3 to the iridium center. A similar shortening was also observed on going from [**4**]$^+$ to [**6**]$^+$ (Me_2-tpa has an unsubstituted pyridine ring in an axial position, which decreases the steric hindrance around the metal center hereby allowing N3 to approach the iridium center at a closer distance).

The significant shortening of the C1-C2 distance by ~ 0.07 Å and the elongation of the Ir-C1 distance by ~ 0.09 Å on going from [**4**]$^+$ to [**36**]$^{2+}$ indicates weakening of the iridium-ethene interaction upon oxidation of iridium(I) to iridium(II). Since a decreased ethene $\rightarrow$ Ir σ-bonding is unlikely, the weaker Ir-ethene interaction apparently results from a decreased Ir $\rightarrow$ ethene π-backbonding on going from [**4**]$^+$ to [**36**]$^{2+}$.

5.2.2 DFT calculations on $[36]^{2+}$

DFT calculations were performed on both $[\mathbf{4}]^+$ and $[\mathbf{36}]^{2+}$. The geometries of the optimized DFT structures match quite well with the X-ray structures of $[\mathbf{4}]^+$ and $[\mathbf{36}]^{2+}$ (*tbp* geometry for $[\mathbf{4}]^+$, *sqpy* geometry for $[\mathbf{36}]^{2+}$). The HOMO of $[\mathbf{4}]^+$ and the SOMO of $[\mathbf{36}]^{2+}$ both mainly consist of the same iridium 5*d*-orbital, with bonding contributions of the ethene π^* orbital and antibonding contributions of orbitals on N3 and N4 (Figure 5.4). In other words, this is the molecular orbital describing most of the Ir $\rightarrow$ ethene π-backdonation.

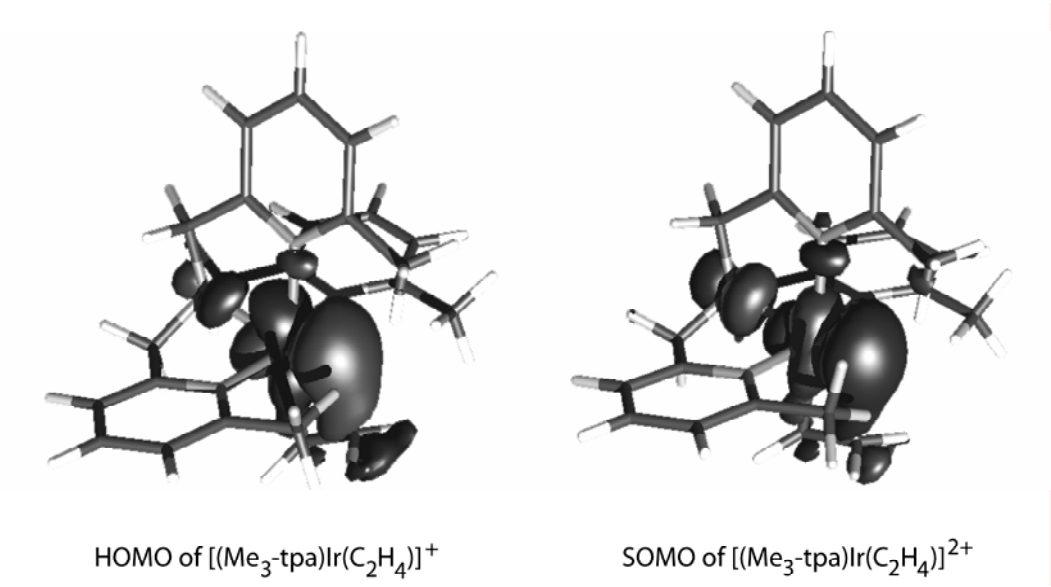

Figure 5.4 *HOMO of $[\mathbf{4}]^+$ (left) and SOMO of $[\mathbf{36}]^{2+}$ based on DFT B3-LYP calculations*

Since oxidation of $[\mathbf{4}]^+$ to $[\mathbf{36}]^{2+}$ removes one electron from this orbital, Ir$\rightarrow$ ethene π-backbonding decreases and the Ir1-N3/Ir1-N4 σ-interaction increases on going from $[\mathbf{4}]^+$ to $[\mathbf{36}]^{2+}$. Actually, we observe that only the Ir1-C1 distance increases and only the Ir1-N3 distance decreases**.** This is probably because Ir1-C2 in $[\mathbf{4}]^+$ is already long as a result of steric hindrance by the axial Py-*Me* substituents, whereas Ir1-N4 in $[\mathbf{4}]^+$ is already short as a result of geometrical constraints by the κ^4-Me_3-tpa ligand. The C-C double bond of the olefin is shortened due to a decreased π-backdonation.

In the $[(por)M^{II}(ethene)]^+$ complexes reported [1], [2], [5] the unpaired electron has a relatively high density on the ethene moiety, inducing some metal(III)-ethyl-radical character on these transient species. In contrast, in $[\mathbf{36}]^{2+}$ the spin density is mainly located on the iridium center, only a small part is located on the olefin moiety and the N_4 ligand.

5.2.3 EPR spectra of the iridium(II) ethene complexes

Solutions of $[\mathbf{36}]^{2+}$ and $[\mathbf{37}]^{2+}$ in acetone/MeOH (2:3) were cooled down to 10 K and subsequently X-band EPR spectra were measured (Figure 5.5 on the next page).

As can be seen from Figure 5.5, the EPR spectrum of Me_2-tpa complex $[\mathbf{37}]^{2+}$ is virtually identical to that of the Me_3-tpa complex.

The (super)hyperfine coupling pattern for the g_{33} signals could be satisfactorily simulated by assuming hyperfine coupling with iridium and superhyperfine coupling with one nitrogen. Contributions from other N-nuclei are not resolved in this direction. The g_{22} signal reveals no resolved hyperfine-coupling in either case. At first the nature of the observed 5-line pattern of the g_{11} signals was not understood. However, as a result from a combination of DFT calculations and more elaborate simulations, It was recently [15] shown that this signal actually results from quadrupole distortion of iridium hyperfine coupling patterns. The exact nature of this thesis is beyond the scope of this thesis.

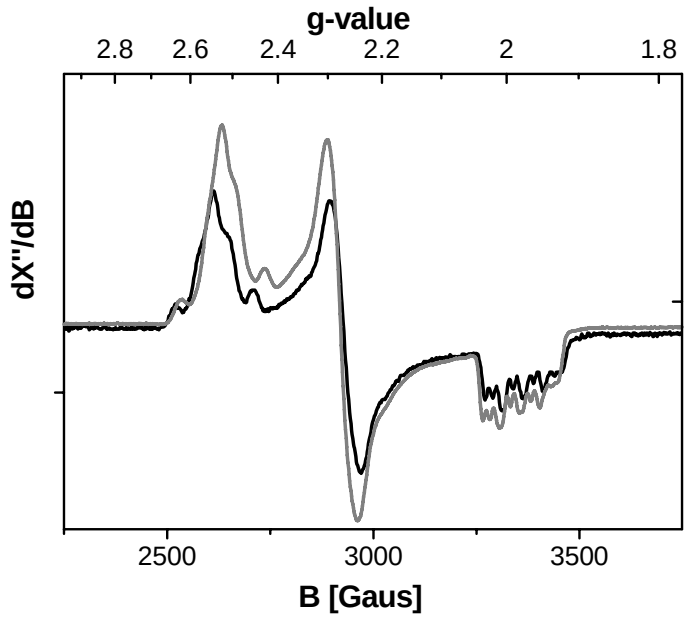

Figure 5.5 *X-band EPR spectrum of [**36**]$^{2+}$ (black) and [**37**]$^{2+}$ (grey)*

5.3 Formation of ethylene-bridged dinuclear complexes: M-C coupling of iridium(II) and iridium(II)-ethene species

Since not only [(por)M^{II}(ethene)] (M= Rh [1], [2], Ir [5]) have been reported to undergo bimolecular M-C and C-C coupling reactions, but also other metal(II) complexes, [3], [7] – [11] it was at first thought quite remarkable, that iridium(II) complexes [**36**]$^{2+}$ and [**37**]$^{2+}$ did *not* spontaneously dimerize. However, as will be shown, whether radical coupling takes place or not depends strongly on the solvent.

It is clear from the electrochemical data presented in Table 5.1 of § 5.2 that [**37**]$^{2+}$ has a reduced stability in acetonitrile compared to the less coordinating solvents acetone and CH_2Cl_2. [**36**]$^{2+}$ can be reversibly oxidized in all solvents tested (scan rate 100 mV/second).
However, it will be shown in this paragraph that both iridium(II) ethene complexes display a reduced stability in acetonitrile at r.t..

5.3.1 Reaction in acetonitrile

In acetonitrile Me_3-tpa complex [**36**]$^{2+}$ is moderately stable, and slowly and selectively converts to diamagnetic product [**38**]$^{4+}$ (Figure 5.6). Full conversion of [**36**]$^{2+}$ to [**38**]$^{4+}$ requires approx. 90 min.
Me_2-tpa complex [**37**]$^{2+}$, is much more reactive in acetonitrile and instantaneously and selectively converts to [**39**]$^{4+}$. Due to the chirality of [**37**]$^{2+}$, dinuclear complex [**39**]$^{4+}$ is formed as a mixture of the two diastereomers [**39a**]$^{4+}$ (rac, C_2-symmetric) and [**39b**]$^{4+}$ (meso, C_i-symmetric). The diastereomers are formed in approximately 1:1 ratio. ^{1}H-NMR signals of [**39a**]$^{4+}$ partially overlap with those of [**39b**]$^{4+}$, but separated signals for Py-*H6*, Py-*Me*, Ir-NC*CH$_3$* and Ir-*CH$_2$CH$_2$*-Ir fragments clearly reveal the presence of [**39a**]$^{4+}$ in equimolar amounts to [**39b**]$^{4+}$. Isomer [**39b**]$^{4+}$ preferentially crystallized from a mixture of acetonitrile and methanol.

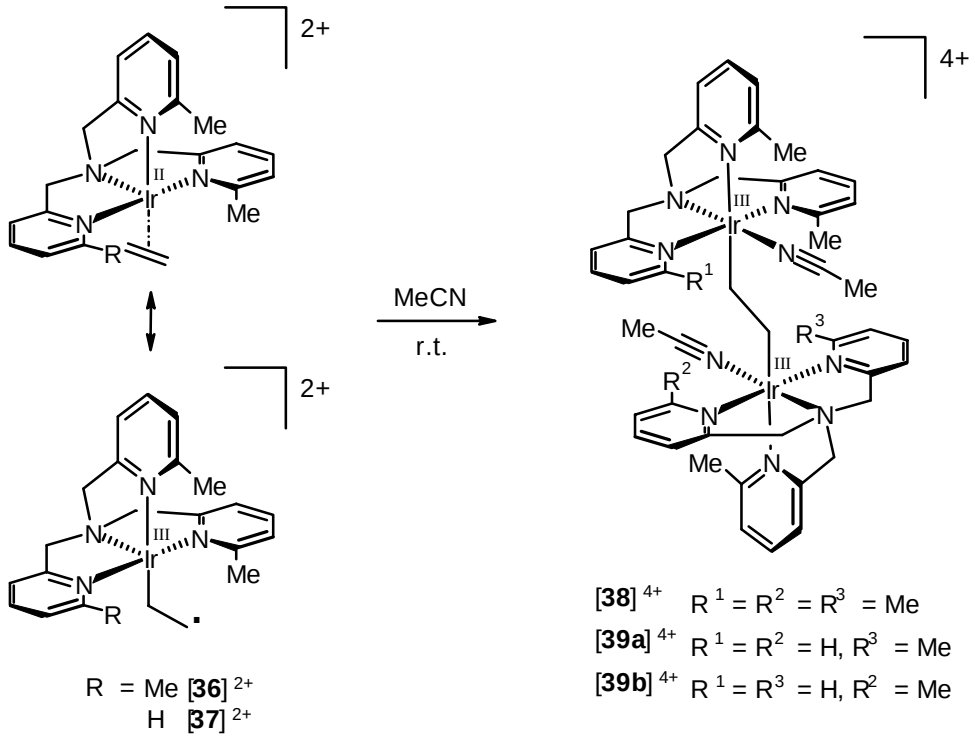

Figure 5.6 *Formation of ethylene bridged dinuclear species from $[\mathbf{36}]^{2+}$ and $[\mathbf{37}]^{2+}$ in MeCN*

Thus, whereas $[\mathbf{36}]^{2+}$ and $[\mathbf{37}]^{2+}$ are relatively stable in weakly coordinating solvents like acetone and CH_2Cl_2, the stronger donor acetonitrile apparently triggers ethene dissociation and M-C coupling of an iridium(II) and an iridium(II)-ethene species. This reaction is more general: in benzonitrile a similar reaction takes place. The observation that the reaction rate increases on going from Me_3-tpa complex $[\mathbf{36}]^{2+}$ to the more accessible Me_2-tpa complex $[\mathbf{37}]^{2+}$ suggest that the reaction proceeds via an associative mechanism.

In view of the radical type mechanisms proposed for the formation of ethylene and butylene bridged dinuclear species from $[(por)M^{II}]$ and ethene, [21] it is tempting to propose a similar radical pathway for formation of $[\mathbf{38}]^{4+}$ and $[\mathbf{39a}]^{4+}/[\mathbf{39b}]^{4+}$ (see Figure 5.7 on the next page): Rate-limiting substitution of ethene by acetonitrile via an associative (A) or associative interchange (I_a) mechanism could be followed by a radical coupling of iridium(II) and iridium(II)-ethene species. The associative substitution at these Me_n-tpa-iridium(II) centers apparently requires 'hard' donors (e.g. acetonitrile), since $[\mathbf{36}]^{2+}$ and $[\mathbf{37}]^{2+}$ do not seem to have any affinity for CO (see § 5.2).

Clearly the iridium(III)-ethyl-radical character of $[\mathbf{36}]^{2+}$ and $[\mathbf{37}]^{2+}$ is insufficient to induce a C-C radical coupling to butylene bridged dinuclear species, but M-C radical coupling with *in situ* generated (more reactive) metal centered radicals $[(Me_n\text{-tpa})\text{-}Ir^{II}(NCMe)]^{2+}$ could well be a route to the ethylene bridged species $[\mathbf{38}]^{4+}$ and $[\mathbf{39a}]^{4+}/[\mathbf{39b}]^{4+}$ as depicted in Figure 5.7.

Some calculations reported recently [15] show that the spin density on the ethene moiety, and thus the ethyl-radical character, increases on coordination of MeCN.

In the absence of further evidence, we cannot exclude alternative mechanisms. For example, electron-transfer (induced by coordination of acetonitrile) might generate intermediate iridium(I) and iridium(III) species which couple via electrophilic attack of iridium(III) at iridium(I)-ethene or nucleophilic attack of iridium(I) at iridium(III)-ethene, thus forming $[\mathbf{38}]^{4+}$and $[\mathbf{39a}]^{4+}/[\mathbf{39b}]^{4+}$. However, in the remainder of this chapter we will *assume* the path illustrated in Figure 5.7.

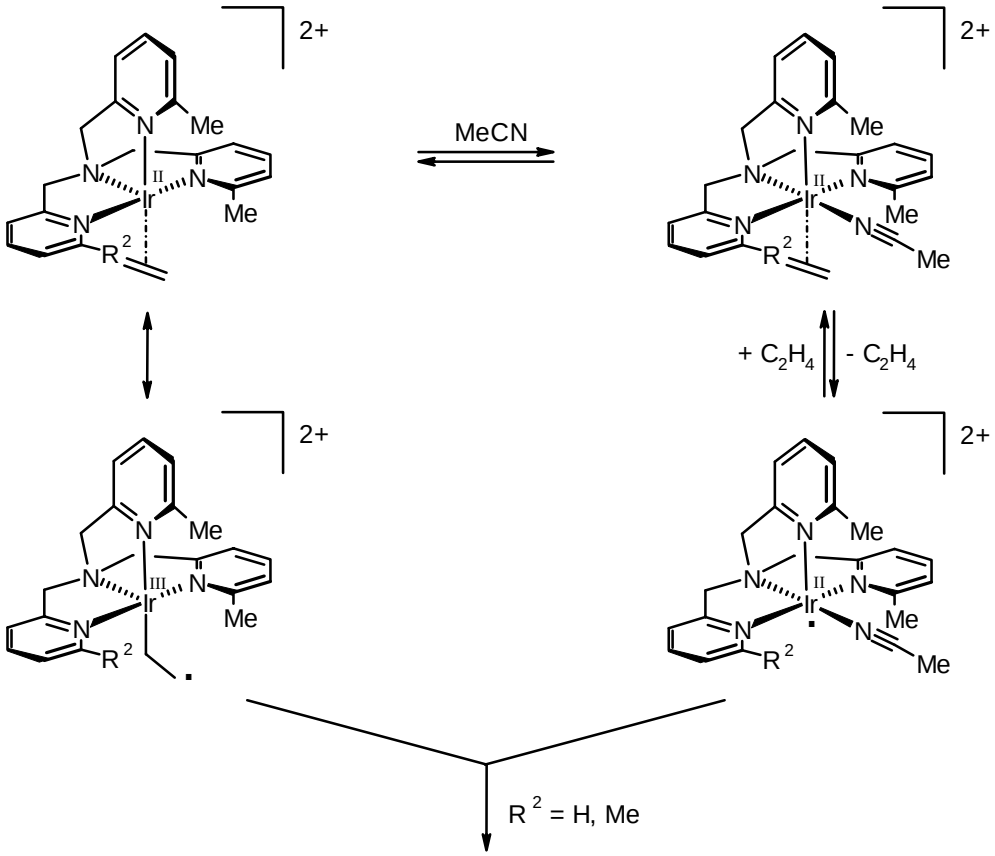

Figure 5.7 *Proposed mechanism for formation of [**38**]$^{4+}$ and [**39a**]$^{4+}$/[**39b**]$^{4+}$*

The irreversible oxidation of [(tpa)Ir^{I}(ethene)]$^{+}$ and [(Me-tpa)Ir^{I}(ethene)]$^{+}$ in acetonitrile, as observed with cyclic voltammetry (see Table 5.1, § 5.2), is probably also related to a rapid M-C coupling reaction (probably even faster than for [**37**]$^{2+}$) similar to the one described above.

We attempted to generate the corresponding iridium(II) complexes *in situ* with [Fc]PF_6 in acetonitirile. Small amounts of ethylene bridged dinuclear species are formed. However, these reactions are very fast and non-selective.

When comparing the chemistry of [(por)M^{II}] (M=Rh, Ir) and the Me$_n$-tpa-iridium(II) complexes discussed in this chapter, it becomes clear that in both systems steric shielding is the key to controlling stability and reactivity. On increase of the steric bulk around the metal center of the por^{2-} complexes, the reactivity changes from the formation of metal-metal bonds [1], [22], [23] via ethylene bridged species [2], [12], [24] to even butylene bridged species. [1], [2], [24]

For the Me$_n$-tpa complexes, on the other hand, increase of the steric bulk does not result in spontaneous dimerization via a C-C coupling reaction, but in a higher stability of the corresponding iridium(II)-olefin complexes.

Although from DFT calculations it is clear that our iridium(II) ethene complexes do have some ethyl-radical character, this is apparently not strong enough to form a butylene bridged complex. However, they do react with an *in situ* generated (more reactive) metal radical species [(Me$_n$-tpa)Ir^{II}(MeCN)]$^{2+}$.

Me$_n$-tpa iridium(II) ethene complexes also have a higher affinity for σ-donor ligands (like acetonitrile), whereas the por^{2-} complexes seem to prefer π-acceptor ligands (like CO). [12] This difference might be due to the stronger σ-donor character of the anionic por^{2-} ligands compared to the neutral Me$_n$-tpa ligands.

Finally, the coordination geometries of the two systems are completely different. In contrast to Me_n-tpa, the por^{2-} ligands maintain *trans*-vacant sites and thus do not allow *cis*-reactivity patterns of substrate fragments. This will probably result in marked differences in reactivity between the radical species $[(Me_n\text{-tpa})M^{II}]^{2+}$ and $[(por)M^{II}]$.

X-ray structures of $[38]^{4+}$ and $[39b]^{4+}$

Crystals of $[\mathbf{38}]^{4+}$ and $[\mathbf{39b}]^{4+}$ suitable for X-ray diffraction were obtained from DMSO/MeOH. The structures obtained are shown in Figure 5.8 and Figure 5.9 on the next page.

Although [(por)M-CH_2CH_2-M(por)] (M=Rh, Ir) species have been reported for a variety of por^{2-} ligands, they have not been structurally characterized.

The structures of $[\mathbf{38}]^{4+}$ and $[\mathbf{39b}]^{4+}$ are very similar. Both dinuclear complexes have a slightly distorted octahedral geometry around each metal center. Complex $[\mathbf{39b}]^{4+}$ has an inversion center. The Me_3-tpa complex does not have any crystallographically imposed symmetry. A few carbon atoms of one of the pyridine rings of Me_3-tpa complex $[\mathbf{38}]^{4+}$ showed large disorder and were split into two partially occupied parts. Further more, some of the atoms of the PF_6 and DMSO moieties of $[\mathbf{39b}]^{4+}$ show a large positional disorder.

The Me_2-tpa ligand seems to be somewhat stronger coordinated to the metal center (shorter Ir-N bonds) than Me_3-tpa. This phenomenon was already observed for the corresponding iridium(I) complexes (§ 5.2). Probably as a result MeCN and the ethylene bridge are somewhat more weakly bound. With regard to the remaining structural features the structures of $[\mathbf{38}]^{4+}$ and $[\mathbf{39b}]^{4+}$ are practically identical.

The C-C bond of the olefin moiety has clearly elongated on going from the iridium(II) ethene complex (1.38 Å for $[\mathbf{36}]^{2+}$) to the corresponding ethylene bridged dinuclear complex (1.50 Å for $[\mathbf{38}]^{4+}$ and $[\mathbf{39a}]^{4+}$/$[\mathbf{39b}]^{4+}$) reflecting the change from a C=C to a C-C bond.

Table 5.3 *Selected bond lengths [Å] and angles [°] of $[\mathbf{38}]^{4+}$ and $[\mathbf{39b}]^{4+}$* [3]

	$[\mathbf{38}]^{4+}$	$[\mathbf{39b}]^{4+}$
Ir1-N1	2.093(4)	2.041(5)
Ir1-N2	2.103(5)	2.073(5)
Ir1-N3	2.270(4)	2.257(5)
Ir1-N4	2.041(4)	2.034(5)
Ir1-N9 or Ir1-N5	2.007(4)	2.020(5)
Ir1-C1	2.105(5)	2.116(5)
C1-C4 or C1-C1a	1.501(7)	1.510(11)
N5-C2	1.138(7)	1.135(7)
C2-C3	1.445(8)	1.446(8)
Ir1-C1-C4 or Ir1-C1-C1a	117.7(4)	118.0(5)
N9-Ir1-N3 or N5-Ir1-N3	100.90(18)	102.42(19)
C1-Ir1-N9 or C1-Ir1-N5	85.8(2)	83.0(2)

[3] Since $[\mathbf{39b}]^{4+}$ has an inversion center and $[\mathbf{38}]^{4+}$ has not, the atom numbering is different in both complexes. Therefore we chose to display the atom numbering of $[\mathbf{39b}]^{4+}$ in Table 5.2 and relate them to the corresponding bond lengths in $[\mathbf{38}]^{4+}$.

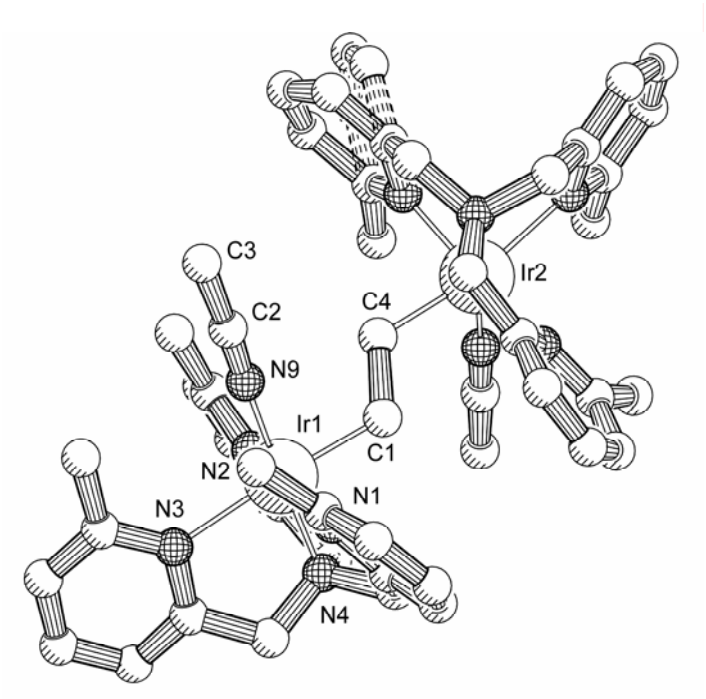

Figure 5.8 *X-ray structure of $[(Me_3\text{-tpa})(CH_3CN)Ir^{III}(\mu_2\text{-}\eta^1,\eta^1\text{-}C_2H_4)Ir^{III}(Me_3\text{-tpa})(CH_3CN)](PF_6)_4$ Hydrogen atoms and anions omitted for clarity*

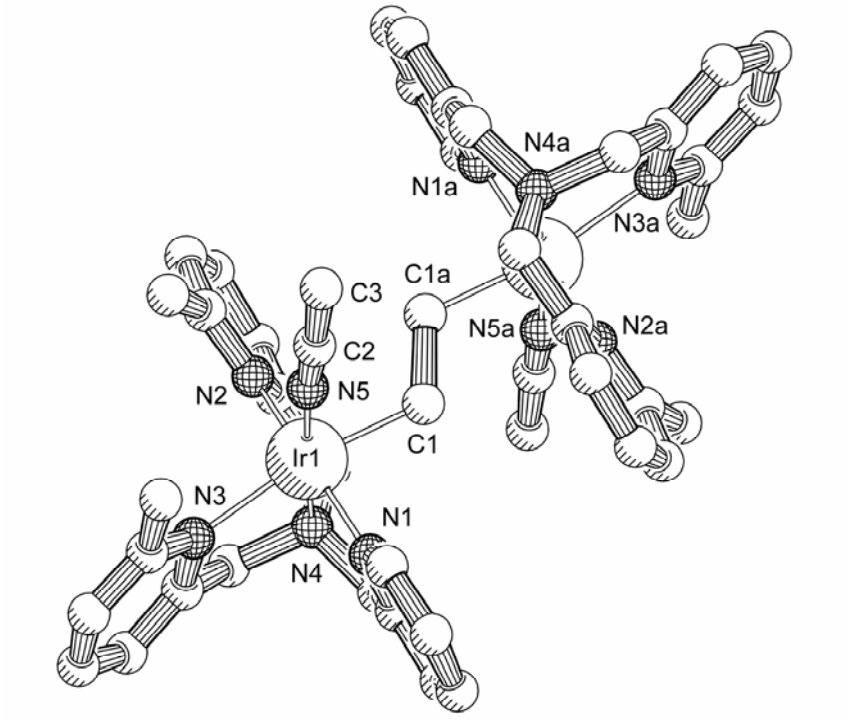

Figure 5.9 *X-ray structure of $[(Me_2\text{-tpa})(CH_3CN)Ir^{III}(\mu_2\text{-}\eta^1,\eta^1\text{-}C_2H_4)Ir^{III}(Me_2\text{-tpa})(CH_3CN)](PF_6)_4.2(CH_3)_2(SO)$ Hydrogen atoms, anions and solvent molecules omitted for clarity*

5.3.2 Reaction of [6]PF_6 with [Fc]BF_4 in CH_2Cl_2/MeOH

When the reaction of Me_2-tpa complex [**6**]$^+$ with [Fc]$^+$ is carried out in a mixture of CH_2Cl_2 and MeOH [4], again a mixture of two diastereomeric compounds is obtained. Now a 1:2 mixture is obtained of [**40a**]$^{2+}$ (rac, C_2-symmetric) and [**40b**]$^{2+}$ (meso, C_i-symmetric), of which [**40b**]$^{2+}$ preferentially crystallized from the reaction mixture (Figure 5.10).

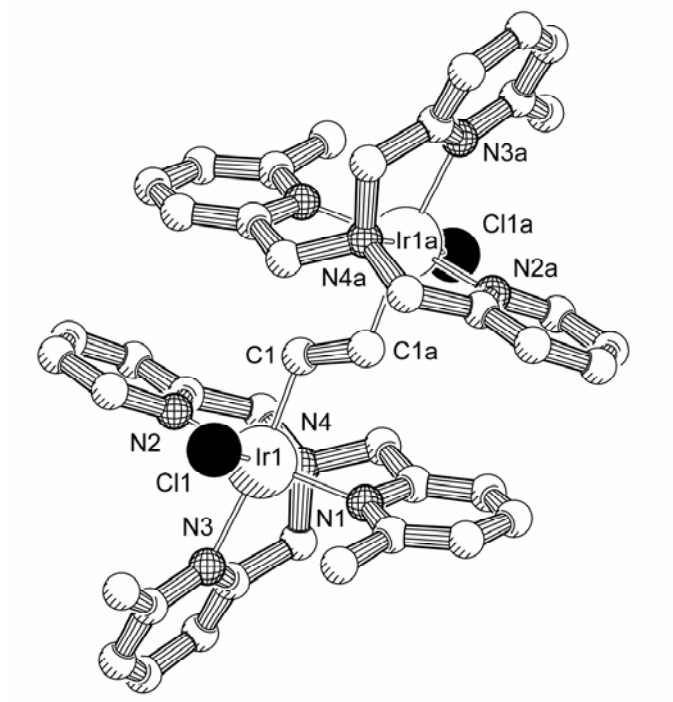

Figure 5.10 *X-ray structure of [$(Me_2$-tpa$)(Cl)Ir^{III}(\mu_2$-η^1,η^1-$C_2H_4)Ir^{III}(Me_2$-tpa$)(Cl)](PF_6)_2$ Per unit cell: ½{[**40b**]$(PF_6)_2$}. All hydrogen atoms and anions are omitted for clarity.*

Table 5.4 *Selected bond lengths and angles of [**40**]$^{2+}$*

Bond length [Å]		Angle [°]	
Ir1-N1	2.087(3)	Ir1-C1-C1a	117.7(4)
Ir1-N2	2.040(3)	C1-Ir1-Cl1	82.70(13)
Ir1-N3	2.281(3)	Cl1-Ir1-N3	102.99(9)
Ir1-N4	2.043(3)		
Ir1-C1	2.102(4)		
C1-C1a	1.518(8)		
Ir1-Cl1	2.3787(11)		

The structure of [**40b**]$^{2+}$ is similar to those of [**38**]$^{4+}$ and [**39b**]$^{4+}$ but contains chloro ligands instead of MeCN. Also this dinuclear complex has a slightly distorted octahedral geometry around each metal center and an inversion center.

Apparently the dinuclear Me_2-tpa complex does not seem to undergo significant sterical or electronic changes when the neutral MeCN ligand is replaced by a mono-anionic chloride ligand: The Ir-N_{PyMe} distances increase only slightly, probably due to the fact that a chlorine atom occupies more space than a MeCN-nitrogen.

[4] [Fc]BF_4 instead of [Fc]PF_6 is used in this case to circumvent solubility problems.

It is clear that the chloride in [**40**]$^{+}$ derives from the solvent, but apart from that we do not know how the product is formed. Hetterscheid [15] found that treatment of [**37**]$^{2+}$ with chloride yields traces of [**40**]$^{2+}$ (~ 5% according to ^{1}H NMR), in this case as a 1:1 mixture of the two diastereomers [**40a**]$^{2+}$ and [**40b**]$^{2+}$.

5.4 Reaction of [36]$^{2+}$ towards oxidizing agents

As will be shown below, the radical character of the iridium(II) ethene complexes is also reflected in their reactivity towards molecular oxygen.

5.4.1 Reactivity of [36]$^{2+}$ towards dioxygen

In the solid state [**36**]$^{2+}$ is air stable. Upon exposure of a solution of [**36**]$^{2+}$ in acetonitrile, benzonitrile, acetone or acetone/MeOH (2:3) to air or O_2 at -10 ºC, the color of the solution changes from brown to purple. Upon warming up these solutions to ambient temperature, the purple color vanishes, the solutions become colorless, and ^{1}H-NMR reveals formation of *diamagnetic* products.

In acetonitrile the main product (~ 70% based on ^{1}H-NMR) was identified as formylmethyl complex [**41**]$^{2+}$ (Figure 5.11). [5]When the reaction with dioxygen is performed in acetone, several different species are formed. Supporting ESI^{+}-MS studies indicate the formation of several species containing one or two oxygen atoms. Iridium(II)-ethene complex [**36**]$^{2+}$ thus seems capable of O_2 activation and C-O bond formation. In marked contrast, oxidation of iridium(I)-ethene complex [**4**]$^{+}$ with O_2 in solution did *not* result in C-O bond formation, but yielded the peroxo-ethene complex [(κ^3-Me$_3$-tpa)Ir^{III}(O_2)(C_2H_4)]$^{+}$ in 25 % isolable yield (§ 4.2.1).

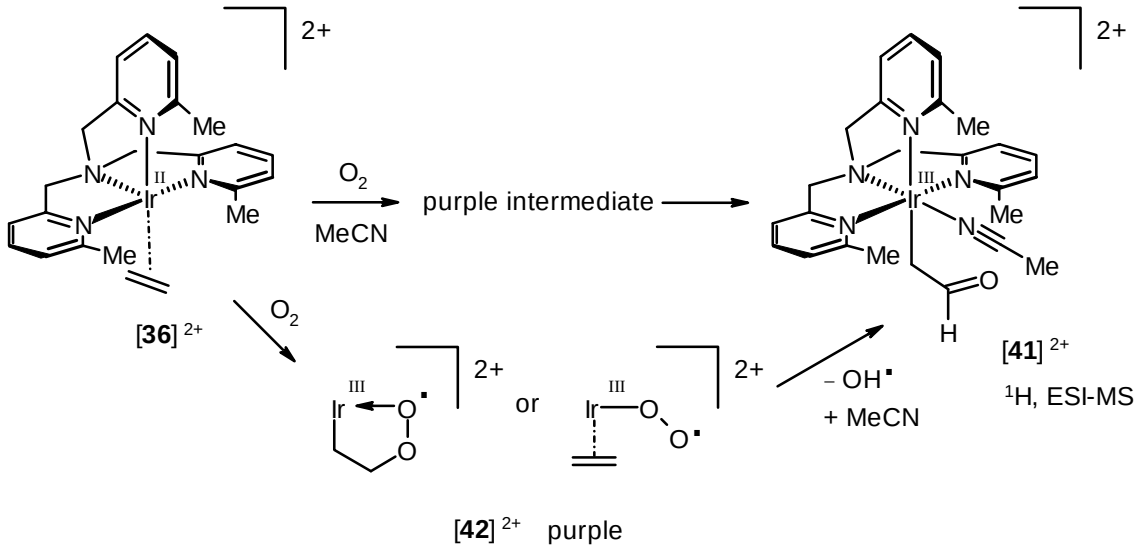

Figure 5.11 *Product and proposed intermediates of the reaction of [**36**]$^{2+}$ with O_2 in MeCN and acetone*

The initial color change from brown to purple in the conversion of [**36**]$^{2+}$ to [**41**]$^{2+}$ at -10 ºC indicates the formation of an intermediate ([**42**]$^{2+}$). The EPR spectrum of [**42**]$^{2+}$ is shown in Figure 5.12.

[5] Other formylmethyl M(III) species (M= Rh, Ir) have been reported previously.[25] – [27]

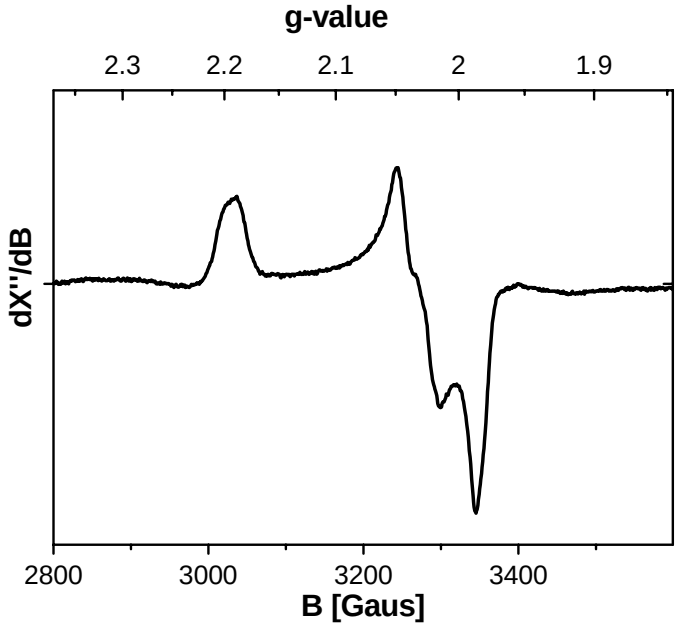

Figure 5.12 *X-band EPR spectrum of intermediate [**42**]$^{2+}$*

Simulation of the rhombic spectrum yields g_{11}= 1.987, g_{22}= 2.030 and g_{33}= 2.191. The line shape for g_{22} suggests a small iridium hyperfine coupling. Thus, on going from [**36**]$^{2+}$ to [**42**]$^{2+}$ a marked decrease in anisotropy of the EPR signal is observed (compare the EPR spectrum of [**36**]$^{2+}$in Figure 5.5 with that of [**42**]$^{2+}$ in Figure 5.12). This might indicate a shift in spin-density from the metal center to a coordinated superoxy or superoxy-ethyl radical as proposed in Figure 5.11.

The radical character of iridium(II)-olefin (or iridium(III)-ethyl radical) complex [**36**]$^{2+}$ could well be responsible for the facile C-O bond formation upon contact with O_2 (Figure 5.13).

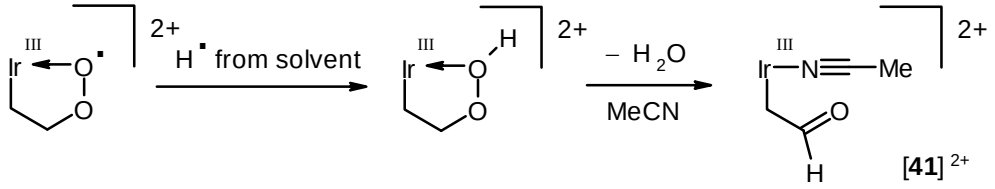

Figure 5.13 *Proposed mechanism for the formation of [**41**]$^{2+}$*

The hydroxy radical that is released, could react further with another iridium(II) ethene complex.

In acetone, the solvent in which the EPR spectrum in Figure 5.5 was taken, an aselective reaction takes places resulting a mixture of unidentifiable products. No conclusions can be drawn whether in this reaction C-O bonds have been formed or not.

5.4.2 Reaction of [36]$^{2+}$ with superoxide (O_2^-)

One possible mechanism for the reaction of solid tpa metal(I) ethene complexes with dioxygen starts with SET followed by reaction of the resulting metal(II) complex with the superoxide anion (O_2^-) to give metal(III) dioxolane complexes. [28]
We already showed that iridium(II) ethene complex [**36**]$^{2+}$ can undergo C-O bond formation in a reaction with dioxygen. Now we are interested whether C-O bond formation can also take place upon reaction with the superoxide anion.

Therefore, [**36**]$^{2+}$ was stirred with a suspension of solid KO_2 in acetonitrile. The solubility of KO_2 is small in this solvent but proved to be sufficient to allow reaction with [**36**]$^{2+}$. ^{1}H-NMR showed that [**36**]$^{2+}$ had been *reduced* rather than oxidized by superoxide. The reaction was also performed as solid phase metathesis as described by Sawyer *et al.* [29] in the synthesis of a soluble superoxide. After 48 hours the products were extracted with dichloromethane under a nitrogen atmosphere. Again ^{1}H-NMR clearly gave a clear spectrum of the iridium(I) ethene complex.

A possible explanation can be derived by looking at the 1-electron oxidation reaction:

$$O_2 + [(Me_3\text{-tpa})Ir^{I}(C_2H_4)]^{+} \rightarrow O_2^{-} + [(Me_3\text{-tpa})Ir^{II}(C_2H_4)]^{2+}$$

The equilibrium constant calculated for this reaction from redox potentials is $K_{eq} \cong 4.2 \times 10^{-15}$, so the reduction of the iridium(II) complex by O_2^- can hardly be considered surprising.

Therefore, it seems unlikely that dioxolanes can be a result from a reaction of a metal(II) complex with the superoxide anion.

5.5 Conclusions

Unique N_4 iridium(II)-ethene complexes have been synthesized through one-electron oxidation of the corresponding iridium(I)-ethene complexes.

From the reactivities described in this chapter it is clear that steric shielding is the key to control their stability and reactivity: an increase in the accessibility of the vacant 6th coordination site at iridium (e.g. on going from Me_3-tpa to the less hindered analogue Me_2-tpa) results in a higher reactivity of the corresponding iridium(II)-olefin complexes, and even more open analogues could not be prepared at all.

The metal(III)-ethyl-radical character of the iridium(II)-olefin complexes is probably responsible for the formation of the ethylene-bridged species as well as for the facile C-O bond formation upon contact with O_2. The observed reactivity towards O_2 points to a possible role of metal(II)-olefin species in rhodium and iridium catalyzed oxidation of olefins by O_2. Such insight is of importance for the development of catalytic olefin oxygenation by group VIII metal centers.

5.6 Experimental section

5.6.1 General methods

All procedures were performed under a nitrogen atmosphere using standard Schlenck techniques, unless indicated otherwise. Solvents (p.a.) were deoxygenated by bubbling through a stream of nitrogen or by the freeze-pump-thaw method. The temperature indication r.t. corresponds to ca. 20 ºC.

NMR experiments were carried out on a Bruker DPX200 (200 MHz and 50 MHz for ^{1}H and ^{13}C respectively), a Bruker AC300 (300 MHz and 75 MHz for ^{1}H and ^{13}C respectively), a Varian Inova 400 (400 MHz and 100 MHz for ^{1}H and ^{13}C respectively). Solvent shift references for ^{1}H-NMR are: CD_2Cl_2 δ (^{1}H) = 5.31 ppm, CD_3CN δ (^{1}H) = 1.94 ppm, methanol-d4 δ (^{1}H) = 3.35 ppm and acetone-d6 δ (^{1}H) = 2.05 ppm. Solvent shift references for ^{13}C-NMR are: CD_3CN δ (^{13}C) = 1.24 (and 118.25), CD_2Cl_2 δ (^{13}C) = 54.20, methanol-d4 δ (^{13}C) = 49.3 ppm and acetone-d6 δ (^{13}C) = 29.83 ppm (and 206.18 ppm). Abbreviations used are: s = singlet, d = doublet, dd = double doublet, ddd = double doublet of doublets, t = triplet, dt = double triplet, q = quartet, qq = quartet of quartets, m = multiplet, dm = double multiplet, br. = broad.

Elemental analysis (C,H,N) were carried out on a Carlo Erba NCSO-analyser.

Mass spectra (ESI- or FAB-MS) were recorded on a Finnigan MAT 900S (Radboud University Nijmegen), a Finnigan TSQ 700 (ETH-Zurich) or a Finnigan TSQ 7000 (ETH-Zurich). All spectra were obtained in the positive ion mode. Daughter ion spectra were measured on the TSQ 700 and TSQ 7000 using argon as a collision gas.

Cyclic voltammetry measurements were performed using an Eco Chemie Autolab PGSTAT20. A conventional three-electrode cell, with Pt working and auxiliary electrodes and 0.1 M $[(n\text{-}Bu)_4N]PF_6$ (TBAH) electrolyte was used. An Ag/AgI reference electrode (grain of AgI, 0.02 M $[(n\text{-}Bu)_4N]I$ (TBAI) and 0.1 M TBAH) was employed. [6]

Experimental X-band EPR spectra were recorded on a Bruker ER220 spectrometer. The spectra were simulated by iteration of the anistropic g values, (super)hyperfine coupling constants, and line widths.

Bpa-Me [25], bpa-Bz [18], tpa [30], Me-tpa [31], Me_3-tpa [31], $[(bpa\text{-}Me)Rh(C_2H_4)]PF_6$ [25], $[(bpa\text{-}Bz)Rh(C_2H_4)]PF_6$ [25], $[(tpa)Rh(C_2H_4)]PF_6$ [32], $[(Me\text{-}tpa)Rh(C_2H_4)]PF_6$ [32], $[(tpa)Ir(C_2H_4)]PF_6$ [28], $[(Me\text{-}tpa)Ir(C_2H_4)]PF_6$ [28], $[\{(C_2H_4)_2Rh(\mu\text{-}Cl)\}_2]$ [33] and $[\{(coe)_2Ir(\mu\text{-}Cl)\}_2]$ [34] were prepared according to literature procedures.

All other chemicals are commercially available and were used without further purification, unless stated otherwise.

5.6.2 X-ray diffraction

*$[(Me_3\text{-}tpa)Ir^{II}(C_2H_4)](PF_6)_2$ ([**36**]PF_6)*

Dark brown crystals suitable for X-ray diffraction were obtained from an acetone solution top-layered with hexane at 4 ºC.

A single crystal was sealed in a glass-capillary under N_2. Intensity data were collected on an Enraf-Nonius CAD4 diffractometer, using graphite monochromatized MoK_α radiation (λ = 0.71073 Å). Data were collected at 293 K ($\omega/2\theta$-scan mode). Unit cell dimensions were determined from the angular setting of 25 reflections. The structure was solved by the program system DIRDIF [35] using the program PATTY [36] to locate the heavy atoms and were refined with standard methods (refinement against F^2 of reflections with $I_o > 2\sigma(I_o)$ using SHELXL-97 [37] with anisotropic parameters for the nonhydrogen atoms. The hydrogen atoms were initially placed at calculated positions, refined isotropically in riding mode, and were subsequently refined without constraints.

From the anisotropic thermal displacement parameters for the PF_6 moieties of [**36**]$(PF_6)_2$, it is clear that some atoms show a large positional disorder. Although it is possible to use several partially occupied positions for these atoms, no physically reasonable models result from these parameters, at least not any better than the models presented here.

Geometrical calculations (PLATON [38]) revealed neither unusual geometric features, nor unusual short intermolecular contacts. The calculations revealed no higher symmetry and no (further) solvent accessible areas.

*$[(Me_3\text{-}tpa)(CH_3CN)Ir^{III}(\mu\text{-}\eta^2\text{-}C_2H_4)Ir^{III}(Me_3\text{-}tpa)(CH_3CN)](PF_6)_2$ ([**38**]$(PF_6)_4$) and*
*$[(Me_2\text{-}tpa)(CH_3CN)Ir^{III}(\mu_2\text{-}\eta^1,\eta^1\text{-}C_2H_4)Ir^{III}(Me_2\text{-}tpa)(CH_3CN)](PF_6)_2$ ([**39b**]$(PF_6)_4$)*

Colorless crystals suitable for X-ray diffraction were obtained from DMSO/MeOH.

Single crystals were sealed in a glass-capillary under N_2. Intensity data were collected on an Enraf-Nonius CAD4 diffractometer using graphite monochromatized MoK_α radiation (λ = 0.71073 Å). Data were collected at 293 K (ω/2θ-scan mode). Unit cell dimensions were determined from the angular setting of 25 reflections. The structure was solved by the program system DIRDIF [35] using the program PATTY [36] to locate the heavy atoms and were refined with standard methods (refinement against F^2 of reflections with $I_o > 2\sigma(I_o)$ using SHELXL-97 [37] with anisotropic parameters for the nonhydrogen atoms. The hydrogen atoms were placed at calculated positions, and refined isotropically in riding mode.

Geometrical calculations (PLATON [38]) revealed neither unusual geometric features, nor unusual short intermolecular contacts. The calculations revealed no higher symmetry and no (further) solvent accessible areas.

In the case of [**38**]$(PF_6)_4$ a few atoms of one pyridyl fragment of one ligand, C53, C54 and C55, showed large disorder and were split into two partially occupied parts. Even then one of the two parts still shows large disorder, but further splitting does not improve the physical model. The same holds for some of the anion fluorine atoms for which no other models could be found that would result in a stable refinement.

For [**39b**]$(PF_6)_4$ it is clear from the anisotropic thermal displacement parameters for the PF_6 and DMSO moieties that some atoms show a large positional disorder. Although it is possible to use several partially occupied positions for these atoms, no physically reasonable models result from these parameters, at least not any better than the models presented here. The

[6] Electron withdrawing ligands coordinated to the metal center cause a shift in anionic direction: the CV potential goes to a less negative or a more positive value with respect to Fc/Fc^+. In other words, the metal can attract more easily electrons.

assignment of atomic species in the DMSO moiety is based on bond distances and equivalent isotropic thermal displacement parameters.

*[(Me_2-tpa)(Cl)Ir^{III}(μ^2-η^1,η^1-C_2H_4)Ir^{III}(Me_2-tpa)(Cl)](PF_6)$_2$ ([**40**](PF_6)$_4$)*

Light yellow crystals suitable for X-ray diffraction were obtained from CH_2Cl_2/MeOH.

A single crystal was sealed in a glass-capillary under N_2. Intensity data were collected on an Enraf-Nonius CAD4 diffractometer, using graphite monochromatized MoK_α radiation (λ = 0.71073 Å). Data were collected at 150 K (area detector, φ and ω scan mode). Unit cell dimensions were determined from the angular setting of 41246 reflections.

The structure was solved by the program system DIRDIF [35] using the program PATTY [36] to locate the heavy atoms and were refined with standard methods (refinement against F^2 of reflections with $I_o > 2\sigma(I_o)$ using SHELXL-97 [37] with anisotropic parameters for the nonhydrogen atoms. The hydrogen atoms were placed at calculated positions, and refined isotropically in riding mode.

The hydrogen atoms attached to C1 were found from a difference fourier map.

Geometrical calculations (PLATON [38]) revealed neither unusual geometric features, nor unusual short intermolecular contacts. The calculations revealed no higher symmetry and no (further) solvent accessible areas.

Selected bond lengths and angles are summarized in Table 5.2 - 5.4. Drawings were generated with the program PLATON. [38] Other relevant crystal data are summarized in Table 5.5.

Table 5.5 *Crystallographic data for [**36**](PF_6)$_2$, [**38**](PF_6)$_4$, [**39b**](PF_6)$_4$ and [**40**](PF_6)$_2$*

	[**36**](PF_6)$_2$	[**38**](PF_6)$_4$.CH_3CN	[**39b**](PF_6)$_4$.2($_{CH3}$)$_2$SO	[**40**](PF_6)$_2$
Empirical formula	$C_{23}H_{28}F_{12}IrN_4P_2$	$C_{50}H_{61}F_{24}Ir_2N_{11}P_4$	$C_{25}H_{33}F_{12}IrN_5OP_2S$	$C_{21}H_{24}ClF_6IrN_4P$
Crystal size [mm]	0.40 x 0.18 x 0.18	0.42 x 0.26 x 0.18	0.50 x 0.18 x 0.11	0.18 x 0.14 x 0.12
Crystal color	Black	Transparent colorless	Transparent colorless	Transparent light yellow
Formula weight	842.63	1780.38	933.76	705.06
T [K]	293(2)	293(2)	293(2)	150(2)
Crystal system	Monoclinic	Triclinic	Triclinic	Monoclinic
Space group	P 2_1/a	P -1	P -1	P 2_1/n
a [Å]	13.072(2)	12.1371(10)	12.500(2)	10.5432(2)
b [Å]	12.454(2)	14.9716(12)	12.837(4)	16.3409(3)
c [Å]	18.860(3)	19.096(2)	13.093(5)	13.4964(3)
α [°]	90	73.115(8)	61.49(3)	90
β [°]	109.734(11)	80.005(8)	75.105(19)	94.8074(9)
γ [°]	90	73.965(8)	68.503(18)	90
V [$Å^3$]	2890.0(8)	3174.7(5)	1709.0(9)	2317.05(8)
$\rho_{calcd.}$ [gcm^{-3}]	1.937	1.862	1.815	2.021
Z	4	2	2	4
Diffractometer (scan)	Enraf-Nonius CAD4 (ω/2θ-scan)	Enraf-Nonius CAD4 (ω/2θ-scan)	Enraf-Nonius CAD4 (ω/2θ-scan)	Enraf-Nonius CAD4 (area detector, φ and ω scan)
Radiation	MoK_α (graphite mon.)	MoK_α (graphite mon.)	MoK_α (graphite mon.)	MoK_α (graphite mon.)
Wavelength [Å]	0.71073	0.71073	0.71073	0.71073
F(000)	1636	1736	914	1364
θ range [°]	2.82 to 27.42	2.70 to 27.49	2.93 to 27.47	1.96 to 27.40
Index ranges	-16<=h<=0 -16<=k<=0	-15<=h<=15 0<=k<=19	-16<=h<=0 -16<=k<=15	-13<=h<=13 -21<=k<=20

	[**36**]$(PF_6)_2$	[**38**]$(PF_6)_4.CH_3CN$	[**39b**]$(PF_6)_4.2(_{CH3})_2SO$	[**40**]$(PF_6)_2$
	-23<=l<=24	-23<=l<=24	-16<=l<=16	-17<=l<=17
Measured reflections	6860	15112	8189	41246
Unique reflections	6569	14554	7831	5253
Observed refl. [$I_o>2\sigma(I_o)$]	5292	11003	6621	3981
Refined parameters	382	857	430	315
Goodness-of-fit on F^2	1.051	1.065	1.093	1.023
R [$I_o > 2\sigma(I_o)$]	0.0393	0.0379	0.0408	0.0285
wR^2 [all data]	0.1011	0.0966	0.1101	0.0536
ρ_{fin} (max/min) [e. $Å^{-3}$]	1.589 and -2.017	1.162 and -0.809	1.159 and -0.914	1.832 and -1.015

5.6.3 Calculations

All calculated structures shown in this chapter and the orbital-pictures of the HOMO en SOMO as presented in § 5.2 were visualized using the Molden program. [39]

*DFT calculations on the HOMO of [**4**]$^{+}$ and the SOMO of [**36**]$^{2+}$*

Geometries were optimized at the B3LYP level [40] – [42] using the Gaussian98 suite of programs. [43] Basis sets used include the LANL2DZ basis and pseudo potential [44], [45] for the iridium center and STO3G [46] – [48] on all other atoms.

5.6.4 Synthesis

*[(Me$_3$-tpa)Ir^{II}(C$_2$H$_4$)]$^{2+}$ ([**36**](PF$_6$)$_2$)*

230 mg (0.33 mmol) of complex [**4**]PF_6 was added to a solution of 86 mg (0.26 mmol) [Fc]PF_6 in 12 ml CH_2Cl_2. The resulting green/brown mixture was stirred for 30 minutes at room temperature. The resulting brown precipitate was collected by filtration. Yield 186 mg (0.221 mmol, 85%) [**36**]$(PF_6)_2$ (analytically pure). Yield after crystallization: 72 mg (0.085 mmol, 33%).

^{1}H-NMR (200.13 MHz, acetone-d6, 298 K): δ (ppm) = 20.5 (br), 10.63 (br), 10.17 (br), 8.0-7.0 (pyridine region, many peaks), some signals between 3.5 and 1.0 , 0.2 (br). Since [**36**]$^{2+}$ is paramagnetic, it is difficult to interpret these signals.

ESI$^+$-MS: m/z = 276.5 [**36**]$^{2+}$, 698 {[**36**](PF_6)}$^+$.

Calculated for $C_{23}H_{28}N_4IrP_2F_{12}$: C 32.78, H 3.35, N 6.65; Found: C 32.64, H 3.33, N 6.67.

EPR (microwave frequency = 9.30195 GHz, microwave power = 1 mW, field modulation amplitude = 2 Gauss, temperature = 10 K, acetone/MeOH (2:3)): g_{11}= 2.54 (five-line pattern (1:4:6:4:1), A_{11}^{Ir} = 45 cm^{-1}, NQI_{11} = -10 cm^{-1}), g_{22}= 2.265 (no resolved hyperfine couplings, NQI_{22} = -16 cm^{-1}) and g_{33}= 1.9755 (A_{33}^{Ir} = 46x10^{-4} cm^{-1}, A_{33}^{N} = 17x10^{-4} cm^{-1}, NQI_{33} = 26 cm^{-1} (η = 0.23)).

X-Ray diffraction.

*[(Me$_2$-tpa)Ir^{II}(C$_2$H$_4$)]$^{2+}$ ([**37**](PF$_6$)$_2$)*

The synthesis of [**37**]$^{2+}$ follows the same procedure as for [**36**]$^{2+}$. Only now the reaction time is about 1.5 hour and a dark-brown colored powder is obtained.

ESI$^+$-MS: m/z = 269.5 [**37**]$^{2+}$

Due to the instability of [**37**]$(PF_6)_2$, reliable elemental analytical data were not obtained..

EPR (microwave frequency = 9.299 GHz, microwave power = 1 mW, field modulation amplitude = 2 Gauss, temperature = 40 K, acetone/MeOH (2:3)): The EPR spectrum of [**37**]$^{2+}$ is almost identical to that of [**36**]$^{2+}$, with slightly different g-values and hyperfine interactions: g_{11} = 2.52 (five-line pattern (1:4:6:4:1), A^{Ir}_{11}≈ 47x10^{-4} cm^{-1}, NQI_{11} = -10 cm^{-1}), g_{22}= 2.27 (no resolved hyperfine couplings, NQI_{22} = -16 cm^{-1}), g_{33}= 1.98 (A_{33}^{Ir}= 43x10^{-4} cm^{-1}, A_{33}^{N}= 18x$10^{-4}$$cm^{-1}$, NQI_{33} = 26 cm^{-1} (η = 0.23)).

*[(Me$_3$-tpa)(CH$_3$CN)Ir^{III}(μ_2-η^1,η^1-C$_2$H$_4$)Ir^{III}(Me$_3$-tpa)(CH$_3$CN)](PF$_6$)$_4$ ([**38**](PF$_6$)$_4$)*

[**36**](PF$_6$)$_2$ was dissolved in MeCN at r.t. and stirred for 90 minutes. Quantitative conversion to the corresponding yellow colored ethylene bridged dinuclear complex [**38**](PF$_6$)$_4$ takes place.

^{1}H-NMR (200.13 MHz, CD$_3$CN, 298 K): δ (ppm) = 7.9-7.1 (18H, Py-*H3*, Py-*H4* and Py-*H5*), 4.78 (4H, d[AB], J(H,H) = 16.4 Hz, N-C*H$_2$*-Py), 4.55 (4H, d[AB], J(H,H) = 16.4 Hz, N-C*H$_2$*-Py), 4.54 (4H, s, N-C*H$_2$*-Py), 3.02 (6H, s, Py-C*H$_3$*), 2.72 (s, 6H, IrNC-C*H$_3$*), 2.68 (12H, s, Py-C*H$_3$*), 2.17 (4H, s, Ir-C*H$_2$*-C*H$_2$*-Ir).

^{13}C{^{1}H}-NMR (50.32 MHz, CD$_3$CN, 298 K): δ (ppm) = 165.5, 163.8, 162.5, 157.5, 140.6, 140.1, 128.3, 127.5, 124.3, 122.0 and 120.4 (Py-*C2*, -*C3*, -*C4*, -*C5* and -*C6*), 74.4 and 70.7 (N-*C*H$_2$-Py), 27.1 and 26.7 (Py-*C*H$_3$), 5.03 (NC*C*H$_3$), 3.05 (Ir-*C*H$_2$-*C*H$_2$-Ir). The N*C*CH$_3$ signal was obscured by the solvent signal.

Calculated for C$_{48}$H$_{59}$N$_{11}$Ir$_2$P$_4$F$_{24}$: C 32.62, H 3.78 N 8.62; Found: C 33.54, H 3.47, N 8.68.

X-Ray diffraction.

*[(Me$_2$-tpa)(CH$_3$CN)Ir^{III}(μ_2-η^1,η^1-C$_2$H$_4$)Ir^{III}(Me$_2$-tpa)(CH$_3$CN)](PF$_6$)$_4$ ([**39**](PF$_6$)$_4$)*

[**37**](PF$_6$)$_2$ was dissolved in MeCN at r.t. Instantaneous quantitative conversion to the corresponding yellow colored ethylene bridged dinuclear complexes [**39a**](PF$_6$)$_4$/[**39b**](PF$_6$)$_4$ takes place. [**39b**](PF$_6$)$_4$ preferentially crystallizes from MeCN/MeOH. two diastereomers [**39a**]$^{4+}$ (rac, C$_2$-symmetric) and [**39b**]$^{4+}$ (meso, C$_i$-symmetric) in equimolar presence.

Quantitative conversion to the corresponding ethylene bridged dinuclear complex takes place.

Data for [**39b**]$^{4+}$:

^{1}H-NMR (200.13 MHz, CD$_3$CN, 298 K): δ (ppm) = 8.45 (2H, d, Py-*H6*); 7.94-7.16 (18H, Py-*H3*, -*H4* and -*H5*); 4.85-4.30 (12H, six [AB]-type doublets, N-C*H$_2$*-Py); 2.92 (s, 6H, Py-C*H$_3$*), 2.78 (s, 6H, Py-C*H$_3$*), 2.71 (s, 6H, IrNC-C*H$_3$*), 1.68 (2H, m, AA'BB', Ir-C*H$_2$*C*H$_2$*-Ir), 1.55 (2H, m, AA'BB', Ir-C*H$_2$*C*H$_2$*-Ir).

^{13}C{^{1}H}-NMR (50.32 MHz, CD$_3$CN, 298 K): δ (ppm) = 165.3, 164.2, 162.9, 162.3, 157.5, 150.9, 140.8, 140.7, 140.4, 127.6, 127.2, 124.5, 122.7 and 120.5 (Py-*C2*, -*C3*, -*C4*, -*C5* and -*C6*), 75.0, 70.6 and 70.4 (N-*C*H$_2$-Py), 27.9 and 26.7 (Py-*C*H$_3$), 5.26 (NC*C*H$_3$), 4.98 (Ir-*C*H$_2$-*C*H$_2$-Ir). N*C*CH$_3$ signal obscured by the solvent signal.

Calculated for C$_{46}$H$_{54}$N$_{10}$Ir$_2$P$_4$F$_{24}$: C 32.29, H 3.18 N 8.18; Found: C 32.11, H 3.24, N 8.12.

X-Ray diffraction of [**39b**]$^{4+}$.

*[(Me$_2$-tpa)(Cl)Ir^{III}(μ_2-η^1,η^1-C$_2$H$_4$)Ir^{III}(Me$_2$-tpa)(Cl)](PF$_6$)$_2$ ([**40**](PF$_6$)$_2$)*

113 mg (0.16 mmol) [**6**]PF$_6$ dissolved in 10 ml CH$_2$Cl$_2$ was toplayered with one equivalent of [Fc]BF$_4$ in 10 mL MeOH. Transparant light-yellow, air-stable crystals were obtained after 2 months.

When the reaction of Me$_2$-tpa complex [**6**]$^+$ with [Fc]$^+$ is carried out in a mixture of CH$_2$Cl$_2$ and MeOH (This time [Fc]BF$_4$ instead of [Fc]PF$_6$ is used in this case to circumvent solubility problems), again a mixture of two diastereomeric compounds is obtained. Now a 1:2 mixture is obtained of [**40a**]$^{2+}$ (rac, C$_2$-symmetric) and [**40b**]$^{2+}$ (meso, C$_i$-symmetric), of which [**40b**]$^{2+}$ preferentially crystallized from the mixture.

Quantitative conversion to the corresponding light-yellow colored ethylene bridged dinuclear complex takes place.

^{1}H-NMR (200.13 Mhz, CD$_3$CN, 298 K): δ (ppm) = 9.0-8.93 (2H, Py-*H6*), 7.7-7.0 (18H, Py-*H3*, -*H4* and -*H5*), 5.72-4.66 (12H, d[AB], N-C*H$_2$*-Py), 3.16 (6H, s, Py-C*H$_3$*), 2.98-2.76(12H, s, Py-C*H$_3$*). The Ir-C*H$_2$*-C*H$_2$* moiety overlaps with the solvent.

^{13}C{^{1}H}-NMR (75 Mhz, acetone-d6, 298 K): δ (ppm) = 166.3, 165.5, 164.0, 158.2, 149.9, 138.9, 138.5, 138.1, 126.7, 125.9, 125.0, 122.5, 121.0 and 120.5 (Py-*C2*, -*C3*, -*C4*, -*C5* and -*C6*), 74.1, 71.5 and 70.9 (N-*C*H$_2$-Py), 27.4 and 26.0 (Py-*C*H$_3$), 5.96 (Ir-CH$_2$-CH$_2$-Ir).

X-Ray diffraction of [**40b**]$^{4+}$.

*Reaction of [**36**]$^{2+}$ with dioxygen:*
*formation of [(Me$_3$-tpa)Ir^{III}(formylmethyl)(CD$_3$CN)](PF$_6$)$_2$ ([**41**](PF$_6$)$_2$)*

Exposure of a solution of [**36**](PF$_6$)$_2$ in MeCN to O$_2$ leads to a yellow colored mixture of ~ 70% [**41**](PF$_6$)$_2$ and ~ 30% of yet unidentified products. From this mixture [**41**](PF$_6$)$_2$ was characterized.

Data for [**41**]$^{2+}$:

^{1}H-NMR (200 MHz, CD$_3$CN, 298 K): δ (ppm) = 9.44 (t, 1H, ^{3}*J*(H,H) = 4.55 Hz, IrCH$_2$C(=O)*H*), 7.81 (t, 2H, ^{3}*J*(H,H) =7.6 Hz, Py^A-*H4*), 7.69 (t, 1H, ^{3}*J*(H,H)=7.6 Hz, Py^B-*H4*), 7.40-7.10 (m, 6H, Py^A- and Py^B-*H3/H5*), 5.32 (d[AB], 2H, ^{2}*J*(H,H) = 16.4 Hz, N-C*H$_2$*-Py^A), 4.90 (d[AB], 2H, ^{2}*J*(H,H) = 16.4 Hz, N-C*H$_2$*-Py^A), 4.71 (s, 2H, N-C*H$_2$*-Py^B), 3.55 (d, 2H, ^{3}*J*(H,H)= 4.55 Hz, IrC*H$_2$*C(=O)H), 3.18 (s, 3H, Py^B-C*H$_3$*), 2.96 (2, 3H, Ir-NCC*H3*), 2.82 (s, 6H, Py^A-C*H$_3$*).

$^{13}C\{^1H\}$-NMR (50 MHz, CD_3CN, 298K): δ = 208.5 ($IrCH_2C(=O)H$), 166.0,164.4, 163.4 and 159.3 (Py^A- and Py^B-*C2*, Py^A- and Py^B-*C6*), 141.3 (Py^B-*C4*), 140.7 (Py^A-*C4*), 128.6 (Py^B-*C3*), 128.2 (Py^A-*C3*), 122.7 (Py^B-*C5*), 120.4 (Py^A-*C5*), 74.9 (N-CH_2-Py^A), 71.4 (N-CH_2-Py^B), 27.3 (Py^B-CH_3), 27.2 (Py^A-CH_3), 10.4 (Ir-$CH_2C(=O)H$), 5.6 (Ir-$NCCH_3$) (Ir-$NCCH_3$ signal obscured by solvent signal).

ESI^+-MS (sample prepared in CD_3CN): m/z = 306 $[M-(PF_6)_2]^{2+}$, 284 $[M-(PF_6)_2-CD_3CN]^{2+}$, 757 $[M-PF_6]^+$.

FT-IR (KBr, cm^{-1}): 2848, 2733 (C-H of CH=O), 1676 (C=O of CH=O), 825, 556 (P-F).

*Reaction (1) of [**36**]$^{2+}$ with KO_2*

To a solution of 6 mg (0.007 mmol) of [**36**]$(PF_6)_2$ in dry-acetonitrile-d3, 1 mg (0.014 mmol) of KO_2 was added, immediately change of colour from orange to yellow was observed.

^1H-NMR (200.13 MHz, CD_3CN, 298 K): all peaks for [**4**]$^+$ and diamagnetic peaks of [**36**]$^{2+}$ in acetonitrile.

*Reaction (2) of [**36**]$^{2+}$ with KO_2*

10 mg (0.14 mmol) of KO_2 and 3 mg (0.0035 mmol) of [**36**]$(PF_6)_2$ and 15 glass beans (3 mm) were mixed (solid phase metathesis) under vacuum for 48 hours, the products were abstracted with CD_2Cl_2.

^1H-NMR (200.13 MHz, CD_2Cl_2, 298 K): all peaks for [**4**]$^+$ and a second unknown product: 7.62 (t), 3.28 (s, ^1H, Py-CH_3), 2.96 (s, 2H, Py-CH_3), other signals could not be assigned.

5.7 References

[1] D. G. de Wit, *Coord. Chem. Rev.,* **1996**, *147*, 209-246
[2] B. B. Wayland, A. E. Sherry and A. G. Bunn, *J. Am. Chem. Soc.,* **1993**, *115 (17)*, 7675-7684
[3] L. Brammer, N. G. Connelly, J. Edwin, W. E. Geiger, A. G. Orpen and J. B. Sheridan, *Organometallics,* **1988**, *7 (6)*, 1259-1265
[4] K. K. Pandey, *Coord. Chem. Rev.,* **1992**, *121*, 1-42
[5] H. L. Zhai, A. Bunn and B. Wayland, *Chem. Commun.,* **2001**, *(14)*, 1294-1295
[6] M. P. Garcia, M. V. Jimenez, L. A. Oro, F. J. Lahoz and P. J. Alonso, *Angew. Chem. - Int. Edit.,* **1992**, *31 (11)*, 1527-1529
[7] C. F. Zou, K. J. Ahmed and M. S. Wrighton, *J. Am. Chem. Soc.,* **1989**, *111 (3)*, 1133-1135
[8] L. N. Novikova, B. A. Mazurchik, N. A. Ustynyuk, Y. F. Oprunenko, V. Y. Rochev and V. G. Bekeshev, *J. Organomet. Chem.,* **1995**, *498 (1)*, 25-27
[9] T. D. Newbound, A. M. Arif, D. R. Wilson, A. L. Rheingold and R. D. Ernst, *J. Organomet. Chem.,* **1992**, *435 (1-2)*, 73-84
[10] R. D. Ernst, H. Ma, G. Sergeson, T. Zahn and M. L. Ziegler, *Organometallics,* **1987**, *6 (4)*, 848-853
[11] W. E. Geiger, T. Gennett, G. A. Lane, A. Salzer and A. L. Rheingold, *Organometallics,* **1986**, *5 (7)*, 1352-1359
[12] L. Basickes, A. G. Bunn and B. B. Wayland, *Can. J. Chem. - Rev. Can. Chim.,* **2001**, *79 (5)*, 854-856
[13] B. de Bruin, S. Thewissen, T. W. Yuen, T. P. J. Peters, J. M. M. Smits and A. W. Gal, *Organometallics,* **2002**, *21 (21)*, 4312-4314
[14] B. de Bruin, T. P. J. Peters, S. Thewissen, A. N. J. Blok, J. B. M. Wilting, R. de Gelder, J. M. M. Smits and A. W. Gal, *Angew. Chem. - Int. Edit.,* **2002**, *41 (12)*, 2135-2138
[15] D. G. H. Hetterscheid, J. Kaiser, E. Reijerse, T. P. J. Peters, S. Thewissen, A. N. J. Blok, J. M. M. Smits, R. de Gelder and B. de Bruin, *J. Am. Chem. Soc.,* **2005**, in press
[16] H. C. Brown, *J. Am. Chem. Soc.,* **1945**, *67*, 378 and 1452
[17] H. C. Brown, H. Bartholomay Jr. and M. D. Taylor, *J. Am. Chem. Soc.,* **1944**, *66*, 435
[18] B. de Bruin, J. A. Brands, J. J. J. M. Donners, M. P. J. Donners, R. de Gelder, J. M. M. Smits, A. W. Gal and A. L. Spek, *Chem. - Eur. J.,* **1999**, *5 (10)*, 2921-2936
[19] J. March, *"Advanced Organic Chemistry; Reactions, Mechanisms and Structure"*, John Wiley & Sons, New York, **1992**
[20] F. A. Cotton, G. Wilkinson and P. L. Gaus*, Basic Inorganic Chemistry, 3rd Edition*, Eds., John Wiley & Sons, **1995**
[21] A. G. Bunn and B. B. Wayland, *J. Am. Chem. Soc.,* **1992**, *114 (17)*, 6917-6919
[22] E. B. Boyar and S. D. Robinson, *Coord. Chem. Rev.,* **1983**, *50*, 109
[23] T. R. Felthouse, *Prog. Inorg. Chem.,* **1982**, *29*, 73
[24] B. B. Wayland and A. E. Sherry, *J. Am. Chem. Soc.,* **1992**, *114*, 6917
[25] B. de Bruin, J. A. W. Verhagen, C. H. J. Schouten, A. W. Gal, D. Feichtinger and D. A. Plattner, *Chem. - Eur. J.,* **2001**, *7 (2)*, 416-422
[26] M. Krom, R. G. E. Coumans, J. M. M. Smits and A. W. Gal, *Angew. Chem. - Int. Edit.,* **2002**, *41 (4)*, 576-579
[27] D. Milstein and J. C. Calabrese, *J. Am. Chem. Soc.,* **1982**, *104 (13)*, 3773-3774
[28] M. Krom, T. P. J. Peters, R. G. E. Coumans, T. J. J. Sciarone, J. Hoogboom, S. I. ter Beek, P. P. J. Schlebos, J. M. M. Smits, R. de Gelder and A. W. Gal, *Eur. J. Inorg. Chem.,* **2003**, *6*, 1072-1087

[29] D. T. Sawyer, T. S. Calderwood, K. Yamaguchi and C. T. Angelis, *Inorg. Chem.,* **1983**, *22 (18)*, 2577-2583
[30] G. Anderegg and F. Wenk, *Helv. Chim. Acta,* **1967**, *50 (8)*, 2330
[31] H. Nagao, N. Komeda, M. Mukaida, M. Suzuki and K. Tanaka, *Inorg. Chem.,* **1996**, *35 (23)*, 6809-6815
[32] B. de Bruin, M. J. Boerakker, J. A. W. Verhagen, R. de Gelder, J. M. M. Smits and A. W. Gal, *Chem. - Eur. J.,* **2000**, *6 (2)*, 298-312
[33] R. Cramer, J. A. McCleverty and J. Bray, *Inorg. Synth.,* **1990**, *28*, 86
[34] J. L. Herde, J. C. Lambert and C. V. Senoff, *Inorg. Synth.,* **1974**, *15*, 18-20
[35] P. T. Beurskens, G. Beurskens, W. P. Bosman, R. de Gelder, S. Garcia-Granda, R. O. Gould, R. Israel and J. M. M. Smits, *"DIRDIF-96. A computer program system for crystal structure determination by Patterson methods and direct methods applied to difference structure factors"*; Laboratory of Crystallography, Department of Inorganic Chemistry, University of Nijmegen: The Netherlands, **1996**
[36] P. T. Beurskens, G. Beurskens, M. Strumpel and C. E. Nordman, *Patterson and Pattersons*, Vol. Eds. J. P. Glusker, B. K. Patterson and M. Rossi, Clarendon Press, Oxford, **1987**, page 356
[37] G. M. Sheldrick, *"SHELXL-97. Program for the refinement of crystal structures"*; University of Goettingen, Germany, **1997**
[38] A. L. Spek, *"PLATON-93. Program for display and analysis of crystal and molecular structures"*; University of Utrecht, The Netherlands, **2003**
[39] G. Schaftenaar and J. H. Noordik, *J. Comput. - Aided Mol. Des.,* **2000**, *14 (2)*, 123-134
[40] A. D. Becke, *J. Chem. Phys.,* **1993**, *98 (7)*, 5648-5652
[41] B. Miehlich, A. Savin, H. Stoll and H. Preuss, *Chem. Phys. Lett.,* **1989**, *157 (3)*, 200-206
[42] C. T. Lee, W. T. Yang and R. G. Parr, *Phys. Rev. B,* **1988**, *37 (2)*, 785-789
[43] M. J. Frisch, G. W. Trucks, H. B. Schlegel, G. E. Scuseria, M. A. Robb, J. R. Cheeseman, V. G. Zakrzewski, J. A. Montgomery Jr., R. E. Stratmann, J. C. Burant, S. Dapprich, J. M. Millam, A. D. Daniels, K. N. Kudin, M. C. Strain, O. Farkas, J. Tomasi, V. Barone, M. Cossi, R. Cammi, B. Mennucci, C. Pomelli, C. Adamo, S. Clifford, J. Ochterski, G. A. Petersson, P. Y. Ayala, Q. Cui, K. Morokuma, D. K. Malick, A. D. Rabuck, K. Raghavachari, J. B. Foresman, J. Cioslowski, J. V. Ortiz, A. G. Baboul, B. B. Stefanov, G. Liu, A. Liashenko, P. Piskorz, I. Komaromi, R. Gomperts, R. L. Martin, D. J. Fox, T. Keith, M. A. Al-Laham, C. Y. Peng, A. Nanayakkara, M. Challacombe, P. M. W. Gill, B. Johnson, W. Chen, M. W. Wong, J. L. Andres, C. Gonzalez, M. Head-Gordon, E. S. Replogle and J. A. Pople, *"Gaussian 98, Revision A.9"*; Gaussian, Inc., Pittsburgh PA, **1998**
[44] J. B. Collins, P. V. R. Schleyer, J. S. Binkley and J. A. Pople, *J. Chem. Phys.,* **1976**, *64 (12)*, 5142-5151
[45] W. J. Hehre, R. F. Stewart and J. A. Pople, *J. Chem. Phys.,* **1969**, *51 (6)*, 2657
[46] P. J. Hay and W. R. Wadt, *J. Chem. Phys.,* **1985**, *82 (1)*, 270-283
[47] W. R. Wadt and P. J. Hay, *J. Chem. Phys.,* **1985**, *82 (1)*, 284-298
[48] P. J. Hay and W. R. Wadt, *J. Chem. Phys.,* **1985**, *82 (1)*, 299-310

Chapter 6

Gas-Phase Fragmentation Behavior of N_3 and N_4 Rhodium and Iridium Complexes

6.1 Introduction

As discussed in § 2.3.7, the m/z ratio of a compound alone is not highly informative of the absolute structure and isomeric descriptions should always be considered. However, Collisional Activation (CA, in the tube lens region) and Collision Induced Dissociation (CID, in the octopole region) measurements are excellent ways to obtain structural information from mass spectra. In biochemical studies the typical fragmentation behavior of enzymes allows elucidation of the amino acid sequence. [1] – [4] Threshold measurements on non-covalent complexes provide information of binding strengths of these non-covalent bonds. [5] – [12] Observed gas-phase fragmentation behavior could also provide indications on deactivation pathways in solution.

In this chapter the results of CID (and in § 6.4 of CA) measurements performed on several rhodium and iridium complexes will be discussed. It will be shown that from these measurements conclusions can be drawn about atom connectivity and electronic structures and decomposition pathways. Most fragmentation reactions were performed in the daughter-ion scan mode by collision with argon in RC 2. The fragmentation behavior of the N_3 and N_4 rhodium ethene and peroxo complexes discussed in § 6.4 was measured by collisional activation of the complexes in the tube lens region.

6.2 About energy transfer during gas-phase collisions

The energy at which ions can collide with neutral gas molecules can be varied in some of the reaction regions. In the tube lens region increase of the potential applied to the tube lenses results in an increase of the velocity of the ions and thus in an increase of the energy with which they will collide with gas molecules. At the entrance of RC 2 another a potential can be applied with which the ions can be accelerated before entering RC 2. In order to be able to compare the reaction conditions for ions with different m/z ratios and for different collision gasses, we need to know how the potential V applied relates to the maximum amount of energy that can be transferred in a collision, $E_{(cm)}$, the energy that will be displayed in most diagrams of gas-phase reactions in the present chapter and in Chapter 7.

At the entrance of RC 2 ions (with charge q_{ion}) are accelerated by a certain potential V. The kinetic energy in the laboratory frame, $E_{(lab)}$, can be calculated using equation 6.1.

$$E_{(lab)} = q_{ion} * V \qquad (6.1)$$

It is not possible to convert this kinetic energy completely into internal energy during a collision, since conservation of the total impulse of the ion-molecule collision requires conservation of the kinetic energy of the center of mass of both collision partners. The maximum amount of energy that can be converted into

internal energy to overcome reaction barriers is equal to the relative kinetic energy of the collision partners in the center of mass system.

The maximum amount of energy that can be transferred in a collision can be calculated using conservation of impulse and energy. This energy corresponds to the kinetic energy, $E_{(cm)}$, of both collision partners in the center of mass frame at a completely inelastic collision (equation 6.2). [13], [14]

$$E_{(cm)} = E_{(lab)} * \frac{m_{gas}}{m_{gas} + m_{ion}} = q_{ion} * V * \frac{m_{gas}}{m_{gas} + m_{ion}} \qquad (6.2)$$

In this equation:

$E_{(cm)}$ is the kinetic energy of the ion in the center of mass coordinate system.

$E_{(lab)}$ is the kinetic energy of the ion in the laboratory system; the velocity of the gas molecules is taken to be zero, which is valid as long as $E_{(lab)} >> k * T$.

m_{ion} and q_{ion} are the mass and the charge of the ion involved in the collision.

m_{gas} is the mass of the gas molecule the ion collides with.

V is the potential difference over which the ions are accelerated just before entering RC 2.

In the tube lens region it is difficult to estimate the kinetic energy of the ions in the laboratory frame. This is due to the fact that the pressure in this region is much higher than the one used in RC 2 (compare 0.5 - 1.0 Torr with 10^{-3} Torr). As a result, the mean free path of the ions is extremely short and it will not be possible for the ions to be accelerated over the total potential difference applied between the tube lenses. They will collide with other molecules and in these collisions transfer some of the kinetic energy they have just acquired. Therefore, the ions will obtain only a fraction of $E_{(lab)}$ and their true kinetic energy in the tube lens region, $E_{(lab,\,TL)}$, can be described by equation 6.3, in which α is an unknown constant.

$$E_{(lab,TL)} = \alpha * q_{ion} * V \qquad (6.3)$$

For convenience we will assume $\alpha = 1$ in the remainder of this chapter, but one should always keep in mind that $0 < \alpha << 1$.

To get an idea of trends of reaction in the tube lens region we need to convert $E_{(lab)}$ to $E_{(cm)}$. The tube lens region contains a mixture of gas molecules with which the ions can collide (air, solvent molecules, other ions). We decided to use the mass of a dioxygen molecule for $\underline{m_{gas}}$ in equation 6.2.

6.3 Trends in binding energy of ethene in $[(N_3)M(C_2H_4)]^+$

N_3 rhodium and iridium ethene complexes[1] were collided in RC 2 with 0.4 mTorr argon at collision energies varying between 0 and 30 eV (laboratory frame). The main fragment observed at this collision-gas pressure and at these collision energies was the "naked" species[2], $[(N_3)M]^+$.[3] When the intensity of this fragment is plotted against the collision energy in the center of mass frame, $E_{(cm)}$, a clear picture is obtained reflecting the trend in the binding energies of ethene upon change of the ligand and the metal center (Figure 6.1).

[1] For M = Rh: N_3 = bpa, bpa-Me, bpa-Bz, Me_2-bpa-Me, Me_2-bpa-Bz. For M = Ir: N_3 = Me_2-bpa-Me.

[2] The term "naked species" will be used throughout this thesis for species of the form $[(L_N)M]^+$: an organometallic complex consisting of only a nitrogen donor ligand L_N and a metal center M.

[3] The intensities of fragments other than $[(L_N)M]^+$ were negligible. If the intensity of these fragments would have been added to the TIC (= Total Ion Current) and the total intensity of all the fragments would have been shown instead of only that of $[(L_N)M]^+$, Figure 6.1 would still have looked the same.

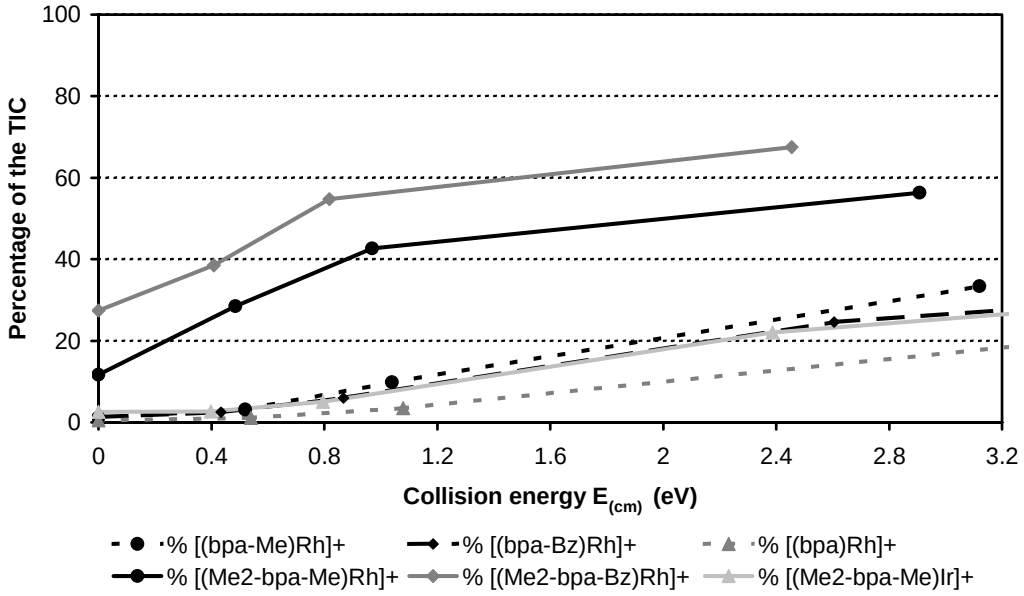

Figure 6.1 *Intensity of $[(N_3)M]^+$ upon collision of the ethene complex with 0.4 mTorr argon in RC 2* [4]

In the case of the more sterically hindered Me_2-bpa-R complexes the olefin seems to be less strongly bound to the metal center than in the case of the bpa-R complexes. Already at near zero-collision-energy quite a percentage of the Me_2-bpa-R rhodium ethene ions has already lost its ethene moiety.
As expected, the olefin binding is stronger for the Me_2-bpa-Me iridium complex than for the corresponding rhodium ethene complex.

The trends in binding energies as observed in the collision experiments are in line with the binding energies obtained via DFT calculations (Table 6.1 on the next page and Appendix A). In both cases the olefin moieties are less strongly coordinated to the bulky Me_2-bpa-R complexes, both for rhodium and iridium.

When the same fragmentation experiments are performed at a higher argon pressure, 0.8 mTorr, the difference in behavior between the N_3 rhodium ethene species is much smaller, probably due to the higher collision frequency.
As can be seen in Figure 6.2 on the next page at this pressures fragmentation occurs to a much larger extent. Now also the bpa-R complexes display significant fragmentation at near-zero collision energies, although they remain more resistant to fragmentation than their Me_2-bpa-R counterparts.
A difference with the measurements at 0.4 mTorr argon is that now not only loss of ethene is observed, but also loss of parts of the N_3 ligands.[5] Therefore in Figure 6.2 the total fragment intensity (and not just the intensity of $[(N_3)Rh]^+$) is plotted against the collision energy $E_{(cm)}$.

[4] TIC = the Total Ion Current generated by all the ions hitting the detector.

[5] For a more detailed description of the types of fragments see § 6.4.

Table 6.1 *Binding energies of ethene in $[(N_3)M(C_2H_4)]^+$ obtained from DFT calculations* [6]

M	L_N	$\Delta H_{0\ Kelvin}$ [7]	
		kcal/mol	eV/mol
Rh	bpa	-30.2	-1.31
	bpa-Me	-30.6	-1.33
	Me_2-bpa[8]	-13.9	-0.60
	Me_2-bpa-Me	-14.9	-0.65
Ir	bpa	-39.5	-1.71
	bpa-Me	-39.3	-1.70
	Me_2-bpa	-20.5	-0.89
	Me_2-bpa-Me	-21.2	-0.92

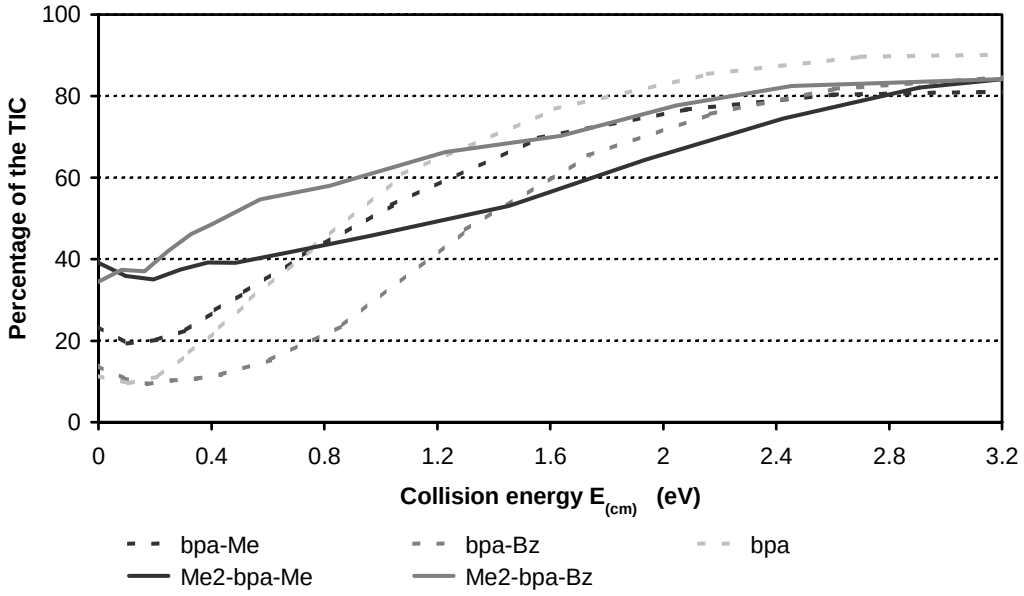

Figure 6.2 *Total fragment intensity upon collision of $[(N_3)Rh(C_2H_4)]^+$ with 0.8 mTorr argon in RC 2*

[6] Relative to the naked species $[(N_3)M]^+$.

[7] As already mentioned in § 3.6 and § 4.4, the most appropriate energy quantity for a description of reactions occurring in solution is the Gibbs free energy at (in this thesis) 25 ºC: $\Delta G_{298\ K,\ 1\ bar}$.

If molecules are isolated from each other and then suddenly obtain internal energy (e.g. through a single high-energy collision), the energy distribution will not resemble a Boltzmann distribution. Statistical arguments are not appropriate any more, the energy distribution over the collided molecules will be narrow, and the temperature is not well-defined. Under these circumstances, one expects that molecules can overcome a particular barrier if their internal energy is higher than "pure" activation barrier $E_{electronic}$+ZPE, which is identical to the enthalpy at 0K, $\Delta H_{0\ K}$.

Therefore, when considering the reactions occurring in RC 2 the enthalpy $\Delta H_{0\ K}$ is probably the appropriate quantity to use. In RC 1 and the tube lens region the collision gas pressures are so high that it is not clear whether use of the enthalpy $\Delta H_{0\ K}$ or of the free free energy $\Delta G_{343\ K,\ 0.001\ bar}$ (70 ºC and 0.001 bar, spectrometer conditions) is more appropriate.

In Appendix A for a bpa-R, Me_2-bpa-R, tpa and Me_3-tpa rhodium and iridium compounds relevant for the reaction with O_2 all three types of energies are listed.

Interestingly, the aromatic C-H activation that takes place in acetone for the Me_2-bpa-Bz rhodium ethene complex $[\mathbf{23}]^+$ (resulting in ethyl complex $[\mathbf{24}]^+$, see Figure 6.3) as described in § 3.5.1, could also be followed by these collision experiments with argon.

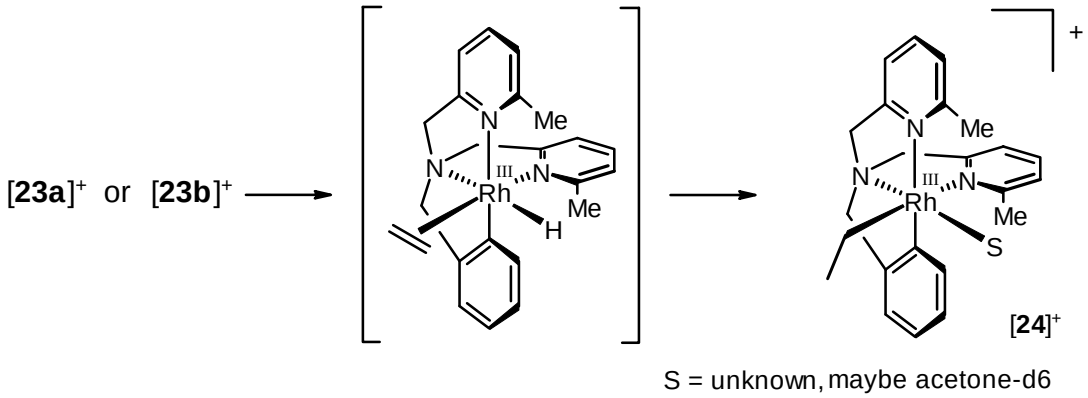

Figure 6.3 *Rearrangement in solution in acetone of $[(Me_2\text{-bpa-Bz})Rh(C_2H_4)]^+$*

ESI^+-MS spectra of an acetone solution of the ethene complex were measured within the first 20 minutes after dissolving (Figure 6.4a). The solution was allowed to stand for 2 hours (no other measurements were performed in the meantime) and then sprayed again (Figure 6.4b). It is known from ^{1}H-NMR experiments that after 2 hours the ethene complex will have fully rearranged to the corresponding ethyl complex.
The "ethyl" complex that was mass selected after 2 hours, $[(Me_2\text{-bpa-Bz}^{\#})RhC_2H_5]^+$, had probably rearranged to the corresponding ethene hydride complex before entering RC 2 (as was also observed for other rhodium ethyl complexes in § 2.3.7), since it has no solvent coordinated anymore to occupy the sixth coordination site. In this second measurement the signal stability had increased tremendously. Also a clear difference in fragmentation behavior of $[(Me_2\text{-bpa-Bz})Rh^{I}(C_2H_4)]^+$ *versus* $[(Me_2\text{-bpa-Bz}^{\#})Rh^{III}C_2H_5]^+$ could be observed, when these isobaric species were collided with 0.8 mTorr argon in RC 2.

As can be concluded from Figure 6.4a and Figure 6.4b on the next page, immediately after dissolving the ethene complex, the olefin moiety dissociates much more easily than 2 hours later, especially at lower collision energies. At higher collision energies ($E_{(cm)}$ > 1.5 eV) the difference in fragmentation behavior becomes less pronounced. During both measurements above $E_{(cm)}$ = 1.5 eV parts of the N_3 ligand start to dissociate.

An explanation for this difference in behavior cannot easily be given.

Assuming that the species entering RC 2 after 2 hours truly has the ethene-hydride structure, then apparently the olefin is more strongly bound to a rhodium(III) center than to a rhodium(I) center. This is rather unexpected. Due to the higher electron density metal(I) centers are capable of stronger π-backdonation to the olefin. Therefore, we would have expected the olefin moiety to be more strongly coordinated during the initial measurements than during those after 2 hours.

It could also be that for some reason the structure of the complex entering RC 2 after 2 hours is not an ethene-hydride species, but a totally different, isobaric one. It could be that for such a species the olefin is stronger bound to the metal center than in the case of the rhodium(I) ethene complex. However, it remains puzzling why we never observed any such species in the ^{1}H-NMR spectra of this C-H activation reaction.

From the mass spectra we can conclude that the structure of the compound has changed and that the complex formed is isobaric with the previously dissolved rhodium(I) ethene complex. However, we do not know what has happened during those 2 hours in solution or upon transferring the complex present in solution from solution to the gas phase.

[8] If R = H in Me_2-bpa-R, then we name the ligand Me_2-bpa (in analogy with the bpa-ligand).

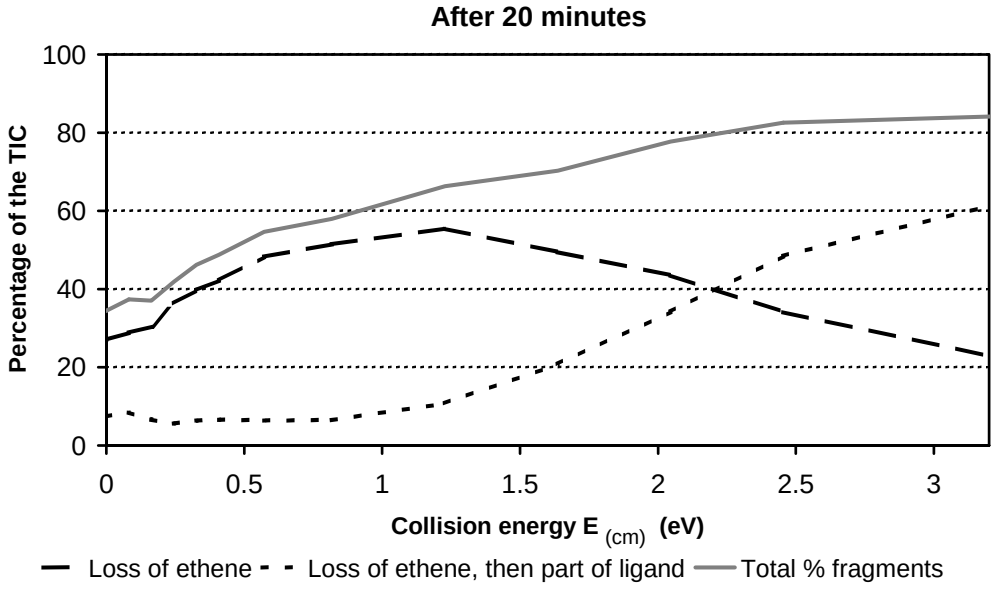

Figure 6.4a *Intensity of $[(Me_2\text{-bpa-Bz})Rh]^+$ upon collision of the ethene complex with 0.8 mTorr argon 20 minutes after sample preparation*

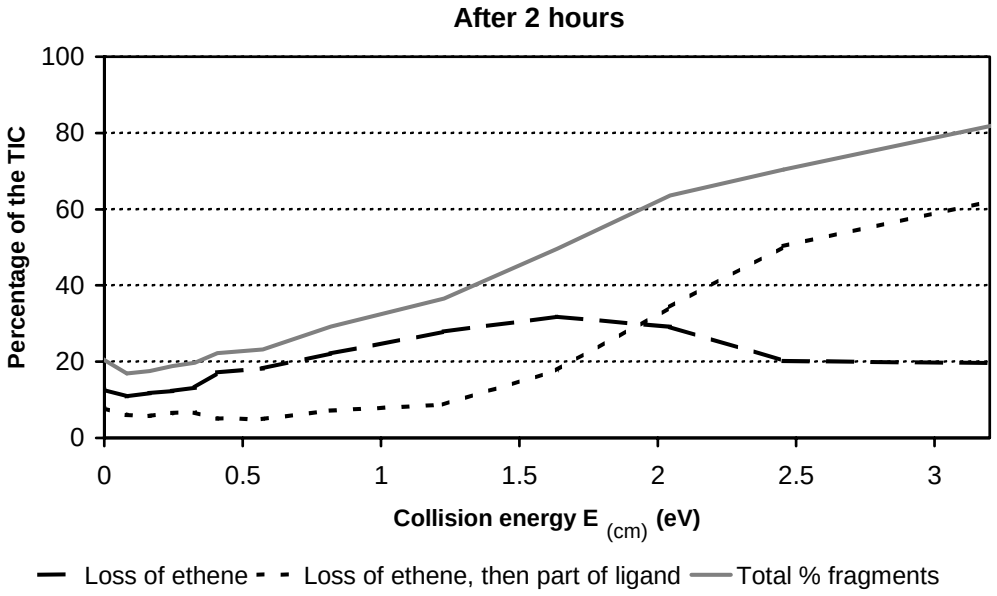

Figure 6.4b *Intensity of $[(Me_2\text{-bpa-Bz})Rh]^+$ upon collision of the ethene complex with 0.8 mTorr argon 2 hours after sample preparation*

6.4 Fragmentation behavior of peroxo *versus* ethene and naked complexes, or homolytic bond splitting *versus* loss of a neutral non-radical species

The fragmentation behavior of some N_3 and N_4 rhodium ethene and peroxo complexes and their naked species $[(L_N)Rh]^+$ [9] was investigated by collisional activation of the ions in the tube lens region[10] (the tube lens

[9] N_4 = tpa, Me-tpa, Me_2-tpa, Me_3-tpa, N_3 = bpa-R (R = H, Me, Bz) and Me_2-bpa-R (R = Me, Bz)

potential was varied from 5 to 145 Volt). Since all species that are transferred to the gas phase in the atmospheric pressure chamber enter the tube lens region, in some cases one could debate whether certain fragments really belong to the parent as presented in this chapter. In those cases, daughter-ion experiments were performed of the parents by collision with argon in the octopole region to confirm our assignments. Upon comparison of $[(L_N)Rh(C_2H_4)]^+$, $[(L_N)Rh]^+$ and $[(L_N)Rh(O_2)]^+$ two different ways of fragmentation were observed.

The ethene complexes $[(L_N)Rh(C_2H_4)]^+$ lose the olefin (**1**), or another *neutral non-radical* molecule like a pyridine fragment (**2**, Figure 6.5) or a fragment in which the amine-substituent is involved (**3a** – **3c**). Loss of H_2 from bpa rhodium ethene complex is especially pronounced. This is probably due to the highly acidic nature of the amine proton upon coordination of the amine to rhodium.

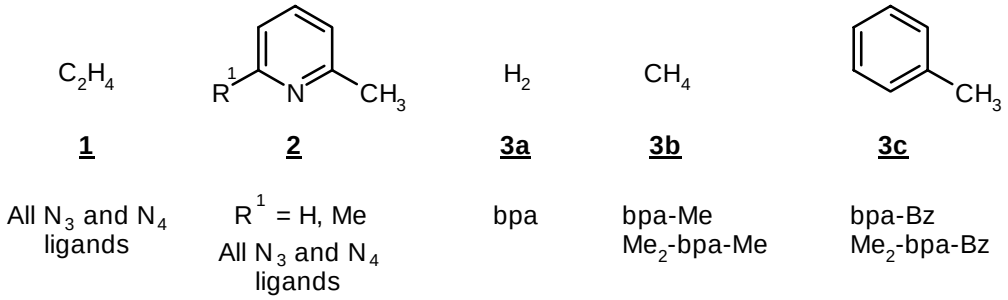

Figure 6.5 *Types of fragments observed for $[(L_N)Rh(C_2H_4)]^+$ in the tube lens region*

For the naked species $[(L_N)Rh]^+$ the same type of fragmentation as the one shown in Figure 6.5 was observed (**2** – **3c**). A difference is that although loss of one H_2 molecule is again most pronounced for the bpa complex, multiple loss of H_2 (up to 3 times!) was observed for all nine $[(L_N)Rh]^+$ complexes. The methylene protons, N-CH_2-Py, are probably involved in this fragmentation reaction.
All these fragments are probably formed in the same type of fragmentation reaction (Figure 6.6).

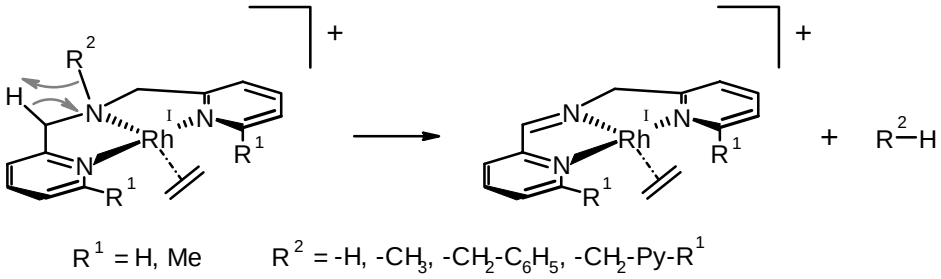

Figure 6.6 *Fragmenation pathway of $[(L_N)Rh(C_2H_4)]^+$ and of $[(L_N)Rh]^+$ upon collision with argon*

This type of fragmentation behavior is similar to that observed for quaternary ammonium ions. [15] – [23]
For gaseous R_4N^+ions it has been reported by Beranovà *et al.* [17] that they dissociate after rate-determining isomerization to ion-dipole complexes $R_3N^{\bullet+}/R^\bullet$ (R = alkyl, C_6H_5, $C_6H_5CH_2$) or R^+/NR_3 (R = $C_6H_5CH_2$). All major primary fragments arise by simple dissociation of the complex: loss of $R^\bullet$ or NR_3 and by elimination of RH or R-R' from the complex. The latter reaction involves atom (or group) transfer within the ion/dipole intermediate, which requires overcoming an additional though smaller barrier, but leads to thermodynamically more stable products; its yields become, therefore, substantially larger as the internal energy of the ammonium cation increases. R' (often R minus CH_2) is in this case formed by fission of a C-C bond α to the nitrogen of a

[10] As explained in § 2.2.1, the background pressure in the tube lens region of 0.5 - 1.0 Torr consists of air and gaseous solvent molecules. The exact composition of the background gas cannot be determined; neither can it be varied at will.

neighbouring R group. Thus $[Me_4N]^+$ shows elimination of CH_4, [17] $[Et_4N]^+$ shows elimination of C_2H_6 and C_3H_8, [17] $[(n\text{-}Pr)_4N]^+$ shows elimination of C_3H_8 and C_5H_{12} [16], [20] and $[(n\text{-}Bu)_4N]^+$ shows elimination of C_4H_{10} and C_7H_{16}. [16], [18] – [20]
If the ammonium ion contains two different substituents, the weaker N^+-C bond is preferentially broken.
For the complexes Beranovà had investigated the N^+-bonds became stronger in the order
$N^+\text{-}C_{benzyl} < N^+\text{-}C_{alkyl} < N^+\text{-}C_{phenyl}$.
Since the internal energy of the cationic organometallic complexes discussed above is quite high, it is likely that the preferred fragmentation is loss of these neutral non-radical fragments R-H instead of $R^\bullet$ radicals.

For the peroxo complexes we found a different fragmentation behavior.
On the basis of collision experiments with argon in RC 2 we know that most peroxo complexes $[(L_N)Rh(O_2)]^+$ preferably lose the dioxygen moiety (**1b**, Figure 6.7), except for the bpa-Bz and Me_2-bpa-Bz rhodium peroxo complexes, which lose H_2O (**1a**). The bpa rhodium peroxo complex can lose both O_2 and H_2O. For the bpa complex loss of H_2O is probably due to the highly acidic amine-proton that can easily be transferred to one of the oxygen atoms, whereas for the benzyl-containing complexes probably the benzylic methylene protons are highly acidic; deprotonation would result in the formation of the hydroperoxo complexes for which loss of H_2O is expected. This same behavior was also observed in the tube lens region.
Apparently the N-CH_2-Py methylene protons are not acidic enough to protonate the coordinated dioxygen molecule or proton transfer is hindered by geometric constraints, since loss of H_2O is not observed for any of the other bpa- or tpa-type of complexes.
In addition, instead of O_2/H_2O the peroxo complexes can also lose *neutral radical* fragments: either a pyridyl radical (**2**, Figure 6.7) or the amine-substituent (**3a**, **3b**). In other words, the peroxo complexes preferably undergo *homolytic bond splitting* of the N-C bond, a fragmentation path never observed for the ethene complexes, but one encountered before by Beranovà *et al.* [17] for quaternary ammonium ions as described before.

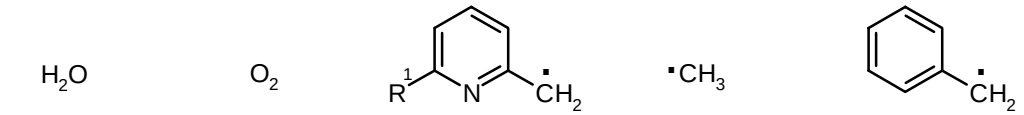

1a	**1b**	**2**	**3a**	**3b**
bpa bpa-Bz Me_2-bpa-Bz	The rest of the N_3 and N_4 ligands	R^1 = H, Me All N_3 and N_4 ligands	bpa-Me Me_2-bpa-Me	bpa-Bz Me_2-bpa-Bz

Figure 6.7 *Types of fragments observed for $[(L_N)Rh(O_2)]^+$ in the tube lens region*

Especially for the peroxo complexes of the N_4 ligands, besides loss of O_2 (**1b**) homolytic bond splitting (**2**) is the only type of fragmentation observed.
For the benzyl-containing N_3 ligands loss of H_2O (**1a**) is a favorite fragmentation at lower collision energies, but at higher collision energies loss of the benzyl radical (**3b**) is the main fragmentation, and some loss of a pyridyl radical (**2**) is also observed.
For the bpa and bpa-Me complexes the distinction in fragmentation behavior between the olefin and the peroxo complex is less pronounced. These peroxo complexes can lose *both* types of fragments: neutral non-radical (**2**, **3b**, Figure 6.5) and neutral radical species (**2**, **3a**, Figure 6.7).

The fragmentation behavior of peroxo complexes can vary strongly. Schwarz *et al.* [24] have already shown that $[MO_2]^+$ species demonstrate radical-type reactivity for M = Ti, Zr abstracting hydrogen atoms from water and methane. In marked contrast, they found that for M = V, Nb no radical reactions occur and $[MO_2]^+$ behave like a closed-shell species. These reactivity patterns were in accord with the calculated bonding schemes. They

found for M = V, Nb a singlet ground state, whereas for M = Ti, Zr a doublet ground state (an oxygen-centered radical) was predicted.

Since we also observed a radical-type fragmentation for our peroxo complexes, we calculated the energies of the singlet and the triplet states of some $[(N_3)Rh(O_2)]^+$ species (N_3 = bpa-Me, Me_2-bpa-Me).[11]
Indeed the triplet energies lie at least 7 kcal/mol below those of the singlets. For the naked species $[(N_3)Rh]^+$, the ethene complex $[(N_3)Rh(C_2H_4)]^+$ and the solvent-coordinated peroxo complex $[(N_3)Rh(O_2)(solvent)]^+$ the singlet state is more stable than the triplet state.
From these results, one would indeed expect (bi)radical behavior during fragmentation at least for the N_3 peroxo complexes (as shown in Figure 6.8).

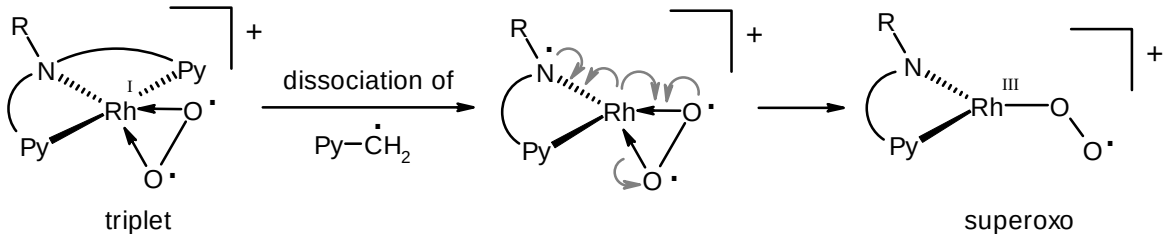

Figure 6.8 *Proposed reactivity of five-coordinate triplet rhodium peroxo complexes*

6.5 Structure determination

Each molecule has its own typical fragmentation behavior, which can provide important information on its atom connectivity. This comes in handy when one is interested in distinguishing between isobaric species or species containing moieties of the same molecular formula but a different structure.
Some examples and some problems related to them will be presented in the next paragraphs.

6.5.1 Peroxo-ethene *versus* dioxolane *versus* hydroxyl-formylmethyl

These three species all contain a nitrogen donor ligand L_N [12], a metal center and a $C_2H_4O_2$ moiety, $[(L_N)MC_2H_4O_2]^+$ (see Figure 6.9). It would be useful if one could distinguish between them using mass spectrometry.

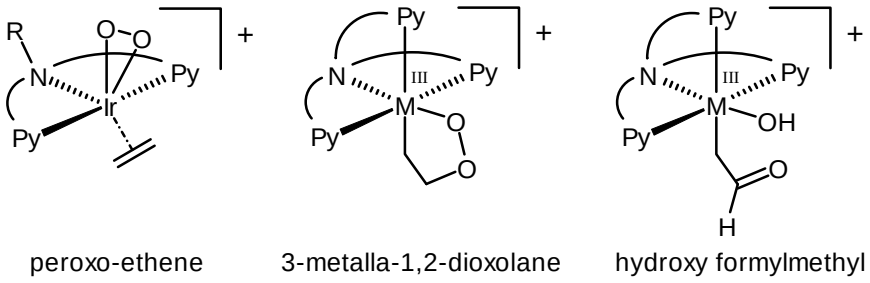

Figure 6.9 *Structures of three $[(L_N)M(C_2H_4O_2)]^+$ species*

[11] These species can only be found in the gas phase. In solution the sixth coordination site is always occupied (presumably with a solvent molecule).

[12] Peroxo-ethene: M = Ir; L_N = Me_3-tpa, Me_2-bpa-Me. 3-Metalla-1,2-dioxolane: M = Rh, Ir; L_N = tpa, Me-tpa. Hydroxy-formylmethyl: M = Rh, Ir; L_N = tpa, Me-tpa.

Distinguishing the peroxo-ethene complexes from the other two types of complexes upon collision with argon is fairly easy:

- They preferably lose the olefin first (it is less strongly bound than the dioxygen molecule, see Appendix A) leaving a peroxo complex.
- First loss of O_2 (leaving an ethene complex behind) is a relatively unimportant fragmentation pathway.

The dioxolane and the hydroxy-formylmethyl lose neither ethene nor O_2 fragments. Their spectra are actually quite similar. (Figure 6.10 and Figure 6.11). A small amount of dissociation of a species with mass 28 (probably CO, *not* C_2H_4, signal **2**) is observed.

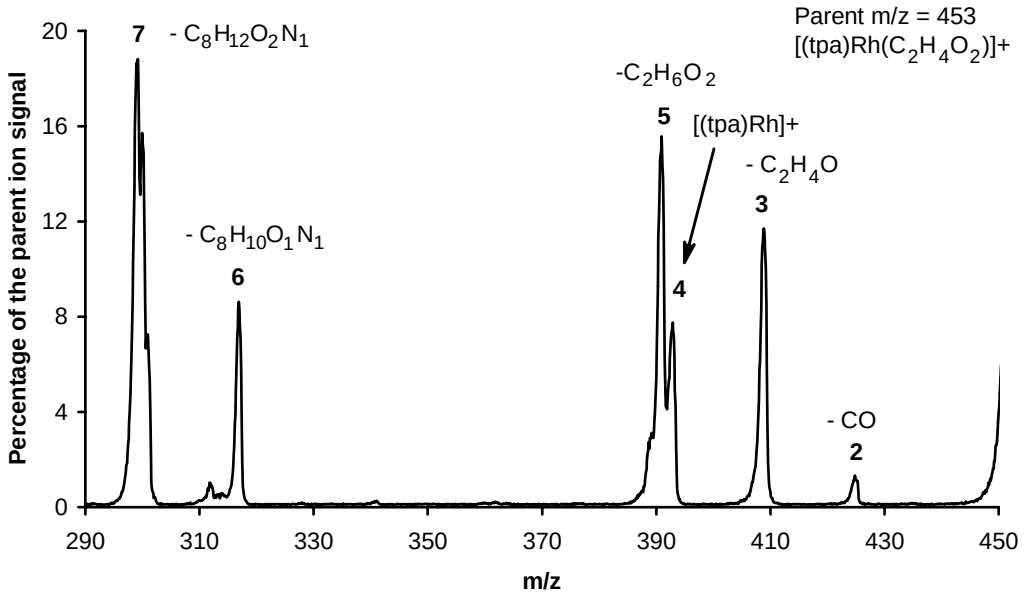

Figure 6.10 *Fragmentation of $[(tpa)Rh(C_2H_4O_2)]^+$ in RC 2 (0.2 mTorr argon, $E_{(cm)}$ = 4.9 eV)*

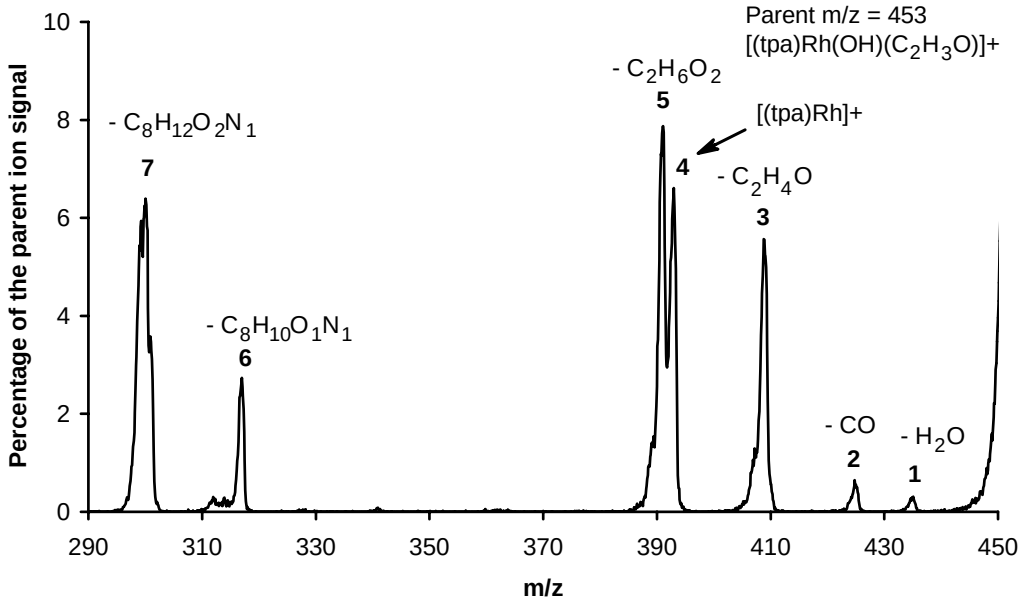

Figure 6.11 *Fragmentation of $[(tpa)Rh(OH)(C_2H_3O)]^+$ in RC 2 (0.2 mTorr argon, $E_{(cm)}$ = 4.9 eV)* [13]

[13] In both Figure 6.10 and Figure 6.11 the intensity of the parent is set to 100 %.

Other fragments that dissociate from both complexes are [14]:

- The $C_2H_4O_2$ moiety can be lost as a whole (signal **4**), after which a neutral non-radical picoline molecule [$C_5H_4NCH_3$] (signal **7**) can dissociate.
- Primary dissociation of a C_2H_4O moiety, presumably acetaldehyde (signal **3**) and then there are two possibilities: either H_2O (signal **5**) and subsequently a picolyl radical [$C_5H_4NCH_2$] (signal **7**), or only the picolyl radical [$C_5H_4NCH_2$] (signal **6**).

This loss of a radical fragment is similar to that described in § 6.4 for rhodium peroxo complexes.

There are also a few subtle differences between the spectra:

- The intensity of the daughters is lower for the hydroxy formylmethyl than for the dioxolane complex, suggesting that fragmentation of the former complex is more difficult.
- Only the hydroxy formylmethyl spectrum shows loss of H_2O from the parent (signal **1**, Figure 6.11).

It is known that the dioxolane species can easily convert to the corresponding hydroxy formylmethyl species either photochemically or in the presence of acid. [25] – [27] The similarity of the two sets of spectra makes it tempting to think that during the spraying process or upon collision with argon the dioxolane species converts into the hydroxy formylmethyl complex. However, this does not immediately explain the subtle differences between the spectra mentioned above. If isomerization *does* occur, the higher yield of daughter ions from the dioxolane might be due to the higher internal energy of the hydroxy formylmethyl ions generated via the isomerization from the dioxolane.

The main problem, however, is the exclusive loss of water from the hydroxy formylmethyl. If the dioxolane indeed isomerizes to the hydroxy formylmethyl in the mass spectrometer, *both* spectra should show loss of water. If isomerization does not occur, larger differences between the spectra would be expected.

It remains possible that signal **1** derives from an unknown species that is isobaric with the hydroxy formylmethyl complex, and is not present in the dioxolane samples we measured. However, the presence of such a species was never revealed by ^{1}H-NMR.

In conclusion, we are able to distinguish a peroxo-ethene complex from the other two complexes. We also see some differences in fragmentation patterns between the dioxolane and hydroxy formylmethyl complexes. The difference in daughter ion intensities seems real and explainable. The exclusive loss of water from the hydroxy formylmethyl remains puzzling; at present we do not have enough information to establish whether this difference is really due to different fragmentation pathways or is instead caused by the presence of an impurity in the sample of the hydroxy formylmethyl complex.

6.5.2 $[(L_N)M('O')]^+$: oxo species or not?

We were interested in the structures of the complexes left behind after dissociation of acetaldehyde from the tpa rhodium dioxolane and hydroxy formylmethyl species (signal **3**, Figure 6.10 and Figure 6.11). They have a molecular formula that corresponds to either an oxo species, $[(tpa)Rh('O')]^+$, or a hydroxy species formed by proton abstraction from the N_4 ligand at some point during the fragmentation process, $[(tpa–H^+)Rh(OH)]^+$. Therefore we compared the fragmentation behavior of these complexes with those of two compounds for which we expected the oxo-form $[(L_N)M('O')]^+$.

[14] Orders of fragmentation presented here are chosen to describe the mass spectra in a systematic way. They are consistent with the mass spectra presented here. Of course one could always imagine other routes that can lead to the same daughter signals.

Formation of $[(N_4)Rh('O')]^+$ in RC 1: Reaction with N_2O

Since N_2O is known for its single-oxygen donating properties, N_3 and N_4 rhodium and N_4 iridium ethene complexes[15] were collided with N_2O in the RC 1 (the first octopole of the TSQ 7000 [16]).
Only for the Me_2-tpa and Me_3-tpa rhodium ethene complexes a reaction took place. In both cases a signal became visible with an m/z corresponding to $[(N_4)Rh('O')]^+$, that increased upon increasing the collision gas pressure. Under the reaction conditions applied the Me_2-tpa complex is clearly less reactive than the Me_3-tpa complex: for the latter there is a large increase of a signal with an m/z corresponding to $[(L_N)Rh('O')]^+$ (see Table 6.2).

Table 6.2 *Intensities (% of the TIC) upon collision with N_2O at a manifold pressure of 6.5 10^{-6} Torr* [17]

L_N	Conditions	$[(L_N)Rh(C_2H_4)]^+$	$[(L_N)Rh('O')]^+$	$[(L_N)Rh]^+$
Me_2-tpa	Without N_2O in RC 1	95	0.4	5
	With N_2O in RC 1	90	5	5
Me_3-tpa [18]	Without N_2O in RC 1	69	5	25
	With N_2O in RC 1	38	46	15

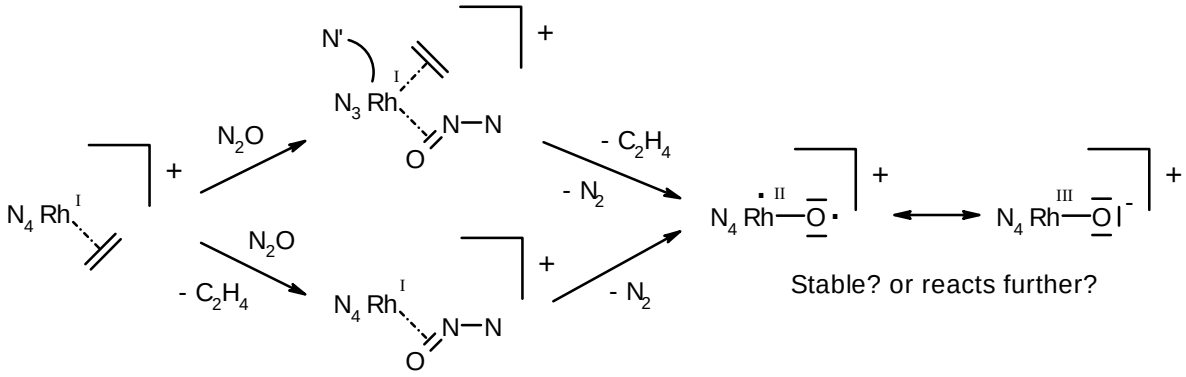

Figure 6.12 *Proposed pathways for the reaction of $[(L_N)Rh(C_2H_4)]^+$ with N_2O in RC 1*

[15] $[(Me_2\text{-bpa-Bz})Rh(C_2H_4)]^+$, $[(bpa\text{-Bz})Rh(C_2H_4)]^+$, $[(bpa)Rh(C_2H_4)]^+$, $[(tia)Rh(C_2H_4)]^+$, $[(Me_2\text{-tpa})Rh(C_2H_4)]^+$, $[(Me_3\text{-tpa})Rh(C_2H_4)]^+$, $[(tpa)Ir(C_2H_4)]^+$ and $[(Me_3\text{-tpa})Ir(C_2H_4)]^+$.

[16] As already shown in § 2.2.3, the velocity of the ions before entering RC 1 cannot be adjusted in any way. They collide with the collision gas molecules at near-zero-collision-energy. Since in RC 1 higher collision gas pressures can be used than in RC 2, higher yields are to be expected. For the TSQ 7000 it is not possible to read the collision gas pressure in RC 1 from a gauge. However, since entering a collision gas in RC 1 has its influence on the manifold pressure, increase of the manifold pressure was used as an indicator for increase of the collision gas pressure in RC 1. The manifold pressure was varied: 5.5, 6.0, 6.5 and 7.0 10^{-6} Torr.

[17] The amount of $[(L_N)Rh('O')]^+$ already present before entering N_2O in RC 1 is probably due to a reaction with air in solution in the capillary prior to the spraying process or during the spraying process in the atmospheric pressure chamber.

[18] For the Me_3-tpa complex a constant signal with an m/z corresponding to $\{[(Me_3\text{-tpa})Rh(C_2H_4)] + 16\}^+$ (oxetane?) comprises up to 1 % of the TIC. Its intensity does not change when N_2O is allowed to enter RC 1. Therefore, it was probably formed in a reaction with air in solution, prior to the spraying process. $[(L_N)Rh(\text{oxetane})]^+$ and $[(L_N)Rh(N_2O)]^+$ are isobaric species. However, since the intensity of that signal does not change upon entering N_2O in RC 1, we do not have any indication that $[(Me_3\text{-tpa})Rh(N_2O)]^+$ is formed in RC 1 upon collision of $[(Me_3\text{-tpa})Rh(C_2H_4)]^+$ with N_2O.

For both complexes the intensity of the naked species remains nearly the same during the reaction and the intensity of the ethene complex decreases. In other words, it appears as if it is only the ethene complex that is responsible for product formation and not just the naked species $[(N_4)Rh]^+$. This is however, not very likely: the naked species are expected to be highly reactive and are known to react with dioxygen in the gas phase (as will be shown in § 7.5.1). There is no reason to expect that towards N_2O they would be less reactive. Therefore, we propose the reaction paths for the reaction with dinitrogenmonoxide in RC 1 shown in Figure 6.12.

Since the oxo species formed is expected to be a very strong base, rapid formation of a 2-rhodaoxetane would be expected in those cases where the olefin is still bound to the metal center as soon as N_2 has dissociated. Formation of such a species upon collision with N_2O is, however, not observed.

For the iridium complexes it is expected that their kinetics is too slow for such a reaction to be observed in RC 1. However, why none of the N_3 rhodium complexes investigated is reactive towards N_2O although they should have a coordination site available for N_2O, we do not know.

The huge decrease in reactivity on removal of one of the methyl substituents of the N_4 ligand suggests that (at least for the N_4 complexes) dissociation of the olefin or a pyridyl donor could be the rate-limiting step[19].

As shown by Schröder *et al.* [28] two types of bonding schemes can be proposed for oxo species in general: (i) a low-spin M=O species having a formal double bond between the metal and oxygen (early transition metals), and (ii) a diradicaloid high-spin $M^{\bullet}$-$O^{\bullet}$ with a covalent σ-bond and resonating π-interactions (for example iron). A recent theoretical study [29] suggests that for tpa-like rhodium and iridium complexes a zwitterionic description M^+-O^- is more appropriate (see Figure 6.12 on the right).

That the Me_2-tpa and Me_3-tpa rhodium oxo species do have a radical character becomes visible when looking at their fragmentation behavior (Figure 6.13).

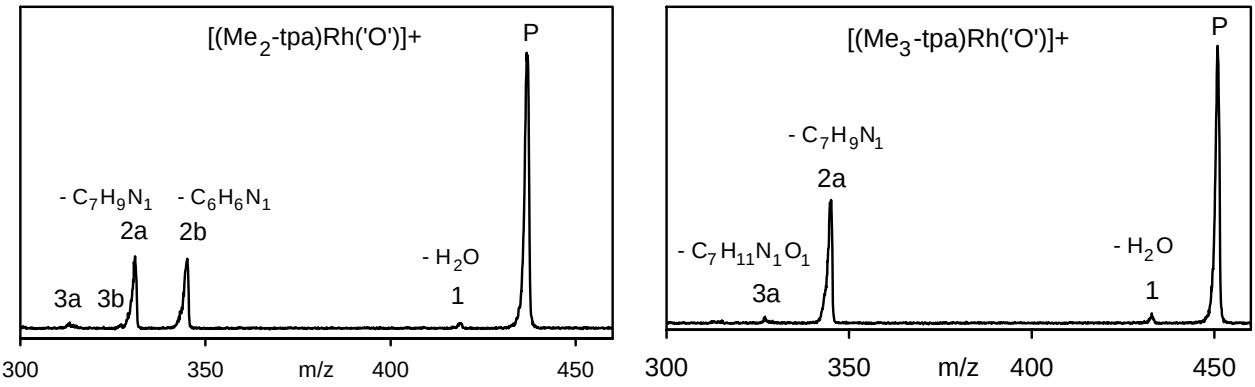

Figure 6.13 *Fragmentation of $[(L_N)Rh('O')]^+$ upon collision with 0.2 mTorr argon in ($E_{(lab)}$ = 50 eV)* [20]

Only small amounts of H_2O (signal **1**) are lost. Mainly lutidyl (signal **2a**) or picolyl (signal **2b**) radicals are dissociated from these oxo species. Once H_2O is lost, it is also possible to lose those same lutidyl (signal **3a**) or picolyl (signal **3b**) radicals.

Oxo species are quite rare for the late transition metals. The low stability of these oxo species is due to the lack of M-O π-bonding. [30] The reason for this is that the π-orbitals of these metal(III) species into which the di-anionic oxo ligand, O^{2-}, could have donated its electron density, are already occupied. Therefore, the M-O bond order will be less than 2. [29], [30]

[19] The olefin is more strongly bound to the metal center in the tpa complex than in the Me_3-tpa complex (Appendix A).

[20] This corresponds to an $E_{(cm)}$ for the Me_3-tpa complex of 4.0 eV and for the Me_2-tpa complex of 4.2 eV.

As a result such late transition metal oxo species are expected to be highly reactive: (i) abstracting protons of other ligands coordinated to the metal center, hereby favoring dissociation of parts of these ligands, or (ii) insertion of the oxo moiety into one of the bonds of one these ligands.

It is therefore remarkable to see that upon collision with N_2O relatively "stable" oxo species [21] are formed.

Comparison of the fragmentation behavior of the different $[(L_N)Rh('O')]^+$ species

The fragmentation behavior of the Me_2-tpa and Me_3-tpa rhodium oxo species (Figure 6.13) is compared with that of the species left behind after dissociation of C_2H_4O from the tpa rhodium dioxolane or hydroxy formylmethyl species (a species with an m/z corresponding to $[(tpa)Rh('O')]^+$ or $[(tpa–H^+)Rh(OH)]^+$, Figure 6.14).

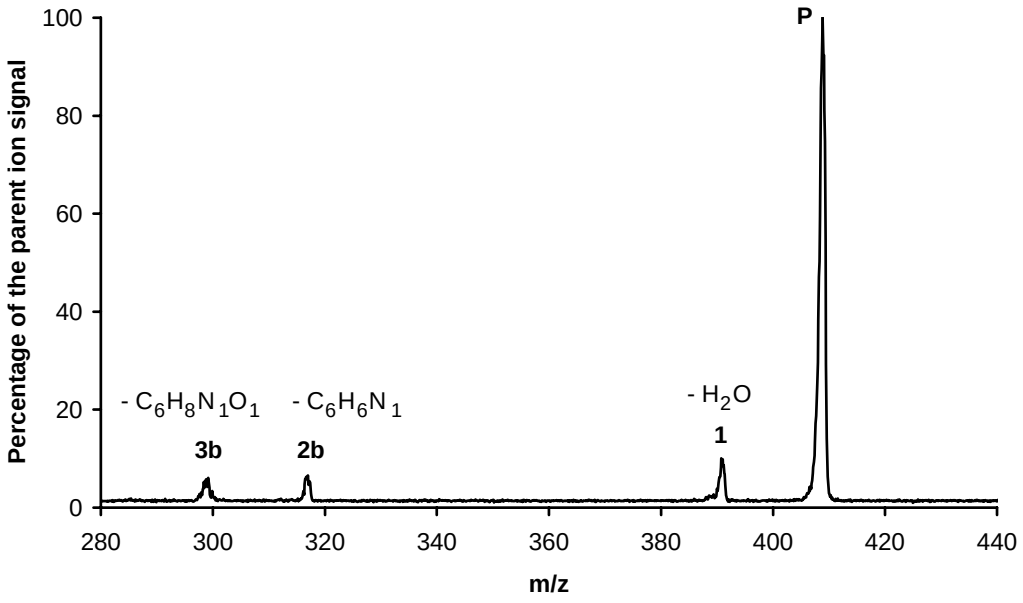

Figure 6.14 *Fragment of the dioxolane species: $[(tpa)Rh('O')]^+$ or $[(tpa–H^+)Rh(OH)]^+$? Fragmentation behavior upon collision with 0.2 mTorr argon ($E_{(lab)}$ = 40 eV or $E_{(cm)}$ = 3.6 eV)*

In all three spectra loss of H_2O (signal **1**) constitutes a minor pathway: the ratio between the parent signal and signal **1** is in all three mass spectra small. Once H_2O has been lost, a picolyl radical (signal **3a** and **3b**) can be lost for all three complexes. In Figure 6.14 the intensity of signal **3b** is somewhat higher than that of signals **3a** and **3b** in Figure 6.13, as if loss of H_2O might be somewhat more favorable for the tpa complex.

If the mass spectra displayed in Figure 6.13 truly belong to oxo complexes, then a somewhat decreased loss of H_2O could be explained by proposing another reaction path for these species besides proton abstraction from the N_4 ligand, e.g. insertion of the oxygen into a rhodium-pyridine bond after which no loss of H_2O is expected anymore.

Loss of part of the N_4 ligand (picolyl radical: signal **2b**; lutidyl radical: signal **2a**) is suppressed for the tpa complex compared to the Me_3-tpa and Me_2-tpa species displayed in Figure 6.13.

From the experiments, we conclude that the Me_2-tpa and Me_3-tpa species formed upon collision with N_2O seem to behave like oxo species, whereas the species left behind when the tpa dioxolane and hydroxy formylmethyl species have lost C_2H_4O appears to be a hydroxo species in which a hydrogen atom has been abstracted from the N_4 ligand.

[21] Although we believe we are dealing with oxo species here, we cannot exclude that upon formation they might have rapidly rearranged e.g. to energetically more favorable hydroxo species.

6.6 Concluding remarks

Collision experiments are an excellent way of getting an idea of differences in binding strengths of certain ligands to a metal center (e.g. ethene) in favorable cases. Structural changes in solution during which the m/z of a species does not change (e.g. aromatic C-H activation) can easily be noticed.

Our results suggest that the fragmentation patterns also provide some information about the electronic ground state of the complexes: neutral non-radical species preferably dissociate from species with a singlet ground state (e.g. $[(L_N)M(C_2H_4)]^+$, $[(L_N)M]^+$), whereas neutral radical species preferably dissociate from species with a ground state that has apparently more radical character (e.g. $[(L_N)M(O_2)]^+$, $[(L_N)M('O')]^+$).

Mass spectrometric measurements have given us some clues on the structures of compounds. However, obtaining conclusive evidence using mass spectrometry alone remains difficult.

6.7 Experimental section

6.7.1 General methods

All procedures were performed under a nitrogen atmosphere using standard Schlenck techniques, unless indicated otherwise. Solvents (p.a.) were deoxygenated by bubbling through a stream of nitrogen or by the freeze-pump-thaw method. Some solvents were distilled under a nitrogen atmosphere to remove last traces of water and dioxygen: acetonitrile was distilled over potassium, THF over CaH_2 and CH_2Cl_2 also over CaH_2. The temperature indication r.t. corresponds to ca. 20 ºC.

Tpa [31], tia [32], bpa-Bz [33], $[(tpa)Rh(C_2H_4)]PF_6$ [34], $[(tia)Rh(C_2H_4)]PF_6$ [27], $[(bpa\text{-}Bz)Rh(C_2H_4)]PF_6$ [35], (tpa)Rh(dioxolane)]BPh_4 and [(tpa)Rh(OH)(formylmethyl)]BPh_4 [25], [26], [36], $[\{(C_2H_4)_2Rh(\mu\text{-}Cl)\}_2]$ [37] were prepared according to literature procedures.

All other chemicals are commercially available and were used without further purification, unless stated otherwise.

6.7.2 Calculations

All geometry optimizations were carried out with the Turbomole program [38] coupled to the PQS Baker optimizer. [39], [40] Geometries were fully optimized as minima at the bp86 [41], [42] level using the Turbomole SV(P) basis set [22] [43] on all atoms. Improved energies were obtained from single-point calculations at the b3-lyp level [44] – [47] using the TZVPP basis [48]. Entropy corrections (to obtain $\Delta G_{343\,K,\,0.001\,bar}$ and $\Delta G_{298\,K,\,1\,bar}$) were performed to take into account that the number of reactants is not always the same as the number of products. They were performed according to standard formulas of statistical thermodynamics. [47]

6.7.3 ESI^+-MS measurements

General ESI-MS setup for the experiments

The electrospray ionization (ESI) mass spectra were measured either on a slightly modified Finnigan MAT TSQ 7000 or on a modified Finnigan MAT TSQ 700 as previously described. [49] – [67]

Typically solutions with a concentration of 10^{-5} M of the desired compounds (prepared in the glove-box under a nitrogen atmosphere) were electrosprayed at a flow-rate of 3 – 15 µl/min at 3 – 5 kV and a capillary temperature of 150 ºC. In some cases dinitrogen was used as a sheath gas. The tube lens potential was varied between 35 and 140 V (referenced to m/z = 500) depending on the complex.

For most of the measurements either solutions in pure THF or in 0.02 % MeCN in THF were used depending on the solubility of the compounds. For the measurements in the tube lens region as described in § 6.4 for the Me_2-bpa-Me, tpa and Me_2-bpa-Bz also measurements were performed in acetone to see if the product yield changed upon changing the solvent. The solvent appeared to be not of influence. The tpa rhodium dioxolane and hydroxy formylmethyl complexes were dissolved in pure MeCN.

Daughter-ion spectra were recorded in daughter-ion mode, that is, the first quadrupole was used to mass select ions of a single mass-over-charge ratio, which were then collided with a target gas in the second reaction chamber (RC 2). The second

[22] Turbomole basis set library, Turbomole Version 5, see reference 38.

quadrupole was operated in scanning mode in order to detect the ionic fragments. The collision energy could be varied by applying different potentials (to a lens in front of the second octopole), which altered the velocity of the ions on their way into the collision region (the collision energies are given in eV, lab frame).

The pressure in RC 2 of the TSQ 700 was read both from a Pirani gauge and with a Capacitance gauge. The pressure in the 24-pole (RC 1 of the TSQ 700) was also read from a Pirani gauge. The pressures of the Pirani gauges were calibrated to those displayed by the Capacitance gauge (see for more details the Experimental of Chapter 2). The pressure in RC 2 of the TSQ 7000 was measured by a cold-cathode gauge. All gauges are directly attached to the housing of the multipoles.

Reactions in the 24-pole region (RC 1)

Experiments with pickup of substrates/ligands in the 24-pole region (RC 1) were carried out by first setting the tube lens potential such as to optimize the yield of the desired complex ion and then bleeding in the gaseous ligand with a needle valve. The liquid ligands used as reactants were thoroughly degassed by freeze–pump techniques.

Mass spectra have been measured at 4 or 5 different pressures to see if the yield if any increases upon increase of the collision gas pressure. Collision-induced dissociation (CID) experiments on the generated ions can then be performed by collision with argon in RC 2 (in which the collision energy can be varied by applying different field potentials which alters the velocity of the ions on their way into the collision region).

As already shown in § 2.2.3, the velocity of the ions before entering RC 1 cannot be adjusted in any way. They collide with the collision gas molecules at near-zero-collision-energy. Since in RC 1 higher collision gas pressures can be used than in RC 2, higher yields are to be expected. For the TSQ 7000 it is not possible to read the collision gas pressure in RC 1 from a gauge. However, since entering a collision gas in RC 1 has its influence on the manifold pressure, increase of the manifold pressure was used as an indicator for increase of the collision gas pressure in RC 1 during the N_2O experiments. The manifold pressure was varied (5.5, 6.0, 6.5 and 7.0 10^{-6} Torr) in order to maintain a same collision gas pressure during all measurements.

Reactions in the octopole region (RC 2)

All CID measurements in RC 2 were carried out in daughter-ion mode, i.e. the first quadrupole was used to mass select ions of a single m/z, which were then collided with a target gas in the octopole region (RC 2). The second quadrupole Q2 was operated in scanning mode and served to detect the ionic collision products. The tube lens potential was again set such as to optimize the yield of the desired complex ion.

For the measurements described in § 6.3 argon pressures of either 0.4 or 0.8 mTorr were used. For the measurements described in § 6.5 an argon pressure of 0.2 mTorr was used. The collision energy can be varied by applying different potentials (to a lens in front of the second octopole), which serves to alter the velocity of the ions on their way into the collision region. The collision energies (eV) given in the laboratory frame, $E_{(lab)}$, are then converted to the center of mass frame, $E_{(cm)}$ as described in § 6.2.

6.8 References

[1] F. Galliano, R. Saletti, V. Cunsolo, S. Foti, D. Marletta, S. Bordonaro and G. D'Urso, *Rapid Commun. Mass Spectrom.*, **2004**, *18 (17)*, 1972-1982
[2] P. Ferranti, *Eur. J. Mass Spectrom.*, **2004**, *10 (3)*, 349-358
[3] V. Cunsolo, S. Foti and R. Saletti, *Eur. J. Mass Spectrom.*, **2004**, *10 (3)*, 359-370
[4] C. Koy, M. Resch, K. Tanaka and M. O. Glocker, *Eur. J. Mass Spectrom.*, **2004**, *10 (3)*, 393-399
[5] A. P. M. de Brouwer, C. Versluis, J. Westerman, B. Roelofsen, A. J. R. Heck and K. W. A. Wirtz, *Biochemistry*, **2002**, *41 (25)*, 8013-8018
[6] J. A. A. Demmers, A. van Dalen, B. de Kruijff, A. J. R. Heck and J. A. Killian, *FEBS Lett.*, **2003**, *541 (1-3)*, 28-32
[7] M. I. Catalina, N. J. de Mol, M. J. E. Fischer and A. J. R. Heck, *Phys. Chem. Chem. Phys.*, **2004**, *6 (10)*, 2572-2579
[8] S. D. Friess, J. M. Daniel, R. Hartmann and R. Zenobi, *Int. J. Mass Spectrom.*, **2002**, *219 (1)*, 269-281
[9] K. M. Koshy and J. M. Boggs, *J. Biol. Chem.*, **1996**, *271 (7)*, 3496-3499
[10] G. Hopfgartner, F. Vilbois and C. Piguet, *Rapid Commun. Mass Spectrom.*, **1999**, *13 (5)*, 302-306
[11] H. Rogniaux, A. Van Dorsselaer, P. Barth, J. F. Biellmann, J. Barbanton, M. van Zandt, B. Chevrier, E. Howard, A. Mitschler, N. Potier, L. Urzhumtseva, D. Moras and A. Podjarny, *J. Am. Soc. Mass Spectrom.*, **1999**, *10 (7)*, 635-647
[12] P. J. Vollmerhaus, F. W. A. Tempels, J. J. Kettenes-van den Bosch and A. J. R. Heck, *Electrophoresis*, **2002**, *23 (6)*, 868-879
[13] Y. M. Chen and P. B. Armentrout, *J. Chem. Phys.*, **1995**, *103 (2)*, 618-625
[14] D. Feichtinger, *PhD Thesis ETH No. 13595 "Untersuchung der intrinsischen Reaktivitaet von metallorganischen Katalysatoren mittels Elektrospray Tandem Massenspektrometrie"*, **2000**
[15] A. G. Harrison, *J. Mass Spectrom.*, **1999**, *34 (12)*, 1253-1273

[16] N. L. Bosma and A. G. Harrison, *Can. J. Chem. - Rev. Can. Chim.*, **1994**, *72 (11)*, 2205-2211
[17] S. Beranova and C. Wesdemiotis, *Int. J. Mass Spectrom. Ion Process.*, **1994**, *134 (2-3)*, 83-102
[18] H. Mestdagh, N. Morin and C. Rolando, *Org. Mass Spectrom.*, **1988**, *23 (4)*, 246-251
[19] H. J. Veith, *Org. Mass Spectrom.*, **1983**, *18 (4)*, 154-158
[20] M. Ohashi, R. P. Barron and W. R. Benson, *J. Am. Chem. Soc.*, **1981**, *103 (13)*, 3943-3945
[21] W. Wagner, H. Heimbach and K. Levsen, *Int. J. Mass Spectrom. Ion Process.*, **1980**, *36 (2)*, 125-142
[22] M. Fischer and H. J. Veith, *Helv. Chim. Acta*, **1978**, *61 (8)*, 3038-3049
[23] H. H. Gierlich, F. W. Rollgen, F. Borchers and K. Levsen, *Org. Mass Spectrom.*, **1977**, *12 (6)*, 387-390
[24] J. N. Harvey, M. Diefenbach, D. Schröder and H. Schwarz, *Int. J. Mass Spectrom.*, **1999**, *183*, 85-97
[25] M. Krom, R. G. E. Coumans, J. M. M. Smits and A. W. Gal, *Angew. Chem. - Int. Edit.*, **2002**, *41 (4)*, 576-579
[26] M. Krom, T. P. J. Peters, R. G. E. Coumans, T. J. J. Sciarone, J. Hoogboom, S. I. ter Beek, P. P. J. Schlebos, J. M. M. Smits, R. de Gelder and A. W. Gal, *Eur. J. Inorg. Chem.*, **2003**, *6*, 1072-1087
[27] M. Krom, *PhD Thesis "Mono- and Dioxygenation of Rhodium and Iridium Olefin Fragments, Solution versus Solid State Reactivity"*, **2003**
[28] D. Schröder, H. Schwarz and S. Shaik, "*Characterization, orbital description, and reactivity patterns of transition-metal oxo species in the gas phase*", *Metal-Oxo and Metal-Peroxo Species in Catalytic Oxidations*, Vol. 97, Eds. Springer-Verlag, Berlin, **2000**, 91-123
[29] P. H. M. Budzelaar and A. N. J. Blok, *Eur. J. Inorg. Chem.*, **2004**, *(11)*, 2385-2391
[30] T. R. Cundari, *Chem. Rev.*, **2000**, *100 (2)*, 807-818
[31] G. Anderegg and F. Wenk, *Helv. Chim. Acta*, **1967**, *50 (8)*, 2330
[32] K. J. Oberhausen, R. J. Obrien, J. F. Richardson and R. M. Buchanan, *Inorg. Chim. Acta*, **1990**, *173 (2)*, 145-154
[33] B. de Bruin, J. A. Brands, J. J. J. M. Donners, M. P. J. Donners, R. de Gelder, J. M. M. Smits, A. W. Gal and A. L. Spek, *Chem. - Eur. J.*, **1999**, *5 (10)*, 2921-2936
[34] B. de Bruin, M. J. Boerakker, J. A. W. Verhagen, R. de Gelder, J. M. M. Smits and A. W. Gal, *Chem. - Eur. J.*, **2000**, *6 (2)*, 298-312
[35] B. de Bruin, J. A. W. Verhagen, C. H. J. Schouten, A. W. Gal, D. Feichtinger and D. A. Plattner, *Chem. - Eur. J.*, **2001**, *7 (2)*, 416-422
[36] M. Krom, R. G. E. Coumans, J. M. M. Smits and A. W. Gal, *Angew. Chem. - Int. Edit.*, **2001**, *40 (11)*, 2106-2108
[37] R. Cramer, J. A. McCleverty and J. Bray, *Inorg. Synth.*, **1990**, *28*, 86
[38] R. Ahlrichs, M. Bär, H.-P. Baron, R. Baurernschmitt, S. Böcker, M. Ehrig, K. Eichkorn, S. Elliot, F. Furche, F. Haase, M. Häser, C. Hättig, H. Horn, C. Huber, U. Huniar, M. Kattannek, A. Köhn, C. Kölmel, M. Kollwitz, K. May, C. Ochsenfeld, H. Öhm, A. Schäfer, U. Schneider, O. Treutler, K. Tsereteli, B. Unterreiner, M. von Arnim, F. Weigend, P. Weis and H. Weiss, *"Turbomole Version 5"*; Theoretical Chemistry Group, University of Karlsruhe, **January 2002**
[39] *"PQS version 2.4"*; Parallel Quantum Solutions, Fayetteville, Arkansas, USA (the Baker optimizer is available seperately from PQS upon request), **2001**
[40] J. Baker, *J. Comput. Chem.*, **1986**, *7 (4)*, 385-395
[41] A. D. Becke, *Phys. Rev. A*, **1988**, *38 (6)*, 3098-3100
[42] J. P. Perdew, *Phys. Rev. B*, **1986**, *33 (12)*, 8822-8824
[43] A. Schäfer, H. Horn and R. Ahlrichs, *J. Chem. Phys.*, **1992**, *97 (4)*, 2571-2577
[44] A. D. Becke, *J. Chem. Phys.*, **1993**, *98 (2)*, 1372-1377
[45] A. D. Becke, *J. Chem. Phys.*, **1993**, *98 (7)*, 5648-5652
[46] C. T. Lee, W. T. Yang and R. G. Parr, *Phys. Rev. B*, **1988**, *37 (2)*, 785-789
[47] P. W. Atkins, *"Physical Chemistry"*, Oxford University Press, Oxford, **1994**
[48] A. Schäfer, C. Huber and R. Ahlrichs, *J. Chem. Phys.*, **1994**, *100 (8)*, 5829-5835
[49] C. Hinderling, D. Feichtinger, D. A. Plattner and P. Chen, *J. Am. Chem. Soc.*, **1997**, *119 (44)*, 10793-10804
[50] C. Hinderling, D. A. Plattner and P. Chen, *Angew. Chem. - Int. Edit.*, **1997**, *36 (3)*, 243-244
[51] D. Feichtinger, D. A. Plattner and P. Chen, *J. Am. Chem. Soc.*, **1998**, *120 (28)*, 7125-7126
[52] C. Hinderling and P. Chen, *Angew. Chem. - Int. Edit.*, **1999**, *38 (15)*, 2253-2256
[53] C. Hinderling and P. Chen, *Int. J. Mass Spectrom.*, **2000**, *196*, 377-383
[54] G. Gerdes and P. Chen, *Organometallics*, **2003**, *22 (11)*, 2217-2225
[55] P. Chen, *Angew. Chem. - Int. Edit.*, **2003**, *42 (25)*, 2832-2847
[56] D. A. Plattner, *Int. J. Mass Spectrom.*, **2001**, *207 (3)*, 125-144
[57] C. Hinderling, C. Adlhart and P. Chen, *Angew. Chem. - Int. Edit.*, **1998**, *37 (19)*, 2685-2689
[58] C. Adlhart and P. Chen, *Helv. Chim. Acta*, **2000**, *83 (9)*, 2192-2196
[59] C. Adlhart, M. A. O. Volland, P. Hofmann and P. Chen, *Helv. Chim. Acta*, **2000**, *83 (12)*, 3306-3311
[60] C. Adlhart and P. Chen, *Helv. Chim. Acta*, **2003**, *86 (4)*, 941-949
[61] Y. M. Kim and P. Chen, *Int. J. Mass Spectrom.*, **2000**, *202 (1-3)*, 1-7
[62] G. Gerdes and P. Chen, *Organometallics*, **2004**, *23 (12)*, 3031-3036
[63] D. Feichtinger and D. A. Plattner, *Chem. - Eur. J.*, **2001**, *7 (3)*, 591-599
[64] M. A. O. Volland, C. Adlhart, C. A. Kiener, P. Chen and P. Hofmann, *Chem. - Eur. J.*, **2001**, *7 (21)*, 4621-4632
[65] D. A. Plattner, D. Feichtinger, J. El-Bahraoui and O. Wiest, *Int. J. Mass Spectrom.*, **2000**, *196*, 351-362
[66] D. Feichtinger and D. A. Plattner, *J. Chem. Soc. - Perkin Trans. 2*, **2000**, *5*, 1023-1028
[67] D. Feichtinger and D. A. Plattner, *Angew. Chem. - Int. Edit.*, **1997**, *36 (16)*, 1718-1719

Chapter 7

Gas-Phase Reactivities of N_3 and N_4 Rhodium and Iridium Complexes

7.1 Introduction

As we have seen in Chapter 4, the ethene complexes discussed in this thesis react with dioxygen in solution yielding a number of products, depending on the type of metal center and the nitrogen donor ligand used. In the case of rhodium only peroxo complexes could be isolated, in the case of iridium only peroxo-ethene complexes. In all cases in which a reaction towards dioxygen was observed paramagnetic species, which we could not identify, were formed.

In this chapter we investigate the corresponding gas-phase reactions.

Depending on the type of nitrogen donor ligand used, products could be formed via one of the following reactions:

a) An associative mechanism for the N_3 complexes, in which dioxygen coordinates to the metal-olefin complex, resulting in a peroxo-ethene complex, possibly followed by subsequent dissociation of the olefin.

b) A dissociative mechanism for both the N_3 and the N_4 complexes, in which dissociation of ethene is required prior to a reaction with dioxygen.

c) For the N_4 complexes another type of dissociative mechanism is possible: one in which the ligand becomes κ^3-coordinated, via dissociation of one of the pyridyl-arms. Subsequently the κ^3-N_4 ethene complex can react either via an associative mechanism as under **a)**, or via a dissociative mechanism as under **b)**.

d) For both N_3 and N_4 complexes initial formation of paramagnetic species via single-electron transfer (SET) between dioxygen and the metal center could be envisaged, judging from their redox potentials.

7.1.1 A comparison of the proposed gas-phase oxidation reactions

Reaction **d)** is highly unlikely for gas-phase reactions for several reasons. In a SET reaction separation of charge takes place (e.g. an ion-molecule pair with charges +1 / 0 becomes a contact ion pair with charges +2 / -1). Contrary to solution-phase chemistry where the solvent can play an important role in stabilizing this contact ion pair, this separation of charge probably cannot be stabilized in the gas phase. Even if charge separation to the ion pair could occur, the ions would never be able to separate in the gas phase, so the +2 ion would never be detected by MS. Therefore SET reactions should be energetically unfavorable in the gas phase for our mono-cationic metal-olefin complexes. [1, 2]

[1] This is not universally true. It holds only for the mono-cationic complexes discussed.
If, for example, a dicationic complex A^{2+} would be collided with a neutral gas molecule B^0, then a reaction like: $A^{2+} + B^0 \rightarrow A^+ + B^+$ would be more favorable.

The other reason why SET reactions are unlikely to happen in the gas phase is that according to the Marcus theory [1] both reagents (ox and red) need to adjust their geometries towards the product geometries (red' and ox'). According to the Franck-Condon principle [2] the positions of the nuclei are fixed at the timescale of the electron transfer reaction. There are only vertical transitions possible between the potential surfaces of reactants and products as shown in Figure 7.1.

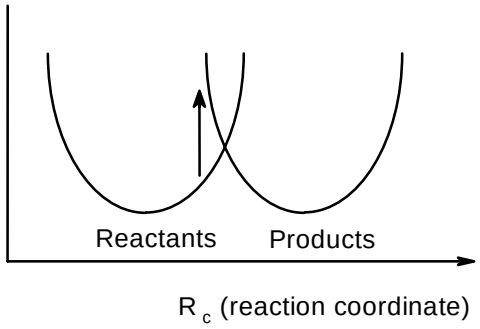

Figure 7.1 *Schematic view of potential surfaces of reactants and products and their crossing point*

Since a transition at the position of the arrow would cost too much energy, the reactants have to rearrange so to adjust their geometry in agreement with the one at the crossing point of the potential surfaces of the reactants and products. At the crossing point electron transfer is possible without a further barrier.

In the gas phase the ion-molecule pair is most probably not long-lived enough to permit the geometric rearrangements for required SET. The barrier for this reorganization is significant, only a small fraction of the molecules will have the right geometry upon collision for a reaction at the moment of collision. Increasing the collision energy does not help much because it also decreases the lifetime of the encounter complex.

Therefore, "pure" single-electron-transfer reactions seem highly unlikely in the gas phase.

Figure 7.2 summarizes the most likely chemistry expected for the remaining three types of reaction: **a)**, **b)** and **c)**. For the N_4 complexes the reaction scheme starts from complex [**A**], for the N_3 complexes from complex [**B**].

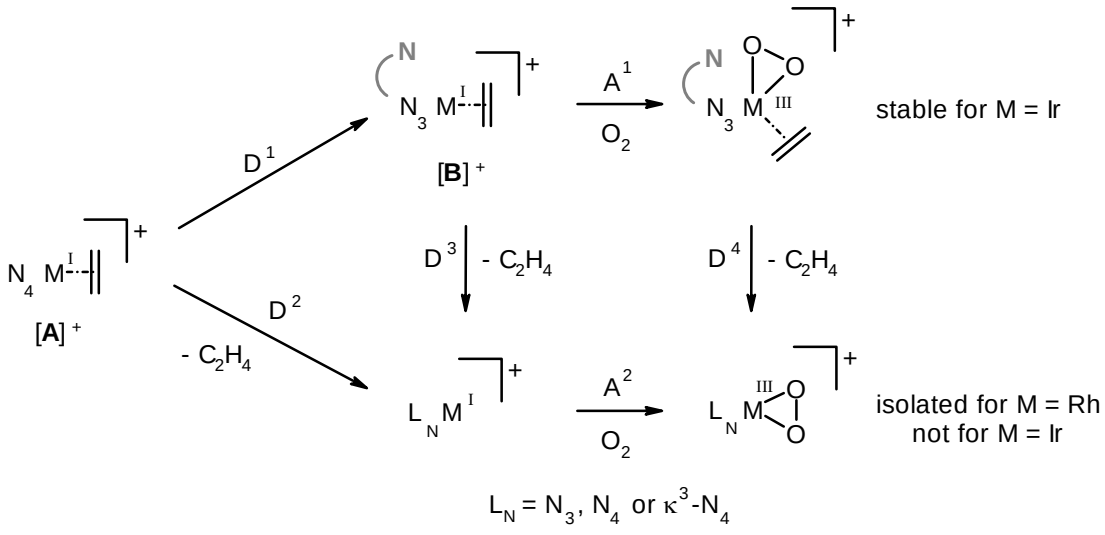

Figure 7.2 *Reactions expected for the reaction of metal-olefin complexes with dioxygen on the basis of an associative ("A") or dissociative ("D") mechanism*

[2] Of course, SET can still play a role as the first step of a series of reactions occurring *within* the ion-molecule pair.

According to the associative mechanism *A*[1] the N_3 metal(I) ethene complexes initially form metal(III) peroxo-ethene complexes, which are either stable or decompose via dissociation of the olefin to the corresponding metal(III) peroxo complexes. Metal(III) centers are less capable of π-back donation in the π^* orbital of the olefin, so olefin loss from these complexes should be easy (see § 4.2.1).

Alternatively, N_3 metal(III) peroxo species could be obtained via dissociation of the olefin followed by reaction of the naked species, $[(N_3)M]^+$, with dioxygen. This will be further addressed as the dissociative mechanism *D*[3].

After dissociation of a pyridyl arm the N_4 ethene complexes could follow a reactivity pattern similar to that of the N_3 complexes.

7.1.2 Associative versus dissociative mechanisms

As already mentioned in § 4.4, in most square-planar systems ligand exchange in solution occurs via an associative mechanism (most kinetic studies of this kind are based on Pt(II) and Pd(II) systems). A five-coordinate intermediate forms first, followed by departure of the leaving ligand. Although dissociative substitution at square planar d8 transition metal complexes is not as common, there are still numerous examples involving dissociation to a T-shaped 3-coordinate intermediate. [3] – [23]

In the field of gas-phase reactions, it was reported by Bossio *et al.* [24] that a square planar rhodium(I) complex, trans-$[Rh(PPh_3)_2(CO)(4\text{-picoline})]^+$, can exchange pyridine for its 4-picoline ligand readily via a dissociative substitution pathway.

Therefore, both reaction pathways, associative and dissociative, have to be considered for gas-phase reactions.

In order to get an idea of the energies associated with the reactions depicted in Figure 7.2, the geometries of all the species proposed were optimized with DFT for some N_3 and N_4 rhodium and iridium complexes as presented in Appendix A. [3] Only for the associative reaction the energy barrier was calculated (= the Minimum Energy Crossing Point (MECP), as presented in § 4.4). Since the results bpa *vs.* bpa-Me as well as Me_2-bpa *vs.* Me_2-bpa-Me are nearly identical, graphical representations of the results for the $\Delta H_{0\,K}$ calculations for the Me_2-bpa-Me and bpa-Me rhodium and iridium species are shown in Figure 7.3a and Figure 7.3b on the next page. [4, 5]

According to the calculations all species involved are much more stabilized with respect to the naked species for the bpa type of complexes than for the Me_2-bpa type of complexes.

---

[3] As already mentioned in Appendix A and § 6.3, in RC 2 the enthalpy $\Delta H_{0\,K}$ is probably the appropriate quantity to use. In RC 1 and the tube lens region the collision gas pressures are so high that it is not clear whether use of the enthalpy $\Delta H_{0\,K}$ or of the free free energy $\Delta G_{343\,K,\,0.001\,bar}$ (70 ºC and 0.001 bar, spectrometer conditions) is more appropriate.

[4] At a MECP the electron movement changes abruptly upon a small change in the nuclei. In other words, the Born-Oppenheimer approximation is not valid anymore and calculation of entropy corrections is not possible. In order to obtain the free energies of the optimized MECP structures after all, we took the difference in $\Delta H_{0\,Kelvin}$ between the MECP structure and the corresponding peroxo-ethene complex and added this to the $\Delta G_{298\,K,\,1\,bar}$ of the peroxo complex.

[5] The reference energy of $^3O_2$ is adjusted upwards by 18 kcal/mol when calculating relative energies (see Appendix A for an explanation).

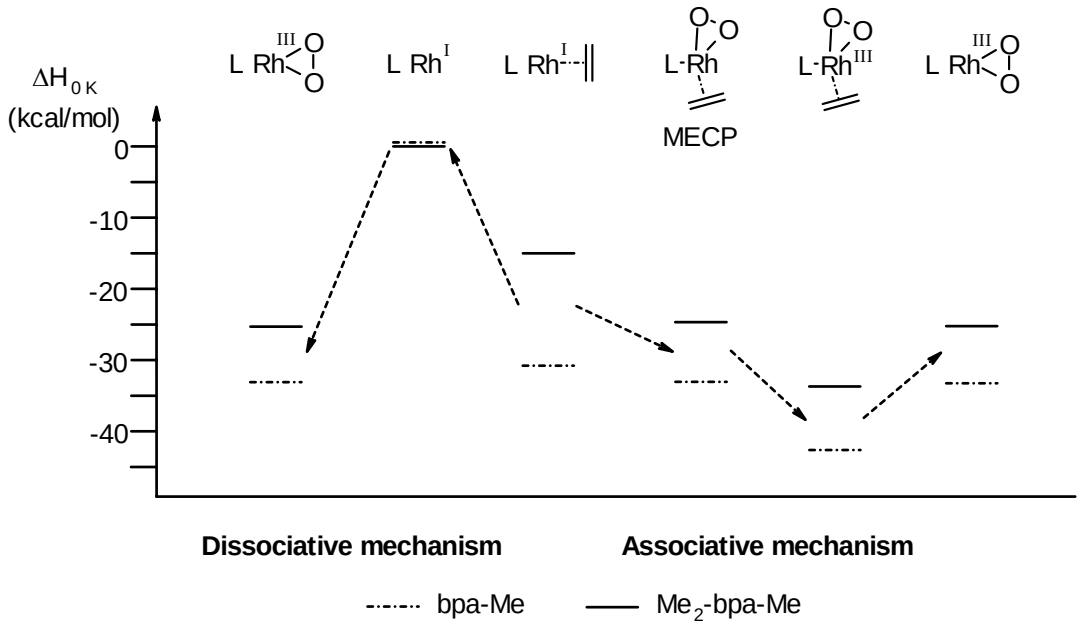

Figure 7.3a *Enthalpies $\Delta H_{0\,K}$ calculated for the bpa-Me and Me_2-bpa-Me rhodium species*

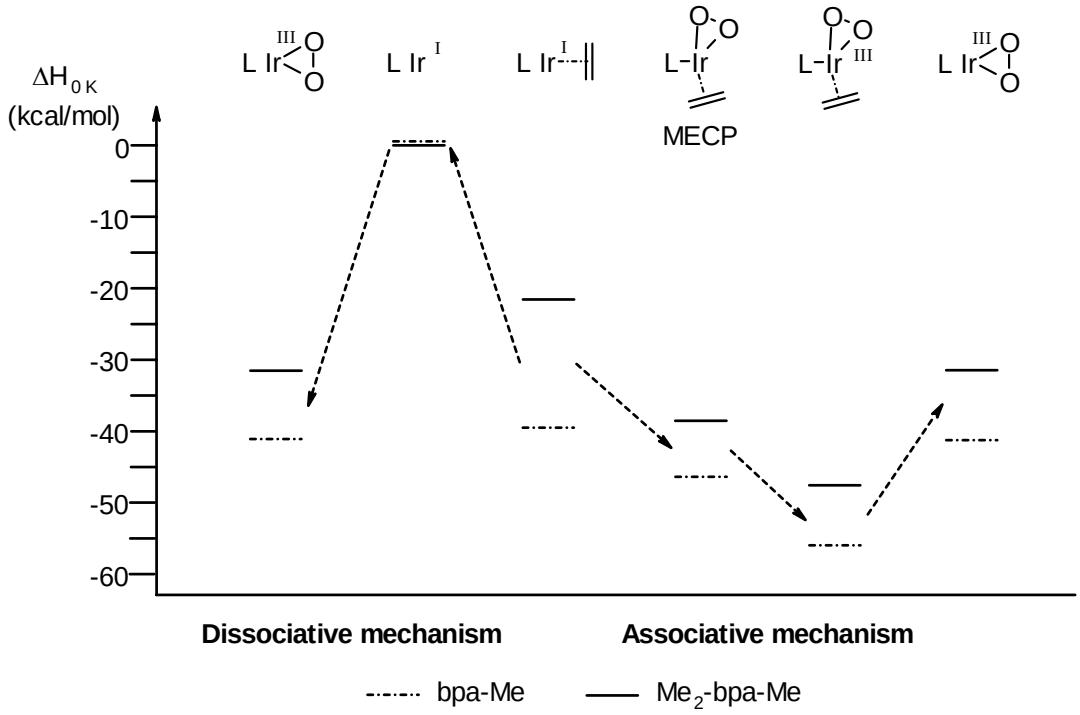

Figure 7.3b *Enthalpies $\Delta H_{0\,K}$ calculated for the bpa-Me and Me_2-bpa-Me iridium species*

When going along the associative pathway the mono-ethene complex can react with dioxygen under formation of the more stable peroxo-ethene complex. The energy of the MECP lies in all cases below that of the olefin complex[6], indicating that the formation of a peroxo-ethene complex should be facile.

If this gaseous product ion can get rid of its excess internal energy by collisions with other gas molecules, the peroxo-ethene complex will be the only product formed. However, if the peroxo-ethene complex cannot get rid of this excess of internal energy, the energy will be dissipated internally, most likely leading to dissociation

[6] For the Me_2-bpa-Me complexes the reaction barrier for the formation of the peroxo-ethene complex is lower than for the bpa-Me complexes. This is probably due to the fact that the Me_2-bpa-Me ethene complexes are already pre-organized for a reaction with dioxygen (as shown in § 4.4).

of ethene to give the peroxo complex (the olefin is less strongly bound than the dioxygen moiety). Although the peroxo complex lies higher in energy than the peroxo-ethene complex [7] (at least 8 kcal/mol for rhodium and 14 kcal/mol for iridium), this reaction should be accessible in the gas phase up to some amounts.

According to Figure 7.3a and Figure 7.3b in all cases the formation of the naked species, $[(L_N)M]^+$, is endothermic.[8] Once this naked species has been formed, formation of the peroxo complex will be quite facile. In other words, for this mechanism the first step will be crucial. Once $[(L_N)Rh]^+$ has been formed, the exothermic reaction of the naked species with dioxygen will occur quite rapidly, provided that the internal energy of the product ion is not too high.

Although we do not know the reaction barrier for the dissociative mechanism we can see that the naked species lies in all cases much higher in energy than the MECP calculated for the associative reaction of the ethene complex with dioxygen. Therefore, an associative pathway could be very favorable for the reaction of N_3 metal ethene complexes with dioxygen.

In this chapter we will describe the reaction of N_3 and N_4 rhodium(I) and iridium(I) ethene complexes, $[(L_N)M(C_2H_4)_p]^+$ [9], towards dioxygen in the gas phase. We will attempt to discriminate between associative and dissociative pathways, which are both likely to occur in the gas phase. As will become clear from this chapter, it depends on the region inside the mass spectrometer which one of the two reactions prevails. In some cases only indirect evidence could be obtained, since it was not always possible to vary every reaction condition at will. In other cases direct evidence for the type of reaction taking place could be obtained. We hope that insight in these gas-phase reactions will help us in understanding via which reaction steps the products from the solution phase reaction could be formed.

7.2 Reaction with air during nebulization?

The atmospheric pressure region, which is filled with 1 bar of air, is the first region in which the organometallic olefin complexes theoretically could react with molecular oxygen. Any reaction here would be best described as a semi-solution phase reaction of a complex with a gas. In other words, one would expect the formation of the same types of products as discussed in Chapter 4, ranging from peroxo and peroxo-ethene complexes to paramagnetic 2+ charged species.

However, for the metal(I) olefin complexes investigated in this thesis no reaction with air seems to take place in this region. Even the use of dinitrogen as a sheath gas was of no influence on the mass spectra obtained. This could either mean that indeed no reaction can take place in the atmospheric pressure chamber[10] or that for

---

[7] A contrast between the $\Delta H_{0\,K}$ presented here and the $\Delta G_{298\,K,\,1\,bar}$ presented in § 4.4 (and Appendix A) is that the $\Delta G_{298\,K,\,1\,bar}$ of N_3 rhodium peroxo complexes lie lower in energy than the corresponding peroxo-ethene complexes. This could be an indication that in should be possible to observe rhodium peroxo-olefin complexes in the gas phase, which appeared not to be possible in solution.

[8] In solution barriers of 15-30 kcal/mol should still be passable. However, in the gas phase, where there is no redistribution of energy due to collisions between the molecules, the equilibrium constant for the dissociation of ethene will determine whether or not such a reaction can take place. This particular equilibrium lies in all cases on the side of the olefin complex making it virtually impossible to spontaneously allow dissociation. However, by applying an external potential (e.g. in the tube lens region or before entering RC 2) the energy available for reaction upon collision can be increased.

[9] M = Rh, Ir; p = 1, 2; L_N = bpa-R and Me_2-bpa-R (R = R^1 = H, Me, Bz), Me_n-tpa (n = 0, 1, 2, 3)

[10] The formation of peroxo and peroxo-ethene complexes is probably too slow to yield a detectable amount of products during nebulization. The nebulization process takes place on the order of milliseconds, whereas the reaction of the most reactive complex, $[(Me_3\text{-tpa})Rh(C_2H_4)]^+$, with dioxygen takes about a minute.

some reasons it is not possible to detect the products formed by ESI^+-MS.[11, 12]
In any case, since no product ions are detected, any reaction that might have occurred will not hinder the study of reactions in subsequent regions of the mass spectrometer either.

7.3 Reaction with molecular oxygen in the tube lens region

7.3.1 General remarks

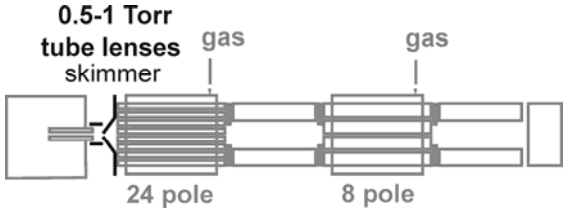

The first region in which a reaction of olefin complexes with dioxygen is observed, is the space between the tube lenses, the so-called tube lens region. As described in § 2.2.1, before entering this region the metal-olefin complexes have been declustered in the heated capillary and the remaining solvent molecules have been evaporated. In other words, reactions taking place in the tube lens region are authentic gas-phase reactions.[13]
The positive potential applied to the tube lenses to converge the diverging ion beam causes the ions to be accelerated in a direction perpendicular to the passageway through the tube lens region. As a result, they will collide with background gas molecules and other ions. Upon collision the kinetic energy of the ions, obtained by this positive potential, can be converted into internal energy, which can be used to overcome activation barriers. As said before, in the tube lens region *high-energy collision experiments at high collision-gas pressures* can be performed (tube lens potential varied between 5 and 150 V).
It was already mentioned in § 6.2 that for the calculation of the kinetic energy of the ions in the tube lens region in the laboratory frame, the ions will never be accelerated over the total potential difference applied[14] and that $E_{(lab)}$ is truly the maximum amount of kinetic energy the ions can obtain. In reality the ions will obtain only a fraction of it and therefore their true kinetic energy in the tube lens region, $E_{(lab,\,TL)}$, can be best described by equation 7.1, in which α is an unknown constant.

$$E_{(lab,TL)} = \alpha * q_{ion} * V \qquad (7.1)$$

For convenience we will use $\alpha = 1$ here, but one should always keep in mind that $0 < \alpha < 1$. Since the mean free path of the ions in this region will be very short due to the high pressure, probably $\alpha << 1$.
Since α is unknown, tube lens measurements will give qualitative insight into certain reactions, showing trends. In order to obtain quantitative reaction cross-sections as a function of energy threshold CID experiments [25] – [29] (in which $\alpha = 1$) should be performed.

---

[11] Dicationic metal(II) species resulting from a SET reaction between dioxygen and the metal(I) complex will be highly reactive and therefore probably undetectable (they will react with anything that comes in their way). As already shown in Chapter 5, only for the most sterically protected N_4 iridium ethene complexes the corresponding iridium(II) species could be isolated. For less sterically shielded complexes and especially for rhodium complexes in general the metal(II) ethene species are expected to be highly unstable and therefore undetectable.

[12] Also the so-called "dominant-ion effect" (as described in § 2.3.4) will prevent detection of (small amounts of) these dicationic species by ESI^+-MS.

[13] Inside the tube lens region a pressure of 0.5 – 1.0 Torr of background gas is present (a pressure of 1 Torr corresponds to 1.33322 mbar). This gas consists of air and gaseous solvent molecules, all of which have entered via the opening in the heated capillary along with the gaseous ions. The exact composition of the background gas cannot be determined. Neither can it be varied at will.

[14] Due to the high pressure in the tube lens region the mean free path of the ions is too short.

In order to be able to calculate the maximum amount of energy that can be transferred in a collision under conservation of impulse and energy [15], we need to know the mass of the gas molecules the ions collide with (see equation 7.2 [16]) [25], [30]. The tube lens region contains a mixture of gas molecules with which the ions can collide (air, solvent molecules, other ions). Since we are only interested in trends and orders of magnitude, we have chosen for m_{gas} the mass of a dioxygen molecule in all cases.

$$E_{(cm)} = E_{(lab,TL)} * \frac{m_{gas}}{m_{gas} + m_{ion}} \qquad (7.2)$$

7.3.2 Reaction in the tube lens region

The influence of the tube lens potential on the type of species appear in the mass spectra has been investigated for N_3 and N_4 rhodium and iridium ethene complexes.

It appears that none of the N_3 and N_4 *iridium* ethene complexes studied reacts with air in the tube lens region. In contrast, all N_3 and N_4 *rhodium* ethene complexes do react.

This difference in behavior is in line with the fact that third-row transition metals like iridium are usually kinetically more inert than their second row congeners. For example, the reaction of Me_3-tpa iridium ethene with dioxygen in solution takes about 30 minutes to complete, whereas the reaction of the corresponding rhodium complex has gone to completion within a minute (Chapter 4).

Interestingly, in all cases in which a reaction in the tube lens region does take place, peroxo complexes $[(L_N)Rh(O_2)]^+$ (Figure 7.4) are the only products formed. This is in contrast to the solution and solid state reactivity of some of these rhodium complexes, which in some cases leads the formation of 3-metalla-1,2-dioxolanes, 2-metallaoxetanes or even paramagnetic species (see Chapter 4, publications by Krom [31] – [33] and Kicken [34]).

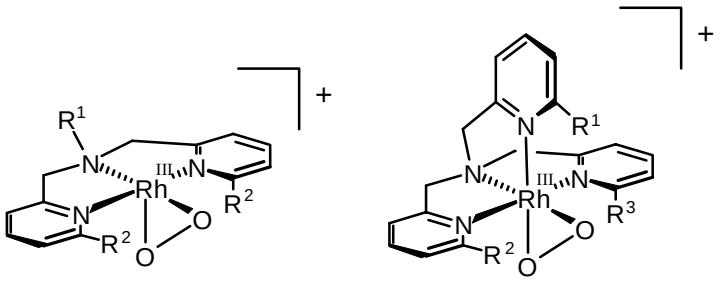

bpa-R : R^2 = H

Me_2-bpa-R : R^2 = Me

R = R^1 = H, Me, Bz

Me_n-tpa

n = 0 : $R^1 = R^2 = R^3$ = H
n = 1 : R^1 = Me, $R^2 = R^3$ = H
n = 2 : $R^1 = R^2$ = Me, R^3 = H
n = 3 : $R^1 = R^2 = R^3$ = Me

Figure 7.4 *Products obtained in the reaction towards air in the tube lens region*

[15] This energy corresponds to the kinetic energy, $E_{(cm)}$, of both collision partners in the center of mass frame at a completely inelastic collision.

[16] V is the potential applied to the tube lenses. It determines the maximum amount of kinetic energy an ion can get; $E_{(cm)}$ is the kinetic energy of the ion in the center of mass coordinate system; $E_{(lab,\,TL)}$ is the kinetic energy of the ion in the tube lens region in the laboratory system; the velocity of the gas molecules is taken to be zero, which is a correct assumption as long as $E_{(lab,\,TL)} > k * T$; m_{ion} and q_{ion} are the mass and the charge of the ion involved in the collision, respectively, and m_{gas} is the mass of the gas molecule the ion collides with, which is in this case taken to be dioxygen.

All rhodium ethene complexes roughly show the same type of behavior when the tube lens potential is increased from 5 to 145 Volts. A typical example (the reactivity of $[(Me\text{-}tpa)Rh(C_2H_4)]^+$) is shown in Figure 7.5. Above a certain tube lens potential peroxo-formation starts, as if there is an activation barrier for this reaction. The influence of the nitrogen donor ligand on the height of this barrier will be discussed in § 7.3.2.

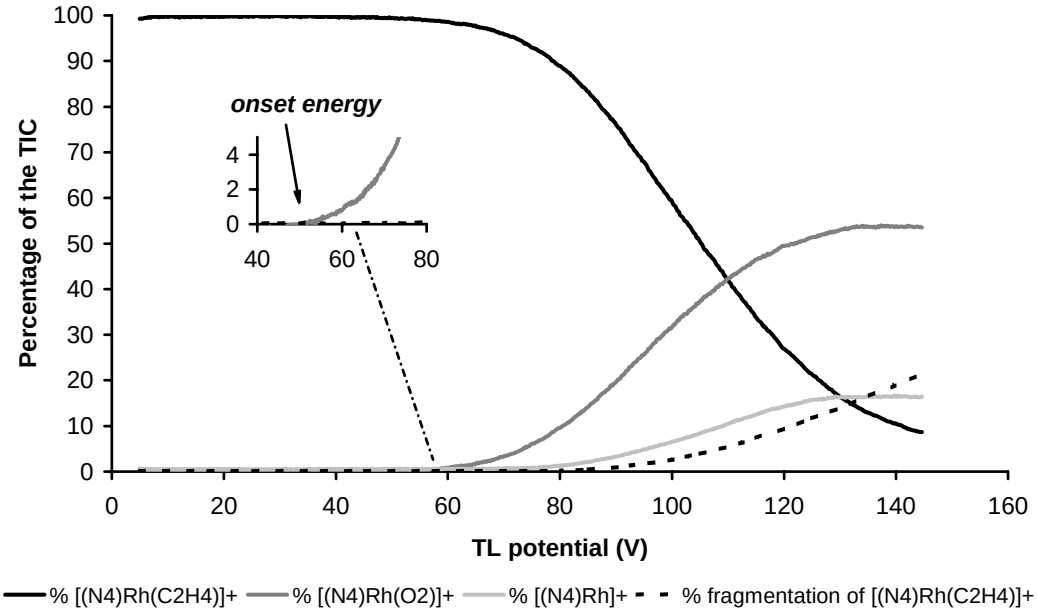

Figure 7.5 *Reaction of $[(Me\text{-}tpa)Rh(C_2H_4)]^+$ towards dioxygen in the tube lens region* [17]

A small amount of peroxo complex is in most cases already present at very low tube lens potentials. This must have been formed during a solution-phase reaction with air in the tubing before spraying (as became clear from § 7.2, it can be excluded that it was formed during the nebulization process). Since we are only interested in the product yield in the tube lens region, this starting amount of peroxo complex is in all cases subtracted from the measured amount of peroxo complex.

Another interesting behavior is that above a certain tube lens potential saturation of the peroxo signal seems to take place. The reason for this maximum yield and its dependence on ligand structure will be discussed in the next paragraph.

7.3.3 Trends in peroxo yields

General remark

Graphs like the one depicted in Figure 7.5 [18] are indicative for dissociative processes taking place: the higher the amount of energy applied, the higher the product yield. Formation of the peroxo complex, $[(L_N)Rh(O_2)]^+$, starts at nearly the same tube lens potential as formation of the naked species, $[(L_N)Rh]^+$. This characteristic behavior was seen for all the rhodium ethene complexes measured. Since the potential at which both species

[17] The signals corresponding to $[(L_N)Rh(O_2)]^+$ and $[(L_N)Rh]^+$ are composed of the summation of the intensities of all fragments and species belonging to them. For example, the peroxo complex can easily lose a pyridyl-radical. Therefore, the intensity of the m/z corresponding to $\{[(L_N)Rh(O_2)]\text{-}C_5H_4NCH_2\}^+$ has been added to the total intensity of $[(L_N)Rh(O_2)]^+$ (For a more detailed description of the fragmentation behavior of the species see § 6.4). The intensities of signals corresponding to fragmented ethene complex were not added to the total $[(L_N)Rh(C_2H_4)]^+$ intensity. All signals in the mass spectra could be classified as deriving from these three species $[(L_N)Rh(C_2H_4)]^+$, $[(L_N)Rh(O_2)]^+$ and $[(L_N)Rh]^+$.

[18] Similar graphs were obtained for the other rhodium ethene complexes.

start to become visible in the spectra shifts for every complex in the same direction, formation of these two species indeed seems to be related.

The conditions in this region are rather harsh, which will entropically favor dissociative processes. Therefore, we propose that in this region only dissociative reactions play a role. Unfortunately this hypothesis cannot be tested by variation of the dioxygen pressure, since neither the background gas composition nor its pressure can be varied at will.

The hypothesis could, however, explain the observed maximum in peroxo yield in the tube lens region. Inside the tube lens region, the horizontal velocity of the ions is only determined by the potential applied between the heated capillary and the skimmer. This potential does not change throughout the measurements. Also the background gas pressure is constant.

If first ethene has to dissociate before dioxygen can come in, then there are certain factors, which determine the percentage of organometallic complex that will react with dioxygen.

- The reaction barrier.
  The energy with which the ions collide with each other and with the background gas molecules can be influenced by variation of the tube lens potential. Upon increase of the tube lens potential the kinetic energy, which can be converted into internal energy, which can be used to overcome reaction barriers, increases.
- The number of collisions.
  This number is determined by the pressure of the background gas the ions collide with during their flight through the tube lens region and the size of the ions and the collision gas molecules.
  This number can therefore be regarded as a constant.
- The probability of reaction upon collision.
  This is a constant, assuming that there is no reaction barrier for peroxo complex formation.
  If this is not correct, then the probability of a reaction taking place upon collision will depend on the collision energy $E_{(cm)}$ versus the activation barrier E_a. E_a is constant, $E_{(cm)}$ is variable.

Upon increase of the tube lens potential the percentage of naked species present in the tube lens region increases, due to an increase in the number of collisions taking place and due to the increase in the energy with which the ions collide. However, once these naked species have been formed, they still have to collide with a dioxygen molecule and react with it. The number of reactive collisions is determined by the number of collisions an ion can undergo in the tube lens region and the probability of reaction upon collision. Since the number of collisions an ion can undergo on its way through the tube lens region can be regarded as a constant, there must also be a maximum number of reactive collisions yielding the peroxo complex.

In other words, the maximum product yield is limited. Since the number of collisions is constant for every complex ion, the probability of reaction determines the height of the maximum yield.

Observed product yields in the tube lens region

For all N_3 and N_4 rhodium ethene complexes that react in the tube lens region such a maximum in product yield can be observed. For each complex this maximum is different and is reached at a different $E_{(cm)}$.[19] Some trends can be observed upon changing the nitrogen donor ligand as displayed in Figure 7.6.

[19] These maximum yields determined were obtained near the highest tube lens potentials possible, e.g. 145 V, due to limitations of the mass spectrometer (a too high potential results in a decrease of the number of ions that is able to pass the tube lens region and reach the detector). Theoretically the peroxo yields could have been somewhat higher if it would have been possible to increase the tube lens potential even more.

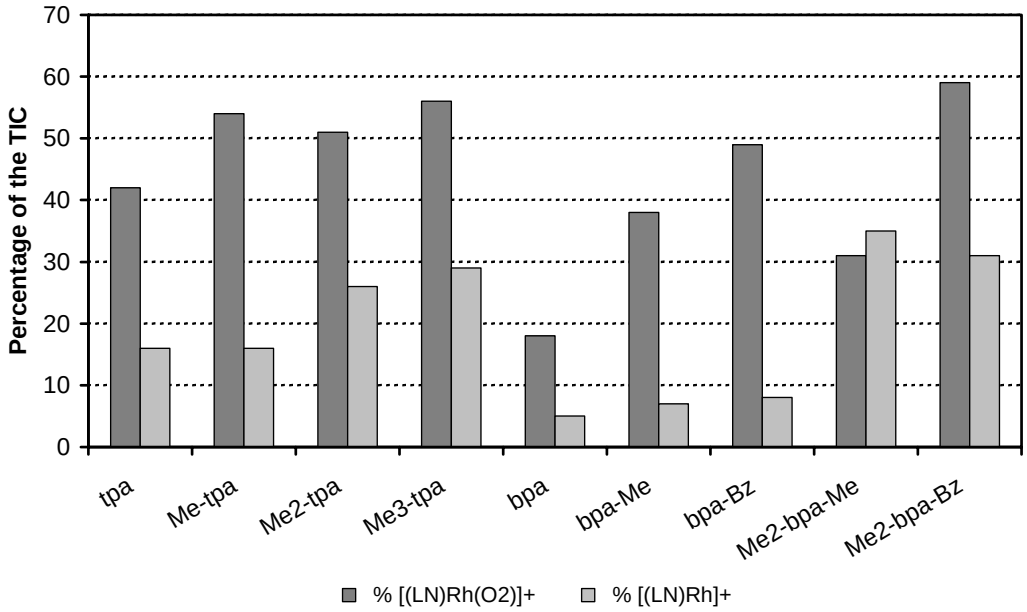

Figure 7.6 *Maximum yields of $[(L_N)Rh(O_2)]^+$ and $[(L_N)Rh]^+$ ($L_N = N_3, N_4$) in the tube lens region* [20]

For the N_4 complexes the steric bulk around the metal center appears to have little influence on the product yield. Maybe the similar yields for all four tpa complexes can be explained by a similar mechanism of reaction for the N_4 complexes in the tube lens region: dissociation of a pyridyl ligand after which a reaction with dioxygen can take place.

For the N_3 complexes, on the other hand, differences in reactivity can be observed upon changing two parameters: the amine-substituent and the steric bulk around the metal centre.

The influence of the steric bulk is not straightforward. There is an increase on going from bpa-Bz to Me_2-bpa-Bz, whereas on going from bpa-Me to Me_2-bpa-Me the product yield decreases somewhat again. It is therefore also not possible to relate the binding strength of the olefin (which decreases on going from bpa-R to Me_2-bpa-R) to the product yield observed.

The first parameter, the substituent on the amine-nitrogen appears to be the most important factor of the two. The reactivity clearly increases upon going from bpa to bpa-Me to bpa-Bz. In other words, upon decrease of the donor strength of the amine nitrogen of the N_3 ligand, the product yield increases drastically.

Possible explanation for the low reactivity of the bpa complex

There are probably two reasons for the low reactivity of the bpa rhodium ethene complex towards O_2. The first is the most obvious explanation that the bpa complex is probably less reactive than the other two N_3 complexes towards dioxygen. Another reason is the fact that the four-coordinate bpa rhodium ethene complex is not stable in the gas phase at those tube lens potentials at which reaction with dioxygen takes place. Loss of H_2 is a major side-reaction observed for this complex. At the tube lens potential at which the maximum product yield is obtained, the intensities of the different species are displayed in Table 7.1 in decreasing order.

[20] All measurements but one were performed in 0.02 % MeCN in THF. Due to the low stability of the electrospray signal for Me_2-bpa-Me an acetone solution was used. Since the tpa and Me_2-bpa-Bz rhodium complexes displayed exactly the same behavior and product yields in both solvents, there appears to be no influence of the solvent on the behavior in the tube lens region.

Table 7.1 *Intensities of bpa rhodium species present at maximum peroxo yield*

Complex or fragment	Percentage of the TIC
$[(bpa)Rh(C_2H_4)]^+$	45.6 %
$\{[(bpa)Rh(C_2H_4)]\text{-}H_2\}^+$	31.2 %
$[(bpa)Rh(O_2)]^+$ incl. its fragments	16.4 %
$\{[(bpa)Rh]\text{-}H_2\}^+$	2.4 %
$[(bpa)Rh]^+$	2.2 %
Other bpa rhodium fragments	2.2 %

The competing reaction, loss of H_2 from the ethene complex, seems to occur about twice as much as formation of the peroxo complex. Not only does loss of H_2 from the ethene complex make it more difficult for a reaction with dioxygen to occur, also the naked species, which according to our working hypothesis is responsible for formation of the peroxo complex in the tube lens region, can lose H_2 again.

In other words, the formation of the bpa rhodium peroxo complex is obscured by this side-reaction.

Would it not have occurred, and would therefore these 31.2 % from the $\{[(bpa)Rh(C_2H_4)]\text{-}H_2\}^+$ species be divided over the other species under conservation of the current ratios between the signals, then roughly about 24 % peroxo complex would have been expected. This is much higher than we observed, but still lower than the yield obtained for the bpa-Me and bpa-Bz rhodium ethene complexes. This could imply that bpa rhodium ethene for some reason really has a lower reactivity towards dioxygen than the other two bpa-R complexes.

One other conclusion that can be drawn from Table 7.1 is, that the naked species, $[(bpa)Rh]^+$, is highly reactive, since there is only 2.2 % of naked species left in the spectrum. Comparing this to the 16.4 % of peroxo complex and assuming a dissociative mechanism taking place, results in a conversion of about 88 %.

In other words, there must be another reason why the bpa rhodium ethene complex is less reactive. Since the steric bulk around the metal center has not changed on going from the bpa to the bpa-Me and bpa-Bz complex, an electronic influence must be responsible for the difference in reactivity.

One could assume that either ethene is more strongly bound to $[(bpa)Rh]^+$ than to $[(bpa\text{-}R)Rh]^+$ making it more difficult for the complex to follow the dissociative pathway,[21] or that the dioxygen molecule is too loosely bound to the rhodium center and dissociates again under the reaction conditions generating a kind of equilibrium concentration of the peroxo complex on the way to the skimmer. Both assumptions concerning the binding energies are, however, not in agreement with the theoretical calculations presented in Appendix A. Therefore, we do not have any explanation for the low reactivity of the bpa complex compared to the high reactivity of the bpa-Me and bpa-Bz complex.

Summary of the reactivities in the tube lens region

In conclusion, upon addition of a substituent to the amine-nitrogen of the bpa-ligand the donor strength of the amine decreases. Despite the fact that upon reaction with dioxygen electron density has to go from the metal center to the O_2 molecule, this decreased electron density results in an increase in the product yields in the tube lens region. Another factor that influences the product yield (for the bpa complex) is the occurrence of a competing reaction like loss of H_2.

[21] This explanation would be in line with our working hypothesis about the reaction path for the gas-phase oxidation of rhodium ethene complexes taking place in the tube lens region. It will decrease the number of $[(L_N)Rh]^+$ species formed, which could react further with dioxygen resulting in a "plateau" for the product yield.

The product yields for the benzyl-containing N_3 complexes and those of the N_4 compounds are very similar. We already proposed that the N_4 complexes all react via the same mechanism. It might be that this mechanism comprises the formation of a complex in which the N_4 ligand is κ^3-coordinated, that would explain the similar conversions of Me_n-tpa and Me_2-bpa-Bz complexes.

7.3.4 Onset energy for peroxo formation

As can be seen in Figure 7.5 there is a specific tube lens potential above which peroxo formation starts, the onset energy. This indicates that the reaction has an activation energy, i.e. a simple collision at zero collision energy is not enough to produce the product. In Table 7.2 the onset enthalpies for the reaction with dioxygen in the tube lens region are listed for all reactive $[(L_N)Rh(C_2H_4)]^+$.

Table 7.2 *Onset enthalpies for the reaction towards dioxygen in the tube lens region*

L_N rhodium ethene complex	H_{onset}		m/z of the ethene complex
	kcal/mol	eV/mol	
$[(bpa)Rh(C_2H_4)]^+$	111	4.8	300
$[(bpa\text{-}Me)Rh(C_2H_4)]^+$	111	4.8	344
$[(bpa\text{-}Bz)Rh(C_2H_4)]^+$	83	3.6	420
$[(Me_2\text{-}bpa\text{-}Me)Rh(C_2H_4)]^+$	74	3.2	372
$[(Me_2\text{-}bpa\text{-}Bz)Rh(C_2H_4)]^+$	65	2.8	448
$[(tpa)Rh(C_2H_4)]^+$	69	3.0	421
$[(Me\text{-}tpa)Rh(C_2H_4)]^+$	78	3.4	435
$[(Me_2\text{-}tpa)Rh(C_2H_4)]^+$	78	3.4	449
$[(Me_3\text{-}tpa)Rh(C_2H_4)]^+$	65	2.8	463

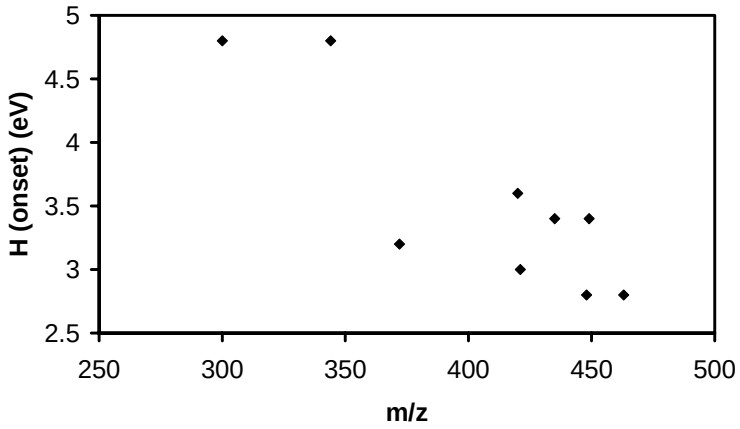

Figure 7.7 *Onset energies versus the m/z of the complexes*

Table 7.3 *Calculated ethene binding enthalpies of ethene for $[(L_N)Rh(C_2H_4)]^+$* [22]

$[(L_N)Rh(C_2H_4)]^+$	$\Delta H_{0\,K}$	
	kcal/mol	eV/mol
$[(bpa)Rh(C_2H_4)]^+$	-30.2	-1.31
$[(bpa\text{-}Me)Rh(C_2H_4)]^+$	-30.6	-1.33
$[(Me_2\text{-}bpa)Rh(C_2H_4)]^+$	-13.9	-0.60
$[(Me_2\text{-}bpa\text{-}Me)Rh(C_2H_4)]^+$	-14.9	-0.65
$[(tpa)Rh(C_2H_4)]^+$	-42.6	-1.85
$[(Me_3\text{-}tpa)Rh(C_2H_4)]^+$	-27.1	-1.18

As already mentioned in § 7.3.1 we propose a dissociative mechanism for the reaction in the tube lens region, since the conditions in this region are rather harsh, which will favor dissociative processes. From the binding energies calculated for some N_3 and N_4 complexes (Table 7.3) it is clear that the onset energies measured for the reaction in the tube lens region are several times as high as the ones obtained by DFT calculations. There also appear to be two groups of compounds (Figure 7.7): one with H_{onset} below 4 eV and an m/z above 400 (all N_4, bpa-Bz and Me_2-bpa-R (R = Me, Bz)) and one with a H_{onset} above 4 eV and an m/z below 350 (bpa, bpa-Me).

For the N_4 complexes there appears to be no influence of the steric bulk on the onset energy. For the N_3 complexes there appears to be an influence of the steric bulk (lower onset for the Me_2-bpa-R complexes), but also of the amine-substituent/mass of the complex (lower onset for benzyl than for methyl and proton).

This different influence of steric size in the N_3 and N_4 series is probably due to the fact that the N_4 complexes react via a different mechanism than the N_3 complexes, *viz.* initial dissociation of one of the pyridyl arms. Since the binding energy of the olefin decreases in the order tpa > Me_3-tpa, bpa, bpa-Me > Me_2-bpa-Me and since the N_4 complexes all have a much lower onset energy than the bpa and bpa-Me complex, dissociation of the olefin is unlikely to be the rate-limiting step for the N_4 complexes.

For the N_3 complexes, on the other hand, there could indeed be an influence of the steric bulk, or the binding strength of the olefin or pre-organization of the olefin c.q. distortion of the energy levels of the orbitals on going from perfectly square planar to distorted square planar. All these factors should result in a lower onset energy for the Me_2-bpa-R complexes.

However, why does for the bpa-R complexes a heavy amine-substituent like a benzyl also result in a decrease of H_{onset}? And why are all onset energies highly overestimated compared to the calculated binding energies of ethene?

A common interpretation of results like these is to ascribe this overestimation of the reaction barriers in part to the kinetic shift, provided the dissociation step is the rate-limiting step. As already explained in § 2.3.8 the amount of energy that is necessary for a reaction to be observed in the laboratory is always higher than the theoretical amount of energy necessary for this reaction (the activation energy). The difference is determined by the number of degrees of freedom (d.o.f.) of the molecules involved in the collision. The larger the molecule and thus the higher the number of d.o.f., the more energy an ion can dissipate among all possible vibrations after collision. This will, for example, be the case for the N_4 and the benzyl-containing N_3 rhodium ethene complexes. Therefore, more energy than just the activation energy has to be supplied to saturate a reactive vibration.

[22] For all L_N metal complexes, the energy of corresponding naked species, $[(L_N)M]^+$, is set to zero kcal/mol.

For the heavy compounds (N_4, Me_2-bpa-Bz and bpa-Bz, which already have a low H_{onset}) the kinetic shift is therefore expected to be largest. As a result, after correction for the kinetic shift [23] the differences between the two groups of compounds will only increase.

Therefore, we do not have an explanation for the observed lowering of the onset on going from low mass to high mass species.

7.4 Reaction towards molecular oxygen in the 24-pole region (RC 1)

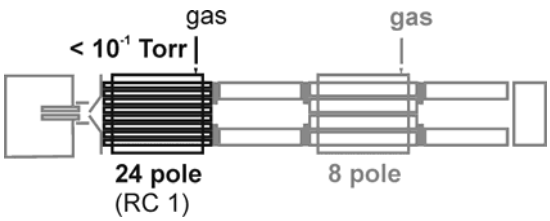

In RC 1, contrary to the tube lens region, pure dioxygen can be used as a collision gas. Also the conditions under which reactions take place are more controllable than in the tube lens region: it is possible to set and measure the exact background gas pressure. Pressures of up to 100 mTorr of collision gas can be applied in this region; this is lower than the pressure in the tube lens region, but still quite high.

As described in § 2.2.3 the kinetic energy of the ions is around zero and cannot be adjusted in any way. And due to the high collision frequency in this region efficient thermalization to 70 °C can take place, which causes species formed in exothermic reactions to easily get rid of their excess of energy.

Complexes that are reactive in RC 1

The reactivities of some N_3 and N_4 ethene complexes of rhodium and iridium towards O_2 have been measured using at least 4 different dioxygen pressures to investigate the effect on the product yield upon increase of the dioxygen pressure.

Remarkably, none of the N_4 complexes investigated [24] seem to react upon collision with dioxygen. A reason for this can be that the first reaction step for these complexes always has to be a dissociative one: of either the olefin or a pyridyl arm. For such a process a certain amount of energy is required, which the complexes do not obtain in RC 1 upon collision with near zero-collision energy with dioxygen molecules. And even if they were able to obtain a certain amount of internal energy upon collision, the N_4 complexes have a higher number of degrees of freedom over which the energy will be dissipated making it more difficult to accumulate enough energy in the required vibration associated with the required dissociation.

The corresponding mono-ethene complexes of the bpa-R and the Me_2-bpa-R rhodium and iridium ethene complexes discussed in this thesis, $[(L_N)M(C_2H_4)_p]^+$, [25] were also tested for their reactivity towards dioxygen in RC 1. As shown in Figure 7.8 *some* of them indeed react upon collision with dioxygen. The structures of the reaction products (peroxo species for rhodium, peroxo-ethene species for iridium) were confirmed by subsequent fragmentation of the product ion m/z by collision with argon in RC 2.

The fact that peroxo-ethene species are obtained for iridium clearly implies that in this region, where mild conditions prevail, reactions go via an associative pathway. It seems likely that this also applies to rhodium but that for this metal the peroxo-ethene complex very readily loses the olefin.

[23] Since the pressure in the tube lens region cannot be varied at will, it will not be possible to perform measurements under single-collision conditions. These measurements would have been required for a *meaningful* application of calculated kinetic shifts. Therefore we did not perform these calculations.

[24] M = Rh, L_N = Me_3-tpa; M = Ir, L_N = Me-tpa, Me_3-tpa.

[25] M = Rh, Ir; L_N = bpa-R (R = R^1 = H, Me, Bz), Me_2-bpa-R (R = R^1 = Me, Bz); p = 1 for Rh and p = 2 for Ir

This hypothesis is in line with the observation that tetradentate nitrogen donor complexes do not react in RC 1, although in the tube lens region, for which a dissociative pathway has been proposed, the N_4 rhodium(I) ethene complexes were quite reactive. In the case of these coordinatively saturated N_4 complexes dissociation

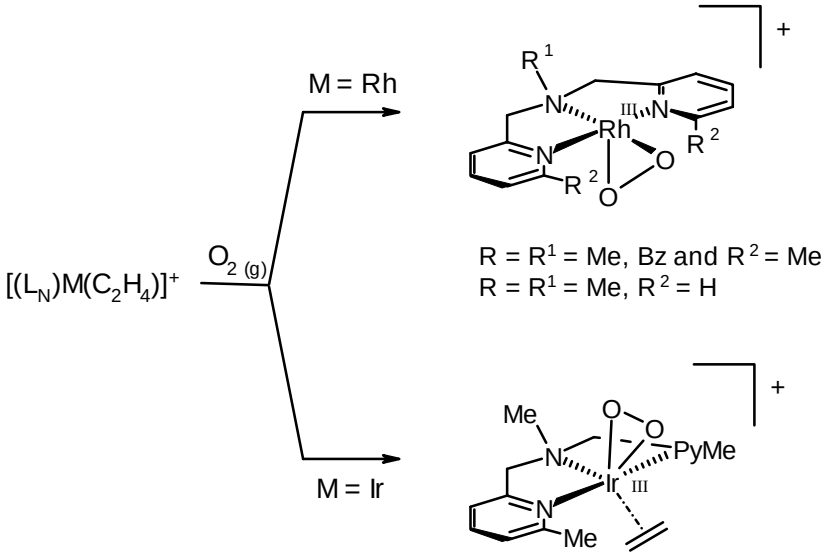

Figure 7.8 *Oxidation products formed in the 24-pole*

of either a pyridyl-arm or the olefin first has to take place before an associative reaction with dioxygen can occur. The energy required for this dissociation cannot come from collision with O_2, which happens at near-zero energy, so it would have to be provided by the environment ("thermal bath" of gas molecules). In solution 70 ºC (the effective temperature in RC 1) would probably have been high enough to allow dissociative reaction with O_2 at the laboratory timescale. The much lower collision frequency inside RC 1 means that all thermal reactions will be slowed down; this effect, combined with the low concentration of O_2, results in the reaction not occurring to a measurable extent within the few milliseconds the molecules take to pass RC 1. For associative reactions, on the other hand, only the (low) reaction barrier for coordination of dioxygen has to be overcome, which is a more likely process for these gaseous ions.

The difference in behavior between the rhodium and iridium complexes could be due to the lower metal-olefin binding energy for rhodium (Appendix A). As a result the peroxo-ethene complexes are less stabilized for rhodium than for iridium. Therefore, even though reactive intermediates are thermalized fairly efficiently in RC 1, the rhodium peroxo-ethene complexes apparently are not stable enough and lose the olefin before leaving the 24-pole region.

Dependence on the dioxygen pressure

Another important phenomenon supporting an associative pathway is that the yields of rhodium peroxo and iridium peroxo-ethene increase upon increase of the dioxygen pressure in RC 1 (see Figure 7.9). The reaction with dioxygen seems to be the rate-determining step.

For iridium it is possible to go up to 100 % product yield if the dioxygen pressure in the 24-pole region is high enough. Interestingly, this maximum yield is much higher than the ~ 25 % of $[(Me_2\text{-bpa-Me})Ir(C_2H_4)(O_2)]^+$ we were able to obtain in solution (where up to 75 % of paramagnetic by-products were formed). We attribute this difference in selectivity to the exclusion of the SET pathway in the gas phase as discussed in § 7.1.1.

From the less steep slope for the Me_2-bpa-Me iridium ethene complex in Figure 7.9 it is also clear that reaction rate of this iridium complex is lower than that of the Me_2-bpa-R rhodium ethene complexes, but apparently it is higher than that of the bpa-Me rhodium ethene complex.

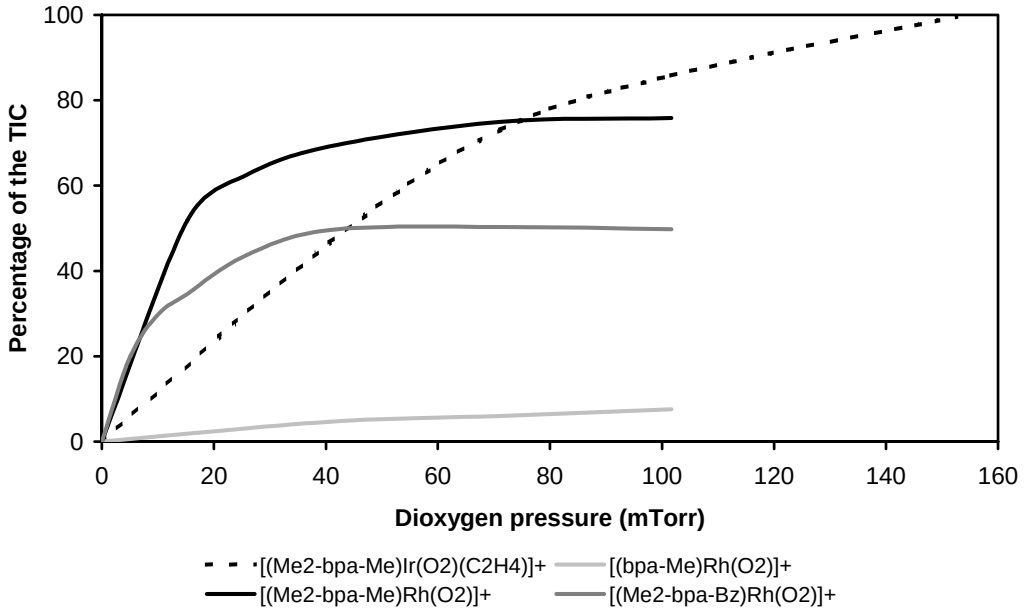

Figure 7.9 *Yields in the 24-pole region* [26]

Interesting aspects of reactivities observed in RC 1

For rhodium a clear influence of the nitrogen donor ligand can be observed. Yields decrease upon going from Me_2-bpa-Me to Me_2-bpa-Bz to bpa-Me. There is clearly an influence of the steric bulk around the metal center on the yield of peroxo complex. An explanation for the difference between bpa-R and Me_2-bpa-R complexes was already given in § 4.4 where it was shown that in order for a reaction with a dioxygen molecule to occur the olefin has to bend down below the plane composed of pyridine rings and the metal center. In the case of the Me_2-bpa-R complexes the olefin is already coordinated in such a way that it is already in a position required for an associative reaction with dioxygen.

Also a methyl substituent attached to the amine nitrogen results in higher yields than a benzyl-substituent. A possible reason for this behavior is, that π-coordination of the benzyl-ring blocks the fifth coordination site by occupation of the free space where the dioxygen molecule is supposed to enter the coordination sphere of the metal. As a result the collision efficiency upon collision with dioxygen will decrease.
The observed difference between a methyl and a benzyl amine-substituent cannot be explained by the occurrence of aromatic C-H activation before entering RC 1 (resulting in solution in a coordinatively saturated ethene-hydride species, § 3.4.1). This reaction takes hours; we found (§ 6.3) that a sample sprayed ~ 20 minutes after preparation showed a fragmentation pattern clearly different from that of the fully metallated species, suggesting that the former still corresponds to the largely unreacted complex. Since the measurements described in this chapter were all performed immediately after sample preparation, the C-H activation reaction, which takes hours, could not have occurred to such an extent as to be of influence here.

For the bpa-Bz rhodium mono-ethene complex π-coordination of the benzyl group, together with the already low yields due to the absence of methyl substituents at the pyridine rings, could explain the apparent lack of reactivity of $[(\text{bpa-Bz})\text{Rh}(C_2H_4)]^+$ in RC 1.

[26] For the calculation of the yields only the intensities of those species the intensity of which changed upon increase in dioxygen pressure were taken into account. The intensities of the other "spectator" complexes (e.g. $[(Me_2\text{-bpa-Me})\text{Ir}(C_2H_4)_2]^+$, $[(\text{bpa-}H_2)\text{Rh}(H_2O)_2]^+$) were omitted in this calculation, since they are proven to be not reactive in the 24-pole region, nor does their intensity change upon change of collision gas pressure.

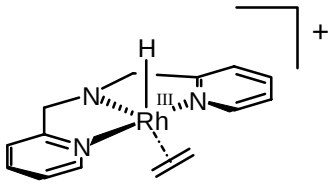

For the gas-phase bpa rhodium ethene complex loss of H_2 is a favorable fragmentation behavior, even at low energy collision conditions. An intermediate structure in this reaction could be the N-H activated rhodium(III) ethene-hydride complex shown on the right. Such a complex would probably not be reactive towards dioxygen anymore due to the already low electron density on the metal center. Maybe the species with m/z corresponding to $[(bpa)Rh(C_2H_4)]^+$ in fact has such an ethene-hydride structure. Since $[(bpa)Rh^{I}(C_2H_4)]^+$ and $[(bpa^{\#})Rh^{III}(H)(C_2H_4)]^+$ are isobaric species, and should have similar fragmentation behavior, the presence of such a rhodium(III) species could explain the lack of reactivity of the bpa rhodium ethene complex in RC 1. However, it then remains puzzling why such a species was never before observed in solution.

For the rhodium complexes the maximum product yield is already obtained at much lower pressures than for the iridium complex in accord with faster kinetics expected for second row transition metals compared to third row transition metals.

Another difference between rhodium and iridium complexes is that for rhodium there seems to be a maximum in the product-yield lower than 100 %. Once this maximum yield is obtained, increase of dioxygen pressure does not have any influence on the yield anymore. This is especially obvious in the case of the Me_2-bpa-R rhodium complexes (R = Me, Bz).

The only explanation that could make sense out of this behavior is that for these rhodium complexes there are apparently two isomers present in the gas phase. One, making up about 75 % of the total intensity in the case of Me_2-bpa-Me rhodium complex (the desired ethene complex?), reacts very rapidly with dioxygen already at low dioxygen pressures. The other isomer is apparently not reactive at all towards dioxygen. If the rearrangement from one isomer to the other is slow (in other words, the other isomer is formed in the tube lens region or in solution and they do not interconvert anymore once the ions have left the tube lens region) then the maximum in product yield will be below 100 % of the total ion current (TIC) and it will not change upon further increase of the dioxygen pressure.

The structures of these isobaric complexes, both having an m/z corresponding to the Me_2-bpa-R rhodium mono-ethene complex, are however unknown. For Me_2-bpa-Bz one could think of an aromatically C-H activated complex. One could perhaps imagine methyl or pyridyl C-H activation reactions for the related Me_2-bpa-Me complexes, but this is pure speculation.

7.5 Reaction with molecular oxygen in the octopole region (RC 2)

7.5.1 Collision with dioxygen

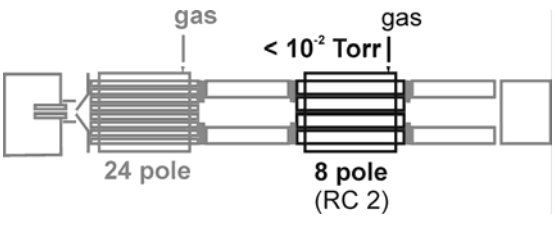

The last region inside the mass spectrometer in which gas-phase reactions towards dioxygen can be performed is the octopole region (RC 2). In this region, just like in the 24-pole region, pure dioxygen is used as a collision gas. Contrary to RC 1, collision gas pressures of up to only a few mTorr can be applied. The mass spectrometer is operated in daughter-ion scan mode, which means that the m/z of the ions we would like to perform reactions with are mass-selected and that only ions with this particular m/z ratio can enter the octopole region. The kinetic energy of the ions $E_{(lab)}$ can be increased from zero up to about 200 eV. Therefore in the octopole region *high-energy collisions at low collision gas pressure* can be performed.

The reactivities of several N_3 and the Me_3-tpa ethene complexes of rhodium and iridium have been measured. Mass spectra have been measured at several different collision energies $E_{(cm)}$ ranging from around zero up to

about 9 eV [27] to see if the product yield, if any, changes upon increase of the collision energy. In a few cases the dioxygen pressure is varied.

One general observation that can be made is that in all those cases where a reaction takes place, it requires collision energies *below* ca. 1.7 eV. The highest yields are obtained around zero-collision energy. Apparently above 1.7 eV the ion-molecule pair formed is too short-lived, making it look like only elastic, unreactive collisions take place leading mainly to fragmentation.

Another general observation is that even in those few cases where a reaction with dioxygen does take place, fragmentation of the olefin complex is the major reaction path; reaction with dioxygen is only a minor one. This is probably due to the low collision gas pressures: transfer of kinetic energy to the internal energy of the complex ion upon collision already occurs at lower collision energies. Since the collision gas pressure is low in the octopole region, the ion cannot get rid of this excess of internal energy by collision with other gas molecules. Therefore it has no other alternative left but to lose a certain fragment, e.g. either C_2H_4 or O_2.

Low reactivity of N_4 rhodium and iridium ethene complexes

As will be shown later on in Table 7.4, for the Me_3-tpa rhodium ethene complex a signal corresponding to the corresponding peroxo complex can be observed in the mass spectra, but only in very low yield (max. 0.6 % of the TIC).

What is the reason for this extremely low activity? This depends of course on the type of reaction taking place: associative or dissociative. One reason could be that the olefin is too strongly bound to the metal center to generate the naked species $[(Me_3\text{-tpa})Rh]^+$, which could react with dioxygen to form a peroxo complex. [28] Another reason could be that for the N_4 ligands the reaction has to go via a κ^3-N_4 ligand. It could be that this process is slow at these collision energies and reaction timescales.

This extremely low activity of N_4 rhodium ethene complexes is very different from the reactivity observed in the tube lens region, in which reaction conditions are proposed to favor dissociative pathways and where for the N_4 rhodium ethene complexes high yields of the corresponding peroxo complexes were obtained. The observed reactivity differs also from the reactivity observed in RC 1, in which reaction conditions are proposed to favor associative pathways and where the N_4 rhodium ethene complexes do not react at all.

The Me_3-tpa iridium ethene complex is even less reactive in the octopole region with dioxygen. This is probably due to the fact that iridium complexes are usually kinetically more inert than their corresponding rhodium analogues.

Reaction of the N_3 rhodium and iridium ethene complexes, Implications for reaction pathways in RC 2

For some of the N_3 rhodium and iridium ethene complexes investigated a higher product yield was observed upon collision with dioxygen.

The one complex for which the reaction in the octopole region was most apparent for $[(Me_2\text{-bpa-Bz})Rh(C_2H_4)]^+$. As can be seen from Figure 7.10, for this complex two product signals could be observed upon collision with dioxygen: one corresponding to the peroxo complex, $[(L_N)Rh(O_2)]^+$, and the other corresponding to one of its fragments, $\{[(L_N)Rh(O_2)]\text{-}H_2O\}^+$ (spectrum measured at a dioxygen pressure of 1.0 mTorr and $E_{(cm)}$ = 0 eV). It was already shown in § 6.4 that the Me_2-bpa-Bz rhodium peroxo complex preferably loses H_2O instead of O_2.

[27] $E_{(lab)}$ was varied from 0 to about 80 eV. The exact $E_{(cm)}$ depends of course on the mass of the ion and of the collision gas molecule, as shown in Equation 6.2 of § 6.2.

[28] In Appendix A it can be seen that the calculated binding enthalpy $\Delta H_{0\,K}$ of ethene to rhodium decreases in the order: tpa > bpa, bpa-Me ≈ Me_3-tpa > Me_2-bpa, Me_2-bpa-Me. This does, however, not explain why the product yields for the bpa and bpa-Me complexes are so much higher than for the Me_3-tpa complex.

As already mentioned, besides a reaction with dioxygen also a large portion of normal fragmentation takes place upon collision with dioxygen due to relatively weak coordination of the olefin to the metal center (Appendix A). This explains the presence of an intense signal corresponding to $[(L_N)Rh]^+$.

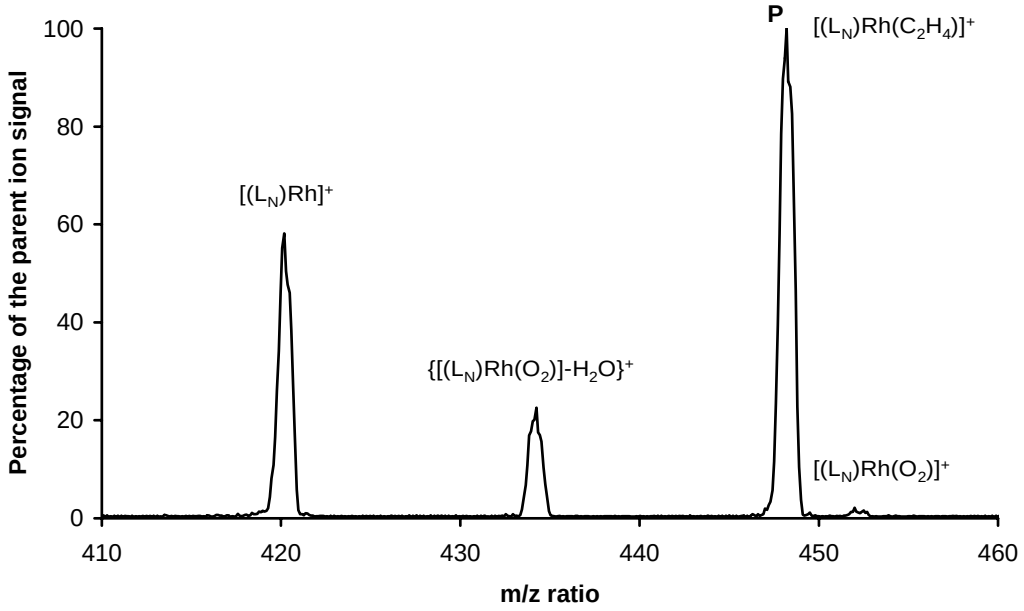

Figure 7.10 *Products obtained upon collision of $[(Me_2\text{-bpa-Bz})Rh(C_2H_4)]^+$ with 1.0 mTorr $O_{2\,(g)}$ in RC 2*

Since the signal corresponding to $\{[(Me_2\text{-bpa-Bz})Rh(O_2)]\text{-}H_2O\}^+$ is much more intense than that of the corresponding peroxo complex, it is clear that the peroxo ions formed indeed have a high internal energy upon formation which results in easy fragmentation. Due to the low collision gas pressures in this region is it not possible for the ions to get rid of this excess of internal energy by collisions with other gas-molecules either (a relaxation process possible in RC 1).

Therefore fragmentation of the peroxo product formed is an understandable phenomenon.

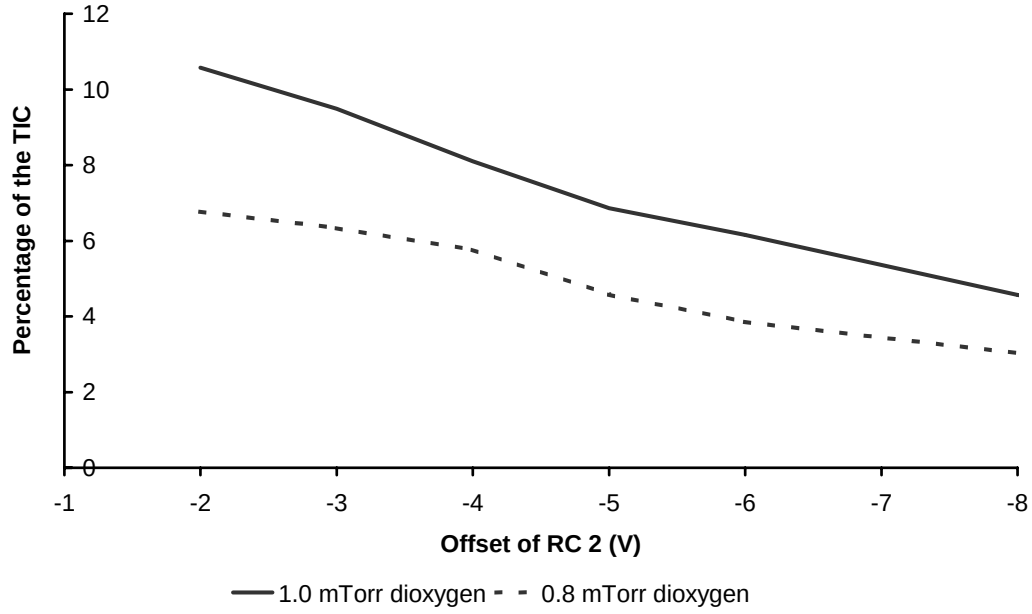

Figure 7.11 *Total yield[29] of $[(Me_2\text{-bpa-Bz})Rh(O_2)]^+$ at different dioxygen pressures in RC 2[30]*

[29] Including the intensity of $\{[Me_2\text{-bpa-Bz})Rh(O_2)]\text{-}H_2O\}^+$.

The reaction with dioxygen in the octopole region clearly depends on the dioxygen pressure. When it is decreased from 1.0 to 0.8 mTorr, the product yield decreases significantly for the Me_2-bpa-Bz rhodium complex, as shown in Figure 7.11.

Such a behavior implies that the reaction with dioxygen is the rate-determining step in the octopole region. Thus either the reaction of $[(L_N)Rh]^+$ with dioxygen or the reaction of $[(L_N)Rh(C_2H_4)]^+$ with dioxygen is rate-limiting.

There was no sign of an rhodium peroxo-ethene signal present in the spectra, which at first does not speak for an associative reaction pathway occurring in the octopole region. Another explanation for the absence of such a peroxo-ethene signal could, of course, also be the fact that the internal energy of the product ions is (as already concluded) quite high. It is known that peroxo-ethene complexes preferably lose the olefin. Such a fragmentation behavior would leave behind the peroxo complex, which is indeed present in the spectra.

In other words, from the absence of the Me_2-bpa-Bz rhodium peroxo-ethene signal, so far, no conclusion can be drawn yet with respect to the type of reaction taking place in the octopole region.

However, the observed behavior that around zero-collision energy the product yield is maximal and that upon increase of the collision energy it decreases again is indicative of an associative reaction taking place (as well).

To get more information on the reaction path leading to the Me_2-bpa-Bz rhodium peroxo complex and to test whether theoretically a dissociative reaction could also occur in the octopole region, we also collided the corresponding naked species, $[(Me_2\text{-bpa-Bz})Rh]^+$ with dioxygen. One of the spectra obtained at 1.0 mTorr dioxygen pressure and $E_{(cm)}$ = 0 eV is shown in Figure 7.12.

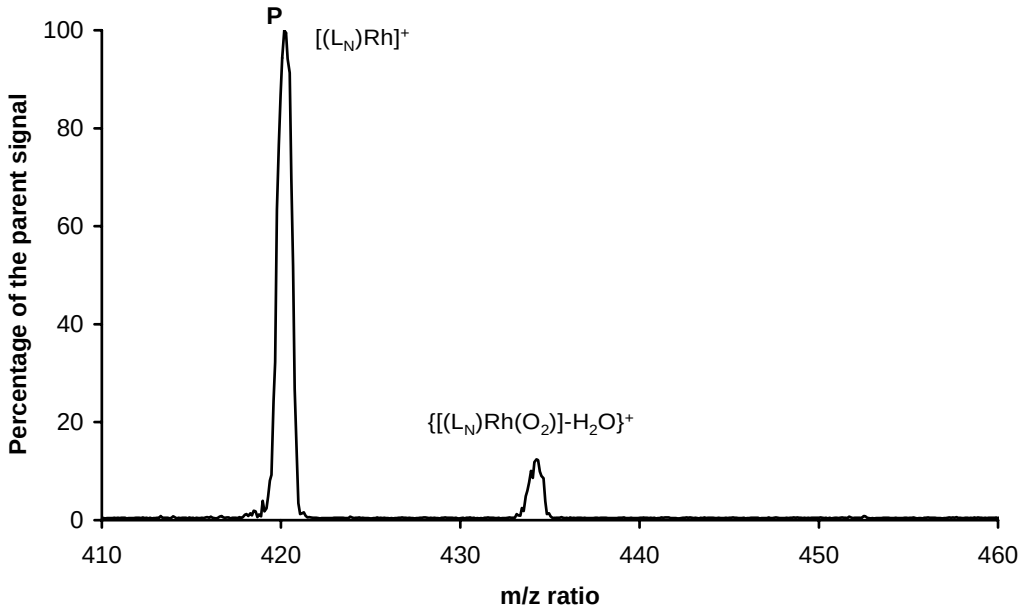

Figure 7.12 *Products obtained upon collision of $[(Me_2\text{-bpa-Bz})Rh]^+$ with 1.0 mTorr $O_{2\,(g)}$ in RC 2*

Indeed the naked species can react with dioxygen in the gas phase, although in somewhat <u>*lower*</u> yields than the ethene complex itself. From this reaction the reactivity of the naked species itself can be deduced. When the

[30] A more negative offset at the entrance of RC 2 results in an increase of the kinetic energy of the ions upon entering the octopole region. Since the ions in the ion beam have a Boltzmann energy distribution, some ions have enough internal energy to fly through RC 2 at less negative offsets of RC 2 than other ions. An offset of -3 V appears to correspond to an average "zero-collision energy" for the ions present in the ion beam (in other words $E_{(lab)} = 3 - V_{offset\ RC\ 2}$). As can be seen in Figure 7.11 the ions in the high-energy tail of the ion beam are also capable of reacting with dioxygen.

ratio $[(L_N)Rh]^+$: $\{[(L_N)Rh(O_2)]\text{-}H_2O\}^+$ = 88 : 12 of Figure 7.12 is used to deduce the amount of peroxo complex obtained via the dissociative pathway in Figure 7.10, then a ratio of dissociative : associative = 4 : 9 is obtained.

On the basis of these Me_2-bpa-Bz rhodium ethene measurements we seem to be able to conclude that probably both pathways, associative and dissociative, can occur in the octopole region. The ratio between the product yields of these two reaction paths will probably change upon variation of not only the nitrogen donor ligand and the metal center, but also of the collision energy (compare the marked difference in reactivity between the tube lens region and RC 1).

Since in the case of the N_4 complexes a dissociative reaction has to be the first reaction step (of either the olefin or one of the pyridyl arms), it can be deduced from the low yield for the Me_3-tpa complex that this pathway is not very favorable in RC 2.

Some of the other N_3 ethene complexes also react with dioxygen in the octopole, but in (much) lower yields. In all cases in which a signal of a reaction product was present in the mass spectra loss of the olefin was the most prominent reaction that took place. The reactivities of all ethene complexes, which display any reactivity at all in the octopole region towards dioxygen, are listed in Table 7.4. For none of these complexes the reaction of the corresponding naked species $[(L_N)M]^+$ towards dioxygen was measured. Therefore we cannot determine the ratio between the dissociative and associative mechanisms for these compounds.

Table 7.4 *Product yields upon collision of $[(L_N)M(C_2H_4)]^+$ with 1.0 mTorr dioxygen in RC 2*

Compound selected for reaction in the octopole	Maximum total product yield [31] (peroxo for Rh, peroxo-ethene for Ir)
$[(Me_2\text{-bpa-Bz})Rh(C_2H_4)]^+$	10.6 %
$[(Me_2\text{-bpa-Me})Rh(C_2H_4)]^+$	3.6 %
$[(bpa\text{-Me})Rh(C_2H_4)]^+$	1.3 %
$[(Me_3\text{-tpa})Rh(C_2H_4)]^+$	0.6 %
$[(bpa)Rh(C_2H_4)]^+$	0.2 %
$[(bpa\text{-Bz})Rh(C_2H_4)]^+$	0.1 %
$[(Me_2\text{-bpa-Me})Ir(C_2H_4)]^+$	0.6 %

In the case of the rhodium compounds the peroxo species was the only product ion that could be observed. Only in the case of bpa-Bz and Me_2-bpa-Bz the peroxo signal was the minor product and the m/z corresponding to $\{[(L_N)Rh(O_2)]\text{-}H_2O\}^+$ was the main product ion signal.
At a first glance at Table 7.4 one would conclude that the Me_2-bpa-Bz and Me_2-bpa-Me rhodium complexes are most reactive and that all other complexes have comparable, very low activities.
However, interpretation of the results appears not to be as straightforward as that. In the case of the Me_2-bpa-Bz and bpa-Bz complex we do know the intensity of the product including its fragments. In other words, we do know that the Me_2-bpa-Bz rhodium complex is highly reactive and the bpa-Bz complex is not.

[31] The product yield corresponds either to the sum of the intensities of the species with an m/z corresponding to $[(L_N)M(O_2)]^+$ and $\{[(L_N)M(O_2)]\text{-}H_2O\}^+$ (bpa-Bz, Me_2-bpa-Bz) or to the intensity of $[(L_N)M(O_2)]^+$ (the other L_N ligands).

In the case of the other complexes, for which the peroxo complex preferably loses O_2, we do not know the intensity of the fragments formed from the peroxo complexes [32], e.g. $[(L_N)M]^+$. On the basis of the behavior for the benzyl-containing complexes, it is expected that such fragments will be formed.

The low reactivity of the bpa-R complexes can probably be explained by the fact that these complexes have to reorganize quite a bit before a reaction with dioxygen can occur (see the MECP structures described § 4.4), which will decrease the probability of a reaction taking place.

In the case of the iridium compound the main product was the peroxo-ethene complex. The corresponding peroxo complex was only formed in minor amounts. A peroxo-ethene complex can only be formed via the associative pathway. This is another indication that associative reactions are possible in the octopole region, though maybe only in small amounts.

For the N_3 iridium ethene complexes, which did not react with dioxygen in RC 2, [33] only fragmentation, e.g. formation of $[(L_N)Ir]^+$ could be observed in the mass spectra. This inactivity is probably mainly due to kinetic reasons. Even the most reactive iridium species, $[(Me_2\text{-bpa-Me})Ir(C_2H_4)]^+$, gave only 0.6 % of the corresponding peroxo complex.

The reactivity in RC 2 shows much resemblance with the one observed in RC 1, both in the nature of products observed (rhodium peroxo and iridium peroxo-ethene complexes) and in the types of complexes that are reactive (mainly bpa-Me, Me_2-bpa-Me and Me_2-bpa-Bz rhodium), although in the octopole region Me_2-bpa-Bz rhodium ethene is more reactive than the corresponding Me_2-bpa-Me complex and in RC 1 this order is reversed.

A difference between the reactivity in RC 2 and RC 1 is that the product yields in the octopole region are much lower, which can of course be explained by the much lower collision frequency in the octopole region due to a dioxygen pressure that is about 100 times lower.

Another difference is that, contrary to the 24-pole region, in which up to 100 % conversion to the corresponding iridium peroxo-ethene was obtained upon going to high dioxygen pressures, the Me_2-bpa-Me iridium ethene complex hardly reacts in the octopole region (max. 0.6 %). This large difference cannot only be due to the lower collision frequency, since the effect is less pronounced for the Me_2-bpa-Bz complex, for example. From Figure 7.9 of § 7.4 it was already clear that in the 24-pole region the iridium complex reacts slower than the Me_2-bpa-R rhodium ethene complexes. But that the iridium complex reacts comparably slow or even seemingly slower than the bpa-Me rhodium ethene complex in the octopole region is not completely in accordance with the 24-pole results (where it seems to be at least twice as active). Perhaps the decrease in yield for the iridium complex is due to the fact that only via an associative reaction a product, the peroxo-ethene, can be obtained (the iridium complexes were not reactive at all in the tube lens region), whereas for the rhodium complexes a significant part of the product intensity in the octopole region can also be attributed to the dissociative pathway.

In all cases in which a reaction occurred in the octopole region a dependence of the product yield on the dioxygen pressure was observed: a decrease in pressure resulted clearly in a decreased yield. Therefore the reaction with dioxygen is really the rate-determining step in the octopole region. However, to which reaction step this rate-determining step corresponds: to a reaction of $[(L_N)M]^+$ with dioxygen or to a reaction of $[(L_N)M(C_2H_4)]^+$ with dioxygen (e.g. a dissociative or an associative reaction), will depend on the type of metal centre and the nitrogen donor ligand. It is clear that, at least for certain compounds, it is possible for both reactions to contribute.

[32] The peroxo fragment for these complexes would be $[(L_N)M]^+$. This species is also a fragment of the parent ion $[(L_N)M(C_2H_4)]^+$. We are not able to determine which part of the $[(L_N)M]^+$ species originate from which complex.

[33] M = Ir, L_N = bpa, bpa-Me, bpa-Bz, Me_2-bpa, Me_2-bpa-Bz

7.5.2 Comparison with other (inert) collision gasses

As already mentioned before, for the bpa-Bz and the Me_2-bpa-Bz rhodium ethene complexes determination of the product yield upon collision with dioxygen seemed quite straightforward, since for these complexes the product ions are $[(L_N)Rh(O_2)]^+$ and $\{[(L_N)Rh(O_2)]\text{-}H_2O\}^+$. In the case of the other N_3 rhodium and iridium complexes, on the other hand, determination of the product yield was a bit more difficult as outlined in Figure 7.13.

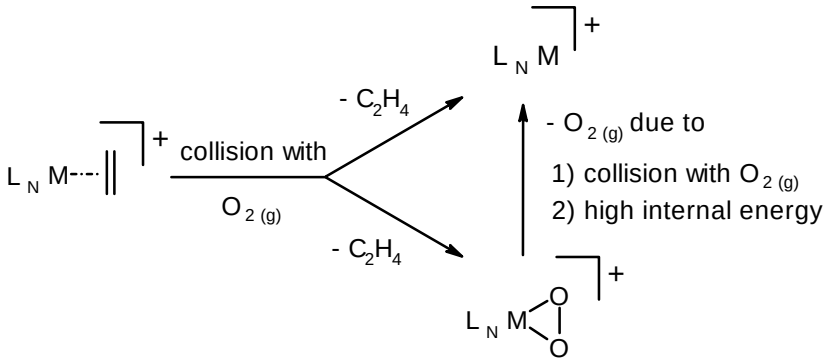

Figure 7.13 *Both reaction and fragmentation of rhodium complexes in RC 2 upon collision with $O_{2\,(g)}$*

When a rhodium ethene complex collides with dioxygen, either a peroxo complex is formed (possibly via a peroxo-ethene complex) or the olefin dissociates, leaving the naked species $[(L_N)Rh]^+$ behind. Due to either the high internal energy of the product ion after formation, or collision with another dioxygen molecule after formation, the peroxo complex can also fragment by loss of O_2, leading to the same $[(L_N)Rh]^+$ species. For the iridium peroxo-ethene complex loss of first ethene and then (in analogy with the rhodium complexes) O_2 is possible.

Therefore, for the complexes investigated part of the observed intensity of the naked species $[(L_N)Rh]^+$ is actually a fragment of the peroxo complex and not of the ethene complex. Thus, it is possible that the product yields in Table 7.4 of § 7.5.1 are underestimated.

In order to be able to correct for this, the N_3 rhodium and iridium complexes investigated [34] were collided with a (supposedly) inert collision gas. Upon comparison of the intensities of the naked species, $[(L_N)M]^+$ (M = Rh, Ir), in the spectra obtained for dioxygen and for the inert collision gas, it should be possible to see whether the peroxo complexes formed also fragment and to which extent this fragmentation occurs.

Collision of $[(L_N)M(C_2H_4)]^+$ with dinitrogen in RC 2

As a collision gas first dinitrogen was chosen, since it is quite similar to dioxygen in three-dimensional structure and vibrational modes. The dinitrogen pressure used (1.0 mTorr) is the same as the one used during the dioxygen measurements. After conversion of $E_{(lab)}$, to collision energies in the center of mass frame, $E_{(cm)}$, it is possible to overlay the spectra obtained for dioxygen and dinitrogen and compare the intensities of the naked species in the spectra at certain collision energies.

An example is given in Figure 7.14 in which for $[(Me_3\text{-tpa})Rh(C_2H_4)]^+$ the increase in intensity of the naked species upon increase of the collision energy $E_{(cm)}$ is shown for both dioxygen and dinitrogen as collision gasses.

The graphs are nearly identical, which implies that no fragmentation of the Me_3-tpa rhodium peroxo species occurs and that the product yield listed in Table 7.4 of § 7.5.1 is correct.

[34] M = Rh or Ir, L_N = bpa-R (R = R^1 = H, Me, Bz) or Me_2-bpa-R (R = R^1 = Me, Bz) or Me_3-tpa.

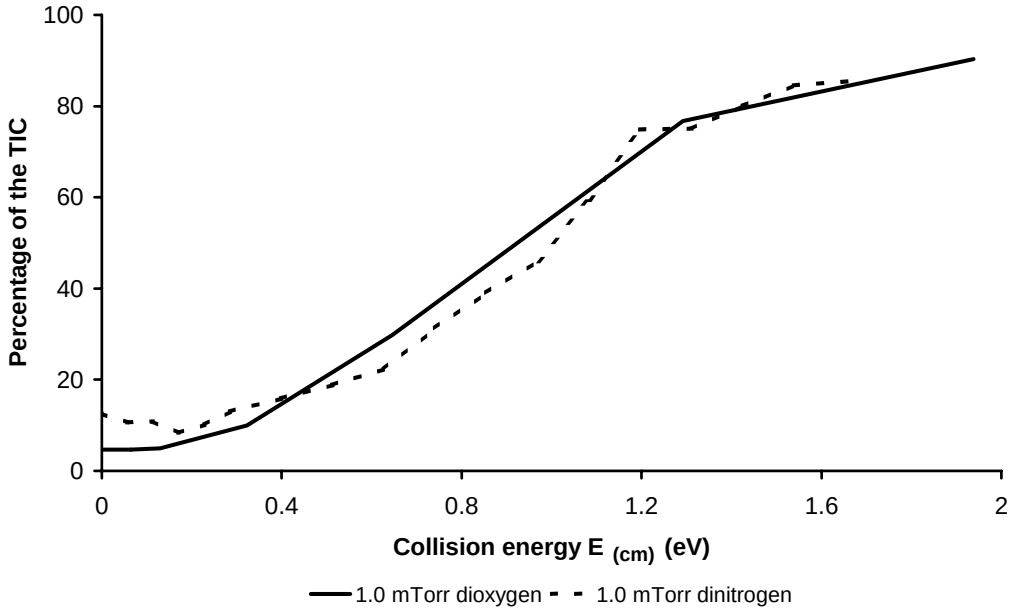

Figure 7.14 *Intensity of $[(Me_3\text{-tpa})Rh]^+$ upon collision of the ethene complex with O_2 or N_2*

For all N_3 rhodium and iridium ethene complexes discussed plots similar to Figure 7.14 could be made. In Figure 7.15 and Figure 7.16 the intensities of the naked species of these complexes are depicted, each graph containing the results per collision gas. To facilitate the interpretation of the results the bulky Me_2-bpa-R rhodium (R = R^1 = Me, Bz) and iridium (R = R^1 = Me) complexes are represented by solid lines and the less bulky bpa-R rhodium complexes (R = R^1 = H, Me, Bz) by dotted lines.

In the case of the bpa-R rhodium complexes no change in behavior takes place upon changing the collision gas. This implies that there is no significant contribution of metal peroxo fragmentation to the observed $[(L_N)M]^+$ yield. Therefore, the product yields as presented in Table 7.4 of § 7.5.1 are correct.
The dinitrogen measurements for the Me_2-bpa-R rhodium (R = R^1 = Me, Bz) and the Me_2-bpa-Me iridium complexes, however, clearly deviate from the dioxygen measurements. Upon collision with dinitrogen much *less* naked species seems to be formed for these complexes.
Since dinitrogen is supposed to be an inert gas, this difference in intensity of the naked species $[(L_N)M]^+$ between the dioxygen and the dinitrogen measurements was ascribed to the extra product yield obtained in the reaction with dioxygen. This seems plausible save for one observation: When only comparing Figure 7.16 with Figure 7.15 the slopes of the different curves (which should represent in a way the binding strength of the olefin/dioxygen molecule to the metal center) have significantly changed. From Figure 7.16 only one would be led to conclude that the olefins of the Me_2-bpa-R rhodium complexes are much more strongly bound to the metal center than the olefins of the bpa-R rhodium complexes, which is not in agreement with the theoretical calculations presented in Appendix A, nor with the already high intensity of $[(Me_2\text{-bpa-R})M]^+$ at a collision energy of 0 eV (above 40 %), which implies that the olefin is not too strongly bound to these Me_2-bpa-R rhodium complexes.

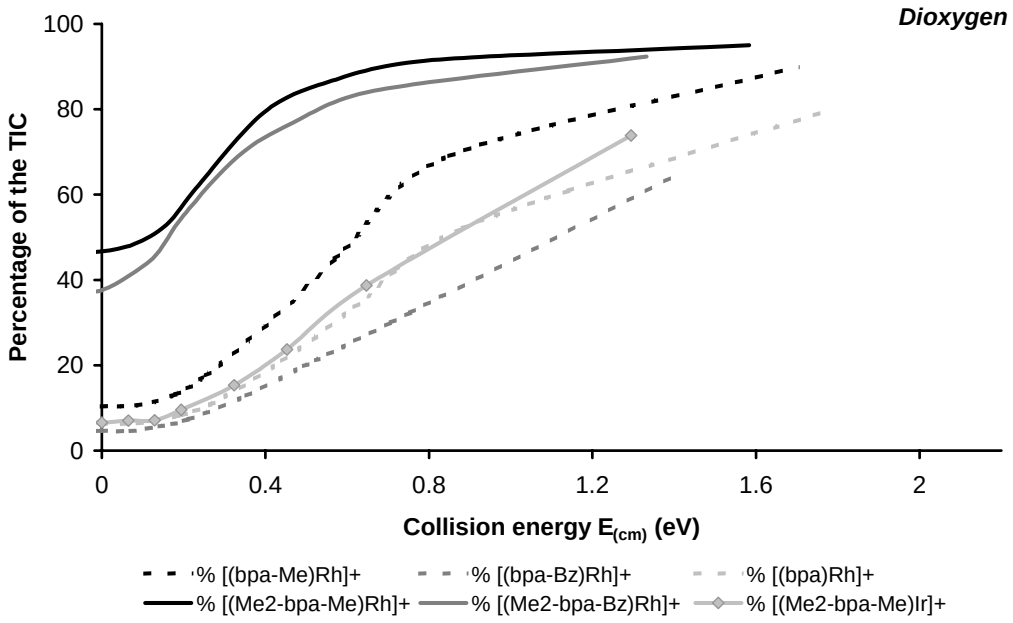

Figure 7.15 *Intensity of $[(N_3)M]^+$ upon collision of the ethene complex with 1.0 mTorr $O_{2\,(g)}$ in RC 2*

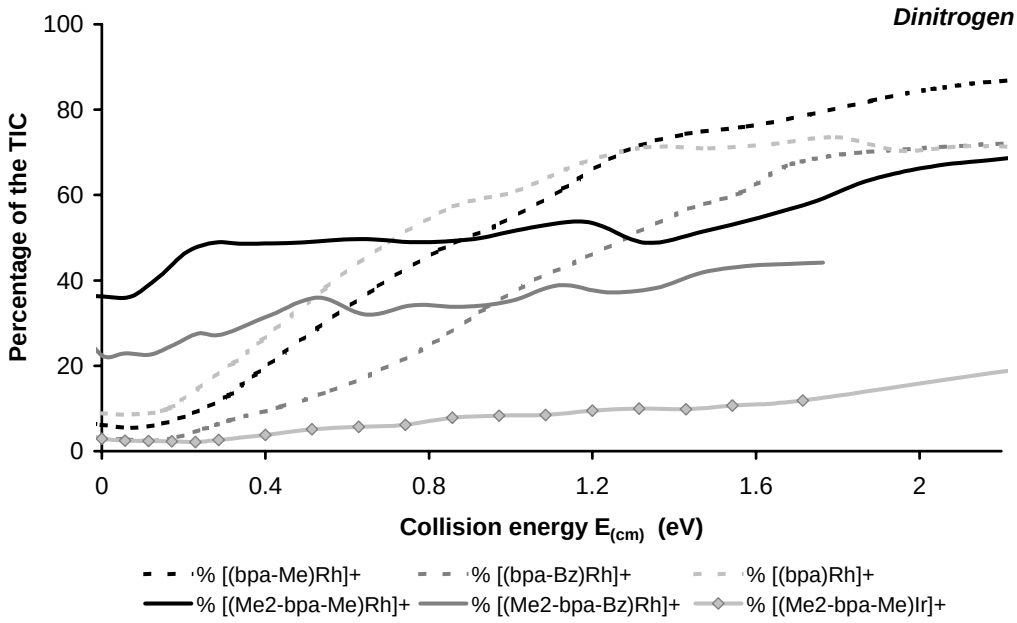

Figure 7.16 *Intensity of $[(N_3)M]^+$ upon collision of the ethene complex with 1.0 mTorr $N_{2\,(g)}$ in RC 2*

How can this sudden change in behavior upon change in collision gas be explained?

To obtain more information we compared the results for dioxygen (Figure 7.15) and dinitrogen (Figure 7.16) with those for argon.[35]

[35] The argon measurements were discussed previously in § 6.3. In Figure 6.2 of § 6.3 the total fragment intensity is displayed, whereas in Figure 7.17 only the intensity of $[(L_N)M]^+$ is shown.

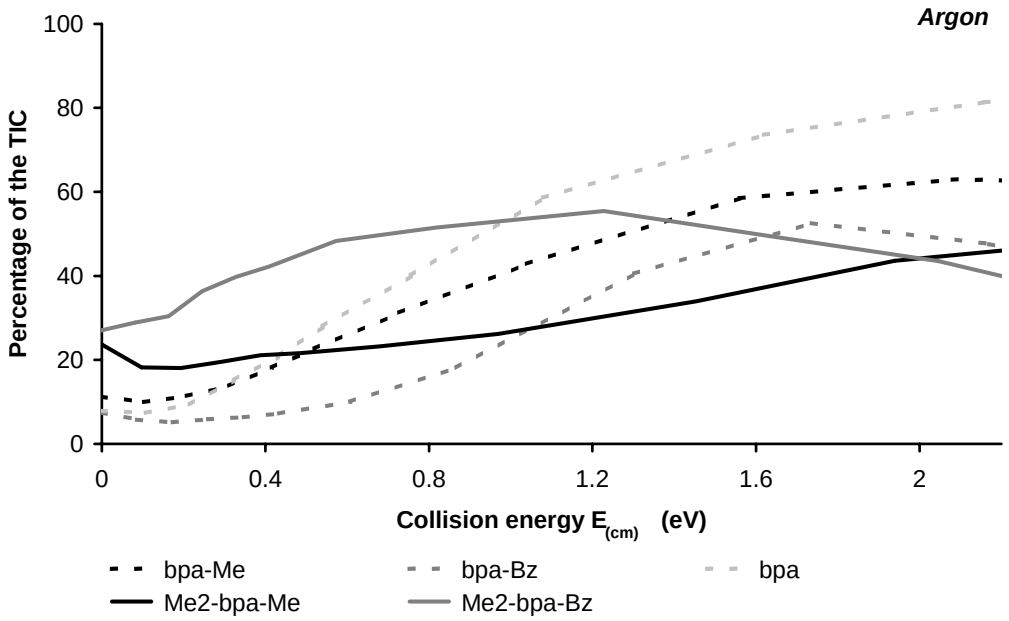

Figure 7.17 *Intensity of $[(N_3)Rh]^+$ upon collision of the ethene complex with 0.80 mTorr argon in RC 2*

The argon measurements of the bpa-R rhodium complexes are comparable [36] to both the dioxygen and the dinitrogen measurements.

Only in the case of the Me_2-bpa-R rhodium complexes we see a clear deviation between the results of the three collision gasses (Figure 7.18). Again the ***dinitrogen*** and ***argon*** measurements are comparable [36].

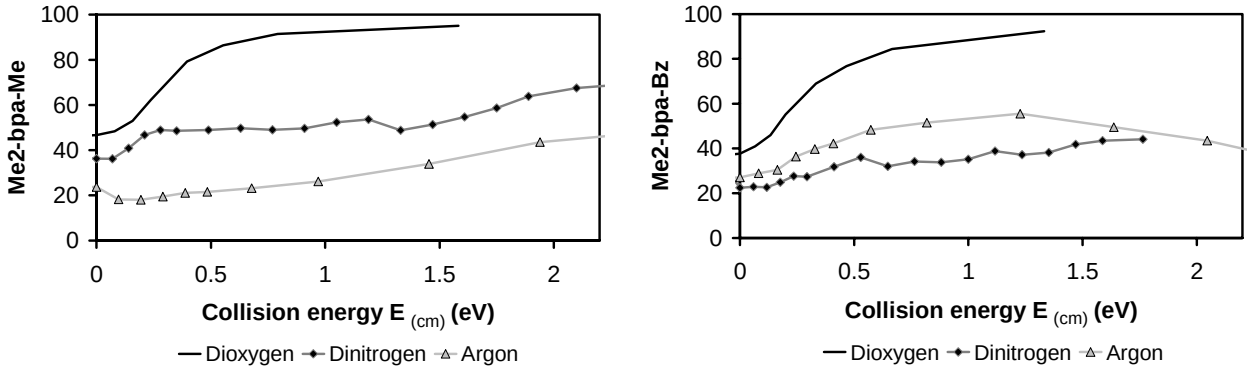

Figure 7.18 *Intensity of $[(Me_2\text{-bpa-R})Rh]^+$ upon collision with 3 different collision gasses in RC 2*

The ***dioxygen*** measurements, on the other hand, deviate a lot from both the dinitrogen and argon measurements. Apparently, above ca. 0.1 eV a reaction with dioxygen takes place for the Me_2-bpa-R rhodium complexes and the yield increases upon increase of the collision energy.

This reaction is expected to be formation of the corresponding peroxo complexes. The increase of the intensity of the naked species $[(Me_2\text{-bpa-R})Rh]^+$ at higher collision energies can then be explained by fragmentation of the increasing amount of peroxo ions that are being formed. This is due to the increase in internal energy upon increase in collision energy.

[36] The argon measurements were performed at a pressure of only 0.8 mTorr instead of 1.0 mTorr (like for O_2 and N_2). If collision with argon results (as expected) in the same kind of fragmentation as collision with N_2, then the $[(L_N)Rh]^+$ intensity is expected to be lower for argon than for N_2 due to the decrease in number of collisions upon decrease of the collision gas pressure. Taking this into account, the intensities observed for these two collision gasses (Figure 7.18) can be considered to be comparable.

Apparently, there is no large difference in reactivity between the Me_2-bpa-Me and Me_2-bpa-Bz complex. The latter is in contrast with the reactivities observed at near zero collision energy in RC 2 as displayed in Table 7.4 of § 7.5.1, in which Me_2-bpa-Bz was clearly more reactive and already yielded about 10 % of peroxo complex.

Since only the Me_2-bpa-R complexes behave differently, it is expected that the distorted square planar structures (which induce an alteration of the energy levels of the orbitals) and maybe pre-organization of the olefin (§ 4.4) are important factors.

The question raised concerning the decrease in slope of the curves on going from bpa-R to Me_2-bpa-R in Figure 7.16 (which was for us a reason to make a comparison with the argon measurements) can be answered by not only considering the intensity of $[(L_N)Rh]^+$ but of all the fragments related to this species. Take for example the graph presented in § 6.3 for the argon measurements (Figure 7.19).

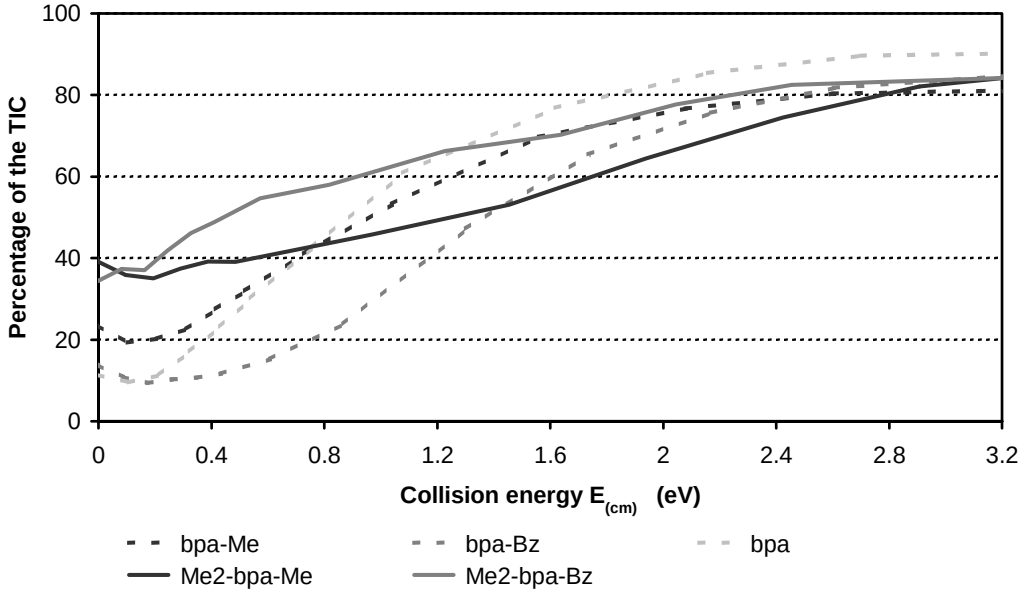

Figure 7.19 *Total fragment intensity upon collision of $[(N_3)Rh(C_2H_4)]^+$ with 0.8 mTorr argon in RC 2*

In this graph the total fragment intensity reaches for all N_3 rhodium complexes a similar value upon increase of the collision energy, indicating that for the Me_2-bpa-R complexes the $[(L_N)Rh]^+$ species fragments more easily than for the bpa-R complexes.

7.5.3 Conclusions from reactions of olefin complexes performed in the octopole region (RC 2)

The reactivity observed in RC 2 shows much resemblance with the one observed in RC 1, for which an associative reaction pathway has been proposed in § 7.4: not only in the nature of the products observed, but also in the pressure dependence of the product yield and in the types of complexes which are reactive. Only a few mainly N_3 rhodium and iridium ethene complexes react with dioxygen.

For most of the complexes investigated the product yield in the octopole region (of peroxo or peroxo-ethene complexes) is maximal at zero-collision-energy and decreases upon increase of the collision energy. Only for the Me_2-bpa-R complexes the product yields increase again above a collision energy of about 0.1 eV. Upon increase of the dioxygen pressure the product yield increases, implying that the reaction with dioxygen is the rate-determining step.

Both associative and dissociative reactions take place around zero collision energy in the octopole region. The ratio between the product yields obtained from these reactions depends on the nitrogen donor ligand and the

metal center. In a few cases it was even possible to estimate this ratio, either because it was possible to compare the reactivity of $[(L_N)Rh]^+$ with that of $[(L_N)Rh(C_2H_4)]^+$ or because clearly an associative product was obtained (iridium peroxo-ethene).
At higher collision energies only dissociative reactions are expected to take place. The difference in reactivity between the N_3 rhodium complexes could then be explained by looking at the calculated binding strengths of ethene (Appendix A): these decrease on going from bpa-R (~ -30kcal/mol) to Me_2-bpa-R (~ -14 kcal/mol).

All iridium ethene complexes investigated but one, the Me_2-bpa-Me iridium complex, are unreactive in RC 2. This is probably both due to kinetic reasons and due to the fact that the iridium complexes only seem to react via the associative pathway, which is less pronounced in RC 2. Even the most reactive iridium-ethene complex (Me_2-bpa-Me) displays only very low activity towards dioxygen in the octopole region.

The reactive complexes are mainly those N_3 rhodium complexes with methyl substituents at the 6-position of both pyridine rings. For reactions following a dissociative path, the weaker metal-olefin bond may be important. For associative paths, the pre-organization present in the Me_2-bpa-R complexes may contribute.
The Me_3-tpa rhodium ethene complex is only slightly reactive towards dioxygen in RC 2.
The low reactivity of N_4 rhodium complexes could be explained by strong metal-olefin bonding (preventing dissociation) and coordinative saturation (preventing association).

Upon collision with argon only fragmentation takes place, displaying clearly the expected trends in binding strength of the olefin to the metal center for the different complexes: decrease upon going from bpa-R to Me_2-bpa-R rhodium and also decrease upon going from iridium to rhodium. These trends are similar to the ones observed when dinitrogen is used as a reagent gas.

7.6 Reaction of peroxo complexes towards α-olefins

7.6.1 Reaction towards 1-butene in RC 2

In the previous section we saw that only one iridium ethene complex reacted in RC 2 with dioxygen under the formation of a product with molecular formula $[(L_N)Ir(C_2H_4O_2)]^+$ and in only very low yields. Such species complexes were never observed for the rhodium ethene complexes. This leaves the question open whether rhodium peroxo-ethene complexes are accessible or not: does rhodium react via a different pathway than iridium or is the rhodium peroxo-ethene complex too unstable due to its high internal energy upon formation. Another interesting question concerns the structure of the $[(L_N)M(C_2H_4O_2)]^+$ product formed: is it a peroxo-ethene complex, which can easily lose C_2H_4 in the gas phase, or is it a five-membered ring 3-rhoda-1,2-dioxolane species? In other words, is it possible for C-O bond formation to take place upon reaction of a rhodium ethene complex with dioxygen in the gas phase or not?

Since upon collision of the rhodium ethene complexes with dioxygen both in RC 1 and RC 2 only peroxo complexes were formed, it does not seem possible to obtain a rhodium peroxo-olefin (or dioxolane) complex starting from the olefin complex.
Therefore, to check whether it is really impossible to obtain such peroxo-olefin or dioxolane complexes in the octopole region for rhodium, the corresponding rhodium peroxo complexes were collided with 1-butene in the octopole region. Butene was chosen as a collision gas instead of ethene, since it is expected that the alkyl tail of this olefin can help in dissipating the excess internal energy of the product after reaction, preventing fragmentation of the initial product.

Several N_3 and N_4 rhodium peroxo complexes,[37] were tested for their reactivity in the reaction with 1-butene in the octopole region. At zero-collision energy the highest product yields, if any, were obtained.
As can be seen in Figure 7.20 three types of product ion signals can be observed in the spectra upon collision of a peroxo complex with 1-butene (besides the normal fragmentation resulting in the formation of $[(L_N)Rh]^+$): the product resulting from an addition reaction, $[(L_N)Rh(O_2)(1\text{-butene})]^+$, the exchange product, $[(L_N)Rh(1\text{-butene})]^+$ and a species in which one oxygen atom has been abstracted, leaving a species with an m/z corresponding to an oxo species behind.
For most complexes some several of these product ion signals were clearly present in the mass spectra (although sometimes in very low yields), as shown in Table 7.5.

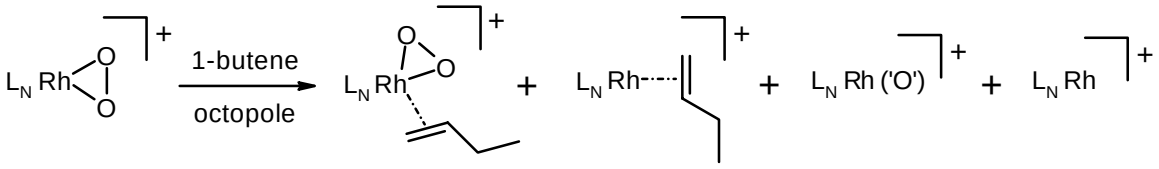

Figure 7.20 *Reaction of $[(L_N)Rh(O_2)]^+$ with 1-butene in RC 2*

Table 7.5 *Yields[a] (% of the TIC) upon collision of $[(L_N)M(O_2)]^+$ with 1-butene in RC 2 at $E_{(cm)} \approx 0$ eV*

Compound	Gas pressure	$[(L_N)M(O_2)(butene)]^+$	$[(L_N)M(butene)]^+$	$[(L_N)M('O')]^+$	$[(L_N)M]^+$
$[(bpa)Rh(O_2)]^+$	0.04 mTorr	5.0	4.0	--	3.0
$[(bpa\text{-}Bz)Rh(O_2)]^+$	0.04 mTorr	0.2[38]	0.2	--	0.2
$[(bpa\text{-}Me)Rh(O_2)]^+$	0.22 mTorr	2.8	2.4	0.7	3.7
$[(Me_2\text{-}bpa\text{-}Me)Rh(O_2)]^+$	0.22 mTorr	1.1	11.9	7.3	25.7
$[(Me_2\text{-}tpa)Rh(O_2)]^+$	0.03 mTorr	--	1.0	--	1.0
$[(Me_3\text{-}tpa)Rh(O_2)]^+$	0.03 mTorr	--	0.7	--	0.7
$[(tia)Rh(O_2)]^+$	0.06 mTorr	0.5	0.5	--	0.6

a) The N_3 rhodium peroxo complexes were collided in the octopole region of the Finnigan TSQ 700, whereas for the N_4 rhodium peroxo complexes the 1-butene measurements were performed at the Finnigan TSQ 7000. Therefore it will be difficult to compare yields between the N_3 and the N_4 rhodium peroxo complexes. Only within a group of complexes (N_3 or N_4) it is possible to compare the yields.

The Me_2-bpa-Bz and tpa rhodium peroxo complexes were not reactive at all towards 1-butene (except for a trace of a signal which could correspond to $[(tpa)Rh(1\text{-butene})]^+$).

Since the measurements for the bpa-Me and Me_2-bpa-Me peroxo complexes were performed at much higher pressures, it is not possible to compare all the observed product yields. What is clear from Table 7.5 is that the most reactive complexes appear to be the bpa, bpa-Me and Me_2-bpa-Me rhodium peroxo species.

For the bpa complex the peroxo-butene complex and the butene complex are generated in almost equal quantities.

[37] L_N = bpa-R (R = R^1 = H, Bz), Me_2-bpa-Bz, tpa, Me_2-tpa, Me_3-tpa, tia (tia = *N*,*N*-di[(1-methyl-1*H*-2-imidazolyl)methyl]-*N*-[(1-methyl-1*H*-3-pyrazolyl)methyl]amine)

[38] For the bpa-Bz rhodium peroxo complex no daughter corresponding to $[(bpa\text{-}Bz)Rh(O_2)(1\text{-butene})]^+$ was present in the spectra, but a daughter corresponding to $\{[(bpa\text{-}Bz)Rh(O_2)(1\text{-butene})]\text{-}H_2O\}^+$, which is present in 0.2 % yield as shown in Table 7.5.

For the bpa-Me complex this is also the case; a small amount of a species with an m/z corresponding to an oxo species is also present in the mass spectra.

For the Me_2-bpa-Me complex the intensity of the peroxo-butene complex is no longer similar to that of the butene complex. This may be due to a reaction taking place upon collision with a butene molecule resulting in the formation of $[(Me_2\text{-bpa-Me})Rh('O')]^+$.[39] Possibly, upon collision with 1-butene one oxygen atom is transferred in the ion-molecule complex before the olefin coordinates to the metal center. C-O bond formation after coordination of the olefin to the metal center seems unlikely, since for the Me_2-bpa-Me *iridium* peroxo-ethene complex such a reaction was never observed in solution.

The structure of the complexes with an m/z corresponding to $[(L_N)Rh('O')]^+$ cannot be determined, since they are generated in RC 2. Oxo species are expected to be highly reactive, as explained in § 6.5.2. It is therefore possible that they rapidly rearrange, e.g. by protonation to hydroxo species or insertion in a rhodium-pyridine bond.

For the N_4 rhodium peroxo complexes and the benzyl-substituted N_3 complexes little or no reaction was observed. Apparently it is difficult for the N_4 complexes to become κ^3-coordinated; this is necessary before they can react with the olefin under the formation of a peroxo-olefin complex. The small amount of $[(N_4)Rh(1\text{-butene})]^+$ observed probably stems from the reaction of the naked species $[(N_4)Rh]^+$ with 1-butene. The lack of reactivity for the benzyl-substituted N_3 peroxo complexes can probably be explained by shielding of the vacant site at the metal center by the benzyl substituent.

7.6.2 Reaction of the bpa rhodium peroxo complex with 1-butene in RC 1

An attempt was made to perform the reaction of the bpa rhodium peroxo complex with 1-butene also in the 24-pole region (the collision gas pressure used during the measurements was however unknown).

All cations that are transferred to the gas phase enter RC 1. Since the intensity of the bpa rhodium peroxo complex is much lower than that of the ethene complex (almost 96 % of the TIC), the main reaction product formed upon collision with 1-butene in RC 1 is $[(bpa)Rh(1\text{-butene})]^+$ (exchange of ethene for 1-butene)[40] and only in minor amounts a peroxo-butene complex is formed.

According to the decrease of the peroxo intensity nearly full conversion of the peroxo complex to a species with a m/z corresponding to $[(bpa)Rh(O_2)(1\text{-butene})]^+$ takes place (a product which was previously observed upon collision of $[(bpa)Rh(O_2)]^+$ with 1-butene in RC 2). The connectivity of the atoms (peroxo-olefin complex or dioxolane) can, however, not be determined from MS data since it was generated in RC 2.

7.6.3 Reaction with ethyl-vinylether in the 24-pole region (RC 1)

From the results in the previous paragraph, it was difficult to determine whether for the bpa complex formed upon collision of the peroxo complex with 1-butene C-O bond formation had taken place (resulting in a dioxolane species) or not (a peroxo-olefin complex). To investigate whether such a C-O bond formation can take place at all in the gas phase ethyl-vinylether, a more activated olefin than 1-butene, was chosen as a

[39] In the tube lens region (§ 6.4), nor upon collision with argon such a loss of a species with a mass of 16 was never observed upon fragmentation of the Me_2-bpa-Me peroxo complex. Therefore it must be attributed to a reaction with 1-butene.

[40] Upon collision of $[(Me_2\text{-bpa-Bz})Rh(C_2H_4)]^+$ with 1-butene in RC 2 (at only 0.04 mTorr pressure and at around 0 eV collision energy), up to 13 % of the ethene complex had already exchanged ethene for 1-butene, which is quite a lot (also fragmentation reaction took place upon collision with 1-butene: 22 % of the TIC corresponded to $[(Me_2\text{-bpa-Bz})Rh]^+$). In other words, it is possible for N_3 rhodium ethene complexes to exchange their olefin in the gas phase for another one, like 1-butene.

collision gas. Three N_3 rhodium peroxo complexes[41] were collided with this substrate in RC 1 at different collision gas pressures.

Already at an ethyl-vinylether pressure of 1.25 mTorr in the 24-pole region two of the rhodium peroxo complexes (L_N = bpa, bpa-Me) underwent full conversion to the corresponding $[(L_N)Rh(O_2)(\text{ethyl-vinylether})]^+$ complexes. The connectivity of the complexes was confirmed by subsequent fragmentation in the octopole region by collision with argon (Figure 7.21).

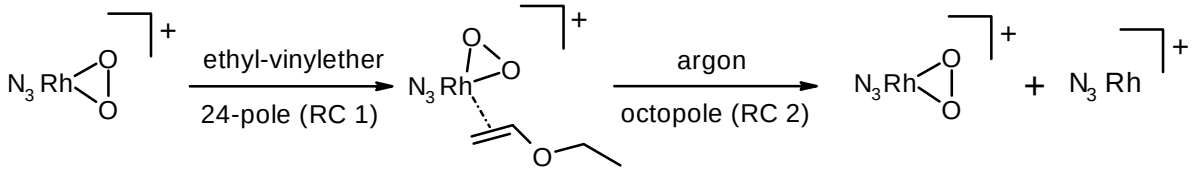

Figure 7.21 *Formation of $[(L_N)Rh(O_2)(\text{ethyl-vinylether})]^+$ in RC 1 (L_N = bpa, bpa-Me)*

For both peroxo-olefin complexes the preferred fragmentation is first loss of the ethyl-vinylether molecule. When the collision energy is increases even more, the dioxygen molecule also dissociates. From this particular fragmentation behavior it can be concluded that the complexes formed are peroxo-olefin complexes formed and that no C-O bond formation takes place (else loss of an aldehyde would have been expected: see § 6.5.1).

The bpa-Bz rhodium peroxo complex did not react in RC 1 with ethyl-vinylether. Complicating reactions like aromatic C-H activation or π-coordination of the aryl-ring, which could shield off the vacant site at the metal center, could play a role here.

7.6.4 Conclusions from gas-phase reactions of peroxo complexes towards olefins

From gas-phase collision experiments of rhodium peroxo complexes with an olefin, like 1-butene and ethyl-vinylether, it is clear that rhodium peroxo-olefin complexes are stable enough to be formed in the octopole region. From the results obtained with ethyl-vinylether, they appear really to be peroxo-olefin complexes.

Why it is possible to obtain a peroxo-olefin complex when peroxo complexes are collided with dioxygen, but not when ethene complexes are collided with dioxygen remains puzzling.

One important factor that can be of influence here is that olefins like 1-butene and ethyl-vinylether can easily dissipate some of the excess of internal energy of the product molecule due to their 'tail' and hereby prevent the peroxo-olefin complex from fragmenting.

Another possible explanation could have something to do with these associative reactions being exothermic. A metal-dioxygen bond is much stronger than a metal-olefin bond. Upon coordination of a dioxygen molecule to a metal-olefin complex the internal energy of the complex would increase with an amount that would exceed the energy necessary for dissociation of the olefin, whereas upon coordination of an olefin to a metal-peroxo complex the internal energy of the complex will increase, but never enough to result in dissociation of the dioxygen moiety.

[41] The sterically less demanding N_3 ligands bpa, bpa-Me and bpa-Bz were chosen, because the steric bulk imposed by methyl substituents at pyridine rings is expected to prevent any C-O bond formation (e.g. in solution for the Me_2-bpa-Me iridium complex only the peroxo-ethene complex could be obtained, which cannot undergo any C-O bond upon activation either, § 4.2.1).
Only N_3, not N_4, rhodium peroxo complexes were chosen to react, because it is expected that a vacant site is necessary for these reactions to occur (the reactivity towards 1-butene was very low for the N_4 complexes).

7.7 Collision of 1-butene complexes with dioxygen in the octopole region

As already mentioned before, bigger ions have a larger density of states (more degrees of freedom), which causes them to fragment slower upon collision with a neutral molecule than smaller ones. This is due to the fact that the internal energy of the ion after collision must accumulate in the reaction coordinate for fragmentation to happen. This becomes less and less probable for bigger systems with more degrees of freedom. Therefore, it was thought that perhaps if rhodium complexes with 1-butene instead of ethene coordinated to the metal center were introduced in RC 2 and collided with dioxygen, formation of rhodium peroxo-olefin complexes indeed might be observed, due to its increased life-time.

The bpa-Me and Me_2-bpa-Me rhodium ethene complexes were collided with 1-butene in the 24-pole region to exchange ethene for 1-butene and the corresponding $[(L_N)Rh(1\text{-butene})]^+$ complex was mass-selected and collided with dioxygen in the octopole.

We only observed loss of the olefin (which appears to be less strongly bound for the Me_2-bpa-Me complex), no reaction product from a reaction with dioxygen (there was only a trace signal present that could correspond to $[(Me_2\text{-bpa-Me})Rh(O_2)]^+$).

An unexpected signal present in the spectra of the bpa-Me complex corresponded to $\{[(bpa\text{-}Me)Rh]\text{-}H_2\}^+$. The intensity of this species was similar to that of $[(bpa\text{-}Me)Rh]^+$. Such a species was never observed when the corresponding ethene instead of 1-butene complex was collided with dioxygen in RC 2. Either it has something to do with a reaction with dioxygen after all (loss of H_2O_2), or the distribution of the vibrational modes has changed to such an extent upon going from the ethene to the 1-butene complex that loss of H_2 has become more favorable.

7.8 Absence of reactivity for the iridium(II) ethene complexes

The Me_2-tpa and Me_3-tpa iridium(II) ethene complexes as described in Chapter 5 were collided both in RC 1[42] and in RC 2[43] with dioxygen. For neither of the complexes a reaction took place in either of the regions. If in the complexes the unpaired electron density would have been mainly on the olefin moiety, giving the complex an ethyl radical character, a reaction would indeed have been expected. Take for example the reaction towards dioxygen in solution in acetonitrile (see § 5.4.1): here the Me_3-tpa complex reacted under formation of the complex $[(Me_3\text{-}tpa)Ir^{III}(formylmethyl)(MeCN)]^{2+}$, a C-O bond was formed.

7.9 Discussion and conclusions

As already postulated in § 7.1.1 no gas-phase single-electron-transfer reactions are expected to take place inside the mass spectrometer upon collision of metal olefin complexes with air or dioxygen. Indeed we do not see the separate ions that would result from these reactions: dicationic metal complexes and superoxide anions. However, we have to keep in mind that if such species are formed, it is possible that due to the expected strong electrostatic interactions they would remain together as an ion pair $\{[(L_N)M(C_2H_4)]^{2+}(O_2)^{\bullet-}\}^+$. In such a case we will not be able to distinguish these complexes from other species with the same molecular formula (peroxo-ethene or dioxolane complexes). Maybe on the basis of fragmentation behavior (easy loss of O_2 instead of C_2H_4 opposite to the fragmentation behavior of the peroxo-ethene complexes) it should be possible to distinguish such ion pairs from complexes in which the dioxygen molecule resides in the first coordination sphere of the metal center.

[42] Pressures of collision gas applied to RC 1: 10, 20, 31 and 51 mTorr.

[43] 1.30 mTorr dioxygen pressure, $0 < E_{(lab)} < 15$ eV.

The type of reaction taking place upon collision of a metal olefin complex with dioxygen depends strongly on the properties of the reaction region in the mass spectrometer.

In the tube lens region reactions are performed at high collision energies and high collision gas pressures. Therefore dissociative processes are favored over associative processes. As a result only N_3 and N_4 *rhodium* ethene complexes are reactive.

In the RC 1, on the other hand, reactions are performed at near zero-collision energy and at relatively high collision gas pressures. In this region only associative pathways are accessible. Therefore none of the N_4 rhodium and iridium ethene complexes are reactive in this region.

In the case of the N_3 complexes, the *distorted* square-planar Me_2-bpa-R (R = R^1 = Me, Bz) rhodium and Me_2-bpa-Me iridium ethene complexes are much more reactive in RC 1 than their almost perfectly square-planar bpa-R counterparts.

The reactions taking place in RC 2 show much resemblance to the ones observed in RC 1; not only in the nature of the products observed, but also in the pressure dependence of the product yield and in the types of complexes which are reactive. For only a few rhodium and iridium ethene complexes a reaction with dioxygen takes place.

When reactions are performed at near zero collision energy, associative and dissociative reactions seem to occur simultaneously in the octopole region. The ratio of the product yields of these two pathways depends on the nitrogen donor ligand and on the metal center. For a few complexes the contributions of both paths could be estimated: they were found to be similar.

At higher collision energies only dissociative reactions are expected to take place. The difference in reactivity between the N_3 rhodium complexes can then probably be explained by the strength of ethene-binding to the metal center.

Upon collision of N_3 rhodium peroxo complexes with olefins, like 1-butene and ethyl-vinylether, it was possible to obtain peroxo-olefin complexes also for rhodium. Why these peroxo-olefin complexes are only obtained starting from the corresponding peroxo complexes and not starting from the olefin complexes (ethene or 1-butene) is not clear. A possible explanation could have something to do with these associative reactions being exothermic. A metal-dioxygen bond is much stronger than a metal-olefin bond. Upon coordination of a dioxygen molecule to a metal-olefin complex the internal energy of the complex would increase with an amount that would exceed the energy necessary for dissociation of the olefin, whereas upon coordination of an olefin to a metal-peroxo complex the internal energy of the complex will increase, but never enough to result in dissociation of the dioxygen moiety.

In most reaction regions most of the N_3 and N_4 iridium ethene complexes are not reactive at all towards dioxygen/air. In the tube lens region and in RC 2 this is probably due to short reaction times, since it is known that iridium complexes are usually kinetically more inert than their rhodium counterparts.

In RC 2, the Me_2-bpa-Me iridium ethene complex still has a lower reaction rate than the corresponding rhodium complex. But since the dioxygen pressure can be increased up to 150 mTorr, it is possible to go up to 100 % conversion for this iridium complex. The high reactivity of this complex is probably due to its distorted square planar structure and the fact that it has a methyl substituent attached to the amine-nitrogen which is not reactive in itself (unlike for example a benzyl-substituent, which can easily undergo aromatic C-H activation).

7.10 Experimental section

7.10.1 General methods

All procedures were performed under a nitrogen atmosphere using standard Schlenck techniques, unless indicated otherwise. Solvents (p.a.) were deoxygenated by bubbling through a stream of nitrogen or by the freeze-pump-thaw method. Some

solvents were distilled under a nitrogen atmosphere to remove last traces of water and dioxygen: acetonitrile was distilled over potassium, THF and CH_2Cl_2 over CaH_2. The temperature indication r.t. corresponds to ca. 20 ºC.

Compounds $[(tia)Rh(C_2H_4)_n]^+$ (n = 1, 2; a mixture), $[(tpa)Rh(C_2H_4)]^+$ and $[(Me\text{-}tpa)Rh(C_2H_4)]^+$ were prepared as described by M.Krom. [35] All other chemicals used were either synthesized according to the experimental section in Chapter 3 or were obtained commercially and used without further purification.

7.10.2 Calculations

All geometry optimizations were carried out with the Turbomole program [36] coupled to the PQS Baker optimizer. [37], [38] Geometries were fully optimized as minima at the bp86 [39], [40] level using the Turbomole SV(P) basis set [44] [41] on all atoms Improved energies were obtained from single-point calculations at the b3-lyp level [42] – [45] using the TZVPP basis [45], [46]. Entropy corrections (to obtain $\Delta G_{343\ K,\ 0.001\ bar}$ and $\Delta G_{298\ K,\ 1\ bar}$) were performed to take into account that the number of reactants is not always the same as the number of products. They were performed according to standard formulas of statistical thermodynamics. [2]

7.10.3 ESI^+-MS measurements

General ESI-MS setup for the experiments

Electrospray ionization (ESI) mass spectra were measured on a modified Finnigan MAT TSQ 700 as previously described. [27], [47] – [64]

Typically solutions with a concentration of 10^{-5} M of the desired compounds (prepared in the glove-box under a nitrogen atmosphere) were electrosprayed at a flow-rate of 3 - 15 ml/min at 3 - 5 kV and a capillary temperature of 150 ºC. In some cases dinitrogen was used as a sheath gas. The tube lens potential was varied between 35 and 140 V (referenced to m/z = 500) depending on the complex.

For most of the measurements either solutions in pure THF or in 0.02 % MeCN in THF were used depending on the solubility of the compounds. For the measurements in the tube lens region as described in § 7.3 for the Me_2-bpa-Me, tpa and Me_2-bpa-Bz also measurements were performed in acetone to see if the product yield changed upon changing the solvent. The solvent appeared to be not of influence.

Daughter-ion spectra were recorded in daughter-ion mode, that is, the first quadrupole was used to mass select ions of a single mass-over-charge ratio, which were then collided with a target gas in RC 2. The second quadrupole was operated in scanning mode in order to detect the ionic fragments. The collision energy could be varied by applying different potentials (to a lens in front of the second octopole), which altered the velocity of the ions on their way into the collision region (the collision energies are given in eV, lab frame).

The pressure in the collision cell (RC 2) was read both from a Pirani gauge and with a Capacitance gauge. The pressure in the 24-pole (RC 1) was also read from a Pirani gauge. The pressures of the Pirani gauges were calibrated to those displayed bye the Capacitance gauge (see for more details the Experimental of Chapter 2). All gauges are directly attached to the housing of the two multipoles.

Subdivision of TIC among the different species in the raw spectra

For determining the exact percentage of the total ion current (TIC) which belongs to the different species, L_N rhodium ethene complex, peroxo complex and naked species, $[(L_N)Rh]^+$, also the intensity of the fragments belonging to each of these species has to be taken into account. Determination of which fragment belongs to which species is done by looking in the daughter scan modus to see how the three species fragment and by looking in the parent scan modus to see if the observed fragment really belongs to one of these species. (see § 6.4 for the typical fragmentation behavior of the three different species: homolytic bond splitting versus loss of a neutral non-radical species).

The intensities of signals corresponding to fragmented ethene complex were not added to the $[(N_4)Rh(C_2H_4)]^+$ intensity in Figure 7.5, instead shown separately, since only the intact ethene complex is reactive. All signals in the mass spectra could be classified as deriving from these three species $[(L_N)Rh(C_2H_4)]^+$, $[(L_N)Rh(O_2)]^+$ and $[(L_N)Rh]^+$.

[44] Turbomole basis set library, Turbomole Version 5, see reference 32.

Reactions in the tube lens region

All measurements were performed on the Finnigan TSQ 700 (ETH-Zurich). Reactions were performed at varying collision energies. The conditions are quite harsh. The exact pressure and composition of the background gas the ions collide with cannot be measured, nor can it be varied at will.

Since for some of the complexes already a reaction with air took place in solution, before the complexes were transferred to the gas phase, the maximum product yield had to be corrected. This was done by abstracting from the percentage of the TIC, which corresponds to the peroxo complex at a certain collision energy, the amount of peroxo complex already present at zero collision energy.

Reactions in the 24-pole region (RC 1)

All reactions were performed on the Finnigan TSQ 700 (ETH-Zurich). Since all cations that are transferred to the gas phase enter RC 1, the tube lens potential was set for every measurement in such a way, that the least fragmentation and reaction took place in the tube lens region.

Reactions were performed at near zero collision energy and at 4 or 5 different dioxygen pressures to see if the yield if any increases upon increase of the dioxygen pressure.

Reaction of ethene complexes in the octopole region (RC 2)

The mass spectrometer is operated in the daughter ion scan mode, which means that the m/z of the ions we would like to perform reactions with are mass-selected and that only ions with this particular m/z ratio can enter the octopole region. Reactions were performed at varying collision energies and in a few cases at two different collision gas pressures (dioxygen: 1.0 and 0.8 mTorr; dinitrogen: 1.0 mTorr; argon: 0.8 mTorr). All measurements were performed on the Finnigan TSQ 700 (ETH-Zurich).

Reaction of peroxo complexes in RC 1 and RC 2

The mass spectrometer is operated in the daughter ion scan mode, which means that the m/z of the ions we would like to perform reactions with are mass-selected and that only ions with this particular m/z ratio can enter the octopole region.

1-Butene in RC 1

This measurement was performed on the Finnigan TSQ 700 (ETH-Zurich) at unknown collision gas pressure. Upon allowing the collision gas to enter the 24-pole region no peroxo complex is present anymore in the spectrum.

1-Butene in RC 2

These measurements were performed on two different mass spectrometers: the TSQ 700(ETH-Zurich) for the bpa, bpa-Bz and Me_2-bpa-Bz rhodium peroxo complex, and on the TSQ 7000 (ETH-Zurich) for the tpa, tia, Me_2-tpa and Me_3-tpa rhodium peroxo complex.

Ethyl-vinylether in RC 2

These measurements were performed on the Finnigan TSQ 700 (ETH-Zurich). Reactions were performed at 4 different collision gas pressures. Already at 1.25 mTorr no peroxo complex was present anymore.

7.11 References

[1] R. A. Marcus, *J. Electroanal. Chem.*, **1997**, *438 (1-2)*, 251-259
[2] P. W. Atkins, *"Physical Chemistry"*, Oxford University Press, Oxford, **1994**
[3] O. Groning, T. Drakenberg and L. I. Elding, *Inorg. Chem.*, **1982**, *21 (5)*, 1820-1824
[4] N. Hallinan, V. Besancon, M. Forster, G. Elbaze, Y. Ducommun and A. E. Merbach, *Inorg. Chem.*, **1991**, *30 (5)*, 1112-1114
[5] P. E. Garrou, *Adv. Organomet. Chem.*, **1984**, *23*, 95-129
[6] R. L. Rominger, J. M. McFarland, J. R. Jeitler, J. S. Thompson and J. D. Atwood, *J. Coord. Chem.*, **1994**, *31 (1)*, 7-18
[7] R. Romeo, L. M. Scolaro, M. R. Plutino, F. F. de Biani, G. Bottari and A. Romeo, *Inorg. Chim. Acta*, **2003**, *350*, 143-151
[8] R. Romeo, *Comments Inorg. Chem.*, **2002**, *23 (1)*, 79-100
[9] A. L. Casado, A. A. Casares and P. Espinet, *Inorg. Chem.*, **1998**, *37 (16)*, 4154-4156
[10] A. Gelling, K. G. Orrell, A. G. Osborne and V. Sik, *J. Chem. Soc. - Dalton Trans.*, **1998**, *(6)*, 937-945
[11] B. B. Coussens, F. Buda, H. Oevering and R. J. Meier, *Organometallics*, **1998**, *17 (5)*, 795-801
[12] M. W. Holtcamp, J. A. Labinger and J. E. Bercaw, *Inorg. Chim. Acta*, **1997**, *265 (1-2)*, 117-125

[13] L. M. Rendina and R. J. Puddephatt, *Chem. Rev.*, **1997**, *97 (6)*, 1735-1754
[14] S. S. Stahl, J. A. Labinger and J. E. Bercaw, *J. Am. Chem. Soc.*, **1996**, *118 (25)*, 5961-5976
[15] J. A. Casares, S. Coco, P. Espinet and Y. S. Lin, *Organometallics*, **1995**, *14 (6)*, 3058-3067
[16] A. Yamamoto, T. Yamamoto, S. Komiya and F. Ozawa, *Pure Appl. Chem.*, **1984**, *56 (11)*, 1621-1634
[17] J. D. Scott and R. J. Puddephatt, *Organometallics*, **1983**, *2 (11)*, 1643-1648
[18] R. S. Paonessa and W. C. Trogler, *J. Am. Chem. Soc.*, **1982**, *104 (12)*, 3529-3530
[19] G. M. Whitesides, *Pure Appl. Chem.*, **1981**, *53 (1)*, 287-292
[20] R. Romeo, G. Alibrandi and L. M. Scolaro, *Inorg. Chem.*, **1993**, *32 (22)*, 4688-4694
[21] R. Romeo and G. Alibrandi, *Inorg. Chem.*, **1997**, *36 (21)*, 4822-4830
[22] M. R. Plutino, L. M. Scolaro, R. Romeo and A. Grassi, *Inorg. Chem.*, **2000**, *39 (13)*, 2712-2720
[23] R. Romeo, M. R. Plutino and L. I. Elding, *Inorg. Chem.*, **1997**, *36 (25)*, 5909-5916
[24] R. E. Bossio, N. W. Hoffman, T. R. Cundari and A. G. Marshall, *Organometallics*, **2004**, *23 (1)*, 144-148
[25] D. Feichtinger, *PhD Thesis ETH No. 13595 "Untersuchung der intrinsischen Reaktivitaet von metallorganischen Katalysatoren mittels Elektrospray Tandem Massenspektrometrie"*, **2000**
[26] C. Hinderling, *PhD Thesis ETH No. 13158 "Elektrospray-Tandem-Massenspektrometrie als vielseitiges Werkzeug zum mechanistischen Studium von organometallischen Reaktionen"*, **1999**
[27] C. Hinderling, D. Feichtinger, D. A. Plattner and P. Chen, *J. Am. Chem. Soc.*, **1997**, *119 (44)*, 10793-10804
[28] M. T. Rodgers, K. M. Ervin and P. B. Armentrout, *J. Chem. Phys.*, **1997**, *106 (11)*, 4499-4508
[29] M. T. Rodgers and P. B. Armentrout, *J. Chem. Phys.*, **1998**, *109 (5)*, 1787-1800
[30] Y. M. Chen and P. B. Armentrout, *J. Chem. Phys.*, **1995**, *103 (2)*, 618-625
[31] M. Krom, R. G. E. Coumans, J. M. M. Smits and A. W. Gal, *Angew. Chem. - Int. Edit.*, **2001**, *40 (11)*, 2106-2108
[32] M. Krom, R. G. E. Coumans, J. M. M. Smits and A. W. Gal, *Angew. Chem. - Int. Edit.*, **2002**, *41 (4)*, 576-579
[33] M. Krom, T. P. J. Peters, R. G. E. Coumans, T. J. J. Sciarone, J. Hoogboom, S. I. ter Beek, P. P. J. Schlebos, J. M. M. Smits, R. de Gelder and A. W. Gal, *Eur. J. Inorg. Chem.*, **2003**, *6*, 1072-1087
[34] R. J. N. A. M. Kicken, *PhD Thesis "Oxidation of Iridium Olefin Complexes by H_2O_2 and O_2"*, **2001**
[35] M. Krom, *PhD Thesis "Mono- and Dioxygenation of Rhodium and Iridium Olefin Fragments, Solution versus Solid State Reactivity"*, **2003**
[36] R. Ahlrichs, M. Bär, H.-P. Baron, R. Baurernschmitt, S. Böcker, M. Ehrig, K. Eichkorn, S. Elliot, F. Furche, F. Haase, M. Häser, C. Hättig, H. Horn, C. Huber, U. Huniar, M. Kattannek, A. Köhn, C. Kölmel, M. Kollwitz, K. May, C. Ochsenfeld, H. Öhm, A. Schäfer, U. Schneider, O. Treutler, K. Tsereteli, B. Unterreiner, M. von Arnim, F. Weigend, P. Weis and H. Weiss, *"Turbomole Version 5"*; Theoretical Chemistry Group, University of Karlsruhe, **January 2002**
[37] *"PQS version 2.4"*; Parallel Quantum Solutions, Fayetteville, Arkansas, USA (the Baker optimizer is available seperately from PQS upon request), **2001**
[38] J. Baker, *J. Comput. Chem.*, **1986**, *7 (4)*, 385-395
[39] A. D. Becke, *Phys. Rev. A*, **1988**, *38 (6)*, 3098-3100
[40] J. P. Perdew, *Phys. Rev. B*, **1986**, *33 (12)*, 8822-8824
[41] A. Schäfer, H. Horn and R. Ahlrichs, *J. Chem. Phys.*, **1992**, *97 (4)*, 2571-2577
[42] A. D. Becke, *J. Chem. Phys.*, **1993**, *98 (7)*, 5648-5652
[43] A. D. Becke, *J. Chem. Phys.*, **1993**, *98 (2)*, 1372-1377
[44] C. T. Lee, W. T. Yang and R. G. Parr, *Phys. Rev. B*, **1988**, *37 (2)*, 785-789
[45] All calculations were performed using the Turbomole functional "b3 lyp", which is not identical to the Gaussian "B3LYP" functional.
[46] A. Schäfer, C. Huber and R. Ahlrichs, *J. Chem. Phys.*, **1994**, *100 (8)*, 5829-5835
[47] D. A. Plattner, *Int. J. Mass Spectrom.*, **2001**, *207 (3)*, 125-144
[48] C. Hinderling, D. A. Plattner and P. Chen, *Angew. Chem. - Int. Edit.*, **1997**, *36 (3)*, 243-244
[49] D. Feichtinger, D. A. Plattner and P. Chen, *J. Am. Chem. Soc.*, **1998**, *120 (28)*, 7125-7126
[50] C. Hinderling and P. Chen, *Int. J. Mass Spectrom.*, **2000**, *196*, 377-383
[51] C. Hinderling and P. Chen, *Angew. Chem. - Int. Edit.*, **1999**, *38 (15)*, 2253-2256
[52] G. Gerdes and P. Chen, *Organometallics*, **2003**, *22 (11)*, 2217-2225
[53] P. Chen, *Angew. Chem. - Int. Edit.*, **2003**, *42 (25)*, 2832-2847
[54] C. Adlhart and P. Chen, *Helv. Chim. Acta*, **2000**, *83 (9)*, 2192-2196
[55] C. Adlhart and P. Chen, *Helv. Chim. Acta*, **2003**, *86 (4)*, 941-949
[56] C. Adlhart, M. A. O. Volland, P. Hofmann and P. Chen, *Helv. Chim. Acta*, **2000**, *83 (12)*, 3306-3311
[57] Y. M. Kim and P. Chen, *Int. J. Mass Spectrom.*, **2000**, *202 (1-3)*, 1-7
[58] G. Gerdes and P. Chen, *Organometallics*, **2004**, *23 (12)*, 3031-3036
[59] D. Feichtinger and D. A. Plattner, *Chem. - Eur. J.*, **2001**, *7 (3)*, 591-599
[60] M. A. O. Volland, C. Adlhart, C. A. Kiener, P. Chen and P. Hofmann, *Chem. - Eur. J.*, **2001**, *7 (21)*, 4621-4632
[61] D. A. Plattner, D. Feichtinger, J. El-Bahraoui and O. Wiest, *Int. J. Mass Spectrom.*, **2000**, *196*, 351-362
[62] D. Feichtinger and D. A. Plattner, *J. Chem. Soc. - Perkin Trans. 2*, **2000**, *5*, 1023-1028
[63] D. Feichtinger and D. A. Plattner, *Angew. Chem. - Int. Edit.*, **1997**, *36 (16)*, 1718-1719
[64] C. Hinderling, C. Adlhart and P. Chen, *Angew. Chem. - Int. Edit.*, **1998**, *37 (19)*, 2685-2689

Chapter 8

Comparison of Gas-Phase, Solution and Solid/Gas Reactivities

8.1 Introduction

In the previous chapters we have presented separately the results obtained for solution, solid/gas reactions and for pure gas-phase reactions. In this chapter we will draw our comparative conclusions. This is of interest from a perspective of frequently observed complex organometallic reactivity in solution. The present work shows that this complexity does not decrease on going from solution to the gas phase, but only changes in ***type***. Compounds that seem stable dissolved in a certain solvent appear to react rapidly with that same solvent upon transfer to the gas phase. ESI-MS spectra can provide useful information hard to obtain from solution studies, but one needs to be careful with the interpretation, which is not always straightforward and often hampered by the presence of isomeric and isobaric species.

8.2 Stability in solution versus the gas phase

Some phenomena observed in the ***gas phase*** for the bpa- and tpa-type rhodium(I) and iridium(I) ethene complexes presented in this thesis correlate well with stabilities seen in ***solution***. The acidic nature of the amine-nitrogen of the bpa ligand is reflected both by easy loss of H_2 in the gas phase for *both rhodium and iridium* and by the formation of dinuclear iridium ethyl complexes in solution.

Also the phenomenon of aromatic C-H activation of the benzyl substituent attached to the amine nitrogen of the N_3 ligands is encountered both in solution and in the gas phase.

The stronger olefin binding for rhodium compared to iridium is shown not only by the fact that the olefin dissociates much more easily for rhodium upon collision with argon in the gas phase, but also by the observation of bis-olefin complexes for iridium and the fact that in a strong coordinating solvent like acetonitrile bpa rhodium ethene complexes almost instantaneously lose the olefin, whereas the corresponding iridium complexes are much more stable.

8.3 Reaction with dioxygen in solution or the solid state

In the reaction of the N_3 and N_4 rhodium(I) and iridium(I) ethene complexes discussed in the present work with dioxygen we have seen that in ***solution*** products could be isolated only for the sterically hindered complexes. In these reactions substitution of dioxygen for ethene takes place for rhodium and formation of mixed peroxo-ethene complexes for iridium.

For *rhodium*, four nitrogen donor ligands appear to be necessary to stabilize peroxo complexes. Thus, isolation of N_3 rhodium peroxo complexes requires use of an additional ligand (MeCN). In favorable cases, formation of peroxo complexes can be quantitative.

For *iridium* peroxo-ethene complexes were never isolated in yields higher than 25 %.

In the ***solid state*** none of the complexes with sterically hindered ligands appeared to be reactive.

The sterically less hindered N_3 complexes rapidly react with dioxygen in *solution*, but these reactions were never selective. In the *solid state* only the rhodium complexes react rapidly and non-selectively with dioxygen yielding again mixtures of unidentifiable products. In both cases the products usually contain both diamagnetic and paramagnetic species.
In all those cases in which mixtures of products were obtained we cannot distinguish whether the by-products are a result of electron transfer reactions between O_2 and the metal center taking place or of decomposition of highly unstable oxygenated product species.

The reactivities for sterically hindered N_4 complexes presented above are in marked contrast with the ones that were reported for less sterically hindered N_4 complexes (tpa, Me-tpa). As shown in Figure 8.1 in *solution* very low yields of 2-irida(III)oxetane species [1], whereas in the *solid state* selective reactions were observed which yielded 3-metalla(III)-1,2-dioxolane species [2] – [4].

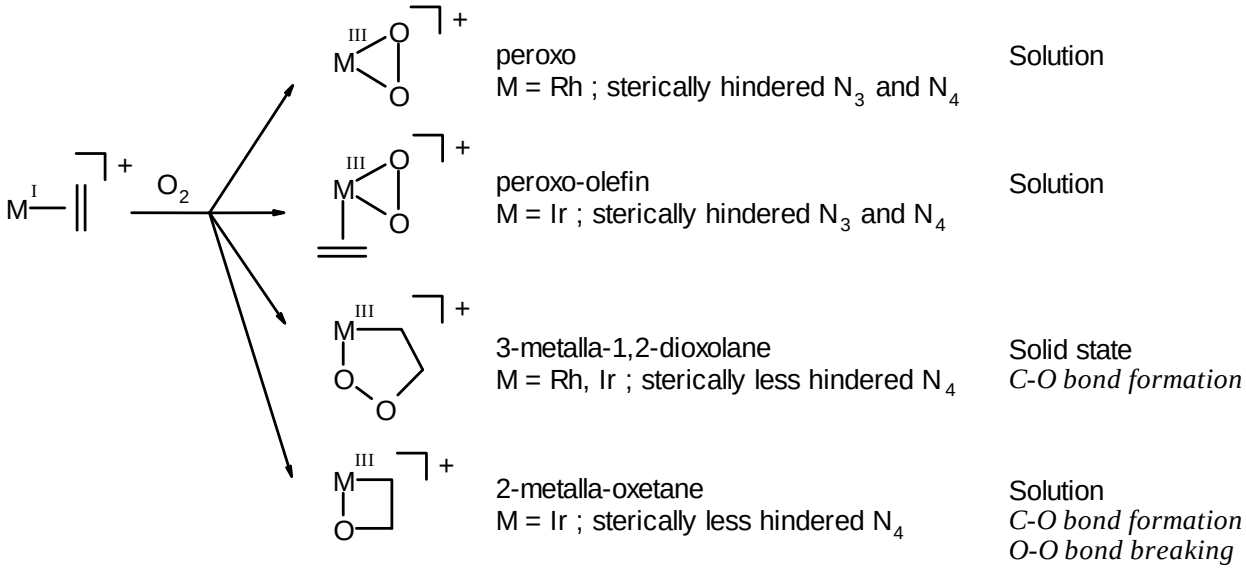

Figure 8.1 *Observed oxygenations of [(N-ligand)M^{I}(olefin)]$^{+}$ (M=Rh, Ir) by O_2*

Formation of a C-O bond and breaking of the O-O bond was conspicuously absent in the reactions of the sterically hindered complexes described in this thesis. One could perhaps have expected our peroxo-olefin complexes to undergo C-O bond formation, but this was never observed. This could in part be due to the steric hindrance imposed by the methyl-substituents attached to the 6-position of the pyridine rings.

8.4 Reactivity of iridium(II)-ethene complexes

In the *gas phase* the Me_3-tpa iridium(II) complex does not react with dioxygen at all. Also in the *solid state* this complex is not reactive. In contrast, in *solution* in acetonitrile and acetone a reaction with dioxygen does take place. The reaction in acetonitrile shows that metal(II)-olefin complexes can indeed be capable of forming a C-O bond and breaking the O-O bond. This is important, since this points to a possible role of metal(II)-olefin species in rhodium and iridium catalyzed oxidation of olefins by O_2. Such a role was already proposed in the reactions of the sterically less hindered N_4 complexes yielding dioxolane and oxetane species. [5] This insight is of importance in the development of catalytic olefin oxidation by group VIII metal centers. From the reaction in acetone no conclusions could be drawn concerning the occurrence of C-O bonds formation.

It was recently reported [6] that in acetonitrile the Me_3-tpa complex displays a metal(III)-ethyl-radical character rather than the metal-centered radical proposed in Chapter 5.

The involvement of the solvent could explain the observed differences in reactivity of the iridium(II)-ethene complexes in the different phases. For a metal(III)-ethyl-radical species a direct reaction of the radical with dioxygen would have been expected. For metal(II) ethene species a reaction is expected to be more difficult. In the Me_3-tpa complex the iridium center is strongly sterically shielded preventing a direct reaction of dioxygen with the iridium center. In order for dioxygen to enter the coordination sphere of the metal, a pyridyl arm of the N_4 ligand would have to dissociate. This process is opposed by an increase in the binding strength of the iridium-pyridyl$_{equatorial}$ bond upon going from iridium(I) to iridium(II).

DFT calculations have shown that the spin density of the unpaired electron in $[(Me_3\text{-tpa})Ir^{II}(C_2H_4)]^{2+}$ is mainly located on the iridium center, only a small part is located on the olefin moiety and the N_4 ligand giving to the structure on the left in Figure 8.2. The computational results seem to be confirmed by the absence of reactivity in the *gas phase* and in the *solid state*. In *solution*, on the other hand, coordination of MeCN induces the ethyl-radical character which appears to be responsible for the reaction with dioxygen.

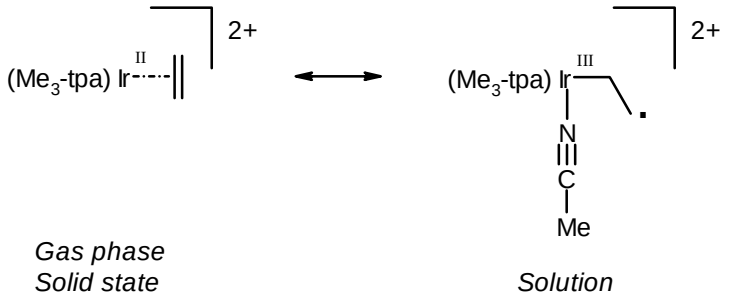

Figure 8.2 *Resonance structures for the Me_3-tpa iridium(II) ethene complex in the different phases*

Going from Me_3-tpa to Me_2-tpa (a sterically less demanding, but also more electron donating ligand) results in an increase in the reactivity of the corresponding iridium(II) complex.

8.5 Reaction towards dioxygen in the gas phase: a comparison

In contrast to solution phase reactivities presented in this work and reported by others [1] – [4], in the gas phase (Table 8.1) for <u>*rhodium*</u> the formation of peroxo complexes was observed for *all* of the N_3 and N_4 complexes, even for the *sterically less demanding* ligands. For the N_3 complexes with only a proton or a methyl group at the amine nitrogen the yields are lowest. Interestingly, in the gas phase N_3 rhodium peroxo complexes can be obtained in absence of the fourth N-donor ligand, which was obligatory for product isolation in solution.

For <u>*iridium*</u>, only for the Me_2-bpa-Me ligand, not for any other N_3 or N_4 ligand, a product was obtained: a peroxo-ethene complex, a reactivity corresponding to solution phase chemistry. In contrast to solution phase reactivity full conversion could be obtained in the gas phase.

Table 8.1 *Products obtained from a gas-phase reaction of $[(L_N)M(C_2H_4)]^+$ with O_2*

Metal	Ligands	Tube lens region	RC 1	RC 2
Rh	Sterically hindered N_3	Peroxo	Peroxo	Peroxo
	Sterically less hindered N_3	Peroxo	Peroxo (bpa-Me)	Peroxo
	Sterically hindered N_4	Peroxo	--	Peroxo (Me_3-tpa)
	Sterically less hindered N_4	Peroxo	--	--

Metal	Ligands	Tube lens region	RC 1	RC 2
Ir	Sterically hindered N_3	--	Peroxo-ethene (Me_2-bpa-Me)	Peroxo-ethene (Me_2-bpa-Me)
	Sterically less hindered N_3	--	--	--
	Sterically hindered N_4	--	--	--
	Sterically less hindered N_4	--	--	--

These differences in products and yields between solution and gas phase can be attributed to two phenomena:

- In the gas phase no electron transfer reactions can take place. No metal(II) ethene species will be formed for which it is expected that they could undergo C-O bond formation.
  In those cases where electron-transfer processes compete with formation of peroxo or peroxo-ethene species, the paramagnetic pathway is shut off in favor of the diamagnetic pathway.
- Highly reactive species can be studied intact in the gas phase, whereas they react further/decompose in solution.

For some complexes products containing both O_2 and the olefin moiety were observed in the gas phase. In some cases we were able to determine the structure of these species and found that they were in the peroxo-olefin form. However, we cannot state conclusively that in the gas phase dioxolane species were never formed.

Mechanistic implications on the basis of a comparative conclusion between gas phase and solution

It has been shown that there are clear differences between gas-phase reactivities on the one hand and solution and solid/gas reactivities on the other hand. By combining information obtained from different phases more insight can be obtained in the reaction steps belonging to the certain reactivities.

Take, for example, the solution phase reaction of N_4 rhodium ethene complexes with dioxygen. There are indications[1] that in solution the formation of peroxo complexes goes via a dissociation step (of either the olefin or a pyridyl group) and subsequent coordination of dioxygen. For the N_4 iridium complex we were even able to isolate a peroxo-ethene complex.

In the gas phase this behavior is confirmed, since we see only reaction in the tube lens region (a region in which dissociative processes are favored over associative processes) and no reaction in the RC 1 or RC 2 (regions in which either only associative reactions can take place or the gas pressure is so low that the probability of reaction has become too low). We even have indications that in the tube lens region the formation of the naked species $[(L_N)Rh]^+$ is related to the formation of the corresponding peroxo complex. This suggests that also for solution-phase chemistry olefin dissociation or dissociation of a pyridyl arm might be the rate-determining step.

For the iridium complexes, on the other hand, we are only able to isolate the associative product from solution, a peroxo-ethene (although in low yields). In the gas phase we are only able to generate these same complexes. Peroxo complexes (possibly a result from dissociative pathways) were never observed. This can be taken as an indication that for iridium associative reactions will be more important, also in solution.

[1] A decrease in the steric bulk around the metal center (and thus in a weakened metal-olefin bond) results in a decrease in reaction rate.

8.6 Added value of studying reactions in the gas phase

A general remark on the term "gas phase"

As described in Chapter 7, there are several regions inside the mass spectrometer in which reactions between our rhodium and iridium olefin complexes can take place. These regions each have their own conditions. This influences the path via which the reaction can take place in each region: associative *versus* dissociative.

One could argue whether results obtained from ESI-MS measurements really resemble real "gas-phase" reactivities. This depends among other things on the definition of "gas phase" used. If "gas phase" is taken to mean colliding molecules at atmospheric pressure gently with each other due to their thermal energy, then shooting an ion through a chamber filled with low pressures of gas does not really correspond to a gas phase (as is done in the tube lens region and in RC 2).

However, even the first definition is ambiguous. There is a sliding scale of gas phase conditions starting from very low pressures (reactions of individual molecules, which can only use their thermal energy to overcome reaction barriers) to more and more dense gas phase conditions with reactions in supercritical CO_2 being the upper limit. In the latter situation the gas phase is so dense that it is not possible anymore to distinguish between the solution phase and the gas phase.

So, who decides which range of conditions corresponds to real "gas phase" chemistry?

Transferring ionic species to the gas phase and thus studying these species under gas-phase conditions other than by ESI-MS is very difficult. Also, the thermal energy of molecules ($3kT$) alone is not high enough to overcome reaction barriers. Acceleration is necessary to increase the internal energy upon collision. Only coordinatively unsaturated and thus reactive species can react without this increase in kinetic energy. Such species are capable of reacting with a gas in RC 1, a region that can be considered to most closely approach "gas phase" conditions with its collision gas pressures of up to 0.1 Torr and around zero-collision energies of the ions in this region.

Whether or not ESI-MS conditions can be labeled as "real" gas-phase conditions, electrospray is a convenient way of transferring ionic species to the gas phase and studying reactions under these conditions can provide valuable additional information.

General conclusions on the ESI-MS technique

There are a few characteristics of ESI-MS important for future gas-phase studies.

In order to be able to perform all the desired experiments an advanced MS setup is necessary.
Two reaction chambers, RC 1 and RC 2, when working with quadrupole type mass spectrometers are necessary luxury. Due to the use of highly diluted solutions for electrospray, the transfer of highly reactive species to the gas phase can be hampered by reactions during the spraying process, from electron-transfer reactions at the spraying tip to reactions with air, the solvent itself or with traces of impurities present in the solvent like water [7].

The reactions performed in the gas phase in RC 2 take place under cleaner conditions than they will ever be in solution, since it is possible to selectively collide only the particles with the m/z ratio of the species of interest with the reactant gas and observe only the products of this reaction.
No other particles like counterions or solvent molecules can influence the reaction.

A drawback of reactions in RC 2 is, that the structure of the particles that are selected is not known, only the m/z ratio. Isobaric and isomeric species always have to be considered. Adding a third reaction chamber to the TSQ's or going to an FT-ICR (MS^n) would solve such a problem.

The reactions to be investigated must not have too high reaction barriers; else it will not be possible to observe any reaction at all. Slow reactions do not have enough time to occur inside the mass spectrometer (~ milliseconds). High reaction barriers could in principle be overcome by increase of the collision energy, but if the collision energy is too high the encounter complexes will be too short-lived for a reaction to occur and only fragmentation of the ions will be observed.

In our experiments investigating dissociative reactions was less difficult than studying associative processes, especially when extensive rearrangement of the ions is necessary for an associative reaction to occur.

If the associative reactions investigated are exothermic, then due to the highly diluted nature of collision experiments in RC 2 the products will have difficulty getting rid of their excess of internal energy and the products will fragment before detection. It is possible to increase the probability of detection of the original products, instead of the product fragments, by increasing the number of degrees of freedom of the product ion. For example attaching a floppy tail to the molecule, i.e. increasing the kinetic shift, could increase its lifetime enough to allow detection. This was used to good effect in a polymerization study of $[Cp_2ZrMe]^+$ complexes. [7] For 1-butene as a reactant gas much neater spectra were obtained than for ethene or propene.

Even though the products formed in gas-phase reactions can fragment upon formation, it will still be possible to draw conclusions on how easy it is for a reaction to occur; it will not be possible to tell how a reaction will proceed.

Under the right circumstances, ESI-MS can provide useful information about complex reactions. In particular, reactions in which the rate-limiting step is generation of a coordinatively unsaturated, highly reactive species lend themselves well to this approach, because such species can often be generated cleanly in a mass spectrometer and their subsequent reactivity studied. In contrast, reactions where the rate-determining step is a slow associative reaction are problematic, because that reaction will simply not occur within the mass spectrometers. In cases where the nature of the rate-determining step is unknown, gas-phase studies may provide useful clues but generally no complete answer.

The study of gas-phase reactivities of larger systems like organometallic complexes is still a pioneering area. It is therefore understandable that some limitations have not yet been solved. However, our results show that a comparison of the reactivities in each phase can provide more insight into the steps of a reaction mechanism than would be obtained from solution phase studies alone.

8.7 References

[1] R. J. N. A. M. Kicken, *PhD Thesis "Oxidation of Iridium Olefin Complexes by H_2O_2 and O_2"*, **2001**
[2] M. Krom, R. G. E. Coumans, J. M. M. Smits and A. W. Gal, *Angew. Chem. - Int. Edit.*, **2001**, *40 (11)*, 2106-2108
[3] M. Krom, R. G. E. Coumans, J. M. M. Smits and A. W. Gal, *Angew. Chem. - Int. Edit.*, **2002**, *41 (4)*, 576-579
[4] M. Krom, T. P. J. Peters, R. G. E. Coumans, T. J. J. Sciarone, J. Hoogboom, S. I. ter Beek, P. P. J. Schlebos, J. M. M. Smits, R. de Gelder and A. W. Gal, *Eur. J. Inorg. Chem.*, **2003**, *6*, 1072-1087
[5] B. de Bruin, P. H. M. Budzelaar and A. W. Gal, *Angew. Chem. - Int. Edit.*, **2004**, *43 (32)*, 4142-4157
[6] D. G. H. Hetterscheid, J. Kaiser, E. Reijerse, T. P. J. Peters, S. Thewissen, A. N. J. Blok, J. M. M. Smits, R. de Gelder and B. de Bruin, *J. Am. Chem. Soc.*, **2005**, in press
[7] D. Feichtinger, D. A. Plattner and P. Chen, *J. Am. Chem. Soc.*, **1998**, *120 (28)*, 7125-7126

Appendix A

Computational Results

In most square-planar d^8 systems, ligand exchange in solution occurs via an associative mechanism (most kinetic studies of this kind are based on Pt(II) and Pd(II) systems). A five-coordinate intermediate forms first, followed by departure of the leaving ligand. However, there are also several examples involving dissociation to a T-shaped 3-coordinate intermediate. [1] – [21]

In order to get a feeling for the stability of the species involved in the oxidation reactions proposed in this thesis, several N_3 and N_4 rhodium and iridium complexes and their possible intermediates in associative and dissociative reactions have been studied by DFT methods. In order to be able to distinguish electronic and steric influences, the tridentate nitrogen donor ligand was varied from bpa to bpa-Me, Me_2-bpa and Me_2-bpa-Me. For tetradentate nitrogen donor ligands the influence of the methyl substituent on the 6-position of the pyridine ring was investigated (tpa, Me_3-tpa).

All geometry optimizations were carried out with the Turbomole program [22] coupled to the PQS Baker optimizer. [23], [24] Geometries were fully optimized as minima at the ridft bp86 [25], [26] level using the Turbomole SV(P) basis set [1] [27] on all atoms (def-SVP pseudopotential basis on rhodium and iridium). Improved energies were obtained from single-point calculations at the dft b3-lyp level [28] – [31] using the TZVPP [31], [32] basis set on all atoms (def-TZVPP pseudopotential basis on rhodium and iridium). Thermal corrections (entropy and enthalpy) were calculated according to standard formulas of statistical thermodynamics [33] for two sets of conditions: 293 K, 1 bar (corresponding to ordinary laboratory conditions) and 343 K, 0.001 bar (corresponding roughly to parts of a mass spectrometer).
All calculated structures were visualized using the Molden program. [34]

The most appropriate energy quantity for a description of reactions occurring in solution at r.t. is the Gibbs free energy, $\Delta G_{298\ K,\ 1\ bar}$. Relative rates can be computed directly from relative free energies of activation using Boltzmann-type expressions. Use of free energies assumes that molecules acquire energies needed for reactions through frequent collisions: this ensures that there is a Boltzmann distribution of internal energies over the molecules, corresponding to a well-defined temperature (in this case 25 ºC).
If molecules are isolated from each other and then suddenly obtain internal energy (e.g. through a single high-energy collision), the energy distribution will not resemble a Boltzmann distribution. Statistical arguments are not appropriate any more, the energy distribution over the collided molecules will be narrow, and the temperature is not well-defined. Under these circumstances, one expects that molecules can overcome a particular barrier if their internal energy acquired by collision is higher than "pure" activation barrier $E_{electronic}$+ZPE, which is identical to the enthalpy at 0K, $\Delta H_{0\ K}$.
Therefore, in RC 2 of a mass spectrometer the enthalpy $\Delta H_{0\ K}$ is probably the appropriate quantity to use. In RC 1 and the tube lens region the collision gas pressures are so high that it is not clear whether use of the

[1] Turbomole basis set library, Turbomole Version 5, see reference 22, Appendix A

enthalpy $\Delta H_{0\,K}$ or of the free energy $\Delta G_{343\,K,\,0.001\,bar}$ (70 ºC and 0.001 bar, spectrometer conditions) is more appropriate.

Since all three sets of energy values are used in this thesis, all the calculated energies are listed in Table A.1, Table A.2 and Table A.3.

Unfortunately, the DFT methods used do not reproduce the O_2 singlet-triplet gap satisfactory, making $^3O_2$ far too stable (by ~ 18 kcal/mol [2]). If the computed results were to be taken at face value, this would result in O_2 complexation being endothermic in many cases, contrary to experimental observations. Therefore, we adjusted the reference energy of $^3O_2$ upwards by 18 kcal/mol when calculating relative energies.

For all L_N metal complexes, the energy of corresponding naked species, $[(L_N)M]^+$, is set to zero kcal/mol.

The MECP structures as described in § 4.4 are not stationary points on any potential energy surface, so the standard formulas for thermal corrections cannot be applied. In order to obtain approximate free energies for the MECP structures, we added the thermal correction calculated for the peroxo-ethene complex to the $\Delta H_{0\,K}$ for the MECP structure.

Table A.1 *Computational results for N_3 rhodium species*

Compound	$\Delta H_{0\,K}$		$\Delta G_{343\,K,\,0.001\,bar}$		$\Delta G_{298\,K,\,1\,bar}$	
	kcal/mol	eV/mol	kcal/mol	eV/mol	kcal/mol	eV/mol
$[(bpa)Rh]^+$	(0.0)	(0.00)	(0.0)	(0.00)	(0.0)	(0.00)
$[(bpa)Rh(C_2H_4)]^+$	-30.2	-1.31	-11.4	-0.49	-18.1	-0.78
$[(bpa)Rh(O_2)]^+$	-31.7	-1.37	-12.5	-0.54	-21.1	-0.92
$[(bpa)Rh(C_2H_4)(O_2)]^+$	-42.0	-1.82	-3.3	-0.14	-18.7	-0.81
$[(bpa)Rh(C_2H_4)_2]^+$ (*fac*)	-26.5	-1.15	9.3	0.41	-3.7	-0.16
$[(bpa)Rh(C_2H_4)_2]^+$ (*mer*)	-29.7	-1.29	8.3	0.36	-5.0	-0.22
$[(bpa\text{-}Me)Rh]^+$	(0.0)	(0.00)	(0.0)	(0.00)	(0.0)	(0.00)
$[(bpa\text{-}Me)Rh(C_2H_4)]^+$	-30.6	-1.33	-12.1	-0.53	-18.7	-0.81
$[(bpa\text{-}Me)Rh(O_2)]^+$	-32.7	-1.42	-13.6	-0.59	-22.3	-0.97
MECP for the reaction with O_2	-37.3	-1.62	1.3	0.06	-14.1	-0.61
$[(bpa\text{-}Me)Rh(C_2H_4)(O_2)]^{+,}$	-42.5	-1.84	-3.9	-0.17	-19.3	-0.84
$[(bpa\text{-}Me)Rh(C_2H_4)_2]^+$ (*fac*)	-25.3	-1.10	11.0	0.48	-2.0	-0.09
$[(bpa\text{-}Me)Rh(C_2H_4)_2]^+$ (*mer*)	-29.5	-1.28	8.5	0.37	-4.8	-0.21
$[(Me_2\text{-}bpa)Rh]^+$	(0.0)	(0.00)	(0.0)	(0.00)	(0.0)	(0.00)
$[(Me_2\text{-}bpa)Rh(C_2H_4)]^+$	-13.9	-0.60	5.4	0.24	-1.3	-0.06
$[(Me_2\text{-}bpa)Rh(C_2H_4)]^+$ *(cis)* [3]	-2.3	-0.10	18.1	0.79	11.2	0.48
$[(Me_2\text{-}bpa)Rh(O_2)]^+$ [4]	-23.7	-1.03	-2.8	-0.12	-11.7	-0.51
$[(Me_2\text{-}bpa)Rh(C_2H_4)(O_2)]^+$	-33.9	-1.47	6.2	0.27	-9.5	-0.41
$[(Me_2\text{-}bpa)Rh(C_2H_4)_2]^+$ (*fac*)	-16.4	-0.71	21.6	0.94	8.2	0.36
$[(Me_2\text{-}bpa)Rh(C_2H_4)_2]^+$ (*mer*)	-16.2	-0.70	22.7	0.99	9.2	0.40

[2] The energy difference between $^1O_2$ and $^3O_2$ is reported [35] to be 22-24 kcal/mol. We found in our calculations a difference of 41 kcal/mol.

[3] *(cis)* refers to the location of the olefin relative to the ligand N-R fragment.

[4] It was not possible to obtain a structure in which the dioxygen molecule is also in the *cis* position (as described in footnote 3).

Compound	$\Delta H_{0\ K}$		$\Delta G_{343\ K,\ 0.001\ bar}$		$\Delta G_{298\ K,\ 1\ bar}$	
	kcal/mol	eV/mol	kcal/mol	eV/mol	kcal/mol	eV/mol
$[(Me_2\text{-bpa-Me})Rh]^+$	(0.0)	(0.00)	(0.0)	(0.00)	(0.0)	(0.00)
$[(Me_2\text{-bpa-Me})Rh(C_2H_4)]^+$	-14.9	-0.65	4.1	0.18	-2.5	-0.11
$[(Me_2\text{-bpa-Me})Rh(C_2H_4)]^+$ *(cis)*	-1.8	-0.08	18.7	0.81	11.7	0.51
$[(Me_2\text{-bpa-Me})Rh(O_2)]^+$	-25.2	-1.09	-4.6	-0.98	-13.6	-0.58
$[(Me_2\text{-bpa-Me})Rh(O_2)]^+$ *(cis)*	-22.9	-0.99	-2.9	-0.13	-11.7	-0.51
MECP for the reaction with O_2	-29.7	-1.29	10.2	0.44	-5.4	-0.23
$[(Me_2\text{-bpa-Me})Rh(C_2H_4)(O_2)]^+$	-33.9	-1.47	6.1	0.26	-9.6	-0.42
$[(Me_2\text{-bpa-Me})Rh(C_2H_4)_2]^+$ (*fac*)	-15.3	-0.66	22.8	0.99	9.4	0.41
$[(Me_2\text{-bpa-Me})Rh(C_2H_4)_2]^+$ (*mer*)	-14.9	-0.65	23.9	1.03	10.4	0.45

Table A.2 *Computational results for N_3 iridium species*

Compound	$\Delta H_{0\ K}$		$\Delta G_{343\ K,\ 0.001\ bar}$		$\Delta G_{298\ K,\ 1\ bar}$	
	kcal/mol	eV/mol	kcal/mol	eV/mol	kcal/mol	eV/mol
$[(bpa)Ir]^+$	(0.0)	(0.00)	(0.0)	(0.00)	(0.0)	(0.00)
$[(bpa)Ir(C_2H_4)]^+$	-39.5	-1.71	-20.7	-0.90	-27.3	-1.19
$[(bpa)Ir(O_2)]^+$	-41.2	-1.79	-22.4	-0.97	-31.0	-1.34
$[(bpa)Ir(C_2H_4)(O_2)]^+$	-55.9	-2.42	-17.2	-0.75	-32.6	-1.41
$[(bpa)Ir(C_2H_4)_2]^+$ (*fac*)	-40.7	-1.77	-3.9	-0.17	-17.1	-0.74
$[(bpa)Ir(C_2H_4)_2]^+$ (*mer*)	-42.9	-1.86	-4.8	-0.21	-18.1	-0.79
$[(bpa\text{-Me})Ir]^+$	(0.0)	(0.00)	(0.0)	(0.00)	(0.0)	(0.00)
$[(bpa\text{-Me})Ir(C_2H_4)]^+$	-39.3	-1.70	-20.8	-0.90	-27.3	-1.19
$[(bpa\text{-Me})Ir(O_2)]^+$	-41.3	-1.79	-22.3	-0.97	-31.0	-1.34
MECP for the reaction with O_2	-46.7	-2.02	-8.0	-0.35	-23.4	-1.02
$[(bpa\text{-Me})Ir(C_2H_4)(O_2)]^+$	-55.9	-2.42	-17.2	-0.74	-32.6	-1.41
$[(bpa\text{-Me})Ir(C_2H_4)_2]^+$ (*fac*)	-38.6	-1.67	-0.8	-0.04	-14.2	-0.61
$[(bpa\text{-Me})Ir(C_2H_4)_2]^+$ (*mer*)	-41.9	-1.82	-3.7	-0.16	-17.1	-0.74
$[(Me_2\text{-bpa})Ir]^+$	(0.0)	(0.00)	(0.0)	(0.00)	(0.0)	(0.00)
$[(Me_2\text{-bpa})Ir(C_2H_4)]^+$	-20.5	-0.89	-0.1	0.00	-7.0	-0.30
$[(Me_2\text{-bpa})Ir(O_2)]^+$	-30.3	-1.31	-10.0	-0.43	-18.8	-0.82
$[(Me_2\text{-bpa})Ir(C_2H_4)(O_2)]^+$	-47.8	-2.07	-7.7	-0.33	-23.4	-1.01
$[(Me_2\text{-bpa})Ir(C_2H_4)_2]^+$ (*fac*)	-29.9	-1.30	9.1	0.40	-4.4	-0.19
$[(Me_2\text{-bpa})Ir(C_2H_4)_2]^+$ (*mer*)	-29.3	-1.27	9.5	0.41	-4.0	-0.17
$[(Me_2\text{-bpa-Me})Ir]^+$	(0.0)	(0.00)	(0.0)	(0.00)	(0.0)	(0.00)
$[(Me_2\text{-bpa-Me})Ir(C_2H_4)]^+$ [5]	-21.2	-0.92	-1.2	-0.05	-8.1	-0.35
$[(Me_2\text{-bpa-Me})Ir(O_2)]^+$	-31.4	-1.36	-11.3	-0.49	-20.1	-0.87
MECP for the reaction with O_2	-38.7	-1.68	1.4	0.06	-14.3	-0.62

[5] Contrary to for rhodium were we not able to obtain a structure in which the olefin moiety or the dioxygen molecule are in a *cis* position (see footnote 3)

Compound	$\Delta H_{0\ K}$		$\Delta G_{343\ K,\ 0.001\ bar}$		$\Delta G_{298\ K,\ 1\ bar}$	
	kcal/mol	eV/mol	kcal/mol	eV/mol	kcal/mol	eV/mol
$[(Me_2\text{-bpa-Me})Ir(C_2H_4)(O_2)]^+$	-47.5	-2.06	-7.5	-0.32	-23.1	-1.00
$[(Me_2\text{-bpa-Me})Ir(C_2H_4)_2]^+$ (*fac*)	-28.1	-1.22	9.7	0.42	-3.6	-0.16
$[(Me_2\text{-bpa-Me})Ir(C_2H_4)_2]^+$ (*mer*)	-27.4	-1.19	11.4	0.49	-2.1	-0.09

Table A.3 *Computational results for N_4 rhodium and iridium species*

Compound	$\Delta H_{0\ K}$		$\Delta G_{343\ K,\ 0.001\ bar}$		$\Delta G_{298\ K,\ 1\ bar}$	
	kcal/mol	eV/mol	kcal/mol	eV/mol	kcal/mol	eV/mol
$[(tpa)Rh]^+$	(0.0)	(0.00)	(0.0)	(0.00)	(0.0)	(0.00)
$[(tpa)Rh(C_2H_4)]^+$	-42.6	-1.85	-30.2	-1.31	-29.8	-1.29
$[(tpa)Rh(O_2)]^+$	-61.3	-2.66	-50.0	-2.17	-49.7	-2.15
$[(Me_3\text{-tpa})Rh]^+$	(0.0)	(0.00)	(0.0)	(0.00)	(0.0)	(0.00)
$[(Me_3\text{-tpa})Rh(C_2H_4)]^+$	-27.1	-1.18	-13.6	-0.59	-13.4	-0.58
$[(Me_3\text{-tpa})Rh(O_2)]^+$	-52.2	-2.26	-37.6	-1.63	-37.9	-1.64
$[(tpa)Ir]^+$	(0.0)	(0.00)	(0.0)	(0.00)	(0.0)	(0.00)
$[(tpa)Ir(C_2H_4)]^+$	-31.8	-1.38	-31.8	-1.38	-31.6	-1.37
$[(tpa)Ir(O_2)]^+$	-54.2	-2.35	-52.8	-2.29	-52.9	-2.29
$[(Me_3\text{-tpa})Ir]^+$	(0.0)	(0.00)	(0.0)	(0.00)	(0.0)	(0.00)
$[(Me_3\text{-tpa})Ir(C_2H_4)]^+$	-18.8	-0.82	-17.3	-0.75	-17.4	-0.75
$[(Me_3\text{-tpa})Ir(O_2)]^+$	-46.6	-2.02	-42.6	-1.85	-43.1	-1.87

Some conclusions can be drawn immediately from these tables:

- The binding energies of both ethene and dioxygen decrease upon addition of methyl substituents to the 6-position of the pyridine rings.
- Neither rhodium nor iridium is predicted to form stable bis-ethene complexes. For rhodium this is in accord with experimental observations. For iridium the calculations apparently underestimate the metal-olefin bond strength (see also a report by Budzelaar and Blok [36]), possibly because relativistic effects are not really included (except for indirect effects included in the effective core potentials).
- The bis-ethene complex with the N_3 ligand *meridionally* coordinated lies for bpa-R complexes <u>*lower*</u> in energy than those in which the N_3 ligand is *facially* coordinated. For the Me_2-bpa-R complexes, on the other hand the *mer*-N_3 complexes lie <u>*higher*</u> in energy.
- The energy difference between the bis-ethene and the mono-ethene complexes is larger for the bpa-R complexes (e.g. these complexes are less stable) than for the Me_2-bpa-R complexes, these differences being smaller for the iridium than for the rhodium complexes.
  This corresponds well to what we have seen in solution, i.e. here *fac*-Me_2-bpa-R and *mer*-bpa-R iridium bis-ethene complexes were formed, the Me_2-bpa-R bis-ethene complexes being least stable, and for rhodium only Me_2-bpa-R bis-ethene complexes could be observed with ^{1}H-NMR in solution.
- For *iridium* the $\Delta G_{298\ K,\ 1\ bar}$ and the $\Delta H_{0\ K}$ of the peroxo complexes lie higher in energy than the corresponding peroxo-ethene species and indeed we were only able to generate the latter species both in

solution (§ 4.2.1) and in the gas phase (Chapter 7).
In contrast, for *rhodium*, when looking at the $\Delta G_{298\ K,\ 1\ bar}$ the peroxo complexes $[(L_N)Rh(O_2)]^+$ lie somewhat lower in energy than the peroxo-ethene complexes. When looking at the $\Delta H_{0\ K}$ the peroxo complexes lie higher in energy than the peroxo-ethene complexes again. Coordinatively unsaturated $[(N_3)Rh(O_2)]^+$ could only be generated in the gas phase (Chaper 7), in solution these N_3 rhodium complexes need a fourth nitrogen donor (acetonitrile) for stabilization (§ 4.3.2). In the gas phase we were able to generate rhodium peroxo-olefin complexes, but only when peroxo complexes were collided with an olefin, not when olefin complexes were collided with dioxygen (Chapter 7).

– For all complexes the energy of the MECP lies below that of the corresponding naked species $[(L_N)M]^+$, this energy difference becoming larger on going from rhodium to iridium and from bpa-Me to Me_2-bpa-Me.
When looking at the $\Delta H_{0\ K}$ the energy of the MECP structure is even lower than that of the corresponding ethene complex, indicating a reaction with dioxygen to form the peroxo-ethene complex energetically favorable in the gas phase.
In the case of the $\Delta G_{298\ K,\ 1\ bar}$ contrary to the Me_2-bpa-Me complexes the energy of the bpa-Me MECP structures lie somewhat above that of the corresponding ethene complex, indicating that a solution phase reaction of the bpa-Me complexes with dioxygen to form peroxo-ethene complexes should be more difficult than for the Me_2-bpa-Me complexes.
We do not have any information on the barriers associated with the dissociative pathway.[6]
However, on the basis of our calculations for both the rhodium and the iridium N_3 complexes the associative pathway seems to be more favorable than the dissociative one.

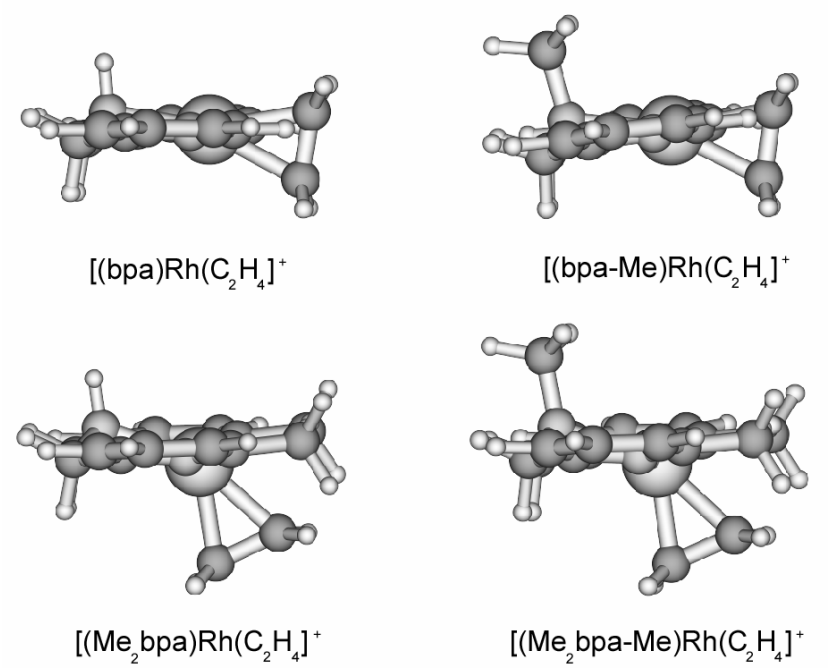

Figure A.1 *Structures obtained from DFT calculations for the bpa, Me_2-bpa, bpa-Me and Me_2-bpa-Me rhodium ethene complexes*

In Figure A.1 the structures obtained from geometry optimization are shown for N_3 rhodium ethene complexes. It is clear that upon addition of methyl substituents to the 6-position of the pyridine rings the olefin

[6] We do not have any information on the barriers related to the formation of $[(L_N)M]^+$. One could imagine that for naked T-shaped $[(N_3)M]^+$ species no rearrangement due to steric hindrance is necessary, since dioxygen can easily approach the metal centre. There should be no barrier for the binding interaction for either $^1O_2$ or $^3O_2$.

is forced to bend out of the plane made up by the pyridine rings and the metal center. From the results in Table A.1 and Table A.2 it is clear that the preferred position of the olefin is away from the amine-substituent. For the rhodium Me_2-bpa-R complexes we were also able to calculate the structures of mono-ethene complexes in which the olefin was situated *cis* to the amine-substituent. These *cis* complexes both lie at least 12 kcal/mol above the complexes displayed in Figure A.1.

References

[1] O. Groning, T. Drakenberg and L. I. Elding, *Inorg. Chem.*, **1982**, *21 (5)*, 1820-1824
[2] N. Hallinan, V. Besancon, M. Forster, G. Elbaze, Y. Ducommun and A. E. Merbach, *Inorg. Chem.*, **1991**, *30 (5)*, 1112-1114
[3] P. E. Garrou, *Adv. Organomet. Chem.*, **1984**, *23*, 95-129
[4] R. L. Rominger, J. M. McFarland, J. R. Jeitler, J. S. Thompson and J. D. Atwood, *J. Coord. Chem.*, **1994**, *31 (1)*, 7-18
[5] R. Romeo, L. M. Scolaro, M. R. Plutino, F. F. de Biani, G. Bottari and A. Romeo, *Inorg. Chim. Acta*, **2003**, *350*, 143-151
[6] R. Romeo, *Comments Inorg. Chem.*, **2002**, *23 (1)*, 79-100
[7] A. L. Casado, A. A. Casares and P. Espinet, *Inorg. Chem.*, **1998**, *37 (16)*, 4154-4156
[8] A. Gelling, K. G. Orrell, A. G. Osborne and V. Sik, *J. Chem. Soc. - Dalton Trans.*, **1998**, *(6)*, 937-945
[9] B. B. Coussens, F. Buda, H. Oevering and R. J. Meier, *Organometallics*, **1998**, *17 (5)*, 795-801
[10] M. W. Holtcamp, J. A. Labinger and J. E. Bercaw, *Inorg. Chim. Acta*, **1997**, *265 (1-2)*, 117-125
[11] L. M. Rendina and R. J. Puddephatt, *Chem. Rev.*, **1997**, *97 (6)*, 1735-1754
[12] S. S. Stahl, J. A. Labinger and J. E. Bercaw, *J. Am. Chem. Soc.*, **1996**, *118 (25)*, 5961-5976
[13] J. A. Casares, S. Coco, P. Espinet and Y. S. Lin, *Organometallics*, **1995**, *14 (6)*, 3058-3067
[14] A. Yamamoto, T. Yamamoto, S. Komiya and F. Ozawa, *Pure Appl. Chem.*, **1984**, *56 (11)*, 1621-1634
[15] J. D. Scott and R. J. Puddephatt, *Organometallics*, **1983**, *2 (11)*, 1643-1648
[16] R. S. Paonessa and W. C. Trogler, *J. Am. Chem. Soc.*, **1982**, *104 (12)*, 3529-3530
[17] G. M. Whitesides, *Pure Appl. Chem.*, **1981**, *53 (1)*, 287-292
[18] R. Romeo, G. Alibrandi and L. M. Scolaro, *Inorg. Chem.*, **1993**, *32 (22)*, 4688-4694
[19] R. Romeo and G. Alibrandi, *Inorg. Chem.*, **1997**, *36 (21)*, 4822-4830
[20] M. R. Plutino, L. M. Scolaro, R. Romeo and A. Grassi, *Inorg. Chem.*, **2000**, *39 (13)*, 2712-2720
[21] R. Romeo, M. R. Plutino and L. I. Elding, *Inorg. Chem.*, **1997**, *36 (25)*, 5909-5916
[22] R. Ahlrichs, M. Bär, H.-P. Baron, R. Baurernschmitt, S. Böcker, M. Ehrig, K. Eichkorn, S. Elliot, F. Furche, F. Haase, M. Häser, C. Hättig, H. Horn, C. Huber, U. Huniar, M. Kattannek, A. Köhn, C. Kölmel, M. Kollwitz, K. May, C. Ochsenfeld, H. Öhm, A. Schäfer, U. Schneider, O. Treutler, K. Tsereteli, B. Unterreiner, M. von Arnim, F. Weigend, P. Weis and H. Weiss, *"Turbomole Version 5"*; Theoretical Chemistry Group, University of Karlsruhe, **January 2002**
[23] *"PQS version 2.4"*; Parallel Quantum Solutions, Fayetteville, Arkansas, USA (the Baker optimizer is available seperately from PQS upon request), **2001**
[24] J. Baker, *J. Comput. Chem.*, **1986**, *7 (4)*, 385-395
[25] A. D. Becke, *Phys. Rev. A*, **1988**, *38 (6)*, 3098-3100
[26] J. P. Perdew, *Phys. Rev. B*, **1986**, *33 (12)*, 8822-8824
[27] A. Schäfer, H. Horn and R. Ahlrichs, *J. Chem. Phys.*, **1992**, *97 (4)*, 2571-2577
[28] A. D. Becke, *J. Chem. Phys.*, **1993**, *98 (7)*, 5648-5652
[29] A. D. Becke, *J. Chem. Phys.*, **1993**, *98 (2)*, 1372-1377
[30] C. T. Lee, W. T. Yang and R. G. Parr, *Phys. Rev. B*, **1988**, *37 (2)*, 785-789
[31] All calculations were performed using the Turbomole functional "b3 lyp", which is not identical to the Gaussian "B3LYP" functional.
[32] A. Schäfer, C. Huber and R. Ahlrichs, *J. Chem. Phys.*, **1994**, *100 (8)*, 5829-5835
[33] P. W. Atkins, *"Physical Chemistry"*, Oxford University Press, Oxford, **1994**
[34] G. Schaftenaar and J. H. Noordik, *J. Comput. - Aided Mol. Des.*, **2000**, *14 (2)*, 123-134
[35] F. Wilkinson, W. P. Helman and A. B. Ross, *J. Phys. Chem. Ref. Data*, **1995**, *24 (2)*, 663-1021
[36] P. H. M. Budzelaar and A. N. J. Blok, *Eur. J. Inorg. Chem.*, **2004**, *(11)*, 2385-2391

Summary

New bpa- and tpa-type[1] rhodium(I) and iridium(I) ethene complexes have been synthesized. The steric bulk around the metal center has been varied to investigate the influence on the reactivity. The stability and reactivity towards dioxygen have been investigated in solution, in the solid state and in the gas phase. The comparison of solution with gas-phase behavior may give information about solvation effects; in the gas phase the intrinsic reactivity of a metal complex can be investigated without interference of solvent molecules and counter ions.

For most species in solution initially bis-ethene complexes (with the nitrogen donor ligand in a κ^3-*fac* or a κ^3-*mer* fashion) are formed which are either stable or spontaneously decompose under ethene loss to give mono-ethene complexes. The olefin is more strongly bound to iridium(I) than to rhodium(I) center. As a result some stable iridium bis-ethene complexes were isolated. Upon increasing the temperature some of the N_3 iridium bis-ethene complexes undergo N-H or aromatic C-H activation in solution resulting in the formation of dinuclear complexes.

In order to obtain a better understanding of the mechanism of rhodium and iridium catalyzed oxygenation of olefins these newly synthesized metal(I) ethene complexes were reacted with molecular oxygen. *In solution*, only for the sterically hindered complexes products could be isolated: rhodium peroxo (displacement of the olefin) and iridium peroxo-ethene complexes. For the isolation of rhodium peroxo complexes four nitrogen donor ligands are required. For the sterically less hindered complexes we were not able to isolate species from the complex reaction mixture (paramagnetic species were among the products formed). *In the solid state*, the sterically hindered complexes are not reactive at all. The sterically less hindered N_3-ligand complexes react very rapidly with dioxygen, but again in a non-selective manner (paramagnetic species are among the products formed). This is in contrast to the reactivity reported[2] for sterically less hindered N_4-ligand (tpa and pyridinophane) complexes where 3-metalla-1,2-dioxolane species were isolated.

Since paramagnetic species were among the products many times and since for the formation of dioxolane species in the solid state electron transfer between dioxygen and the organometallic complex was proposed as a key step in the C-O bond formation proces, we were interested in the reactivity of metal(II) olefin complexes towards dioxygen. Therefore two new sterically hindered N_4 iridium(II) ethene complexes were synthesized and their reactivity towards dioxygen was investigated. Increasing the steric bulk imposed by the nitrogen donor ligand increases the stability of the iridium(II) ethene complex. The iridium(II) ethene complexes undergo metal-ligand coupling to form ethylene bridged dinuclear complexes. Strong coordinating solvents like acetonitrile are necessary to induce this reactivity.

In contrast to the iridium(I) ethene complexes, the iridium(II) species are capable of C-O bond formation upon reaction with dioxygen. This points to a possible role of metal(II)-olefin species in rhodium and iridium catalyzed oxidation of olefins by dioxygen. Such insight is of importance for the development of catalytic olefin oxygenation by group VIII metal centers.

[1] bpa = *N*,*N*-di(2-pyridylmethyl)amine (amine substituent has been varied), tpa = *N*,*N*,*N*-tri(2-pyridylmethyl)amine

[2] M. Krom *et al.*, *Angew. Chem. - Int. Edit.*, **2002**, 41 (4), 576-579 and *Eur. J. Inorg. Chem.*, **2003**, 6, 1072-1087.

Gas-phase behavior of the rhodium(I) and iridium(I) ethene complexes correlates well with stabilities in solution. The acidic nature of the amine-nitrogen of the bpa ligand is reflected by emphasized loss of H_2 from the (N-ligand)M^{I}(ethene) complexes (M=Rh, Ir) in the gas phase and by the occurrence of N-H activation in solution. Aromatic C-H activation is encountered both in solution and in the gas phase. The stronger olefin binding for iridium compared to rhodium is also reflected by gas-phase measurements: 1) easy dissociation of the olefin for rhodium upon collision with argon, 2) only observation of bis-olefin iridium complexes in the gas phase.

Upon collision with dioxygen in the gas phase only diamagnetic products are formed: peroxo complexes for rhodium and peroxo-ethene complexes for iridium. The type of complexes that are reactive in the gas phase and the mechanism via which they react depends on the region of the mass spectrometer. In each region the reaction conditions differ, which determines whether associative or dissociative reactions (or both) can take place.

There are clear differences between solution, solid state and gas-phase reactivities. In contrast to reactions in solution, no electron transfer reactions take place in the gas phase. Thus, on going from solution to the gas phase, it is possible to separate paramagnetic from diamagnetic pathways (which occur simultaneously in solution). We note that the reactivity in the gas phase differs significantly from the reactivity in solution on some interesting other points. In the gas phase:

1) For ***all*** tpa-type rhodium ethene complexes the formation of peroxo species was observed,
2) There is no necessity of a fourth nitrogen donor for the formation of rhodium peroxo complexes and
3) No formation of five-membered ring dioxolane species was observed (possibly due to the absence of electron transfer reactions).

Since the reactivity of organometallic complexes can be very complex in all phases, a comparison of the reactivities in each phase can be very useful and provide more insight into certain steps in a reaction mechanism. Such comparisons may also give information about the reasons for low complex stabilities.

Samenvatting

Nieuwe bpa- en tpa-type[1] rhodium(I) en iridium(I) etheen verbindingen zijn gesynthetiseerd. De invloed van de sterische hinder die wordt uitgeoefend door de stikstofdonorliganden op de reactiviteit is onderzocht. De stabiliteit van deze verbindingen en hun reactiviteit t.a.v. zuurstof is onderzocht zowel in oplossing, de vaste stof als in de gasfase. Een vergelijking van de reacties waargenomen in al deze fasen kan meer informatie verschaffen t.a.v. van de invloed van solvatatie: in de gasfase kan de intrinsieke reactiviteit van een metaal complex onderzocht worden in de afwezigheid van de storende invloeden van oplosmiddelmolekulen en tegenionen.
In de meeste gevallen worden in eerste instantie bis-etheen complexen gevormd (met het stikstofdonorligand κ^3-*fac* of κ^3-*mer* gecoördineerd). Deze zijn hetzij stabiel, hetzij ze verliezen etheen waarbij een mono-etheen verbinding gevormd wordt. De binding tussen etheen en een metaalcentrum is sterker in het geval van iridium(I) dan van rhodium(I), met als resultaat dat voor iridium een aantal stabiele iridium bis-etheen complexen geïsoleerd konden worden. Bij verwarmen ondergaan sommige van de N_3 iridium etheen verbindingen in oplossing N-H of aromatische C-H activering, waarbij dinucleaire verbindingen gevormd worden.

Om meer inzicht te krijgen in het mechanisme volgens welke olefines katalytisch geoxygeneerd worden gebruik makend van rhodium of iridium katalysatoren, hebben we de hierboven genoemde verbindingen laten reageren met zuurstof. *In oplossing* konden alleen voor de verbindingen met sterisch omvangrijke stikstofdonorliganden producten geïsoleerd worden: rhodium peroxo (verdringing van etheen door zuurstof) en iridium peroxo-etheen complexen. Rhodium peroxo verbindingen kunnen alleen geïsoleerd worden indien vier stikstofdonorliganden aanwezig zijn rondom het metaalcentrum. Voor de verbindingen met sterisch minder gehinderde liganden konden geen producten geïsoleerd worden uit de complexe reactiemengsels (deze bevatten o.a. paramagnetische verbindingen). *In de vaste stof* reageren de sterisch gehinderde verbindingen helemaal niet met zuurstof. De sterisch minder gehinderde N_3-verbindingen reageren wel, heel erg snel zelfs, maar niet selectief (weer worden o.a. paramagnetische producten gevormd). Dit is in tegenstelling tot wat er eerder beschreven is in de literatuur[2] voor sterisch minder gehinderde N_4-verbindingen (tpa en pyridinofaan), waarvoor 3-metalla-1,2-dioxolanen geïsoleerd konden worden.

Aangezien in veel van de bovenstaande gevallen paramagnetische verbinding gevormd worden, en aangezien voor de vorming van dioxolanen in de vaste stof elektrontransfer tussen zuurstof en het metaal complex tevens wordt voorgesteld als een belangrijke stap in de vorming van een C-O binding, waren we geïnteresseerd in de reactie van metaal(II) olefine verbindingen met zuurstof. Daarom zijn twee nieuwe iridium(II) etheen verbindingen met sterisch omvangrijke N_4-liganden gesynthetiseerd en onderzocht op hun reactiviteit t.a.v. zuurstof. Toename van de sterische hinder uitgeoefend door het stikstofdonorligand zorgt ervoor dat de stabiliteit van het desbetreffende complex toeneemt. De iridium(II) etheen verbindingen ondergaan metaal-ligand-koppeling waarbij ethyleen-gebrugde dinucleaire verbindingen gevormd worden. Sterk coördinerende oplosmiddelen als acetonitril zijn nodig om deze reactie te doen plaatsvinden.

---

[1] bpa = *N*,*N*-di(2-pyridylmethyl)amine (amine substituent is gevarieerd, N_3 ligand),
tpa = *N*,*N*,*N*-tri(2-pyridylmethyl)amine (N_4 ligand)

[2] M. Krom *et al.*, *Angew. Chem. - Int. Edit.*, **2002**, 41 (4), 576-579 en *Eur. J. Inorg. Chem.*, **2003**, 6, 1072-1087.

In tegenstelling tot de iridium(I) etheen verbindingen kunnen de iridium(II) verbindingen wel een C-O binding vormen in de reactie met zuurstof. Dit kan een indicatie zijn dat de metaal(II) olefine verbindingen een rol kunnen spelen in de door rhodium en iridium gekatalyseerde oxidatie van olefins met zuurstof. Een dergelijk inzicht is van belang bij de verdere ontwikkeling van Groep VIII metaal katalysatoren voor de oxidatie van olefines.

Het gedrag van de rhodium(I) en iridium(I) etheen complexen in de gasfase komt netjes overeen met de mate van stabiliteit die reeds waargenomen was in oplossing. Bijvoorbeeld de zuurte van het amine-proton van het bpa-ligand komt zowel tot uiting door toename in verlies van H_2 in de gasfase door de (N-ligand)M^{I}(etheen) complexen (M = Rh, Ir) als door het plaatsvinden van activering van de N-H binding in oplossing. Activering van een aromatische C-H binding wordt zowel waargenomen in oplossing als in de gasfase. Ook uit de gasfase experimenten blijkt dat de metaal-olefine binding sterker is voor iridium(I) dan voor rhodium(I) centra. Dit komt enerzijds tot uiting in het feit dat voor rhodium het olefine makkelijker dissocieert bij botsing met argon dan voor iridium en anderzijds doordat aleen voor iridium bis-etheen verbindingen in de gasfase konden worden waargenomen.

Bij botsing met zuurstof worden er in de gasfase alleen diamagnetische producten gevormd: peroxo verbindingen voor rhodium en peroxo-etheen complexen voor iridium. Het type verbindingen dat reageert in de gasfase en het mechanisme volgens welke deze reageert hangt sterk af van de regio binnenin de massaspectrometer waarin de reactie plaatsvindt. De reactiecondities zijn in elke regio verschillend en bepalen of associatieve en/of dissociatieve reacties kunnen plaatsvinden.

Er zijn duidelijke verschillen tussen de reactiviteiten waargenomen in oplossing, de vaste stof en in de gasfase. In tegenstelling tot wat is waargenomen voor reacties in oplossing, vindt er in de gasfase geen elektrontransfer plaats. M.a.w. door te kijken naar gasfase reacties is het mogelijk om het diamagnetische en het paramagnetische reactiepad van elkaar te scheiden (in oplossing vinden deze reacties gelijktijdig plaats).

Op nog een aantal andere punten verschillen gasfase reacties significant van die in oplossing:

1) In de gasfase wordt voor ***alle*** tpa-type rhodium etheen complexen de vorming van peroxo verbindingen waargenomen.
2) In tegenstelling tot in oplossing is in de gasfase voor de waarneming van rhodium peroxo verbindingen de aanwezigheid van vier stikstofdonorliganden rondom het metaalcentrum niet noodzakelijk.
3) Tijdens geen enkele reactie in de gasfase is de vorming van dioxolanen waargenomen (dit wordt waarschijnlijk veroorzaakt door de afwezigheid van elektrontransferreacties).

Aangezien reacties van organometaalverbindingen erg complex kunnen zijn, kan een vergelijking van reactiviteiten in de verschillende fasen erg nuttig zijn en kan meer inzicht geven in het mechanisme volgens welke een reactie plaastvindt. Een dergelijke vergelijking kan ook informatie verschaffen over de reden waarom sommige complexen zo'n instabiel zijn.

Curriculum Vitae

Simone Thewissen werd op 10 november 1975 geboren te Geleen en groeide op in Beek (L).

In 1994 behaalde zij haar Gymnasium β diploma cum laude (8 vakken) aan de Scholengemeenschap Sint Michiel te Geleen (inmiddels genaamd Graaf Huyn College).

In datzelfde jaar begon zij haar studie scheikunde aan de Katholieke Universiteit Nijmegen (inmiddels genaamd Radboud Universiteit Nijmegen), waarvan zij in augustus 1999 het doctoraal examen behaalde. Haar hoofvakstage in de organometaalchemie, met als onderwerp "Synthese en reactiviteit van rhodium en iridium olefine complexen met tetradentaat liganden" voerde Simone uit op de afdeling Anorganische Chemie van Prof. Dr. A.W. Gal onder begeleiding van Dr. P.H.M. Budzelaar. De bijvakstage in de Industriële Chemie werd gedaan bij een research afdeling van DSM, BC-ICC, te Geleen, onder leiding van Drs. P. van Geem en P. Hoogendoorn van DSM en Prof. Dr. A.W. Gal.

Naast haar studie was Simone ook werkzaam als studentassistente tijdens praktika van lagere-jaars studenten.

In september 1999 begon Simone op de afdeling Anorganische Chemie van de Radboud Universiteit Nijmegen o.l.v. Prof. Dr. A.W. Gal en Dr. B. de Bruin te Nijmegen aan het promotieonderzoek in de organometaalchemie dat tot het huidige proefschrift leidde. Dit onderzoek werd gedeeltelijk uitgevoerd in Nijmegen (oplossings- en vaste stof chemie) en gedeeltelijk aan de Eidgenössische Technische Hochschule (ETH) in Zürich, Zwitserland, o.l.v. Prof. Dr. P. Chen en Prof. Dr. D.A. Plattner (gasfase chemie).

In november 2001 ontving Simone de "Ecomagic Award 2001" uitgereikt door Akzo Nobel Catalysts (inmiddels genaamd Albemarle Catalysts).

In september 2004 werd door de Universiteit van Kaapstad (UCT) aan Simone een Postdoctoral Fellowship toegekend, die zij gebruikte om vanaf januari 2005 daar te gaan werken als post-doc onderzoeker in de Katalyse Onderzoeksgroep van het departement Chemical Engineering o.l.v. Prof. Dr. J.C.Q. Fletcher en Dr. W. Böhringer, en waar zij op het moment nog steeds werkzaam is.

Simone Thewissen was born in Geleen, the Netherlands, on November 10, 1975 and grew up in Beek (in the very south of the Netherlands).

In 1994 she graduated cum laude from her pre-university education (Gymnasium-β, science) at the "Scholengemeenschap Sint Michiel" in Geleen, the Netherlands (now called "Graaf Huyn College").

That same year she commenced her chemistry studies at the University of Nijmegen, the Netherlands (now called Radboud University Nijmegen). In 1999 she graduated cum laude with a major in the field of Metal-Organic Chemistry at the Department of Inorganic Chemistry under supervision of Prof.Dr. A.W. Gal and Dr. P.H.M. Budzelaar ("Synthesis and reactivity of rhodium and iridium olefin complexes of tetradentate ligands"). Simone fulfilled a minor thesis in Industrial Chemistry at the Base Chemicals - Industrial Chemistry and Catalysis department (BC-ICC) of the DSM research devision in Geleen, the Netherlands, under supervision of Drs. P. van Geem, P. Hoogendoorn and Prof. Dr. A.W. Gal.

During her study Simone assisted in practical courses in the field of organic and metal-organic syntheses.

In September 1999 Simone started a PhD research project in the field of metal-organic chemistry at the Department of Inorganic Chemistry of the Radboud University Nijmegen under supervision of Prof. Dr. A.W.

Gal and Dr. B. de Bruin. This thesis was a collaboration with Prof. Dr. P. Chen and Prof. Dr. D.A. Plattner at the Swiss Federal Institute of Technology Zurich (ETH-Zürich) in Switserland. The present thesis describes the research she carried out during this project. The gas-phase measurements were performed in Switzerland.

In November 2001 Simone received the "Ecomagic Award 2001" granted by Akzo Nobel Catalysts (now called Albemarle Catalysts).

In September 2004 Simone was awarded a Postdoctoral Fellowship by the University of Cape Town (UCT), South Africa, which she used to start working as a Postdoctoral Fellow at the Catalysis Research Unit of the Department of Chemical Engineering under auspices of Prof. J.C.Q. Fletcher, from January 2005 on.